NASA
TT
F-494
v.2
c.1

NASA TECHNICAL TRANSLATION

NASA TT F-519

LOAN COPY
AFWL (
Kirtland A.

0068972
TECH LIBRARY KAFB, NM

NASA TT F-519

HELICOPTERS - CALCULATION AND DESIGN

Volume II. Vibrations and Dynamic Stability

by M. L. Mil', et al.

"Mashinostroyeniye" Press
Moscow, 1967

NATIONAL AERONAUTICS AND SPACE ADMINISTRATION • WASHINGTON, D. C. • MAY 1968

TECH LIBRARY KAFB, NM
0068972

NASA TT F-519

HELICOPTERS - CALCULATION AND DESIGN

Volume II. Vibrations and Dynamic Stability

By M. L. Mil', et al.

Translation of "Vertolety. Raschet i proyektirovaniye. 2. Kolebaniya i dinamicheskaya prochnost'." "Mashinostroyeniye" Press, Moscow, 1967.

NATIONAL AERONAUTICS AND SPACE ADMINISTRATION

For sale by the Clearinghouse for Federal Scientific and Technical Information
Springfield, Virginia 22151 – CFSTI price $3.00

ANNOTATION

/2*

The work "Helicopters, Calculation and Design" is published in three volumes:

Vol.I - Aerodynamics;
Vol.II - Vibrations and Dynamic Strength;
Vol.III - Design.

The second volume gives an account of certain problems of the theory of vibrations and methods of calculating stresses set up during such vibrations in helicopters in flight, and, in particular, in the rotor blade.

Methods are presented for calculating the service life of a structure and for calculating helicopter vibrations which permit determining the amplitudes of these vibrations and comparing them with the norms of comfort. For the first time in Soviet literature, the problem of coupled vibrations of rotor and fuselage is examined.

The theory of self-excited oscillations of a special type known as "ground resonance" is discussed in detail. The characteristics of the occurrence of such vibrations in a helicopter on the ground, during takeoff and landing run, and under flight conditions are examined.

Special cases, little elucidated in the general literature, of calculating bearings that operate under specific conditions of rolling are examined in a separate chapter. The same chapter gives an account of the theory and method of calculating a new type of thrust bearing of high load capacity and bearings under compound loads.

The book is intended for engineers of design offices, scientific workers, graduate students, and teachers of higher institutes of learning. It might be useful to engineers of helicopter manufacturers and to students for furthering their knowledge of the vibrations and dynamic strength of helicopters. Certain sections of the book will be useful also to flight and technical staffs of helicopter flight units.

There are 35 tables, 246 illustrations, and 47 references.

Cand. Tech. Sci. R.A.Mikheyev, Reviewer

---

* Numbers in the margin indicate pagination in the foreign text.

PREFACE /3

The first volume of the work "Helicopters, Calculation and Design", published in 1966, was devoted to aerodynamics: theory and methods of calculating the aerodynamic characteristics of rotors and an aerodynamic calculation of helicopters of various configurations.

That volume included an account of the theory of rotor flutter which usually belongs to the category of aeroelasticity - an area between aerodynamics and mechanical strength.

The present, second volume is a logical continuation of the first and is devoted to vibrations and dynamic strengths of helicopters.

The problems of the static strength of helicopters comprise no fundamentally new aspects in comparison with what is known in aircraft construction. With respect to vibrations and dynamic strength, helicopters exhibit a number of peculiarities which were recognized when they first appeared as a new type of flying machine. These peculiarities loomed large during - if one may use the expression - the "struggle for existence" of this new type of craft in the overall system of air transport means not requiring airfields.

The recital of the problems of vibration and dynamic strength of the helicopter begins with a description of a method of calculating the elastic vibrations of its rotor blade, which are similar in fundamental equations and methods of solution to those used in the theory of flutter but have a different trend since ultimately the calculation reduces mainly to a solution of the purely mechanical strength problem, namely to a determination of variable stresses acting in the blade, and then, with the use of data on the fatigue limits of a specific structure, to a determination of service life, i.e., blade life.

Problems of vibrations and dynamic strength are important not only from the viewpoint of reliability of the craft. Also the service life of machines, and hence their economy, depends on the solution of these problems.

In particular, this volume examines current methods of calculating elastic vibrations of a blade, performed on high-speed electronic computers which permits determining the variable stresses set up in the blade.

Investigations of the "ground resonance" mode of vibration, just as a study of the vibrations of a structure, constitute the principal theme of the theory of helicopter vibrations.

Elimination of "ground resonance" vibrations which, if they arise and develop further, lead to destruction of the craft on the ground and, in the case of multirotor configurations, also in the air, has always been one of the main problems confronting the designer. The problem of vibrations of helicopter parts, examined from the viewpoint of crew and passenger comfort, is also quite important. It is not difficult to estimate the acuteness of this problem when

thinking of the power of the constant source of such vibrations - a huge rotor operating in a highly variable velocity field. /4

The last chapter of this volume is devoted to a calculation of special bearings, a necessity in designing many of the helicopter components and thus representing a transitional chapter to the third volume on "Helicopter Design".

The volume "Design" will give a brief study of the main problems in layout of helicopters, selection of the basic parameters of helicopters including winged types, and auxiliary propulsion units such as tractor propellers or supplementary jet engines. Economic considerations of aviation engineering, of importance in designing, will also be presented.

This volume also presents a discussion of problems of balancing, controllability, and stability from the viewpoint of selecting parameters for the control system, as well as problems of designing individual components of the helicopter.

M.Mil'

*

The second volume "Vibrations and Dynamic Strength" was written by: Introduction, M.L.Mil'; Chapter I, A.V.Nekrasov, Chapters II and III, L.N. Grodko; Chapter IV, M.A.Leykand. Section 11 of Chapter I was written by A.V. Nekrasov in collaboration with engineer Z.Ye.Shnurov.

In preparing the manuscript the authors were assisted by engineers F.L. Zarzhevskaya, V.M.Kostromin, and I.V.Kurov.

In this volume, we made use of the results of calculations performed by engineers Yu.A.Myagkov, O.P.Bakhov, V.F.Khvostov, S.A.Golubtsov, V.M.Pchelkin, S.Ye.Sno, V.G.Pashkin, N.F.Shevnyakova, N.M.Kiseleva, L.V.Artamonova, V.F.Semina, N.A.Matskevich, V.I.Kiryushkina, and A.G.Orlova.

The reviewer, R.A.Mikheyev, offered many valuable comments.

Engineer L.G.Rudnitskiy was in charge of the final preparation of the manuscript for publication.

The authors express their sincere gratitude to these coworkers.

TABLE OF CONTENTS

	Page
Preface	iii
Introduction	1
CHAPTER I ELASTIC VIBRATIONS AND BLADE STRENGTH	11
Section 1. Problems of Calculation, Basic Assumptions, and Derivation of Differential Equations of Blade Bending Deformations	12
1. Ultimate Purpose of Calculating Elastic Blade Vibrations	12
2. Calculation of Blade Strength	13
3. Flight Regimes Detrimental to the Fatigue Strength of the Structure	14
4. Assumption of a Uniform Induced Velocity Field	15
5. Assumptions in Calculating Aerodynamic Loads on the Blade Profile	15
6. Relation of Deformations due to Bending in Two Mutually Perpendicular Directions and Corresponding Assumptions for Calculation	16
7. Consideration of Torsional Deformation of a Blade in Calculations of Flexural Vibrations	17
8. Two Calculation Steps in Blade Design: Calculation of Natural Vibration Frequency and Calculation of Stresses	18
9. Idealized Blade Models Used in Calculation	18
10. Derivation of the Differential Equation of Blade Bending in a Centrifugal Force Field at Vibrations in the Flapping Plane	20
11. Differential Equation of Blade Bending in the Rotor Plane of Rotation	22
Section 2. Free Vibrations of the Blade of a Nonrotating Rotor	22
1. Method of Calculation for Solution of the Integral Equation of Blade Vibrations	22
2. Calculation of the Natural Vibration Modes and Frequencies of a Blade Model with Discretely Distributed Parameters	24
3. Condition of Orthogonality and Calculation of Successive Natural Vibration Harmonics	26
4. Characteristics of Calculation of Natural Vibration Frequencies and Modes of a Hinged Blade	27
5. Calculation of the Natural Vibration Modes and Frequencies of a Blade as a Simply Supported Beam	28
Section 3. Approximate Method of Determining the Natural Blade	

Page

Vibration Frequencies in a Centrifugal Force Field 29
1. Use of B.G.Galerkin's Method for Determining the Natural Blade Vibration Frequencies 29
2. Resonance Diagram of Blade Vibrations 31
3. Selection of Blade Parameters to Eliminate Resonance during Vibration in the Flapping Plane 32
4. Selection of Blade Parameters to Eliminate Resonances in the Plane of Rotation 34
Section 4. Calculation of Natural Blade Vibration Modes and Frequencies in a Centrifugal Force Field 36
1. Purpose and Problems of Calculation 36
2. Limits of Applicability of Calculation Methods Reducing to a Solution of the Integral Equation of Blade Vibrations 37
3. Possible Methods of Calculating Free Blade Vibrations in a Centrifugal Force Field 39
4. Three-Moment Method for Calculating Natural Blade Vibration Modes and Frequencies in a Centrifugal Force Field 39
5. Determination of Bending Moments on the Basis of Known Forces 46
6. Determination of Displacements from Known Bending Moments 48
7. Case of a Blade Rigidly Attached at the Root .. 50
8. Possible Simplifications in Calculating the Coefficients 50
9. Certain Results of Calculating the Natural Blade Vibration Modes and Frequencies 51
Section 5. Torsional Vibrations of a Blade 57
1. Problems Solved in Calculating Torsional Vibrations 57
2. Differential Equation of Torsional Blade Vibrations 58
3. Determination of the Natural Torsional Blade Vibration Modes and Frequencies 60
4. Determination of the Natural Vibration Modes and Frequencies of a Rotor as a Whole 64
Section 6. Combined Flexural and Torsional Blade Vibrations .. 65
1. Coupling of Flexural and Torsional Vibrations .. 65
2. Method of Calculating Binary Vibrations 66
3. Effect of Coupling between Bending and Torsion at Natural Vibration Frequency 71
Section 7. Forced Blade Vibrations 77
1. Use of B.G.Galerkin's Method for Calculating Blade Deformations. Determination of Static Deformations of a Blade 77
2. Determination of Blade Deformations with Periodic Application of an External Load 79

Page

3. Simplified Approach to Calculation of Forced Blade Vibrations 81
4. Amplitude Diagram of Blade Vibrations 83
5. Calculation of Vibrations at Application Phase of External Load Variable over the Blade Length 84
6. Aerodynamic Load on a Rigid Blade 85
7. Determination of the Blade Flapping Coefficients 89
8. Simplified Calculation of Elastic Blade Vibrations 93

Section 8. Calculation of Bending Stresses in a Blade at Low and Moderate Flying Speeds 97
1. Characteristics Distinguishing Flying Regimes at Low and Moderate Speeds 97
2. Method of Calculating Stresses 97
3. Assumptions in Determining Induced Velocities 98
4. Mathematical Formulas for Induced Velocity Field Determination 100
5. Transformations of Mathematical Formulas in Particular Cases 102
6. Numerical Determination of the Integrals $J(\bar{P}_m)$ and $J(\bar{\bar{P}}_m)$ 103
7. Assumptions Adopted in Aerodynamic Force Determinations 107
8. Mathematical Formulas 107
9. Conversion to an Equivalent Rotor 111
10. Basic Assumptions Used in Calculation of Bending Stresses 111
11. Differential Equation of Blade Vibrations and its Solution 112
12. Determination of the Coefficients on the Left-Hand Side of the Equations in Table 1.8 .. 113
13. Determination of the Coefficients on the Right-Hand Side of the Equation of Table 1.8 116
14. System of Equations after Substitution of Eqs.(8.34) and (8.38) 117
15. General Computational Scheme 118
16. Determination of Deformation Coefficients 118
17. Computational Program 120
18. Comparison of Calculation with Experiment at Low Flying Speed 122
19. Comparison of Calculation with Experiment at Moderate-Speed Mode 124
20. Possibilities of Further Refinement of Calculation Results 125

Section 9. Calculation of Blade Bending Stresses, with Consideration of the Nonlinear Dependence of

Page

Aerodynamic Coefficients on Profile Angle of Attack and Mach Number 127
1. Flight Regimes 127
2. Determination of Aerodynamic Loads 127
3. Method of Blade Calculation as a System whose Motion is Coupled by Prescribed Vibration Modes 129
4. Mathematical Formulas for a Blade Model with Discrete Parameters 133
5. Consideration of a Variable Induced Velocity Field 134
6. Characteristics of Numerical Integration of Differential Equations of Elastic Blade Vibrations 135
7. Numerical Integration Method Proposed by L.N.Grodko and O.P.Bakhov 143
8. Sequence of Operations in Recalculation and Practical Evaluation of Different Integration Steps 144
9. Comparison of Results by Numerical Integration Methods with Calculation of Harmonics 147
10. Some Calculation Results 148

Section 10. Calculation of Flexural Vibrations with Direct Determination of the Paths of Motion of Points of the Blade 151
1. Principle of the Method of Calculation 151
2. Determination of Elastic Forces Applied to a Point of the Blade by Adjacent Segments 153
3. Characteristics of Numerical Integration of Eqs.(10.1) 156
4. Equations of Motion for a Multihinge Articulated Blade Model 158
5. Sequence of Operations in Calculating Elastic Vibrations by the Numerical Integration Method 161
6. Method of Calculation with Inverse Order of Determining Variables in Numerical Integration 163
7. Comparative Evaluation of Various Methods of Calculating Flexural Blade Vibrations 165

Section 11. Fatigue Strength and Blade Life 168
1. Testing a Structure to Determine its Service Life 168
2. Dispersion of the Characteristics of Endurance in Fatigue Tests 169
3. Basic Characteristics of the Fatigue Strength of Structure 170
4. Stresses Set Up in the Blade Structure in Flight 173

Page

5. Hypothesis of Linear Summation of Damage Potential and Average Equivalent Amplitude of Alternating Stresses 175
6. Dispersion of the Amplitudes of Alternating Stresses in an Assigned Flight Regime 179
7. Method of Calculating Service Life with the Use of Reliability Coefficients 180
8. Method of A.F.Selikhov for Calculating the Required Safety Factor with Respect to the Number of Cycles η_N 183
9. Determination of $S_{\log N}$ at Given Fiducial Probability 187
10. Dispersion in the Stress Levels for Various Structural Specimens and Reliability Margin with Respect to the Amplitude of Alternating Stresses η_σ 189
11. Method of Determining the Reliability Margin η_σ Proposed by A.F.Selikhov 194
12. Example of Calculation of Service Life 198
13. Possible Ways of Determining the Minimum Endurance Limit of a Structure 202
14. Advantages and Disadvantages of Various Approaches in Determining the Necessary Reliability Margins, and Estimation of their Accuracy 205
15. Blade Strength Requirements in Design Selection 206
16. Strength of a Blade with Tubular Steel Spar 207
17. Strength of a Blade with Duralumin Spar 211
18. Effect of Service Conditions on Fatigue Strength of Spars 212

CHAPTER II HELICOPTER VIBRATIONS 214

Section 1. Forces Causing Helicopter Vibrations 214
1. Excitation Frequencies 214
2. Dependence of the Frequency Spectrum of Exciting Forces on the Harmonic Content of Blade Vibrations 217

Section 2. Flexural Vibrations of the Fuselage as an Elastic Beam 227
1. Calculation of Forced Vibrations of an Elastic Beam by the Method of Expansion in Natural Modes 228
2. Dynamic Rigidity of a Beam. Resonance and Antiresonance 234
3. Application of the Method of Dynamic Rigidity to the Vibration Analysis of Side-by-Side Helicopters 237

Page

4. Method of Auxiliary Mass 241
5. Effect of Damping Forces. Vibrations at Resonance 242
Section 3. Vibration Analysis with Consideration of Fuselage Characteristics 247
1. Fuselage Characteristics. Lateral and Vertical Vibrations 247
2. Calculation of Fuselage Vibrations in the Plane of Symmetry by the Method of Residues ... 251
3. Consideration of the Effect of Shearing Deformation 258
Section 4. Combined Vibrations of the System Fuselage-Rotor .. 259
1. Vibrations of the System Fuselage-Rotor 259
2. Calculation of the Natural Rotor Blade Vibrations in the Plane of Rotation, with Consideration of Elasticity of the Rotor Shaft and Attachment to the Fuselage 263

CHAPTER III GROUND RESONANCE 274

Section 1. Stability of Rotor on an Elastic Base 275
1. Statement of Problem and Equations of Motion 275
2. Stability Analysis and Basic Results 281
3. Physical Picture of Rotor Behavior in the Presence of Ground Resonance 292
4. Rotor on an Isotropic Elastic Base 298
Section 2. Lateral Vibrations of a Single-Rotor Helicopter .. 299
1. Preliminary Comments 299
2. Lateral and Angular Stiffness of Landing Gear. Flexural Center 300
3. Natural Lateral Vibrations of a Helicopter 304
4. Determination of Damping Coefficients 308
5. Combined Action of the System Shock Strut-Pneumatic Tire 310
6. Reduction of the Problem to Calculation of a Rotor on an Elastic Base 312
7. Analysis of the Results of Ground Resonance Calculations 314
Section 3. Characteristics of Damping of Landing Gear and Blade. Influence on Ground Resonance 315
1. Determination of the Damping Coefficient of the Landing Gear Shock Absorber 315
2. Effect of Locking of the Shock Absorber as a Consequence of Frictional Resistance of the Gland and Self-Excited Vibrations of the Helicopter 318
3. Characteristics of Blade Dampers and their Analysis 322

Page

4. Effect of Flapping Motion of Rotor on Ground Resonance 325
Section 4. Ground Resonance of a Helicopter during Ground Run 330
1. Stiffness and Damping of a Wobbling Tire 330
2. Calculation of Ground Resonance and Results ... 335
3. Ground Resonance on Breaking Contact of the Tires with the Ground 337
Section 5. Ground Resonance of Helicopters of Other Configurations 339
1. General Comments 339
2. Calculation of Lateral Natural Vibrations with Consideration of Three Degrees of Freedom 340
3. Calculation of Natural Helicopter Vibrations in the Plane of Symmetry (Longitudinal Vibrations) 347
4. Reduction of the Problem to Calculation of a Rotor on an Elastic Base 352
5. Self-Excited Vibrations in Flight of a Helicopter with an Elastic Fuselage 354
Section 6. Selection of Basic Parameters of Landing Gear and Blade Dampers. Design Recommendations 356
1. Selection of Blade Damper Characteristics 357
2. Rotor with Interblade Elastic Elements and Dampers 361
3. Selection of Stiffness and Damping Characteristics for Landing Gears 364
4. Certain Recommendations for Landing Gear Design 367

CHAPTER IV THEORETICAL PRINCIPLES OF CALCULATING BEARINGS OF MAIN HELICOPTER COMPONENTS 369

Section 1. Equations of Static Equilibrium of Radial and Radial-Thrust Ball Bearings under Combined Load .. 370
Section 2. Calculation of Radial and Radial-Thrust Ball Bearings under Combined Loads, for Absence of Misalignment of the Races 377
1. Pressure on Balls 377
2. Reduced Loads 384
3. Statistical Theory of Dynamic Load-Carrying Capacity 385
4. Effect of Axial Load on Bearing Performance ... 393
5. Approximate Solutions of Equations (2.1) and (2.2) 397
6. Relative Displacements of Races 403
Section 3. Certain Problems in Calculating Radial-Thrust Ball Bearings with Consideration of Misalignment of their Races under Load 405

Page

1. Basic Relationships 405
2. Case of "Pure" Moment 409
3. Simultaneous Action of Moment and Axial Force 413
4. Limit Dependences on Small Loads 4.5
5. Distribution of Load between Rows of Balls of Double-Row Radial-Thrust Ball Bearings 421
6. Examples of Calculation 424

Section 4. Calculation of Tapered Roller Bearings under Combined Loads 426

1. Calculation of Single-Row Tapered Roller Bearings 426
2. Remarks on Calculation of Bearing Assemblies of Two Tapered Roller Bearings 431

Section 5. Calculation of Vibrating Bearings 433

1. Characteristics of the Mechanism of Wear of Antifriction Bearings under Vibration Conditions 434
2. Lubrication of Highly Loaded Vibrating Bearings in the Presence of Small Vibration Amplitudes 435
3. Calculation of Hub Bearings in Main and Tail Rotors 441
4. Calculation of Bearings for the Pitch Control and Control Mechanisms 450

Section 6. Theory and Selection of Basic Parameters of Thrust Bearings with "Slewed" Rollers 453

1. Determination of the Time T_c 454
2. Selection of Angles of Slope of Cage Seats 459
3. Friction Losses 463
4. Additional Considerations of Optimal Thrust Bearing Design with "Slewed" Rollers 465
5. Example of Calculating a Thrust Bearing with "Slewed" Rollers 466

References 468

INTRODUCTION /5

As soon as an aircraft engine of sufficient power and light in weight had been created and the first helicopter took off from the ground, problems of balancing, controllability, and stability of this craft arose. These were mainly aerodynamic problems. If we consider the first flight of de la Cierva's autogiros in 1925-1926 to be the start of flight of rotary-wing aircraft, then we can say that the stated problems were mainly solved in the first decade (1926-1936) of their development. The new type of flying machine was thus cured of its "childhood diseases".

However, as soon as the first series-produced machines appeared and they were placed in service, more serious deficiencies of helicopters became apparent such as, for example, fatigue due to insufficient dynamic strength of certain structural members.

New dynamic problems arose with the wider practical use of autogiros and especially of helicopters, which entered the scene at the end of the Thirties and beginning of the Forties on a new improved technical basis. These problems pertained primarily to oscillations and vibrations of individual structural elements and of the helicopter as a whole, which are harmful owing to the stresses set up in this case, or are impermissible from the viewpoint of necessary crew and passenger comfort, and also include the problem of service life of structural elements operating under high variable stresses. The latter problem, namely the increase in service life, is constantly gaining in importance since the amortization and overall life of a helicopter, determined by the lifetimes of its components, has an effect on the cost-effectiveness in its use as a means of transportation. The service life, in turn, is determined mainly by the level of the variable stresses set up in the structure; therefore, the accuracy with which these are calculated is one of the basic problems of a dynamic strength analysis of helicopters.

A tractor propeller of a conventional aircraft operates practically in an axial flow and, like an engine, sets up no noticeable variable stresses in the structural members. Only takeoff, landing, and flight under conditions of atmospheric turbulence (and, on military aircraft, maneuvers) create appreciable dynamic loads on the aircraft structure, but at relatively few load cycles (of the order of tens and hundreds of thousands of cycles) during the lifetime of the aircraft. In this case, one can speak about repeated static loads.

The loads on the helicopter are quite different. Its main structural members are loaded dynamically, the number of loadings often exceeding tens of millions of cycles during its lifetime. This is due primarily to the asymmetric flow past the rotor, which rotates and simultaneously advances. In so doing, /6 the blade is subject to variable aerodynamic loads as a consequence of the change in relative flow velocity and angles of attack of its sections. All forces and moments acting on the blade are transmitted to the hub and rotor controls. The forces and moments arriving from different blades are mutually compensated, with the exception of loads acting with frequencies whose ratio to the rotor rpm is

a multiple of the blade number. These loads are transmitted to the fuselage and to the nonrotating part of the rotor control system and there set up noticeable variable stresses.

Thus, the problem of vibrations and dynamic strengths in helicopter construction is not only much broader than in aircraft construction but, in many cases, has no direct analogy in the latter.

Recognition of the importance of the problems of dynamic strength was not immediately obvious. Thus, even the causes of the first accidents of autogiros in 1936-1937, during which these craft overturned in the air, were attributed for long to insufficient dynamic stability. In this respect, in particular, investigations of the dynamics of a rotor with hinged blades at curvilinear motion of the craft were undertaken (see Sect.2, Chapt.II of Vol.I). This theory later found wide application in the elaboration of problems of dynamic stability and controllability of helicopters. However, it never uncovered the true cause of the above-mentioned accidents. As was subsequently realized, the cause was insufficient dynamic strength of the rotor blades.

These problems were recognized literally by hit and miss. The first experimental autogiros and helicopters were small and thus had a rather high structural rigidity. However, the first increase in size immediately encountered considerable difficulties. For instance, on the A-4 autogiro, which had a diameter somewhat larger than its predecessor the 2EA autogiro, serious difficulties arose owing to insufficient torsional rigidity of the blade. The blade angle, in the first flight, increased so much due to torsional deformation that autorotation was impossible and the flight almost ended in crackup.

The investigation of this phenomenon was completed with the publication of a paper on the dynamic twisting of a rotor blade in flight [see (Ref.2)], in which the first suggestions were made as to the necessity of matching the center of gravity and the center of pressure, and in which considerations of the effect of blade profile on static stability and controllability of the craft were examined. This investigation resulted in asymmetric profiles, ensuring a large reserve of autorotation, which were adopted in the engineering practice of Soviet helicopter construction. A set of different profiles was used for the blade arrangement. The recommendations in the above paper were sufficient to prevent flutter in the first Soviet helicopters which had a rotor span of about 14 m.

The development of the Soviet helicopter industry is characterized by larger steps than that of the helicopter industry in other countries (this also enabled Soviet designers, who had started later to build helicopters, to create machines vastly superior to modern foreign helicopters with respect to lift capacity and size). Whereas, after the first successful flight of the Sikorsky S-51 with a rotor span of 14 m built in 1947, the Americans, in 1950-1951, began working on a craft with a rotor of 15.5 m diameter (S-55), the Soviet designers, after creating the Mi-1 helicopter with a 14-m rotor, constructed as early as 1952 the Mi-4 and Yak-24 helicopters with 21-m rotors. It is not surprising that such a jump in size led to a new previously unencountered phenomenon: In both craft, the rotor began to flutter during the first takeoff. We readily /7 coped with this problem, but problems of the theory of flutter had to wait a long time for solution.

We first encountered this new phenomenon in April 1952 with the Mi-4 helicopter, when it was ready for its maiden takeoff. At onset of overspeeding, the blades began to flap in a random manner, bending to an ever increasing extent and threatening to strike the airframe. The test crew realized that this was a new phenomenon never before encountered. This constituted so-called flutter of the rotor blades. At that time, no one thought of the fact that this was the very same type of flutter under study by many scientists in the USSR and other countries. According to the data available at that time, flutter was not expected since it was thought to arise at about 500 rpm rather than at a rotor rpm of 100-110, as actually happened in the Mi-4 helicopter. The decisive factor for the occurrence of flutter in this case was the fact that the large forces generated on a rotor of such a diameter produced appreciable deformation of the swashplate of the automatic pitch control, which is equivalent to a decrease in torsional rigidity of the blades, and also the fact that a large value of the coefficient of the flapping compensator (close to unity) had been selected for these machines; this point had been disregarded in earlier investigations of flutter. As a result there was no reason to think of helicopter flights, since flutter set in appreciable before the operating rpm of the rotor was reached.

It became clear, in studying the pattern of flutter (flapping, bending, and twisting of the blades) that this phenomenon could be prevented only by utilizing the torques from the inertia forces generated during displacement of the blade sections on flapping. Without associating rotor flutter with wing flutter where - as known for long - the mutual position of center of gravity, flexural axis, and center of pressure is of prime importance, we simply attached counterweights to several points along the blade length to create moments of inertia of opposite sign during vibrations and then repeated start-up of the rotor; we immediately understood that we had in hand a reliable means of stopping flutter.

Thus, within a short time this problem was practically solved, and by May 1952 the first flights with the Mi-4 helicopter were made.

At the same time, flutter occurred also on the Yak-24 helicopter which had the same hub and automatic pitch control as did the Mi-4 helicopter but the blades were of different design (with larger flexural and torsional rigidity). However, as a consequence of the fact that the rigidity of the automatic pitch control and the parameters of the flapping compensator were decisive in the occurrence of flutter, we also encountered flutter of the very same form and at the same rpm on the blades of the Yak-24 helicopter as well as on the Mi-4 helicopter.

Thus, within several weeks a practical solution was found for preventing flutter, which is used even now. The scientific theory, however, to determine whether flutter will or will not occur and - if it did occur - at what rpm and in what form, was developed by us during the subsequent four years.

It should be stated that, after completion of studies of flutter on the ground (by shifting the centering of the blade forward it was possible to "drive" it beyond the limits of the working rpm and even beyond the maximum permissible rpm of the engine on the ground), there still existed the possibility of its occurrence in flight. This led to detrimental happenings. In January 1953,

crash of a Mi-4 helicopter took place, whose causes were not satisfactorily defined for almost three years. Inspection revealed traces of impact of the blades on the cockpit. This had never been observed before. We should note that, during normal flapping motion, the blade does not come into contact with the cabin unless the lower restrictors of blade overhang or coning stops are ruptured in the air. /8

It is obvious that our search for the cause of this accident was diligent, when realizing that the crash did not stop either actual flights or series production of this prototype.

During 1954, a number of pilots observed an unusual phenomenon in flight, which came to be known as "Kalibernyy effect" (after the pilot who was the first to notice it). Kalibernyy established that in a power descent at a blade setting angle of about 6 - 7°, the blades began to flap out of their coning angle. This stopped after resetting the blades that had a somewhat different transverse centering. However, two years later, when flight-testing a set of blades for absence of the "Kalibernyy effect", i.e., during a power descent with an angle of pitch of 6 - 7°*, this phenomenon became so predominant, at such strong flapping of the blades, that it was difficult to make a forced landing with the craft. It should be mentioned here that close to the ground, upon changing to another regime, the blade flapping stopped and the craft behaved normally. A visual inspection of the helicopter after the flight revealed ruptured blade footings (so-called movable slotted trailing edge of the blade), which indicated bending of the blade in the plane of rotation. Everything else was in good working order. It was decided to make a detailed checkout of this helicopter with the same set of blades. Flight tests were carried out to check and study this phenomenon.

Measurements of the blades showed that the centering had shifted by about 1% of the chord more rearward than its position at the time of the blades leaving the manufacturer. This can be explained as follows: The blades were sheathed with plywood. The center of gravity of plywood is about at 50% of the chord. Therefore, as soon as the wood swells and increases in weight due to the absorbed moisture, the center of gravity of the entire blade will shift toward the trailing edge. The above happening with the helicopter occurred in autumn when the humidity was high.

During these tests it was also conclusively established that the character of blade flapping and the motions of the control stick during flight in a "Kalibernyy effect" regime are completely analogous to the flapping and motion of the stick recorded in ground tests where blades are caused to flutter by an artificially created tail-heaviness. This complex procedure made it possible to establish that the phenomenon occurring in flight was identical with that noted on the ground. Thus it was established that the "Kalibernyy effect" is none other than the onset of flutter in flight. On the basis of this conclusion it was conjectured that the earlier unexplained flight accident in which the blades struck the cockpit was also nothing else than flutter of the blades in flight arising at a rotor rpm at which it did not appear when operating on the ground.

---

* On the Mi-4 helicopter, flutter sets in primarily in this regime.

The vibrations of a hinged blade in flutter, unlike the vibrations of a conventional aircraft wing, are capable of a flapping motion whose amplitude builds up until the blade impacts on the coning stops and, after breaking these, strikes the cabin.

That this phenomenon was not uncovered for a long time can be attributed /9 to the erroneous assumption based on model tests that, if flutter on the ground is eliminated, it cannot occur in air during forward motion. However, practical experience and, later, more rigorous experiments with helicopters and, finally, corresponding theories have shown that there are flight regimes in which flutter at the operating rpm of the rotor will not occur on the ground but may occur in flight.

It should be stated that, as established in investigations, the phenomenon of flutter also had been observed earlier on helicopters. Already in 1949, the Mi-1 helicopter was equipped with a rotor with wider blades to increase the safety factor relative to flow separation. In flight, this rotor produced buffeting which could not be eliminated. After the theory of flutter had been worked out and all aspects of this phenomenon had been clarified, it became possible not only to attribute the jolting of the Mi-1 helicopter with wide blades to an approach of the regime to flutter but also, and without further difficulty, to design and construct (in 1956) a 35-meter rotor for the Mi-6 and Mi-10 helicopters. Perfection of this rotor was confirmed by the fact that a week after the initial takeoff the new heavy Mi-6 helicopter was able to complete the training flight for participation in the Air Parade on Aviation Day at Tushino. Neither then nor later did anything detrimental, associated with flutter, occur with these craft. This constitutes the historical aspect of the flutter problem.

Of no less importance is the problem of determining variable stresses in blades, which is solved by studying their forced vibrations.

During the first decade of their development, helicopter rotors were actually designed without precalculation of variable stresses arising in flight. At that time, calculation was cumbersome and inaccurate and often completed only after the craft was at the airfield. It was only the development of computational methods for variable stresses, allowing the use of high-speed digital computers, that permitted designing blades with deliberate selection of rigidity and mass distribution so as to avoid harmful resonance, reduce the stress level, and thus ensure long service life and blade reliability.

It should be noted that refinement of stress analysis for blades led to further development in depth and elaboration of the aerodynamic theory. As shown in the first volume, refinement of the calculation of flight data did not make it necessary to develop the complex and cumbersome vortex theory of a rotor. Nevertheless, it is only the vortex theory that permits determining the nonuniformity of the induced velocity field, causing variable blade loading at frequencies that excite flexural vibrations of the blades of second, third, and higher harmonics. Therefore, in stress analysis, only the vortex theory can give results close to those observed in reality.

Vibrations constituted another no less important problem. This problem has always been one of the most difficult in the development of rotary wing aircraft.

Dozens of Soviet and foreign designs, interesting from the viewpoint of conception and flight data, never came to completion owing to the high level of vibration.

In conventional aircraft, the sources of vibration are not as powerful as in helicopters. Furthermore, both engines and propellers which are the main vibration exciters in conventional aircraft can be adequately isolated from the structure by means of special shock absorbers. High-frequency resonance /10
produced by such exciters can be eliminated quite easily by comparatively minor modifications of the structure. In a helicopter, in addition to the fact that the perturbing forces produced by the rotors are appreciably greater than in a conventional aircraft, the frequencies from the slowly rotating rotor are rather low and, in combination with the natural oscillation frequencies of the fuselage, engine, wing, or tail unit, give rise to resonance leading to appreciable vibrations with an amplitude of displacement which, in steady flight regimes, reaches magnitudes of the order of 0.3 - 0.4 mm and in short-time regimes, prior to landing of the helicopter, even 1 - 2 mm in the crew cabin.

Resonance with fundamental tones of the natural fuselage vibrations often are practically impossible to damp out by changing the rigidity of the structure in an already built machine. Therefore, it is important to make a correct estimate of the natural vibration frequency of the fuselage and to calculate the vibration amplitude in designing the craft.

In overcoming vibrations, main emphasis must be on reducing the magnitudes of variable forces produced by the rotor and acting on the fuselage. These forces are caused by blade vibration. In turn, such blade vibrations may be larger or smaller depending on the closeness of their natural frequencies to the frequencies of the external excitation sources.

In all cases, closeness to resonance will lead to an increase in blade stresses. However, if the vibrations occur with the harmonic frequency $z_b + 1$ (or $z_b - 1$ for vibrations in the plane of rotation of the rotor) or with the harmonic frequency z_b for vibrations in the flapping plane (where z_b is the number of blades), then the forces are summed and transmitted over the hinges to the hub and through it to the fuselage, causing vibration.

Vertical vibrations, which are the type most disagreeably perceived by man, are largely caused by forces acting in the plane of rotation of the rotor, since these forces, applied high above the center of gravity of the helicopter, create appreciable moments that excite flexural vibrations of the fuselage. In this case, it is natural that the greatest vibration amplitudes (antinodes) are reached at the ends of the fuselage and hence in the cockpit.

It was found that, in determining the natural vibration frequencies of helicopter blades, it must be considered that the rotor hub does not remain fixed during the vibration since it is attached to an elastic fuselage. Thus, in an analysis of vibrations, the craft should be treated as a single dynamic system with elastic blades hinged to a hub attached to an elastic fuselage.

It is obvious that it is only lately that such a calculation scheme could be developed and made available for study. As far as we know, we are the first,

in this book, to present a method of calculating helicopter vibrations in the design stage.

Later in this volume, we will discuss self-excited oscillations of a helicopter, generally known as "ground resonance".

Designers first encountered the phenomenon of ground resonance more than 30 years ago when one of the first Soviet autogiros, the A-6 (designed by V.A. Kuznetsov), was equipped with low-pressure tires which were new at that time. The oleo struts were removed from this helicopter. An unexpected vibration occurred in the first takeoff attempt. The helicopter rocked from wheel to wheel at constantly increasing amplitude, finally jumping upward so that the wheels broke contact with the ground. The takeoff ended in failure.

Since the tests were recorded by a motion-picture camera, it was possible /11 to establish that the blades had executed increasingly stronger vibrations about the drag hinge. These vibrations, which occurred in a centrifugal force field, produced a periodic displacement of the center of gravity of the entire lifting system relative to the center of the hub and thus excited vibrations of the helicopter standing on the ground. It is obvious that, if the frequency of displacements of the rotor center of gravity coincides with the frequency of natural vibrations of the helicopter on pneumatic tires, such vibrations are able to increase. It would seem that the physical aspect of the phenomenon is clear. The energy that fed these increasing vibrations was either the energy of the engine turning the rotor or, with the engine cut out, the kinetic energy of the rotating rotor.

However, numerous investigations, which are still in progress, were needed to develop the theory of ground resonance and to study its new manifestations, possibly in new basically differing configurations and structures.

The first theoretical work explaining the nature of self-oscillations of the "ground resonance" type was done as early as 1936 by I.P.Bratukhin and B.Ya. Zherebtsov. In particular, the results of their investigations made it possible to eliminate ground resonance in the world's largest autogiro, the A-15 with a rotor span of 18 m which was constructed in 1936 from the design by V.A.Kuznetsov and M.L.Mil'. In the design of the hub of this autogiro, springs mounted to the blade-vibration restrictor around the drag hinge were used. The springs were given the natural vibration frequency of the blades in the plane of rotation, which eliminated "ground resonance".

There is no doubt that, at the time, the phenomenon of ground resonance was also known in the Western Countries and had undergone some study there, since even the first successful de la Cierva autogiros, for example the C-19, had elastic couplings (shock absorbers) connected to the blades over friction dampers.

However, many designers continued for some time to produce autogiros without dampers in the drag hinges. A model of such a machine was the A-7 autogiro developed in 1937 by N.I.Kamov. It made successful flights without dampers on the rotor hub. The secret of the success was the fact that this was the first time a tricycle landing gear was used, which ensured a practically vertical

position of the rotor axis during engine revving before takeoff and after the landing stop. This caused small initial perturbations due to deflection of the blades in the plane of rotation, since the initial deflections of the blades are produced by the projection of the force of gravity onto the plane of rotation. Another important point was the friction force in the hinges (at that time, bronze bushings were used in the hinges), which cannot be disregarded in the presence of appreciable centrifugal forces; in this case they produced sufficiently large damping. On one occasion, the pilot S.A.Korzinshchikov after one of the flights forgot to push the control stick immediately after landing and thus did not change the craft from a three-point landing (tail skid and main landing gear) to a standard position (with support on the front leg); ground resonance occurred after subsequent decrease in rotor rpm owing to the large initial disturbance in blade deflections in the plane of rotation (the axis of rotor rotation was inclined at an angle of 14° to the ground), causing the blades to break and the helicopter to be damaged.

Thus, the problem assumed constantly newer aspects from one experimental model to another.

Since, at that time, no exact calculation of the required damping of blade vibrations existed (in the presence of ground resonance vibrations, the damping of vibrations of the craft by shock absorbers on the landing gear is of equal /12 importance), designers attempted to select a minimum value of the friction moment of the hub damper. This was dictated by the desire to reduce variable bending moments set up in the presence of a damper during forced vibrations of the blades in flight.

As is known, friction dampers cause vibrations at threshold excitation. If the excitation is small, i.e., the excitatory moment is smaller than the friction moment, no vibrations will appear. However, vibrations may suddenly arise in a helicopter which is fail-proof with respect to ground resonance and had already been in actual service. This can be attributed to the fact that, in a given case, the initial perturbations may be greater than usual. This case occurred in the Mi-1 helicopter when taxiing obliquely across deep ruts made by a truck. In this case, a random disturbance of tilt strongly rocked the craft on its pneumatic tires, causing it to acquire such large vibration amplitudes that the available damping in the hub became inadequate and ground resonance arose. The pilot G.A.Tinyakov remedied this in a simple manner by taking off; this stopped the vibrations since the elastic coupling, i.e., the coupling with the ground, was broken.

This case suggested the need for making use of viscous friction, i.e., installing hydraulic blade vibration dampers in the hub, for which the moment of friction does not remain constant but increases with the vibration amplitude.

However, practice constantly required improvement and development of the theory in this area. One merely need recall the generation of ground resonance when the helicopter is attached to its moorings, with the engine operating.

Several cases of ground resonance were observed also when the wheels of the helicopter, in taxiing during takeoff or landing, had only slight ground contact, so that the propulsive force of the rotor came close to the weight of the craft

and the shock struts with the usual pretightening were fully extended. The difference between the weight and the propulsive force of the craft was absorbed only by the pneumatic tires.

It is obvious that, in this case, not only will the vibration frequencies of the craft change but there also will be no damping of the struts. Thus, ground resonance occurred here which had never been observed in a helicopter that was not moored or was not taxiing, at very small wheel loading.

To avoid such cases, we began using so-called two-chamber landing-gear struts, which were shock struts provided with a second low-pressure chamber for absorbing the vibration energy of the craft when it made only slight ground contact with the pneumatic tires while the main struts were not operative.

Problems of the theory of ground resonance are especially important for twin-rotor configurations when the elastic system coupling both rotors, be it the fuselage in the fore-and-aft or the wing in the side-by-side configuration, has low natural vibration frequencies. In the presence of such vibrations, appreciable displacements of the rotor hub may take place, creating the possibility of energy transfer between blade oscillations and oscillations of the lifting structure. Vibrations of this type are possible not only on the ground but also in flight.

A similar problem arises in designing tail rotors with drag hinges mounted to a flexible tail boom.

The development of harmonic and improved craft is possible only if the designer is sufficiently competent not only in general problems of design but also in special problems having to do with the theory and calculation of the indi- /13
vidual elements.

A modern helicopter contains many essential highly loaded mechanical components whose reliability and service life depend in many respects on the performance of the bearing assemblies. Consequently, helicopter designers should be familiar with the theory and calculation of roller bearings. This pertains specifically to cases of the work of roller bearings in complex combinations of external loads and in the presence of rocking motion of low amplitude.

For this reason, we included a chapter giving answer to problems of the theory and calculation of bearing assemblies of hubs, cyclic pitch control, and other units. One of the most interesting problems described in Chapter IV is the theory of special thrust roller bearings in which, owing to the positioning of the rollers at an angle to the radial direction, the cage - during the rocking motion - not only vibrates along with the movable collar but also continuously rotates in one direction. This prevents local wear of the raceways and increases the lifetime of the bearing.

It should be noted that the use of such bearings in the feathering hinge of rotor hubs resulted in an appreciable increase in service life.

Helicopter engineering requires a high general level of theoretical and scientific training of the design engineer, since dynamic problems are of much

greater importance for helicopters (rotary wing aircraft) than for regular aircraft (prototypes with fixed wing, although lately also including tilt wings and variable sweep). This is confirmed by the fact that the few designers who made notable contributions to the development of helicopter engineering and especially those who had practical success, were simultaneously outstanding scientific theorists. These include B.N.Yur'yev, Prof. A.M.Cheremukhin, and Prof. I.P. Bratukhin who, in the Thirties, were the developers of the first Soviet helicopters from the 1EA to the 11EA prototypes; Prof. Focke, the designer of the FW-61 and FA-223 helicopters in Germany; one of the pioneers of aviation Louis Breguet; Prof. Doran who created the first French helicopters; and many others.

It should be noted that the present level of theoretical training of designers working for the foremost helicopter engineering firms of the world is very high, as far as can be judged from the literature. For this reason, neither the engineer-calculator nor the designer working in helicopter engineering should have any difficulty in assimilating the material presented below.

The authors hope that this second volume will find readers and be found useful.

* *
*

The inserts show photographs of the main Soviet helicopters in series production. These are the first Soviet series-produced helicopters with piston engines Mi-1 and Mi-4, developed in 1949 and 1952. Having been produced in large numbers, these prototypes range now among the most widespread variants of helicopters.

Other photographs show the Mi-6 helicopter with two turboprop engines /14
developed in 1957 and the Mi-10 helicopter (1962) which is a flying crane with a high landing gear, adapted for lifting and transporting heavy stores rigidly mounted on the underbelly. In 1965, a world lifting record for helicopters was established with this cargo craft: 25 tons were lifted to a height of 2830 m.

The next pictures give the Mi-2 and Mi-8 helicopters which are a second generation of Soviet light and medium versions. The lifting systems of the Mi-1 and Mi-4 were retained on these, but the single piston engine was replaced by two turboprop engines.

CHAPTER I /15

ELASTIC VIBRATIONS AND BLADE STRENGTH

Calculation of elastic vibrations is a necessary element in the process of developing new blade designs. It forms an inseparable part of the calculation of blade strength.

To develop helicopter blades it is necessary to solve many presently quite complex technological and design problems. In their solution, account must be taken of the most diverse requirements and primarily of the requirement of high fatigue strength of the structure.

The work of designing blades usually involves the following basic steps:
Selection of materials for individual structural members, determination of optimal parameters, and design of the blade.
Selection of the best technological processes ensuring highest fatigue strength of its main stressed elements, and manufacture of the blade.
Flight tests with analysis of stresses set up in flight.
Dynamic tests and evaluation of the blade service life.
Performance of the complex of finalizing, including work on reduction of active stresses and increase in fatigue strength of the structure.
Acceptance tests and start of series production.
Analysis of operation of series-produced blades under various high-load and endurance conditions and layout of final designs for blade series based on the analytical data.

Calculations of elastic blade vibrations are required at many stages of this work, but primarily at the initial stage which terminates with the actual blade design.

In selecting the blade parameters and its structural materials, one of the main criteria is the magnitude of alternating stresses set up in flight and the correlation between these stresses and others characterizing the fatigue strength of the structure. It is only by calculations that the magnitude of these stresses can be determined and an estimate made of the strength of the structure at this stage. To design the blade within the required - usually rather short - period, the designer should have available modern methods and computational means to obtain a rapid solution to any number of possible problems.

Of similar importance is the calculation in the finalizing stage. As a rule, in new blade designs the variable stresses are excessive, confronting the designer with the problem of their reduction. For this, the occurrence pattern of stresses measured in flight must be confirmed by calculation, followed by devising means for their reduction by varying some of the parameters. To attempt a solution of this problem without calculation generally means excessive loss of time in checking unverified assumptions and waste of considerable funds in manufacturing a blade that might be rejected after flight testing. /16

A reduction of alternating stresses is extremely important and permits not only an increase in the reliability and service life of the blade but also an improvement in mechanical and flying qualities of a helicopter such as, for example, flying speed and lift capacity, which in modern helicopters are often limited because of strength conditions.

Solution of all these problems would not be excessively difficult if the calculation results would sufficiently well coincide with those observed during in-flight stress analysis. Unfortunately, this is not always the case since calculation does not necessarily give results satisfactory for practice.

Calculations for determining the natural vibration frequencies are most reliable. Usually, an accuracy of the order of ±2% is achieved. Therefore, all calculations on the exclusion of resonance yield high reliability. Calculations of alternating stresses at cruising and maximum flying speeds are noticeably less reliable. The stress values obtained in these calculations usually are 15-25% lower than stresses measured in flight. Consequently, the stress analyses in these regimes do not always satisfy the designer. Nevertheless, the error can be compensated to a certain extent by introducing into the calculation a correction allowing for a constant divergence from experiment.

A still greater error is possible in calculations of alternating stresses at low flying speeds.

It is obvious from the above that the calculation methods for alternating blade stresses require further elaboration. Nevertheless, practice has shown that parameter selection and blade finishing without even these imperfect methods is rather ineffective. Therefore, this Chapter will give a detailed account of various calculation methods. In our opinion, this will give the reader an idea of all features of blade loading in flight, showing possible approaches for calculation, for determining and estimating the advantages and shortcomings of various methods and, finally, providing engineers concerned with such problems bases for extension of studies and improvements of calculation methods.

Along with a description of various methods of calculating elastic blade vibrations, on which main emphasis is placed, this Chapter also presents the basic principles of stress analysis for blades and of service life determination (Sect.11).

With respect to specific data on the selection of blade parameters, we thought it preferable to include this problem in the Section "Blade Design" forming part of the third volume of this book.

Section 1. Problems of Calculation, Basic Assumptions, and Derivation of Differential Equations of Blade Bending Deformations

1. Ultimate Purpose of Calculating Elastic Blade Vibrations

The calculation of elastic blade vibrations is necessary in solving a number of problems created in the designing and debugging of a helicopter. The

Mi-1 Helicopter.

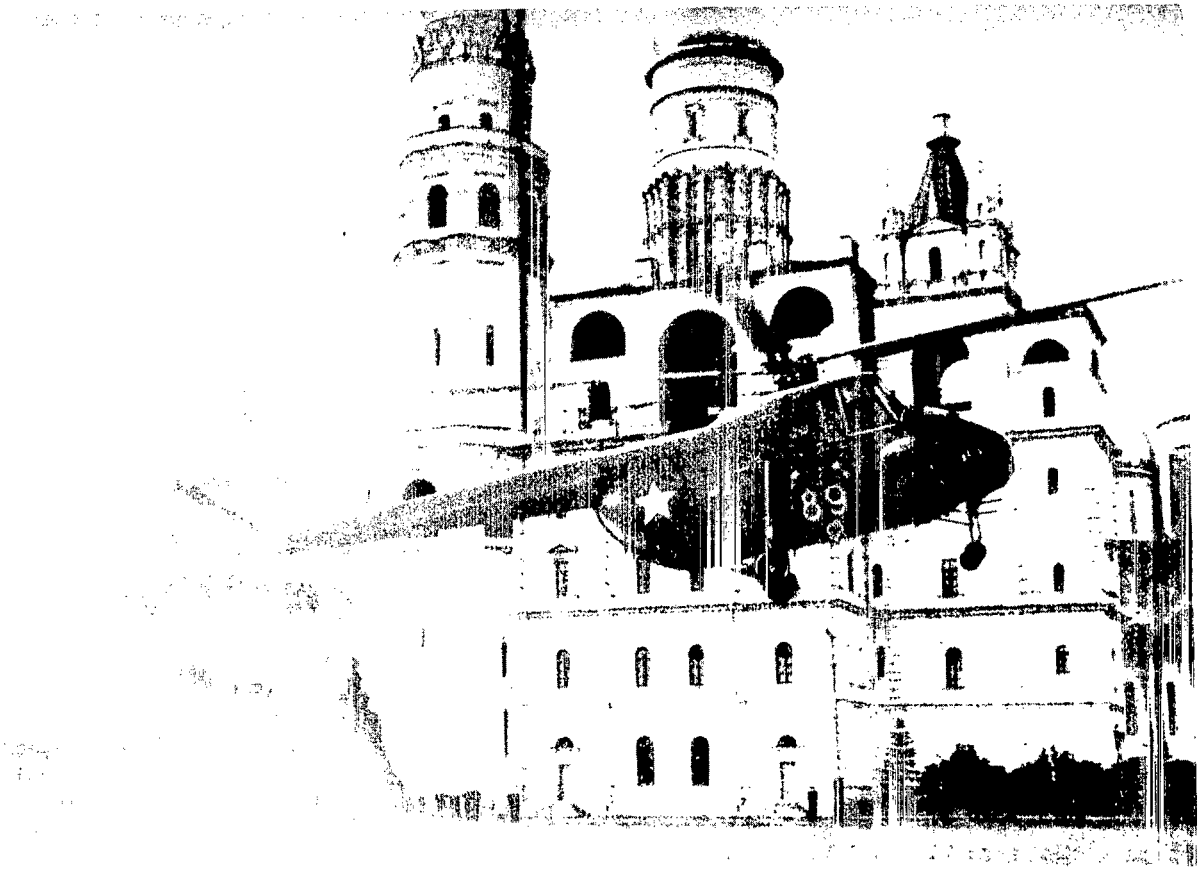

Mi-4 Helicopter.

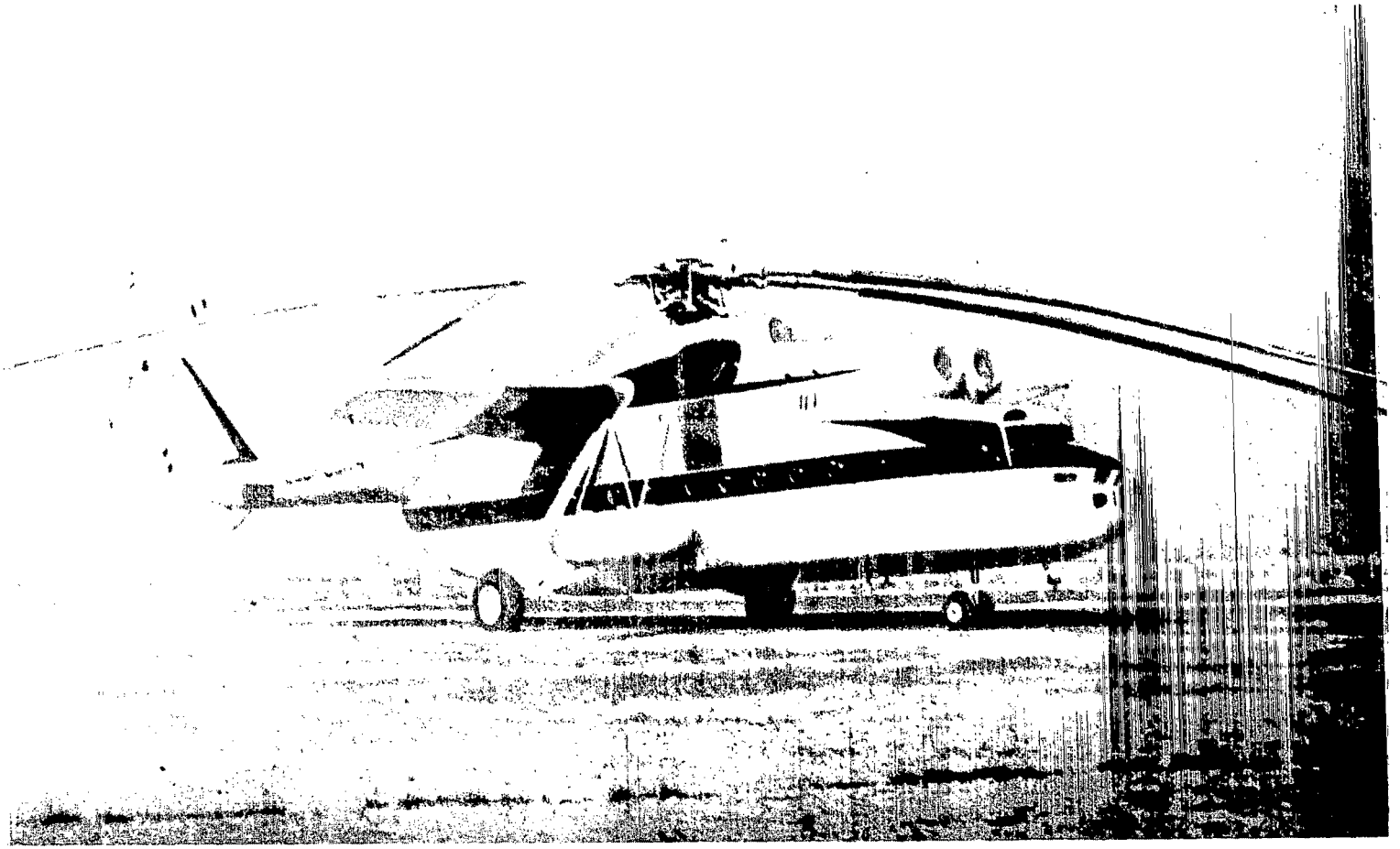

Mi-6 Helicopter.

Mi-10 Helicopter Crane.

Mi-2 Helicopter.

Mi-8 Helicopter.

most important of these is the problem of determining alternating blade bending stresses. Determination of these stresses forms the major part of the strength calculation. Therefore, the main problem in this Chapter is to determine the /17 elastic vibrations of a blade for calculating its strength.

A determination of blade vibrations is necessary also for solving many other problems. Without calculating these vibrations it is impossible to determine the loads acting on the helicopter, the hub, its controls, and on the transmission of the engine drive. A determination of alternate loads exerted on the helicopter by the rotor blades largely solves the problem of analyzing helicopter vibrations.

Also of interest is the problem of the effect of blade vibrations on the handling qualities of the helicopter. The limitations imposed on the flying qualities by flow separation due to the rotor blades are determined primarily by the permissible amplitude of blade vibrations. With an increase in these amplitudes, the variable forces in the controls and the vibrations of the helicopter increase. Therefore, a calculation of elastic blade vibrations permits the most accurate estimate of the limits of helicopter flight regimes with respect to flow-separation conditions.

To some extent, blade vibrations - and primarily torsional vibrations - affect the aerodynamic characteristics of the rotor even when far removed from regimes with flow separation.

We will discuss the first of the above problems in greater detail.

2. Calculation of Blade Strength

Calculation of blade strength involves a determination of the constant and variable stresses at all points of the blade structure, under different loading conditions. The most dangerous of these will be singled out as typical cases calculated for structural strength.

Usually, in the development of new blades, when the time alloted for performing and processing the calculations is limited, it is desirable to reduce the number of calculated cases to a minimum. Experience has shown that it suffices to examine a single case of blade loading under ground operating conditions of the helicopter and several cases in flight at different flight regimes.

The first case necessitates calculating a blade supported on the vertical restrictor of the hub after full or partial stoppage of the effect of centrifugal forces. This occurs when the rotor is not rotating or is in the initial stage of overspeeding or else is stopped after the flight. In the absence of centrifugal forces, the gravitational forces or inertia forces arising upon impact of the blade against the coning stop set up appreciable bending stresses. In this case, compressive stresses are especially dangerous for blade strength. Experiments show that individual blade overloads, at which considerable compressive stresses are set up, may affect the fatigue strength of the structure and hence its service life. Usually, static stresses due to bending of the blade under the effect of its own weight are limited to values of $\sigma_G = 25 - 28$ kg/mm^2 for a

blade with a steel spar and of σ_c = 7.0 - 7.5 kg/mm^2 for a blade with a duralumin spar.

From the computational viewpoint, this case presents no difficulties; therefore, we will not further discuss it here.

Other cases pertain to different helicopter flight regimes when constant and variable stresses from blade bending are added to the permanent stresses due to centrifugal forces. This combination of loads is highly detrimental to the fatigue strength of the blade structure.

3. Flight Regimes Detrimental to the Fatigue Strength of the Structure /18

In-flight stress analyses have shown that helicopter blades are subject to appreciable alternate loads having a detrimental effect on the structural strength in two different types of flight regimes.

The first type of flight regime includes low-speed modes, when the flying speed is 3 - 8% of the blade tip speed (μ = 0.03 - 0.08). In these regimes there is a marked increase in the flexural vibration amplitudes of the blades, causing a corresponding increase in the variable stresses.

The helicopter uses the above range of flying speeds in acceleration, horizontal flight at steady low speed, and in the braking regime. Usually the greatest variable stresses arise in the braking regime. Appreciable stresses may arise also in a steep descent at low horizontal speed.

With respect to the conditions of loading of the structure, flights at low speeds generally are short-term regimes, at least for helicopters used for transport missions. However, because of the high stresses present, it is precisely these regimes that often determine the service life of the blade with respect to fatigue.

The second type of regime detrimental to fatigue strength has to do with high-speed modes. These comprise primarily flights at cruising and maximum speeds. A flight at cruising speed is usually the longest flight mode and thus imposes considerable fatigue stresses on the structure.

A marked increase in variable stresses at low speeds can be attributed primarily to the appreciable nonuniformity of the induced velocity field created, during these regimes, in the flow through the rotor. Moreover, in absolute magnitude, the induced velocities here reach maximum values in comparison with all other flight modes. Therefore, their influence on the magnitude of stresses increases greatly at low speeds. The variable induced velocity field leads to variable aerodynamic blade loading. Under the effect of these loads the blade executes flexural vibrations which set up considerable variable stresses.

At high flying speeds, variable aerodynamic loads are generated mainly as a consequence of fluctuations in the relative flow velocity and changes in angles of attack of the blade sections with respect to the rotor azimuth. The variable

induced velocity field in these regimes has little effect on the magnitudes of the aerodynamic load.

In strength calculations it is sometimes necessary to allow for rotor overspeeding which might occur in flight at a steep rise in centrifugal forces. This will also cause an increase in the constant component of stresses in the blade.

4. Assumption of a Uniform Induced Velocity Field

It is obvious from the above that a calculation of variable aerodynamic loads at low speeds is impossible without consideration of the variable induced velocity field.

On an increase in flying speed, the absolute magnitude of induced velocities decreases. The effect of their nonuniformity on the magnitudes of aerodynamic loads also diminishes. Therefore, beginning with average flying speeds, when $\mu \geq 0.2$, it can be approximately assumed in calculating variable blade stresses that the induced velocity field is uniform, i.e., that the induced velocities are constant over the rotor disk area. This assumption leads to /19
significant simplifications of all computations and to a marked decrease in calculation time. For this reason, it is widely used in practical calculations.

However, the accuracy of the results, with consideration of this assumption, often is unsatisfactory to the designer. Thus, it is often necessary to abandon this assumption when calculating moderate and high-speed modes.

5. Assumptions in Calculating Aerodynamic Loads on the Blade Profile

In all methods of calculation presented in this Chapter it is assumed that aerodynamic forces acting on the blade profile can be determined by making use of aerodynamic coefficients for steady flow past an infinitely long wing in a plane-parallel stream. An unsteady state of the flow is taken into account only at values of the profile angles of attack at which downwash is introduced.

Consequently, to determine forces acting on a profile member, it is sufficient to determine its angle of attack α and the relative velocity U of the flow past it. Then, knowing α and $M = \frac{U}{a_{so}}$ (where a_{so} is the velocity of sound), we can determine from the profile polar the coefficients c_y and c_x and hence the forces acting on the profile. If necessary, one can also determine the coefficient m_z.

If, in the flight mode under study, the profile angle of attack does not exceed $\alpha \approx 9^\circ$ and if the Mach number is not higher than $M \approx 0.5$, then we can disregard its influence and assume that

$$c_y = c_y^\alpha \alpha, \tag{1.1}$$

where c_y^{α} is the tangent of the angle of slope for the relation $c_y = f(\alpha)$.

This assumption is used in calculating loads in flight modes sufficiently far from separation in which, furthermore, we can disregard the compressibility effect of the flow.

The possibility of using various assumptions in the method of determining aerodynamic forces is of great value in selecting the method of stress analysis to be used in the case in question. As a consequence, it is suggested to use different methods of calculation for different regimes. Below, we will differentiate between three types of regimes for each of which optimum results can be obtained by different methods of calculation. These are low-, moderate-, and high-speed modes.

In the low-speed mode, it is unavoidable to take account of the variable induced velocity field but linear aerodynamics can be used at average blade loading. At moderate flying speeds, the variable induced velocity field need be considered only in solving special problems raised by the necessity of differentiating individual high harmonics of the aerodynamic loads. It is almost always unnecessary at these speeds to consider nonlinear relations in determining the aerodynamic coefficients. Finally, in the high-speed mode which is close to the separation limit, consideration of these nonlinearities becomes mandatory, whereas the variability of the induced velocity field can be disregarded in most cases.

The above considerations result in individual methods of calculation tied /20 in with specific flight regimes.

6. Relation of Deformations due to Bending in Two Mutually Perpendicular Directions and Corresponding Assumptions for Calculation

Usually, a helicopter blade is designed such that the principal elastic moments of inertia of its sections differ substantially in magnitude. Therefore, the blade is considered as a bar extended by centrifugal forces, each portion of which has different rigidities in two mutually perpendicular directions. To characterize these directions, let us lay planes through the axis of the bar along the direction of the principal axes of the section, which will be designated as planes of maximum and minimum rigidity (Fig.1.1).

Frequently, to produce aerodynamic blade twist not only the frame forming its contour is twisted but also its spar. In this case, the directions of the principal elastic axes of the section vary over the length of the blade, changing it into a geometrically twisted bar. In other cases, aerodynamic twist is obtained only by turning the frame of the blade relative to the spar.

In flight, external forces act on the blade profile in widely differing directions. This changes the problem of blade bending into a highly complex three-dimensional problem.

In addition, the degree of geometric twist of helicopter blades is only

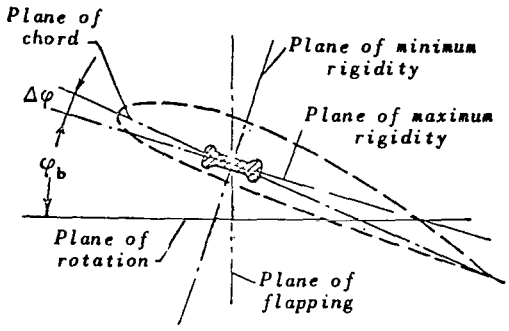

Fig.1.1 Position of the Spar at Geometric Twist Obtained by Turning the Frame Relative to the Spar (φ_b = const).

moderate (of the order of 6 - 12°) and appreciably less than is feasible in aircraft propellers or in compressor and turbine blades. As shown by various estimates, the effect of such twist on the calculation results is only slight. Therefore, in all the methods of calculation presented here we will disregard the degree of twist of the elastic axes of the blade spar and will assume that the direction of the plane of maximum and minimum blade rigidity is constant over its length.

This assumption permits projecting all external forces onto these planes and solving two elastically unrelated two-dimensional problems of blade bending in two mutually perpendicular directions. After performing the stress analyses for various points of the blade section, the results of both calculations can be summed.

The blade section profile permits increasing the size of the spar in the chord plane and limits the chords in a perpendicular direction. Thus, the plane of maximum rigidity is usually close to a plane passing through the blade chord. This circumstance, as well as the fact that the magnitude of the aerodynamic forces in the chord plane is usually smaller than in the plane perpendicular to it, causes the magnitude of the bending stresses to be greater in the plane of minimum rigidity and lower in the plane of maximum rigidity. A study of modern blade designs, where the fatigue strength is approximately identical in omnidirectional bending, indicates that bending in the plane of minimum rigidity is /21 considerably more dangerous. In practice, all difficulties usually have to do with the need of ensuring adequate bending strength in this plane. Therefore, we will here discuss methods of calculating blade vibrations only in the plane of minimum rigidity. For calculations in this plane, we can use the additional assumptions that the plane of minimum rigidity coincides with the plane going through the rotor axis. Below, we will designate this plane as the flapping plane.

7. Consideration of Torsional Deformation of a Blade in Calculations of Flexural Vibrations

Torsional deformations change the angles of attack of the blade sections and hence the aerodynamic forces acting on them. Therefore, these deformations should be taken into account in the calculation of aerodynamic loads and vibrations of a blade. However, the consideration of torsional blade vibrations entails considerable difficulties and greatly complicates the calculation.

At the same time, this does by no means always lead to substantially improved results. Therefore, torsional deformation should be taken into account only in cases of actual need, for example whenever the flexural blade vibrations

are amplified on approach to bending flutter; however, this implies an inadequate margin of safety with respect to flutter and must be considered impermissible.

To allow for torsional deformations, a system of differential equations of bending-torsional blade vibrations must be solved. Its solution is obtained by calculation of flutter. Such a method of calculation, known as the general method of calculation of blade flutter and bending stress, has been given in the first volume of this book (Sect.7, Chapt.IV).

Here, we will describe only methods of calculating free torsional (Sect.5) and bending-torsional vibrations (Sect.6).

8. Two Calculation Steps in Blade Design: Calculation of Natural Vibration Frequency and Calculation of Stresses

If a newly designed helicopter blade does not differ excessively in geometric and mass characteristics from an already manufactured and tested blade, it can be asserted that in identical flight regimes the variable blade stresses will be approximately the same as in the prototype blade. However, this rule is violated when, as a consequence of some change in its parameters, the blade is in resonance with some harmonic of the external forces.

Blade-design practice shows that sufficiently reliable blades can be developed only if none of its natural frequencies coincides with the frequencies of the external forces and actually these are far apart. This pertains to blade vibrations both in the plane of minimum rigidity and in that of maximum rigidity. Naturally, it is obvious that not all harmonics of external forces, but only those whose magnitude is sufficient to set up high stresses, are detrimental to the strength of material. Usually, absence of resonance is mandatory for harmonics not higher than the 8^{th} relative to the rotor rpm. Higher harmonics of external forces have little effect.

Thus, if a rough error in selecting the blade characteristics is impermissible, variable stresses can be kept within permissible limits by preventing /22
the occurrence of resonance. In this case, there is no need to calculate the variable stress amplitudes. Thus, the experimental designer can often limit himself to the first stage of blade calculation: determination of its natural vibration frequencies and plotting of the resonance diagram.

It follows from the above that the calculation of blade frequencies and natural vibration modes is not only an auxiliary step in stress analysis but has an independent value as a preliminary step in blade strength calculations.

9. Idealized Blade Models Used in Calculation

In performing the calculation, the blade must be represented as some idealized mechanical model for which all adopted initial assumptions would hold, so that later - during the calculations - there would be no need to use approximate mathematical operations.

With calculation on computers, the problem should be programmed such that its solution becomes possible with any prescribed accuracy attainable by the computer.

As shown by practical experience, calculation methods utilizing approximate mathematical operations often lead to other misconcepts. In many cases, it is impossible to complete the calculation because of some inaccuracy in the computations. For example, in calculating the natural vibration modes by the method of successive approximations an entire series of integrals must be calculated. This is often done by the trapezoidal method. At a limited number of integration intervals, this method results in such a large error that, in calculating the vibration modes of higher harmonics whose ordinates are calculated in the form of small differences of large quantities, the method of successive approximations ceases to converge.

This fact necessitates special caution in using approximate methods of calculation. Consequently, it is preferable to introduce a simplified idealized blade model which could be calculated at maximum permissible accuracy on the computer.

Three different types of mechanical models are known, which are frequently used in calculations.

Beam model with continuously distributed parameters. In this model, the blade is represented as a beam with continuously distributed rigidities EI, linear mass m, and parameters determining the magnitude of the linear aerodynamic load.

Such a model is highly convenient in deriving initial differential equations and in applying known approximate solution methods to them but is unsuitable for performing numerical calculations. Below, we will frequently refer to such a model in deriving working formulas so that, in the stage of numerical calculation, we can use formulas derived by analogy and pertaining to a model with discrete parameters. In these formulas, all integrals of functions depending on the blade radius are replaced by the sums of discrete quantities pertaining to a series of fixed blade radii.

Beam model with concentrated weights. In this model, the blade is represented as a system of coupled concentrated weights. The coupling between these weights is accomplished by small weightless beams having a longitudinal constant flexural rigidity equal to the rigidity of the corresponding blade elements.

In determining the aerodynamic forces, it is assumed that to each weight is attached a separate small wing whose area is equal to the area of the corresponding blade element. Usually, it is assumed that the area is /23

$$S_i = \frac{1}{2}(l_{i-1,i} + l_{i,i+1})\, b_i, \qquad (1.2)$$

where $l_{i-1,i}$ and $l_{i,i+1}$ = lengths of adjacent segments into which the blade is divided in the calculation;
b_i = blade chord in the section between these segments.

This model most accurately reflects the properties of a real blade. For this reason, it will be used in practical calculations in almost all cases.

However, we should mention that the beam model has these favorable properties only if the number of parts z is equal to 25 - 30 or more. As soon as this number decreases, the type of deformations of the beam model begins differing greatly from that of the deformations of the blade. This will be illustrated in more detail in Section 10, Subsection 3. Furthermore, the use of the beam model often leads to a rather complicated system of equations and at times even interferes with the calculation. In such cases, the simpler hinge blade model can be used.

Hinge model of blade. In this model, the blade is represented as a multihinge chain consisting of absolutely rigid weightless links whose masses are concentrated in the hinges. The flexural rigidity of the blade is simulated by elastic members concentrated in the hinges. Under the action of external forces, the axis of this chain takes the form of a broken line rather than of a smooth line as in the beam-type model. This fact, just as the task of selecting the rigidity of the elastic members, introduces a certain error when changing from a blade to a mechanical model.

At the same time, the use of the hinge model leads to such great simplification of the working formulas that it often becomes possible to use improved methods of calculation which were not feasible when using the beam model. This compensates the faults inherent to this model.

It should be mentioned that, on a decrease in the number of segments into which the blade is separated in the calculation, the properties of the models begin to differ markedly from the properties of a real blade. However, for the hinge model these errors do not increase as rapidly as for the beam model. As a consequence, the hinge model may be more suitable in rough methods of calculation, when the blade is divided into a small number of segments, say of the order of 10 - 12.

10. Derivation of the Differential Equation of Blade Bending in a Centrifugal Force Field at Vibrations in the Flapping Plane

Let us represent the blade as a beam with continuously distributed parameters. For our study, let us isolate an element of the beam of length dr. The forces acting on this element are plotted in Fig.1.2.

Let us then construct the equation of equilibrium of this element, limiting the calculation to values of the first order of smallness. Then, the sum of the projections of the forces onto the y-axis can be written as

$$W dr + dQ = 0, \tag{1.3}$$

and the sum of the moments of all forces relative to the point A

$$Q dr + dM - N dy = 0, \tag{1.4}$$

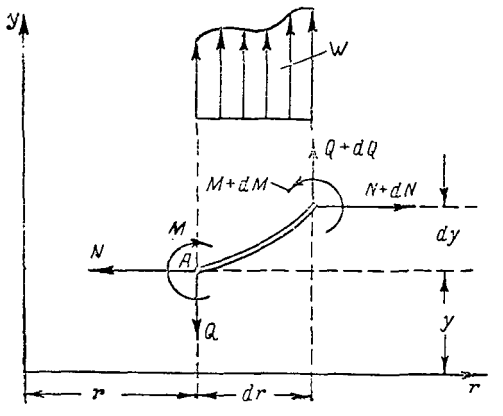

Fig.1.2 Diagram of Forces Acting on a Blade Element.

where

W = linear external load on the blade;
Q = shearing force in the blade section;
M = bending moment; /24
N = centrifugal force in the blade section.

From eq.(1.3) we obtain

$$W=-Q'. \tag{1.5}$$

Here and below the prime denotes differentiation with respect to the blade radius.

After differentiation of eq.(1.4), we obtain

$$Q'=-M''+[Ny']'. \tag{1.6}$$

Setting M = EIy" and substituting eq.(1.6) into eq.(1.5), we obtain the known differential equation of bending deformations of a blade in a centrifugal force field:

$$[EIy'']''-[Ny']'=W. \tag{1.7}$$

Let us represent the external load W, consisting of aerodynamic and inertia loads, in the form

$$W=T-m\ddot{y}, \tag{1.8}$$

where

T = linear aerodynamic load;
m = linear mass of the blade.

Here, the two dots denote differentiation with respect to time.

After substituting eq.(1.8) into eq.(1.7), we obtain the differential equation of blade vibrations

$$[EIy'']''-[Ny']'+m\ddot{y}=T. \tag{1.9}$$

In a vacuum, when the aerodynamic load T is equal to zero, eq.(1.9) will describe free blade vibrations in a centrifugal force field:

$$[EIy'']''-[Ny']'+m\ddot{y}=0. \tag{1.10}$$

The solution of this equation offers certain difficulties. For this reason,

Section 2 will first give its solution for the case N = 0 pertaining to a nonrotating blade.

11. Differential Equation of Blade Bending in the Rotor Plane of Rotation

On bending of the blade in the plane of rotation, owing to concentricity of the centrifugal force field, the blade element will be subject to an additional force which did not enter the equations in the flapping plane. With consideration of this, eq.(1.8) should be rewritten in the form

$$W=Q+\omega^2 mx-m\ddot{x}, \tag{1.11}$$

where

Q = aerodynamic force in the plane of rotation;
x = displacement of the blade elements in the plane of rotation.

After substituting eq.(1.11) into an equation analogous to eq.(1.7) but written for the plane of rotation, we obtain the differential equation of blade bending in this plane /25

$$[EI_x x'']''-[Nx']'-\omega^2 mx+m\ddot{x}=Q. \tag{1.12}$$

This equation differs from eq.(1.9) only by the additional term $\omega^2 mx$.

Section 2. Free Vibrations of the Blade of a Nonrotating Rotor

1. Method of Calculation for Solution of the Integral Equation of Blade Vibrations

Calculation of the natural vibration modes and frequencies of the blade of a nonrotating rotor has been extensively described in the literature [see, for example (Ref.1)]. In this Section, we will briefly repeat certain fundamental premises and somewhat refine the formulas used for practical calculations.

Let us examine the differential equation of vibrations derived for the model of a blade with continuously distributed parameters. If we set N = 0 in eq.(1.10), it will take the form

$$[EIy'']''+m\ddot{y}=0. \tag{2.1}$$

Setting

$$y=\bar{y}\sin pt \tag{2.2}$$

and substituting into eq.(2.1), we obtain

$$[EI\bar{y}'']''-p^2 m\bar{y}=0. \tag{2.3}$$

In our further computations, we will omit the vinculum over y. Let us

integrate eq.(2.3) with consideration of the boundary conditions of the blade attachment. For simplicity, let us take the case of a blade rigidly attached at the root, with the following boundary conditions:

at r = 0; y = 0; y′ = 0;
at r = R; M = 0; Q = 0.

By quadruple integration, eq.(2.3) is transformed into an integral equation of the form

$$y = p^2 \int_0^r \int_0^r \frac{dr^2}{EI} \int_r^R \int_r^R m y dr^2. \tag{2.4}$$

Equation (2.4) is solved by the conventional method of successive approximations. Prescribing an arbitrary form of y, normalized in some manner, for example

$$y_R = 1, \tag{2.5}$$

let us substitute it into the right-hand side of eq.(2.4).

After integration, we obtain a function

$$u = \int_0^r \int_0^r \frac{dr^2}{EI} \int_r^R \int_r^R m y dr^2, \tag{2.6}$$

such that $y = p^2 u$.

From this, using the condition (2.5), we obtain /26

$$p^2 = \frac{1}{u_R}, \tag{2.7}$$

where u_R is the value of u at r = R.

We then repeat the same operation, taking the new value

$$y = p^2 u. \tag{2.8}$$

After carrying out the above operations several times, it will be found that the vibration mode y and the frequency p converge to definite values which constitute the solution of the integral equations (2.4).

The method of successive approximations, applied in this manner, yields a determinable mode y converging to the mode of the lower harmonic of the natural blade vibrations.

To determine the subsequent harmonics, it is necessary to satisfy the condition of orthogonality of the natural vibration overtones. This condition will be discussed in Subsection 3.

In practical application of the calculation method presented here, it is important to select a sufficiently exact method for calculating the integral equation (2.6). If the blade parameters are given in the form of continuous

functions, then the simplest method of calculation of the integrals (2.6) is the trapezoidal method generally employed in such cases. However, as already indicated above, in calculating higher vibration overtones the uncertainty introduced by this operation leads to such extensive errors that the method becomes useless for practical purposes. This drawback is eliminated if, in calculating the integrals (2.6), we use the method obtained from a study of the mechanical model of a blade with discretely distributed parameters.

2. Calculation of the Natural Vibration Modes and Frequencies of a Blade Model with Discretely Distributed Parameters

For the calculation, we will use a beam-type model with concentrated loads (see Sect.1, Subsect.9). For this, let us divide the blade into z segments. The length of the individual segments can be different. The weight of the blade is concentrated along the edges of these segments in the form of individual discrete loads with mass m_i. The flexural rigidity of the blade is represented by a stepped curve, so that it remains constant over the length of each segment (Fig.1.3).

Just as in Subsection 1, we will first examine the case of a blade fixed at the root. The operation defined by eq.(2.6) can be carried out exactly here.

Actually, let us use an arbitrary form of displacement of the loads of the model y_i. Here, the system of discrete values of y_i (i = 0, 1, 2, 3, ... z being the serial number of the concentrated loads of the model) will be designated as the mode of displacement. As above [see eq.(2.5)], we set $y_z = 1$. If the displacements y_i are known, we can determine the inertia forces of the loads on their vibrations with a frequency p = 1. These are determined by the expression

$$F_i = m_i y_i. \tag{2.9}$$

Knowing the inertia forces, we can determine all bending moments by a system of simple recursive formulas of the form

$$M_i = l_{i,\,i+1}\,[F_{i+1} - a_{i+1}M_{i+1} - b_{i+1}M_{i+2}], \tag{2.10}$$

where $l_{i,i+1}$ is the length of the blade section between the i-th and i+1-th concentrated mass.

The coefficients a_i and b_i are determined by the formulas /27

$$b_i = \frac{1}{l_{i,i+1}};$$

$$a_l = -b_{l-1} - b_l.$$

A calculation of the bending moments by eqs.(2.10) should start from the end of the blade, first putting i = z - 1 and then equating the bending moments M_z and M_{z+1} to zero.

After defining the bending moments, it is easy to determine the blade deformations. As above, the blade deformations during vibrations with a frequency p = 1 will be denoted by the symbol u.

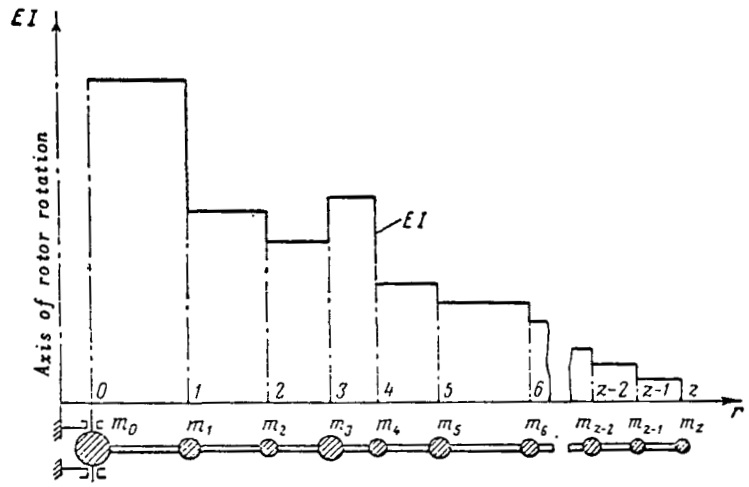

Fig.1.3 Calculation Model of Blade.

The magnitude of these deformations is determined by recursive formulas of the type

$$u_i = l_{i-1,\,i}\,[D_{i-1} - b_{i-2}u_{i-2} - a_{i-1}u_{i-1}], \tag{2.11}$$

where

$$D_{i-1} = d_{i-1}M_{i-1} + c_i M_i + d_i M_{i+1}. \tag{2.12}$$

Here,

$$\left.\begin{aligned} d_i &= \frac{l_{i,\,i+1}}{6EI_{i,\,i+1}}, \\ c_i &= 2(d_{i-1} + d_i). \end{aligned}\right\} \tag{2.13}$$

Calculation of the deformation u_i should begin from the blade root, after setting $u_0 = 0$, in conformity with the boundary conditions adopted here. All quantities with negative subscript should also be equated to zero.

Thus, carrying out the operations (2.10) and (2.11), applicable to a beam model with a discrete distribution of parameters, leads to calculation of exact values of u_i.

After determining p^2 in the same manner as before [see eq.(2.7)]

$$p^2 = \frac{1}{u_z} \tag{2.14}$$

and using the new values

$$y_i = p^2 u_i, \tag{2.15}$$

we repeat all operations until the method of successive approximations converges. Usually, the calculation is considered completed as soon as the difference in the values of y_i, in two successive approximations, is less than the prescribed accuracy ε_y. /28

3. Condition of Orthogonality and Calculation of Successive Natural Vibration Harmonics

The above method of successive approximations permits a determination of the lower harmonic of natural vibrations. In determining the higher harmonics, it is necessary to satisfy the conditions of independence of the vibrations with respect to different harmonics.

Let us imagine that free blade vibrations in vacuum occur simultaneously with respect to two modes $y_i^{(j)}$ and $y_i^{(m)}$. The vibration energy for each of the modes can be determined separately from the amplitude values of the kinetic energy*:

$$\left.\begin{aligned} K_j &= \sum_i m_i \left[p_j y_i^{(j)}\right]^2; \\ K_m &= \sum_i m_i \left[p_m y_i^{(m)}\right]^2. \end{aligned}\right\} \tag{2.16}$$

On the other hand, the total energy of the system vibrating simultaneously with respect to two modes can be determined from the amplitude value of the total kinetic energy:

$$K_\Sigma = \sum_i m_i \left[p_j y_i^{(j)} + p_m y_i^{(m)}\right]^2. \tag{2.17}$$

The system has this kinetic energy at that instant of time when the blade, during vibration, passes the neutral position simultaneously with respect to the two modes $y_i^{(j)}$ and $y_i^{(m)}$. Owing to the difference in the values of the natural vibration frequency, such a position arises relatively seldom, but can be easily created artificially by prescribing the appropriate vibration phases at the initial instant.

If the amplitudes with respect to each of the component modes of vibration do not change in time, then their energy, determined by eqs.(2.16), also remains constant.

The total vibration energy should always be equal to the sum of the energies of the component motions, i.e.,

$$K_\Sigma = K_j + K_m. \tag{2.18}$$

---

* For simplicity, here and below the constant 1/2 is omitted in the values of the kinetic and potential energy of vibrations.

As follows from eq.(2.17), this is possible only if

$$\sum_i m_i y_i^{(j)} y_i^{(m)} = 0. \tag{2.19}$$

This condition is known as the condition of orthogonality of the natural vibration harmonics. A more rigorous derivation of this condition will be given in Section 2 of Chapter II.

In calculating any j-th harmonic, all previous harmonics to which the subscript m = 0, 1, 2, ..., j - 1 corresponds, should already have been calculated.

To satisfy the condition of orthogonality in determining the mode of the /29
j-th harmonic by the method of successive approximations, we will represent the unknown mode $y_i^{(j)}$ as

$$y_i^{(j)} = p^2 \left[u_i - \sum_{m=0}^{m=j-1} C_m y_i^{(m)} \right], \tag{2.20}$$

where $y_i^{(m)}$ are previously determined natural vibration modes.

The constants C_m are determined from the condition of orthogonality (2.19) by the formulas

$$C_m = \frac{\sum_i m_i u_i y_i^{(m)}}{\sum_i m_i \left[y_i^{(m)} \right]^2}. \tag{2.21}$$

The value of the frequency of the j-th harmonic is calculated from

$$p_j^2 = \frac{1}{u_z - \sum_{m=0}^{m=j-1} C_m}. \tag{2.22}$$

Knowing p^2, we can determine the vibration mode from eq.(2.20).

4. Characteristics of Calculation of Natural Vibration Frequencies and Modes of a Hinged Blade

All above-presented computations pertaining to a rigidly fixed blade can easily be extended to a blade with hinge attachment at the root.

For this case, the integral equation (2.4) takes the following form:

$$\bar{y} = p^2 \left[\int_0^r \int_0^r \frac{dr^2}{EI} \int_r^R \int_r^R m y dr^2 + C_0 r \right], \tag{2.23}$$

where the constant C_0 is determined from the condition of equating to zero the sum of the moments of all inertia forces relative to the hinge. For a model with a discrete distribution of the parameters, this condition can be written as

$$\sum_i m_i y_i (r - r_0) = 0. \tag{2.24}$$

It is obvious that this condition satisfies the condition of orthogonality to the vibration mode, which we will tentatively call the fundamental vibration mode. If this mode is normalized in conformity with the condition (2.5), then it can be written as

$$y_i^{(0)} = \frac{r - r_0}{R - r_0}. \tag{2.25}$$

Thus, in calculating a hinged blade it must be taken into account that the mode of its fundamental is known beforehand and is prescribed by means of eq.(2.25) and, in calculating all subsequent harmonics beginning with the first, it is also necessary to satisfy the condition of orthogonality to the fundamental (2.24). Here, we can determine the functions u_i by the same formulas as those given in Subsection 2.

5. Calculation of the Natural Vibration Modes and Frequencies of a Blade as a Simply Supported Beam

/30

It frequently is necessary to calculate the frequency of synchronous vibrations of the blade and helicopter fuselage. In this case the rotor hub itself, being the point of attachment of the blade, may be displaced together with the helicopter fuselage. The calculations of such vibrations are very easy to perform when using a blade model representing a simply supported beam. Then, in determining the synchronous vibrations of rotor and fuselage, it suffices to calculate the mass of the fuselage m_0 reduced to the rotor (see Fig.1.3) and then calculate the natural vibration frequencies of the blade.

Calculation of the blade as a simply supported beam can be performed by the formulas given in Subsection 2, except that all natural vibration modes should be additionally orthogonalized to the mode of the second fundamental:

$$y_i^{(0)} = 1 = \text{const}, \tag{2.26}$$

which is equivalent to satisfying the condition of equating to zero the sum of all inertia forces acting during the vibrations.

This method of calculation, with slight refinements, can be used also for calculating the natural vibration modes and frequencies of the fuselage, which will be taken up in Chapter II.

Section 3. Approximate Method of Determining the Natural Blade Vibration Frequencies in a Centrifugal Force Field

1. Use of B.G.Galerkin's Method for Determining the Natural Blade Vibration Frequencies

The method of B.G.Galerkin is widely used for solving various problems of elastic blade vibrations.

The idea of Galerkin's method and its application to the solution of differential equations is rather thoroughly covered in the literature [see, for example, the manual "Mashinostroyeniye" (Mechanical Engineering), Vol.1, Book 1, Mashgiz, 1947].

Here, we will not repeat conclusions that can be found in other sources but will illustrate the use of this method on a number of simple examples.

In Subsection 10 of Section 1 in this Chapter, we derived a differential equation of blade vibrations in a centrifugal force field. On substituting into it the quantity y in the form of eq.(2.2), then this equation takes the following form (we have omitted here the vinculum of y):

$$[EIy'']''-[Ny']'-p^2my=0. \tag{3.1}$$

Let us assume that the natural blade vibration modes in a centrifugal force field do not differ from the corresponding modes calculated for the case N = 0. Then, taking into account that the vibration modes $y^{(j)}$ are known, let us substitute some mode $y^{(j)}$ into eq.(3.1) and, after multiplying all terms of the equation by this same mode $y^{(j)}$, integrate the obtained expressions over the blade length.

The obtained equation, after certain transformations, can be represented in the form

$$\int_0^R EI\,[(y^j)'']^2\,dr+\int_0^R N\,[(y^j)']^2dr-p^2\int_0^R m\,(y^j)^2\,dr=0. \tag{3.2}$$

The integrals entering this equation /31

$$C_{EI}=\int_0^R EI\,[(y^j)'']^2\,dr, \tag{3.3}$$

$$C_N=\int_0^R N\,[(y^j)']^2\,dr \tag{3.4}$$

have a well-defined physical meaning, namely:

C_{EI} = elastic potential energy accumulated by the blade as soon as, during flexural vibrations with respect to the mode of the j-th

harmonic, the blade shows extreme deflections from the equilibrium position*;

C_N = potential energy accumulated by the blade while bending in a centrifugal force field. Here, just as in eq.(3.3), different harmonics of the natural vibrations can be studied.

The total potential energy accumulated by the blade while bending in a centrifugal force field according to the formula of $y^{(j)}$ can be written as

$$C_\Sigma = C_{EI} + C_N. \tag{3.5}$$

In flexural vibrations when the blade passes through the equilibrium position, the rate of displacement of its points reach maximum values:

$$\dot{y}^{(j)} = py^{(j)}. \tag{3.6}$$

In this case, the kinetic energy of the blade can be determined by the formula

$$K_j = p^2 \int_0^R m\,[y^{(j)}]^2\,dr. \tag{3.7}$$

In free vibrations, the potential energy accumulated by the blade while bending with respect to the mode $y^{(j)}$ is converted into kinetic energy when the blade passes the equilibrium position. The equality of the amplitude values of the potential and kinetic energy of the blade is expressed by eq.(3.2).

From eq.(3.2), the frequency of the j-th harmonic of natural blade vibrations in a centrifugal force field can be obtained. This frequency is determined by the formula

$$p_j^2 = p_{0j}^2 + \kappa_j \omega^2, \tag{3.8}$$

where

p_{0j} = natural vibration frequency of the blade without consideration of centrifugal forces;

k_j = a coefficient allowing for the effect of centrifugal forces.

Here,

$$p_{0j}^2 = \frac{\int_0^R EI\,[(y^j)'']^2\,dr}{\int_0^R m\,[y^j]^2\,dr}; \tag{3.9}$$

* This holds with an accuracy to within a constant equal to 1/2, which is omitted in eqs.(3.3), (3.4), and (3.7).

$$\kappa_j = \frac{\int_0^R N_{\omega=1}[(y^j)']^2\,dr}{\int_0^R m[y^j]^2\,dr}. \qquad (3.10)$$

In eq.(3.10), $N_{\omega=1}$ is the centrifugal force in the blade section at $\omega = 1$. /32

Equation (3.9) for the natural vibration frequency without consideration of centrifugal forces can be obtained if the method of B.G.Galerkin is applied to eq.(2.3) in the same manner.

The expressions derived here for the natural blade vibration frequency in a centrifugal force field are approximate. However, calculations show that, in many cases, these expressions give an accuracy completely satisfactory for practical purposes. A more thorough evaluation of the accuracy of the results of these calculations will be given in Section 4.

2. Resonance Diagram of Blade Vibrations

As mentioned above, in blade designing calculations are required to preclude possible resonances of natural blade vibration frequencies with the harmonics of external forces, which might set up appreciable variable stresses. As stated before, the harmonic components of aerodynamic forces acting on a blade in flight are of substantial magnitude, up to harmonics not exceeding the 8th. Higher harmonics of aerodynamic forces are so small in magnitude that they can be disregarded.

The frequencies of forced vibrations, which are a source of concern in blade calculations, can be determined by means of the formula

$$\nu = n\omega, \qquad (3.11)$$

where n = 1, 2, 3, ..., 8.

Equation (3.8) permits constructing the dependence of natural vibration frequencies of various harmonics on the angular velocity of rotation of the rotor. Equations (3.8) and (3.11), plotted jointly on one graph, are usually called the blade resonance diagram. Figures 1.4 and 1.5 give resonance diagrams constructed for blades with different parameters encountered in practice. These diagrams are plotted in relative values. Both the natural vibration frequency p and the rotor rpm refer to a certain operating value of the rpm, n_{op}.

The resonance diagram permits tracing, in graphic form, the direction toward which the blade parameters should be changed so as to eliminate resonance in the entire range of operating rotor rpm.

3. Selection of Blade Parameters to Eliminate Resonance during Vibration in the Flapping Plane

A scrutiny of the resonance diagrams, constructed for the diverse blades, shows that they do not differ greatly. The existing difference can mostly be attributed to the difference in the flexural blade rigidity. Less often and to a lesser degree, the cause is a deviation in the blade mass characteristics. This can be explained in a simple manner. Actually, the designer must be guided by a large number of various requirements, which limit the possibilities of varying the blade parameters and ultimately lead to the creation of blades with closely adjacent characteristics.

The following conditions place the main restriction on extensive variations in blade parameters:

1. The height of the spar is limited by the blade profile and cannot be increased much, since an increase in relative profile thickness will automatically deteriorate the L/D ratio of the rotor. This places an upper limit on the magnitude of flexural rigidity of the blade. /33

2. The bending deflection of the blade under its own weight should not be excessive, since it will lead to difficulties in laying out the helicopter. Bending stresses in the spar, set up by dead weight, should not exceed known magnitudes which are selected from strength conditions with consideration of possible dynamic overloadings. These considerations limit the possibilities of reduction in blade rigidity.

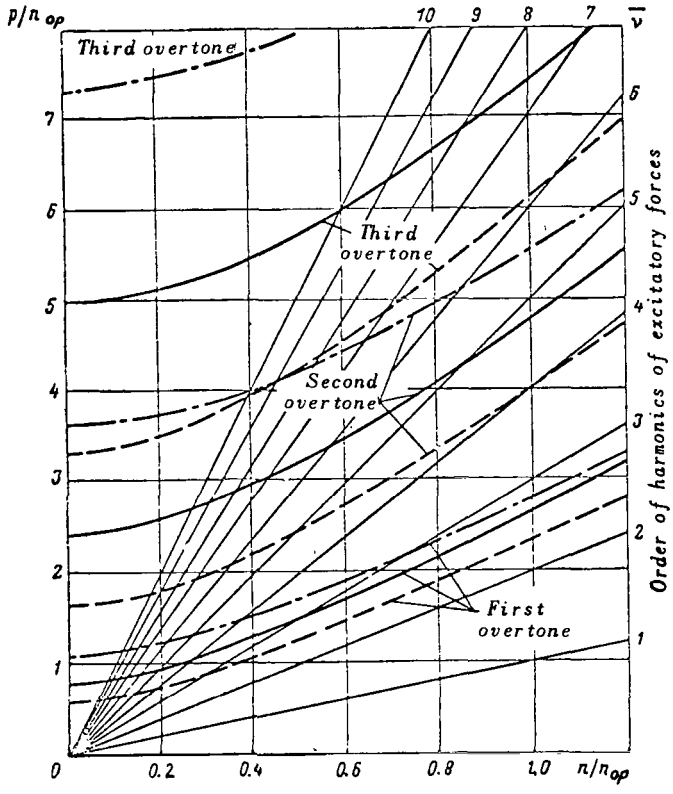

Fig.1.4 Resonance Diagrams of Various Types of Blades in the Flapping Plane.

3. The weight of the blade is confined within even closer limits. The endeavor to increase the weight factor of a helicopter forces the designer to reduce the blade weight to a minimum. However, this leads to an increase in variable stresses due to bending, acting in the blade during flight and hence leading to a decrease in its service life. Therefore, the blade weight usually is decreased until the spar starts being subject to increasing variable stresses. As a result, blade weight is strictly dependent on rotor

size and on the strength characteristics of the material from which the rotor spar is fabricated.

As a consequence, the resonance diagrams of different blades vary in practice within limits that are bounded on one hand by the feasibility of a highly rigid blade and on the other by the feasibility of an adequate service life of low-rigidity blades.

For a given total structural weight, a blade of maximal rigidity is obtained if the spar material is arranged along the contour of the profile, i.e., if the spar is inscribed in the blade profile. In this case a large percentage of the blade weight can be put into its power member, the spar. Such blades usually are most advantageous from the aspect of magnitude of effective stresses, but they are difficult to manufacture. Blades with a free form of the spar cross section (for example, of tubular shape) which are not inscribed in the blade profile are simpler to manufacture. However, such blades have little resistance to bending and provide the least favorable resonance diagram during vibrations in the flapping plane. /34

The following blade types can be distinguished with respect to dynamic characteristics in the flapping plane:

Blades of low rigidity in the flapping plane. Such blades are usually employed in a structure made of tubular steel spars, with a frame not subject to bending. In Fig.1.4 the broken line shows the resonance diagrams for a blade whose rigidity in the flapping plane is at the lower limit of rigidity encountered in practice. With such parameters, the blade enters into resonance of the second tone with the fourth harmonic and of the third tone with the sixth harmonic of the exciting forces, which is the reason for the creation of appreciable stresses of the same frequencies (see also Fig.1.66). These resonances are especially manifest at low speeds where the stresses of a blade of this type are even higher than at maximum speed (Fig.1.64). Therefore their service life, as a rule, is limited by the length of their stay in low-speed modes.

Blades of low rigidity are usually unfavorable with respect to strength and service life but are often used since they are the easiest to manufacture.

Blades of moderate rigidity in the flapping plane. With an increase in rigidity, the natural vibration frequencies of the blade move away from these resonances. This permits the designing of rather successful blades. In Fig.1.4 the resonance diagram of this blade is shown as a solid line. As follows from the diagram, the second tone of vibrations of such a blade has still not approached the fifth harmonic, while the third tone was somewhere between the seventh and eighth harmonics. Designwise, these are usually blades with a contour (or close to this shape) spar inscribed in the profile. The spar can be either steel or duralumin.

It is impossible to obtain a further increase in rigidity without increasing the blade weight. Moreover, even a slight increase in rigidity may lead to resonance of the second tone with the fifth harmonic of the external forces. Therefore, only heavy blades of greatly increased rigidity can be the next possible type in the sequence of increasing rigidity.

Heavy blades of high rigidity in the flapping plane. In increasing the weight of a given blade, putting this weight into the structure of the spar, the rigidity can be increased so much that the frequency of the second tone will be above the fifth harmonic. In this case, the resonance diagram shown in Fig.1.4 by the dot-dash line is possible. Lower variable stresses will act in the spar of a blade with this resonance diagram, but the blades will be somewhat heavier in comparison with blades of moderate rigidity. However, for small helicopters in which the relative rotor weight is low, such an increase in blade weight is feasible.

It should be noted that, in evaluating the dynamic characteristics of various blades in the flapping plane, the position of the first tone of blade vibration has been completely disregarded. Usually the first tone lies between the second and third harmonics and its location can be changed substantially only /35 in structures differing by some special features, for example, jet rotors with engines on the blade tip or rotors with nonhinged blades. The negligible displacement in natural frequency of the first tone observed for ordinary rotors generally does not greatly affect the magnitudes of the effective variable stresses.

4. Selection of Blade Parameters to Eliminate Resonances in the Plane of Rotation

In designing a blade, absence of resonance must be ensured also in the plane of maximum blade rigidity, which can be approximately considered to coincide with the plane of rotation of the rotor. The plane of maximum blade rigidity usually coincides with the plane of the chord. Therefore, the rigidity characteristics of a blade in this plane may vary in wider limits than in the flapping plane. Beginning with a circular tube, the cross section of the spar can increase to a size occupying practically the entire profile from the leading to the trailing edge. However, there are certain limitations also in this plane. Thus, an increase in the width of the spar with respect to the chord is certain to lead to a shift in blade centering toward the trailing edge, which is usually impermissible from the viewpoint of requirements for the prevention of flutter. Furthermore, an increase in width of the spar may be accompanied by an increase in variable stresses. A decrease in rigidity of the spar by reduction of its width automatically leads to a decrease in torsional rigidity of the blade. This constitutes one of the factors preventing the creation of blades of low rigidity in the plane of rotation.

In evaluating the resonance characteristics in the plane of rotation it is mainly necessary to investigate the first and sometimes also the second harmonic of blade vibration. The excitation of vibrations by higher harmonics is not as likely.

Blades can be subdivided into the following types, based on their dynamic characteristics in the plane of maximum rigidity:

Blades of minimum rigidity in the plane of rotation. This type of blade usually includes those with a tubular spar and a frame not subject to bending. The natural vibration frequencies of this type of blade in the plane of rotation

are approximately the same as in the thrust plane or even somewhat lower, due to the fact that the value of the coefficient k_1 [see eq.(3.8)] in the plane in question is somewhat lower (this will be taken up in Sect.4, Subsect.4). The first harmonic vibrations in this case is generally somewhat higher than the second harmonic of external forces so that no serious trouble is created by this resonance. The situation becomes worse for the second harmonic. This might enter into resonance with the fourth harmonic of external forces. Generally, this leads to a substantial increase in stresses of this particular frequency in the plane of rotation. In Fig.1.5 the dashed line represents the resonance diagram for a blade whose rigidity in the plane of rotation lies at the lower limit of rigidity encountered in practice. This blade is close to resonance of the second harmonic with the fourth harmonic of external forces.

Blades of low rigidity in the plane of rotation. If the rigidity of a blade in the plane of rotation is somewhat increased, so that its first tone remains between the second and third harmonics and the second tone gets out of resonance with the fourth harmonic, then the blade will be adequate with respect to stresses in the plane of rotation. It should be noted that, with an increase in rigidity, resonance of the second tone with the fifth harmonic to the rotor /36 rpm must be prevented. Practice has shown that, at this resonance, the stresses in the plane of rotation increase rather strongly, which might even affect their service life. The resonance diagram of blades of low rigidity in the plane of rotation, for which the second tone is between the fifth and sixth harmonics, is shown in Fig.1.5 by solid lines.

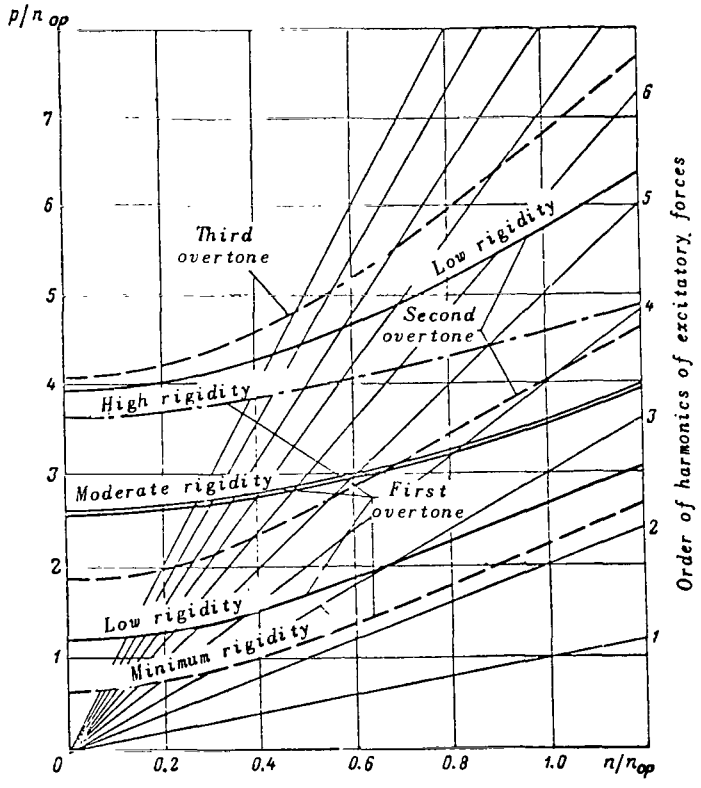

Fig.1.5 Resonance Diagrams of Various Types of Blades in the Plane of Rotation.

Blades of low rigidity in the plane of rotation are widely used in practice, and as a rule, cause no troubles associated with vibrations in this plane. However, their rigidity characteristics in the plane of flapping are often close to those for blades of low rigidity in the flapping plane, which are distinguished by high stresses at low flying speeds. On increasing the blade rigidity in the flapping plane, the rigidity in the plane of rotation often is simultaneously increased.

This makes it necessary to use blades of even greater rigidity in the plane of rotation.

Blades of moderate and high rigidity in the plane of rotation. Blades of moderate rigidity in the plane of rotation usually include those whose fundamental lies between the third and fourth harmonics of external forces, while the second tone is located in a frequency range with such weak excitations that it can be disregarded. In Fig.1.5, the frequency of the fundamental of these blades is shown by a double line.

Blades of high rigidity in the plane of rotation include those whose frequency in the fundamental lies above the fourth harmonic of external forces (dot-dash line in Fig.1.5). /37

Blades of moderate and high rigidity in the plane of rotation can be fabricated with moderate stresses. However, in the practical use of such blades difficulties often arise, associated with a decrease in blade frequency as a consequence of elasticity of the rotor attachment point to the fuselage. This must definitely be taken into account in designing blades of this type.

Section 4. Calculation of Natural Blade Vibration Modes and Frequencies in a Centrifugal Force Field

1. Purpose and Problems of Calculation

As mentioned in Section 1, Subsection 8, the natural vibration modes and frequencies of the blade must be determined in solving two types of technical problems that impose different demands on the method of calculation.

The first type includes problems in which the calculation of modes and frequencies is carried out to select blade parameters that will prevent the appearance of resonance. In this case, the calculation is completed by construction of the resonance diagrams, and the natural vibration modes play only the role of intermediate results and are not used later. Therefore, in current calculations of this type, the natural vibration mode of a given blade in a centrifugal force field is assumed to coincide with the mode of a nonrotating blade. The effect of centrifugal forces is taken into account only in the values of frequencies computed from energy relationships determined by eq.(3.8). Such a rather simple method of calculation is fully adequate for the purposes involved.

The second type includes problems in which the natural vibration modes and frequencies are used for calculating forced vibrations, with a determination of variable stresses set up in the blade structure. To obtain sufficiently accurate results here, it is important to allow for characteristics that introduce tensile centrifugal forces into the vibration mode.

It will be shown in this Section that centrifugal forces substantially change the natural vibration mode of the blade. The effect of centrifugal forces is especially manifest in the form of curvature distribution of an elastic line over the blade length and, to a lesser extent, in the mode of displacement of its elements. A change in the form of curvature distribution naturally leads

to a redistribution of bending stresses over the blade. The effect of centrifugal forces on the distribution of stresses over the blade length is felt most at sites of a marked drop in flexural rigidity and at sites of concentrated loadings.

It should be noted that, in determining the natural vibration modes with consideration of centrifugal forces, certain difficulties are encountered that must be examined in greater detail.

2. Limits of Applicability of Calculation Methods Reducing to a Solution of the Integral Equation of Blade Vibrations

To calculate the free vibrations of a blade in a centrifugal force field, it is convenient to use the same method as for the blades of a nonrotating rotor. However, the method of successive approximations (see Sect.2), which involves solving the integral equation (2.1), cannot be applied in all cases to the solution of eq.(3.1) describing natural blade vibrations in a centrifugal force field. /38

It was shown in Section 2, Subsection 1 that, with a fourfold integration of eq.(2.1), the problem reduces to solving the integral equation (2.4). This equation can be written in a somewhat different form

$$y = p^2 \int_0^r \int_0^r \frac{M_{inert}\, dr^2}{EI}, \tag{4.1}$$

where $M_{inert} = \int_r^R \int_r^R mydr^2$ is the bending moment due to inertia forces arising upon blade vibrations with a frequency p = 1.

In the same manner, on integrating eq.(3.1) the problem reduces to solving an equation of the following form:

$$y = p^2 \int_0^r \int_0^r \frac{(M_{inert} - \gamma M_{cf})\, dr^2}{EI}, \tag{4.3}$$

where $M_{c.f}$ is the bending moment due to centrifugal forces at an angular velocity of rotation of the rotor ω = 1:

$$M_{cf} = \int_r^R myrdr - y \int_r^R mrdr; \tag{4.4}$$

$$\gamma = \frac{\omega^2}{p^2}. \tag{4.5}$$

The method of successive approximations applied to eq.(4.1) yields satisfactory convergence in all cases of rotor calculation but, applied to eq.(4.3), it will converge only in a certain range of values of the parameter γ.

Figure 1.6 gives the resonance diagram for a conventional helicopter blade with hinged attachment to the hub. In this graph, the rotor rpm is laid off on the abscissa and the natural vibration frequencies on the ordinate.

The values for the natural frequencies, obtained by solving eq.(4.3) with the method of successive approximations, are shown in Fig.1.6 by dots. Opposite each dot, we entered the corresponding value of the parameter γ and the number of approximations s necessary for achieving the required accuracy of 0.001. The graph indicates that, at certain values of γ, the value of s begins to increase rapidly and the method of successive approximations ceases to converge.

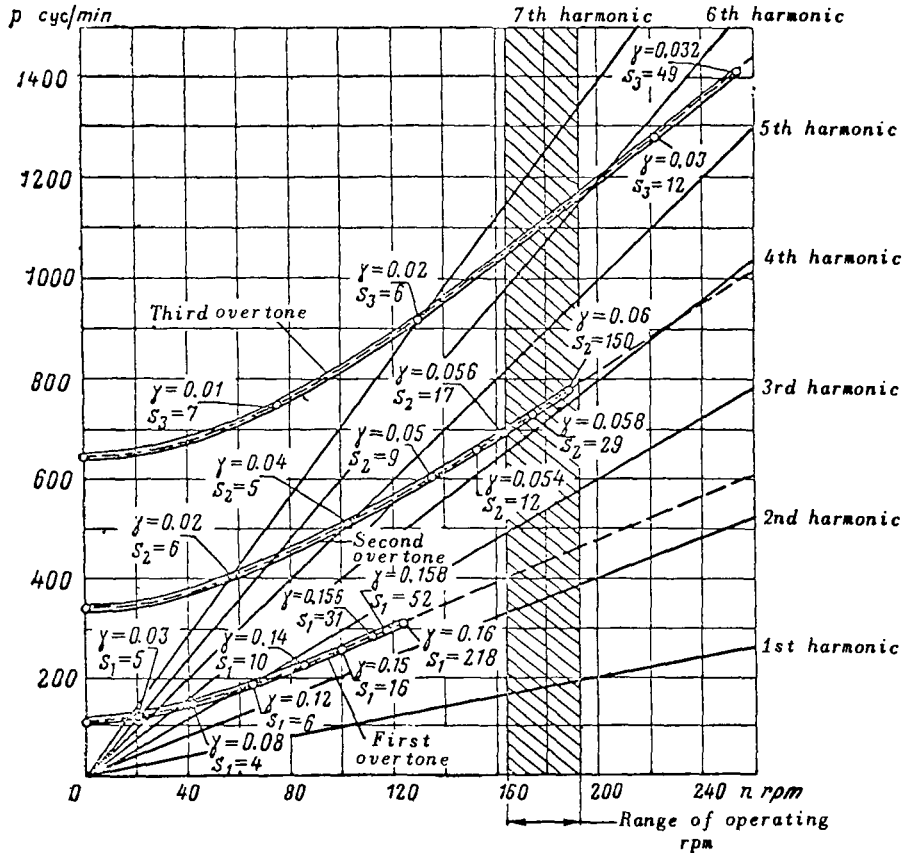

Fig.1.6 Resonance Diagram of Helicopter Blade in the Thrust Plane, Constructed by the Method of Successive Approximations.

If follows from Fig.1.6 that, in the operating rpm range for helicopter blades, this method permits a determination of natural frequencies of the third and higher harmonics but only if all harmonics of the vibrations are determined for a constant value of the parameter γ, which only approximately corresponds to conditions of the formulated physical problem. If, in the process of successive approximations, the parameter γ is refined for a given value of angular velocity ω, then the method will converge only in an rpm range appreciably smaller than the operating rpm.

This requires the use of other methods that afford a more reliable result in the entire rpm range of the rotor.

3. Possible Methods of Calculating Free Blade Vibrations in a Centrifugal Force Field /39

Various methods can be used for calculating the natural vibration frequencies and modes in a centrifugal force field. Of Soviet work, published on this subject matter, we should mention three papers (Ref.4, 8, 10). Papers were also published in other countries (Ref.33, 34). In these, a rather cumbersome method is presented which, moreover, does not yield a high accuracy of the final results despite the fact that the calculation should be carried out to not less than the 10th to 12th significant figure.

Here, we will present a method which, in our opinion, is the most convenient for calculating the natural vibration frequencies of the blade in a centrifugal force field. The process is based on the three-moment method used by T.Morris and W.Tye (Ref.32) in calculating bending stresses in a blade extended by centrifugal forces. The Morris and Tye method is also presented elsewhere (Ref.12).

The three-moment method, applied to calculation of a blade extended by centrifugal forces, has a number of significant advantages, the main one being that it does not require a high accuracy in the calculation process. The calculations can even be carried out with an ordinary slide rule.

The three-moment method has long been in use for calculating natural /40
frequencies, and has been programmed on the electronic computers "Strela" and M-20. Calculation of the first eight harmonics of natural vibrations takes only about 3 minutes on the "Strela" computer. A large number of the most diverse calculations have been performed. The results indicate the extreme convenience and great reliability of this method.

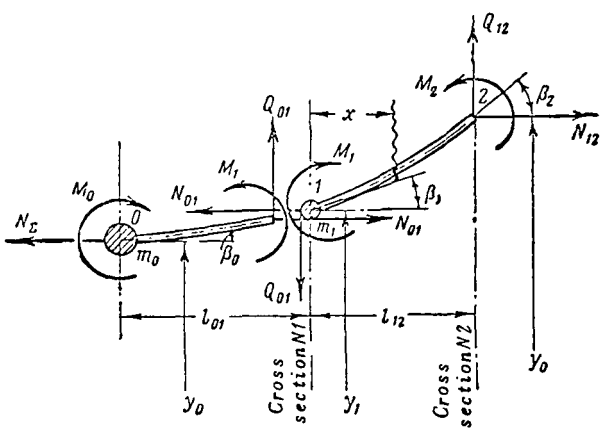

Fig.1.7 Polygon of Forces Acting on Two Adjacent Blade Elements.

It should be noted that, when using a computer program for such a calculation, there is no need for any simplified methods of calculation, for example, those mentioned in Section 3.

4. Three-Moment Method for Calculating Natural Blade Vibration Modes and Frequencies in a Centrifugal Force Field

To derive the computational formulas, we used the blade beam model with concentrated loads, discussed

already in Section 2, Subsection 2. As before, we present the flexural rigidity of the blade as a stepped curve, so that it remains constant over the length of each segment (see Fig.1.3). We will assume the centrifugal force to be applied only to the loads. Therefore, this value will be constant over the length of each segment. We will also assume that the centrifugal force is absorbed by a special attachment of zero weight, free to move vertically.

It is obvious that such an idealized calculation scheme will be reliable if the number of segments z is taken as sufficiently large. Usually the blade is divided into no less than 25 - 30 segments (elements).

The method proposed later consists in determining the natural oscillation modes and frequencies of such an idealized scheme, without additional assumptions.

Let us examine two adjacent blade segments, deflected under the effect of inertia forces from the plane of rotation of the rotor (Fig.1.7). As usual, we will examine only small deflections.

The equation of equilibrium of each of the segments under the effect of forces external to the given segment can be written in the form of zero-equality of the sum of the moments of all these forces relative to some point. In this case, we must include in the sum of the moments of these forces the shearing force Q and the bending moment M acting in the cross section.

Then, the sum of the moments of forces acting on the blade segment 0 - 1 /41 relative to the point 0 can be written as

$$M_1 - M_0 - N_{01}(y_1 - y_0) + Q_{01} l_{01} = 0. \tag{4.6}$$

The sum of the moments of forces acting on the segments 1 - 2 relative to the point 1 reads

$$M_2 - M_1 - N_{12}(y_2 - y_1) + Q_{12} l_{12} = 0. \tag{4.7}$$

Here,

$$Q_{01} = -\sum_{1}^{z} m_i \ddot{y}_i;$$

$$Q_{12} = -\sum_{2}^{z} m_i \ddot{y}_i.$$

After dividing eqs.(4.6) and (4.7), respectively, by $l_{01}N_{01}$ and $l_{12}N_{12}$ and adding them, we obtain the following equation of equilibrium:

$$b_0 y_0 + a_1 y_1 + b_1 y_2 = m_0 M_0 + n_1 M_1 + m_1 M_2 + \frac{Q_{12}}{N_{12}} - \frac{Q_{01}}{N_{01}}. \tag{4.8}$$

The notations introduced here, as well as in eqs.(4.12), (4.13), (4.14), and (4.15), are given below [see eqs.(4.18) - (4.25)].

In the same manner as eq.(4.8), we can write the equations of equilibrium for all other blade segments.

Examining, as usual, only small displacements of the blade elements, we first determine the deformations of the segment 1 - 2. The equation of deformations of the element 1 - 2 can be written, as conventional [see eq.(3.1)],

$$[EI_{12}y']''-[N_{12}y']'=0.$$

The inertia term is absent here, since inertia forces are applied only at the boundaries of the segment. Taking into consideration that EI = const and N = const over the length of the segment and also that EIy″ = M, we obtain

$$\frac{\partial^2 M}{\partial x^2}-\mu_1^2 M=0, \tag{4.9}$$

where

$$\mu_1^2=\frac{N_{12}}{EI_{12}}.$$

The solution of eq.(4.9) can be written in terms of hyperbolic functions, in the following manner:

$$M_x=A\sinh\mu_1 x+B\cosh\mu_1 x. \tag{4.10}$$

The coefficients A and B are found from the following boundary conditions:
for x = 0 $M_x = M_1$;
for x = l_{12} $M_x = M_2$.
From this, it follows that

$$A=\frac{M_2}{\sinh\alpha_1}-\frac{M_1}{\tanh\alpha_1};$$
$$B=M_1,$$

where $\alpha_1 = \mu_1 l_{12}$.

Substituting these values into eq.(4.10), we obtain <u>/42</u>

$$M_x=EI_{12}y''=\left[\frac{M_2}{\sinh\alpha_1}-\frac{M_1}{\tanh\alpha_1}\right]\sinh\mu_1 x+M_1\cosh\mu_1 x. \tag{4.11}$$

Twice integrating eq.(4.11), assuming $y' = \beta_1$, $y = y_1$ at x = 0 and $y' = \beta_2$, $y = y_2$ at x = l_{12}, we obtain either

$$\left.\begin{aligned} b_1(y_2-y_1)&=d_1M_2+e_1M_1+\beta_1,\\ b_1(y_2-y_1)&=-e_1M_2-d_1M_1+\beta_2. \end{aligned}\right\} \tag{4.12}$$

or

The equation of deformations for the segment 0 - 1 can be written by analogy

with the second equation of the system (4.12):

$$b_0(y_1-y_0)=-e_0M_1-d_0M_0+\beta_1. \tag{4.13}$$

After changing all signs in eq.(4.13) to the opposite and adding to the first equation of the system (4.12), we obtain

$$b_0y_0+a_1y_1+b_1y_2=d_0M_0+c_1M_1+d_1M_2. \tag{4.14}$$

Substituting the left-hand side of eq.(4.14) for the bending moments into the equation of equilibrium of the elements [eq.(4.8)], we obtain the following equation:

$$h_0M_0+g_1M_1+h_1M_2=\frac{Q_{12}}{N_{12}}-\frac{Q_{01}}{N_{01}}. \tag{4.15}$$

Repeating the calculations for other segments of the blade, we obtain a system of differential equations with respect to the unknown functions of time y_i and M_i, which is written out below.

This system, expressed in the form of tables, consists of two systems of equations (4.16) and (4.17), each of which comprises z + 1 equations.

Any of the equations occupying one row in Table 1.1 represents a polynomial whose coefficients are entered in the squares. All terms of the polynomial represent the products of some coefficient determined by eqs.(4.18), (4.21), (4.23) and (4.24) - (4.27) as well as the unknown functions M_i and y_i or the second derivative of y_i with respect to time.

Only the coefficients of these functions are entered in the squares of Table 1.1 while the functions themselves, simultaneously entering several equations, are given in a separate row above the tables.

The described system of equations also includes equations of the type of eq.(4.12), pertaining only to the root and tip segments of the blade and containing the boundary values β_0 and β_z. These equations are needed for calculating the boundary value problems.

The obtained system of equations has the following form:

/43

Table 1.1

β_0	M_0	M_1	M_2	...	...	M_{z-1}	M_z	β_z		$\ddot{y}_0$	$\ddot{y}_1$	$\ddot{y}_2$	$\ddot{y}_3$	...	$\ddot{y}_{z-1}$	$\ddot{y}_z$
1	g_0	h_0								0	t_{01}	t_{02}	t_{03}	...	$t_{0,z-1}$	t_{0z}
	h_0	g_1	h_1								s_1	t_{12}	t_{13}	...	$t_{1,z-1}$	t_{1z}
		h_1	g_2	h_2								s_2	t_{23}	...	$t_{2,z-1}$	t_{2z}
			...	...	...				=				...	...	...	...
				h_{z-3}	g_{z-2}	h_{z-2}								s_{z-2}	$t_{z-2,z-1}$	$t_{z-2,z}$
					h_{z-2}	g_{z-1}	h_{z-1}								s_{z-1}	$t_{z-1,z}$
						h_{z-1}	g_z	1								s_z

(4.16)

$$
\begin{array}{|c|c|c|c|c|c|c|c|c|}
\hline
\beta_0 & M_0 & M_1 & M_2 & \cdots & \cdots & M_{z-1} & M_z & \beta_z \\
\hline
1 & c_0 & d_0 & & & & & & \\
 & \alpha_0 & c_1 & d_1 & & & & & \\
 & & d_1 & c_2 & d_2 & & & & \\
 & & & \cdots & \cdots & \cdots & & & \\
 & & & & d_{z-3} & c_{z-2} & d_{z-2} & & \\
 & & & & & d_{z-2} & c_{z-1} & d_{z-1} & \\
 & & & & & & d_{z-1} & c_z & -1 \\
\hline
\end{array}
=
\left\{
\begin{array}{|c|c|c|c|c|c|c|}
\hline
y_0 & y_1 & y_2 & \cdots & y_{z-2} & y_{z-1} & y_z \\
\hline
\alpha_0 & b_0 & & & & & \\
b_0 & \alpha_1 & b_1 & & & & \\
 & b_1 & \alpha_2 & b_2 & & & \\
 & & \cdots & \cdots & \cdots & & \\
 & & & b_{z-3} & \alpha_{z-2} & b_{z-2} & \\
 & & & & b_{z-2} & \alpha_{z-1} & b_{z-1} \\
 & & & & & b_{z-1} & \alpha_z \\
\hline
\end{array}
\right\}
\tag{4.17}
$$

The following notations were adopted in constructing the above equations:

$$
\left.
\begin{aligned}
&b_0=\frac{1}{l_{01}};\quad a_0=-b_0;\\
&b_i=\frac{1}{l_{i,\,i+1}};\quad a_i=-b_{i-1}-b_i;\\
&b_z=0;\quad a_z=-b_{z-1}.
\end{aligned}
\right\}
\tag{4.18}
$$

$$
\left.
\begin{aligned}
&m_0=\frac{1}{l_{01}N_{01}};\quad n_0=-m_0;\\
&m_i=\frac{1}{l_{i,\,i+1}N_{i,\,i+1}};\quad n_i=-m_{i-1}-m_i;\\
&m_z=0;\quad n_z=-m_{z-1}.
\end{aligned}
\right\}
\tag{4.19}
$$

$$
\left.
\begin{aligned}
&\alpha_0=\sqrt{\frac{N_{01}l_{01}^2}{EI_{01}}};\\
&\alpha_i=\sqrt{\frac{N_{i,i+1}l_{i,\,i+1}^2}{EI_{i,\,i+1}}};\\
&\alpha_z=0.
\end{aligned}
\right\}
\tag{4.20}
$$

$$
\left.
\begin{aligned}
&d_0=m_0\left(1-\frac{\alpha_0}{\sinh\alpha_0}\right);\\
&d_i=m_i\left(1-\frac{\alpha_i}{\sinh\alpha_i}\right);\\
&d_z=0.
\end{aligned}
\right\}
\tag{4.21}
$$

/44

$$
\left.
\begin{aligned}
&e_0=m_0\left(\frac{\alpha_0}{\tanh\alpha_0}-1\right);\\
&e_i=m_i\left(\frac{\alpha_i}{\tanh\alpha_i}-1\right);\\
&e_z=0.
\end{aligned}
\right\}
\tag{4.22}
$$

$$
\left.
\begin{aligned}
&c_0=e_0;\\
&c_i=e_{i-1}+e_i;\\
&c_z=e_{z-1}.
\end{aligned}
\right\}
\tag{4.23}
$$

$$\left.\begin{aligned} h_0 &= d_0 - m_0; \\ h_i &= d_i - m_i; \\ h_z &= 0. \end{aligned}\right\} \tag{4.24}$$

$$\left.\begin{aligned} g_0 &= c_0 - n_0; \\ g_i &= c_i - n_i; \\ g_z &= c_z - n_z. \end{aligned}\right\} \tag{4.25}$$

In eqs.(4.26) and (4.27), given below, m_i is the mass of the i-th load

$$\left.\begin{aligned} s_0 &= 0; \\ s_i &= \frac{m_i}{N_{i-1,i}}; \\ s_z &= \frac{m_z}{N_{z-1,z}}. \end{aligned}\right\} \tag{4.26}$$

$$\left.\begin{aligned} t_{0i} &= m_i\left(-\frac{1}{N_{01}}\right); \\ t_{ki} &= m_i\left(\frac{1}{N_{k-1,k}} - \frac{1}{N_{k,k+1}}\right); \\ t_{z-1,z} &= m_z\left(\frac{1}{N_{z-2,z-1}} - \frac{1}{N_{z-1,z}}\right). \end{aligned}\right\} \tag{4.27}$$

Here, the subscript k denotes the number of the row in Table 1.1.

To solve the system of equations in Table 1.1, it is convenient to use the method of successive approximations. With respect to this system of equations, this involves the following: The functions of time $y_i(t)$, $M_i(t)$, and $\beta_i(t)$ entering into the systems (4.16) and (4.17) are represented in the following form:

$$\begin{aligned} y_i(t) &= y_i \sin pt; \\ M_i(t) &= M_i \sin pt; \\ \beta_i(t) &= \beta_i \sin pt, \end{aligned}$$

where the letters y_i, M_i, and β_i now denote only amplitude values of these functions.

Then, bearing in mind that $\ddot{y}_i(t) = -p^2 y_i \sin pt$ and canceling for sin pt, we obtain a system of algebraic equations analogous to the system (4.16) and (4.17). Only the values of p^2 will appear on the right-hand sides of the system of equations analogous to eq.(4.16).

Let us begin the method of successive approximations after assigning some /45 function y_{i_0} as the zeroth approximation. The second subscript here denotes the number of the approximation. The function y_{i_0} taken as the zeroth approximation should somehow be normed, for example

$$y_z = 1. \tag{4.28}$$

If the function y_i is known, then the inertia forces entering the right-hand side of eqs.(4.16) can be determined with an accuracy to within a constant factor p^2.

For the time being, we will assume $p^2 = 1$. Then, eqs.(4.16) will yield the values of the bending moments M_i and the angle of rotation of the blade at the root β_0. Next, from the known values of M_i and β_0 we can determine, over eqs.(4.17), the displacements of the blade axis during deformation which, for the case $p^2 = 1$, we will denote by u_i such that

$$y_i = p^2 u_i. \tag{4.29}$$

After determining the displacements u_i we can define the natural vibration frequency p. Its value is obtained on the basis of eqs.(4.28) and (4.29) in the following manner:

$$p^2 = \frac{y_z}{u_z} = \frac{1}{u_z}. \tag{4.30}$$

Then, in conformity with eq.(4.29) we determine the refined (after the first approximation) function

$$y_{i_1} = p^2 u_{i_1}. \tag{4.31}$$

The entire process is repeated until the required accuracy is achieved.

This method of successive approximations results in the determined mode y_i being reduced to the mode of the lower harmonic of the natural blade vibrations.

In determining successive harmonics, the condition of orthogonality must be satisfied. The operations required when obeying the condition of orthogonality are the same as for a blade of a nonrotating rotor (see Subsect.3 of Sect.2).

The above equations are equally suitable for calculating the natural vibration frequencies in the flapping plane and in the plane of rotation of the rotor. When calculating in the plane of rotation, the above values of the frequencies should be corrected by the formula

$$p^2_{pl.rot} = p^2_{pl.fl} - \omega^2, \tag{4.32}$$

where ω is the angular velocity of rotation of the rotor.

The method of calculating the natural vibration modes remains the same, irrespective of the plane in which the calculation is performed.

Let us make a more detailed study of certain operations in performing one approximation.

5. Determination of Bending Moments on the Basis of Known Forces

Let us begin with a determination of the bending moments on the basis of known inertia forces entering the right-hand side of eq.(4.16), which we determine in each approximation, assigning at first the value $p^2 = 1$.

After prescribing some vibration mode y_i, the coefficients of the right-hand side of eqs.(4.16) can be determined which will be denoted here by F_k.

The coefficients F_k can be determined from the formulas /46

$$F_k = s_k y_k + \sum_{l=k+1}^{z} t_{kl} y_l \tag{4.33}$$

or, still better, from

$$F_k = \frac{Q_{k-1,k}}{N_{k-1,k}} + \frac{Q_{k,k+1}}{N_{k,k+1}}, \tag{4.34}$$

where $Q_{k-1,k} = \sum_{k}^{z} m_i y_i$.

Then, the system of equations (4.16) can be rewritten in the following form (Table 1.2):

Table 1.2

β_0	M_0	M_1	M_2	...	...	M_{z-1}	M_z	β_z	
1	g_0	h_0							p^2F_0
	h_0	g_1	h_1						p^2F_1
		h_1	g_2	h_2					p^2F_2
			...	...	...				= ...
				h_{z-3}	g_{z-2}	h_{z-2}			p^2F_{z-2}
					h_{z-2}	g_{z-1}	h_{z-1}		p^2F_{z-1}
						h_{z-1}	g_z	-1	p^2F_z

(4.35)

To solve this system, we must know two additional equations which take the boundary condition into consideration. These equations can be the following:

at rigid attachment of the blade root

$$\beta_0 = 0;$$

at rigid attachment of the blade tip

$$\beta_z = 0.$$

At hinged attachment of the blade tips or with completely free tips, we have $M_0 = 0$ and $M_z = 0$.

Below, we will discuss only the two most common cases where the blade tip is free ($M_z = 0$) while the root either has a hinged support ($M_0 = 0$) or a rigid attachment ($\beta_0 = 0$).

Let us examine the first case in which the blade is hinged, i.e., $M_0 = 0$. Here, to determine the bending moments we use only the equations encased by a solid line in the system (4.35); from the first equation we can then determine the value of the angle of blade rotation in the hinge β_0. From the last equation of the system (4.35) we could also determine the value of β_z. However, we do not need this value for further solution. The equation itself is used only if $\beta_z = 0$, a case rarely encountered in practice.

In solving the system (4.35), it may easily happen that the wrong path is selected, leading to the appearance, during solution, of small differences of large quantities, which might completely ruin the result even when using a computer providing an accuracy to 10 decimal places.

We propose here a repeatedly verified procedure, which permits performing /47 the calculation on an ordinary slide rule.

We divide the first equation of the system (4.35), written for a hinged blade, by g_1 and the second equation by h_1:

$$M_1 + \frac{h_1}{g_1} M_2 = \frac{F_1}{g_1}; \tag{4.36}$$

$$M_1 + \frac{g_2}{h_1} M_2 + \frac{h_2}{h_1} M_3 = \frac{F_2}{h_1}. \tag{4.37}$$

Subtracting eq.(4.36) from eq.(4.37) and introducing the following notations:

$$g_2^* = \frac{g_2}{h_1} - \frac{h_1}{g_1};$$

$$h_2^* = \frac{h_2}{h_1};$$

$$F_2^* = \frac{F_2}{h_1} - \frac{F_1}{g_1},$$

we obtain an equation analogous to eq.(4.36):

$$M_2 + \frac{h_2^*}{g_2^*} M_3 = \frac{F_2^*}{g_2^*}. \tag{4.38}$$

In combination with the next equation of the system (4.35), this equation forms a system of two equations analogous to eqs.(4.36) and (4.37). Repeating the described operations a certain number of times, we ultimately obtain one equation of the following form:

$$M_{z-1} = \frac{F_{z-1}^*}{g_{z-1}^*}. \tag{4.39}$$

After determining the moment M_{z-1}, we determine the moment M_{z-2}, and so on up to the moment M_1. In other words, the moment M_i is determined each time when the moment M_{i+1} is already determined. The formula for determining the moment M_i can be written on the basis of eqs.(4.36) and (4.38) in the following manner:

$$M_i=\frac{F_i^*}{g_i^*}-\frac{h_i^*}{g_i^*}M_{i+1}. \tag{4.40}$$

After obtaining the bending moments, the angle of rotation of the blade in the root hinge β_0 is determined by means of the formula

$$\beta_0=F_0-h_0M_1. \tag{4.41}$$

The second step in the method of successive approximations involves determining the blade deformations from known values of the bending moments M_i and the angle of blade rotation in the hinge β_0.

6. Determination of Displacements from Known Bending Moments

Displacements of the blade in deformation which - in conformity with the above - are denoted by u_i can be determined from the system (4.17). However, it can be demonstrated that the equations of the system (4.17) are inadequate for determining all values of u_i.

Actually, for determining the position of the curve at a known curvature distribution over the length, when given the values of M_i, and at a known value of the angle of rotation at one point β_0, one more condition imposed on the values of displacements is necessary. In this case, the last equation of the system (4.17), which incorporates the value of the angle of rotation at another point β_z, is actually identical with the first equation so that it can be written out exclusively by analogy with the system (4.16). /48

Thus, the auxiliary condition either will be the condition

$$u_0=0, \tag{4.42}$$

if there is a support at the blade root, or else the condition

$$\sum_{i=0}^{z} m_iu_i=0, \tag{4.43}$$

if the blade is regarded as free on two sides of the beam. The condition (4.43) coincides with the expression obtained from the condition of orthogonality with the fundamental of the vibrations

$$y_i^{(0)}=1=\text{const.}$$

Calculating the coefficients that comprise the already determined values of M_1 and β_0 and leaving only the first of the two identical equations, we obtain the following system of equations which, in combination with eqs.(4.42) and (4.43), permits determining all values of u_i (see Table 1.3)

Table 1.3

u_0	u_1	u_2	u_3	$\bullet\bullet\bullet$	u_{z-1}	u_z		
u_0	b_0						=	D_0
b_0	a_1	b_1					=	D_1
	b_1	a_2	b_2				=	D_2
		b_2	a_3	b_3			=	D_3
			$\bullet\bullet\bullet$	$\bullet\bullet\bullet$	$\bullet\bullet\bullet$		=	$\bullet\bullet\bullet$
				b_{z-2}	a_{z-1}	b_{z-1}	=	D_{z-1}
					b_{z-1}	a_z	=	D'_z

(4.44)

Here, we have introduced the following notations:

$$D_i = d_{i-1}M_{i-1} + c_iM_i + d_iM_{i+1}. \tag{4.45}$$

In this formula, at i = -1, it is necessary to substitute β_0 for the values of M_{-1} and to consider the value of d_{-1} as equal to unity ($d_{-1} = 1$).

With the condition (4.42), the solution of the system (4.44) reduces to determining the values of u_i from simple recurrence relations of the type of

$$u_l = \frac{1}{b_{l-1}}[D_{l-1} - b_{l-2}u_{l-2} - a_{l-1}u_{l-1}]. \tag{4.46}$$

On solving the system (4.44) with the condition (4.43), the values of u_i /49 can be represented as

$$u_i = u_0 + \bar{u}_i, \tag{4.47}$$

where $\bar{u}_0 = 0$, and we can determine $\bar{u}_1$ from eqs.(4.46), after which the value of u_0 can be determined by means of the formula

$$u_0 = -\frac{\sum_{l=0}^{l=z} m_l\bar{u}_l}{\sum_{l=0}^{l=z} m_l}. \tag{4.48}$$

The further course of successive approximations has been described above.

In the examined case of hinged blade attachment at the root, the method of successive approximations leads at first to a determination of the mode of the fundamental, which, when the blade hinge coincides with the axis of rotation of the rotor, will coincide with a straight line. It is natural that, in this particular case, the calculations should begin directly with determination of the first harmonic, carrying out in each approximation orthogonalization to the fundamental which will be assumed as coinciding with a straight line.

In most designs, the root hinge of a helicopter blade is set off from the axis of rotation of the rotor by some amount r_0, which may be as much as 3 - 10% of the blade radius. The presence of this offset causes the mode of the fundamental of a hinge-suspended blade to deviate slightly from a straight line and the natural frequency to differ noticeably from an amount equal to the rpm of the rotor. To illustrate this effect, we will present (see Fig.1.14) a graph of the mode of the fundamental, for a large offset of the axis of rotor rotation from the root hinge.

7. Case of a Blade Rigidly Attached at the Root

The calculation of the natural vibration mode for a blade rigidly fixed at the root differs little from the above case of hinged attachment.

The first stage of the calculation, involving a determination of the bending moments M_1, is carried out in the same manner as described above, except that we now solve the system outlined by a broken line in the table of eq.(4.35). This system incorporates one more equation in which, by virtue of the boundary conditions, we set $\beta = 0$.

This condition is used also in solving the system (4.44), in which the coefficient D_0 is calculated from the formula

$$D_0 = c_0 M_0 + d_0 M_1.$$

8. Possible Simplifications in Calculating the Coefficients

We would like to emphasize that, in cases in which the blade is divided into a sufficiently large number of segments so that the value of the coefficients α_i in eqs.(4.20) is less than 0.05 - 0.08, it is possible to simplify eqs.(4.21) and (4.22) on replacing their hyperbolic functions by the first terms of their expansion in series.

Actually, in eqs.(4.21) and (4.22) we set

$$\sinh \alpha = \alpha + \frac{\alpha^3}{3!} + \frac{\alpha^5}{5!} + \ldots \cong \alpha + \frac{\alpha^3}{6};$$

$$\tanh \alpha = \alpha - \frac{\alpha^3}{3} + \frac{2\alpha^5}{15} - \ldots \cong \alpha - \frac{\alpha^3}{3}$$

and neglect the values α^2 with respect to unity. Then the coefficients d_i /50

and e_i can be calculated from the approximate formulas

$$d_i = \frac{l_{i,i+1}}{6EI_{i,i+1}};$$

$$e_i = \frac{l_{i,i+1}}{3EI_{i,i+1}} = 2d_i.$$

These simplifications render the calculation somewhat less laborious, which is important when using manual means.

9. Certain Results of Calculating the Natural Blade Vibration Modes and Frequencies

Here we distinguish two problems which are of prime interest from our point of view.

The first problem concerns the refinements yielding final results for the calculation of natural blade vibration frequencies and modes in a centrifugal force field, in comparison with the approximate method of calculations presented in Section 3. After this, we will give a discussion of the occurrence of sharp bends in the blade under the effect of local phenomena of the distribution of rigidity and mass parameters over the blade length. The occurrence of such flexures is characteristic for beams extended by centrifugal forces and is never observed in the absence of extension by centrifugal forces.

TABLE 1.4

Harmonic of Vibrations	Natural Vibration Frequency	
	Approximate Method	Exact Method
Hinged suspension at blade root		
First	405.3	404.3
Second	708.5	705.9
Third	1069.7	1069.0
Rigid attachment at blade root		
First	212.1	194.7
Second	463.7	461.9
Third	821.5	817.5

Let us begin with the first problem: We already noted in Subsection 1 of Section 3 that the approximate method of calculation of natural blade frequencies in a centrifugal force field, which is based on the assumption that the natural vibration modes do not differ in the presence or absence of centrifugal forces, yields completely satisfactory results at these frequency values.

To confirm this assumption, let us present the values of the natural vibration frequencies of the first three harmonics of hinged and rigid helicopter blades in a centrifugal force field. The values of the frequencies calculated by the approximate energy method (see Sect.3) are shown in the second column of Table 1.4. For comparison, the third column contains the exact values of frequencies calculated by the method presented in this Section.

A comparison of the frequency values presented in Table 1.4 shows that, at hinged suspension of the blade, the difference in their values is quite small. At rigid attachment, the difference is somewhat greater but still moderate. Therefore, as pointed out above, in calculations with the purpose of preventing the possible occurrence of resonance, the approximate method gives satisfactory results.

Centrifugal forces have a stronger effect on the natural vibration modes and especially on the distribution of bending moments and curvature of the elastic line over the blade length. /51

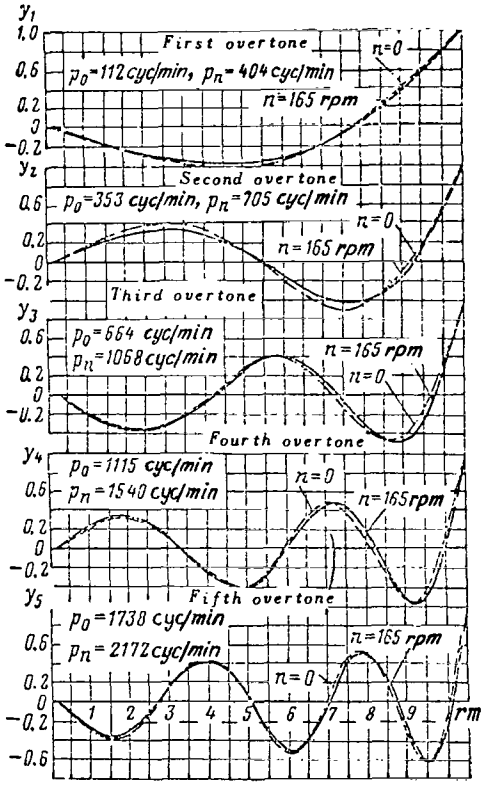

Fig.1.8 Modes of the First Five Harmonics of a Blade in a Centrifugal Force Field and at n = 0.

Figure 1.8 shows hinged modes of the first five harmonics (excluding the fundamental) for the same blade as in Table 1.4, while Fig.1.9 gives the distribution of bending moments corresponding to these modes. The solid lines in Figs.1.8 and 1.9 (just as in Figs.1.10, 1.11, and 1.12) represent the natural vibration modes in a centrifugal force field, and the broken lines indicate the same modes for a nonrotating blade.

Figure 1.10 shows the natural vibration modes and the corresponding bending moments for the first two harmonics of a blade fixed at the root.

As indicated by all these graphs, consideration of centrifugal forces, in certain blade sections, has a noticeable effect on the natural vibration mode, a point especially manifest in bending moment diagrams and hence in the distribution of bending stresses over the blade length. This effect is stronger, the lower the harmonics of natural vibration.

The distribution of bending moments over the blade length during its vibration in a centrifugal force field is characterized by an increase in bending moments in certain blade segments due to their decrease in adjacent segments. We will call this local increase in bending moments a "concentration of bending moments". The occurrence of such concentrated bending moments is associated with the presence of large concentrated loads and marked decreases in flexural rigidity in the blade structure.

Concentrated bending moments lead to an intensification of bending stresses at various blade segments, caused by sharp flexures of the blade at these segments.

This is of considerable interest for practice and thus should be studied in greater detail.

The nature of blade vibrations in a centrifugal force field is largely determined by the correlation between the magnitudes of elastic and centrifugal forces. If the flexural rigidity of the blade is sufficiently great (as is often the case, especially in the plane of rotation of the rotor) and if the centrifugal forces are insignificant (low rpm of rotor), then the vibration mode will differ little from that of a nonrotating blade.

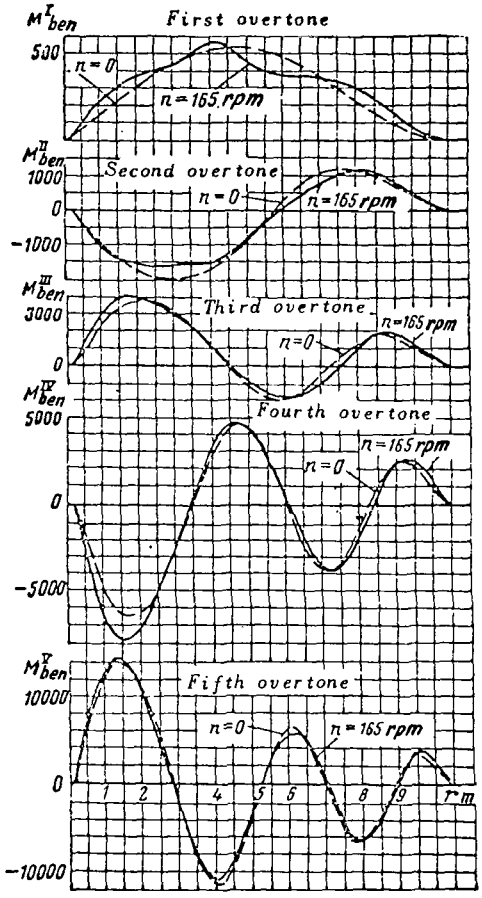

Fig.1.9 Distribution of Bending Moments over a Blade Vibrating with Respect to the Modes of the First Five Harmonics in a Centrifugal Force Field and when n = 0.

If, on the other hand, the flexural rigidity of the blade is low and the centrifugal forces are appreciable, then the form of blade deformation is determined mainly by inertia and centrifugal forces and depends little on the elastic properties of the blade. In this case, the form of blade deformation during vibration differs little from the form of deformation of an ideal flexible heavy string stretched by centrifugal forces. This phenomenon is generally observed during vibrations in the thrust plane of blades in modern helicopters. /52

Quantitatively, the relation between elastic and centrifugal forces can be estimated from the coefficient α which represents the ratio of the elastic potential energy to the potential energy accumulated by the blade due to bending in the centrifugal force field:

$$\alpha = \frac{C_{EI}}{C_N}.$$

The values of C_{EI} and C_N are described in eqs.(3.3) and (3.4).

When $\alpha > 1$, the effect of the elastic properties of the blade is greater than the effect of centrifugal forces. When $\alpha < 1$, the opposite is observed.

Table 1.5 gives the values of the coefficients α for a hinged blade whose modes of operation are shown in Figs.1.8 and 1.9. This blade can be regarded as a typical helicopter blade.

The values of the coefficients α given in Table 1.5 confirm the assumption that the helicopter blade, with respect to its characteristics in the flapping plane, approximates an ideal flexible heavy string extended by centrifugal forces, for which $\alpha = 0$.

The properties of a blade and of an elastic string draw closer together, the lower the overtone of the natural vibrations.

A basic feature of an extended ideal elastic string is that its axis undergoes sharp bends at the points of application of concentrated lateral forces and at sites where the string makes contact with rigid elements. Such a sharp flexure generally occurs at the site where the string is embedded or clamped. If a rigid segment is inserted into the string, sharp bends will form along the edges of this segment. Therefore, in cases when the properties of the blade and those of the stretched string approach more closely, the same characteristics become manifest also in deformations of the blade. Of course, an elastic blade, no matter how low its flexural rigidity might be, cannot undergo such sharp bends. Nevertheless, sharp bends inherent to an ideal elastic string are transmitted to the blade and cause sharp alternating bendings of its axis. These bends are accompanied by concentrations of bending moments and an increase in bending stresses at the points of flexure. /53

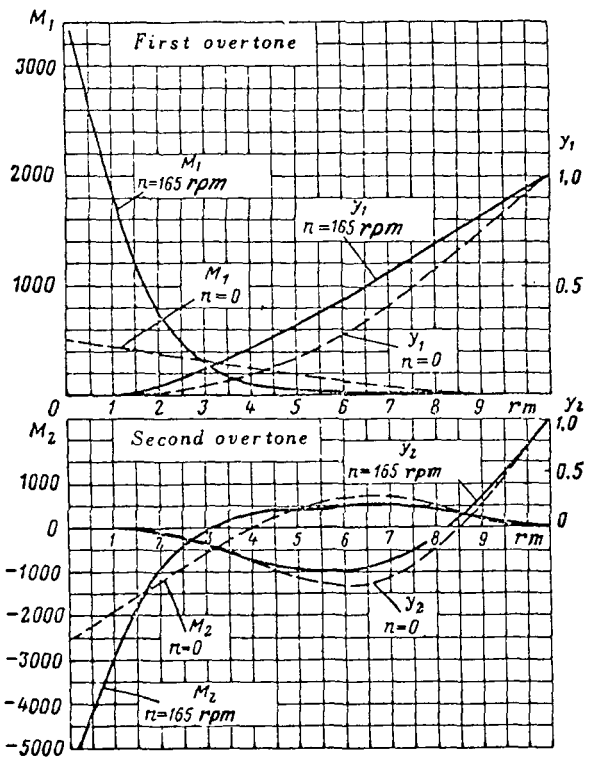

Fig.1.10 Modes of First and Second Overtones of Natural Vibrations of a Rigid Blade.

Let us examine several examples that confirm this assumption.

Figure 1.11 shows the distribution of bending moments over the blade length, corresponding to the natural vibration modes of the first and second harmonics with a load almost equal to the weight of the blade and located at a relative radius $\bar{r} = 0.48$.

At the point of attachment of the load, there is a marked concentration of bending moments leading to an increase in stresses by a factor of almost 2 in comparison with a nonrotating blade. The introduction into the blade of a segment of high rigidity leads to a concentration of bending moments in the area of this segment (Fig.1.12). However, since an increase in flexural rigidity leads to an increase in the moment of resistance over the length of the rigid

TABLE 1.5

Harmonic of Vibrations	Coefficient a for	
	Deformation in Flapping Plane	Deformation in Plane of Rotation
First	0.083	2.2
Second	0.332	3.7
Third	0.629	7.7
Fourth	1.116	—

segment, the greatest stresses will arise along the edges of the segment, /54 i.e., where the ideal rigid string would undergo sharp bends.

The occurrence of the same properties of an ideal elastic stretched string explains the occurrence of sharp concentrations of bending moments in the case of rigid blade attachment, since a flexible string would have, at the site of attachment, the same sharp bend as a hinged blade.

The bending moment corresponding to the first harmonic in the case of a rigid blade rises by a factor of almost 6 (see Fig.1.10) in comparison with the moment of a nonrotating blade. Such a sharp concentration of bending moments has a noticeable effect even on the values of the natural vibration frequencies (see Table 1.4). This greatly reduces the feasibility of an approximate method (see Sect.3), as applied to a calculation of a blade with rigid attachment at the root.

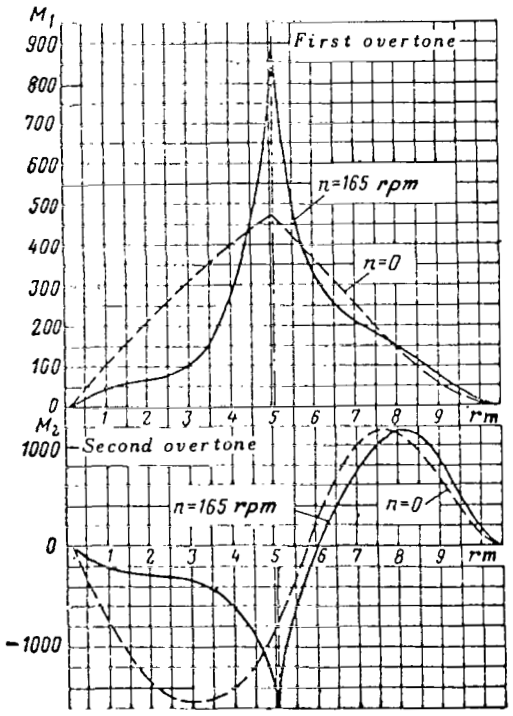

Fig.1.11 Bending Moment during Vibrations with Respect to the First and Second Overtone, for a Load at Radius $\bar{r} = 0.48$ Close in Weight to the Weight of the Blade.

In practice it is often necessary to introduce additional hinges into the rotor blade or to shift the position of the hinges already present in the hub design. The necessity of providing additional hinges has to do with the need to reduce the bending stresses at some blade segment or with the change in its natural vibration frequency.

Let us now investigate the manner in which bending deformations of a blade are affected by the introduction of an additional hinge. It was mentioned earlier that the blade of a helicopter is close in its characteristics to a stretched elastic string. A stretched chain, with hinges continuously distributed over its length, behaves like an elastic string. Therefore, we can assume that a helicopter blade takes approximately the same shape as an extended multihinged chain during deformation. Thus, it is logical that the introduction of an additional

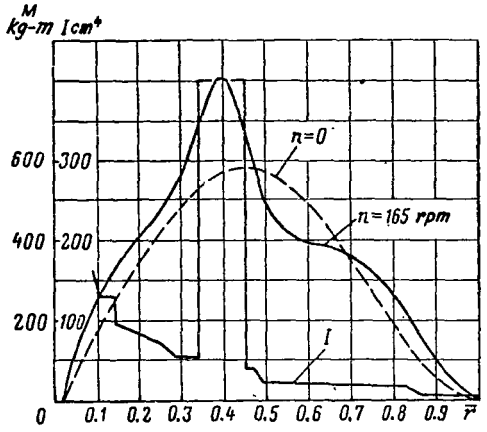

Fig.1.12 Mode of Bending Moment with Respect to the First Harmonic, for a Blade with a Segment of High Rigidity.

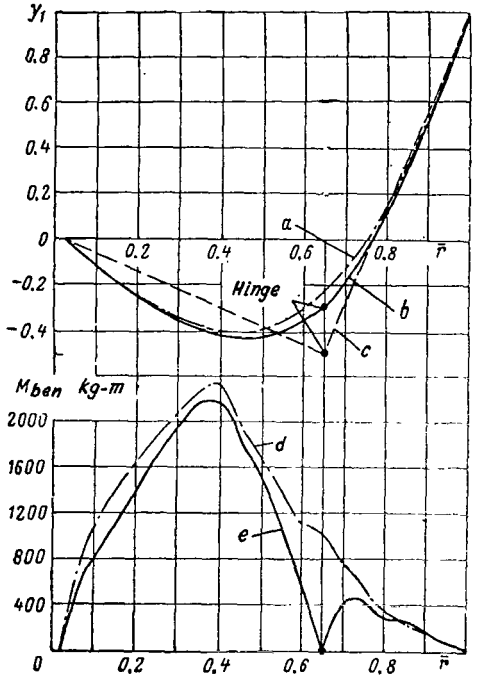

Fig.1.13 Mode of First Harmonic of Natural Vibrations of a Blade with and without Additional Hinge.
a and b - Modes of first harmonic in a centrifugal force field without hinge (a) and with hinge (b); c - Mode of first harmonic of nonrotating blades with hinge; d and e - Modes of bending moment with respect to first harmonic in a centrifugal force field without hinge (d) and with hinge (e).

hinge into the blade cannot substantially affect the mode of its deformation. This is illustrated in Fig.1.13 which gives the mode of the first harmonic of natural vibrations of a blade with and without an additional hinge. It is also seen from Fig.1.13 that the addition of an auxiliary hinge has a noticeable effect on the mode of the bending moment only in a small segment close to the hinge. Its influence is negligible in segments remote from the hinge.

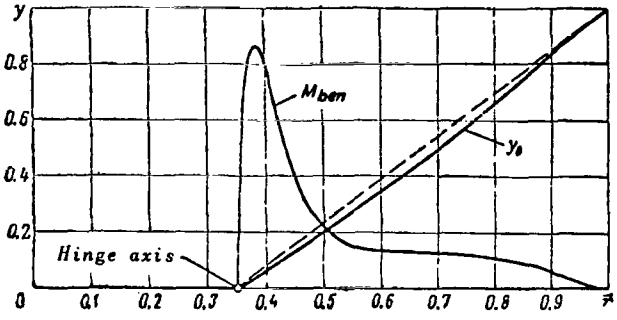

Fig.1.14 Modes of Lower Harmonic of Natural Vibrations of a Blade with Hinge Set Off from the Axis of Rotation and the Bending Moment Corresponding to this Mode (on Vibration in the Flapping Plane $p_0/n = 1.35$, on Vibration in the Plane of Rotation $p_0/n = 0.91$).

It is especially necessary to note that, in the case in question in which the blade has two hinges, its vibration modes /56 in a centrifugal force field differ greatly from the oscillation modes of a nonrotating blade. The nonrotating blade is not deformed at all in first-harmonic vibrations. Therefore, in the given case the approximate energy method of frequency calculation, in the form in which it is presented in Section 3, is not applicable.

Nor can we disregard the centrifugal force field in studying the blade deformations in a Dorschmidt-type rotor with a hinge far removed from the axis of rotation. The vibration mode of the lower harmonic of the blade of this rotor and the corresponding bending moment are shown in Fig.1.14. Without consideration of centrifugal forces the mode of the blade would coincide with a straight line and it would be impossible to find the magnitude of the bending moment plotted in Fig.1.14, which is very great for this rotor and actually determines the possibility of its use.

These examples show that, in many cases, the natural vibration modes in a centrifugal force field substantially differ from the corresponding modes of a nonrotating blade. This must be taken into account when designing a blade. Therefore, in the design office, if the calculations are all carried out on electronic computers and the degree of complexity of the method is of no import, there is no sense in resorting to approximate methods.

Section 5. Torsional Vibrations of a Blade

1. Problems Solved in Calculating Torsional Vibrations

It was noted above in Sections 1 and 4 that the calculation of the modes and frequencies of natural flexural blade vibrations not only has a secondary value (for stress analysis) but also an independent value as a method for selecting blade parameters that prevent the occurrence of bending resonance. This problem does not arise in calculating free torsional vibrations since vibrations

of noticeable amplitude caused by torsional resonance are never encountered in practice. As a rule, appreciable torsional vibrations are set up only during flutter or during forced vibrations under conditions close to flutter. Therefore, the magnitude of the frequency of natural torsional vibrations is of no practical interest in itself (if we do not regard it as a parameter characterizing the torsional rigidity of a blade), and the results of the calculation /57
of natural vibration modes and frequencies are only of secondary significance for calculating flutter or for calculating bending stresses computed with consideration of torsional blade deformations. The other problem does not arise when calculating free torsional blade vibrations.

Two main problems are encountered in calculating forced torsional vibrations. The first is the determination of elastic blade deformations whose consideration is necessary for the calculation of bending stresses; the second is the determination of the magnitudes of the hinge moments necessary for calculating the rotor control system.

2. Differential Equation of Torsional Blade Vibrations

Let us represent a blade in the form of a cantilever straight bar with a torsional rigidity GT_t variable over its length. The mass moment of inertia of the bar sections relative to its axis I_m will be assumed, just as the torsional rigidity, to be a continuous function variable over the length of the bar, the centers of gravity of all sections of the bar to lie on its axis, and the mounting of the bar to be torsionally elastic.

It is logical that reducing the problem of blade vibrations to calculation of such a model presupposes the use of numerous simplifying assumptions. Let us assume that the flexural axis of the blade is rectilinear and coincides with the axis of the feathering (axial) hinge of the rotor hub. Let us equate the flapping compensator ν to zero.

Allowance for displacement of the centers of gravity and determination of the effect of the flapping compensator on the natural frequencies will be examined in Section 6.

Use of the above assumptions permits solving the problem of torsional blade vibrations completely independently, without relating them with the flexural blade vibrations.

Let us construct the differential equation of torsional blade vibrations. The torque in the blade section can be determined from the differential equation:

$$[M_t]' = -\mathfrak{M}, \tag{5.1}$$

where $\mathfrak{M}$ is the linear torque of external and inertia forces acting on a blade element.

Under the effect of torque, each element of the blade is twisted through an angle of

$$d\varphi = \frac{M_t}{GT_t}\, dr, \tag{5.2}$$

where φ is the elastic angle of rotation of the blade section.

The value of the torque, derived from eq.(5.2), is substituted into eq.(5.1). Then, the differential equation of torsional deformations of the blade can be written in the form

$$[GT_t\ \varphi']' + \mathfrak{M} = 0. \tag{5.3}$$

Let us examine the torsional vibrations of a rotor blade rotating in a vacuum. The linear torque in this case will be equal to

$$\mathfrak{M} = -I_m\ddot{\varphi} - \omega^2 (I_y - I_x)\varphi, \tag{5.4}$$

where I_y and I_x are the mass moments of inertia of the blade section relative to its principal axes of inertia.

If the length of the profile along the x-axis is appreciably greater than along the y-axis (and this is usually the case), then we can set approximately /58

$$I_y - I_x \cong I_m, \tag{5.5}$$

where I_m is the linear mass moment of inertia of the blade section relative to an axis going through its flexural axis.

After substituting eq.(5.4), with consideration of eq.(5.5), into eq.(5.3), we obtain the differential equation of torsional vibrations of a rotor blade rotating in a centrifugal force field:

$$[GT_t\ \varphi']' - I_m(\ddot{\varphi} + \omega^2\varphi) = 0. \tag{5.6}$$

The blade model discussed here has the following boundary conditions:

$$\left.\begin{array}{ll} \text{at } r=0: & [GT_t\ \varphi']_0 = c_{con}\,\varphi_0; \\ \text{at } r=R: & [GT_t\ \varphi']_R = 0, \end{array}\right\} \tag{5.7}$$

where

c_{con} = rigidity of the rotor control system reduced to the axial hinge of the hub (the control rigidity determines the magnitude of rigidity of the elastic blade attachment at the root);

φ_0 = rotation of the blade in the axial (feathering) hinge as a consequence of deformation of the rotor control system.

3. Determination of the Natural Torsional Blade Vibration Modes and Frequencies

Here, we will use the method of solution presented in Subsection 1 of Section 2 for determining the flexural vibration modes and frequencies. Let us pose

$$\varphi(t)=\varphi\sin\nu t. \tag{5.8}$$

Substituting eq.(5.8) into eq.(5.6), we obtain

$$[GT_t\ \varphi']'+(\nu^2-\omega^2)\,I_m\varphi=0. \tag{5.9}$$

It immediately follows from this equation that the natural torsional vibration modes of a rotating and nonrotating blade are identical and that the frequencies are correlated by a simple relation of the form

$$\nu^2=\nu_0^2+\omega^2, \tag{5.10}$$

where

ν = natural frequency in a centrifugal force field;
ν_0 = natural frequency of blade of a nonrotating rotor.

Integrating eq.(5.9), with consideration of the boundary conditions (5.7) for the case $\omega = 0$ will yield

$$\varphi=\nu^2\left[\int_0^r\frac{dr}{GT_t}\int_r^R I_m\varphi dr+\frac{1}{c_{con}}\int_0^R I_m\varphi dr\right]. \tag{5.11}$$

Here and below, we will omit the superscript of ν, which denotes that the natural frequency is determined for $\omega = 0$.

Equation (5.11) is solved by the method of successive approximations, just as had been done in solving eq.(2.4) in Section 2.

Let us prescribe an arbitrary vibration mode φ. This mode should be normed in some manner, for example /59

$$\varphi_R=1, \tag{5.12}$$

where φ_R is the elastic angle of twist of the blade tip.

Then, performing the operations prescribed by eq.(5.11), we determine the function

$$\vartheta=\int_0^r\frac{dr}{GT_t}\int_r^R I_m\varphi dr+\frac{1}{c_{con}}\int_0^R I_m\varphi dr. \tag{5.13}$$

We can determine the natural torsional blade vibration frequency from the

norming condition for eq.(5.12)

$$\nu^2 = \frac{1}{\vartheta_R}, \tag{5.14}$$

where ϑ_R is the value of the function ϑ at r = R.

After prescribing a new value of the function

$$\varphi = \nu^2 \vartheta \tag{5.15}$$

and performing the operations (5.13) and (5.14) as many times as necessary for securing the required accuracy, we obtain the final values of ν and φ. As in the determination of the modes and frequencies of natural flexural vibrations, this method of successive approximations leads to determination of the lower harmonic of natural torsional vibrations. When determining the next harmonics, the condition of orthogonality

$$\int_0^R I_m \varphi^{(j)} \varphi^{(m)} dr = 0. \tag{5.16}$$

must be satisfied.

Here the index j denotes the mode of the unknown harmonic of vibrations, while the index m gives the modes of already determined lower harmonics. Putting

$$\varphi^{(j)} = \nu^2 \left[\vartheta - \sum_{m=1}^{m=j-1} c_m \varphi^{(m)} \right], \tag{5.17}$$

we obtain from the condition (5.16) the following expressions for the constant coefficients c_m:

$$c_m = \frac{\int_0^R I_m \vartheta \varphi^{(m)} dr}{\int_0^R I_m [\varphi^{(m)}]^2 dr}. \tag{5.18}$$

The natural vibration frequencies of subsequent harmonics are determined in each approximation from the formula

$$\nu_j^2 = \frac{1}{\vartheta_R - \sum_{m=1}^{m=j-1} c_m}. \tag{5.19}$$

Upon completing the determination of all natural vibration modes and frequencies needed for further calculations it is necessary to correct the frequencies by means of eq.(5.10) which takes into account the effect of centrifugal forces.

Calculations of the natural torsional vibration modes and frequencies of a blade in actual helicopters show that the rigidity of the rotor control system is of decisive importance in determining the magnitudes of lower-harmonic vibration frequencies. The torsional blade rigidity is almost always much higher than the rigidity of the control system. Figure 1.15 shows the modes of the first harmonic of natural torsional blade vibrations for different helicopters in mass service. /60

Based on the relationship between the torsional deformations of the blade and rotor control system in first-harmonic vibrations, it is possible to estimate the extent of torsional rigidity of the blade in comparison with the rigidity of the control system. The correlation between these rigidities is estimated by the coefficient α (see Fig.1.15). This coefficient determines the portion of the total angle of rotation of the blade tip due to deformations of only the blade.

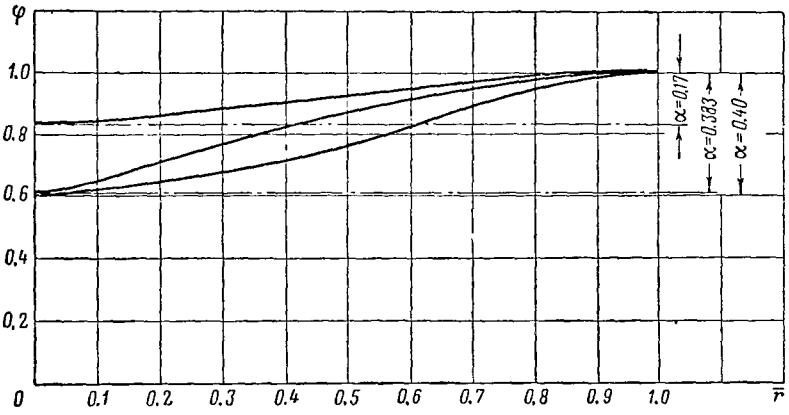

Fig.1.15 Natural Torsional Blade Vibration Modes; for Various Correlations of Blade and Control System Rigidities.

The described characteristic in the correlation between blade and control rigidities permits in certain calculations the assumption that the torsional blade deformations are small in comparison with the control deformations, thus making it possible to use only the blade twist due to deformation of the control. This assumption is often used in the calculation of flutter (see Chapt.IV of Vol.I).

The results of the calculation by the above method permit an estimate of the type of layout of the natural torsional vibration frequencies of a blade relative to the harmonic components of aerodynamic forces. Figure 1.16 gives the resonance diagram of torsional vibrations of a blade constructed for one of the existing helicopters, while Fig.1.17 shows the modes of the first three harmonics.

It was noted in Subsection 1 of this Section that the variable external forces producing blade twist are small so that, even in the presence of resonance, the torsional vibration amplitudes do not become dangerous for the strength of

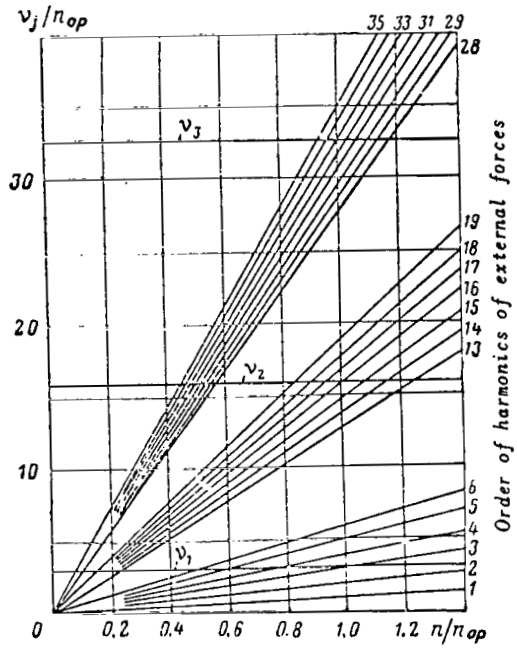

Fig.1.16 Resonance Diagram of Torsional Blade Vibrations.

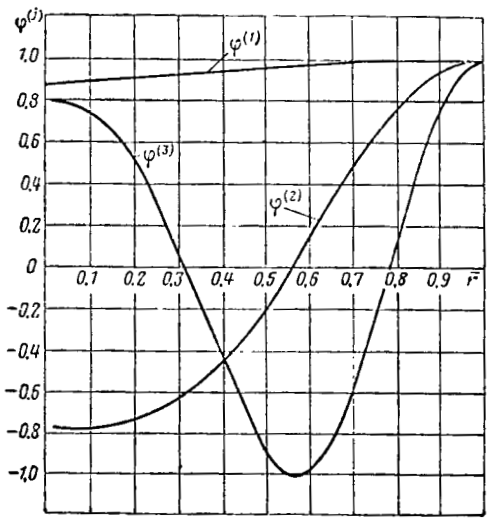

Fig.1.17 Modes of First Three Harmonics of Torsional Blade Vibrations.

the blade. In view of this, one usually does not try to avoid torsional resonance, and the resonance diagram presented in Fig.1.16 is given only for estimating the absolute magnitude of the torsional vibration frequencies.

It follows from Fig.1.16 that even the second harmonic of torsional vibrations at the operating rpm n_{op} proves to be higher than the 15th harmonic of the rotor rpm. The frequencies of subsequent overtones are even higher. Therefore, probably only the frequency of the first harmonic of natural torsional blade vibrations can be of practical interest.

All of the above considerations pertain to torsional vibrations of a rotor blade treated as an isolated blade, without consideration of the relations superimposed on the vibrations by the design of blade attachment at the hub. It was found that the interconnection of torsional vibrations of individual rotor blades across the control system may substantially change the entire pattern of vibrations. /62

4. Determination of the Natural Vibration Modes and Frequencies of a Rotor as a Whole

Figure 1.18 gives the diagram of the blade-setting control system used on most modern helicopters. Designwise this system is laid out so that loading of one or another control loop depends on the combination of forces generated at the swashplate of the pitch control by the blades. The form of this combination depends on the vibration mode of the rotor, i.e., on the distribution of vibration phases with respect to the blades. For example, when all blades vibrate with the same phase, the control loop is loaded only by the total pitch. When opposite blades vibrate in opposite phase, the lateral and longitudinal control loops are loaded. Finally, if the number of rotor blades is more than three, vibration modes become possible at which all forces arriving from the blades are locked on the swashplate of the pitch control.

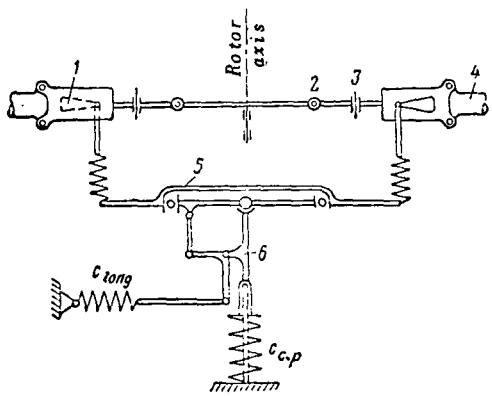

Fig.1.18 Diagram of Pitch Control.
1 - Blade turning lever; 2 - Flapping hinge; 3 - Drag hinge; 4 - Blade; 5 - Swashplate of control; 6 - Slide.

Variable forces during vibrations cause deformations of the control loops loaded by these forces. On deformation of individual control loops, the swashplate of the pitch control is set in oscillation; these vibrations impose definite phases on the blade vibrations. For example, during vertical vibrations of the swashplate generated by deformation of the collective pitch control loop, rotor vibrations are excited having a mode in which the phases of all blades are identical.

If the swashplate of the pitch control is inclined during vibration, opposite blades are excited in opposite phase. Thus, the swashplate of the pitch control couples the vibrations of individual rotor blades. As a result, blade vibrations can occur only with well-defined vibration modes of the entire rotor as a whole, and the number of such modes will coincide with the number of rotor blades. Here, each vibration mode corresponds to its value of control rigidity reduced to the feathering hinge of the blade, which depends on the rigidity of the control loop loaded at this mode. Accordingly, each mode of rotor vibration is characterized by its own frequency value of the natural torsional blade vibrations.

Consequently, for a rotor with a number of blades z_b there are z_b different natural vibration frequencies corresponding to each harmonic of torsional blade vibration. Each natural vibration frequency is characterized by its own specific mode of distribution of angles of twist over the blade length, but qualitatively all modes corresponding to a specific harmonic of vibrations do not differ; for example, they have an identical number of vibration nodes. /63

As a typical example we can cite the values of the natural vibration frequencies of the first harmonic for the four-blade rotor of the Mi-4 helicopter.

The lower frequency values at stressing of the longitudinal and lateral controls, relative to the operating rpm of the rotor, are $\frac{\nu_1}{n_{op}} = 3.4$ to 3.5. Upon loading the collective pitch control, this quantity takes the value $\frac{\nu_{1c.p}}{n_{op}} = 4.6$ while, upon locking all forces from the rotor on the swashplate, we have $\frac{\nu_{1s.p}}{n_{op}} = 6.6$.

A very important circumstance is that only the first harmonic of natural torsional blade vibrations lies within the limits of the vibration frequencies corresponding to harmonics of the rotor rpm, with respect to which the external forces have a noticeable magnitude. All subsequent harmonics of vibrations lie higher and therefore are of no practical interest.

Section 6. Combined Flexural and Torsional Blade Vibrations

1. Coupling of Flexural and Torsional Vibrations

Above, we discussed free flexural and torsional blade vibrations as two unrelated, independent problems. In a real blade, torsional and flexural vibrations are always related. The intensity of such coupling will be demonstrated below. We will examine blade vibrations in vacuum, when the coupling between torsional and flexural vibrations is produced exclusively by displacement of the centers of gravity of the sections relative to the flexural axis of the blade and as a consequence of the kinematic coupling over the flapping compensator. We will use the method of calculation constructed on the basis of the three-moment method described in Section 4, as applied to calculation of flexural vibrations.

The possibility of calculating the natural flexural and torsional (binary) vibration frequencies is useful to the designer in solving numerous specific practical problems.

For example, such a calculation becomes necessary if it is desired to place outrigger balancers on the blade to prevent resonance. Here we have in mind the relatively rare cases when the use of balancers is proposed not to eliminate flutter but to change the natural frequencies.

The designer may wish to take into account the coupling between flexural and torsional vibrations also when the calculation of natural blade frequencies for some reason does not coincide with experiment. Here it can be shown in many cases that this difference is due to disregard of such coupling. We can hope that the calculation results presented below will facilitate settling these doubts.

We should note, however, that calculation of natural frequencies in vacuum cannot give the answer to many questions in practical use having to do with the appearance of high variable stresses of some frequency in the blade, which are evaluated as resonance since aerodynamic forces often introduce substantial corrections into the picture of the phenomenon. /64

2. Method of Calculating Binary Vibrations

Calculation of natural binary vibration modes and frequencies is greatly simplified if we only consider blades of a definite conventional type, for whose calculation the following assumptions can be used:

1. The flexural axis of the blade is a straight line coinciding with the axis of the feathering (axial) hinge.

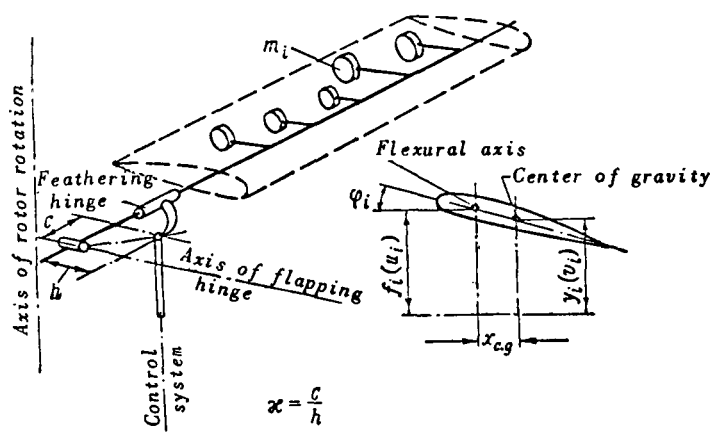

Fig.1.19 Design Model of Blade.

The method of calculation does not fundamentally change when these axes do not coincide. It is then only necessary to introduce, into the calculation formulas, a number of additional terms which take into account the distance between these axes. For simplicity of computation, we will assume that the flexural axis goes through the axis of rotation of the rotor.

2. The plane of minimum blade rigidity is considered to coincide with the flapping plane.

3. The blade performs torsional vibrations as a consequence of torsional deformations of the blade itself, deformation of the pitch control, and kinematic coupling over the flapping compensator with blade vibrations in the flapping plane.

These assumptions permit representing the blade as a weightless free beam divided into z segments, along whose edges loads are placed of a mass m_i at some stagger $x_{c.g_i}$ (Fig.1.19). Each load, in addition to the mass m_i concentrated at the center of gravity of the corresponding blade element, has a certain moment of inertia $I_{c.g_i}$ relative to an axis going through the center of gravity of the load and parallel to the elastic axis of the blade.

Let us represent the flexural and torsional rigidities in the form of stepped curves, such that they remain constant over the length of each segment.

The presence of a flapping compensator leads to a kinematic coupling between the flexural and torsional vibrations, which can be expressed by the formula /65

$$\varphi_0 = \frac{M_{t_0}}{c_{con}} - \varkappa\beta_0, \tag{6.1}$$

where

φ_0 = angle of blade rotation in the feathering hinge;
M_{t_0} = twisting moment relative to the feathering hinge;
c_{con} = rigidity of the pitch control reduced to the feathering hinge;
$\varkappa$ = flapping compensator;
β_0 = angle of blade rotation relative to the flapping hinge.

Furthermore, the boundary conditions at the root of the hinged blade somewhat change during its vibrations in the thrust plane. These conditions, in the presence of a flapping compensator, can be written as

$$M_0 = \varkappa M_{t_0}, \tag{6.2}$$

where M_0 is the bending moment and M_{t_0} is the twisting moment at the blade root.

In constructing the differential equations of blade vibrations in the flapping plane, we will use the three-moment method in the form as presented in Section 4. Application of this method to the case examined here leads to the following equations:

$$\left.\begin{aligned} h_{i-1}M_{i-1}+g_iM_i+h_iM_{i+1}&=\frac{Q_{i,i+1}}{N_{i,i+1}}-\frac{Q_{i-1,i}}{N_{i-1,i}};\\ d_{i-1}M_{i-1}+c_iM_i+d_iM_{i+1}&=b_{i-1}f_{i-1}+a_if_i+b_if_{i+1}. \end{aligned}\right\} \tag{6.3}$$

Here,

$$\left.\begin{aligned} Q_{i,i+1}&=-\sum_{i+1}^{z}m_i\ddot{y}_i;\\ Q_{i-1,i}&=-\sum_{i}^{z}m_i\ddot{y}_i \text{ (where } i=0,1,2,\ldots,z); \end{aligned}\right\} \tag{6.4}$$

where

f_i = vertical displacement of points of the elastic blade axis (see Fig.1.19);

y_i = vertical displacement of the centers of gravity of the loads m_i.

The expressions for the constants a_i, b_i, c_i, h_i, and g_i are given in Section 4; see eqs.(4.18) - (4.25).

The displacements of the elastic axis f_i and the centers of gravity of the blade elements y_i are related by

$$f_i=y_i+x_{c.g\,i}\varphi_i, \tag{6.5}$$

where φ_i is the angle of rotation of the blade elements about its elastic axis.

To determine the binary vibration modes and frequencies of a blade, eqs.(6.3) must be supplemented by the equations of torsional vibrations.

The twisting moment, if it is considered constant in magnitude over the length of each blade segment, can be defined as

$$M_{t\,i-1,i}=-\sum_{i}^{z}I_{c.g\,i}\ddot{\varphi}_i-\omega^2\sum_{i}^{z}I_{c.g\,i}\varphi_i+\omega^2\sum_{i}^{z}m_ix_{c.g\,i}r_if_i'+\sum_{i}^{z}m_ix_{c.g\,i}\ddot{y}_i. \tag{6.6}$$

From the magnitude of the twisting moment, we can determine the torsional deformations of the blade /66

$$\varphi_i=\sum_{0}^{i}\frac{M_{t\,i-1,i}\,l_{i-1,i}}{GT_{t\,i-1,i}}-\varkappa\beta_0, \tag{6.7}$$

where $GT_{t_{i-1,i}}$ is the torsional rigidity of a blade segment having a length equal to $t_{i-1,i}$ while φ_0 is determined by eq.(6.1).

When using the three-moment method, the boundary conditions of the problem are taken into account in the coefficients of the equation of the system. Thus, in the case examined here, the boundary condition (6.2) leads to a change of the coefficients of the first two equations of the system (6.3). For a blade with hinged attachment at the root these equations can be written in the following manner:

first equation of the system (6.3), from which the value β_0 is determined:

$$\beta_0+\varkappa g_0 M_{t_0}-h_0 M_1=\frac{Q_{01}}{N_{01}}; \tag{6.8}$$

second equation of the system (6.3):

$$\varkappa h_0 M_{t_0}+g_1 M_1+h_1 M_2=\frac{Q_{12}}{N_{12}}-\frac{Q_{01}}{N_{01}}. \tag{6.9}$$

Thus, the system of equations that includes eqs.(6.3), (6.5), (6.6), and (6.7) represents a system of differential equations of binary blade vibrations. The solution of this system permits determining the modes and frequencies of natural binary blade vibrations, which also enters into the calculation problem.

If we assume that the variables entering the differential equations (6.3), (6.5), (6.6), and (6.7) vary in accordance with a sine law of the type

$$y_i(t)=y_i \sin pt,$$

then these equations can be transformed into a system of algebraic equations relative to unknowns representing the amplitude values of the previous variables. The parameters p^2 and $\gamma = \frac{\omega^2}{p_2}$ will enter as cofactors only into certain coefficients of these equations. If we set $p^2 = 1$, then these equations can be rewritten in the form

$$\left.\begin{aligned} h_{i-1}\overline{M}_{i-1}+g_i\overline{M}_i+h_i\overline{M}_{i+1}&=\frac{\overline{Q}_{1,i+1}}{N_{i,i+1}}-\frac{\overline{Q}_{i-1,i}}{N_{i-1,i}};\\ d_{i-1}\overline{M}_{i-1}+c_i\overline{M}_i+d_iM_{i+1}&=b_{i-1}u_{i-1}+a_iu_i+b_iu_{i+1};\end{aligned}\right\} \tag{6.10}$$

$$\overline{M}_{t\ i-1,i}=(1-\gamma)\sum_i^z I_{c.g_i}\varphi_i+\gamma\sum_i^z m_i x_{c.g_i} r_i f_i'-\sum_i^z m_i x_{c.g_i} y_i; \tag{6.11}$$

$$\vartheta_i=\sum_0^i \frac{\overline{M}_{t\ i-1,i}\, l_{i-1,i}}{GT_{t\ i-1,i}}-\varkappa\overline{\beta}_0; \tag{6.12}$$

/67

$$v_i=u_i-x_{c.g_i}\vartheta_i, \tag{6.13}$$

where

$$\overline{Q}_{1,i+1}=\sum_{i+1}^z m_i\overline{y}_i;$$

$$\overline{Q}_{i-1,i}=\sum_i^z m_i\overline{y}_i.$$

The quantities entering these equations obey the following relations:

$$\left.\begin{aligned} y_i &= p^2 v_i; \\ f_i &= p^2 u_i; \\ \varphi_i &= p^2 \vartheta_i; \\ M_i &= p^2 \overline{M}_i; \\ M_{t\,i-1,i} &= p^2 \overline{M}_{t\,i-1,i}; \\ \beta_0 &= p^2 \overline{\beta}_0. \end{aligned}\right\} \qquad (6.14)$$

The system of equations (6.10), (6.11), (6.12), and (6.13) can be conviently solved by the method of successive approximations. In so doing, in each approximation we should refine the parameter γ for the angular velocity of rotation of the rotor ω prescribed in the calculation.

The successive approximations are carried out in the following sequence:

Assign a certain magnitude of the parameter γ and an arbitrary form of the zeroth approximation of the functions y_{i_0} and φ_{i_0}.

Normalize the functions taken as the zeroth approximation, for example

$$y_z = 1.$$

After this, derive the function f_{i_0} from eq.(6.5). Then, from eq.(6.11), determine the quantity $\overline{M}_{t_0}$ needed for solving the system of equations (6.10). At the same time $\overline{M}_{t_{i-1,i}}$ is determined.

After solving the system of equations (6.10) and determining u_i from the first equation of this system, determine $\overline{\beta}_0$:

$$\overline{\beta}_0 = \frac{\overline{Q}_{01}}{N_{01}} - h_0 \overline{M}_1 - \varkappa g_0 \overline{M}_{t_0}. \qquad (6.15)$$

Then, from eq.(6.12), determine ϑ_i and from eq.(6.13) the values of v_i, which, furthermore, should satisfy the condition $\sum_0^z m_i v_i = 0$.

Determine the natural frequency from the condition of normalization on the basis of the first relation in the system (6.14), thus:

$$p^2 = \frac{1}{v_z}. \qquad (6.16)$$

After this, determine the functions y_i and φ_i from eq.(6.14) and use them in the next approximations which are performed in the same sequence. At the same time, refine the parameter γ.

This method of successive approximations leads to a determination of the /68
frequency and mode of the lower harmonic of natural vibrations. To determine the next harmonic, we use the condition of orthogonality which for binary vibrations has the following form:

$$\sum_{0}^{z} \left[m_i y_i^{(j)} y_i^{(m)} + I_{c.g_i} \varphi_i^{(j)} \varphi_i^{(m)} \right] = 0. \qquad (6.17)$$

Here, the index j denotes the mode of the sought harmonic and the index m the modes of already determined lower harmonics.

The use of this method of calculation gives results that are completely satisfactory for practice.

It should be mentioned that, in cases in which the natural frequencies of two successive harmonics have sufficiently close values, this method of calculation does not give a converging solution. In practice, however, this is of no great import since it can happen only when the coupling between torsional and flexural vibrations is very weak and the corresponding vibration modes can be determined separately without consideration of this coupling.

3. Effect of Coupling between Bending and Torsion at Natural Vibration Frequency

Here, we will define the extent of the difference of natural binary blade vibration frequencies from corresponding partial frequencies, i.e., frequencies obtained without consideration of coupling between bending and torsion.

Calculations show that the coupling between bending and twisting has the greatest influence on natural blade vibrations in regions in which the partial frequencies of bending and torsion approach closely. Therefore, we should investigate only these regions. Outside these zones, the partial frequencies of the blade and the frequencies of the coupled binary vibrations practically coincide.

It is known that the partial frequencies of natural vibrations of bending of a hinged blade, for all modern helicopters, lie in very narrow well-defined zones whose position relative to the harmonics of external excitation cannot be changed substantially. In Fig.1.20, these zones are superposed on a resonance diagram of the blade. This diagram is constructed for the frequency range that includes only a series of first harmonics of rotor rpm, since external forces acting on the blade with higher harmonics are insignificant in magnitude and cannot cause noticeable blade vibrations. Only the first three overtones of the partial frequencies of the blade in bending fall within this region. In practice only these overtones are of interest in blade design. The natural flexural vibration frequencies can leave the indicated zones only for rotors with an unusual method of blade attachment to the hub, such as - for example - in rotors with rigid blade attachment or with a gimbaled hub.

The partial frequencies of natural torsional blade vibrations may vary

within wider limits, mainly as a consequence of the difference in the rigidities of the rotor control system whose designs may vary widely. Nevertheless, with respect to the magnitudes of the partial frequencies of natural torsional blade vibrations a very important conclusion can be drawn, involving the following: Only the first harmonic of torsional vibrations can fall within the frequency range of interest here. The second harmonic of torsional vibrations generally will be in a region not below the 15th harmonic of the rotor rpm (see Fig.1.16), i.e., beyond the limits of the region of interest to the designer. Usually, /69 vibrations of relatively large amplitude do not arise with such frequencies. Therefore, only the first harmonic of natural torsional vibrations of a blade is of practical interest from the aspect of possible occurrence of resonance.

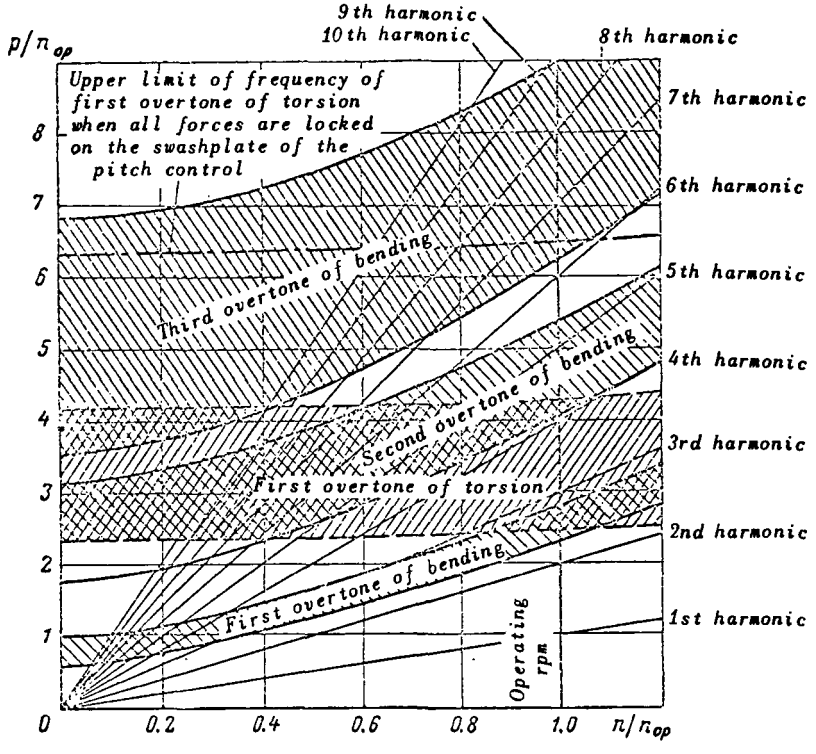

Fig.1.20 Regions on the Resonance Diagram of the Frequencies of Natural Vibrations of the First, Second, and Third Overtone of Bending and the First Overtone of Torsion for Blades of Different Helicopters.

Here, it should be recalled that the helicopter rotor blade may have several first overtones of torsional vibrations with different frequencies, depending on the vibration mode of the rotor as a whole and on what control loop is loaded at this mode. The difference in natural vibration frequency of these modes will be determined exclusively by the difference in the rigidities of the control loops being loaded.

In flight, each harmonic of external forces is able to excite only one well-defined vibration mode. Therefore, in investigating the possibility of the occurrence of resonance it is necessary to check whether the control rigidity adopted in the calculation corresponds to this mode, with which resonance is possible. In this Section, we will discuss only natural vibrations of the system. Therefore, we will not further discuss this problem.

Figure 1.20 shows the region which usually comprises the frequencies of the first harmonic of natural vibrations of a blade in torsion, for all modes of rotor vibrations when both cyclic and collective pitch control loops are loaded. For rotors with a blade number greater than three, a vibration mode is possible in which all forces arriving from the blades lock on the swashplate of the pitch control. The control rigidity corresponding to this mode generally is very high. In Fig.1.20, the upper limit of the region of torsional vibrations for this case is shown by a dot-dash line. /70

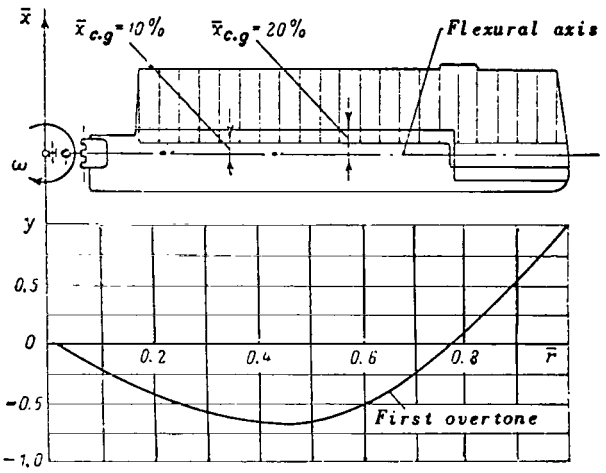

Fig.1.21 Stepped Centering of Blade with a Change of Sign at the Node of the First Overtone of Natural Flexural Vibrations.

Let us examine the most common case in which partial frequencies of the first harmonic of bending and the first harmonic of torsion coincide in magnitude in the zone of operating rpm of the rotor. Let us discuss two versions of the blade center-of-gravity distribution over its length.

In both versions, we will assume - in conformity with the above-adopted assumptions - that the flexural axis of the blade is rectilinear and coincides with the axis of the feathering hinge of the hub. The distance to the centers of gravity of the sections will be reckoned from the flexural axis in percentages of the blade chord. All investigations will be conducted applicable to a helicopter blade with a pressed duralumin spar with a chord constant over its length. Such a blade has roughly a constant linear weight over the length. Its chord comprises about 1/20 of the rotor radius.

So that the results of the calculations will be more graphic, we will assume that, upon variations in blade centering, the mass moments of inertia of its sections relative to an axis going through the centers of gravity do not change, i.e., that the position

$$I_{c.g} = \text{const},$$

is maintained.

First, let us examine the case in which the centerings of the blade sections are constant over its length, i.e.,

$$\bar{x}_{c.g}=\frac{x_{c.g}}{b}=\text{const},$$

where b is the blade chord.

This version of the distribution of centerings is considered quite widespread in practice. Furthermore, it permits tracing - in a very graphic form - the effect of centering and evaluating its significance as a factor of the coupling between flexural and torsional vibrations.

Figure 1.22 shows the resonance diagram of a blade for this case. The solid lines represent the partial frequencies of bending and twisting of the /71 blade, and the dashed lines give the frequencies of binary vibrations calculated for a displacement of the centering relative to the flexural axis, equal to 10% of the blade chord. The calculations were performed for the case of $\varkappa = 0$. Therefore, the sign of the shift of centering is of no significance.

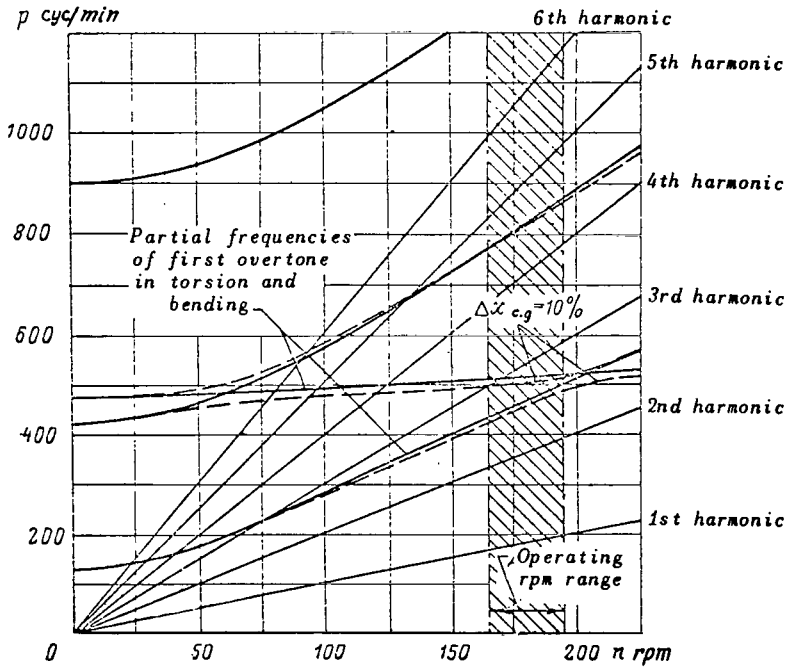

Fig.1.22 Resonance Diagram of Blade at Displacement of Centering Constant over the Length and Amounting to 10% of the Chord.

Here and below, we will intentionally examine a very wide range of variation in centerings, so as to trace its influence in a more concise form. In practice, the design capabilities and the conditions imposed by flutter permit

changing of the centering only within very narrow limits. Usually, for rotor blades the centering varies within limits from 20% to 25% of the blade chord (here, values reckoned from the leading edge of the blade are given), i.e., the entire range of variation in centering amounts to only about 5% of the blade chord. Thus, we can conclude from a study of Fig.1.22 that a displacement of centering, constant over the blade length, has only a negligible effect on the values of natural frequencies.

In the second case examined here, the distribution of centering is selected such that its influence is strongest during vibrations with a frequency close to the partial bending frequency of the first harmonic. The centering is assumed as constant over the blade length, but its sign changes at the node of the first harmonic of the partial bending mode.

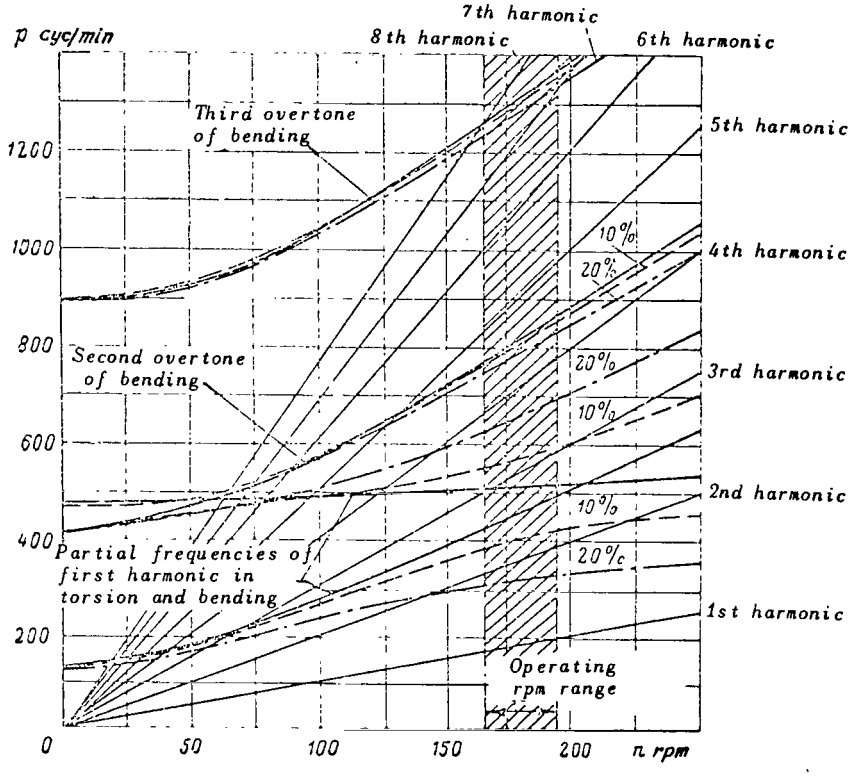

Fig.1.23 Frequencies of Natural Binary Blade Vibrations with a Stepped Law of Change of Centering over the Blade Length, at 10 and 20% Displacement with Respect to the Chord from the Flexural Axis.

An offset centering can be created for a blade when the anti-flutter balancer is introduced into the design not over the entire length but only over a small segment at the blade tip. Results of the calculation of this version of centering distribution are given in Fig.1.23. The effect of centering is

rather strong in this case. Therefore, at such a distribution over the length, the coupling between bending and torsion must be taken into account when calculating the blade.

It is also necessary to examine the effect of a concentrated load shifting over the chord. Let us take the magnitude of the load as equal to 8% of the blade weight. This probably is the maximum value of a load that can actually be attached to a blade. The most effective site of attaching such a load from the viewpoint of producing strong coupling factors for flexural and torsional vibrations is the point of the blade where the displacements in the thrust plane are maximum. Therefore, we will discuss the case in which the load is attached at the blade tip. /72

Figure 1.24 shows the results of calculation for this case. The effect of a concentrated load on the natural vibration frequency for large offset of the load can be considered substantial; however, the use of such a means for eliminating resonance cannot be recommended to the designer. Nevertheless, the attachment of a load can be regarded as a temporary means for treating blades subject to large variable stresses due to resonance.

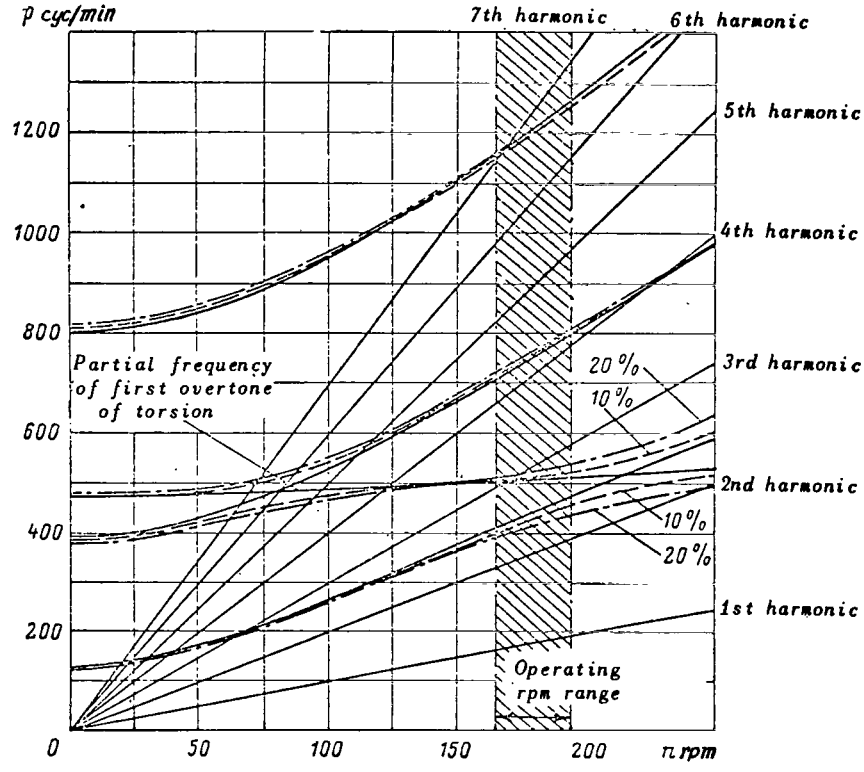

Fig.1.24 Effect of a 10 and 20% Displacement with Respect to the Chord of a 10-kg Tip-Concentrated Load on the Magnitude of the Natural Binary Blade Vibration Frequencies.

The last parameter which should be regarded as a coupling factor between bending and torsion is the flapping compensator. To evaluate its effect on the magnitude of the natural binary vibration frequencies, we made calculations with a flapping compensator $\varkappa = 1.0$. This is the maximum value of a flapping compensator of the type ever used in practice. All the data presented above were obtained with $\varkappa = 0$.

It follows from the calculations that the effect of the flapping compensator is negligible. /73 However, consideration of the flapping compensator can be justified to some extent, since it introduces some refinement into the form of the distribution of the bending moment at the blade root.

Section 7. Forced Blade Vibrations

1. Use of B.G.Galerkin's Method for Calculating Blade Deformations. Determination of Static Deformations of a Blade

The problem of the determination of blade deformations reduces to a solution of the above differential equation (1.9) whose derivation is given in Section 1:

$$[EIy'']'' - [Ny']' + m\ddot{y} = T, \tag{7.1}$$

where T is a linear external load on the blade, distributed over the radius and varying in time.

In Sections 2, 3, and 4, we discussed the solution of a similar equation for T = 0 describing the free vibrations of a blade. Here, we will examine forced vibrations of a blade when T is some periodic function varying with the frequency ν.

In the particular case when $\nu = 0$, the problem reduces to a determination of the static blade deformations due to a load T_0 constant in time.

The simplest method of solving eq.(7.1) is that given by B.G.Galerkin. /74

To illustrate the application of Galerkin's method to the determination of blade deformations, let us examine the static problem, when the external load is time-invariant. In this case, $\ddot{y} = 0$ and eq.(7.1) can be written as

$$[EIy'']'' - [Ny']' = T_0. \tag{7.2}$$

Let us represent the blade deformations in the form

$$y = \sum_j \delta_j y^{(j)}, \tag{7.3}$$

where

y^j = natural vibration modes of the blade with respect to the j-th harmonic;

δ_j = certain coefficients which will be called coefficients of blade deformation. The coefficients of deformation in all further computations in which the Galerkin method is used will play the role of generalized coordinates of the system.

Let us substitute eq.(7.3) into eq.(7.2), multiply all terms of the equation in turn by $y^{(0)}$, $y^{(1)}$, $y^{(2)}$, etc. and integrate them with respect to the blade radius.

By virtue of the orthogonality of the functions $y^{(j)}$, the performed operation transforms the differential equation (7.2) into a series of independent equations of the form

$$C_j\delta_j = A_j, \tag{7.4}$$

where

$$\left.\begin{aligned} C_j &= \int_0^R EI\,[y'']_j^2\,dr + \int_0^R N\,[y']_j^2\,dr; \\ A_j &= \int_0^R T_0 y^{(j)}\,dr. \end{aligned}\right\} \tag{7.5}$$

We will designate the quantity C_j as the generalized rigidity of the blade during deformation with respect to the mode of the j-th harmonic in a centrifugal force field. It follows from an examination of eqs.(7.5) that the generalized blade rigidity C_j is equal to double the potential energy accumulated by the blade during its elastic deformation in a centrifugal force field with respect to the normalized mode of the j-th harmonic. Let us call the quantity A_j the generalized external force deforming the blade with respect to the mode of the j-th harmonic. The magnitude of the generalized force A_j is equal to double the work done by the external linear forces T_0 during deformation of the blade with respect to the normalized mode of the j-th harmonic of its natural vibrations.

From eq.(7.4) we can determine the coefficients of blade deformation δ_j:

$$\delta_j = \frac{A_j}{C_j}, \tag{7.6}$$

after which eq.(7.3) will yield the mode of static blade deformation.

The more natural vibration modes are used in the calculation, the more accurate can the mode of deformations be determined. However, for practical purposes it is sufficient to limit ourselves to the first four harmonics of blade vibrations.

If the coefficients of deformation δ_j are known, then it is easy to determine the bending moments and the bending stresses in the blade. These are determined from the formulas /75

$$\left.\begin{aligned} M &= \sum_j \delta_j M^{(j)}; \\ \sigma &= \sum_j \delta_j \sigma^{(j)}. \end{aligned}\right\} \tag{7.7}$$

Here, $M^{(j)}$ and $\sigma^{(j)}$ are the modes of distribution of bending moments and bending stresses in normalized deformations of the blade with respect to the j-th harmonic of its natural vibrations.

The quantities entering eqs.(7.7) are governed by the relations:

$$\left.\begin{aligned} \sigma &= \frac{M}{W}; \\ \sigma^{(j)} &= \frac{M^{(j)}}{W}, \end{aligned}\right\} \tag{7.8}$$

where W is the moment of resistance of the blade sections.

2. Determination of Blade Deformations with Periodic Application of an External Load

Let us here discuss the case in which the external load varies in accordance with the law:

$$T = T_v \sin \nu t. \tag{7.9}$$

To solve this problem, we will again use Galerkin's method. Representing the blade deformations in the form of eq.(7.3), we first substitute eqs.(7.3) and (7.9) into eq.(7.1), multiply all terms of the obtained equations in turn by $y^{(j)}$ and integrate over the blade length. By virtue of orthogonality of the function $y^{(j)}$, we obtain a series of independent differential equations of the form

$$m_j \ddot{\delta}_j + C_j \delta_j = A_j \sin \nu t, \tag{7.10}$$

where

$$\left.\begin{aligned} m_j &= \int_0^R m [y^{(j)}]^2 dr; \\ A_j &= \int_0^R T_v y^{(j)} dr. \end{aligned}\right\} \tag{7.11}$$

We will designate the quantity m_j as the equivalent mass of the blade during its vibrations with respect to the mode of the j-th harmonic. If the vibration modes $y^{(j)}$ are normed so that $y_R^{(j)} = 1$, then m_j will be the equivalent mass of the blade reduced to its tip. It also follows from the first equation of the system (7.11) that the equivalent blade mass is equal to double its kinetic energy and that the blade elements are displaced at a rate of $y^{(j)}$.

To determine the steady motion, we pose

$$\delta_j = \delta^{(j)}_{dyn} \sin \nu t.$$

Substituting this expression into eq.(7.10) and canceling all terms of the equation by the quantity sin νt, we obtain

$$-\nu^2 m_j \delta^{(j)}_{dyn} + C_j \delta^{(j)}_{dyn} = A_j, \tag{7.12}$$

according to which the value of the amplitude of blade deformation is equal to /76

$$\delta^{(j)}_{dyn} = \frac{A_j}{C_j\left(1 - \frac{\nu^2}{C_j/m_j}\right)}. \tag{7.13}$$

It is not difficult to note that the ratio C_j/m_j is equal to the natural vibration frequency of the j-th harmonic of the blade. Actually, if we set $A_j = 0$ in eq.(7.12), then the value of ν in this case will determine the natural frequency of the blade and can be obtained from eq.(7.12):

$$\nu^2 = p_j^2 = C_j/m_j. \tag{7.14}$$

In conformity with eq.(7.6) the ratio A_j/C_j determines the magnitude of deformation if the load T_ν were to be applied statically.

Equation (7.13) is conveniently represented in the form

$$\delta^{(j)}_{dyn} = \lambda_{dyn}\, \delta^{(j)}_{st}, \tag{7.15}$$

where

$\delta^{(j)}_{st}$ = coefficient determining the magnitude of deformation at a statically applied external load T_ν; below, this coefficient will be called the coefficient of quasi-static blade deformation;

λ_{dyn} = coefficient of dynamic increase in vibration amplitude.

For the case in question, we have

$$\lambda_{dyn} = \frac{1}{1 - \frac{\nu^2}{p_j^2}}. \tag{7.16}$$

It follows from eq.(7.16) that during resonance, when the frequency of forced vibrations ν is equal to the frequency of the natural vibrations p_j, the coefficient of dynamic increase in amplitude becomes infinite. This result is regular for problems in which forced vibrations without damping are examined.

In reality, a helicopter blade operating in air undergoes appreciable aero-

dynamic damping during vibration. Aerodynamic damping limits the amplitude of blade vibrations in resonance and must be taken into account if a determination of blade vibrations, under conditions of resonance, enters into the problem of the calculation.

In determining the vibrations of a helicopter blade, when vibrations arise under the effect of aerodynamic forces, it is very difficult to make a strict separation between forces of aerodynamic damping and aerodynamic forces causing blade vibrations. Such a separation can be made only conditionally. However, a number of simplified calculation methods do use such a division. Therefore, we will discuss this approach in some detail.

3. Simplified Approach to Calculation of Forced Blade Vibrations

Let us assume that the external aerodynamic loads acting on an elastic blade in flight can be divided into two parts: external loads acting on the blade and forces of aerodynamic damping. We will stipulate, in first approximation, that the external loads acting on an elastic blade coincide with loads acting on an ideal flexurally rigid blade. Then, for performing the calculation it remains only to determine the forces of aerodynamic damping.

Usually the forces of aerodynamic damping are determined for a regime /77
with axial flow past the rotor, whereupon it is assumed that, in all other flight regimes with oblique flow past the rotor, the coefficients of aerodynamic damping do not change.

In a regime with axial flow past the rotor, the force of aerodynamic damping can be determined on the basis of the following:

During vibration, the blade elements move with a velocity $\dot{y}$. As a consequence, the angles of attack of all blade elements change by the quantity

$$\Delta\alpha = -\frac{\dot{y}}{\omega r}.$$

Upon a change in the angle of attack, the blade elements become subject to the action of additional forces of aerodynamic damping

$$T_{damp} = \frac{1}{2} c_y^{\alpha} \rho b \omega^2 r^2 \Delta\alpha = -\frac{1}{2} c_y^{\alpha} \rho b \omega r \dot{y}. \tag{7.17}$$

Let us assume that the aerodynamic load T can be represented as consisting of two components:

$$T = T_{rig} + T_{damp}, \tag{7.18}$$

where

T_{rig} = aerodynamic load acting on a rigid blade;
T_{damp} = additional load due to aerodynamic damping produced during elastic

blade vibrations.

Then, eq.(7.1) can be rewritten in the following form:

$$[EIy'']''-[Ny']'+m\ddot{y}+\frac{1}{2}c_y^a\varrho b\omega r\dot{y}=T_{rig}. \tag{7.19}$$

Let us examine blade vibrations due to the sinusoidal component of the aerodynamic load, varying according to the law

$$T_{rig}=T_\nu \sin \nu t.$$

If we represent blade deformations in the form of eq.(7.3) and apply B.G. Galerkin's method to eq.(7.19), then we arrive at a system of ordinary differential equations relative to the coefficients of deformation δ_j. Individual equations of this system will be correlated by terms into which the following integral enters:

$$D_{lm}=\int_0^R br y^{(j)} y^{(m)} dr,$$

where $y^{(j)}$ and $y^{(m)}$ are the natural vibration modes corresponding to different harmonics ($j \neq m$).

In simplified methods of calculation, the integrals D_{jm} are usually equated to zero although, in many cases, such an assumption is impossible to justify.

If we nevertheless make use of this assumption, then application of Galerkin's method yields a series of independent differential equations of the form

$$m_l\ddot{\delta}_l+\xi_l\dot{\delta}_l+C_l\delta_l=A_l \sin \nu t, \tag{7.20}$$

where the coefficient ξ_j determines the magnitude of aerodynamic damping: /78

$$\xi_l=\frac{1}{2}\, c_y^a\varrho\omega\int_0^R br[y^{(l)}]^2 dr. \tag{7.21}$$

After dividing all terms of eq.(7.20) by m_j, we obtain an equation of the form

$$\ddot{\delta}_l+2n_j\dot{\delta}_l+p_j^2\delta_l=p_j^2\delta_{st}^{(j)} \sin \nu t, \tag{7.22}$$

where

$$2n_l=\frac{\xi_j}{m_j};$$

$$\delta_{st}^{(j)} = \frac{A_j}{C_j}.$$

Usually, for the characteristic of the magnitude of damping we use the relative damping coefficient

$$\bar{n}_j = \frac{n_j}{p_j}.$$

Its magnitude, as applied to aerodynamic damping of a blade, is calculated by means of the formula

$$\bar{n}_j = \frac{1}{4} c_y^a \frac{\omega}{p_j} \cdot \frac{1}{m_j} \int_0^R br [y^{(j)}]^2 dr. \tag{7.23}$$

The solution of eq.(7.22), performed in the same manner as that used above in solving eq.(7.10), leads to the formula

$$\delta_{dyn}^{(j)} = \lambda_{dyn} \delta_{st}^{(j)},$$

where the coefficient of the dynamic increase in vibration amplitude is

$$\lambda_{dyn} = \frac{1}{\left[1 - \left(\frac{\nu^2}{p_j}\right)\right]^2 + 4\bar{n}_j^2 \left(\frac{\nu}{p_j}\right)^2}. \tag{7.24}$$

Thus, the solution of the problem examined here consists in determining the quasi-static coefficients of deformation $\delta_{st}^{(j)}$ and their subsequent multiplication by the value of the coefficient of dynamic increase in amplitude λ_{dyn}.

Such an approach is subject to certain inaccuracies because of the artificial separation of aerodynamic forces into two components by eq.(7.18), the inadequately founded assumption that $D_{jm} = 0$, and the approximate determination of the coefficients of aerodynamic damping for a regime with axial flow past the rotor. Therefore, in Sections 8 and 9 we will present methods of calculation in which the above assumptions are not used.

Nevertheless, a simplified approach of this type fairly well describes the qualitative aspect of phenomena observed during blade vibrations.

4. Amplitude Diagram of Blade Vibrations

/79

As indicated above in Section 3, the resonance diagram of a blade is widely used in evaluating the character of blade vibrations. The resonance diagram permits estimating the extent to which the natural vibration frequencies of the blade differ from the excitation frequencies and determining the possible hazard of the occurrence of resonance vibrations. However, in cases in which the natu-

ral frequencies and the excitation frequencies do not differ greatly, it is of interest to estimate the extent to which blade vibration amplitudes can be reduced. Such an estimate can be made by using the amplitude diagram of blade vibrations. This diagram, constructed for a blade with ordinary mass and rigidity characteristics, is given in Fig.1.25.

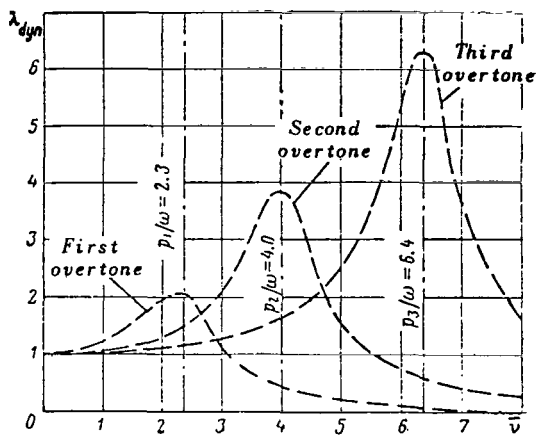

Fig.1.25 Amplitude Diagram of Blade Vibrations.

In this diagram, the abscissa gives the excitation frequency referred to the angular velocity of rotation of the rotor,

$$\bar{\nu} = \frac{\nu}{\omega}. \qquad (7.25)$$

The ordinate gives the coefficients of dynamic increase in vibration amplitude. The diagram is constructed only for the first three harmonics of elastic blade vibrations, using the damping coefficients calculated from eq.(7.23).

5. Calculation of Vibrations at Application Phase of External Load Variable over the Blade Length

In Subsection 3 of this Section we presented formulas for the case when the external load is represented as

$$T_{rig} = T_\nu \sin \nu t.$$

This form of notation of the load is possible only if the phase of its application over the blade length is constant. As a rule, this does not happen during vibrations of a helicopter blade. The phase of the external load varies over the blade length, so that the load should be represented in the form

$$T_{rig} = \bar{T}_\nu \cos \nu t + \bar{\bar{T}}_\nu \sin \nu t, \qquad (7.26)$$

where the components of the external load $\bar{T}_\nu$ and $\bar{\bar{T}}_\nu$ vary over the blade length in accordance with different laws.

After substituting eq.(7.26) into eq.(7.19), using Galerkin's method, and /80 assuming that $D_{jm} = 0$, we obtain

$$m_j \ddot{\delta}_j + \xi_j \dot{\delta}_j + C_j \delta_j = \bar{A}_j \cos \nu t + \bar{\bar{A}}_j \sin \nu t, \qquad (7.27)$$

where

$$\bar{A}_j = \int_0^R \bar{T}_\nu y^{(j)} \, dr;$$

$$\overline{\overline{A}}_j = \int_0^R \overline{\overline{T}}_\nu y^{(j)}\, dr.$$

Let us pose

$$\delta_j = \bar{\delta}^{(j)}_{dyn} \cos \nu t + \bar{\bar{\delta}}^{(j)}_{dyn} \sin \nu t. \tag{7.28}$$

Then,

$$\left.\begin{aligned} \bar{\delta}^{(j)}_{dyn} &= \frac{\left[1 - \frac{\nu^2}{p_j^2}\right] \bar{\delta}^{(j)}_{st} - 2\bar{n}_j \frac{\nu}{p_j} \cdot \bar{\bar{\delta}}^{(j)}_{st}}{\left[1 - \frac{\nu^2}{p_j^2}\right]^2 + 4\bar{n}_j \frac{\nu^2}{p_j^2}}; \\ \bar{\bar{\delta}}^{(j)}_{dyn} &= \frac{\left[1 - \frac{\nu^2}{p_j^2}\right] \bar{\bar{\delta}}^{(j)}_{st} + 2\bar{n}_j \frac{\nu}{p_j} \bar{\delta}^{(j)}_{st}}{\left[1 - \frac{\nu^2}{p_j^2}\right]^2 + 4\bar{n}_j \frac{\nu^2}{p_j^2}}, \end{aligned}\right\} \tag{7.29}$$

where

$$\left.\begin{aligned} \bar{\delta}^{(j)}_{st} &= \frac{\overline{A}_j}{C_j} = \frac{\overline{A}_j}{p_j^2 m_j}; \\ \bar{\bar{\delta}}^{(j)}_{st} &= \frac{\overline{\overline{A}}_j}{C_j} = \frac{\overline{\overline{A}}_j}{p_j^2 m_j} \end{aligned}\right\} \tag{7.30}$$

are the coefficients of quasi-static blade deformation.

Equations (7.29) permit determining the dynamic coefficients of blade deformation if the quasi-static coefficients of deformation obtained for the aerodynamic loads $\overline{T}_\nu$ and $\overline{\overline{T}}_\nu$ are known.

6. Aerodynamic Load on a Rigid Blade

In flight, a helicopter blade is acted upon by variable loads with frequencies that are multiples of the rotor rotations. In this case, as already mentioned, the greatest variable stresses in the blade are caused by the first six to eight harmonics of the aerodynamic load relative to the rotor rotations. Higher harmonics usually are so small as to cause no noticeable stresses in the blade, even in resonance.

A calculation of the variable aerodynamic loads on a blade encounters certain difficulties. These have to do primarily with the necessity of determining the variable induced velocity field, consideration of nonlinearity in the dependence of the aerodynamic coefficients on the angle of attack of the profile, the Mach number (M), and coupling of the loads with the torsional vibrations of the blade. The consideration of these characteristics is discussed in the respective Sections. Here, we will construct formulas for determining variable

aerodynamic loads acting on a blade rigid in flexure and torsion, under the following assumptions.

a) We assume that the inlet angle to the blade profile Φ (Fig.1.26) is small so that we can set approximately: /81

$$\Phi = \tan^{-1}\frac{U_y}{U_x} \approx \frac{U_y}{U_x}, \tag{7.31}$$

where

Φ = inlet angle;

U_x and U_y = mutually perpendicular components of the relative flow velocity lying in a plane normal to the blade axis (see Fig.1.26). Here, the velocity U_x is parallel to the plane of rotation of the rotor.

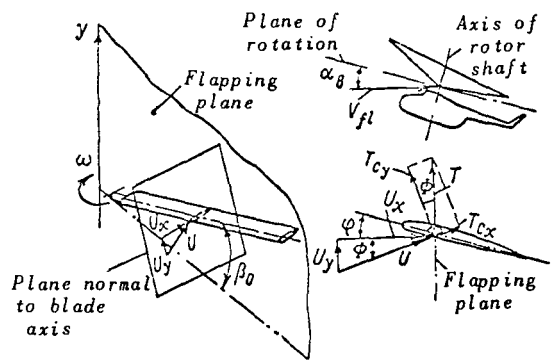

Fig.1.26 Diagram of Flow Past a Blade Rigid in Flexure and Torsion.

Assuming also that $\cos\Phi \cong 1$, we will consider that the unknown load T acting in the flapping plane does not differ from the load T_{cy}, perpendicular to the inlet to the blade profile (Fig.1.26).

b) We assume that the magnitude of relative velocity of the flow (U) past the profile differs little from the quantity U_x:

$$U \cong U_x. \tag{7.32}$$

c) We assume that, in determining the loads in the flapping plane, the profile drag can be neglected and that we can set $c_x = 0$.

We stipulate that the profile lift coefficient c_y depends linearly on the profile angle of attack α:

$$c_y = c_y^\alpha \cdot \alpha. \tag{7.33}$$

d) We assume that the induced velocity of the flow v passing through the rotor is constant over the entire area swept by the rotor:

$$v = \text{const}. \tag{7.34}$$

With these assumptions, only the constant portions of the first two harmonics of aerodynamic forces are of substantial magnitude, and then only at medium and high flying speeds of the helicopter. The high harmonics are small and their calculation under the above assumptions is of no interest.

Using these assumptions, the linear aerodynamic load on the blade can be determined by the formula

$$T=\frac{1}{2}c_y^{\alpha}\cdot\alpha\rho bU_x^2. \tag{7.35}$$

We will assume furthermore that the profile angle of attack is

$$\alpha=\varphi_r+\frac{U_y}{U_x}, \tag{7.36}$$

where φ_r is the angle of blade profile setting in a section at distance r from the axis of rotation.

Then, eq.(7.35) can be transformed into the form /82

$$T=\frac{1}{2}c_y^{\alpha}\rho b\left[\varphi_r U_x^2+U_x U_y\right]. \tag{7.37}$$

For an ideal flexurally rigid blade, suspended at the hub by a flapping hinge, the velocities entering eq.(7.37) can be determined by means of the following formulas:

$$\left.\begin{aligned} U_x&=\omega R(\bar{r}+\mu\sin\psi);\\ U_y&=\omega R\left(\lambda_0-\mu\cos\psi\beta_0-\frac{\bar{r}}{\omega}\dot{\beta}_0\right). \end{aligned}\right\} \tag{7.38}$$

Here,

β_0 = flapping angle of the blade relative to the flapping hinge;

$\dot{\beta}_0=\frac{\partial\beta_0}{\partial t}$ = time derivative of the angle β_0;

λ_0 = relative velocity of the flow through the rotor;

$$\lambda_0=\mu\,tan\alpha_{rot}+\bar{v}_0,$$

where

α_{rot} = rotor angle of attack at the shaft axes;

$\bar{v}_0$ = induced velocity of the flow referred to ωR, which is constant over the rotor disk.

The blade angle can be written as

$$\varphi_r=\theta_0+\Delta\varphi-\theta_1\sin\psi-\theta_2\cos\psi-\varkappa\beta_0, \tag{7.39}$$

where

θ_0 = blade angle at the relative radius $\bar{r}$ = 0.7 or at any other radius adopted for reckoning θ_0 at β_0 = 0;

$\Delta\varphi$ = geometric twist of the blade;
θ_1 and θ_2 = angles of cyclic pitch control of the blade prescribed by the swashplate.

If we represent the flapping motion of the blade in the form of a series

$$\beta_0 = a_0 - \sum_n (a_n \cos n\psi + b_n \sin n\psi) \tag{7.40}$$

and retain there only the first two harmonic components, since the higher harmonics are small at the adopted assumptions, then eq.(7.37) can be transformed into

$$T = \frac{1}{2} c_y^{\alpha} \varrho b_{0.7} \omega^2 R^2 \left[\bar{P}_0 + \sum_n (\bar{P}_n \cos n\psi + \bar{\bar{P}}_n \sin n\psi) \right], \tag{7.41}$$

where

$$\left.\begin{aligned}
\bar{P}_0 &= \bar{b}\left[\bar{r}\lambda_0^* + \left(\bar{r}^2 + \frac{1}{2}\mu^2\right)\varphi_r - \frac{1}{4}\mu^2 \varkappa a_2 + \frac{1}{4}\mu^2 b_2\right];\\
\bar{P}_1 &= \bar{b}\left[-\mu\bar{r}a_0 + \left(\bar{r}^2 + \frac{1}{4}\mu^2\right) b_1^* - \frac{1}{2}\mu\bar{r}a_2 + \mu\bar{r}\varkappa b_2\right];\\
\bar{\bar{P}}_1 &= \bar{b}\left[\mu\lambda_0^* + 2\mu\bar{r}\varphi_r + \left(-\bar{r}^2 + \frac{1}{4}\mu^2\right)a_1^* - \mu\bar{r}\varkappa a_2 - \frac{1}{2}\mu\bar{r}b_2\right];\\
\bar{P}_2 &= \bar{b}\left[-\frac{1}{2}\mu^2\varphi_r + \mu\bar{r}a_1^* + \varkappa\left(\bar{r}^2 + \frac{1}{2}\mu^2\right)a_2 + 2\bar{r}^2 b_2\right];\\
\bar{\bar{P}}_2 &= \bar{b}\left[-\frac{1}{2}\mu^2 a_0 + \mu\bar{r}b_1^* - 2\bar{r}^2 a_2 + \varkappa\left(\bar{r}^2 + \frac{1}{2}\mu^2\right)b_2\right].
\end{aligned}\right\} \tag{7.42}$$

In performing these transformations we used a substitution that permits changing over to the so-called equivalent rotor. /83

An equivalent rotor is a rotor whose shaft is imagined as turned relative to a real rotor through an angle such that the same angles of attack of the blade sections are achieved without cyclic pitch control. All formulas written out for an equivalent rotor can be used without change for a real rotor without an automatic pitch control. An equivalent rotor usually is also given the properties of a rotor without a flapping compensator. In this case, the formulas are equivalent only to an accuracy to within the first harmonic of flapping.

Transformation of the formulas for aerodynamic loads, as applied to the equivalent rotor, was performed under application of the following substitutions:

$$\left.\begin{aligned}
\varphi_r &= \varphi_{real} + \Delta\varphi = \theta_0 - \varkappa a_0 + \Delta\varphi;\\
a_1^* &= a_1 - \varkappa b_1 + \theta_1;\\
b_1^* &= b_1 + \varkappa a_1 - \theta_2;\\
\lambda_0^* &= \lambda_0 + \mu(\varkappa b_1 - \theta_1),
\end{aligned}\right\} \tag{7.43}$$

where

φ_{real} = real blade angle with consideration of the effect of a flapping compensator at the radius adopted for reading this angle;

a_1^*, b_1^* and λ_0^* = flapping coefficients and relative velocity of flow through the blades for an equivalent rotor.

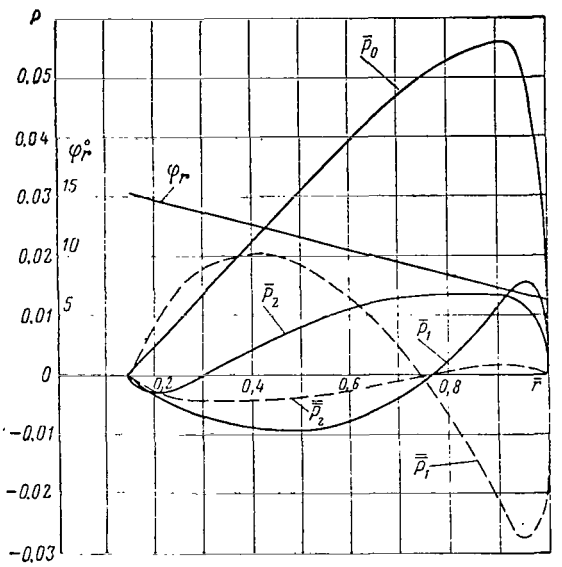

Fig.1.27 Distribution of Harmonic Components of Aerodynamic Load over the Blade Radius, for $\mu = 0.28$.

Here, we will not discuss higher harmonics of the aerodynamic load.

Figure 1.27 shows the constant portion and cosinusoidal and sinusoidal components of the first two harmonics of the aerodynamic load, for a typical helicopter blade derived from eqs.(7.42) for horizontal flight of a helicopter at $\mu = 0.28$. /84

In Figs.1.28 and 1.29 these loads are summed; the diagram also gives the total relative aerodynamic load P acting on a blade in the longitudinal plane of the rotor at $\psi = 0^\circ$ and $\psi = 180^\circ$ (Fig.1.28) and in the lateral plane at $\psi = 90^\circ$ and $\psi = 270^\circ$ (see Fig.1.29).

7. Determination of the Blade Flapping Coefficients

To determine aerodynamic loads by means of eq.(7.42), it is necessary to know the flapping coefficients of a flexurally rigid blade.

The flapping coefficients can be determined from the differential equation (7.1) if we represent the solution of the equation in the form

$$y = \beta_0 y^{(0)}, \tag{7.44}$$

where $y^{(0)}$ is the mode of blade vibrations with respect to the fundamental.

For a rigid blade, this vibration mode coincides with a straight line

$$y^{(0)} = \frac{r - l_{h.h}}{1 - l_{h.h}/R}.$$

If the distance from the axis of rotation to the horizontal or flapping hinge is equal to zero ($l_{h.h} = 0$), then /85

$$y^{(0)} = r, \tag{7.45}$$

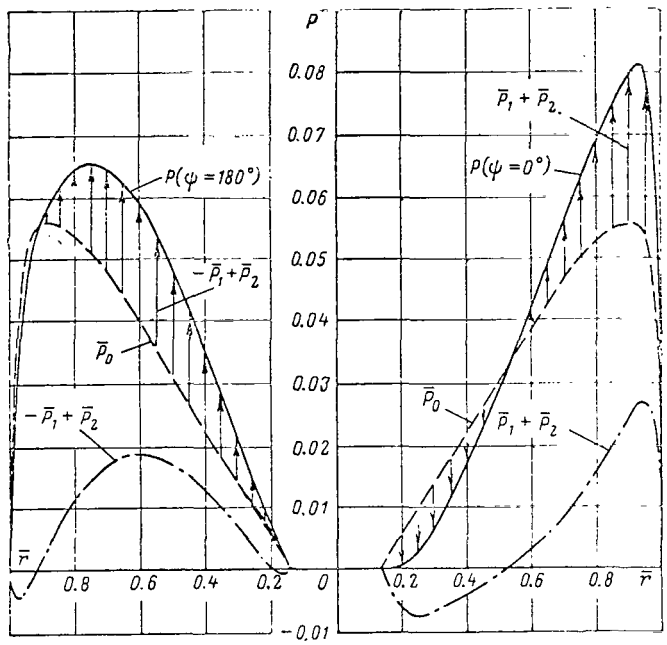

Fig.128 Relative Aerodynamic Load Acting on a Blade in the Longitudinal Plane of the Rotor.

which is valid both for rigid and elastic blades (see Sect.4).

Setting $i_{h.h} = 0$, let us substitute eq.(7.45) into the differential equations (7.1) and apply Galerkin's method to it. This operation leads to a differential equation of flapping vibrations of the blade

$$I(\ddot{\beta}_0 + \omega^2\beta_0) = \int_0^R T dr, \qquad (7.46)$$

where I is the moment of inertia of the blade relative to the flapping hinge.

Equation (7.46) can also be derived by equating to zero the moment of all forces relative to the flapping hinge.

Substituting eqs.(7.40) and (7.41) into eq.(7.46) and equating the coefficients of like harmonic azimuthal functions, we obtain a system of equations from which we can determine all flapping coefficients. This system is written out as a table (see Table 1.6).

Each equation of the derived system represents the sum of the products of /86 certain coefficients, entered in the squares of Table 1.6, while the unknown flapping coefficients of the blade simultaneously entering several equations are set apart vertically in a separate row above the table. The known coefficients of each equation occupy one row in Table 1.6. On the right-hand side of the

table, a special column contains the coefficients Φ making up the right-hand side of the equations. The empty squares of the table correspond to coefficients equal to zero.

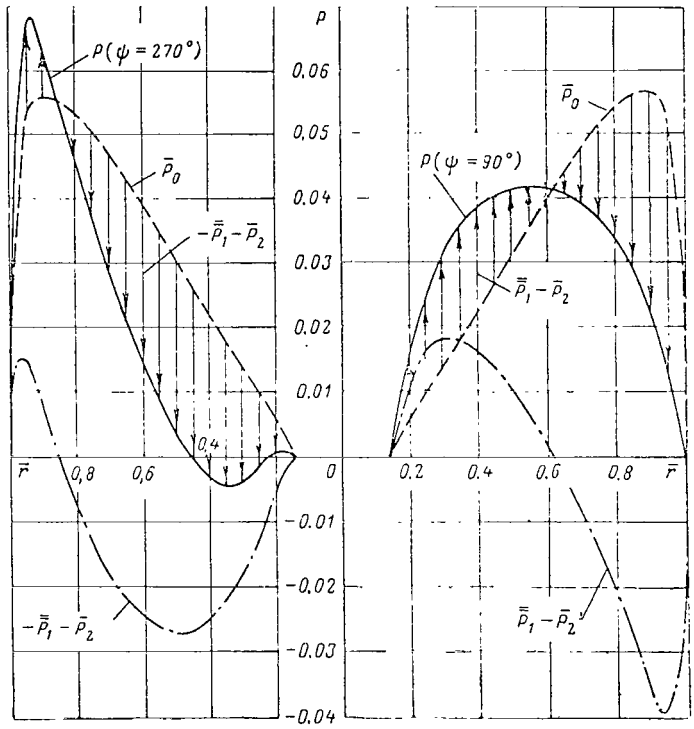

Fig.1.29 Relative Aerodynamic Load Acting on a Blade in the Lateral Plane of the Rotor.

Table 1.6

a_0	a_1^*	b_1^*	a_2	b_2		Φ
$1/\gamma$			$\frac{1}{4}\mu^2 \varkappa C$	$-\frac{1}{4}\mu^2 C$	=	$\lambda_0^* B + A^\varphi + \frac{1}{2}\mu^2 C^\varphi$
μB		$-A - \frac{1}{4}\mu^2 C$	$\frac{1}{2}\mu B$	$-\mu \varkappa B$		
	$A - \frac{1}{4}\mu^2 C$		μB	$\frac{1}{4}\mu B$	=	$\mu \lambda_0^* C + 2\mu B^\varphi$
	$-\mu B$		$\frac{3}{\gamma_0} - \varkappa(A + \frac{1}{2}\mu^2 C)$	$-2A$	=	$-\frac{1}{2}\mu^2 C^\varphi$
$\frac{1}{2}\mu^2 C$		$-\mu B$	$2A$	$\frac{3}{\gamma_0} - \varkappa(A + \frac{1}{2}\mu C)$		

The following notations were used in compiling the table:

$$\left.\begin{aligned} A &= \int_0^1 \bar{b}\bar{r}^3 d\bar{r}; \\ B &= \int_0^1 \bar{b}\bar{r}^2 d\bar{r}; \\ C &= \int_0^1 \bar{b}\bar{r} d\bar{r}. \end{aligned}\right\} \tag{7.47}$$

$$\left.\begin{aligned} A^{\varphi} &= \int_0^1 \bar{b}\bar{r}^3 \varphi_r d\bar{r}; \\ B^{\varphi} &= \int_0^1 \bar{b}\bar{r}^2 \varphi_r d\bar{r}; \\ C^{\varphi} &= \int_0^1 \bar{b}\bar{r} \varphi_r d\bar{r}. \end{aligned}\right\} \tag{7.48}$$

The mass characteristic of a rigid blade γ is determined by the expression

$$\gamma = \frac{c_y^{\alpha} \rho b_{0.7} R^4}{2I}. \tag{7.49}$$

On solving this system of equations, it is found that the coefficient a_2 and b_2 are appreciably smaller than the coefficients a_0, a_1^*, and b_1^*. Thus, they can be neglected in determining the coefficients a_0, b_1^*, and a_1^*. This assump- /87 tion leads to simple formulas for determining the flapping coefficients of the blade

$$\left.\begin{aligned} a_0 &= \gamma\left[\lambda_0^* B + A^{\varphi} + \frac{1}{2}\mu^2 C^{\varphi}\right]; \\ a_1^* &= \frac{\mu\left[\lambda_0^* C + 2B^{\varphi}\right]}{A - \frac{1}{4}\mu^2 C}; \\ b_1^* &= \frac{\mu B a_0}{A + \frac{1}{4}\mu^2 C}; \\ a_2 &= \frac{\gamma_x^2}{18 + 8A^2\gamma_x^2}\left[\mu\left(4ABb_1^* + \frac{6B}{\gamma_x}a_1^*\right) - \mu^2\left(2ACa_0 + \frac{3C^{\varphi}}{\gamma_x}\right)\right]; \\ b_2 &= \frac{\gamma_x^2}{18 + 8A^2\gamma_x^2}\left[\mu\left(-4ABa_1^* + \frac{6B}{\gamma_x}\cdot b_1^*\right) + \mu^2\left(2AC^{\varphi} - \frac{3C}{\gamma_x}\cdot a_0\right)\right], \end{aligned}\right\} \tag{7.50}$$

where

$$\gamma_x = \frac{\gamma}{1 - \frac{1}{3}\varkappa\gamma\left(A + \frac{1}{3}\mu^2 C\right)}.$$

8. Simplified Calculation of Elastic Blade Vibrations

Based on the simplifying assumptions adopted in this Section, we can construct the calculation of elastic vibrations and bending stresses in a blade for horizontal flight regimes of the helicopter. Such a calculation, of course, cannot give positive results when applied to low flying speeds where a major role is played by variable stresses having to do with the nonuniform induced velocity field; the same is true for high speeds where it is impossible to disregard the nonlinearity of the dependence of aerodynamic coefficients on the angle of attack and phenomena associated with flow compressibility.

In conformity with the above formulas, the calculation is conveniently performed along the axes of an equivalent rotor.

The calculation of elastic blade vibrations is carried out in the following sequence:

1. First, determine the parameters of the flight regime at which the calculation of stresses is to be carried out. These are the following parameters:
   a) rotor angle of attack α_{eq};
   b) angular velocity of rotation of the rotor ω;
   c) altitude and flying speed represented in the calculation by the coefficients ρ and μ.

2. Calculate the relative velocity of flow through the rotor from the formula

$$\lambda_0^* = \mu \tan\alpha_{eq} + \frac{C_T}{4\sqrt{\mu^2 + (\lambda_0^*)^2}}, \qquad (7.51)$$

where C_T is the thrust coefficient of the rotor.

3. Next, calculate the blade angle at the control section relative to which the geometric twist of the blade is prescribed.

Without consideration of forces related with the second harmonic of flap- /88
ping, this angle can be determined by the formula

$$\varphi_{real} = \frac{t/\sigma - B^{\Delta\varphi} + \frac{1}{2}\mu^2 D^{\Delta\varphi} + \lambda_0^* C}{B + \frac{1}{2}\mu^2 D}. \qquad (7.52)$$

Here,

$$\left.\begin{aligned} B^{\Delta\varphi} &= \int_0^1 \bar{b}\bar{r}^2 \Delta\varphi d\bar{r}; \\ D &= \int_0^1 \bar{b} d\bar{r}; \\ D^{\Delta\varphi} &= \int_0^1 \bar{b}\Delta\varphi d\bar{r}, \end{aligned}\right\} \tag{7.53}$$

t = coefficient of thrust;
σ = solidity ratio of the rotor.

4. By means of eqs.(7.50), determine the flapping coefficients of the blade, and by means of eqs.(7.41) and (7.42) the external loads on the blade.

5. To determine the bending stresses, calculate the natural vibration modes and frequencies of the blade.

6. If such a calculation is performed, eqs.(7.30) will yield the quasi-static coefficients of deformation with respect to different harmonics of blade vibration from the constant component of the first and second harmonics of the aerodynamic load.

Substituting eq.(7.41) into eq.(7.30), we obtain the values of the quasi-static coefficients of deformation with respect to the j-th harmonic blade vibration

$$\left.\begin{aligned} \bar{\delta}_0^{(j)} &= \frac{\omega^2}{p_j^2}\cdot\gamma_j\left[\lambda_0^* B_j + A_j^\varphi + \frac{1}{2}\mu^2 C_j^\varphi\right]; \\ \bar{\delta}_1^{(j)} &= \frac{\omega^2}{p_j^2}\cdot\gamma_j\left[-\mu B_j a_0 + \left(A_j + \frac{1}{4}\mu^2 C_j\right) b_1^*\right]; \\ \bar{\bar{\delta}}_1^{(j)} &= \frac{\omega^2}{p_j^2}\gamma_j\left[\mu\lambda_0^* C_j + 2\mu B_j^\varphi - \left(A_j - \frac{1}{4}\mu^2 C_j\right) a_1^*\right]; \\ \bar{\delta}_2^{(j)} &= \frac{\omega^2}{p_j^2}\cdot\gamma_j\left[-\frac{1}{2}\mu^2 C_j^\varphi + \mu B_j a_1^* + \varkappa\left(A_j + \frac{1}{2}\mu^2 C_j\right) a_2 + 2A_j b_2\right]; \\ \bar{\bar{\delta}}_2^{(j)} &= \frac{\omega^2}{p_j^2}\cdot\gamma_j\left[-\frac{1}{2}\mu^2 C_j a_0 + \mu B_j b_1^* - 2A_j a_2 + \varkappa\left(A_j + \frac{1}{2}\mu^2 C_j\right) b_2\right]. \end{aligned}\right\} \tag{7.54}$$

Here, the subscripts of the coefficients of quasi-static blade deformation correspond to the order of the harmonic of the aerodynamic forces. The index j denotes coefficients pertaining to the j-th overtone of blade vibrations; γ_j is the mass characteristic of the blade in deformations with respect to the j-th overtone:

$$\gamma_j = \frac{1/2 c_y^\alpha \varrho b_{0.7} R^2}{m_j}. \tag{7.55}$$

The following notations are adopted for the integrals entering eqs.(7.54):/89

$$\left.\begin{aligned} A_j &= \int_0^1 \bar{b}\bar{r}^2\bar{y}^{(j)}\,d\bar{r};\\ B_j &= \int_0^1 \bar{b}\bar{r}\bar{y}^{(j)}\,d\bar{r};\\ C_j &= \int_0^1 \bar{b}\bar{y}^{(j)}\,d\bar{r};\\ A_j^{\varphi} &= \int_0^1 \bar{b}\bar{r}^2\varphi_r\bar{y}^{(j)}\,d\bar{r};\\ B_j^{\varphi} &= \int_0^1 \bar{b}\bar{r}\varphi_r\bar{y}^{(j)}\,d\bar{r};\\ C_j^{\varphi} &= \int_0^1 \bar{b}\varphi_r\bar{y}^{(j)}\,d\bar{r}, \end{aligned}\right\} \qquad (7.56)$$

where $\bar{y}^{(j)}$ is the mode of blade vibrations with respect to the j-th overtone normed such that $\bar{y}^{(j)} = 1$ for $\bar{r} = 1$.

7. Then, write the blade deformations in the following form:

$$\begin{aligned} y = {} & [c_0 - c_1\cos\psi - d_1\sin\psi - c_2\cos 2\psi - d_2\sin 2\psi]\,y^{(1)} + \\ & + [e_0 - e_1\cos\psi - f_1\sin\psi - e_2\cos 2\psi - f_2\sin 2\psi]\,y^{(2)} + \\ & + [g_0 - g_1\cos\psi - h_1\sin\psi - g_2\cos 2\psi - h_2\sin 2\psi]\,y^{(3)} + \ldots \end{aligned} \qquad (7.57)$$

Here, in determining the blade deformation, the mode of the fundamental which, in the case of $r_0 = 0$, coincides with a straight line, is replaced by the first three harmonics of natural vibration of the blade $y^{(1)}$, $y^{(2)}$, and $y^{(3)}$ normed such that $y^{(j)} = R$ at $r = R$. Then, the coefficients of blade deformation entering eq.(7.57) can be determined in terms of the quasi-static coefficients of deformation in accordance with eq.(7.29).

As a typical example, let us write out the formulas for determining the coefficients of deformation with respect to the first harmonic:

$$\left.\begin{aligned} c_0 &= \bar{\delta}_0;\\ c_1 &= \frac{-\left[1-\frac{\omega^2}{p_1^2}\right]\bar{\delta}_1^{(1)} + 2\bar{n}_1\frac{\omega}{p_1}\cdot\bar{\delta}_1^{(1)}}{\left[1-\frac{\omega^2}{p_1^2}\right]^2 + 4\bar{n}_1^2\frac{\omega^2}{p_1^2}}; \end{aligned}\right\} \qquad (7.58)$$

$$d_1 = \frac{-\left[1-\frac{\omega^2}{p_1^2}\right]\bar{\delta}_1^{(1)} + 2\bar{n}_1 \frac{\omega}{p_1}\cdot\bar{\delta}_1^{(1)}}{\left[1-\frac{\omega^2}{p_1^2}\right]+4\bar{n}_1^2\frac{\omega^2}{p_1^2}};$$

$$c_2 = \frac{-\left[1-\frac{4\omega^2}{p_1^2}\right]\bar{\delta}_2^{(1)} + 2\bar{n}_1 \frac{2\omega}{p_1}\bar{\delta}_2^{(1)}}{\left[1-\frac{4\omega^2}{p_1^2}\right]+4\bar{n}_1^2\cdot\frac{4\omega^2}{p_1^2}};$$

$$d_2 = \frac{-\left[1-\frac{4\omega^2}{p_1^2}\right]\bar{\delta}_2^{(1)} - 2\bar{n}_1\cdot\frac{2\omega}{p_1}\bar{\delta}_2^{(1)}}{\left[1-\frac{4\omega^2}{p_1^2}\right]^2+4\bar{n}_1^2\frac{4\omega^2}{p_1^2}}.$$

/90

(7.58)

If the dynamic coefficients of deformation are known, it is easy to determine any components of the stresses set up in the blade. This will be discussed in more detail in Subsection 17 of Section 8 and in Subsection 8 of Section 9.

In the simplified method of calculation presented here, a large number of additional assumptions of a computational nature applicable to almost all stages of the calculation are used in place of the initial assumptions pertaining to the physical properties of a blade model adopted in deriving eq.(7.1) and in calculating the right-hand side of this equation, which reduces to eq.(7.35). All these simplifications, although they make the method of calculation quite suitable for manual computation, introduce numerous indeterminacies that are poorly amenable to a quantitative evaluation. Despite this shortcoming, the described simplified method of calculation has one important advantage, namely its clear presentation. In principle, all calculation results obtained by other more improved methods are evaluated and analyzed on the basis of dependences presented here in a simplified form.

However, even with the use of all these assumptions, pencil-and-paper computing by this method takes one month of work for one calculator. The current flow of blade designing cannot be maintained when one calculation takes that long. Therefore, the calculation of elastic vibrations of a blade used for selecting the blade design parameters can be performed only on high-speed electronic computers. Naturally, there is no need then to use assumptions that facilitate the computational process.

Consequently, in Section 8 we will present a method of calculation based on the same initial assumptions, provided we neglect all variable induced velocities; the method uses no assumptions of a computational nature.

Section 8. Calculation of Bending Stresses in a Blade at Low and Moderate Flying Speeds

1. Characteristics Distinguishing Flight Regimes at Low and Moderate Speeds

Low and moderate speeds of a helicopter are regarded here as regimes sufficiently remote from flow separation in which, furthermore, phenomena associated with flow compressibility can be neglected. On this basis, in calculating aerodynamic loads it is assumed approximately that

$$c_y = c_y^{\alpha} \cdot \alpha. \tag{8.1}$$

This assumption greatly simplifies the calculations necessary for constructing design formulas.

On the other hand, low-speed modes can be regarded as regimes especially /91 detrimental to fatigue strength and often conducive to the generation of maximum bending stresses in the blade.

These considerations justify the use of a method of calculation suitable only for low and moderate flying speeds but not for high speeds nor for regimes in which phenomena associated with the nonlinear character of the dependence $c_y = f(\alpha)$ and with flow compressibility become determining factors.

It should be noted that the assumption (8.1) does not always hold for low-speed modes. In cases in which the rotor blade accounts for an extremely large load, the calculation should be performed with consideration of the nonlinear dependence of the aerodynamic coefficients on the angle of attack of the profile. The method of such a calculation will be discussed in Section 9.

The blade overloading can be estimated from the value of the thrust coefficient of the rotor t. Calculations show that the assumption (8.1) can be used for low-speed modes without introduction of substantial errors into the results at $t < 0.18$.

In regimes with vertical overloads such as, for example, the braking regime of a helicopter before landing, an infringement of this inequality might occur in rotors which show such overloads in steady flight. All this must be taken into account in selecting the calculation method.

2. Method of Calculating Stresses

This Section presents the conventional method of calculating variable stresses, based on Galerkin's method with expansion of the deformation coefficient in a Fourier series in harmonics.

Because of the possibility of using this method for calculating low-speed modes, the harmonic components of the induced field are introduced into all calculation formulas, and the problem of blade deformation is solved simultaneously

with the problem of determining the induced velocities.

However, such an approach is not a "must" for the method proposed here. In calculating stresses at moderate flying speeds when the variable induced velocities do not cause excessive refinements in the results, it can be disregarded. In this case the method of calculation is greatly simplified.

If the assumption (8.1) is used, the aerodynamic load will be a linear function of the displacements of the blade element, and the problem of calculating the bending deformations will reduce to solving the linear differential equation (1.9). To solve this equation we use the B.G.Galerkin method. The blade deformations are represented as a series with respect to eigenfunctions, while the time coefficients of this series are expanded in a Fourier series. The use of Galerkin's method transforms the differential equation of blade vibrations into a system of algebraic equations relative to the unknown coefficients of the Fourier series, and the determination of the blade bending deformations reduces to a calculation of these unknown coefficients. Such a method of calculation will be presented here.

3. Assumptions in Determining Induced Velocities

When calculating the bending stresses at low flying speeds when their value is determined mainly by the degree of nonuniformity of the induced velocity /92 field, the assumptions on whose basis this field is determined become of great importance.

In the first volume (Chapt.II, Sect.5), it was mentioned that induced velocities can be represented as the sum of the extrinsic and intrinsic induced velocities. This subdivision is somewhat arbitrary but proves useful since it permits an evaluation of the effect of individual induced velocity components by analogy with the evaluation conventional for the wing of a regular aircraft; this justifies the adoption of certain assumptions important for further presentation.

The flow past a helicopter blade with a nonuniform induced velocity field is analogous to the flow past the wing of a regular aircraft in flights in turbulent air, when the wing constantly encounters airflows of differing velocity and direction. During rotation of a rotor, the blade also encounters in its path a nonuniform velocity field, except that this field is not caused by atmospheric turbulence but by the induced action of the entire vortex system of the rotor. This field, by analogy with a wing, is usually called the extrinsic induced velocity field, unlike the velocity field induced in the blade region by the vortices shed by the blade due to a change in circulation with respect to time and blade radius. That these vortices create appreciable induced velocities at the blade is due exclusively to the fact that they are at a very short distance from it. Upon removing the vortices a distance of 20 - 30° from the rotor azimuth, their influence on the aerodynamic load on the blade will decrease.

Just as in calculating a wing, the "steady-flow hypothesis" can be used in determining the aerodynamic loads on a blade. According to this hypothesis it is assumed that, in a nonsteady flow past a profile, the loads acting on the profile behave as though the flow pattern produced at a given instant of time would

remain unchanged for an arbitrary length of time. In conformity with this hypothesis, in calculating the aerodynamic loads on a wing allowance is made only for the change in angle of attack produced by the extrinsic velocity field, while the effect of the intrinsic induced velocities is disregarded.

We will use an analogous approach for the case of a blade. In determining the aerodynamic loads, we will take into account only the extrinsic induced velocity field.

In the calculation of this field, certain additional assumptions relative to the characteristics of the vortex system in the low-speed mode can be used.

Figure 1.30 gives a planview of a system of free vortices shed by the blade tips of a five-blade rotor in a flight regime with a speed corresponding to $\mu = 0.05$. At this speed, the variable stresses in the rotor blades reach a maximum.

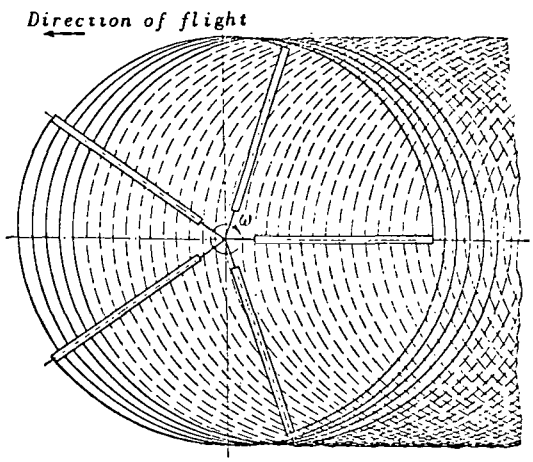

Fig.1.30 View of a Vortex System Shed by the Blade Tip in the $\mu = 0.05$ Regime.

The picture conveyed by this sketch is incomplete, since only free vortices shed from the blade tips are shown while the vortices shed from all other blade radii are omitted. The radial (transverse) vortices are also left off. However, even this pattern already gives an idea on the close spacing of vortices in low-speed regimes. Due to this characteristic of the vortex system, the induced actions of individual vortices will merge and appear as the total nonuniformity of the entire velocity field. No sharp induced velocity peaks, characteristic for the vortex system, with widely spaced vortices occur. Therefore, at low flying speeds and especially for rotors with a large number of blades, the induced velocities can be determined from the theory covering the configuration of a rotor with an infinite number of blades.

With an increase in flying speed, the free vortex system starts extending /93 and shows wider spacing. The vortex system also changes in the same sense on a decrease in the number of rotor blades. This reduces the accuracy of calculation for a configuration with an infinite number of blades.

On changing from a given rotor to a configuration with an infinite number of blades, the local effect due to the vortices immediately adjacent to the blade is reduced so greatly that, in first approximation, it can be assumed that this design does not allow for the influence of adjacent vortices so that the velocity field determined on its basis will practically coincide with the extrinsic induced velocity field.

The considerations presented above lead to the conclusion that, for calculating elastic blade vibrations at low flying speeds, the vortex theory based on a scheme with an infinite number of blades can be used.

At low flying speeds, one usually measures variable stresses of which a major portion is made up of high harmonics of the rotor rpm, generally located between the fourth and sixth harmonic. Therefore, still another important requirement must be imposed on the method of determining induced velocities. Such a method should determine the induced velocity field with an accuracy of at least to the sixth harmonic, which is possible only if the circulation values are determined with an accuracy to the same harmonic. Consequently, all methods not satisfying this requirement are worthless and cannot be used for calculating elastic vibrations.

As stated above, we will present a method of calculating stresses in which all variables are expanded in Fourier series in harmonics. Therefore, it is convenient to use the method of determining the induced velocity field, in which these velocities are determined also in the form of an expansion in harmonics.

These stipulations are best met by the theory developed by V.E.Baskin [(Ref.3); see also Sect.5, Chapt.II of Vol.I]. Therefore, this theory will be used here for our stress analysis.

4. Mathematical Formulas for Induced Velocity Field Determination

Let us examine the system of formulas proposed by V.E.Baskin for calculating the induced velocity field in the plane of rotation of a rotor.

We will represent the field of these velocities as the sum of its harmonic components. In so doing, both the total flow velocity and the harmonic components of this velocity are related to the tip speed of the rotor blades ωR: /94

$$\lambda = \mu \tan \alpha_{rot} + \bar{\lambda}_0 + \sum_n (\bar{\lambda}_n \cos n\psi + \bar{\lambda}_n \sin n\psi). \qquad (8.2)$$

Here,

λ = total velocity of the flow passing through the rotor, relative to ωR;

$\bar{\lambda}_0$ = constant induced velocity component, also relative to ωR;

$\bar{\lambda}_n$ and $\bar{\lambda}_n$ = harmonic induced velocity components;

ψ = azimuthal blade angle reckoned from an axis coinciding in direction with the tail boom of a single-rotor helicopter;

$$\mu = \frac{V \cos \alpha_{rot}}{\omega R},$$

where

V = flying speed of the helicopter;

α_{rot} = rotor angle of attack at the shaft axes.

The linear aerodynamic load acting on the blade is represented in the form

$$T=\frac{1}{2}\,c_y^{\alpha}\varrho b_{0,7}\omega^2R^2P, \tag{8.3}$$

where

c_y^{α} = angle of slope of the dependence $c_y = f(\alpha)$, which here is taken to be linear in the form of eq.(8.1);
ρ = air density;
$b_{0.7}$ = value of blade chord at the relative radius $\bar{r} = 0.7$.

Henceforth, the value of P entering this expression will be designated as "relative aerodynamic load".

We represent the value of P in the form

$$P=\overline{P}_0+\sum_m(\overline{P}_m\cos m\psi+\overline{\overline{P}}_m\sin m\psi). \tag{8.4}$$

The harmonic velocity components λ_n are represented as the sum of the so-called partial induced velocities, each of which is induced only by one harmonic of the aerodynamic load

$$\left.\begin{aligned}\bar{\lambda}_n&=\sum_m\bar{\lambda}_{nm};\\ \bar{\bar{\lambda}}_n&=\sum_m\bar{\bar{\lambda}}_{nm}.\end{aligned}\right\} \tag{8.5}$$

In these expressions, the sum total induced velocity components have one subscript n, while the partial components have two subscripts n and m.

The values of the partial harmonic induced velocity components are determined by the following expressions:

$$\left.\begin{aligned}&\text{at } n=0:\\ &\quad\bar{\lambda}_{0m}=-\frac{1}{8}\,c_y^{\alpha}\sigma A_0(-1)^m\tau^m J(\overline{P}_m);\\ &\text{at } n\neq 0:\\ &\quad\bar{\lambda}_{nm}=-\frac{1}{8}\,c_y^{\alpha}\sigma A_0\,[\tau^{n-m}+(-1)^m\tau^{n+m}]\,J(\overline{P}_m)\cdot\\ &\quad\bar{\bar{\lambda}}_{nm}=-\frac{1}{8}\,c_y^{\alpha}\sigma A_0\,[\tau^{n-m}-(-1)^m\tau^{n+m}]\,J(\overline{\overline{P}}_m).\end{aligned}\right\} \tag{8.6}$$

If the power to which τ is raised is negative ($n - m < 0$), we must set $\tau^{n-m} = (-\tau)^{m-n}$ in eqs.(8.6). /95

The coefficients entering eqs.(8.6) have the following values:

$$\left.\begin{aligned} A_0 &= \frac{1}{\sqrt{\mu^2+\lambda_{oav}^2}}; \\ \tau &= \frac{\sqrt{\mu^2+\lambda_{oav}^2}-|\lambda_{oav}|}{\mu}; \\ \sigma &= \frac{z_b b_{0,7}}{\pi R}, \end{aligned}\right\} \tag{8.7}$$

where

σ = solidity ratio of the rotor;
z_b = number of blades of rotor.

The value of the disk flow ratio averaged over the blade radius λ_{oav} is determined from the formula

$$\lambda_{oav} = \mu \tan\alpha_{rot} + 2\int_0^1 \bar{\lambda}_0 \bar{r}\, d\bar{r}. \tag{8.8}$$

To determine the functions $J(\bar{P}_m)$ and $J(\bar{\bar{P}}_m)$ entering eqs.(8.6), the following formulas are obtained from V.E.Baskin's theory:

$$\left.\begin{aligned} J(\bar{P}_m) &= \int_0^\infty J_n(z\bar{r})z\left[\int_0^1 \bar{P}_m(\bar{\varrho})J_m(z\bar{\varrho})d\bar{\varrho}\right]dz; \\ J(\bar{\bar{P}}_m) &= \int_0^\infty J_n(z\bar{r})z\left[\int_0^1 \bar{\bar{P}}_m(\bar{\varrho})J_m(z\bar{\varrho})d\bar{\varrho}\right]dz, \end{aligned}\right\} \tag{8.9}$$

where

$J_n(z\bar{r})$ and $J_m(z\bar{r})$ = Bessel functions of the first kind of order n and m, respectively;
z = integration parameter.

Here, to specify the parameter over which integration is carried out, a new notation is introduced for the relative blade radius $\bar{\rho}$. This notation will be used only in calculating the integrals (8.9).

5. Transformations of Mathematical Formulas in Particular Cases

Equations (8.6) are greatly simplified in particular cases. Thus, in the case of n = m = 0, we have

$$\lambda_{00} = -\frac{1}{8} c_y^\alpha \sigma A_0 \frac{\bar{P}_0}{\bar{r}}. \tag{8.10}$$

For further calculations, the result obtained for the case of n = m is especially important. It will be found that the coinciding harmonics of the aero-

dynamic load and induced velocity are uniquely related by the expressions: /96

$$\left.\begin{aligned}\bar{\lambda}_{nn}&=\bar{\alpha}_n\frac{\bar{P}_n}{\bar{r}};\\ \bar{\bar{\lambda}}_{nn}&=\bar{\bar{\alpha}}_n\frac{\bar{\bar{P}}_n}{\bar{\bar{r}}},\end{aligned}\right\} \tag{8.11}$$

where

$$\left.\begin{aligned}\bar{\alpha}_n&=-\frac{1}{8}c_y^{\alpha}\sigma A_0[1+(-1)^n\tau^{2n}];\\ \bar{\bar{\alpha}}_n&=-\frac{1}{8}c_y^{\alpha}\sigma A_0[1-(-1)^n\tau^{2n}].\end{aligned}\right\} \tag{8.12}$$

This formulation makes it expedient to separate the induced velocity components into two types: principal induced velocity components due to the same harmonic of the aerodynamic load as the harmonic of the induced velocity, and secondary components due to all other harmonics of the aerodynamic load.

This separation permits writing eqs.(8.5) in the form

$$\left.\begin{aligned}\bar{\lambda}_n&=\bar{\alpha}_n\frac{\bar{P}_n}{\bar{r}}+\bar{\lambda}_n^s;\\ \bar{\bar{\lambda}}_n&=\bar{\bar{\alpha}}_n\frac{\bar{\bar{P}}_n}{\bar{\bar{r}}}+\bar{\bar{\lambda}}_n^s,\end{aligned}\right\} \tag{8.13}$$

where the principal induced velocity components are determined by eq.(8.11), whereas the sum of all secondary induced velocity components is introduced into the equation by means of the new notations $\bar{\lambda}_n^s$ and $\bar{\bar{\lambda}}_n^s$:

$$\left.\begin{aligned}\bar{\lambda}_n^s&=\sum_{m=0}^{m=n-1}\bar{\lambda}_{nm}+\sum_{m=n+1}^{m=z_h}\bar{\lambda}_{nm};\\ \bar{\bar{\lambda}}_n^s&=\sum_{m=0}^{m=n-1}\bar{\bar{\lambda}}_{nm}+\sum_{m=n+1}^{m=z_h}\bar{\bar{\lambda}}_{nm}.\end{aligned}\right\} \tag{8.14}$$

Here, z_h is the number of harmonic induced velocity components taken into account in the calculation.

At n = 0, the first members of these expressions should be equated to zero, and at $n = z_h$ the same should be done with the second members. In constructing the equations for stress analysis, the induced velocities will be represented in the form of eq.(8.13).

6. Numerical Determination of the Integrals $J(\bar{P}_n)$ and $J(\bar{\bar{P}}_n)$

At $m \neq n$, a calculation of the integrals (8.9) encounters certain difficulties. To determine the values of these integrals, V.E.Baskin proposed a

method in which the aerodynamic load components are approximated by trigonometric polynomials. For this, it is necessary to determine the values of P_m at prescribed blade radii not coinciding with those used in the overall calculation. This is not too convenient for the method proposed here. Therefore, we will use another method more suitable for the given case, in which calculation of the integrals $J(\bar{P}_m)$ and $J(\bar{\bar{P}}_m)$ is carried out approximately in the same form /97 in which the integrals are computed when calculating the blade stresses. To this end, the blade is divided into individual segments within whose limits the aerodynamic load is represented in a form suitable for integration. Here, it is logical to divide the blade into the same segments in all cases, both when calculating the stresses and when calculating the integrals (8.9). We will represent the load $P_m(\bar{\rho})$ such that, at each segment of integration, this load will vary in accordance with the law

$$P_m(\bar{\rho}) = \frac{P_m(\bar{\rho}_k)}{\bar{\rho}_k^{m+1}} \bar{\rho}^{m+1}. \qquad (8.15)$$

Here,

$\bar{\rho}$ = current values of relative blade radius; after integration and substitution of the limits, the value of $\bar{\rho}$ will no longer be contained in formulas without an index;

$\bar{\rho}_k$ = same value of relative radius but with the subscript k, which means that the radius in question coincides with the radius at which the relative aerodynamic load $P_m(\rho_k)$ is calculated.

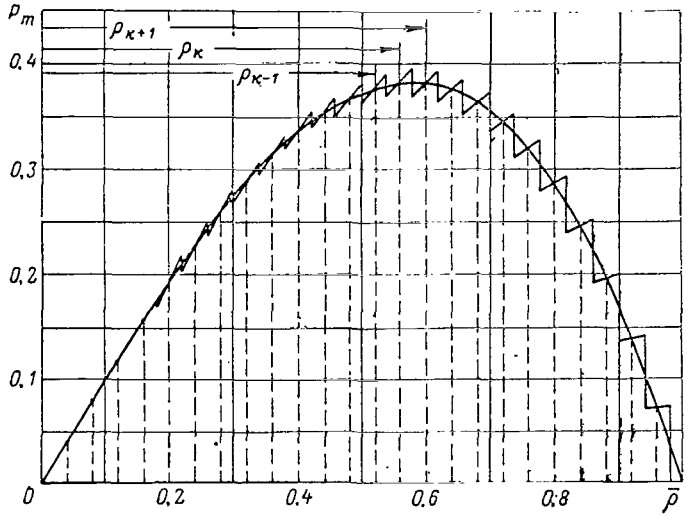

Fig.1.31 Shape of the Relative Aerodynamic Load Adopted for the Calculation of Induced Velocities.

Henceforth, as already stated, let us differentiate the relative radii $\bar{\rho}_k$, at which the value of the aerodynamic load is taken, from the relative radii $\bar{r}_i$

at which the induced velocity is calculated. This prevents possible confusion.

Let us assume that the relative aerodynamic load varies in accordance with the law (8.15) over the length of each segment bounded by the relative radii

$$\bar{Q}=\frac{1}{2}(\bar{Q}_{k-1}+\bar{Q}_k) \text{ and } \bar{Q}=\frac{1}{2}(\bar{Q}_k+\bar{Q}_{k+1}).$$

In Fig.1.31, the solid stepped line gives the shape of the distribution of the relative aerodynamic load over the blade length, represented for calculating the induced velocities from eq.(8.15) in the case m = 0. Such a form of representation of the aerodynamic load naturally may introduce certain errors into the values of the induced velocities. However, calculations performed to estimate the magnitude of this error demonstrated that the error is small and is /98 unable to cause substantial changes in the calculation results.

On substituting the value of the relative aerodynamic load expressed in the form of eq.(8.15) into the expression of the integrand of eq.(8.9), then the interior integral on the right-hand side of this equation can be represented as some sum of definite integrals:

$$\int_0^1 P_m(\bar{Q})\,J_m(z\bar{Q})\,d\bar{Q}=\sum_k \frac{P_m(\bar{Q}_k)}{\bar{Q}_k^{m+1}}\int_{1/2(\bar{Q}_{k-1}+Q_k)}^{1/2(\bar{Q}_k+\bar{Q}_{k+1})}\bar{Q}^{m+1}J_m(z\bar{Q})\,d\bar{Q}. \tag{8.16}$$

The definite integrals entering this expression can be calculated analytically [see (Ref.11)]. Substituting the integration limits into the obtained expressions, we can write:

$$\int_0^1 P_m(\bar{Q})\,J_m(z\bar{Q})\,d\bar{Q}=\sum_k A_k\frac{1}{z}J_{m+1}\left(z\cdot\frac{\bar{Q}_k+\bar{Q}_{k+1}}{2}\right), \tag{8.17}$$

where

$$A_k=\frac{\bar{Q}_k+\bar{Q}_{k+1}}{2}\left[\frac{P_m(\bar{Q}_k)}{\bar{Q}_k^{m+1}}-\frac{P_m(\bar{Q}_{k+1})}{\bar{Q}_{k+1}^{m+1}}\right].$$

Substituting the resultant value of the interior integral into eqs.(8.9), we obtain

$$\begin{aligned}J(\bar{P}_m)&=\int_0^\infty J_n(z\bar{r})\,z\left[\int_0^1 P_m(\bar{Q})\,J_m(z\bar{Q})\,d\bar{Q}\right]dz=\\&=\sum_k A_k\int_0^\infty J_n(z\bar{r}_i)\cdot J_{m+1}\left(z\cdot\frac{\bar{Q}_k+\bar{Q}_{k+1}}{2}\right)dz.\end{aligned} \tag{8.18}$$

Or, if we write this in a simpler form,

$$J(\bar{P}_m)=\sum_k A_k\varepsilon_k(\bar{r}_i), \tag{8.19}$$

where

$$\varepsilon_k(\bar{r}_i)=\int_0^\infty J_n(z\bar{r}_i)\,J_{m+1}\left(z\cdot\frac{\bar{\varrho}_k+\bar{\varrho}_{k+1}}{2}\right)dz. \tag{8.20}$$

The integral (8.20) is a discontinuous integral known as the Weber-Schafheitlin integral (Ref.11). Its analytic expression, as a function of the relation between $\bar{r}_i$ and $\frac{1}{2}(\bar{\rho}_k+\bar{\rho}_{k+1})$, has the following form:

If $\frac{1}{2}(\bar{\varrho}_k+\bar{\varrho}_{k+1})<\bar{r}_i$, then

$$\varepsilon_k(\bar{r}_i)=\int_0^\infty J_n(z\bar{r})J_{m+1}\left(z\,\frac{\bar{\varrho}_k+\bar{\varrho}_{k+1}}{2}\right)dz=\frac{\left(\frac{\bar{\varrho}_k+\bar{\varrho}_{k+1}}{2}\right)^{m+1}\cdot\Gamma\left(\frac{m+2+n}{2}\right)}{\bar{r}_i^{m+2}\,\Gamma(m+2)\cdot\Gamma\left(\frac{n-m}{2}\right)}\times \tag{8.21}$$

$$\times F\left[\frac{m+2+n}{2};\ \frac{m+2-n}{2};\ m+2;\ \left(\frac{\bar{\varrho}_k+\bar{\varrho}_{k+1}}{2\bar{r}_i}\right)^2\right].$$

If $\frac{1}{2}(\bar{\varrho}_k+\bar{\varrho}_{k+1})>\bar{r}_i$, then /99

$$\varepsilon_k(\bar{r}_i)=\int_0^\infty J_n(z\bar{r}_i)\,J_{m+1}\left(z\,\frac{\bar{\varrho}_k+\bar{\varrho}_{k+1}}{2}\right)dz=$$

$$=\frac{\bar{r}_i^n\,\Gamma\left(\frac{m+2+n}{2}\right)}{\left(\frac{\bar{\varrho}_k+\bar{\varrho}_{k+1}}{2}\right)^{n+1}\Gamma(n+1)\,\Gamma\left(\frac{m+2-n}{2}\right)}\times \tag{8.22}$$

$$\times F\left[\frac{m+2+n}{2};\ \frac{n-m}{2};\ n+1;\ \left(\frac{2\bar{r}_i}{\bar{\varrho}_k+\bar{\varrho}_{k+1}}\right)^2\right].$$

Here,

Γ = gamma function with different arguments;
F = hypergeometric function of the argument α, β, γ, z.

These arguments, as indicated by eqs.(8.21) and (8.22), may have different values depending upon the relation between $\bar{r}_i$ and $\frac{1}{2}(\bar{\rho}_k+\bar{\rho}_{k+1})$. For example, in eq.(8.21), we have

$$\alpha=\frac{m+2+n}{2};$$

$$\beta=\frac{m+2-n}{2};$$

$$\gamma=m+2;$$

$$z=\left(\frac{\bar{\varrho}_k+\bar{\varrho}_{k+1}}{2\bar{r}_i}\right).$$

When performing the calculation on a digital computer, these functions are easy to program. Therefore, their calculation presents no difficulties.

7. Assumptions Adopted in Aerodynamic Force Determinations

In determining the aerodynamic loads, the assumption (8.1) is supplemented by the same assumptions used in determining the rigid blade loadings (Sect.7, Subsect.6), with the exception of the assumption (7.34).

1. Let us assume that the inflow angle to the blade profile Φ is small and that we thus can assume approximately:

$$\Phi = \tan^{-1}\frac{U_y}{U_x} \approx \frac{U_y}{U_x}, \tag{8.23}$$

where

Φ = inflow angle;

U_x and U_y = mutually perpendicular components of the relative flow velocity in a plane normal to the elastic blade axis (Fig.1.32); here, the velocity U_x is parallel to the plane of rotation of the rotor.

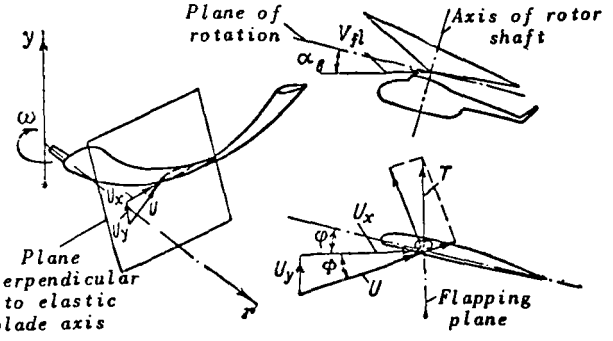

Fig.1.32 Diagram of Flow Past a Blade, Used in Stress Analysis at the Low-Speed Mode.

2. Let us assume that the magnitude of the relative velocity of circulation flow U around the profile differs little from the magnitude of U_x. Therefore, we can assume that $U \cong U_x$.

3. Let us assume that, in determining the loads in the flapping plane (plane going through the axis of rotation of the rotor), the profile drag can be neglected and it can be assumed that $c_x = 0$.

4. Stipulating that $\cos \Phi = 1$, let us assume that the load in the flapping plane does not differ from the load perpendicular to the inflow to the blade profile (see Fig.1.32). /100

8. Mathematical Formulas

When using the assumptions given in Subsection 7, the value of the relative aerodynamic load P entering eq.(8.3) can be determined from the formula:

$$P = \bar{b}_r [\varphi \bar{U}_x^2 + \bar{U}_x \bar{U}_y], \tag{8.24}$$

where

$\bar{b}_r$ = value of the blade chord at the radius in question, relative to the chord at a radius $\bar{r} = 0.7$;

$\bar{U}_x$ and $\bar{U}_y$ = same relative flow velocity components as in eq.(8.23) but relative to the tip speed of the rotor blades ωR:

$$\left.\begin{aligned} \bar{U}_x &= \bar{r} + \mu \sin\psi; \\ \bar{U}_y &= \lambda - \mu\cos\psi \qquad \beta - \frac{1}{\omega R}\cdot \dot{y}. \end{aligned}\right\} \tag{8.25}$$

Here,

λ = relative velocity of the flow through the rotor; this velocity is determined from eq.(8.2);

y = displacements of the elastic blade axis in a plane perpendicular to the plane of rotation from which these displacements are calculated;

$\beta = y'$ = angle of slope of the elastic blade axis.

Here the prime denotes differentiation with respect to the blade radius and the dot, with respect to time.

The blade setting angle can be written in the form

$$\varphi = \theta_0 + \Delta\varphi - \theta_1 \sin\psi - \theta_2 \cos\psi - \varkappa_0\beta_0. \tag{8.26}$$

Here,

θ_0 = blade setting angle at a relative radius $\bar{r} = 0.7$ or at some other radius adopted for calculating θ_0, when the angle of rotation of the blade in the flapping hinge β_0 is equal to zero;

$\Delta\varphi$ = geometric blade twist;

θ_1 and θ_2 = cyclic pitch control angles prescribed by the automatic pitch control;

$\varkappa$ = flapping compensator;

β_0 = angle of rotation of the blade in the flapping hinge.

Let us represent blade deformations in the form /101

$$y = \sum_j \delta_j y^{(j)}, \tag{8.27}$$

where

δ_j = coefficients of blade deformation corresponding to the j-th harmonic of its natural vibrations; these coefficients are functions of time and therefore are also called time factors;

$y^{(j)}$ = natural blade vibration modes in vacuum normed such that $y_R^{(j)} = R$.

Let us expand the time factors δ_j in a Fourier series in harmonics. Then, the blade deformations can be represented as

$$y=\left[a_0-\sum_n\left(a_n\cos n\psi+b_n\sin n\psi\right)\right]y^{(0)}+\cdot$$
$$+\left[c_0-\sum_n\left(c_n\cos n\psi+d_n\sin n\psi\right)\right]y^{(1)}+$$
$$+\left[e_0-\sum_n\left(e_n\cos n\psi+f_n\sin n\psi\right)\right]y^{(2)}+ \qquad (8.28)$$
$$+\left[g_0-\sum_n\left(g_n\cos n\psi+h_n\sin n\psi\right)\right]\cdot y^{(3)}+\ldots$$

This form of notation of the solution is a continuation of the conventional form of notation for the flapping motion of a blade (7.40).

After differentiating eq.(8.28) with respect to radius and time and substituting y, together with its derivatives and eqs.(8.2) and (8.26), into eq.(8.25), and then substituting the resultant formulas for $\bar{U}_x$ and $\bar{U}_y$ into eq.(8.24), we finally obtain the expression from which all harmonic components of the relative aerodynamic load P can be determined.

These components can be represented in the form

$$\left.\begin{aligned}\bar{P}_n&=\bar{b}_r\left[\bar{f}_n+\bar{r}\bar{\lambda}_n-\frac{1}{2}\mu\left(\bar{\lambda}_{n-1}-\bar{\lambda}_{n+1}\right)\right];\\ \bar{\bar{P}}_n&=\bar{b}_r\left[\bar{\bar{f}}_n+\bar{r}\bar{\bar{\lambda}}_n+\frac{1}{2}\mu\left(\bar{\lambda}_{n-1}-\bar{\lambda}_{n+1}\right)\right].\end{aligned}\right\} \qquad (8.29)$$

Here, $\bar{f}_n$ and $\bar{\bar{f}}_n$ are certain functions determining the value of this component of the aerodynamic load, which does not depend on the magnitude of the induced velocities.

If now the induced velocities $\bar{\lambda}_n$ and $\bar{\bar{\lambda}}_n$ are represented in the form of the sum of the main and secondary components and if the main components are expressed in terms of $\bar{P}_n$ and $\bar{\bar{P}}_n$ with respect to eqs.(8.11), then the values of $\bar{P}_n$ and $\bar{\bar{P}}_n$ will appear both on the left- and right-hand sides of eqs.(8.29).

After determining from these equations the values of $\bar{P}_n$ and $\bar{\bar{P}}_n$, we obtain the following expressions: /102

$$\left.\begin{aligned}\bar{P}_n&=\bar{B}_n\left[\bar{f}+\bar{r}\bar{\lambda}_n^s-\frac{1}{2}\mu\left(\bar{\lambda}_{n-1}-\bar{\lambda}_{n+1}\right)\right];\\ \bar{\bar{P}}_n&=\bar{\bar{B}}_n\left[\bar{\bar{f}}+\bar{r}\bar{\bar{\lambda}}_n^s+\frac{1}{2}\mu\left(\bar{\lambda}_{n-1}-\bar{\lambda}_{n+1}\right)\right],\end{aligned}\right\} \qquad (8.30)$$

where

$$\left.\begin{aligned}\overline{B}_n &= \frac{\overline{b}_r}{1+\frac{1}{8}c_y^{\alpha}\sigma A_0[1+(-1)^n\tau^{2n}]\overline{b}_r};\\ \overline{\overline{B}}_n &= \frac{\overline{b}_r}{1+\frac{1}{8}c_y^{\alpha}\sigma A_0[1-(-1)^n\tau^{2n}]\overline{b}_r}.\end{aligned}\right\} \qquad (8.31)$$

Below, the values of $\overline{B}_n$ and $\overline{\overline{B}}_n$ will be denoted as equivalent chords of the blade since, in the calculation, they play the same role as the actual chords and, in eqs.(8.30), appear at the same place at which the values of $\overline{b}_r$ are located in eqs.(8.29).

Thus, the harmonic components of aerodynamic loads, with consideration of variable induced velocities, should be determined by substituting only secondary induced velocity components into the formulas and replacing the real chords by the equivalent blade chords. The values of the equivalent blade chords may differ depending on the flight regime and on the order of the harmonic of aerodynamic load being determined. However, they always prove to be smaller than the real chords. Consequently, all harmonic aerodynamic load components are smaller than the values they would have if the main induced velocity components were equal to zero and are also smaller as many times as the equivalent chords are smaller than the real chords. The introduction of equivalent chords leads to a decrease of all aerodynamic load components, both exciting and damping the blade vibrations. Therefore, there will also be a decrease in the values of the relative coefficients of aerodynamic damping which determines the vibration amplitudes in resonance. This causes a decrease in the variable blade deformations far from resonance, whereas those in resonance remain approximately the same as in calculations without consideration of this effect.

Expressions of the type of eq.(8.30), written for all harmonic components of the aerodynamic load, are found to be interrelated over the induced velocity components. Hence, these constitute a certain complex system of equations relative to unknown loads, which can be solved only if the values of $\overline{f}_n$ and $\overline{\overline{f}}_n$ are known. These values, however, depend on the magnitude of the coefficients of blade deformation. Therefore, to solve this system of equations it is necessary to construct equations for determining the deformation coefficients. This will be carried out below.

If the values of $\overline{f}_n$ and $\overline{\overline{f}}_n$ entering eqs.(8.30) are described in detail, the expressions for the harmonic aerodynamic load components can be represented in the form of Table 1.7.

The expression for each harmonic component of the loads $\overline{P}_n$ and $\overline{\overline{P}}_n$ occupies one row in the table and represents the sum of the products formed by the coefficients entered in the squares of the table with the unknown factors simultaneously contained in several expressions and entered vertically in a special row /103 at the top of the table. These factors, as already mentioned above, are called the coefficients of blade deformation. The right-hand side of the table contains a number of terms f_n^{θ}, f_n^{α}, f_n^{φ}, and f_n^{λ}, not related with the unknown coefficients of deformation.

To determine the values of $\overline{P}_n$ and $\overline{\overline{P}}_n$, it is necessary to multiply the sum of the products of the terms of each row and the unknown coefficients of deformation, which sum is added to terms independent of the coefficients of deformation, by the values of $\overline{B}_n$ and $\overline{\overline{B}}_n$. These values are entered on the left-hand side of the table.

The number of terms entering the expressions for $\overline{P}_n$ and $\overline{\overline{P}}_n$ depends on the number of harmonics and overtones of the natural vibrations being taken into account in the calculation. In Table 1.7, the expressions are given for the case where only two overtones and four harmonics of the variable forces are taken into account in the calculation.

In programs used for calculation on digital computers, four overtones of natural vibrations and six to eight harmonics of variable forces can usually be considered.

9. Conversion to an Equivalent Rotor

In order to demonstrate the possibility of converting to an equivalent rotor, the following equality was used in compiling Table 1.7:

$$\overline{y}^{(0)} = \overline{r},$$

which is valid only when the distance between the axis of rotation and the flapping or horizontal hinge $l_{h.h}$ is equal to zero.

If we now use the known formulas for the coefficients of flapping and angles of attack of an equivalent rotor

$$a_1^* = a_1 - \varkappa b_1 + \theta_1;$$
$$b_1^* = b_1 + \varkappa a_1 - \theta_2;$$
$$\tan \alpha_{eq} = \tan \alpha_{ref} + \varkappa b_1 - \theta_1,$$

then the expressions for $\overline{P}_n$ and $\overline{\overline{P}}_n$ can be somewhat simplified by substituting, in the first row of the table, the values of a_1^* and b_1^* for a_1 and b_1. This will cause the coefficients f_n^{θ} to become equal to zero, and the values of the angles θ_1 and θ_2 will not enter into the equation. In other words, the well-known principle that blade loading does not depend on the deflection of the automatic pitch control at $l_{h.h} = 0$, is completely observed in the expressions of Table 1.7.

However, the simplifications obtained on converting to an equivalent rotor are so insignificant as not to justify the assumption of $l_{h.h} = 0$. Therefore, we will investigate blade vibrations only in the axes of the shaft and will not use the concept of an equivalent rotor.

10. Basic Assumptions Used in Calculation of Bending Stresses

In the calculation of bending stresses in a blade, we will use the assump-

$J = 0$

				$\bar{B}_n$	a_0	a_1	b_1	a_2	b_2
$i=0$		$\bar{P}_0$	$=$	$\bar{B}_0$			$\mu\bar{r}\varkappa_0$	$-\frac{1}{4}\mu^2\varkappa_0$	$\frac{1}{4}\mu^2$
$i=1$									
$i=2$	$\cos\psi$	$\bar{P}_1$	$=$	$\bar{B}_1$	$-\mu\bar{r}$	$\varkappa_0(\bar{r}^2+\frac{1}{4}\mu^2)$	$\bar{r}^2+\frac{1}{4}\mu^2$	$-\frac{1}{2}\mu\bar{r}$	$\mu\bar{r}\varkappa_0$
$i=3$	$\sin\psi$	$\bar{\bar{P}}_1$	$=$	$\bar{\bar{B}}_1$		$-\bar{r}^2+\frac{1}{4}\mu^2$	$\varkappa_0(\bar{r}^2+\frac{3}{4}\mu^2)$	$-\mu\bar{r}\varkappa_0$	$-\frac{1}{2}\mu\bar{r}$
$i=4$	$\cos 2\psi$	$\bar{P}_2$	$=$	$\bar{B}_2$		$\mu\bar{r}$	$-\mu\bar{r}\varkappa_0$	$\varkappa_0(\bar{r}^2+\frac{1}{2}\mu^2)$	$2\bar{r}^2$
$i=5$	$\sin 2\psi$	$\bar{\bar{P}}_2$	$=$	$\bar{\bar{B}}_2$	$-\frac{1}{2}\mu^2$	$\mu\bar{r}\varkappa_0$	$\mu\bar{r}$	$-2\bar{r}^2$	$\varkappa_0(\bar{r}^2+\frac{1}{2})\mu^2$
$i=6$	$\cos 3\psi$	$\bar{P}_3$	$=$	$\bar{B}_3$		$-\frac{1}{4}\mu^2\varkappa_0$	$-\frac{1}{4}\mu^2$	$\frac{3}{2}\mu\bar{r}$	$-\mu\bar{r}\varkappa_0$
$i=7$	$\sin 3\psi$	$\bar{\bar{P}}_3$	$=$	$\bar{\bar{B}}_3$		$\frac{1}{4}\mu^2$	$-\frac{1}{4}\mu^2\varkappa_0$	$\mu\bar{r}\varkappa_0$	$\frac{3}{2}\mu\bar{r}$
$i=8$	$\cos 4\psi$	$\bar{P}_4$	$=$	$\bar{B}_4$				$-\frac{1}{4}\mu^2\varkappa_0$	$-\frac{1}{4}\mu^2$
$i=9$	$\sin 4\psi$	$\bar{\bar{P}}_4$	$=$	$\bar{\bar{B}}_4$				$\frac{1}{4}\mu^2$	$-\frac{1}{4}\mu^2\varkappa_0$

TABLE

a_3	b_3	a_4	b_4	• • •
$\frac{1}{4}\mu^2\varkappa_0$	$\frac{1}{4}\mu^2$			
$-\frac{1}{4}\mu^2$	$-\frac{1}{4}\mu^2\varkappa_0$			
$-\mu\bar{r}$	$\mu\bar{r}\varkappa_0$	$-\frac{1}{4}\mu^2\varkappa_0$	$\frac{1}{4}\mu^2$	
$-\mu\bar{r}\varkappa_0$	$-\mu\bar{r}$	$-\frac{1}{4}\mu^2$	$-\frac{1}{4}\mu^2\varkappa_0$	
$_0(\bar{r}^2+\frac{1}{2}\mu^2)$	$3\bar{r}^2$	$-\frac{3}{2}\mu\bar{r}$	$\mu\bar{r}\varkappa_0$	• • •
$-3\bar{r}^2$	$\varkappa_0(\bar{r}^2+\frac{1}{2}\mu^2)$	$-\mu\bar{r}\varkappa_0$	$-\frac{3}{2}\mu\bar{r}$	• • •
$2\mu\bar{r}$	$-\mu\bar{r}\varkappa_0$	$\varkappa_0(\bar{r}^2+\frac{1}{2}\mu^2)$	$4\bar{r}^2$	• • •
$\mu\bar{r}\varkappa_0$	$2\mu\bar{r}$	$-4\bar{r}^2$	$\varkappa_0(\bar{r}^2+\frac{1}{2}\mu^2)$	• • •
• • •	• • •	• • •	• • •	• • •

$J = 1$

c_0	c_1	d_1	c_2	d_2
	$-\frac{1}{2}\mu\bar{y}^{(1)}+\frac{1}{2}\mu\bar{r}\beta^{(1)}$	$\mu\bar{r}x_1$	$-\frac{1}{4}\mu^2 x_1$	$\frac{1}{4}\mu^2\beta^{(1)}$
$-\mu\bar{r}\beta^{(1)}$	$x_1(\bar{r}^2+\frac{1}{4}\mu^2)$	$\bar{r}\bar{y}^{(1)}+\frac{1}{4}\mu^2\beta^{(1)}$	$-\mu\bar{y}^{(1)}+\frac{1}{2}\mu\bar{r}\beta^{(1)}$	$\mu\bar{r}x_1$
	$-\bar{r}\bar{y}^{(1)}+\frac{1}{4}\mu^2\beta^{(1)}$	$x_1(\bar{r}^2+\frac{3}{4}\mu^2)$	$-\mu\bar{r}x_1$	$-\mu\bar{y}^{(1)}+\frac{1}{2}\mu\bar{r}$
	$\frac{1}{2}\mu\bar{y}^{(1)}+\frac{1}{2}\mu\bar{r}\beta^{(1)}$	$-\mu\bar{r}x_1$	$x_1(\bar{r}^2+\frac{1}{2}\mu^2)$	$2\bar{r}\bar{y}^{(1)}$
$\frac{1}{2}\mu^2\beta^{(1)}$	$\mu\bar{r}x_1$	$\frac{1}{2}\mu\bar{y}^{(1)}+\frac{1}{2}\mu\bar{r}\beta^{(1)}$	$-2\bar{r}\bar{y}^{(1)}$	$x_1(\bar{r}^2+\frac{1}{2}\mu^2)$
	$-\frac{1}{4}\mu^2 x_1$	$-\frac{1}{4}\mu^2\beta^{(1)}$	$\mu\bar{y}^{(1)}+\frac{1}{2}\mu\bar{r}\beta^{(1)}$	$-\mu\bar{r}x_1$
	$\frac{1}{4}\mu^2\beta^{(1)}$	$-\frac{1}{4}\mu^2 x_1$	$\mu\bar{r}x_1$	$\mu\bar{y}^{(1)}+\frac{1}{2}\mu\bar{r}\beta$
			$-\frac{1}{4}\mu^2 x_1$	$-\frac{1}{4}\mu^2\beta^{(1)}$
			$\frac{1}{4}\mu^2\beta^{(1)}$	$-\frac{1}{4}\mu^2 x_1$

c_3	d_3	c_4	d_4	$\cdots$
$-\frac{1}{4}\mu^2 \varkappa_1$	$\frac{1}{4}\mu^2 \beta^{(1)}$			
$-\frac{1}{4}\mu^2 \beta^{(1)}$	$-\frac{1}{4}\mu^2 \varkappa_1$			
$-\frac{3}{2}\mu\bar{y}^{(1)}+\frac{1}{2}\mu\bar{r}\beta^{(1)}$	$\mu\bar{r}\varkappa_1$	$-\frac{1}{4}\mu^2 \varkappa_1$	$\frac{1}{4}\mu^2 \beta^{(1)}$	
$-\mu\bar{r}\varkappa_1$	$-\frac{3}{2}\mu\bar{y}^{(1)}+\frac{1}{2}\mu\bar{r}\beta^{(1)}$	$-\frac{1}{4}\mu^2 \beta^{(1)}$	$-\frac{1}{4}\mu^2 \varkappa_1$	
$\varkappa_1(\bar{r}^2+\frac{1}{2}\mu^2)$	$3\bar{r}\bar{y}^{(1)}$	$-2\mu\bar{y}^{(1)}+\frac{1}{2}\mu\bar{r}\beta^{(1)}$	$\mu\bar{r}\varkappa_1$	$\cdots$
$-3\bar{r}\bar{y}^{(1)}$	$\varkappa_1(\bar{r}^2+\frac{1}{2}\mu^2)$	$-\mu\bar{r}\varkappa_1$	$-2\mu\bar{y}^{(1)}+\frac{1}{2}\mu\bar{r}\beta^{(1)}$	$\cdots$
$\frac{3}{2}\mu\bar{y}^{(1)}+\frac{1}{2}\mu\bar{r}\beta^{(1)}$	$-\mu\bar{r}\varkappa_1$	$\varkappa_1(\bar{r}^2+\frac{1}{2}\mu^2)$	$4\bar{r}\bar{y}^{(1)}$	$\cdots$
$\mu\bar{r}\varkappa_1$	$\frac{3}{2}\mu\bar{y}^{(1)}+\frac{1}{2}\mu$	$-4\bar{r}\bar{y}^{(1)}$	$\varkappa_1(\bar{r}^2+\frac{1}{2}\mu^2)$	$\cdots$
$\cdots$	$\cdots$	$\cdots$	$\cdots$	$\cdots$

Terms, Independent of the Coefficient of Deformation			
f_n^{θ}	f_n^{ω}	f_n^{φ}	f_n^{λ}
$-\mu\bar{r}\theta_1$	$\mu r\, tg\alpha_B$	$(\bar{r}^2+\frac{1}{2}\mu^2)\varphi_r$	$\bar{r}\,\bar{\lambda}_0^n+\frac{1}{2}\mu\bar{\bar{\lambda}}_1$
$(\bar{r}^2+\frac{1}{4}\mu^2)\theta_2$			$\bar{r}\,\bar{\lambda}_1^n+\frac{1}{2}\mu\bar{\bar{\lambda}}_2$
$(\bar{r}^2+\frac{3}{4}\mu^2)\theta_2$	$\mu^2 tg\alpha_B$	$2\mu\bar{r}\varphi_r$	$\bar{r}\,\bar{\bar{\lambda}}_1^n+\mu\bar{\lambda}_0-\frac{1}{2}\mu\bar{\lambda}_2$
$\mu\bar{r}\theta_1$		$-\frac{1}{2}\mu^2\varphi_r$	$\bar{r}\,\bar{\lambda}_2^n-\frac{1}{2}\mu(\bar{\bar{\lambda}}_1-\bar{\bar{\lambda}}_3)$
$-\mu\bar{r}\theta_2$			$\bar{r}\,\bar{\bar{\lambda}}_2^n+\frac{1}{2}\mu(\bar{\lambda}_1-\bar{\lambda}_3)$
$\frac{1}{4}\mu^2\theta_2$			$\bar{r}\,\bar{\lambda}_3^n-\frac{1}{2}\mu(\bar{\bar{\lambda}}_2-\bar{\bar{\lambda}}_4)$
$\frac{1}{4}\mu^2\theta_1$			$\bar{r}\,\bar{\bar{\lambda}}_3^n+\frac{1}{2}\mu(\bar{\lambda}_2-\bar{\bar{\lambda}}_4)$
			$\bar{r}\,\bar{\lambda}_4^n-\frac{1}{2}\mu(\bar{\bar{\lambda}}_3-\bar{\bar{\lambda}}_5)$
			$\bar{r}\,\bar{\bar{\lambda}}_4^n+\frac{1}{2}\mu(\bar{\lambda}_3-\bar{\lambda}_5)$
			• • •

tions adopted in deriving the differential equation (1.9) of blade vibrations in the thrust plane. We will represent the blade as an elastic beam extended by centrifugal forces N. The parameters of this beam - its linear mass m and the flexural rigidity EI - will be considered as continuously distributed over the blade length.

Furthermore, we are adopting the following assumptions: /104

1. We will assume that the plane of minimum blade rigidity coincides with the flapping plane, so that the blade will bend in the flapping plane only under the effect of forces acting in this plane.

2. In determining loads in the flapping plane we will disregard torsional blade deformations (see Sect.7 of Chapt.IV in Vol.I, on consideration of torsional deformation).

3. We will assume the conventional type of rotor with hinged blades and disregard the distance from the axis of rotation to the flapping hinge, i.e., we will pose $i_{h.h} \neq 0$. We will also neglect the frictional forces in the blade hinges.

11. Differential Equation of Blade Vibrations and its Solution

When using these assumptions, the calculation of bending stresses reduces to solving a differential equation whose derivation has been given in Section 1 of this Chapter:

$$[EIy'']'' - [Ny']' + m\ddot{y} = T. \tag{8.32}$$

With the blade attachment in question here, the boundary conditions can be written as

$$\left.\begin{aligned} y_0 &= 0; \quad [EIy'']_R = 0; \\ [EIy'']_0 &= 0; \quad [EIy'']'_R = 0. \end{aligned}\right\} \tag{8.33}$$

The value of the linear aerodynamic load entering the right-hand side of eq.(8.32) is determined from eqs.(8.3), (8.4), and Table 1.7.

After substituting, into this equation, the solution of the form of equation (8.28) and applying Galerkin's method, we obtain a system of algebraic equations relative to the unknown deformation coefficients. This system of equations is represented in the form of Table 1.8.

Each equation of the obtained system represents the sum of the products formed by certain coefficients entered in the squares of the table with the unknown coefficients of deformation simultaneously contained in several equations and entered vertically in a special row at the top of the table. The known coefficients of each equation occupy one row in the table. The right-hand side of the table, in a special column, contains the coefficients $\overline{\Phi}_n$ and $\overline{\overline{\Phi}}_n$ representing

TABLE 1.8

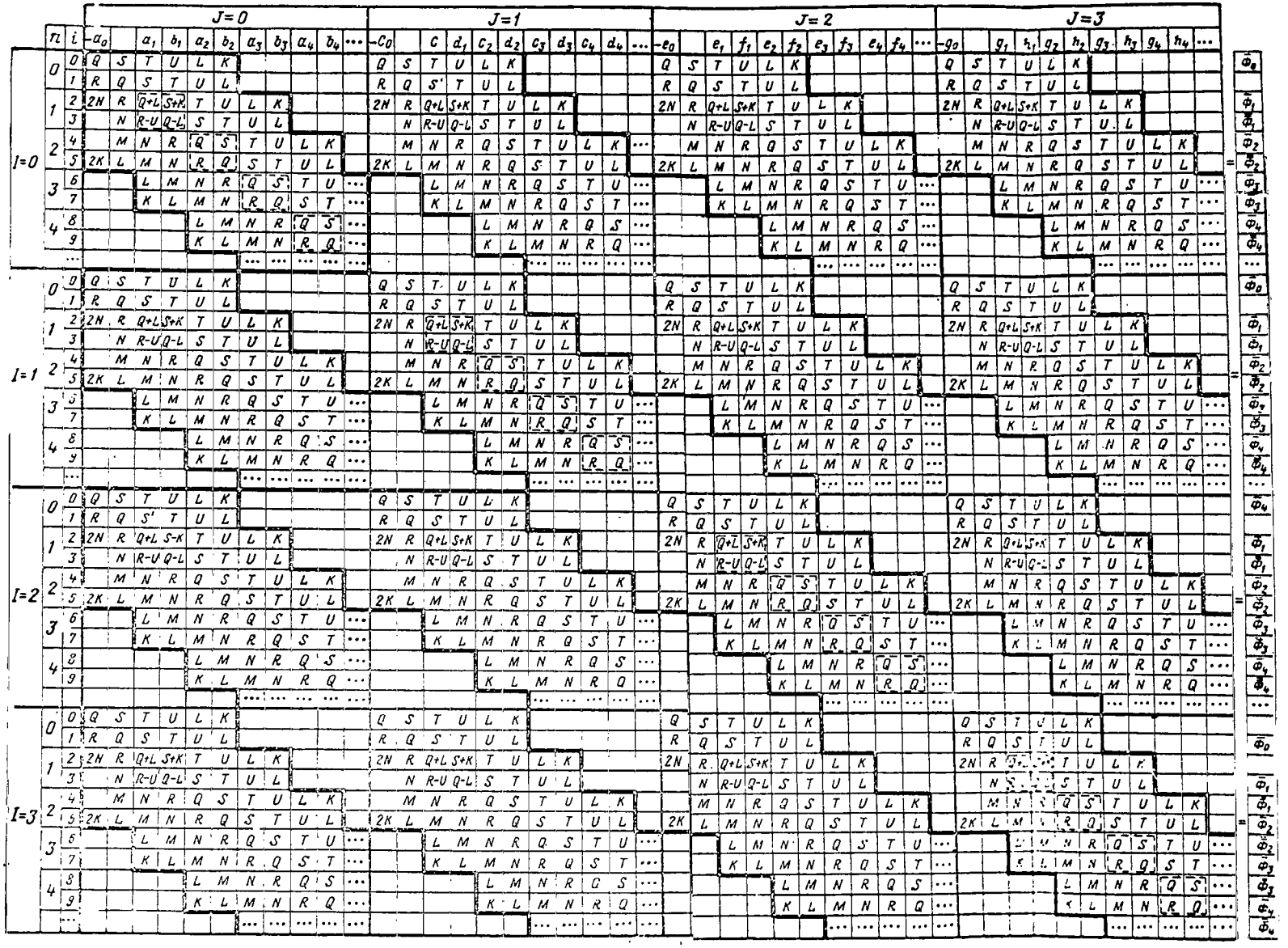

the right-hand side of the equations.

Just as in Tables 1.7 and 1.9 there are empty squares in Table 1.8. This means that the coefficients of the equations for which these squares are intended are equal to zero.

12. Determination of the Coefficients on the Left-Hand Side of the Equations in Table 1.8

To determine the coefficients on the left-hand side of the equations, a special operator must be devised for the computational program. This operator should read out the values for all coefficients of any equation of the system. To render this operator as simple as possible, we will divide the entire table of coefficients into a number of zones relative to the number of harmonics of natural vibrations used in the calculation. These zones are then used for combining, into separate groups, all coefficients that follow a similar path of formation when using Galerkin's method and can be roughly calculated by the same formulas.

The transformation of the differential equation (8.32) by means of Galerkin's method into a system of algebraic equations of Table 1.8 comprises the following operations:

1. Into the differential equation (8.32), we first substitute the solution/105 in the form of eq.(8.28) containing various natural vibration modes. If the modes entering into the solution (8.28) are denoted by the subscript J, then all terms of the equation obtained as result of this operation can be divided into several groups, each of which is characterized by a definite subscript J.

2. Next, all terms of the equations are multiplied in turn by the same natural vibration modes $y^{(I)}$. As a result of this operation, a system of equations is formed in which each equation differs from the others by the harmonic of the natural vibration mode $y^{(I)}$ by which all terms of the equations had been multiplied. Therefore, the resultant equations were numbered in accordance with the values of the index I.

3. Integration over the blade length of all functions obtained as a result of prior operations is the next step in Galerkin's method. As a result of this operation, all terms of the equations which previously had been functions of the blade radius become constants.

4. In the next step, each equation obtained in this manner can be divided into numerous simpler equations if all coefficients of like values of cos $n\psi$ and sin $n\psi$ are equated. As a result of this operation, each equation with the numeral I will be transformed into an entire family of equations. The individual equations entering this family are coordinated by the index i in Table 1.8. Furthermore, each pair of equations pertaining to like harmonics is marked by the index n, equal to the order of the corresponding harmonic.

An analysis of the resultant system of algebraic equations shows that all like coefficients of equations are arranged diagonally in Table 1.8. This arrangement is repeated in all zones corresponding to different indexes J and I.

It should be noted that there are exceptions to this rule, which becomes obvious from a study of Table 1.8.

Using the above indices i, n, J, and I, it is possible to construct general formulas for all coefficients entering into the left-hand side of the equations of Table 1.8. In constructing these formulas, we will use special functions $f_1(a)$ and $f_2(a)$ which assume the following values, depending upon the parity and magnitude of their argument:

$$f_1(a)=\begin{cases}1 & \text{at } a \text{ even;}\\ 0 & \text{at } a \text{ odd;}\end{cases}$$

$$f_2(a)=\begin{cases}1 & \text{at } a=0;\\ 0 & \text{at } a\neq 0.\end{cases}$$

These formulas have the form

$$\left.\begin{aligned}
Q&=\frac{f_2(I-J)}{\gamma_I}\left[n^2-\frac{p_J^2}{\omega^2}\right]-\varkappa_J\left[A_I+\frac{1}{2}\mu^2 C_I\right][1-f_2(i)];\\
R&=nf_1(i+1)D_{JI}+\mu\varkappa_J f_1(i)B_I;\\
S&=-nf_1(i)D_{JI}+\mu\varkappa_J f_1(i+1)B_I;\\
N&=\frac{1}{2}\mu[(1-n)F_{JI}-G_{JI}];\\
T&=\frac{1}{2}\mu[(1+n)F_{JI}-G_{JI}];
\end{aligned}\right\}\qquad(8.34)$$

/106

$$\left.\begin{aligned}
M&=\frac{1}{4}\mu^2 f_1(i)H_{JI}-\mu\varkappa_J f_1(i+1)B_I;\\
U&=\frac{1}{4}\mu^2 f_1(i+1)H_{JI}-\mu\varkappa_J f_1(i)B_I;\\
L&=\frac{1}{4}\mu^2\varkappa_J C_I;\\
K&=-\frac{1}{4}\mu^2 H_{JI}.
\end{aligned}\right\}\qquad(8.34)$$

Here, $\varkappa_J=\varkappa_0\beta_0^{(J)}$,

where

$\beta_0^{(J)}$ = angle of rotation in the horizontal hinge during vibrations with respect to the mode of the j-th harmonic of natural vibrations normed in conformity with eq.(8.27);

γ_I = mass characteristic of the blade during vibrations with respect to the i-th harmonic;

$$\gamma_I=\frac{c_y\rho b_{0.7}R^2}{2m_I^{eq}};\qquad(8.35)$$

m_I^{eq} = equivalent mass of blade during vibrations with respect to the mode of the I-th harmonic:

$$m_I^{eq} = \int_0^R m \left[\bar{y}^{(I)}\right]^2 dr.$$

In the particular case when I = 0 and when we can set $\bar{y}^{(0)} = \bar{r}$, the expression for γ_0 will coincide with the conventional expression (7.49) for the mass characteristic of a rigid blade [eq.(7.49)].

p_J = frequency of natural blade vibrations with respect to the mode of the j-th harmonic; in performing the calculations, the value of the frequency is attributed to the expression

$$p_J^2 = \frac{\int_0^R EI\left[(y^J)''\right]^2 dr + \int_0^R N\left[(y^J)'\right]^2 dr}{\int_0^R m\left[y^J\right]^2 dr}; \qquad (8.36)$$

ω = angular velocity (or rotor rpm, depending on the units in which p_J is determined); the ratio p_J/ω should be dimensionless.

Other quantities entering eqs.(8.34) have the following values:

$$\left.\begin{aligned} A_I &= \int_0^1 B^{(I)} \bar{r}^2 \bar{y}^I d\bar{r}; \\ B_I &= \int_0^1 B^{(I)} \bar{r} \bar{y}^I d\bar{r}; \\ C_I &= \int_0^1 B^{(I)} \bar{y} d\bar{r}; \\ D_{JI} &= \int_0^1 B^{(I)} \bar{r} \bar{y}^J \bar{y}^I d\bar{r}; \end{aligned}\right\} \qquad (8.37)$$

/107

$$\left.\begin{aligned} F_{JI} &= \int_0^1 B^{(I)} \bar{y}^J \bar{y}^I d\bar{r}; \\ G_{JI} &= \int_0^1 B^{(I)} \bar{r}\beta^J \bar{y}^I d\bar{r}; \\ H_{JI} &= \int_0^1 B^{(I)} \beta^J \bar{y}^I d\bar{r}. \end{aligned}\right\} \qquad (8.37)$$

Here,

$B^{(i)}$ = equivalent blade chord determined by eqs.(8.31) and thus having different values depending on the number of the equation:

$$B^{(i)}=\overline{B}_n \quad \text{at} \quad i \quad \text{even};$$
$$B^{(i)}=\overline{\overline{B}}_n \quad \text{at} \quad i \quad \text{odd};$$

$\overline{y}^J$ and $\overline{\overline{y}}^I$ = natural vibration modes of the blade whose harmonic is determined by the value of the indices J and I.

The symbols of these modes are marked by a vinculum. This means that they are normed such that $\overline{y}_R = 1$. At the same time, the values of the first derivative of these modes, following differentiation over the blade radius β^J, are not marked by a vinculum. This means that these derivatives are taken from the vibration modes y^J normed such that $y^J_R = R$.

Equations (8.34) permit determining the vinculi of the coefficients K, L, M, N, R, Q, S, T, U, L, and K for any zone of Table 1.8, if the coordinates of this zone J and I and the number of the equation in the zone i are prescribed. Thus, assigning in sequence the different values of J, I, and i and making use of the operator which includes the operation prescribed by eqs.(8.34), we can determine all coefficients of the left-hand side of the equations in Table 1.8.

13. Determination of the Coefficients on the Right-Hand Side of the Equation of Table 1.8

To determine the coefficients on the right-hand side $\overline{\Phi}_n$ and $\overline{\overline{\Phi}}_n$, it is necessary to derive a special operator for the computational program, in which these coefficients are determined by the following formulas:

$$\left.\begin{aligned}
\overline{\Phi}_0&=-\mu B_I\theta_1+\mu\tan\alpha_{\infty}B_I+A_I^{\circ}+\frac{1}{2}\mu^2C_I^{\circ}+\overline{\Phi}_0^{\wedge};\\
\overline{\Phi}_1&=-\left[A_I+\frac{3}{4}\mu^2C_I\right]\theta_2+\overline{\Phi}_1^{\wedge};\\
\overline{\overline{\Phi}}_1&=-\left(A_I+\frac{3}{4}\mu^2C_I\right)\theta_1+\mu^2\tan\alpha_{\infty}C_I+2\mu B_I^{\circ}+\overline{\overline{\Phi}}_1^{\wedge};\\
\overline{\Phi}_2&=\mu B_I\theta_1-\frac{1}{2}\mu^2C_I^{\circ}+\overline{\overline{\Phi}}_2^{\wedge};\\
\overline{\overline{\Phi}}_2&=-\mu B_I\theta_2+\overline{\Phi}_2^{\wedge};\\
\overline{\Phi}_3&=\frac{1}{4}\mu^2C_I\theta_2+\overline{\Phi}_3^{\wedge};\\
\overline{\overline{\Phi}}_3&=\frac{1}{4}\mu^2C_I\theta_1+\overline{\Phi}_3^{\wedge}.
\end{aligned}\right\} \qquad (8.38)$$

For harmonics above the third (at $n > 3$), we have /108

$$\overline{\Phi}_n=\overline{\Phi}_n^{\lambda};\quad \overline{\overline{\Phi}}_n=\overline{\overline{\Phi}}_n^{\lambda}.$$

In eqs.(8.38), the new notations are used for a series of integrals:

$$\left.\begin{aligned} A_I^{\varphi}&=\int_0^1 B^{(i)}\varphi_r\bar{r}^2\bar{y}^I d\bar{r};\\ B_I^{\varphi}&=\int_0^1 B^{(i)}\varphi_r\bar{r}\bar{y}^I d\bar{r};\\ C_I^{\varphi}&=\int_0^1 B^{(i)}\varphi_r\bar{y}^I d\bar{r};\\ \Phi_n^{\lambda}&=\int_0^1 B^{(i)} f_n^{\lambda}\bar{y}^I d\bar{r}. \end{aligned}\right\} \qquad (8.39)$$

Here,

$$\varphi_r=\varphi_{real}+\Delta\varphi,$$

where

$$\varphi_{real}=\theta_0-\varkappa_0 a_0-\varkappa_1 c_0-\varkappa_2 e_0-\varkappa_3 g_0;$$

φ_r = constant component of blade setting angle, calculated from the plane of rotation of the rotor; over the blade radius, this quantity changes only due to its geometric twist $\Delta\varphi$.

The values of f_n^{λ} are entered in the extreme right-hand column of Table 1.7.

Thus, eqs.(8.38) permit determining all coefficients of the right-hand side of the equations if the value of I is prescribed.

14. System of Equations after Substitution of Eqs.(8.34) and (8.38)

If the values of the coefficients determined from eqs.(8.34) and (8.38) are substituted into the equations of Table 1.8, then this same system of equations can be represented in the form of Table 1.9.

For simplicity, we limited ourselves here to the case in which the calculation is performed with an accuracy to two overtones of vibrations and four harmonics of rotor rpm. However, the above-derived mathematical formulas (8.34) and (8.38) are written in a general form and permit calculation to any desired accuracy.

After evaluating the practical requirements, it becomes possible, in setting up the program, to limit the calculation to consideration of only four overtones of natural vibrations and to six or eight harmonics of the rotor rpm.

TABLE 1.9

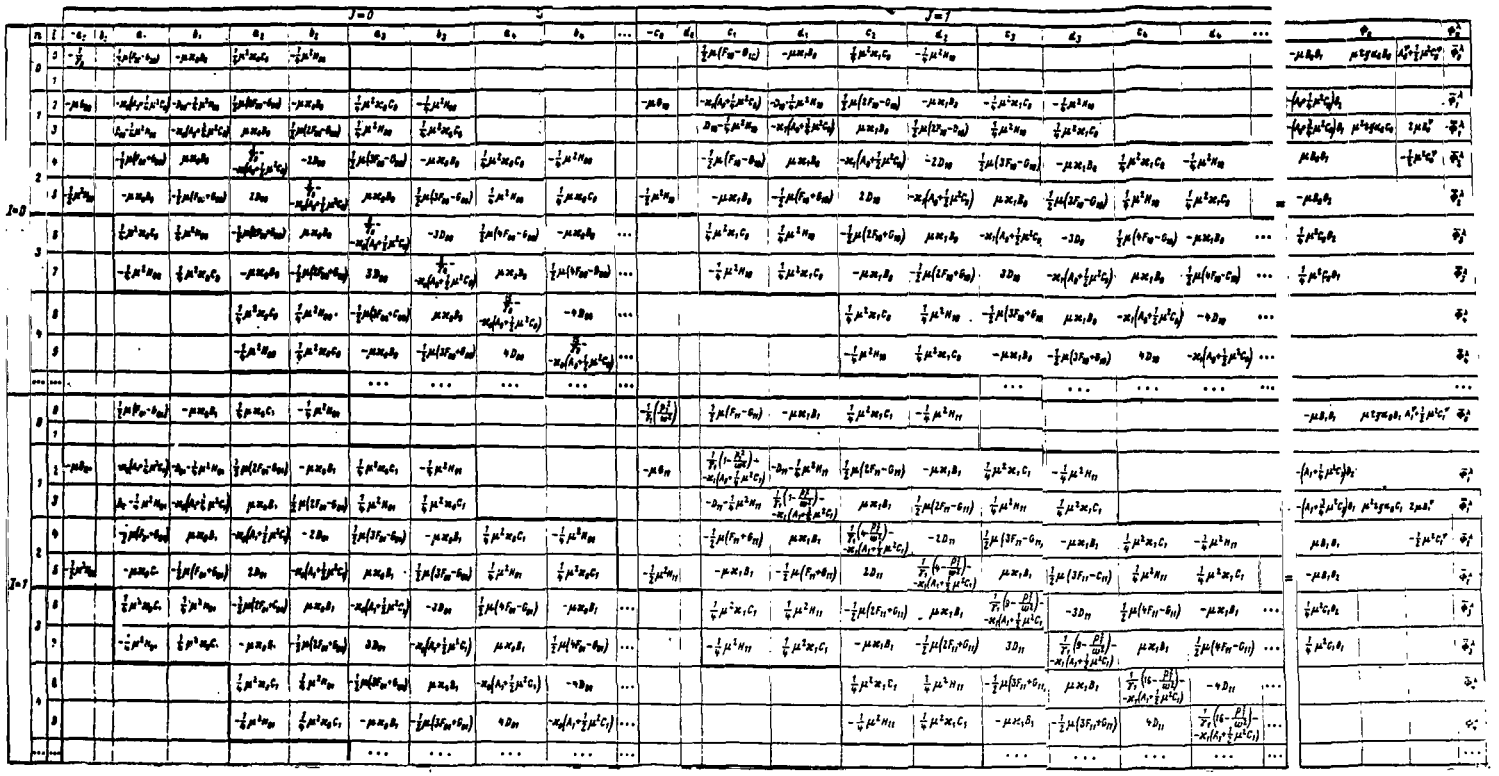

* tg = tan

15. General Computational Scheme

The system of algebraic equations entered in Table 1.8, together with the system of equations presented in Table 1.7, represents a complex system of equations permitting a determination of all unknown quantities entering into it. A determination of these unknowns and primarily of all coefficients of blade deformation constitutes the ultimate purpose of the method of calculation presented here.

Above (Sect.7), in the calculation of bending stresses based on Galerkin's method, we used various simplifications in deriving the equations presented here and in solving them. The use of digital computers greatly facilitates solving this system of equations without additional assumptions; this greatly increases the reliability of the results. In any case, the computational errors can be ascribed solely to the initial assumptions. Performance of all necessary mathematical operations will introduce no errors and can be carried out at any prescribed accuracy. /109

How does one solve this rather complex system of equations? No doubt, the simplest method here is the method of successive approximations in the form in which it will be presented below. This method was used in programming and has been checked by numerous calculations. The method converges rapidly and already three or four approximations suffice for obtaining the necessary accuracy.

In applying the method of successive approximations, the unknown coefficients of deformation are determined in the sequence of ascending indices characterizing their relation to the corresponding harmonic. Therefore, before passing to a description of the sequence of operations in the method of successive approximations, a brief review of the determination of deformation coefficients is required.

16. Determination of Deformation Coefficients

In determining the coefficients of deformation, the same principle is used in all cases, involving the following. The deformation coefficients are determined in pairs from two equations of the system of Table 1.8 pertaining to the cosinusoidal and sinusoidal components of some harmonic. The equations are first transformed in the following manner: Determine the sum of the products of $\Delta\bar{\Phi}_n$ and $\Delta\bar{\bar{\Phi}}_n$ coefficients in Table 1.8 as well as the deformation coefficients derived before performing this operation, with the exception of the products containing the coefficients outlined by a broken line in Table 1.8. These sums of the products are transferred to the right-hand side of the equations. After this, the deformation coefficients pertaining to like harmonics (of course, only in the case of $n > 1$) and to the deformation modes are determined from two algebraic equations of the following form:

$$\left.\begin{aligned} \bar{Q}a_n + Sb_n &= \bar{\Phi}_n^{\text{II}}; \\ Ra_n + \bar{\bar{Q}}b_n &= \bar{\bar{\Phi}}_n^{\text{II}}, \end{aligned}\right\} \qquad (8.40)$$

where

$$\overline{\Phi}_n^{II}=\overline{\Phi}_n-\Delta\overline{\Phi}_n; \quad \overline{\overline{\Phi}}_n^{II}=\overline{\overline{\Phi}}_n-\Delta\overline{\overline{\Phi}}_n.$$

The coefficients a_n and b_n here have a generalized character in that such a notation of the equations is possible also with the coefficients c_n and d_n; e_n and f_n; g_n and h_n.

The coefficients $\overline{Q}$, S, R, and $\overline{\overline{Q}}$ entering eqs.(8.40) are determined by eqs.(8.34) for the case of J = I. The value of i is even for the first equation and odd for the second. Consequently, the coefficients, in this particular /110 case, can be written in accordance with eqs.(8.34) in the form

$$\left.\begin{aligned}&\overline{Q}=\overline{\overline{Q}}=\frac{1}{\gamma_J}\left[n^2-\frac{p_J^2}{\omega^2}\right]-\varkappa_J\left[A_J+\frac{1}{2}\mu^2 C_J\right];\\&S=-nD_J;\\&R=nD_J.\end{aligned}\right\} \tag{8.41}$$

In this case, at J = I, we have

$$D_J=\int_0^1 B^{(i)}\bar{r}\,[\bar{y}^J]^2\,d\bar{r}.$$

Neglecting the second term in the first equation of the system (8.41) and approximately setting $\overline{B}_n = \overline{\overline{B}}_n = \overline{b}_r$, eqs.(8.40) can be transformed into the form used in the simplified methods of calculation (see Sect.7).

In fact, when making these assumptions, we multiply all terms of eq.(8.40) by $\gamma_J\frac{\omega^2}{p_J^2}$.

Let us now introduce new notations. The quantity $\overline{n}_J$, determined by the expression

$$\overline{n}_J=\frac{1}{2}\frac{\omega}{p_J}\gamma_J D_J, \tag{8.42}$$

will be called the relative coefficient of aerodynamic damping.

The quantity $\nu_n = n\omega$ will be called the frequency of excitation of forced vibrations.

Then eq.(8.40) can be rewritten in the form used in Section 7:

$$\left[\left(\frac{\nu_n}{p_J}\right)^2-1\right]a_n-2\overline{n}_J\frac{\nu_n}{p_J}\cdot b_n=\frac{\omega^2}{p_J^2}\gamma_J\overline{\Phi}_n^{II};$$

$$2\bar{n}_J \frac{\nu_n}{p_J} a_n + \left[\left(\frac{\nu_n}{p_J}\right)^2 - 1\right] b_n = \frac{\omega^2}{p_J^2} \gamma_J \bar{\bar{\Phi}}_n^{\text{II}}.$$

From these equations, the amplitude of the coefficients of deformation corresponding to the J-th harmonic of natural vibrations can be determined as

$$\delta_{dyn}^{(J)} = \lambda_{dyn} \delta_{st}^{(J)},$$

where

λ_{dyn} = coefficient of dynamic increase in amplitude;

$\delta_{st}^{(J)}$ = deflection of the blade with respect to the mode of the J-th harmonic under static application of external forces:

$$\left.\begin{aligned} \delta_{st}^{(J)} &= \frac{\omega^2}{p_J^2} \gamma_J \sqrt{(\bar{\Phi}_n^{\text{II}})^2 + (\bar{\bar{\Phi}}_n^{\text{II}})^2}; \\ \lambda_{dyn} &= \frac{1}{\sqrt{\left[\left(\frac{\nu_n}{p_J}\right)^2 - 1\right]^2 + 4\bar{n}_J^2 \left(\frac{\nu_n}{p_J}\right)^2}}. \end{aligned}\right\} \qquad (8.44)$$

Thus, the adopted form of determining the deformation coefficients theoretically coincides with the form used in problems of mechanics when determining the vibration amplitude of a damped system, as described above in Section 7.

It should be noted that, in determining the coefficients of deformation, /111 the equations of the system (see Table 1.8) are transformed into the form of eq.(8.40) only at $n > 1$. In determining the coefficients relative to the first harmonic, certain additional coefficients K, L, and U will enter the left-hand side of eqs.(8.40) which, however, changes nothing in the essential aspect of the matter.

A determination of the coefficients a_0, c_0, e_0 and g_0 which define the constant component of the deformations proves to differ somewhat. These coefficients can be determined for one equation with the number $i = 0$. However, so as not to disrupt the generality of the approach, it is preferable to determine them also in a program of two equations with the numbers $i = 0$ and $i = 1$ whose coefficients are determined by the same formulas [eqs.(8.34)]. In so doing, it is necessary to put $\bar{\bar{\Phi}}_0^{\Sigma} = 0$. Such an approach yields a slight simplification of the computational program.

17. Computational Program

In programming the calculation, the following sequence of performing the necessary operations is used:

1. The natural vibration modes and frequencies of a blade in the thrust plane are determined from a separate program which is absolutely necessary in designing blades and thus must be formulated. The following quantities should be

defined for carrying out this calculation: y^J, β^J, σ^J, and m_j^{eq}. Here, $\sigma^{(J)}$ is the distribution of bending stresses over the blade radius during its vibrations with respect to the normed modes of the J-th harmonic.

2. The parameters characterizing the flight regime of the helicopter are prescribed: μ, ρ, ω, α_{rot}, φ_{real}, θ_1, θ_2. Here, α_{rot} and φ_{real} can be determined from calculation if the required propulsive force and thrust of the rotor are prescribed. The cyclic pitch control angles θ_1 and θ_2 can be determined if the required moments M_x and M_z due to the rotor blades and acting on the hub are determined from the conditions of helicopter balancing. These operations are usually included into the programming.

3. To arrive at the solution of the system of equations entered here in Tables 1.7 and 1.8, it is necessary to determine the coefficients γ_J and $\varkappa_J$. This system of equations is solved by the method of successive approximations where, in each approximation, all unknowns are determined in the sequence given in Table 1.10. First, the coefficients in the first row are determined, then those in the second row, and so on.

4. After determining all quantities given in Table 1.10, the parameters of the flight regime φ_{real}, α_{rot}, θ_1, θ_2 can be refined and the calculation of all coefficients can be carried out in the next approximation in the same sequence.

5. The sequenc of operations, indicated in Table 1.10, is repeated until the difference of like deformation coefficients in two successive approximations is less than the prescribed accuracy of calculating $\varepsilon\delta$. The value of $\varepsilon\delta$ can be taken as equal to 1/1000 or somewhat smaller.

6. The magnitude of the bending stresses in the blade at each azimuth can be determined from the formula

$$\sigma_\psi = \sum_J \delta_J \sigma^J,$$

where the values of δ_J are determined from the deformation coefficients a_0, a_n, b_n, c_0, c_n, b_n, etc., in conformity with eqs.(8.27) and (8.28).

This sequence of operations constitutes the principle of the method of calculation presented here. Performance of these calculation permits obtaining:

bending stresses and form of blade deformation at each rotor azimuth, /113
with simultaneous determination of all harmonic components of these quantities;
field of axial induced velocities in the plane of the rotor and all harmonic components of this field;
angle of attack and blade setting angle in flight regimes with prescribed values of propulsive force and thrust;
angles of deflection of the pitch control swashplate, necessary for creating the moments M_x and M_z required for helicopter balancing.

18. Comparison of Calculation with Experiment at Low Flying Speed

At low flying speeds, the variable stresses measured in the blade are usually highly unstable.

During a single flight regime flown by one pilot, the vibration amplitude may fluctuate in magnitude by a factor of 2 - 3. This can be attributed to the fact that the angle of attack of the rotor and the flying speed in these regimes are extremely difficult to keep constant. The flight mode changes continuously. However, the designer is mainly interested in the maximum variable stress amplitudes, since these generally carry the greatest risk with respect to fatigue in the structure.

TABLE 1.10

Coefficients of Deformation				Harmonic Components of Load	Partial Induced Velocities	Total Induced Velocities	
Determined from eqs. (8.40)				Determined from Table 1.7	Determined from eqs. (8.6)	Determined from eqs. (8.5)	Determined from the Formulas of Table 1.7
Constant component	a_0	c_0	e_0 g_0	$\bar{p}_0$	$\bar{\lambda}_{0n}$	$\bar{\lambda}_n$ and $\bar{\bar{\lambda}}_n$	$\bar{f}_1^{\lambda}$ and $\bar{\bar{f}}_1^{\lambda}$
First harmonic	a_1, b_1	c_1, d_1	e_1, f_1 g_1, h_1	$\bar{p}_1$ and $\bar{\bar{p}}_1$	$\bar{\lambda}_{1n}$ and $\bar{\bar{\lambda}}_{1n}$	$\bar{\lambda}_n$ and $\bar{\bar{\lambda}}_n$	$\bar{f}_2^{\lambda}$ and $\bar{\bar{f}}_2^{\lambda}$
Second harmonic	a_2, b_2	c_2, d_2	e_2, f_2 g_2, h_2	$\bar{p}_2$ and $\bar{\bar{p}}_2$	$\bar{\lambda}_{2n}$ and $\bar{\bar{\lambda}}_{2n}$	$\bar{\lambda}_n$ and $\bar{\bar{\lambda}}_n$	$\bar{f}_3$ and $\bar{\bar{f}}_3^{\lambda}$
Third harmonic	a_3, b_3	c_3, d_3	e_3, f_3 g_3, h_3	$\bar{p}_3$ and $\bar{\bar{p}}_3$	$\bar{\lambda}_{3n}$ and $\bar{\bar{\lambda}}_{3n}$	$\bar{\lambda}_n$ and $\bar{\bar{\lambda}}_n$	$\bar{f}_4$ and $\bar{\bar{f}}_4^{\lambda}$
Fourth harmonic	a_4, b_4	c_4, d_4	e_4, f_4 g_4, h_4	$\bar{p}_4$ and $\bar{\bar{p}}_4$	$\bar{\lambda}_{4n}$ and $\bar{\bar{\lambda}}_{4n}$	$\bar{\lambda}_n$ and $\bar{\bar{\lambda}}_n$	$\bar{f}_5$ and $\bar{\bar{f}}_5^{\lambda}$
Fifth harmonic	a_5, b_5	c_5, d_5	e_5, f_5 g_5, h_5	$\bar{p}_5$ and $\bar{\bar{p}}_5$	$\bar{\lambda}_{5n}$ and $\bar{\bar{\lambda}}_{5n}$	$\bar{\lambda}_n$ and $\bar{\bar{\lambda}}_n$	$\bar{f}_6^{\lambda}$ and $\bar{\bar{f}}_6^{\lambda}$
Sixth harmonic	a_6, b_6	c_6, d_6	e_6, f_7 g_6, h_6	$\bar{p}_6$ and $\bar{\bar{p}}_6$	$\bar{\lambda}_{6n}$ and $\bar{\bar{\lambda}}_{6n}$	$\bar{\lambda}_n$ and $\bar{\bar{\lambda}}_n$	$\bar{f}_0^{\lambda}$

To compare the results of calculation and experiment, one proceeds in the following manner: Check all flight regimes with abrupt braking of the helicopter before landing, in which the blade stresses were measured. From each flight, select the maximum (over the blade radius) amplitude of stresses set up during the entire landing mode. The field of values of these stresses is hatched in Fig.1.33.

Then, calculate the stresses for regimes with different flying speeds and with an identical rotor angle of attack. The flying speed in the given regime will be characterized by μ. The results of these calculations are given in Fig.1.33. The solid lines

show the dependence of the calculated maximum variable blade stresses on flying speed. Here, we examined regimes with an angle of attack $\alpha = 0$, $\alpha = 30^\circ$ which can be achieved in a regime of abrupt braking, as well as with an angle of attack $\alpha = 50^\circ$ which is possible during steep descent at high vertical speed. The dashed line shows the same dependence for $\alpha = 0$ and $\alpha = -6^\circ$, but without consideration of the variable induced velocity field. In performing these calculations, we investigated flight regimes without overload when the thrust of the rotor was equal to the weight.

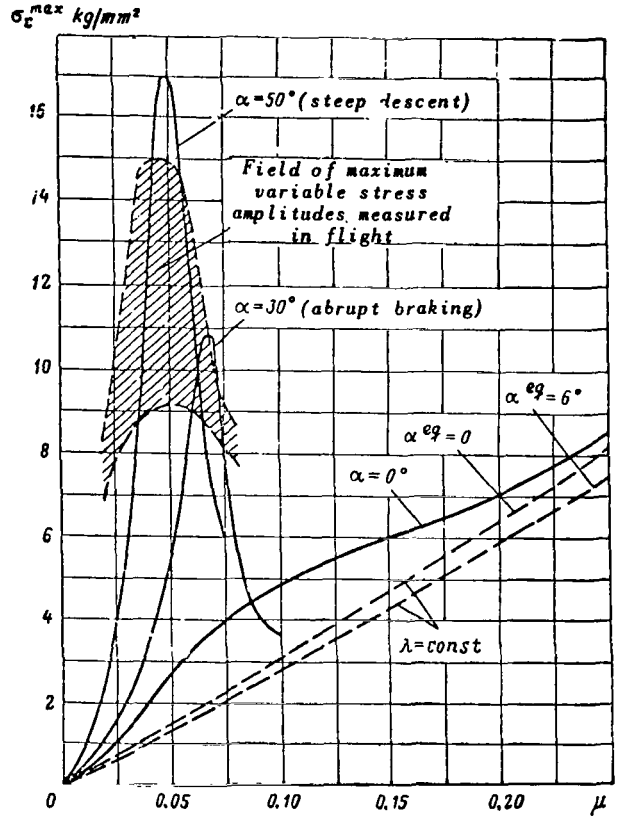

Fig.1.33 Results of Calculating Variable Stresses, with Consideration of a Nonuniform Induced Velocity Field and Comparison with Experiment.

It follows from these calculations, that the greatest increase in variable stresses at low speeds is observed in flight regimes in which the free vortex sheet shed by the blades becomes two-dimensional. When the sheet is farther removed from the rotor plane, the variable stresses decrease greatly and approach, in magnitude, the stresses calculated without consideration of the variable induced velocity field.

A comparison of regimes with identical angles of attack shows a marked increase in variable stresses, in a very narrow range of flying speeds.

The results of the calculation reflect to some degree the pattern of the phenomenon observed in flight. Thus, as in flight, the calculated values of variable stresses increase at low speeds /114 and rise with an increase in rotor angle of attack. However, there is a considerable discrepancy between calculation and experiment.

1. At identical flight regimes, the variable stress amplitudes obtained from calculation were found to be lower than those measured in flight tests.

2. The variable stress amplitudes obtained in calculation and experiment are quantitatively similar when comparing regimes with different angles of attack, using, in the calculation, rotor angles of attack somewhat greater than those occurring in flight.

3. A comparison of flight regimes in which the stress magnitudes obtained

in calculation and experiment coincide shows a substantial difference in their harmonic composition. The content of high harmonics is greater in stresses measured in flight than in calculation. Thus, harmonics from the fourth to the sixth predominate in stresses measured in an abrupt braking regime, which are shown in Fig.1.33. At the same time, stresses of the first, third, and fifth harmonic predominate in variable stresses obtained by calculation. Here, they are listed in the sequence of descending amplitude. As an example, Fig.1.34 shows the distribution of stresses over the blade radius and their harmonic content in a flight regime at $\alpha = 50^{\circ}$ and $\mu = 0.048$.

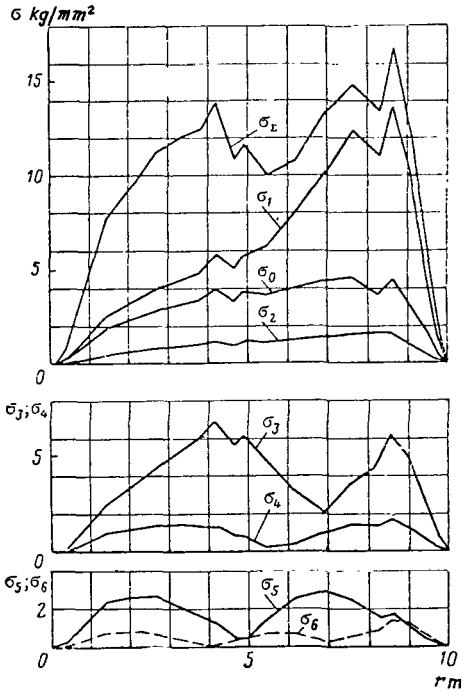

Fig.1.34 Distribution of Stresses over the Blade Radius and their Harmonic Content at Flight Regimes ($\mu = 0.048$ and $\alpha = 50^{\circ}$).

It should be noted that, in the calculation, we investigated a blade with characteristics ensuring the absence of resonance at the operating rpm. Its resonance diagram is shown in Fig.1.35. The operating rpm adopted in the calculation is shown on the resonance diagram by a vertical line. /115

The presented data show that application of the method of calculation, with consideration of moderate induced velocities under the same assumptions as described in Subsection 3, approximates the results of calculation and experiment at low flying speeds. However, further refinements are necessary to obtain results useful for practical purposes.

19. Comparison of Calculation with Experiment at Moderate-Speed Mode

Here, by moderate flying speeds we mean all speeds at which the nonlinearity in the relation $c_y = f(\alpha)$ and the phenomena associated with flow compressibility still have no effect. In many cases, therefore, "moderate flying speeds" comprise the cruising speed of a helicopter; this is especially of interest from the viewpoint of fatigue strength, since the helicopter operates most of the time at this speed.

Figure 1.36 gives a comparison of the amplitudes of variable stresses and their first and second harmonics relative to the rotor rpm, obtained in calculations with stresses measured in the blade at cruising speed for $\mu = 0.25$. The stresses obtained in flight are shown by dots. The dashed line shows stresses calculated with consideration of the assumption that $\lambda = \lambda_{cav} = \text{const}$, and the solid lines with consideration that $\lambda = \text{var}$.

It follows from this diagram that the results from calculation and experiment at cruising speed differ substantially. The total amplitude of calculated stresses amounts to no more than 80% of the values measured in flight. This dis-

crepancy occurs mainly as a consequence of the difference in the values of the second harmonic of the stresses relative to the rotor rpm. The coincidence in the first harmonic of the stresses is rather good. The higher harmonics of stresses in this flight regime are quite small and have no substantial effect on the stress amplitude.

The results presented in Fig.1.36 are typical for flight regimes with μ = = 0.25 and are duplicated on almost all helicopters.

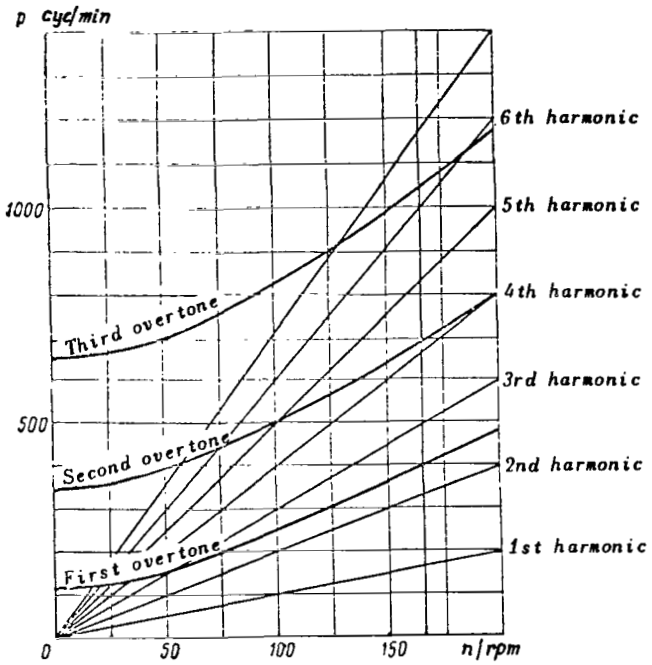

Fig.1.35 Resonance Diagram of Blade.

We also see from Fig.1.36 that consideration of variable induced velocities, in this regime, yields no noticeable refinement in the values of the variable stresses. However, when having to do only with /116 one harmonic - for example, the fourth - it will be found that its value increases greatly when allowance is made for the variable induced velocity field. Therefore, such refinement is highly important if this harmonic is present and determines the magnitude of forces acting on the fuselage and causing it to vibrate.

Above, we have said nothing on the constant component of the bending stresses. Generally their magnitude, obtained on the basis of calculation, proves to be so accurate that it usually is not even measured in flight. Calculation yields more reliable results in this case.

20. Possibilities of Further Refinement of Calculation Results

As follows from the above, a calculation of variable blade stresses still yields no results that could be completely satisfactory to the designer. If, at moderate flying speeds, the results of calculation more or less satisfactorily agree with experiment (although further refinement of the values of the second harmonic is extremely desirable), a rather remote coincidence is observed at low flying speeds.

In this connection, it is highly important to establish the direction in which further refinement of the results is sought. We can propose the following in this respect.

In calculating variable stresses at low flying speeds, the most important refinements comprise:

consideration of the effect of intrinsic induced velocities (abandonment of the "steady-flow hypothesis");

use of the vortex theory which takes into account deformations of the free vortex system (abandonment of the assumption that vortices are shed from a rotor at a constant speed equal to the average disk downwash λ_{oav}). /117

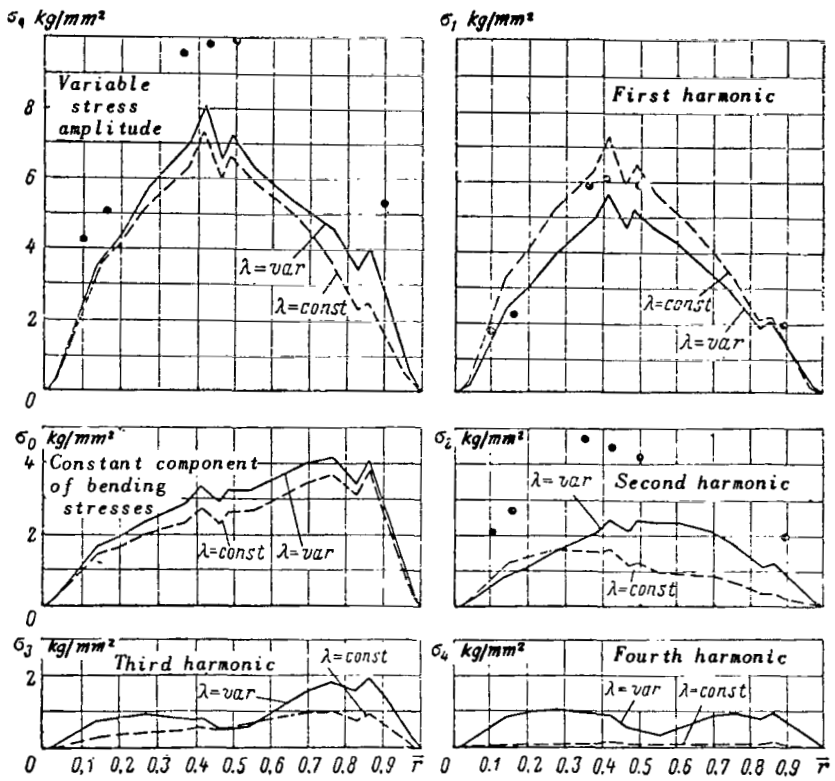

Fig.1.36 Comparison of the Values of Variable Stresses, Calculated under Consideration of a Variable Induced Velocity Field, with Stresses Measured in Flight.

In calculating variable stresses at moderate flying speeds, where the main discrepancy is observed in values of the second harmonic of the stresses, application of the vortex theory for a finite number of blades and introduction into the calculation of the effect of both extrinsic and intrinsic induced velocities would constitute a highly useful refinement.

In cases of a blade of low rigidity in torsion or of excitation by the external forces of a rotor vibration mode coinciding with the flutter mode at a frequency close to the frequency of flutter, a consideration of torsional blade deformations may yield noticeable refinements. The method of such a calculation was presented in Section 7, Chapter IV of Vol.I.

Often, in calculating variable stresses at cruising speed (just as at maximum speed), a consideration of the nonlinear relations $c_y = f(\alpha)$ and of flow compressibility may lead to substantial refinement, a point to be discussed further in the next Section.

Section 9. Calculation of Blade Bending Stresses, with Consideration of the Nonlinear Dependence of Aerodynamic Coefficients on Profile Angle of Attack and Mach Number

/118

1. Flight Regimes

Consideration of the nonlinear dependence of aerodynamic coefficients on the profile angle of attack is necessary in flight regimes in which these angles attain such significant values that it no longer is possible to use linear dependence [eq.(8.1)]. Such regimes pertain to flights at speeds close to maximum and to low-speed modes in which, as a consequence of high blade loading and excessive nonuniformity of the induced velocity field at individual segments of the disk area, the angles of attack enter the nonlinear domain of the dependence $c_y = f(\alpha)$. In a number of cases, consideration of these nonlinearities is necessary also in other regimes, including the cruising-speed mode.

In general, consideration of phenomena associated with flow compressibility is necessary at high flying speeds for helicopters having rotors with high blade tip speeds.

2. Determination of Aerodynamic Loads

In Section 8, we had stipulated that the inflow angle to the blade profile Φ is a small quantity; therefore, the approximate equation (8.23) was used in determining this angle. Here, we stipulate that the angle Φ can vary within limits of 360°; therefore, its magnitude will be calculated by means of the formula

$$\Phi = \tan^{-1}\frac{U_y}{U_x}, \tag{9.1}$$

where the values of U_x and U_y are determined by the expressions

$$\left.\begin{aligned} U_x &= \omega R(\bar{r} + \mu\sin\psi);\\ U_y &= \omega R\left(\lambda - \mu\cos\psi\beta - \frac{1}{\omega R}\dot{y}\right). \end{aligned}\right\} \tag{9.2}$$

Equations (9.2) coincide with the formulas used in Section 8. This means that, in their derivation, it was assumed that blade displacements are small so that we can put

$$\left.\begin{aligned} \sin\beta &\cong \beta;\\ \cos\beta &\cong 1. \end{aligned}\right\} \tag{9.3}$$

The value of the angle Φ determined from eq.(9.1), when carrying out the calculation on a digital computer, is usually read out only in the range $\mp 90^\circ$. This must be taken into account in calculating the angle of attack by means of the formula

$$\alpha = \varphi + \Phi. \tag{9.4}$$

Therefore, we can use eq.(9.1) only at $U_x > 0$. If $U_x < 0$, then, as follows from Fig.1.37, we have

$$\Phi = \pi + \tan^{-1}\frac{U_y}{U_x}. \tag{9.5}$$

The inflow angle determined by eqs.(9.1) and (9.5) varies in the range $-90^\circ < \Phi < 270^\circ$.

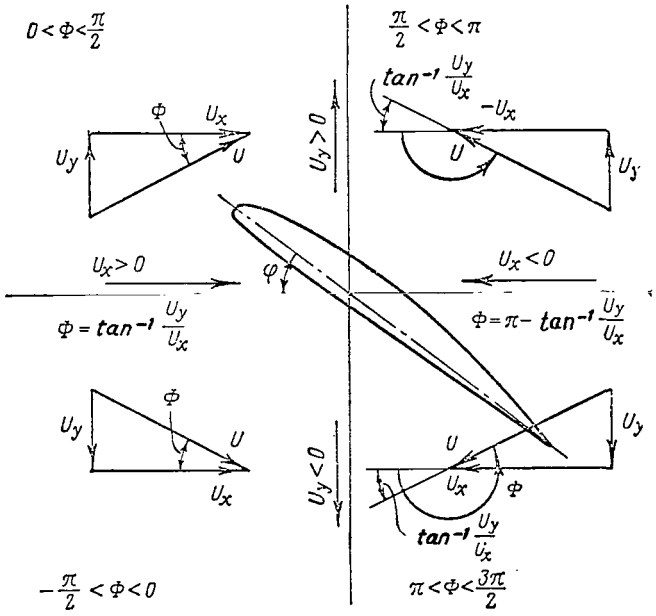

Fig.1.37 Diagram of Flow Past a Profile for Determining the Inflow Angle Φ.

If we assume that the blade setting can be changed from $\varphi = -15^\circ$ to $\varphi = +45^\circ$, then the aerodynamic coefficients should be prescribed within limits of the variation of the angle of attack from -105° to $+315^\circ$. /119

The Mach number needed for determining the aerodynamic coefficients is calculated by means of the formula

$$M = \frac{U}{a_{s\sigma}}. \tag{9.6}$$

Here, $a_{s\sigma}$ is the velocity of sound:

$$a_{s\sigma} = \sqrt{\frac{kp}{\varrho}}, \tag{9.7}$$

where k is the adiabatic exponent and p is the atmospheric pressure.

The aerodynamic coefficients required for the calculation are determined on the basis of wind-tunnel tests with the profile exposed to a circular air stream. In computer calculations, the program compiled by engineer M.N.Tishchenko for determining the aerodynamic coefficients is highly useful. In this program, the effect of the Mach number M on the aerodynamic coefficients is taken into account only in the range of profile angles of attack from $\alpha = -2^\circ$ to $\alpha = +15^\circ$.

In the remaining range of angle-of-attack variation, the aerodynamic coefficients are considered as independent of M.

The dependence of the lift coefficient c_y on the angle of attack α for the profile NACA-230, which was adopted in one of the versions of this program, is shown in Fig.1.38 as a typical example.

/120

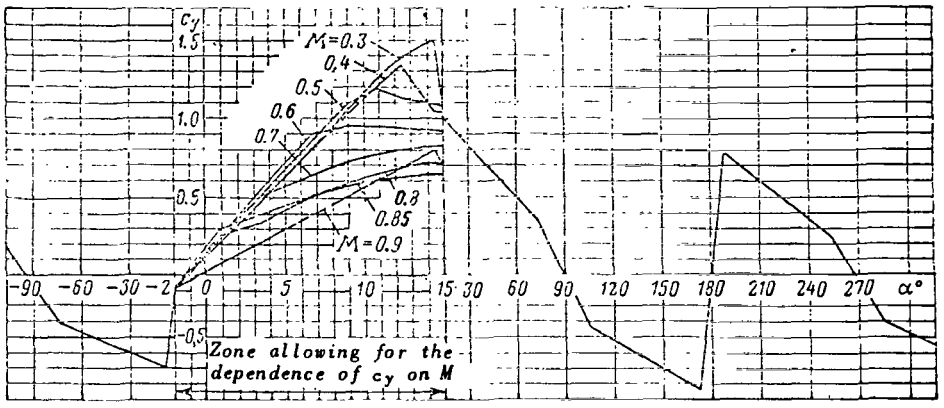

Fig.1.38 Dependence $c_y = f(\alpha, M)$ Adopted in the Program.

If the lift coefficient c_y and the drag coefficient c_x are known, then the aerodynamic forces acting in the flapping plane T and in the plane of rotation Q can be determined from the formulas

$$\left.\begin{aligned} T &= \frac{1}{2}(c_y U_x + c_x U_y)\rho b U; \\ Q &= \frac{1}{2}(c_x U_x - c_y U_y)\rho b U. \end{aligned}\right\} \qquad (9.8)$$

3. Method of Blade Calculation as a System whose Motion is Coupled by Prescribed Vibration Modes

As above in Section 8, the calculation of elastic blade vibrations reduces to solving the differential equation

$$[EIy'']'' - [Ny']' + m\ddot{y} = T, \qquad (9.9)$$

where, with the adopted assumptions, the aerodynamic force T is a nonlinear function of the displacements of the blade elements y.

In this case, it is convenient in solving eq.(9.9) to use a method where the blade motion in time is found by numerical integration of ordinary differential equations obtained from eq.(9.9) by Galerkin's method. In this approach to the problem, these equations are coupled only over the aerodynamic forces. Therefore, if - at some arbitrary time - the aerodynamic forces can be calculated,

then the blade deformations with respect to each vibration mode are determined independently, provided these modes are orthogonal.

Let us represent the blade vibration mode as the sum of a certain number of natural vibration harmonics of the blade:

$$y=\sum_j \delta_j y^{(j)}, \tag{9.10}$$

where

$j = 0, 1, 2, \ldots, j_h$ (j_h being the number of the higher overtone of natural blade vibrations taken into account in the solution);

$y^{(j)}$ = mode of the j-th overtone of natural blade vibrations normed such that $y_R^{(j)} = R$ at $\bar{r} = R$;

δ_j = coefficients determining the magnitude of blade deformation with respect to the j-th overtone.

As above, we will designate the coefficients δ_j as the coefficients of blade deformation. The values of δ_j are functions of time. /121

The coefficients of blade deformation δ_j, in the present method of calculation, are taken as generalized coordinates of the system. Determination of the law of their time-variance constitutes the content of the calculation.

After twice differentiating eq.(9.10) with respect to time, we obtain

$$\left.\begin{aligned} \dot{y}&=\sum_j \dot{\delta}_j y^{(j)};\\ \ddot{y}&=\sum_j \ddot{\delta}_j y^{(j)}. \end{aligned}\right\} \tag{9.11}$$

On substituting eqs.(9.10) and (9.11) into eq.(9.9) and successively multiplying all terms of eq.(9.9) by $y^{(j)}$ (where $j = 0, 1, 2, \ldots, j_h$) and then integrating over the blade radius, eq.(9.9), by virtue of the orthogonality of the natural vibration modes, will decompose into $j_h + 1$ independent equations of the form

$$m_j\ddot{\delta}_j + C_j\delta_j = A_j. \tag{9.12}$$

Here,

$$\left.\begin{aligned} C_j&=\int_0^R EI\,[(y^j)'']^2\,dr+\int_0^R N\,[(y^j)']^2\,dr;\\ m_j&=\int_0^R m\,(y^j)^2\,dr;\\ A_j&=\int_0^R Ty^{(j)}dr. \end{aligned}\right\} \tag{9.13}$$

As mentioned above in Subsections 1 and 2 of Section 7, the quantities entering eq.(9.12) have a well-defined physical meaning. The quantity C_j, known as the generalized blade rigidity in deformation with respect to the mode of the j-th overtone, represents also double the potential energy accumulated by the blade in bending in a centrifugal force field with respect to the mode of the same harmonic. The quantity m_j is the equivalent blade mass reduced to its tip. It is equal also to double the kinetic energy of blade vibrations with respect to the mode of the j-th overtone with a frequency p = 1. The integral A_j on the right-hand side of eq.(9.12) represents the generalized force and is equal to double the work of aerodynamic forces in displacements caused by blade deformations at the j-th overtone.

It is known that the frequency of the j-th overtone of natural blade vibrations can be determined from the formula

$$p_j = \sqrt{\frac{C_j}{m_j}}.$$

Therefore, it is convenient to transform eqs.(9.12), relating all terms to values of m_j. These can then be written as

$$\ddot{\delta}_j + p_j^2 \delta_j = \frac{A_j}{m_j} \tag{9.14}$$

or

$$\ddot{\delta}_j + p_j^2 \delta = \frac{\delta_{st}^{(j)}}{p_j^2}, \tag{9.15}$$

where $\delta_{st}^{(j)}$ is the coefficient of quasi-static blade deformations with respect to the mode of the j-th overtone of aerodynamic forces T (see Sect.7, Subsect.7).

As follows from eqs.(9.8) and (9.2), the magnitude of the aerodynamic force varies with respect to the blade azimuth and depends on the blade deformations or, more precisely, on the values of $\dot{y}$ and β determining the magnitude of the relative flow velocity U_y. Therefore, for calculating the aerodynamic forces, the values of $\dot{y}$ and β must be predetermined by means of /122

$$\left.\begin{aligned} \dot{y} &= \sum_j \dot{\delta}_j y^{(j)}; \\ \beta &= \sum_j \delta_j \beta^{(j)}, \end{aligned}\right\} \tag{9.16}$$

where $\beta^{(j)}$ is the angle of rotation of the elastic blade axis relative to the plane of rotation, corresponding to the normed natural vibration mode of the i-th overtone.

If the coefficients of deformation δ_j and their first derivatives $\dot{\delta}_j$ pertaining to some azimuthal blade position or to some time t are known, the calculation can be performed in the following sequence.

First, determine the values of $\dot{y}$ and β from eqs.(9.16). After this, derive the components of the relative flow velocity U_y and U_x as well as the velocity U from eqs.(9.2):

$$U=\sqrt{U_y^2+U_x^2}. \tag{9.17}$$

Of course, to determine the velocity U_y it is also necessary to know the relative disk flow ratio λ which, in the general case, is a variable changing with respect to blade radius and azimuth. Determination of the quantity λ will be taken up in Subsection 5 of this Section.

If the velocities U_y and U_x are known, then the inflow angle Φ can be determined from eqs.(9.1) and (9.5), and the profile angle of attack α from eq.(9.4). The Mach number is determined by eq.(9.6). These data suffice for determining the aerodynamic coefficients for circular blowing of the profile and hence for obtaining the aerodynamic forces T.

Thus, at the azimuth in question the blade deformation, rate of deformation, and the aerodynamic forces T acting on the blade are known. Consequently, on the basis of eq.(9.14) it becomes possible to derive also the coefficients $\ddot{\delta}_j$ that determine the accelerations of the blade elements:

$$\ddot{\delta}_j=\frac{A_j}{m_j}-p_j^2\delta_j. \tag{9.18}$$

Next, by numerical integration of eqs.(9.14) with respect to time we can determine the new values of the coefficients of blade deformation δ_j and their first derivatives $\dot{\delta}_j$ at the next blade azimuth after a certain time Δt, determined by the integration step. The change from the time t at which the coefficients of deformation δ_j and their first derivatives $\dot{\delta}_j$ and second derivatives $\ddot{\delta}_j$ are known to the next time $t + \Delta t$ can be accomplished by various conventional methods of numerical integration of equations.

As a typical example, we are giving the formulas for such a change, derived from the Euler method:

$$\left.\begin{aligned}\delta_{t+\Delta t}&=\delta_t+\Delta t\dot{\delta}_t;\\ \dot{\delta}_{t+\Delta t}&=\dot{\delta}_t+\Delta t\ddot{\delta}_t.\end{aligned}\right\} \tag{9.19}$$

The characteristics of various methods of numerical integration will be discussed in greater detail below. In particular, it will be shown that the Euler method represented by eqs.(9.19) is not suitable for calculating elastic blade vibrations. /123

Numerical integration of eqs.(9.14) with respect to time permits determining the deformation coefficients and their first derivatives at a new blade azimuth. After determining the new values of aerodynamic forces at this azimuth we can also derive the new coefficients $\ddot{\delta}_j$. This process can be continued until

the coefficients of deformation are determined at all blade azimuths in one rotation of the rotor.

If the initial values of the coefficients δ_j and $\dot{\delta}_j$ are arbitrarily prescribed, an integration of the equations over one rotor revolution will cause the values of δ_j and $\dot{\delta}_j$, obtained by integration at the same azimuth, to differ from the values taken arbitrarily at the initial time. However, if the blade motion is stable, the numerical integration can be continued. Then, after several revolutions of the rotor the motion will be established and will be repeated in each subsequent revolution. This steady motion is the sought solution of eq.(9.9).

Thus, the method of calculation presented here is the solution of the Cauchy problem, with integration of the equations of motion of the blade with respect to time at given initial conditions.

4. Mathematical Formulas for a Blade Model with Discrete Parameters

In practical calculations, a rotor blade is usually conceived as a weightless beam with attached concentrated loads simulating its mass. The aerodynamic forces acting on the blade also can be conveniently represented as a series of concentrated forces. Let us assume that aerodynamic forces are applied at the attachment points of concentrated loads as though a separate flap with a certain area S_i were attached to each load (see Sect.1, Subsect.9). Then, the aerodynamic forces can be determined by formulas analogous to eq.(9.8):

$$T_i = \frac{1}{2}(c_y U_{x_i} + c_x U_{y_i}) \varrho S_i U_i; \tag{9.20}$$

$$Q_i = \frac{1}{2}(c_x U_{x_i} - c_y U_{y_i}) \varrho S_i U_i, \tag{9.21}$$

where the subscript i denotes all quantities pertaining to the blade section of number i (see Fig.1.51). The size of the area of the concentrated flap S_i is determined by eq.(1.2).

For a rotor blade which is not represented as a beam with distributed parameters but as a model with a finite number of elastically coupled concentrated masses, equations analogous to eq.(9.14) can be derived. However, the quantities m_j and A_j entering the equations are not defined as integrals but as sums of the form

$$\left.\begin{aligned} m_l &= \sum_j m_i (y_i^{(j)})^2; \\ A_l &= \sum_i T_i y_i^{(j)}, \end{aligned}\right\} \tag{9.22}$$

where

m_i = values of the concentrated mass of the system;

$y_i^{(j)}$ = values determining the natural vibration mode of the j-th overtone; here, the mode of natural vibrations should be represented by a series of discrete values of the ordinates y_i determining /124 the displacements of the i-th mass of the blade;

T_i = discrete values of aerodynamic forces determined by eq.(9.20).

The calculation of a blade model with discrete parameters differs in no respect from the calculation of a model with parameters continuously distributed over the blade length. However, in digital computer calculations it is much more convenient to investigate a model with discrete parameters.

5. Consideration of a Variable Induced Velocity Field

Application of the calculation method presented above does not preclude the possibility of considering a variable induced velocity field represented by the relative disk flow ratio λ in eq.(9.2). For this, in determinations of aerodynamic forces acting on the blade at the time t in question, the integrodifferential equation of the vortex rotor theory must be solved [see eq.(5.29) in Sect.5, Chapt.II of Vol.I].

Reduction of the problem of elastic vibrations of a blade to the Cauchy problem, at determination of blade motion beginning with some initial time, leads to appreciable simplifications in solving the integrodifferential equations of the vortex theory.

When the rotor advances one step with respect to azimuth, vortices that have to do only with variations in circulation over the length of this particular step will be shed by the blade. All vortices shed from the blade at prior instants of time are merely displaced in space but show no change in their circulation. Therefore, in solving the integrodifferential equation pertaining to some definite time, it is only necessary to find the relation between circulation of the bound vortices and the vortices shed from the blade during its shift after the last integration step. The magnitudes of circulation of all remaining free vortices are already known in this case and are determined by the entire history of the process of motion.

To simplify the problem, we can take at the initial time some schematic model of a vortex system consisting, for example, only of rotor vortices shed from the blade tip with constant circulation over the length. It is assumed that, at the start of calculation, no free vortices can exist since the average induced velocity through the rotor is equal to zero.

The method discussed here yields the maximum accuracy possible in the calculation of induced velocities for a rotor scheme with a finite number of blades. However, use of this scheme in other methods of calculation of elastic blade vibrations will lead to serious complications.

Numerous difficulties are encountered in using calculation methods for induced velocities based on a rotor scheme with an infinite number of blades, as applied to the method of calculation discussed in this Section. Thus, the method of successive approximations generally appears simplest. However, if we use a

method in which the induced velocities are calculated after completing the calculation of blade motion over each revolution of the rotor (when the values of the aerodynamic forces T are known at all blade azimuths and radii so that the values of the circulation at the same point can be determined) and if we introduce these velocities into the calculation of aerodynamic forces during the next revolution of the rotor, it will be found that such a solution process does /125 not converge. Consequently, different methods bypassing these difficulties must be used; as a rule, this leads to appreciable complications which ultimately may prove to be unwarranted.

6. Characteristics of Numerical Integration of Differential Equations of Elastic Blade Vibrations

For a successful calculation of elastic blade vibrations, it is of importance to select the most advantageous method of numerical integration, i.e., a method of high accuracy and requiring a minimum number of operations for solving the differential equations of motion. Most of the machine time in calculation is used for this operation. Its major portion is spent on determining the external forces. Therefore, the computer time is determined mainly by the number of times the equation of motion must be handled. This number is determined by the chosen method and integration step. The smaller the step, the longer the calculation.

An analysis shows that, when seeking a periodic solution of the problem of elastic vibrations, the required integration step varies within very wide limits depending on the type of numerical integration method used. Poor results are obtained by many conventional numerical integration methods, such as the above-mentioned Euler method [see eqs.(9.19)]. The well-known method of solution by Taylor series was found to be just as unsuitable for the problem in question. This method leads to the following formulas for the change-over from the time t to the time t + Δt:

$$\left.\begin{aligned}\delta_{t+\Delta t} &= \delta_t + \Delta t\dot{\delta}_t + \frac{1}{2}\Delta t^2\ddot{\delta}_t;\\ \dot{\delta}_{t+\Delta t} &= \dot{\delta}_t + \Delta t\ddot{\delta}_t.\end{aligned}\right\} \tag{9.23}$$

The value of $\ddot{\delta}_{t+\Delta t} = f(\delta_{t+\Delta t}, \dot{\delta}_{t+\Delta t})$ is determined from a differential equation. Here, Δt is the integration step.

The widely known Runge-Kutta and Adams numerical integration methods are more suitable for the given case but still quite inconvenient.

The best method of checking the applicability of a given numerical integration method to the solution of the problem of blade vibrations is a numerical solution of the equation

$$\ddot{\delta} + 2\bar{n}\dot{\delta} + \delta = \sin \nu t, \tag{9.24}$$

describing vibrations of some mechanical model representing a mass attached to

a spring with a damper (see Fig.1.39).

The rotor blade can be conceived as a set of a certain number of such models, of different natural frequencies and different damping coefficients corresponding to the frequencies and damping coefficients of different harmonics of blade vibration.

At relatively small steps Δt, the use of Taylor series for an integration of eq.(9.24) leads to a solution representing a vibratory process whose amplitude tends to some definite value differing from the exact analytic value by a quantity of the calculation error. With an increase in the integration step, the solution diverges at certain definite values of Δt. If the solution does not diverge, the greatest error arises in resonance, i.e., at $\nu = 1$. Therefore, /126 we will now estimate the error with respect to this most severe case.

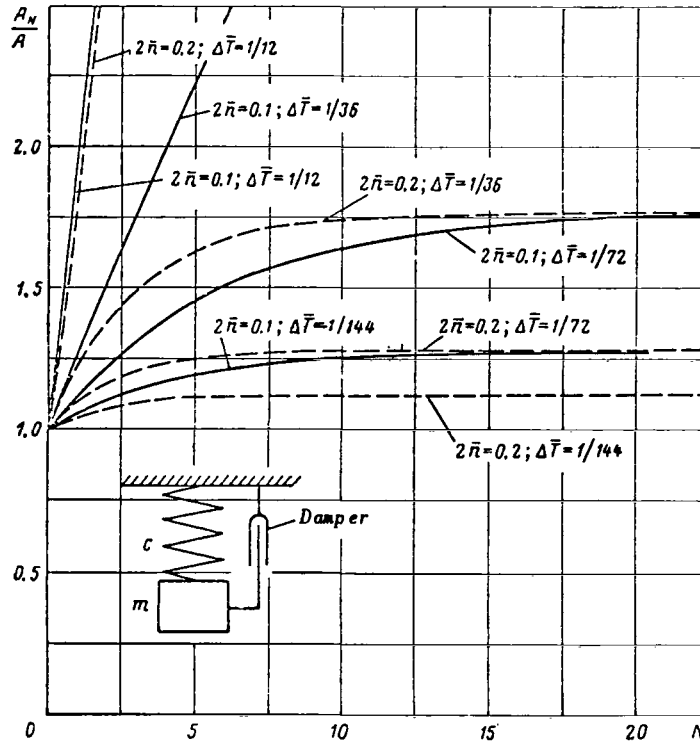

Fig.1.39 Effect of Relative Integration Steps on Accuracy of Solution.

Figure 1.39 shows the change in vibration amplitude values obtained as a result of the numerical solution of eq.(9.24) by means of Taylor series. The exact analytic values of δ_0 and $\dot{\delta}_0$ were taken as the initial values. Cases with relative damping coefficients equal to $2\bar{n} = 0.1$ and $2\bar{n} = 0.2$ and different integration steps were investigated.

The maximum values of δ obtained during the integration period with the ordinal number N were taken as the vibration amplitude A_N at this period and referred to the analytic value of amplitude

$$A=\frac{1}{2\bar{n}}. \tag{9.25}$$

It follows from Fig.1.39 that, during the numerical integration, the solution diverges from the exact analytic curve. A steady vibratory process has an amplitude always greater than the exact value. The larger the relative integration step $\Delta\bar{T}$, the greater will be the error. Here, we will call the relative integration step the quantity

$$\Delta\bar{T}=\frac{\Delta t}{T}, \tag{9.26}$$

where

Δt = integration step with respect to time;
T = vibration period of the model.

The magnitude of the relative damping coefficient $\bar{n}$ also noticeably affects the accuracy of the solution. It follows from the calculations that, to obtain a satisfactory accuracy, the relative integration step should be of the order of 1/200 of the oscillation period or even smaller. /127

In a numerical integration of equations describing elastic vibrations, it is important not only to secure the required accuracy but also to use an integration step in which there would be no divergent solution.

The determination of the limit step of integration, at which the solution will still be stable, can be accomplished in the following manner:

Equations (9.23) and (9.24) can be regarded as some system of difference equations. To determine the stability of the solution, we will discuss a homogeneous system of difference equations [without the right-hand side of eq.(9.24)].

Equations (9.23) are written in a somewhat more general form, introducing some constant coefficient $\varkappa$:

$$\left.\begin{aligned}\delta_{t+\Delta t}&=\delta_t+\Delta t\dot{\delta}_t+\varkappa\Delta t^2\ddot{\delta}_t;\\ \dot{\delta}_{t+\Delta t}&=\dot{\delta}_t+\Delta t\ddot{\delta}_t.\end{aligned}\right\} \tag{9.27}$$

At $\varkappa$ = 0, these formulas coincide with the Euler equations (9.19) while, when $\varkappa=\frac{1}{2}$, they coincide with the Taylor equations (9.23).

From eq.(9.24) for the case of $\sin\nu t = 0$, we derive the value of $\ddot{\delta}_t$; substituting this into eq.(9.27), we obtain the following system of difference equations:

$$\left.\begin{aligned}\delta_{t+\Delta t}&=(1-\varkappa\Delta t^2)\,\delta_t+(\Delta t-2\bar{n}\varkappa\Delta t^2)\,\dot{\delta}_t;\\ \dot{\delta}_{t+\Delta t}&=-\Delta t\delta_t+(1-2\bar{n}\Delta t)\,\dot{\delta}_t.\end{aligned}\right\} \tag{9.28}$$

The solution of this system will be sought in the form of

$$\left.\begin{aligned}\delta_t&=A\alpha^n;\quad \delta_{t+\Delta t}=A\alpha^{(n+1)};\\ \dot{\delta}_t&=B\alpha^n;\quad \dot{\delta}_{t+\Delta t}=B\alpha^{(n+1)}.\end{aligned}\right\} \tag{9.29}$$

Substituting eq.(9.29) into the system of homogeneous difference equations (9.28), we obtain the characteristic equation relative to α. From this equation, we find α:

$$\alpha=1-\Delta t\left(\bar{n}+\frac{1}{2}\varkappa\Delta t\right)\mp\Delta t\sqrt{\left(\bar{n}+\frac{1}{2}\varkappa\Delta t\right)^2-1}. \tag{9.30}$$

To keep the values of δ_t from approaching infinity as $n\to\infty$, the condition

$$|\alpha|\leqslant 1$$

is necessary.

At relatively small Δt and $\bar{n}$, the value of α - as follows from eq.(9.30) - is a complex quantity.

After determining the modulus α, we obtain the condition of a nondivergent solution:

$$\left|\sqrt{1+\Delta t^2-2\Delta t\left(\bar{n}+\frac{1}{2}\varkappa\Delta t\right)}\right|\leqslant 1 \tag{9.31}$$

or

$$\Delta t-2\left(\bar{n}+\frac{1}{2}\varkappa\Delta t\right)\leqslant 0. \tag{9.32}$$

Hence, /128

$$\Delta t\leqslant\frac{2\bar{n}}{1-\varkappa}. \tag{9.33}$$

If the integration step is related to the oscillation period of the system T equal to 2π in the examined simplified model, we obtain the condition of a nondivergent solution

$$\overline{\Delta T}\leqslant\frac{\bar{n}}{\pi(1-\varkappa)}. \tag{9.34}$$

Then, for the Euler method at $\varkappa = 0$, we find that the solution is possible at

$$\overline{\Delta T} \leqslant \frac{\bar{n}}{\pi}, \tag{9.35}$$

and, for the Taylor method at $\varkappa = \frac{1}{2}$,

$$\overline{\Delta T} \leqslant \frac{2\bar{n}}{\pi}. \tag{9.36}$$

Thus, in order to avoid a divergent solution, a step smaller by a factor of 2 is needed in the Euler method than in the Taylor method. Both methods give a divergent solution no matter how small the integration step, provided that the relative damping coefficient n is equal to zero.

With an increase in $\bar{n}$ and Δt, the value of α becomes a real number. In this case, the value of α can never be greater than unity but may be a negative quantity greater than unity in absolute value.

The condition that $\alpha < 1$ is observed if

$$(2\varkappa - 1)\Delta t^2 + 4\bar{n}\Delta t - 4 > 0. \tag{9.37}$$

Hence, instability of the solution for the Euler method at $\varkappa = 0$ will occur at $\Delta\bar{T} > \frac{\bar{n} - \sqrt{\bar{n} - 1}}{\pi}$ if and only if $\bar{n} > 1$, whereas for the Taylor method ($\varkappa = \frac{1}{2}$) this happens at $\Delta\bar{T} \frac{1}{2\pi\bar{n}}$. However, these conditions are usually covered by the more rigorous condition (9.36).

If these results are transferred to a system representing a rotor blade, then the magnitude of the relative step must be selected on the basis of the period of the highest harmonic of vibrations possible in the system, since this will result in the smallest value of the required step at which numerical integration is possible.

Figure 1.40 shows the typical character of variation in the natural vibration period of a blade T_ψ and in the relative coefficient of aerodynamic damping $\bar{n}$ with respect to the number of the harmonic of the vibration j. The value of the vibration period is calculated in degrees with respect to the blade radius. The same diagram shows the dependence of $\sqrt{p_j}$ on the number of the harmonic; p_j is the frequency of the j-th overtone of natural blade vibrations calculated in oscillations per minute. In the range of lower harmonics, the quantity p_j changes greatly with any variation in rotor rpm from n = 0 to the operating rpm $n = n_{op}$.

If we limit ourselves in the calculation to a consideration of only the first four harmonics of natural vibration, including the fundamental, which

usually is sufficient for obtaining the accuracy required in practice, then the integration step must be selected on the basis of the period and coefficient of relative damping of the highest harmonic of natural vibration, the third for this system. /129

If we assume that the vibration period with respect to the third harmonic cannot be shorter than 45° with respect to the rotor azimuth and that the relative coefficient of aerodynamic damping will not be lower than n = 0.07, then - to obtain a nondivergent solution - the integration step in conformity with eq.(9.36) should be less than 2° and in conformity with eq.(9.35) less than 1° with respect to azimuth. The step would have to be shortened much further to obtain satisfactory accuracy (Fig.1.39).

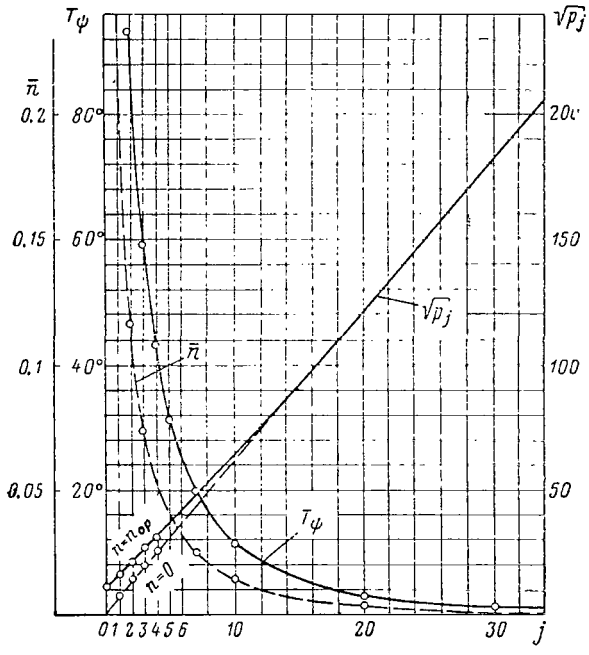

Fig.1.40 Dependence of Vibration Period T_ψ of the Relative Coefficient of Aerodynamic Damping $\bar{n}$ on the Number of the Natural Vibration Overtone j.

This example shows that an application of the above integration methods to blade calculations gives unsatisfactory results. For this particular example, the Runge-Kutta and Adams methods permit using an integration step of the order of 3°, but they are not too suitable since they require storage of an excessive number of variables, calculated for the preceding instants of time, in the computer memory.

Good results are obtained by a previously mentioned integration method (Chapt.IV, Sect.7 in Vol.I) with expansion of the solution in a Taylor series and with recalculation of each integration step. This method is completely suitable in applications to the problem in question and is being used at present in numerous computer programs.

The change-over from the time t to the time t + Δt is accomplished by this numerical integration method, in the following sequence:

First rough calculation: /130

$$\delta^{I}_{t+\Delta t}=\delta_t+\Delta t\dot{\delta}_t+\frac{1}{2}\Delta t^2\ddot{\delta}_t;$$

$$\dot{\delta}^{I}_{t+\Delta t}=\dot{\delta}_t+\Delta t\ddot{\delta}_t.$$

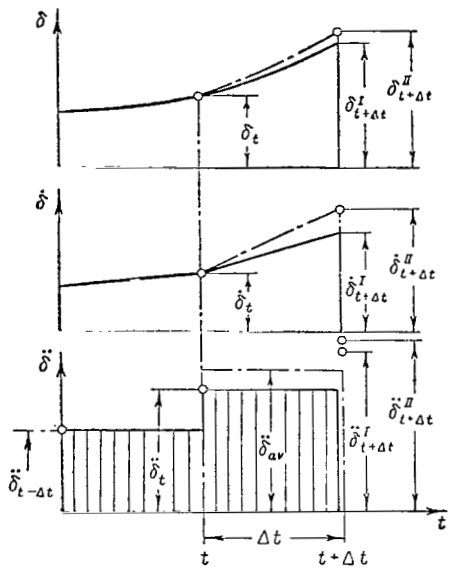

Fig.1.41 Dependence of the Variable δ and its First and Second Derivatives with Respect to Time.

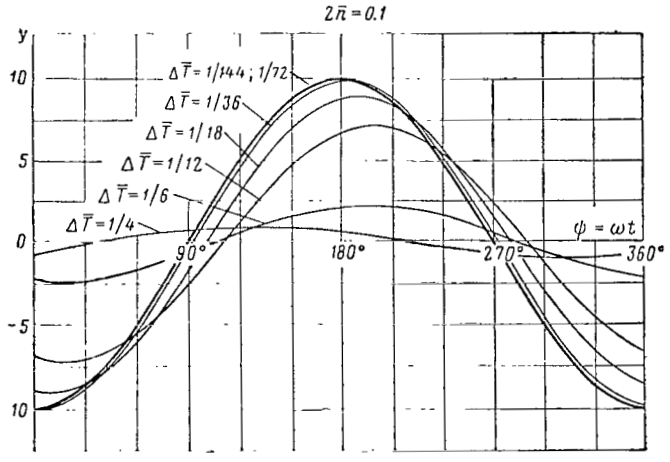

Fig.1.42 Results of Numerical Solution of Eq.(9.26) as a Function of the Relative Integration Step.

At a relative step of

Here, $\ddot{\delta}^{I}_{t+\Delta t} = f(\delta^{I}_{t+\Delta t}, \dot{\delta}^{I}_{t+\Delta t})$ is determined from a differential equation. Then, $\ddot{\delta}_{av}$ is obtained from the formula

$$\ddot{\delta}_{av} = \frac{1}{2}(\ddot{\delta}_t + \ddot{\delta}^{I}_{t+\Delta t}). \qquad (9.38)$$

Recalculation:

$$\delta^{II}_{t+\Delta t} = \delta_t + \Delta t \dot{\delta}_t + \frac{1}{2}\Delta t^2 \ddot{\delta}_{av};$$

$$\dot{\delta}^{II}_{t+\Delta t} = \dot{\delta}_t + \Delta t \ddot{\delta}_{av};$$

Here, $\ddot{\delta}^{II}_{t+\Delta t} = f(\delta^{II}_{t+\Delta t}, \dot{\delta}^{II}_{t+\Delta t})$ is determined from a differential equation.

The values of $\delta^{II}_{t+\Delta t}$, $\dot{\delta}^{II}_{t+\Delta t}$, and $\ddot{\delta}^{II}_{t+\Delta t}$ are considered final for the time t + Δt.

The change of variable δ and its first and second derivatives with respect to time, determined in conformity with eqs.(9.38), is shown in Fig.1.41.

Figure 1.42 gives the steady solution of eq.(9.24) obtained as a result of numerical integration by this method. The solution is given for different values of the integration step. The heavy line shows the exact analytic solution.

At a relative step of 1/72 and less, a numerical integration yields a solution almost exactly coinciding with the analytic solution. At a larger relative step, a substantial difference occurs between the exact and numerical solution, which is apparent from Fig.1.42.

$$\Delta\bar{T} \geqslant \frac{1}{\pi} \qquad (9.39)$$

the solution diverges.

To preclude the possibility of divergent solutions in the system, the integration step should not be greater than about 1/3 of the period of the highest vibration harmonic of the system, which has the smallest period. An important advantage of this method lies in the fact that the limit integration step is practically independent of the magnitude of the relative damping coefficient.

A comparison of the limit steps $\Delta\psi_{lim}$ for the examined integration methods as a function of the number of the higher harmonic j_h of natural vibration of the system is shown in Fig.1.43 for a blade with the parameters shown in the diagram of Fig.1.40.

If we restrict ourselves to a consideration of only the first four harmonics of natural vibration, then in conformity with eq.(9.39) it suffices to have an integration step of about 15° with respect to the blade azimuth, i.e., by a factor of about 7 greater than in the same method without recalculation, in order to obtain a nondivergent solution.

The results of solving eq.(9.24) permit an approximate determination of the error in the amplitude values corresponding to different harmonics of blade vibration as a function of the integration step used. By error, we mean here the difference between the exact analytic value of the vibration amplitude and the value obtained as a result of numerical integration. This difference is always positive in integrations by means of a Taylor series with recursive calculation. This means that the numerical solution always leads to underestimating the vibration amplitude. /132

The calculation errors, in percentage of the exact values of the amplitude for different blade vibration harmonics with ordinary parameters as a function of the step used in an integration by Taylor series with recalculation are given in Table 1.11.

TABLE 1.11

Number of Overtone	Calculation Errors in Percentage of Exact Value of Amplitude for Integration Step in Degrees					
	0.3	1.0	2.5	5	10	20
Fundamental	<0.1%	<0.1%	<0.1%	0.3%	5%	25%
1st	<0.1%	<0.1%	0.4%	6%	12%	50%
2nd	<0.1%	0.3%	5%	25%	45%	80%
3rd	<0.1%	0.4%	15%	30%	75%	
5th	<0.1%	2%	20%	70%		
10th	1%	30%	90%			
20th	40%	Divergent solution				
30th	90%					

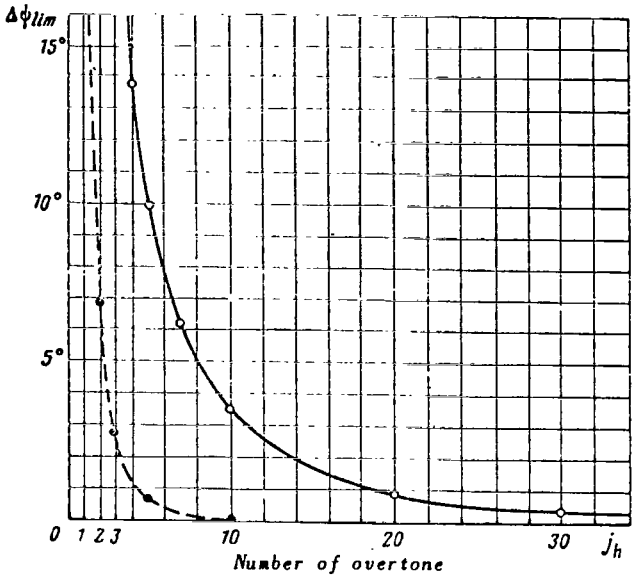

Fig.1.43 Comparison of Limit Steps for Two Numerical Integration Methods.
---- Limit step in integration with expansion of the solution in a Taylor series;
——— Limit step in integration with recalculation by eqs.(9.38).

The presented data show that the magnitude of the required integration step and hence the calculation time are determined mainly by the parameters of the system representing the rotor blade. The more degrees of freedom the system has and the more natural vibration harmonics it possesses, the smaller will be the vibration period of the highest harmonic and the smaller should be the integration step. Therefore, the calculation time is substantially shortened if the number of degrees of freedom of the system is reduced. All these considerations are especially important when using direct calculation methods which do not employ limitations imposed upon the modes of blade vibration. These methods will be examined in Section 10 of this Chapter. /133

7. Numerical Integration Method Proposed by L.N.Grodko and O.P.Bakhov

In the numerical integration of differential equations of elastic vibrations of a blade by the method proposed by L.N.Grodko and O.P.Bakhov, the value of the coefficient $\varkappa$ in eqs.(9.27) is taken as equal to unity.

The stability condition (9.31) is simplified and takes the form

$$\left|\sqrt{1-2\Delta t\bar{n}}\right| \leqslant 1. \tag{9.40}$$

Consequently, at $\varkappa = 1$ there cannot be a divergent solution with a complex value of α. From the stipulation that α is a complex number, the condition (9.40) is valid only for values $\Delta t \leq 2 - 2\bar{n}$.

From the condition (9.37) it follows that the solution cannot be divergent as long as

$$\Delta t \leqslant 2\sqrt{\frac{1}{2\varkappa-1}+\frac{\bar{n}^2}{(2\varkappa-1)^2}}-\frac{2\bar{n}}{2\varkappa-1}. \tag{9.41}$$

Hence, at $\varkappa = 1$, it follows that

$$\bar{T} \leqslant \frac{\sqrt{1+\bar{n}^2}-\bar{n}}{\pi}. \qquad (9.42)$$

As in an integration by a Taylor series with double recalculation, this method does not give a divergent solution at $\bar{n} = 0$ and has approximately the same value of the limit step.

Its accuracy with respect to the solution of problems of elastic vibrations is no worse than that for the preceding method. The volume of computational operations is cut almost in half. Therefore, this method of numerical integration can be recommended for practical use.

8. Sequence of Operations in Recalculation and Practical Evaluation of Different Integration Steps

As a whole, the calculation of elastic blade vibrations is carried out in the following sequence:

1. Assign arbitrary initial values of δ_j and $\dot{\delta}_j$ at the azimuth $\psi = 0$.

2. From eq.(9.20), determine the magnitude of the aerodynamic forces T_i, for whose determination the following parameters should first be calculated: $\dot{y}_i$, β_i, U_{xi}, U_{yi}, Φ_i, α_i, M_i, c_{yi}, and c_{xi}.

3. From eq.(9.18), determine the values of $\ddot{\delta}_j$. The values of m_j and p_j^2 entering this equation are calculated beforehand after determining the natural vibration modes of the blade and remain constant during the calculation.

4. The change-over to the next azimuth is accomplished in conformity with /134 the selected numerical integration method, for example, by means of eqs.(9.38).

$$\left.\begin{aligned}
\delta^{I}_{t+\Delta t} &= \delta_t + \Delta t\dot{\delta}_t + \frac{1}{2}\Delta t^2\ddot{\delta}_t;\\
\dot{\delta}^{I}_{t+\Delta t} &= \dot{\delta}_t + \Delta t\ddot{\delta}_t;\\
\ddot{\delta}^{I}_{t+\Delta t} &= \frac{A_j}{m_j} - p_j^2\delta^{I}_{t+\Delta t};\\
\ddot{\delta}_{av} &= \frac{\ddot{\delta}_t + \ddot{\delta}^{I}_{t+\Delta t}}{2};\\
\delta^{II}_{t+\Delta t} &= \delta_t + \Delta t\dot{\delta}_t + \frac{1}{2}\Delta t^2\ddot{\delta}_{av};\\
\dot{\delta}^{II}_{t+\Delta t} &= \dot{\delta}_t + \Delta t\ddot{\delta}_{av};\\
\ddot{\delta}^{II}_{t+\Delta t} &= \frac{A_j}{m_j} - p_j^2\delta^{II}_{t+\Delta t}.
\end{aligned}\right\} \qquad (9.43)$$

The values of $\delta^{II}_{t+\Delta t}$, $\dot{\delta}^{II}_{t+\Delta t}$, and $\ddot{\delta}^{II}_{t+\Delta t}$ for the time $t + \Delta t$ are considered final. For changing to the next azimuth, the entire cycle is repeated.

This integration method can be recommended as fairly exact and has been quite fully checked in practice in calculations of elastic blade vibrations.

The numerical integration is carried out over several rotations of the rotor, until all values of δ_j in two successive revolutions differ by less than the prescribed accuracy of the calculation. Calculations show that any prescribed accuracy can be achieved in this manner.

In practice, however, it is assumed that the calculation is completed as soon as the accuracy of determining the deformation coefficients becomes equal to R/1000 (R being the rotor radius). If necessary, a greater accuracy can be prescribed.

The magnitudes of bending stresses at each azimuth can be determined by the formula

$$\sigma_\psi = \sum_j \delta_j \sigma^j, \tag{9.44}$$

where σ^j is the normed value of bending stresses, i.e., stresses during blade bending with respect to the normed natural vibration mode of the j-th overtone.

The period of the process of transition to steady motion largely depends on the assigned initial values of the deformation coefficients. At properly posed initial values of δ_j and $\dot{\delta}_j$, the calculation is completed after checking two revolutions of the rotor. At poorly determined initial values of δ_j, the calculation may drag out to 8 - 10 revolutions.

The possibility of refining the flight regime parameters θ_0, α_{rot}, μ, and λ_{oav} after checking each revolution should also be included in the calculation program. The indicated parameters are refined such that the rotor produces the magnitude of thrust and propulsive force prescribed in the initial data. Thus, it is logical that the calculation time is determined also by the correctness of prescribing the parameters of the flight regime.

To refine the flight regime parameters and also to solve other problems, /135
various integral rotor characteristics such as thrust T_{rot}, longitudinal force H, torque M_t, etc. should be determined during the calculation.

On the basis of practical requirements, blade vibrations can be represented sufficiently completely by four natural vibration harmonics. In this case, even considering Table 1.11 which shows that the largest errors arise in resonance, satisfactory accuracy can be obtained at an integration step $\Delta\psi = 2.5^\circ$.

However, for all practical purposes in the absence of well-defined resonance or in the presence of damping forces in the system sufficient to produce a damping coefficient greater than $2\bar{n} = 0.1$, the accuracy of the calculation used in compiling Table 1.11 is not entirely lost, even at a step $\Delta\psi = 5^\circ$ or, at times, even at a step $\Delta\psi = 10^\circ$. This fact is of great importance in saving time when using digital computers of moderate speed. Thus, with the "Strela" computer, only 6 min are required to determine the motion of the blade over one revo-

lution of the rotor, at an integration step of 10°. On decreasing the step, the machine time increases greatly, rising so much at a step of 2.5° that performance of the calculation on this computer becomes difficult. These considerations lose their meaning when the calculation is performed on the high-speed M-20 computer.

/136

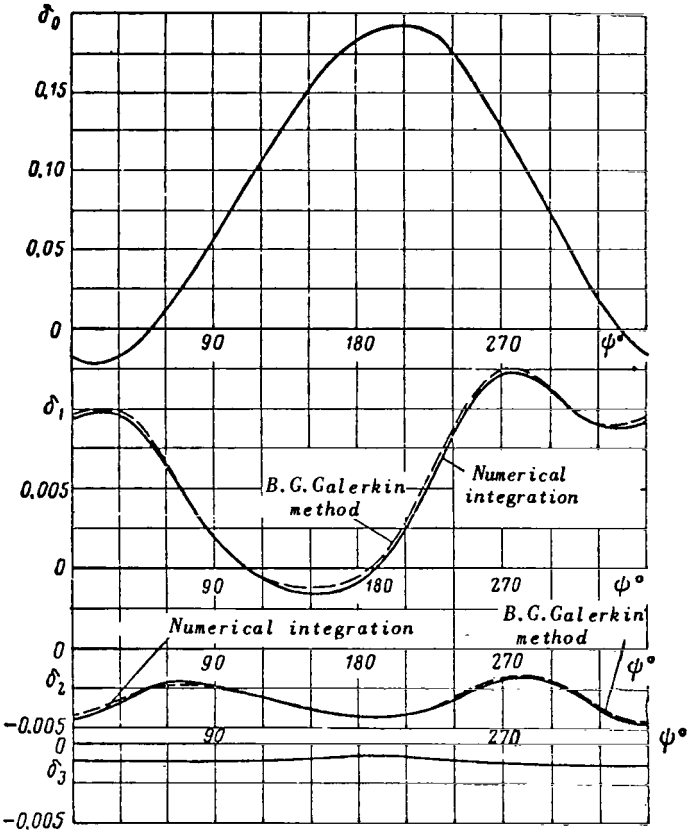

Fig.1.44 Comparison of Deformation Coefficients Obtained by Solving the Equations with Galerkin's Method and with Numerical Integration for $c_y = c_y^{\alpha} \alpha$ and $\mu = 0.3$.

As an example, Fig.1.44 shows the values of the deformation coefficient calculated for a helicopter in a flight regime with a speed corresponding to $\mu = 0.3$. For the helicopter under study, this regime is far from flow separation; therefore, the calculation is performed in a linear setup with the assumptions described in Subsection 3 of Section 8. With these assumptions, the calculation was carried out at integration steps of 2.5°, 5°, and 10°. To all intents and purposes, the results of these calculations, shown in Fig.1.44 by a solid line, coincide fully. On the basis of these data, it can be concluded that, in flight regimes sufficiently remote from flow separation when the linear approach to the solution of the problem is used and low vibration harmonics prevail in the solution, at appreciable forces of aerodynamic damping acting on the blade, the cal-

culation can be performed with an integration step $\Delta\psi = 10^\circ$ without substantial loss of accuracy.

The picture changes for regimes in which onset of flow separation occurs. Such flow separation leads to an increase in vibrations relative to higher harmonics and to a sharp decrease in the coefficients of aerodynamic damping. As a consequence, the integration step must be shortened.

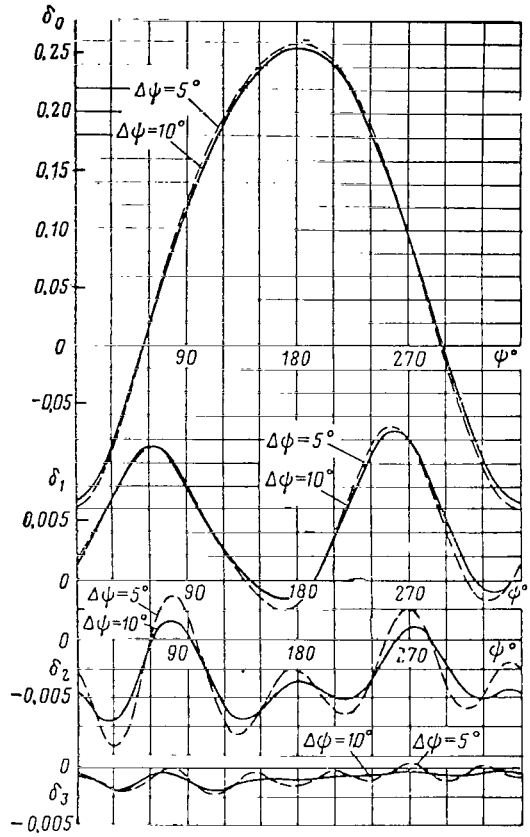

Fig.1.45 Deformation Coefficients at Incipient Flow Separation, for $\mu = 0.4$.

Figure 1.45 gives the computational data for the damping coefficients using the steps $\Delta\psi = 5^\circ$ and $\Delta\psi = 10^\circ$ for the same rotor as above but in a regime at $\mu = 0.4$ with incipient flow separation. The calculation was carried out with consideration of the nonlinear dependence of the aerodynamic coefficients on the profile angle of attack α and on the Mach number M. Flow separation leads to a pronounced increase in the vibration amplitude with respect to the modes of higher harmonics which, as is known, even without separation have lower aerodynamic damping coefficients. Therefore, a decrease in aerodynamic damping at flow separation primarily affects the vibration amplitudes with respect to these modes. Due to this, calculation with the step $\Delta\psi = 10^\circ$ introduces substantial errors into the calculation of the deformation coefficients δ_2 and δ_3. In Fig.1.45 this is illustrated on hand of a comparison of the calculation, at $\Delta\psi = 5^\circ$. Therefore, to reduce the error in calculating deformations in regimes with incipient flow separation the integration step must be reduced to values of the order of $\Delta\psi = (2.5\text{-}5)^\circ$.

9. Comparison of Results by Numerical Integration Methods with Calculation of Harmonics

A method of stress calculation with respect to harmonics was presented above in a linear arrangement, using the assumptions set forth in Subsection 3 of Section 8. Such a method will be successful for flight regimes sufficiently remote from flow separation. It has a number of advantages, the first being the relatively short calculation time.

In Fig.1.44 the deformation coefficients calculated by the harmonic method

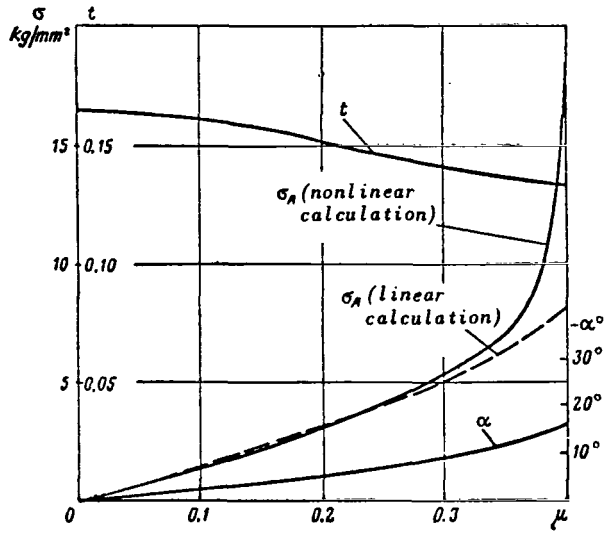

Fig.1.46 Maximum Amplitude of Variable Stresses over the Blade, as a Function of Flying Speed.

presented in Section 8 are shown by a broken line, for comparison in the same flight regimes at $\mu = 0.3$ with a linear dependence $c_y = c_y^{\alpha}\alpha$. A study of the calculation methods shows satisfactory agreement of the results. The slight difference can be attributed to some difference in the initial parameters of the flight regime.

10. Some Calculation Results

We will here present individual results that characterize the new possibilities for theoretical investigations offered by the method of numerical integration with consideration of a nonlinear dependence of the aerodynamic coefficients on the angle of attack α and the Mach number M, in comparison with linear methods of calculation. /137

One of the major advantages of numerical integration is the possibility of making stress analyses under conditions close to flow separation regimes.

Calculation shows that, on approach to flow separation, the aerodynamic damping of blade vibrations decreases steeply and the amplitude of vibrations having harmonics in resonance or close to resonance with the natural blade vibrations increases. A study of the deformation coefficients plotted in Fig.1.45 indicates that vibrations at the first overtone occur mainly with the second harmonic, those at the second overtone with the fourth, and those at the third overtone with the sixth harmonic to the rotor rpm, i.e., only with frequencies close to the natural vibration frequencies of the blade in question. An especially pronounced increase in vibration amplitude takes place with respect to modes of the relatively higher vibration overtones, as demonstrated in Fig.1.45 on the example of the coefficients δ_2 and δ_3.

The onset of flow separation is characterized by a marked increase in the amplitude of the variable blade stresses. Figure 1.46 shows the values of maximum amplitude of variable stresses over the blade radius as a function of flying speed, calculated with consideration of the linear and nonlinear dependence $c_y = f(\alpha, M)$. A marked increase in stresses is a highly useful criterion for determining the onset of separation in calculating the aerodynamic characteristics of a rotor. /139

The harmonic content of the variable stresses set up during flow separation and their distribution over the blade radius are shown in Figs.1.47 and 1.48.

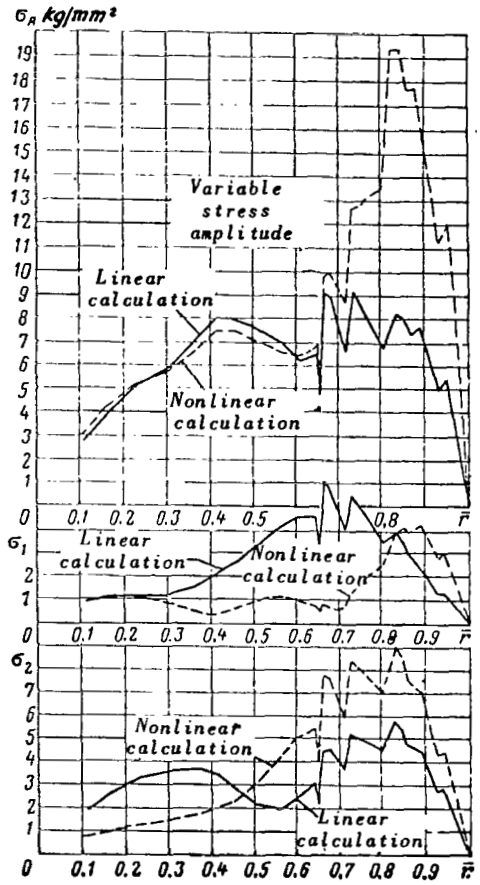

Fig.1.47 Distribution of Variable Stress Amplitudes and the Two First Harmonic Stress Components over the Blade Radius at $\mu = 0.4$.

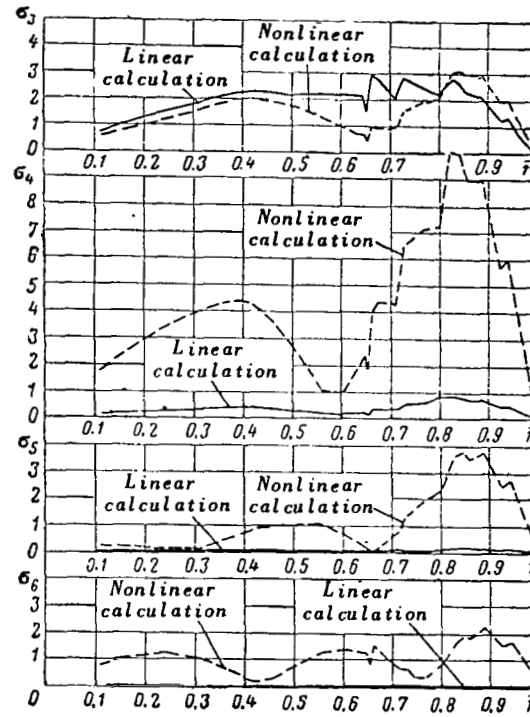

Fig.1.48 Distribution of Amplitude of the Third, Fourth, Fifth, and Sixth Harmonic Components of Stresses over the Blade Radius at $\mu = 0.4$.

It should be noted that a substantial difference is also observed in the results of linear and nonlinear calculations in regimes sufficiently remote from flow separation.

Figure 1.49 gives the deformation coefficients calculated for the same helicopter at $\mu = 0.3$, with a linear and nonlinear dependence $c_y = f(\alpha, M)$; Fig.1.50 shows the corresponding harmonic components of stresses and their amplitude σ_A constructed over the blade radius. As indicated by this diagram, the results differ substantially.

Thus, already the few data presented here show that the calculation of variable blade stresses with consideration of the nonlinear dependence $c_y = f(\alpha, M)$ yields a large number of interesting characteristics that have a substantial influence on the rotor strength.

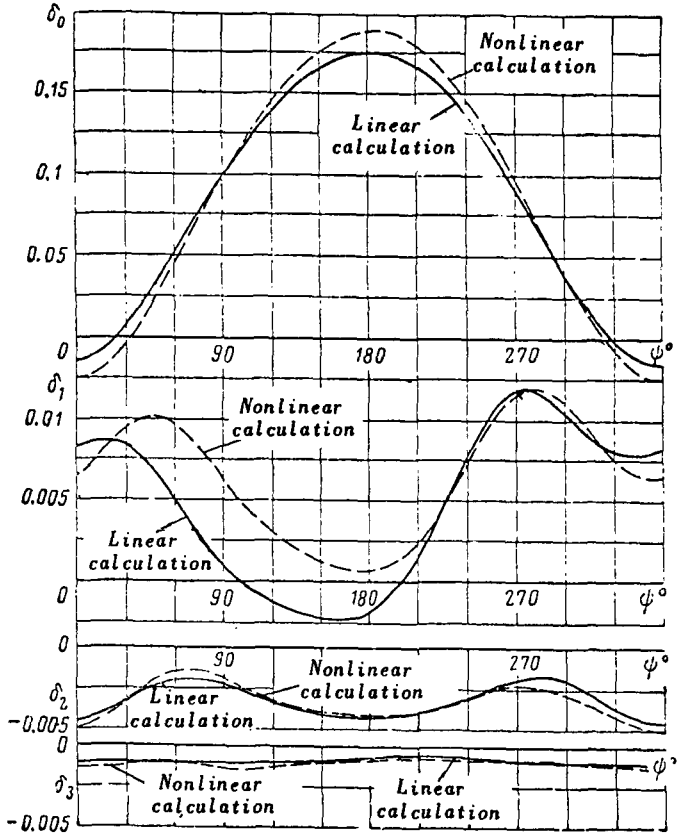

Fig.1.49 Comparison of Deformation Coefficients Calculated with Consideration of the Linear and Nonlinear Dependence $c_y = f(\alpha, M)$ for the Regime $\mu = 0.3$ Far from Flow Separation.

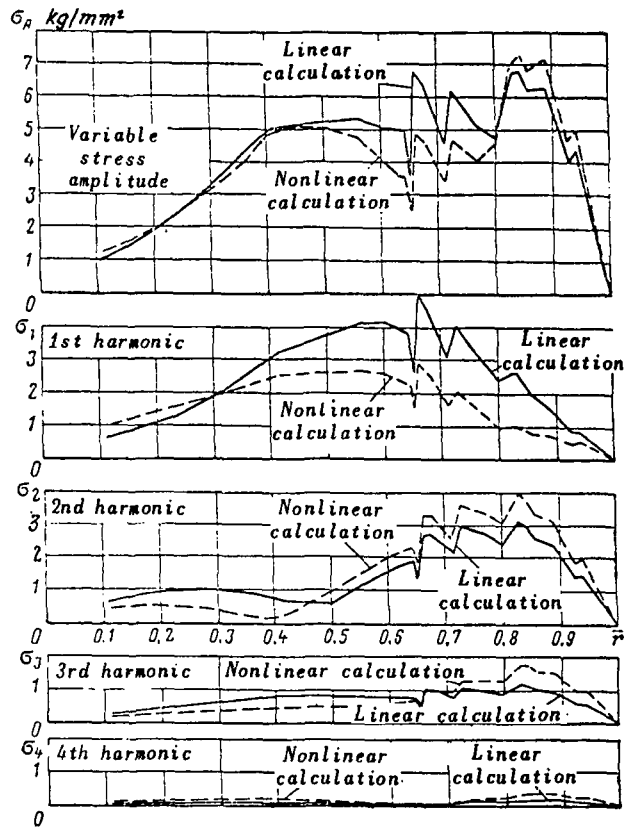

Fig.1.50 Distribution of Variable Stress Amplitudes and the Four First Harmonic Components over the Blade Radius for $\mu = 0.3$.

Section 10. Calculation of Flexural Vibrations with Direct Determination of the Paths of Motion of Points of the Blade

/142

1. Principle of the Method of Calculation

In Sections 7, 8, and 9 we presented methods of calculating flexural blade vibrations where the deformation mode was determined by Galerkin's method. For this purpose, the blade deformations were expanded in a series in prescribed known functions. As such functions, we proposed using the natural flexural vibration modes of a blade in vacuum. In this respect, it was stated that, for practical purposes, it is sufficient to limit the calculation to the first four harmonics of natural vibrations.

Here, we will discuss methods that eliminate this assumption and permit a determination of blade deformations by a direct calculation of the paths of motion of a certain number of points of the blade, without expansion of the vibration mode in known functions*.

To determine the motion of individual points of the blade, it is convenient to use a blade model with discrete parameters. In this case, the mass of the blade is simulated by several concentrated loads distributed over its length.

For such a mechanical model, we can derive a system of differential equations of the form

$$m_i \ddot{y}_i = C_i + T_i, \tag{10.1}$$

where

$i = 0, 1, 2, \ldots, z$;

$\ddot{y}_i$ = second derivative with respect to time for displacements y_i of the i-th concentrated load with mass m_i; the values of y_i are reckoned from the plane of rotation of the rotor;

C_i = elastic force acting on the i-th mass m_i by adjacent segments of the mechanical blade model;

T_i = external aerodynamic force acting on the i-th point of the blade where one of the concentrated loads is situated.

The system of equations (10.1) describes the motion of all masses of the mechanical blade model. Thus, it comprises equations with variables y_i equal in number to the masses of the mechanical model in question.

However, not all variables y_i entering the system (10.1) are independent, since the motion should satisfy the condition of equilibrium of the entire system:

$$\sum_0^z (m_i \ddot{y}_i - T_i) = 0. \tag{10.2}$$

---

* Such a method for calculating a helicopter blade was first used by R.M.Zanozina.

It is preferable to consider that the displacements of all masses, except for the root mass m_0, are independent variables. Then, the motion of the root mass, if we assume $T_0 = 0$, can be determined in conformity with eq.(10.1) as

$$m_0\ddot{y}_0 = C_0,$$

where

$$C_0 = \sum_1^z (T_i - m_i\ddot{y}_i). \tag{10.3}$$

This condition of equilibrium of forces is automatically satisfied when using the formulas presented below. /143

Thus, the system in question can be described by independent variables y_i whose number is lower by one than the number of concentrated masses of the mechanical model. Consequently, the number of degrees of freedom of this system is equal to the number of segments of the calculation scheme and is lower by one than the number of concentrated masses.

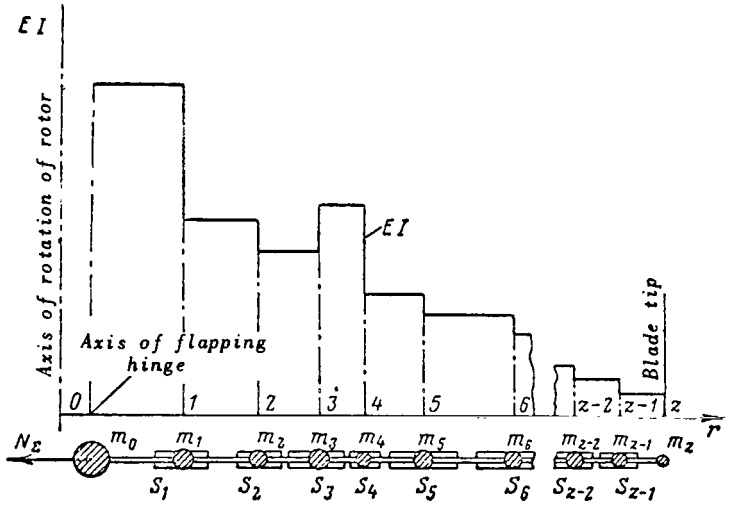

Fig.1.51 Blade Model Examined in the Calculation.

The solution of the system of equation (10.1) can be obtained by numerical integration with respect to time. For this, it is necessary at each instant of time to determine the forces C_i and T_i. The forces T_i can be determined from eqs.(9.20) whose derivation is given in Section 9. A determination of the elastic forces C_i has many peculiarities, which we will discuss here at some length.

2. Determination of Elastic Forces Applied to a Point of the Blade by Adjacent Segments

Let us make a more detailed analysis of the mechanical blade model used in the calculation. First, let us examine a beam-type model. We will represent the blade as a weightless free beam governed by certain boundary conditions at the ends and divided into z segments, along whose edges concentrated loads are placed (Fig.1.51). The lengths of the segments can be different.

As before, we represent the flexural rigidity of the blade as a stepped curve so that it remains constant over each segment. We will assume the centrifugal force as applied only to the loads. Therefore, its magnitude will remain constant over each segment. We will also assume that the aerodynamic forces are applied only at the points of attachment of the loads as if a separate flap with an area S_i were attached to each load.

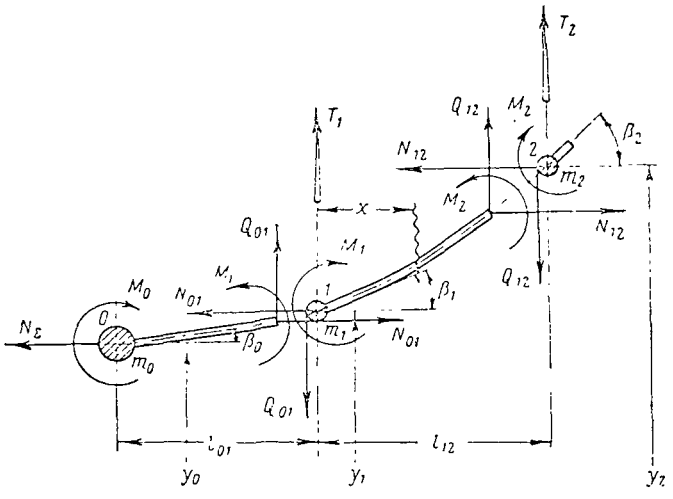

Fig.1.52 Polygon of Forces Acting on Adjacent Blade Elements.

To produce the conditions of blade attachment at the root, we will assume that the centrifugal force is sensed by a special attachment of root mass m_0, able to move freely in vertical direction. When solving this problem it is not necessary to create freedom of vertical motion of the root mass. However, in other problems associated with a determination of synchronous vibration modes of the blade and fuselage, this condition is necessary. If the /144 fuselage vibrations are disregarded and the blade is considered as attached at the hub on a rigid base, the conditions of root attachment in the calculation are established by prescribing the necessary - usually rather large - mass m_0.

It is logical that such an idealized scheme will yield a more accurate description of the real pattern of blade vibration the larger the number of segments into which the blade is divided. The blade can be represented with sufficient accuracy by a scheme in the form of a beam consisting of 25 - 30 segments and of the same number of concentrated loads.

To determine the elastic force C_i, we will construct the equations of blade deformations. Figure 1.52 shows the forces acting on two adjacent segments of a deformed blade. Let us write out the equations of deformation of these segments.

Since the inertia and aerodynamic forces for the mechanical model in question are applied only along the edges of the segments, the deformations of each

segment can be determined by the equation

$$[EIy'']''-[Ny']'=0. \tag{10.4}$$

The magnitude of the flexural rigidity EI and the centrifugal force N remain constant over each segment. Therefore, they can be removed from the differentiation sign. Then, eq.(10.4) can be rewritten in the form

$$M''-\mu^2M=0, \tag{10.5}$$

where M = EIy'' is the bending moment in the blade section and $\mu^2 = \frac{N}{EI}$.

The solution of eq.(10.5) can be written as

$$M_x=A\sinh\mu x+B\sinh\mu x, \tag{10.6}$$

where the coefficients A and B can be obtained from the boundary conditions. /145
Thus, for the segment 1 - 2, we have $M_x = M_1$ at $x = 0$ and $M_x = M_2$ at $x = l_{12}$. Substituting these conditions into eq.(10.6), we obtain

$$\left.\begin{aligned} A&=\frac{M_2}{\sinh\alpha_1}-\frac{M_1}{\tanh\alpha_1};\\ B&=M_1. \end{aligned}\right\} \tag{10.7}$$

Here, $\alpha_1 = \mu_1 l_{12}$ and $\mu_1 = \sqrt{\frac{N_{12}}{EI_{12}}}$.

With consideration of eq.(10.7) and of the fact that $M_x = EI_{12}y''$, eq.(10.6) can be written in the form

$$EIy''=\left[\frac{M_2}{\sinh\alpha_1}-\frac{M_1}{\tanh\alpha_1}\right]\sinh\mu x+M_1\cosh\mu_1 x. \tag{10.8}$$

After twice integrating eq.(10.8) and bearing in mind that at $x = 0$ $y' = \beta_1$; $y = y_1$, and at $x = l_{12}$ $y' = \beta_2$; $y = y_2$, we obtain

$$b_1(y_2-y_1)=d_1M_2+e_1M_1+\beta_1 \tag{10.9}$$

or

$$b_1(y_2-y_1)=-e_1M_2-d_1M_1+\beta_2. \tag{10.10}$$

Here,

$$b_1=\frac{1}{l_{12}};$$
$$d_1=\frac{1}{l_{12}N_{12}}\left(1-\frac{\alpha_1}{\sinh\alpha_1}\right);$$
$$e_1=\frac{1}{l_{12}N_{12}}\left(\frac{\alpha_1}{\tanh\alpha_1}-1\right).$$

The equation of deformation for the segment 0-1 can be written by analogy with eq.(10.10):

$$b_0(y_1-y_0)=-e_0M_1-d_0M_0+\beta_1. \tag{10.11}$$

Changing all signs in eq.(10.11) and adding with eq.(10.9), we obtain

$$d_0M_0+c_1M_1+d_1M_2=A_1, \tag{10.12}$$

where

$$c_1=e_0-e_1;$$
$$A_1=b_0y_0+(b_0+b_1)y_1+b_1y_2.$$

After performing the same operations for other adjacent segments, we obtain a system of z equations of the following form:

Table 1.12

β_0	M_0	M_1	M_2	...	...	M_{z-2}	M_{z-1}		
1	c_0	d_0						=	A_0
	d_0	c_1	d_1					=	A_1
		d_1	c_2	d_2				=	A_2
			...	...	...			=	...
				...	...	...		=	...
					d_{z-1}	c_{z-2}	d_{z-2}	=	A_{z-2}
						d_{z-2}	c_{z-1}	=	A_{z-1}

We have written this system of equations here in the form of a table. /146
Any of the equations of the system represents the sum of the products of coefficients, occupying one row in the rectangular Table 1.12, while the unknown functions M_i simultaneously entering several equations and shown in the vertical column are given in a separate row on top of Table 1.12. The unknown function β_0 entering only the first equation is written in this row. The right-hand sides of the equations A_i are placed in a special column.

The system of equations in Table 1.12 is solved by the method of elimination of unknowns. This method was already described in Subsection 5 of Section 4.

Thus, the system of equations written out above permits determining the values of the angle of rotation of the blade at the root β_0 and all values of the bending moments M_i if the deformation mode of the blade is known as a set of values of y_i.

To determine the elastic force C_i, it is necessary to perform a number of successive operations, the first of which involves solving the system represented in Table 1.12. It is expedient to include in this sequence of operations a determination of the angles of rotation of the elastic blade axis β_i which are needed later for calculating the aerodynamic forces:

$$\beta_i = b_i (y_i - y_{i-1}) - e_{i-1} M_i + d_{i-1} M_{i-1}. \qquad (10.13)$$

From the known values of M_i and from the condition of equilibrium of the elements, we can calculate the shearing force $Q_{i,i+1}$ which is constant over each segment of the blade. Actually, equating the sum of the moments of all forces acting on the segment i, i+1 to zero, we obtain the equation

$$Q_{i,i+1} l_{i,i+1} = N_{i,i+1} (y_{i+1} - y_i) + M_i - M_{i+1}, \qquad (10.14)$$

from which we can determine the value $Q_{i,i+1}$.

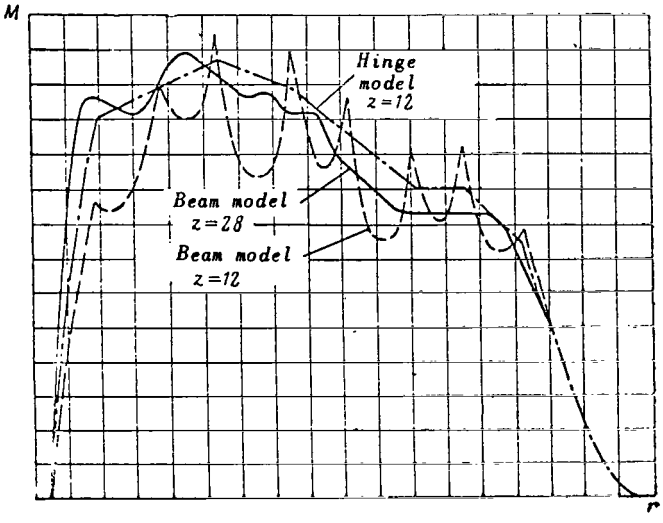

Fig.1.53 Bending Moments with Respect to the First Overtone of Natural Vibrations, Calculated with a Different Number of Masses.

Knowing the value of the shearing forces over the blade length, we can determine also the elastic force C_i applied to the mass m_i by the adjacent segments:

$$C_i = Q_{i,i+1} - Q_{i-1,i}. \qquad (10.15)$$

These computations permit determining all values of elastic forces C_i exerted on the given mass m_i by the adjacent segments, if the deformation mode y_i is known.

3. Characteristics of Numerical Integration of Eqs.(10.1)

In Section 9, we described the basic characteristics of application of numerical integration to the solution of differential equations of elastic blade vibrations. It was shown that the success of numerical integration is largely determined by the magnitude of the limit step, which is directly associated with the smallest vibration period of the mechanical model examined as a blade analog. The limit integration step should not be too small, since calculation in this case will be extremely time-consuming.

A characteristic of the model under study is that it may have as many natu-

ral vibration harmonics as there are segments into which the blade is divided over its length in the calculation. As already mentioned above, to reduce errors when changing from a blade to its mechanical model analog, the blade must be represented by at least 25 - 30 segments with the same number of concentrated masses. Therefore, in determining the limit integration step in this case it is necessary to proceed from the period of the highest (30^{th}) overtone of natural vibrations.

Figure 1.40 shows the relation of the natural vibration frequency and /147
period of an ordinary helicopter blade as a function of the number of the overtone. It follows from this diagram that the period of the 30^{th} overtone of natural vibrations is about 1° with respect to the rotor azimuth. It was stated above that, in using the most suitable method of numerical integration to obtain a nondivergent solution, the integration step should be less than one third of the period of the highest overtone. Consequently, for the method of calculation examined here, the integration step should be at least 0.3° with respect to the rotor azimuth. This stabilizes the solution and permits neglecting the appreciable error in determining the amplitudes corresponding to high vibration overtones, since their magnitudes are usually small and stresses in the blade are determined mainly by several first harmonics of natural vibrations. The vibration amplitude with respect to these harmonics can be determined with satisfactory accuracy.

It becomes understandable from the above considerations that, in using the calculation method with a direct determination of the path of motion of points of a blade, it is advantageous to use a model with a minimum number of concentrated loads. It is desirable to use only models with a number of loads not more than 12 - 15. It should be noted that, with such a small number of segments, the above beam model introduces errors into the calculation associated with specific features of this model. To illustrate this, Fig.1.53 shows the mode of the bending moment corresponding to the first overtone of natural blade vibrations, calculated for $z = 28$ (solid line) and $z = 12$ (dashed line). It follows from Fig.1.53 that, for a small number of segments, the bending moment in the blade model begins to show peculiarities characteristic for highly flexible beams stressed by transverse forces in a field of centrifugal forces in that bending moment concentrations appear at the site where the masses are located. This characteristic was mentioned already in Section 4, Subsection 9. The occurrence of such concentrations substantially reduces the calculation accuracy. Therefore, the use of beam models with a number of segments less than 25 ($z = 25$) is not recommended. For a small number of masses, such errors do not arise when /148
using a multihinge articulated model, although vibration modes of higher harmonics will be severely distorted. In Fig.1.53, the bending moment calculated for a multihinge model with a number of segments $z = 12$ is shown by a dot-dash line.

Proceeding from these considerations, let us examine in greater detail the method presented here as related to a multihinge model. Furthermore, it will be shown in Subsection 6 of this Section that a multihinge model permits applying the calculation of elastic vibrations by numerical integration methods, at an inverse order of determining the variables, which is practically impossible in the beam model.

4. Equations of Motion for a Multihinge Articulated Blade Model

Let us represent the blade as a chain consisting of perfectly rigid weightless links interconnected by hinges. The weight of the blade is concentrated in the hinges of this chain in the form of individual loads with a mass m_i. The flexural rigidity of the blade is also concentrated in the hinges, based on the concept that a spring of rigidity c_i preventing fracture of the blade in this hinge is, so to speak, built into each hinge (Fig.1.54).

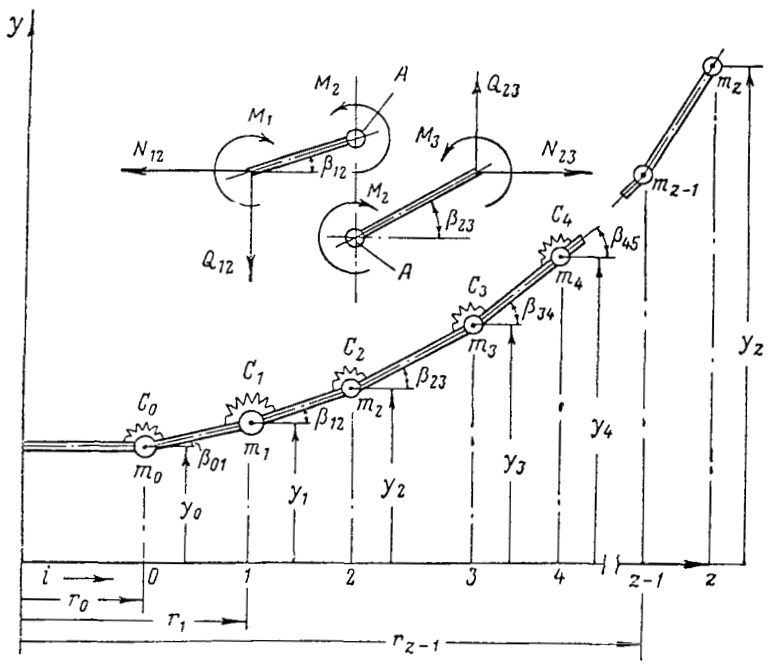

Fig.1.54 Diagram of Multihinge Articulated Blade Model.

The system of differential equations of vibrations pertaining to this blade model will be derived here, starting with the equation describing the equilibrium of the load with the ordinal number i = 2. Then, by analogy, we will construct all remaining equations of the system.

The equation of equilibrium of the load with mass m_2 can be written in the form /149

$$m_2\ddot{y}_2 = C_2 + T_2. \qquad (10.16)$$

The elastic force C_2 exerted on the mass m_2 by the adjacent segments of the model is determined by the formula

$$C_2 = Q_{23} - Q_{12}, \tag{10.17}$$

where Q_{12} and Q_{23} are the shearing forces on segments of the model adjacent to the load.

To determine the magnitude of the shearing forces Q_{12} and Q_{23}, we will derive equations that equate to zero the sum of the moments of all forces relative to the point of the load with a mass m_2 (point A) for both segments of the model adjacent to this load. These equations have the following form:

$$\left.\begin{aligned} Q_{12}l_{12} - N_{12}(y_2 - y_1) + M_2 - M_1 = 0; \\ Q_{23}l_{23} - N_{23}(y_3 - y_2) + M_3 - M_2 = 0. \end{aligned}\right\} \tag{10.18}$$

Determining Q_{12} and Q_{23} from this and substituting these values into formula (10.17), we obtain

$$\begin{aligned} C_2 = Q_{23} - Q_{12} = \\ = \frac{1}{l_{12}} M_1 + \left(\frac{1}{l_{12}} + \frac{1}{l_{23}}\right) M_2 - \frac{1}{l_{23}} M_3 + \\ + \frac{N_{12}}{l_{12}} y_1 - \left(\frac{N_{12}}{l_{12}} + \frac{N_{23}}{l_{23}}\right) y_2 + \frac{N_{23}}{l_{23}} y_3. \end{aligned} \tag{10.19}$$

The bending moment entering this equation can be expressed by blade element displacement, using the formulas

$$\left.\begin{aligned} M_1 = c_1(\beta_{12} - \beta_{01}) = \frac{c_1}{l_{01}} y_0 - c_1\left(\frac{1}{l_{01}} + \frac{1}{l_{12}}\right) y_1 + \frac{c_1}{l_{12}} y_2; \\ M_2 = c_2(\beta_{23} - \beta_{12}) = \frac{c_2}{l_{12}} y_1 - c_2\left(\frac{1}{l_{12}} + \frac{1}{l_{23}}\right) y_2 + \frac{c_2}{l_{23}} y_3; \\ M_3 = c_3(\beta_{34} - \beta_{23}) = \frac{c_3}{l_{23}} y_2 - c_3\left(\frac{1}{l_{23}} + \frac{1}{l_{34}}\right) y_3 + \frac{c_3}{l_{34}} y_4. \end{aligned}\right\} \tag{10.20}$$

Substituting eqs.(10.20) for M_1, M_2, and M_3 into eq.(10.19), we obtain the following equation:

$$C_2 = d_1 y_0 + e_1 y_1 + f_2 y_2 + e_2 y_3 + d_3 y_4, \tag{10.21}$$

where

$$\left.\begin{aligned} d_1 = -\frac{c_1}{l_{01}l_{12}}; \\ d_3 = -\frac{c_3}{l_{23}l_{34}}; \\ e_1 = \frac{c_2}{l_{12}}\left(\frac{1}{l_{01}} + \frac{1}{l_{12}}\right) + \frac{N_{12}}{l_{12}} + \frac{c_2}{l_{12}}\left(\frac{1}{l_{12}} + \frac{1}{l_{23}}\right); \end{aligned}\right\} \tag{10.22}$$

$$e_2 = \frac{c_2}{l_{23}}\left(\frac{1}{l_{12}} + \frac{1}{l_{23}}\right) + \frac{N_{23}}{l_{23}} + \frac{c_3}{l_{23}}\left(\frac{1}{l_{23}} + \frac{1}{l_{34}}\right);$$
$$f_2 = -\frac{N_{12}}{l_{12}} - \frac{c_1}{l_{12}^2} - c_2\left(\frac{1}{l_{12}} + \frac{1}{l_{23}}\right)^2 - \frac{c_3}{l_{23}^2} - \frac{N_{23}}{l_{23}}.$$

If we also write out all remaining values of C_i and substitute them into eq.(10.16), then the system of differential equations of blade vibrations can be represented in the form shown in Table 1.13. /150

Table 1.13

y_0	y_1	y_2	y_3	y_4	y_5	...	y_{z-1}	y_z		
f_0	e_0	d_1							=	$m_0\ddot{y}_0$
e_0	f_1	e_1	d_2						=	$m_1\ddot{y}_1 - T_1$
d_1	e_1	f_2	e_2	d_3					=	$m_2\ddot{y}_2 - T_2$
	d_2	e_2	f_3	e_3	d_4				=	$m_3\ddot{y}_3 - T_3$
		...	...	...	...	...			=	...
			...	...	...	...	...		=	...
				...	...	...	...	...	=	...
					d_{z-2}	e_{z-2}	f_{z-1}	e_{z-1}	=	$m_{z-1}\ddot{y}_{z-1} - T_{z-1}$
						d_{z-1}	e_{z-1}	f_z	=	$m_z\ddot{y}_z - T_z$

Each equation of the obtained system, occupying one row in Table 1.13, represents the sum of the products of the known coefficients d_i, e_i, and f_i and the variables y_i which simultaneously enter several equations. The variables y_i are set off vertically in a special row in the upper portion of Table 1.13. The right-hand sides of the equations, representing the sum of inertia and aerodynamic forces, are given in a separate column to the right of Table 1.13.

This system of equations directly correlates blade deformations with the forces acting on the blade, without intermediate coupling across bending moments, as had been the case in analogous equations pertaining to the beam model described above in Subsection 3 of this Section and in equations used previously in Section 4 for calculating the free vibrations of a blade.

This form of differential equations greatly simplifies the calculations in determining the elastic blade deformations, but it also has certain shortcomings. One of these, as already mentioned, is that the elastic blade axis is not represented as smooth but as a broken line. The mode of the distribution of the bending moment over the blade length is also represented as a broken line. A second shortcoming is the arbitrariness in selecting the hinge rigidities c_i.

Let us present one of the methods of determining these rigidities. For this purpose, we investigated two adjacent blade segments. The value of the

hinge rigidity c_i is determined from the stipulation that the angles of rotation of the ends of adjacent segments β_0 and β_2 of the equivalent beam model coincide with the angles β_{01} and β_{12} for the hinge scheme Fig. 1.55):

$$(\beta_2 - \beta_0)_{beam} = (\beta_{12} - \beta_{01})_{hinge}. \qquad (10.23)$$

If, in comparing these angles, we neglect the effect of centrifugal forces and assume that the bending moment over these two segments is constant ($M_0 = M_1 = M_2 = \text{const}$), then the condition (10.23) will yield the following formula for determining the hinge rigidity: /151

$$\frac{1}{c_i} = \frac{l_{01}}{EI_{01}} + \frac{l_{12}}{EI_{12}}. \qquad (10.24)$$

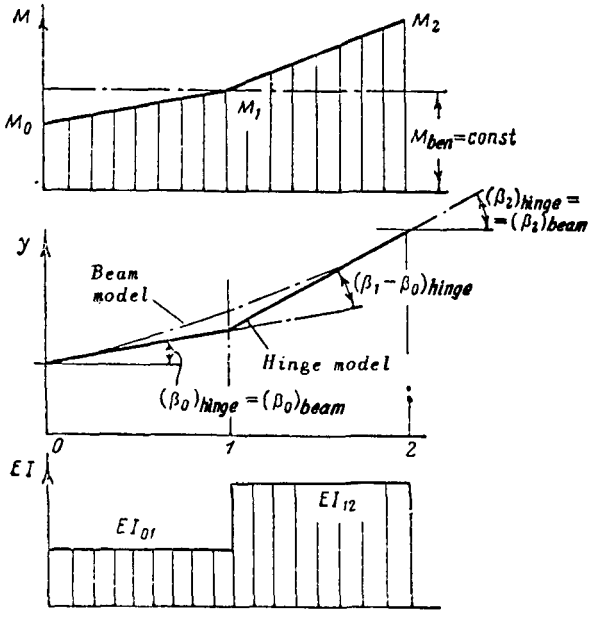

Fig.1.55 For Determination of Hinge Rigidity.

In practice, these assumptions can be obeyed only approximately. This leads to certain errors in using such a calculation method.

5. Sequence of Operations in Calculating Elastic Vibrations by the Numerical Integration Method

As a whole, blade calculations by the proposed method are carried out in the following sequence: At the initial time, which is usually related with the azimuth $\psi = 0$, an arbitrary blade deformation mode y_i and the distribution of the rate of displacement of the masses $\dot{y}_i$ are prescribed. If all values of y_i are known, the elastic forces C_i can be determined by the formulas presented in Subsections 2 and 4 of this Section. The angles of rotation of the elastic blade axis β_i should be calculated at the same time. For the beam model, these are derived from eq.(10.13). For the articulated model, they can be determined as the half-sum of the angles of rotation of two links of the model adjacent to the point in question:

$$\beta_i = \frac{\beta_{i-1,i} + \beta_{i,i+1}}{2}.$$

If the values of β_i and y_i are known, then the aerodynamic forces T_i can be obtained from eqs.(9.20). These data suffice to determine the values $\ddot{y}_i$ by means of eqs.(10.1).

Next, a change-over is made to the next azimuth of the blade by means of formulas analogous to eq.(9.43): /152

$$\left.\begin{aligned}
y^{\mathrm{I}}_{t+\Delta t} &= y_t + \Delta t \dot{y}_t + \frac{1}{2}\Delta t^2 \ddot{y}_t;\\
\dot{y}^{\mathrm{I}}_{t+\Delta t} &= \dot{y}_t + \Delta t \ddot{y}_t;\\
\ddot{y}^{\mathrm{I}}_{t+\Delta t} &= \frac{1}{m}(C^{\mathrm{I}}_{t+\Delta t} + T^{\mathrm{I}}_{t+\Delta t});\\
\ddot{y}_{av} &= \frac{\ddot{y}_t + \ddot{y}^{\mathrm{I}}_{t+\Delta t}}{2};\\
y^{\mathrm{II}}_{t+\Delta t} &= y_t + \Delta t \dot{y}_t + \frac{1}{2}\Delta t^2 \ddot{y}_{av};\\
\dot{y}^{\mathrm{II}}_{t+\Delta t} &= \dot{y}_t + \Delta t \ddot{y}_{av};\\
\ddot{y}^{\mathrm{II}}_{t+\Delta t} &= \frac{1}{m}(C^{\mathrm{II}}_{t+\Delta t} + T^{\mathrm{II}}_{t+\Delta t}).
\end{aligned}\right\} \qquad (10.25)$$

The values of $y^{\mathrm{II}}_{t+\Delta t}$, $\dot{y}^{\mathrm{II}}_{t+\Delta t}$, and $\ddot{y}^{\mathrm{II}}_{t+\Delta t}$ for the time t + Δt are considered final. The index i, referring to the number of the concentrated load, is omitted in eqs.(10.25) so as to prevent excessive complication of the expressions.

All operations are then repeated, to change to the new azimuth. This is continued for several revolutions of the rotor until the motion of the blade becomes stable. The calculation terminates with the revolution at which the solution converges to the established solution, with the prescribed accuracy. The accuracy of the solution is determined by the difference in the ordinates of the mass displacement when calculating the motion in two successive rotor revolutions.

Analysis of the results can be carried out in any manner, depending on the purpose of the calculation. To solve problems of blade strength analysis, the bending moments M_i, every 10° of rotor azimuth, are usually read into the external memory. After calculating the values of M_i and the drag moments of the blade sections, the values of the stresses and their amplitude are determined

$$\sigma^A_i = \frac{\sigma_{\max i} - \sigma_{\min i}}{2} \qquad (10.26)$$

and the stresses are expanded in harmonics.

Calculation of elastic vibrations by the above method comprises a constant repetition of the same operations, which amounts to a determination of the forces C_i and T_i and to the solution of eq.(10.1). Therefore, the computer time primarily depends on the number of such repetitions. This number is determined by only two factors. The first is the duration of the period of changing to a stable process, which depends only on the correspondence of the initial conditions of steady motion and on the physical properties of the rotor and is independent of the method of calculation. The second, already mentioned above, is the required integration step.

6. Method of Calculation with Inverse Order of Determining Variables in Numerical Integration

In Section 9 and in this Section, we discussed direct methods of numerical integration of differential equations for the case in which, on changing to a new time, we determined the variable y and its first derivative $\dot{y}$, and then the second derivative $\ddot{y}$ from the differential equation. Here, we will examine a method of calculation proposed by V.E.Baskin in which these quantities are determined in the opposite order. /153

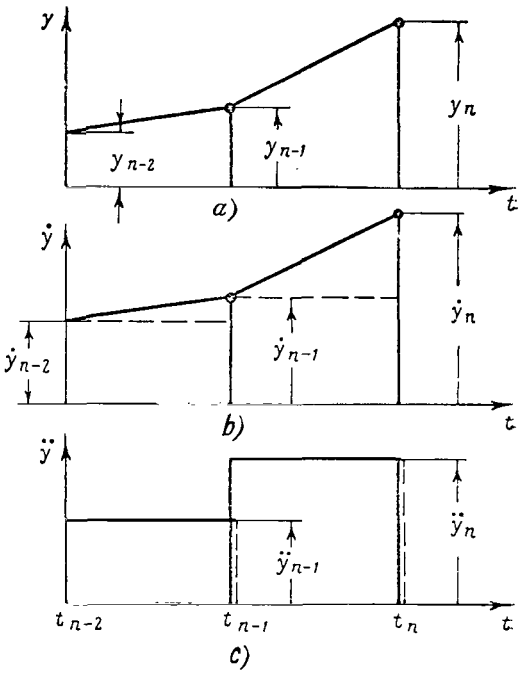

Fig.1.56 Change of Variable y and its Time Derivatives, in Numerical Integration.

In sequence, we will investigate three times: the time t_n at which the blade deformation must be determined, and the two times $t_{n-1} = t_n - \Delta t$ and $t_{n-2} = t_n - 2\Delta t$ preceding this.

Assuming that the second derivative $\ddot{y}$ remains constant over each integration interval, as shown in Fig.1.56c, the value of $\ddot{y}_{n-1}$ can be expressed by $\dot{y}_{n-2}$ and $\dot{y}_{n-1}$:

$$\ddot{y}_{n-1} = \frac{\dot{y}_{n-1} - \dot{y}_{n-2}}{\Delta t}. \qquad (10.27)$$

If we now assume that the first derivative $\dot{y}$ also remains constant over the integration interval, as shown in Fig.1.56b by a broken line, then the values of $\dot{y}_{n-1}$ and $\dot{y}_{n-2}$ can be determined from the formulas

$$\left.\begin{aligned} \dot{y}_{n-1} &= \frac{y_n - y_{n-1}}{\Delta t}; \\ \dot{y}_{n-2} &= \frac{y_{n-1} - y_{n-2}}{\Delta t}. \end{aligned}\right\} \qquad (10.28)$$

Substituting eq.(10.28) into eq.(10.27) yields the expression for $\ddot{y}_{n-1}$:

$$\ddot{y}_{n-1} = \frac{1}{\Delta t^2}(y_n - 2y_{n-1} + y_{n-2}). \qquad (10.29)$$

If the integration step is sufficiently small, then we can put approximately

$$\ddot{y}_n = \ddot{y}_{n-1} \qquad (10.30)$$

and write eq.(10.29) in the form

$$\ddot{y}_n = \frac{1}{\Delta t^2}(y_n - 2y_{n-1} + y_{n-2}). \qquad (10.31)$$

Substituting the values of $\ddot{y}_n$ into the system of differential equations represented by Table 1.13, a system of algebraic equations relative to the unknowns y_n is obtained. As above, this system is written in the form of Table 1.14.

In the variables y in Table 1.14, the index denoting the instant of time is given as superscript, while the index referring to the number of the concentrated load of the model - as before - is given as subscript. /154

In compiling Table 1.14 it was also assumed that the aerodynamic forces calculated for the time t_{n-1} can be set approximately equal to these forces for the time t_n.

Table 1.14

y_0^n	y_1^n	y_2^n	y_3^n	y_4^n	y_5^n	...	y_{z-1}^n	y_z^n		
$f_0 - \frac{m_0}{\Delta t^2}$	e_0	d_1							=	$\frac{m_0}{\Delta t^2}\left[y_0^{(n-2)} - 2y_0^{(n-1)}\right]$
e_0	$f_1 - \frac{m_1}{\Delta t^2}$	e_1	d_2						=	$\frac{m_1}{\Delta t^2}\left[y_1^{(n-2)} - 2y_1^{(n-1)}\right] - T_1^{(n-1)}$
d_1	e_1	$f_2 - \frac{m_2}{\Delta t^2}$	e_2	d_3					=	$\frac{m_2}{\Delta t^2}\left[y_2^{(n-2)} - 2y_2^{(n-1)}\right] - T_2^{(n-1)}$
	d_2	e_2	$f_3 - \frac{m_3}{\Delta t^2}$	e_3	d_4				=	$\frac{m_3}{\Delta t^2}\left[y_3^{(n-2)} - 2y_3^{(n-1)}\right] - T_3^{(n-1)}$
		...	...	...	...	...			=	...
			...	...	...	...	...		=	...
				...	...	...	...	...	=	...
					d_{z-2}	e_{z-2}	$f_{z-1} - \frac{m_{z-1}}{\Delta t^2}$	e_{z-1}	=	$\frac{m_{z-1}}{\Delta t^2}\left[y_{z-1}^{(n-2)} - 2y_{z-1}^{(n-1)}\right] - T_{z-1}^{(n-1)}$
						d_{z-1}	e_{z-1}	$f_z - \frac{m_z}{\Delta t^2}$	=	$\frac{m_z}{\Delta t^2}\left[y_z^{(n-2)} - 2y_z^{(n-1)}\right] - T_z^{(n-1)}$

The assumption (10.30) permits expressing the acceleration $\ddot{y}_n$ at the time t_n in terms of the deformations y_{n-2}, y_{n-1}, and y_n. After determining the inertia forces as the products formed by the masses m_i with the corresponding accelerations and after adding these to the aerodynamic forces, we can obtain the total external forces acting on the blade. Then the deformations y_n are determined as in a conventional static problem. This is based on solving the system of equations in Table 1.14. The only special feature of these equations is the fact that the components of the inertia forces expressed in terms of the still uncalculated values of y_n are transposed to the left-hand side and are determined simultaneously with solving the system of equations.

Thus, the determination of the various parameters of blade motion by this

method is carried out in an unconventional order. As it were, first the accelerations and then the deformations are determined. For this reason, we called this method of solution "inverse method of numerical integration". Another frequently used designation is "implicit method".

The calculation with the inverse method of numerical integration does not result in a divergent solution, even at rather large integration steps. Therefore, the size of the required integration step should be determined only on the basis of the magnitude of errors resulting from the use of this method. The magnitude of the error can be estimated by applying the inverse method of integration to the solution of eq.(9.24). The results of this calculation are plotted in Fig.1.57.

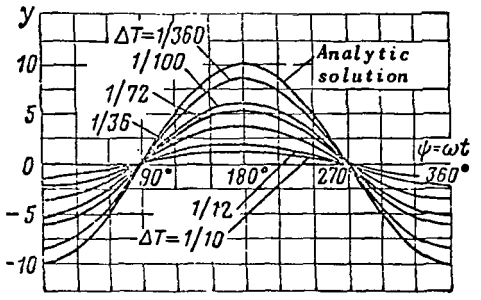

Fig.1.57 Results of Numerical Solution of Eq.(9.26) by the "Inverse Method of Integration", as a Function of the Relative Integration Step.

It follows from these calculations that, to achieve a satisfactory accuracy of the deformation values corresponding to frequencies equal to the rotor rpm, the integration step should be less than 1° with respect to the rotor azimuth $\left(\Delta\bar{T} = \frac{1}{360}\right)$.

In calculating by the method with inverse order of determining the variables, the system of equations in Table 1.14 is solved in sequence at each azimuth, using predetermined values of y_i^{n-2} and y_i^{n-1}. At the initial time, these quantities can be taken arbitrarily. /155

The above method of calculation is more laborious than methods that use expansion of the solution in accordance with prescribed vibration modes, and thus is very time-consuming in calculations on digital computers. However, the method offers valuable advantages in estimating the influence of various concentrated effects on a blade, for example, in estimating the effects produced by blade dampers and in all cases when the solution cannot be represented with sufficient accuracy by a limited number of prescribed modes.

7. Comparative Evaluation of Various Methods of Calculating Flexural Blade Vibrations

In this Chapter, we have presented a large number of methods for calculating flexural blade vibrations; naturally, this raises the question as to what method to select for practical application and what criteria to use as basis for this selection. The answer is quite simple: For practical purposes, the optimum method will always be the one that most fully and accurately takes into account all characteristics of rotor behavior, including the variable induced velocity field and the nonlinear character of the dependence of aerodynamic coefficients on the angle of attack and the Mach number. However, it is impossible here to disregard the existing limitations that the more complete and more accurate the method of calculation, the more time will be required for calculation on digital

TABLE 1.15

		Method of Calculation with Expansion of Solution in Eigenfunctions and Determination of the Coefficients of Expansion of Time Factors in Fourier Series in Harmonics	Method of Calculation with Expansion of the Solution in Eigenfunctions and with Determination of Time Factors by the Method of Numerical Integration of Transformed Equations	Method of Calculation with Direct Determination of the Trajectories of Motion of Individual Points of the Blade
Differential equations		$[EIy'']'' - [Ny']' + m\ddot{y} = T$		$m_i \ddot{y}_i = C_i T_i$
Form of presentation of solution		$y=(a_0-a_1\cos\psi-b_1\sin\psi-a_2\cos 2\psi-b_2\sin 2\psi\ldots)\cdot y^{(0)}+$ $+(c_0-c_1\cos\psi-d_1\sin\psi-c_2\cos 2\psi-d_2\sin 2\psi\ldots)\cdot y^{(1)}+$ $+(e_0-e_1\cos\psi-f_1\sin\psi-e_2\cos 2\psi-f_2\sin 2\psi\ldots)\cdot y^{(2)}+$ $+(g_0-g_1\cos\psi-h_1\sin\psi-g_2\cos 2\psi-h_2\sin 2\psi\ldots)\cdot y^{(3)}$	$y=\sum_j \delta_j y^{(j)}$	$y_i = f(t)$
Method of transformation of equations		Method of B.G. Galerkin		Equations are not transformed
Method of determining time factors		Coefficients of expansion of time factors are determined from a system of algebraic equations	Direct method of numerical integration	Inverse method of numerical integration
Characteristics of method and required computational speed V_{req} for determining stresses in one flight regime within 5-10 min under the following assumptions:	$\lambda = const$ $c_y = c_y^\alpha \alpha$ $c_x = 0$	V_{req} = 5000 operations/sec	$\Delta\psi_{req} = 2.5 \div 5°$ V_{req} = 20000 operations/sec	$\Delta\psi_{req} = 0.5 - 1.0°$ V_{req} = 100000 operations/sec
	$\lambda = var$ $c_y = c_y^\alpha \alpha$ $c_x = 0$	The method is convenient for taking into account a nonuniform induced velocity field expanded in harmonic components V_{req} = 50000 operations/sec	The methods are convenient for taking into account induced velocities determined for a rotor with finite number of blades (for a number of points over the radius $z_r \leq 12$) V_{req} = 100000 operations/sec	V_{req} = 500000 operations/sec
	$\lambda = const$ $c_y = f(\alpha, M)$ $c_x = f(\alpha, M)$	For taking into account the relation $c_y = f(\alpha, M)$ and $c_x = f(\alpha, M)$, this method is unsuitable in practice	The methods are convenient for taking into account the nonlinear relation $c_y = f(\alpha, M)$ and $c_x = f(\alpha, M)$ V_{req} = 500000 operations/sec	V_{req} = 200000 operations/sec
	$\lambda = var$ $c_y = f(\alpha, M)$ $c_x = f(\alpha, M)$		at $z_r = 12$ V_{req} = 250000 operations/sec	V_{req} > 100000 operations/sec

computers. Therefore, in selecting the optimum calculation method, the main criterion is the machine capability which places a limit on the use of the most refined calculation methods.

To select the most suitable calculation method, we compiled Table 1.15 which also gives the required speed of computation for various methods of calculation. The table also shows the basic characteristics of the different methods.

Here, we will present approximate values of the required speed of operation per second V_{req} for carrying out a calculation within 5 - 10 min. The required speed is given for all calculation methods in four variants of the assumptions used. The required capacity of the computer memory is not estimated in Table 1.15 since, in modern computers, this usually constitutes no handicap for the programmer.

It follows from a perusal of the data in Table 1.15 that, for a low-speed /157 computer (speed of the order of 5000 operations/sec), only one method known as the method of calculation in harmonics can be used to any greater extent. In this method, the solution is expanded in eigenfunctions. The time factors in these functions are represented as a Fourier series in harmonics. The coefficients of this series are determined from a system of algebraic equations derived from a differential equation by means of Galerkin's method. This method is described in Section 8.

On low-speed computers, this method can be used only under the assumption of a uniform induced velocity distribution λ = const. For taking into account the nonlinear dependence of aerodynamic coefficients on the profile angle of attack and on the Mach number, the method is practically useless. These relations can be considered in this method only by making extensive assumptions. However, even with such an approach, the computation necessary for constructing the mathematical formulas is so laborious that, for all practical purposes, it is simply unfeasible.

On moderate-speed computers (speed of 20,000 - 50,000 operations/sec), the most convenient method is to expand the solution in eigenfunctions and to determine the time factors of these functions by numerical integration. This method is presented in Section 9, and is quite convenient for taking into account the nonlinear correlation between aerodynamic coefficients, profile angle of attack, and Mach number.

In cases in which the variable induced velocity field must be considered, this method can be used only on high-speed computers. If, in determining the induced velocities, the number of calculated points over the radius and azimuth of the rotor is limited, the calculation can be performed also on moderate-speed computers.

The method of calculation with direct determination of the trajectories of motion of individual blade points (see Sect.10) can be used only on computers with a speed greater than V > 100,000 operations/sec. A consideration of the variable induced velocity fields and of the nonlinear correlations between aerodynamic coefficients, profile angle of attack, and Mach number further increases the speed needed for this method. Only the inverse numerical integration method

is considered in the last column of Table 1.15. In using the direct method of numerical integration, the required computer speed for the method with direct determination of the trajectories of motion of imdividual blade points may increase even more steeply.

The required computer speeds given in Table 1.15 are obtained for the case in which the computations require 5 - 10 min. Within this time, it is possible to make several checkouts required in designing a blade with variation in rotor parameters and flight regime.

If we limit ourselves to a calculation at only one variant of the parameters, a longer computer time is admissible. In this case, the required computer speed shown in Table 1.15 can be reduced accordingly.

Using the above considerations, it is possible - for each individual case - to select the optimum method based on the possibility of using various assumptions and available time in calculations on a computer.

Section 11. Fatigue Strength and Blade Life /158

1. Testing a Structure to Determine its Service Life

The service life of a given structure is usually established on the basis of results of dynamic analysis.

Depending upon how essential the structure is for flight safety, tests of one or several design variants are performed. Frequently, only individual parts of a structure whose strength is decisive for the entire unit as a whole, are tested.

In determining the blade life, it is conventional to test individual spar segments with airframe components that set up stress concentrations in the spar. Specimens of at least three different spar segments are tested. As a rule, these segments include the root butt and two segments along the length of the spar. Sometimes it becomes necessary to test additional specimens to check individual design features of the spar (for example, at points of transition of the spar cross section).

Specimens of blades are almost always tested on resonance stands, with excitation by mechanical vibrators. The length of the test specimen is chosen such that its natural frequency in bending is within the operating range of the vibrator. Usually the tests are conducted at a frequency of 1500 to 2500 cycles per minute. In this case, the length of the specimens is of the order of 3-4 m. In addition to alternating bending stresses, the specimen must be extended by longitudinal forces creating a constant static load close to that which the blade experiences in flight due to the effect of centrifugal forces. Figure 1.58 shows a stand for testing of helicopter blade specimens with a centrifugal force of the order of 100 tons (force).

In general, complete blades rather than individual short specimens are tested, because of the excessive complexity of test stands required for this pur-

pose and the long testing time, since the vibration frequency in this case cannot be higher than 300 - 400 cpm.

2. Dispersion of the Characteristics of Endurance in Fatigue Tests

An appreciable scattering of the test results is observed in fatigue tests on a certain number of specimens manufactured under identical conditions. Failure of specimens tested at the same stress level occurs at a different number of cycles N. The ratio of the greatest number of cycles to the least number often reaches 20 - 40. /159

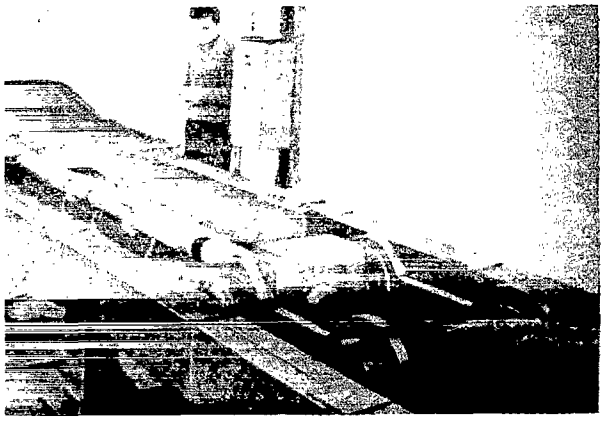

Fig.1.58 Blade Test Stand.

The dispersion of the characteristics of fatigue strength is explained by the inhomogeneity of the structure of the material and by the difference in the conditions of manufacturing and processing the specimens. Failure of specimens always begins from small flaws within the material and on the surface of the specimen. In the overwhelming majority of cases, failure begins from a defect situated on the surface. In this case, the endurance characteristics of the specimen are determined by the type and magnitude of these defects.

The scattering of fatigue failure data in tests of various specimens is usually characterized by a distribution function of the number of cycles N to failure of the specimen. An analysis of the test data indicates that the distribution of logarithms of the number of cycles log N to failure rather closely obeys the normal distribution law at almost all average values of the probability of failure, beginning approximately from a probability of 0.01 - 0.02.

Figure 1.59 shows the distribution of the probability of failure P and the probability density φ, corresponding to the real characteristics of endurance of the structure (solid curves) and those determined by the normal distribution law (broken curves):

$$\varphi(\log N) = \frac{1}{S_{\log N}\sqrt{2\pi}} \cdot e^{-\frac{(\log N - m_{\log N})^2}{2S^2_{\log N}}}; \qquad (11.1)$$

$$P(\log N) = \int_{-\infty}^{\xi} \varphi(\xi)\, d\xi. \qquad (11.2)$$

Here,

$\varphi(\log N)$ = probability density function of failure of the structure;
$P(\log N)$ = probability of failure of the structure at a number of cycles of stress less than N;
$\xi = \log N$ = value of the logarithm of the number of cycles to failure of the structure;
$S_{\log N}$ = mean-square deviation of the distribution of the logarithms of the number of cycles to failure of the structure;
$m_{\log N}$ = mathematical expectation of the distribution of the logarithms of the number of cycles.

In the range of low probability of failure, the distribution function usually deviates from the normal law (Fig.1.59). This has to do with an important feature of the characteristics of endurance. In fact, fatigue failure can take place only after a certain number of cycles of stress N_0 and can never occur earlier. This feature of the characteristics of endurance leads to the concept of a zone of insensitivity to N in which the probability of failure of the structure is equal to zero (P = 0). In particular, this permits an important conclusion as to the possibility of determining the service life of the structure, based on endurance conditions with a probability of failure equal to zero, even in the presence of sufficiently high alternating stresses.

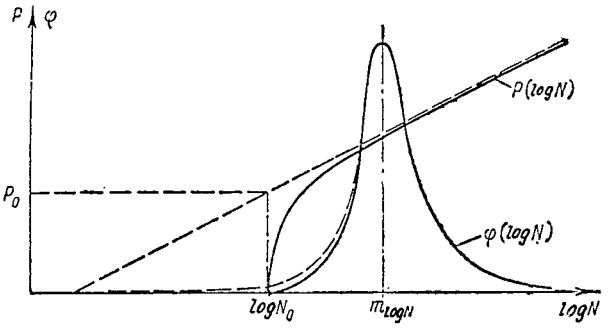

Fig.1.59 Curves for the Distribution of Endurance in Tests and Corresponding to Normal Law.

Unfortunately, a determination of the sensitivity threshold N_0, with any satisfactory accuracy, is virtually impossible. Therefore, in determining the service life of a given structure the distribution law of endurance is usually taken as normal, and the requirement P = 0 is replaced by the requirement of a very low probability of failure.

/160

The deviation of the values of the logarithms of the number of cycles from the normal law should be observed also in the region of high probabilities of failure. At a relatively low level of alternating stresses this happens since there is almost always some specimen that does not fail even at a very large number of cycles of stress.

3. Basic Characteristics of the Fatigue Strength of Structure

The fatigue strength of a structure is characterized usually by the number of cycles N it is able to withstand prior to failure at a given upper limit of alternating stresses σ. The higher the upper limit of alternating stresses σ, the smaller the number of cycles of stress the structure will resist.

The curve characterizing the number of cycles N to failure as a function of the upper limit of alternating stresses σ is called the Wöhler curve.

The Wöhler curve can be approximately described by the equation

$$\left.\begin{aligned} \sigma^m N = \text{const} \quad &at \quad \sigma > \sigma_w \; and \; N < N_w; \\ \sigma = \sigma_w = \text{const} \quad &at \quad N > N_w. \end{aligned}\right\} \tag{11.3}$$

Here,

σ_w = maximum amplitude of stress below which the structure will withstand an indefinitely large number of cycles of stress N without fracture; this peak amplitude is usually called the fatigue limit or endurance limit;

N_w = minimum number of cycles of stress corresponding to the fatigue limit;

m = some exponent whose value is determined from test results.

The Wöhler curve can be plotted for different values of the probability of failure. For this, a batch of test pieces is divided into several groups and tested at different ranges of alternating stresses.

After constructing the distribution functions of endurance for various levels of alternating stresses (Fig.1.60) and connecting points of the same probability of failure, we can obtain the Wöhler curves corresponding to a different probability of failure. Usually, in so doing the dispersion of the characteristics of endurance is smaller, the higher the level of alternating stresses, and the sensitivity threshold N_0 is more distinctly expressed at lower stresses. At low stresses, the sensitivity threshold is reached at relatively high probabilities P, whereas at high stresses it shifts toward such small probabilities that it usually goes unnoted. /161

The test data almost always confirm the presence of a fatigue limit σ_w. At a given stress σ a certain number of specimens usually will not fail even at a very large number of cycles of stress. The existence of a fatigue limit is confirmed also in practical experience of operating various machines and mechanisms. We know of many different components that constantly operate under appreciable alternating stresses and do not fail at a number of cycles of 10^8 and more. There are individual exceptions to this general rule. It has been noted that, for certain structural elements made of aluminum alloys, the fatigue curve continues to drop even at an endurance of the order of $10^8 - 10^{10}$ cycles. However, this drop is so negligible that even in this case the Wöhler curve can be approximately represented in the form of eq.(11.3). In any case, as applied to the basic parts of a helicopter, consideration of this drop yields no substantial refinements.

A definite dispersion is also observed in the values of the endurance limits. The presence of a sensitivity threshold with respect to the amplitude of stresses is characteristic for their distribution. This threshold will henceforth be called the minimum fatigue limit $\sigma_{w\min}$. At stresses below $\sigma_{w\min}$ not a single specimen will fail, even at a very large number of cycles of stress. In con-

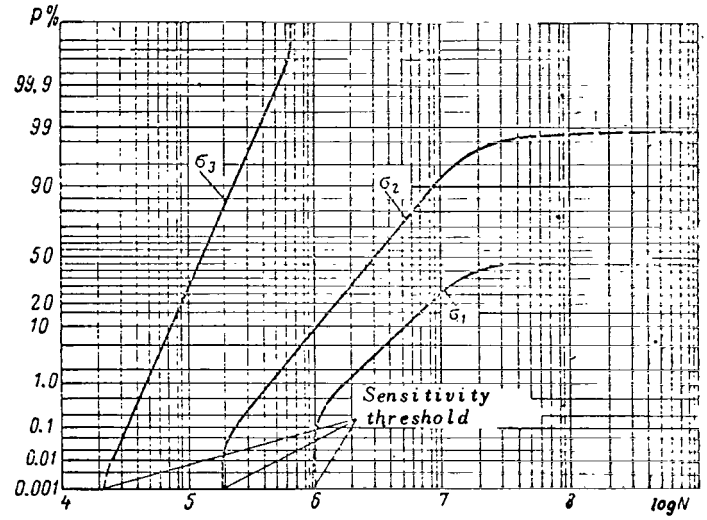

Fig.1.60 Distribution of Endurance at Different Levels of Alternating Stresses.

/162

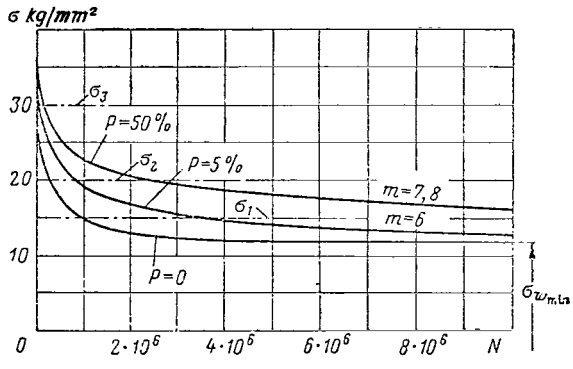

Fig.1.61 Wöhler Curves Corresponding to Different Probability of Failure.

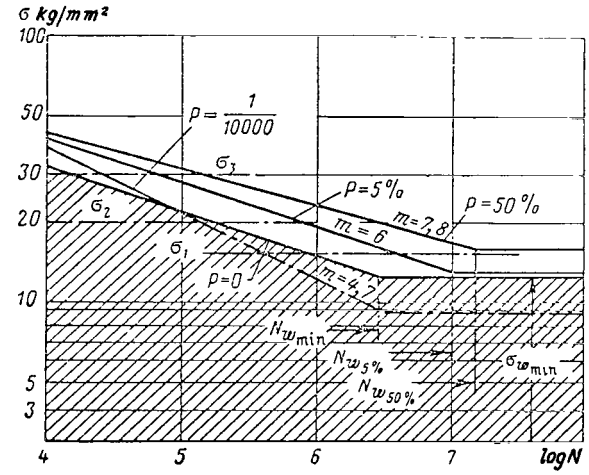

Fig.1.62 Wöhler Curves Corresponding to Different Probability of Failure on a Logarithmic Scale.

formity with the above features of the characteristics of fatigue, the Wöhler curves should have the slope depicted in Fig.1.61.

If the curves corresponding to a different probability of failure are replaced by an approximate analytic relation (11.3), then the Wöhler curves on a logarithmic scale will have the slope shown in Fig.1.62. The zone of insensitivity corresponding to zero probability of failure is hatched in this graph.

At such a plotting of the Wöhler curves, the number of cycles N_w corresponding to the endurance limit and the exponent m differ for curves corresponding to different probabilities of failure.

It should be noted that construction of the Wöhler curves as shown in Figs.1.61 and 1.62 is possible only in tests with small laboratory specimens, since a very large number of test pieces is required.

Construction of such curves is practically impossible when estimating the strength of a structure, since only a very small number of specimens can be used in such estimates. Often this number does not exceed n = 3 - 5 (where n is the number of tested specimens). In this case, the tests yield only n values of the number of cycles to fracture at a prescribed magnitude of loads for a strength estimate. With such a limited number of data, some idea on the fatigue characteristics of a given structure can be gained only on the basis of certain assumptions with respect to the Wöhler curves.

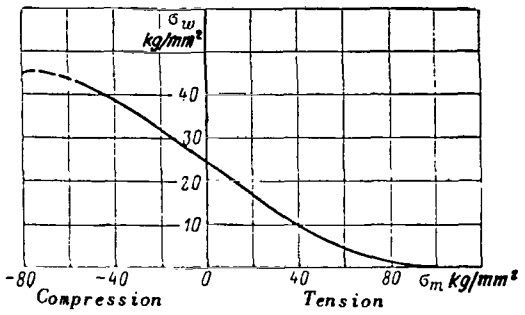

Fig.1.63 Hay's Diagram for Specimens of Tubular Blade Spars.

The range of alternating stresses at which the structure will withstand a prescribed number of cycles N to failure depends also on the magnitude of the constant component of the stresses of the cycle σ_m (static load). The greater the /163 static load, the smaller the range of stresses at which the structure will withstand a given number of cycles. This dependence is usually characterized by Hay's diagram. As an example Fig.1.63 shows the configuration of such a diagram.

For tubular steel spars at σ_m = 20 - 30 kg/mm² an increase in static load by an amount $\Delta\sigma_m$ leads to a decrease in the fatigue limit by an amount $\Delta\sigma_w \approx \approx 0.4\Delta\sigma_m$. For duralumin spars at σ_m = 6 - 8 kg/mm², the value is $\Delta\sigma_w \approx 0.3\Delta\sigma_m$.

It should be mentioned that, in the region of constant compressive stresses, the fatigue limits increase substantially. This fact is utilized when conferring strength to components by cold-working (see Subsects.16 and 17).

4. Stresses Set Up in the Blade Structure in Flight

In Section 1 of this Chapter (Subsect.3) it was mentioned that, under the effect of aerodynamic forces, the blades of a helicopter in flight are subject to appreciable alternating stresses in two different types of regimes designated as low-and high-speed modes.

Figure 1.64 shows the type of variation in amplitudes of alternating stresses with respect to flying speed, for two blade structures: one with a steel and one with a duralumin spar. As indicated in this diagram, maximum alternating stresses can arise both at low speeds (braking regime) and at maximum flying

speed. As demonstrated before, the blades perform flexural vibrations such that, at each point of the spar, the stresses vary in accordance with a periodic law duplicating each revolution of the rotor. As a typical example, Fig.1.65 shows the recording of stresses obtained in blade sections at relative radii $\bar{r} = 0.73$ and $\bar{r} = 0.8$ in horizontal flight at relatively high speed. The same diagram gives the harmonic content of the stresses set up in these blade sections.

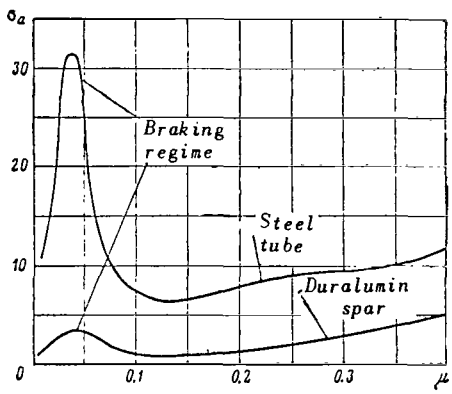

Fig.1.64 Character of Variation in Amplitudes of Alternating Stresses as a Function of Flying Speed in Blades of Low (Tubular Steel) and Moderate (Duralumin Spar) Rigidity in the Flapping Plane.

Usually, in a horizontal flight at $\mu = 0.2 - 0.4$ the first harmonic component of the stresses reaches maximum values. The second harmonic is lower in amplitude and generally amounts to 30 - 70% of the first harmonic. The first and second harmonics, generally totaling 70 - 90%, determine the magnitude of the total alternating blade /164 stresses in these regimes, since the higher harmonics usually are small. Their magnitude almost always decreases with an increase in order of the harmonic. Such a type of variation in magnitude of harmonics can be attributed to a decrease in magnitude of the harmonic components of aerodynamic forces on change-over to higher harmonics.

For all blades there are exceptions to this rule, having to do with the occurrence of or proximity to resonance.

In low-speed modes, the harmonic content of the effective stresses is different. Here the higher harmonics predominate, and harmonics close in frequencies to the frequency of the natural vibrations of the second and third overtones are mainly distinguished. An especially pronounced increase in alternating stresses in these flight regimes (see Fig.1.64) takes place for blades of low rigidity in the flapping plane (see Sect.3, Subsect.3). For such blades, stresses with the fourth and sixth harmonics are predominant (Fig.1.66). Low-speed modes may cause damage to the structure of such blades (see Table 1.21).

For a blade of moderate rigidity in the flapping plane, the increase in alternating stresses at low speeds is appreciably weaker (see Fig.1.64) and predominance of higher harmonics is not so marked (Fig.1.67). For such blades (just as for blades of high rigidity) high-speed flight modes may lead to basic damage potential.

Along with alternating stresses due to flexural vibrations, the blade spar is extended and bent by constant (in magnitude) centrifugal forces and by the constant component of the aerodynamic forces. Therefore, the spar material works under alternating stresses with a large static load. The static load markedly lowers the fatigue strength of the spar.

5. Hypothesis of Linear Summation of Damage Potential and Average Equivalent Amplitude of Alternating Stresses

In different flight regimes, alternating stresses of widely differing magnitude are set up in a structure. In this case, the duration of individual flight regimes may differ substantially. Thus, a flight at cruising speed is usually the regime of longest duration. In helicopters used for cargo transport,

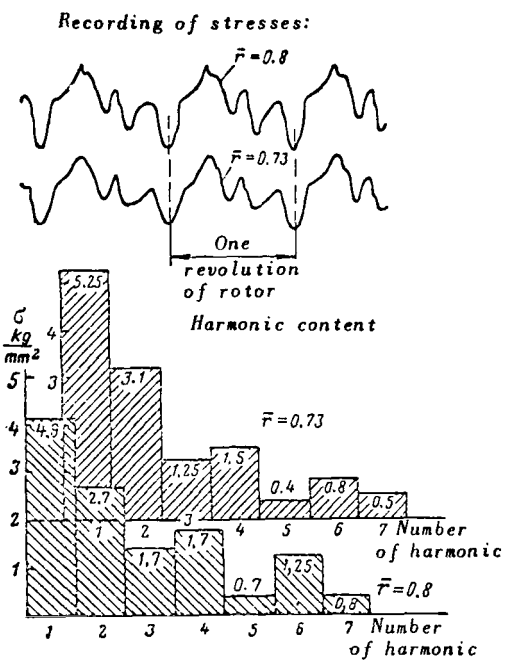

Fig.1.65 Recording of Stresses in Two Sections of a Helicopter Blade in Horizontal Flight Regime (μ = = 0.3) and their Harmonic Content.

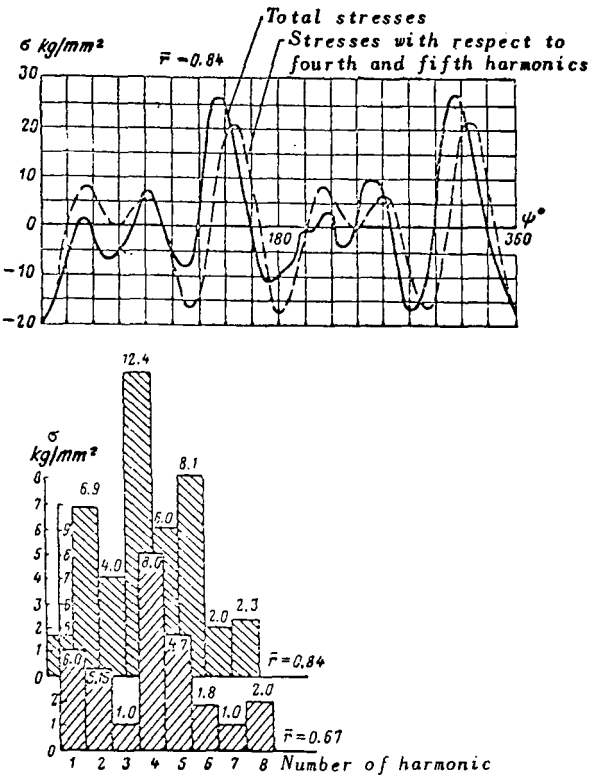

Fig.1.66 Oscillogram of Alternating Stresses in a Blade with a Tubular Steel Spar of Low Rigidity in the Flapping Plane during Braking, and their Harmonic Content.

this regime occupies 60 - 70% of the service life. The maximum flying speed /166
of cargo helicopters used in the national economy is rarely reached. Such helicopters also spend very little time in low-speed modes which generally are only transient regimes during takeoff and approach to landing.

However, helicopters can be used for widely differing types of work, where the duration of individual flight regimes varies. As an example, Table 1.21 gives

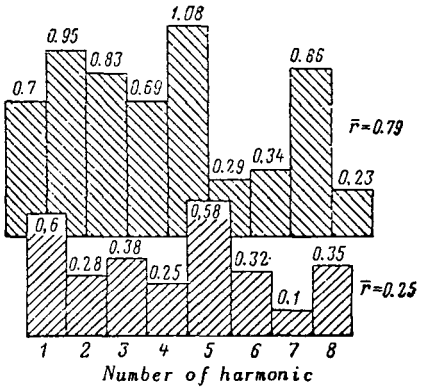

Fig.1.67 Harmonic Content of Alternating Stresses in a Blade of Moderate Rigidity with a Pressed Duralumin Spar in Braking Regime.

the values of the relative duration of different regimes α_i common for one of the military transport helicopters.

The service life of a given structure should be determined with consideration of the time base of a helicopter in flight regimes of differing alternating stress level which contribute to the structure a different portion of fatigue damage potential. To take this into account it is convenient to use the hypothesis of linear summation of damage potentials. This hypothesis presupposes the possibility of summing individual components of damage potential contributed by different stress levels and stipulates that failure of a structure takes place as soon as

where

$$\left.\begin{aligned} \Delta\bar{N}_\Sigma &= 1, \\ \Delta\bar{N}_\Sigma &= \sum_i \frac{\Delta N_i}{N_i}. \end{aligned}\right\} \qquad (11.4)$$

Here,

N_i = number of cycles to failure for a steadily sustained stress level with amplitude σ_i;

ΔN_i = number of cycles of stress with amplitude σ_i experienced by the structure in the i-th flight regime.

The ratio $\Delta\bar{N}_i = \frac{\Delta N_i}{N_i}$ is usually called the damage potential of a structure in a regime with an amplitude of stresses σ_i, while $\Delta\bar{N}_\Sigma$ is designated as total damageability.

It has been proved by other authors that, at a certain alternation of stress regimes, failure of a structure may take place as soon as

$$\Delta\bar{N}_\Sigma < 1.$$

However, the cases discussed in those papers, for the most part, do not cover stress conditions of the helicopter parts. Therefore, we can almost always use eq.(11.4) in the calculations.

As a consequence of the dispersion of the characteristics of endurance, the damage potential of individual specimens of a given structure may differ even for one and the same stress level. Structures with the lowest values of endurance are subject to maximum damageability. Therefore, one can talk of damage potential as corresponding to a certain probability of failure.

If, in eq.(11.4), the values of N_i corresponding to an assigned probability of failure P_{asd} are given, then the probability of failure will also be equal to

P_{asd} at $\Delta\bar{N}_{\Sigma} = 1$. This makes it possible to obtain the formula for calculating the safe number of cycles of stress N_s with the assigned probability of failure P_{asd} determining the service life of structures based on endurance conditions:

$$N_s = \frac{1}{\sum_i \frac{\alpha_i}{N_i}}. \tag{11.5}$$

Here,

$\alpha_i = \frac{\Delta N_i}{N_{s.i}}$ = relative duration of the regime with stress σ_i;

$N_{s.i}$ = number of cycles of stress during the life of the structure when determining the relative duration of individual flight regimes α_i (generally speaking, we can take any arbitrary interval of the service time of a helicopter with a number of cycles N that need not at all be equal to the number of cycles of stress during the rated service life of the structure $N_{s.i}$); /167

N_i = number of cycles of stress of amplitude σ_i at which the probability of failure is equal to that assigned (P_{asd}).

If the acting stresses are lower than the minimum fatigue limit, then damageability is not introduced into the structure. In this case, the number of cycles N_i in eq.(11.5) can be set equal to infinity.

Let us introduce the concept of relative duration of regimes ϵ which add a damage potential to the structure:

$$\varepsilon = \frac{N_d}{N_{s.l}},$$

where N_d is the number of cycles of stress during the life of the structure which contributes to damageability.

Thus, during the service life R, the structure is damaged only during a time equal to ϵR.

It often proves convenient, for greater clarity of the calculations, to introduce the concept of average equivalent amplitude of alternating stresses.

The average equivalent amplitude of stresses is an amplitude constant in time and acting during a part of the service life equal to ϵR, which contributes damageability to the structure equal to the damageability introduced by amplitudes of alternating stresses differing in magnitude in all flight regimes encountered during the service of a helicopter.

In introducing this concept, it is assumed that at stresses greater than the fatigue limit, the endurance of the structure can be determined as

$$N_i = N_w \left(\frac{\sigma_w}{\sigma_i}\right)^m. \tag{11.6}$$

Then, substituting eq.(11.6) into eq.(11.4), we obtain

$$\frac{\sum_i \Delta N_i \sigma_i^m}{N_w \sigma_w^m} \Rightarrow 1, \tag{11.7}$$

where summation is performed only for those regimes that raise the damage potential to the structure.

If we introduce one equivalent stress level with an amplitude σ_{eq} and with a number of cycles determined from the stipulation that stresses σ_{eq} act continuously during a part of the service life εR, i.e., that $N_{eq} = \varepsilon N_{s.l}$, then we can write

$$\sum \Delta N_i \sigma^m \Rightarrow \varepsilon N_{s.l}\, \sigma_{eq}^m. \tag{11.8}$$

Consequently,

$$\sigma_{eq} = \sqrt[m]{\frac{1}{\varepsilon} \sum_i \alpha_i \sigma_i^m}. \tag{11.9}$$

The calculation of equivalent stresses for a blade of a helicopter at the maximally stressed section at a relative radius $\bar{r} = 0.74$ is given as an example in Subsection 12; see also Table 1.21. The spar of this blade is a steel tube squashed into an ellipse over its entire length, beginning from radius $\bar{r} = 0.3$. The minimum fatigue limit of the tubular blade at this station, based on results of dynamic tests, can be taken as equal to $\sigma_{w_{min}} = 13$ kg/mm^2. /168

Stress analysis of a blade with a tubular steel spar is usually carried out in two planes: in the plane of minimum (σ_y) and in the plane of maximum rigidity (σ_x). In this case, it may happen that, at some point of the perimeter of the spar section, the amplitude of alternating stresses reaches a magnitude $\sigma_\Sigma = \sqrt{\sigma_x^2 + \sigma_y^2}$ greater than the amplitude σ_y.

However, usually owing to the phase difference of the stresses acting in these two planes, such a magnitude of alternating stresses is almost never reached. Therefore, in calculating the service life of a blade we can use the approximate formula:

$$\sigma_\Sigma = \sigma_y + \xi \left(\sqrt{\sigma_x^2 + \sigma_y^2} - \sigma_y\right).$$

The coefficient ξ can be calculated if a simultaneous recording of stresses σ_x and σ_y is available. If there are no data for determining ξ, then sufficiently

reliable results can be obtained by assuming $\xi = 0.5$.

6. Dispersion of the Amplitudes of Alternating Stresses in an Assigned Flight Regime

In measuring alternating stresses in flight it has been found that, at an assigned flight regime, the magnitudes of stresses differ during the flight regime and in different flights. This makes it necessary to introduce the average equivalent amplitude of alternating stresses in all flight regimes.

To determine this amplitude, we can use special oscillogram decoders which permit determining the number of amplitudes of stresses n_k located in the range

$$\Delta\sigma_k = \sigma_k - \sigma_{k-1},$$

where σ_k and σ_{k-1} are the amplitude levels of alternating stresses selected for the calculation.

Then, the average equivalent amplitude of alternating stresses in the regime in question can be determined by a formula analogous to eq.(11.9):

$$\sigma_i = \sqrt{\frac{1}{\varepsilon_i}\sum_k \bar{n}_k \sigma_k^m}. \tag{11.10}$$

Here,

$\bar{n}_k$ = relative number of cycles with amplitude σ_k

$$\bar{n}_k = \frac{n_k}{n_\Sigma},$$

where

n_k = number of cycles with amplitude σ_k while n_Σ is the total number of cycles recorded by the decoder;

ε_i = relative number of cycles with stresses greater than the minimum fatigue limit in the i-th flight regime.

Summation with respect to k is carried out only for those time intervals in the i-th regime in which the amplitude of stresses σ_k is greater than the minimum fatigue limit $\sigma_{w_{min}}$.

When determining the average equivalent amplitude during the entire service life of a helicopter by means of eq.(11.9), the amplitude in each flight regime should be calculated from eq.(11.10), while the relative duration of the regimes raising the damage potential of the structure is calculated by the formula

$$\varepsilon = \sum_i \varepsilon_i a_i.$$

To simplify the decoding, it is general practice to replace determination /169 of the equivalent amplitude by the maximum amplitude in each regime; this raises

the reliability margin but leads to some decrease in service life of the structure.

7. Method of Calculating Service Life with the Use of Reliability Coefficients

The problem of determining the service life of a given structure reduces to finding some safe number of cycles of stress in service N_s at which the probability of failure of the structure is very small and equal to the assigned value. If it were possible to test a sufficiently large number of specimens, it would be easy to find N_s after determining the distribution characteristic of their service life (Fig.1.68). Numerous methods of calculation of service life [see, for example (Ref.43)] are based on this approach. However, it is usually necessary to determine the service life of a structure on the basis of dynamic tests of a few specimens n of the structure, where it is impossible to determine the distribution of service life with the required accuracy. Therefore, the method of calculation of service life of a structure, based on the introduction of certain margins of reliability with respect to the number of cycles η_N and amplitude of alternating stresses η_σ, has become popular in practical engineering.

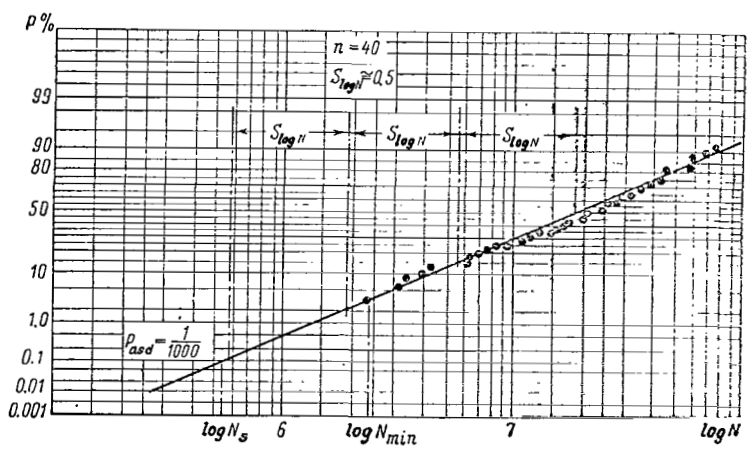

Fig.1.68 Determination of Safe Number of Cycles, Based on the Service Life Distribution Curve.

To calculate the service life by this method, it is necessary to make a stress analysis of a structure in various flight regimes, to determine the equivalent stresses, and to conduct dynamic tests of one or several specimens of the structure at stresses of

$$\sigma_{test} = \eta_\sigma \sigma_{eq} . \qquad (11.11)$$

The margin of reliability η_σ is introduced here to take into account the possible difference in values of alternating stresses in identical units of different helicopters.

After testing the specimens and obtaining the minimum value of cycles to failure N_{min}, we determine the safe number of cycles of stress in service, by means of the formula

$$N_s = \frac{N_{min}}{\eta_N}. \qquad (11.12)$$

The margin of reliability η_N is introduced to take into account the dispersion of the endurance characteristics. /170

Then, the service life of a structure in hours can be determined from the formula

$$R = \frac{N_s}{60f},$$

where f is the frequency of stressing the blade in service (cycles per minute).

In some cases, the endurance of a structure might depend on the frequency of stress application. Therefore, if dynamic tests are carried out at a frequency greater than the frequency of stressing in flight, it will be necessary to introduce an additional margin for the frequency of stressing η_f. This margin is introduced mainly for components made of duralumin and for tests carried out at a frequency which is by a factor of 5 - 10 higher than the frequency of stressing in flight. In this case, the value is taken as equal to $\eta_f = 1.5 - 2.0$. When allowing for these factors, the formula for determining the service life can be written in the form

$$R = \frac{N_{min}}{60f\eta_N\eta_f}. \qquad (11.13)$$

If we assume that the distribution of the endurance characteristics obeys the normal law and that the parameters of this law are known, then, as already mentioned, the magnitudes of the required reliability margins with respect to the number of cycles η_N and amplitude of alternating stresses η_σ could be determined by calculation, after assigning a certain, sufficiently small probability of failure of the structure in service. However, such calculations cannot lay claim to high accuracy. Therefore, we can use the method of assigning the magnitudes of these coefficients on the basis of helicopter operating experience.

On the basis of such experience, the safety factor with respect to the amplitude of alternating stresses η_σ can be taken as equal to 1.2, whereas the factor with respect to the number of cycles of stress η_N varies as a function of the number of tested specimens and the degree of essentiality of the unit for flight safety.

All units and components of a helicopter can be divided into four groups based on degree of essentiality for flight safety:

Group I - units whose failure leads to immediate and complete disruption of

operability and safety, with a difficultly detectable incipient fatigue crack. This group includes blades whose spar is covered and does not permit postflight inspection, a variety of components of the hub and controls of the main and auxiliary rotors not accessible to inspection, the rotor shaft, etc.

Group II - units whose failure could lead to immediate and complete disruption of operability of the structure and flight safety, but where early detection of incipient fatigue cracks is possible. This group includes blades with a reliably operating system signaling the appearance of cracks, as well as all other units classified in Group I provided that incipient fatigue cracks can be detected in preflight inspection.

TABLE 1.16

SAFETY FACTORS WITH RESPECT TO NUMBER OF CYCLES*

Number of Tested Specimens n	Safety Factor η_N			
	Group I	Group II	Group III	Group IV
1	12	6.0	6	2.5
2	8	4.0	4	2.0
3	6	3.0	3	1.5
6	4	2.5	2	1.0

* The factors η_N given for Group I of the units are double the usual values, since they include also the factors η_Σ often introduced to allow for inaccuracy of the hypothesis of linear summation of damageability.

Group III - units whose failure leads to partial loss of operability and endangers flight safety, but permits forced landing without damage to the helicopter. This group includes numerous fuselage parts and even the reduction gear framework if it is redundant.

Group IV - units whose failure causes partial loss of operability, allows continuance of flight, does not lead to rapid failure of other units, and permits detecting rupture in ground inspection. This group includes numerous elements of the fuselage, stabilizer of the helicopter, and of other related structural elements. /171

The more essential the unit, the greater should be the magnitude of the safety factor with respect to the number of cycles. The following values of these factors are proposed here (Table 1.16).

In practice it is possible to realize safety factors for the number of cycles required in Groups I and II of helicopter parts only at a very low frequency of stress alternation in flight. In establishing the service life with such large safety factors for all basic helicopter units, tests up to a very large number of cycles, much greater than 10^7 cycles, would be required; this would take a great deal of time. Therefore, an accelerated method of dynamic tests with a safety factor for the number of cycles of $\eta_N = 1$ or of even less than unity is gaining in popularity. In this case, the required reliability is secured by introducing only the safety factor for stresses. To convert the factor η_N to the factor for η_σ we generally use eq.(11.3) with the exponent $m = 6$. With this approach, the required factor of safety for the amplitude of alternating stresses differs, depending on the number of tested specimens and is greater for duralumin, making it necessary to introduce an additional factor for the difference of the frequency in tests and in flight.

TABLE 1.17

Number of Tested Specimens n	η_σ (η_N=1)	
	Steel	Duralumin
1	1.8	2.0
2	1.7	1.9
3	1.6	1.8
6	1.5	1.7

With consideration of the aforesaid, it is possible to adopt safety factors for the amplitude of alternating stresses indicated in Table 1.17 for Group I of helicopter parts.

In dynamic tests with such safety factors η_σ, the safe number of cycles is determined with respect to the minimum number of cycles of stress of the specimen to failure $N_s = N_{min}$.

It should be borne in mind, however, that the conduction of tests with such large safety factors for the amplitude of alternating stresses is possible only if the character of the stress distribution for different components of the structure does not substantially change on increasing the load. If, upon increasing the loads, there is a redistribution of stresses as a consequence of say flare-out of joints, occurrence of mutual displacements of contacting parts which ordinarily work under loads without such displacements, or for other similar reasons, application of this test method is not recommended.

8. Method of A.F.Selikhov for Calculating the Required Safety Factor with Respect to the Number of Cycles η_N /172

As mentioned above in Subsection 2, the endurance of a structure has a sensitivity threshold with respect to the number of cycles N_0 so that the distribution function in the region of low probabilities of failure deviates from the normal law. Theoretically, one could select a safety factor for the number of cycles η_N such that the probability of failure of the structure would be equal to zero. However, as shown elsewhere (Ref.44), for a sufficiently accurate determination of the sensitivity threshold a large number of specimens is required so that it usually is impossible to determine its magnitude for a structure. Therefore, one generally assumes that the logarithms of the number of cycles to failure log N are distributed according to the normal law and the service life of the structure is not based on the condition that the probability of failure is P = 0 but on the condition that this probability is sufficiently small, say equal to P = 1/10,000. If there actually is a threshold of sensitivity present, then the stipulation of such a small prob-

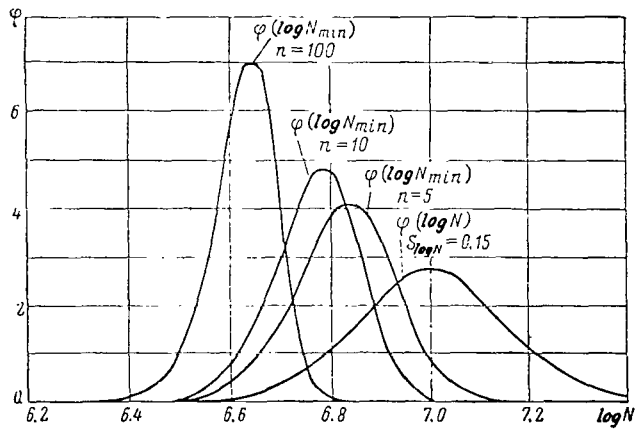

Fig.1.69 Distribution of Minimum Endurance Values for a Different Number of Specimens.

ability of failure, calculated in accordance with the normal law of distribution, tends to be more rigorous than the requirement P = 0 which could be imposed if the value of N_0 were calculable. Therefore, a determination of safety factors on the basis of a somewhat greater probability of failure, say P = 1/1000 and even P = 1/100, is entirely permissible.

To determine the required safety factors for the number of cycles we can use the method proposed by A.F.Selikhov. This method involves the following:

Assuming that the distribution of the logarithms of the numbers of cycles to failure of a structure obeys the normal law

$$\varphi(\log N)=\frac{1}{S_{\log N}\sqrt{2\pi}}\cdot e^{-\frac{(\log N-m_{\log N})^2}{2S^2_{\log N}}}, \qquad (11.14)$$

then the distribution of the minimum endurance values of a certain batch of specimens of this structure can be determined from the formula

$$\varphi_{\min}(\log N)=\frac{n}{2^{n-1}}\left[1+\Phi\left(\frac{m_{\log N}-\log N}{S_{\log N}\sqrt{2}}\right)\right]^{n-1}\varphi(\log N), \qquad (11.15)$$

where

n = number of tested specimens;

$\Phi(x)$ = Laplace function $\left(x=\dfrac{m_{\log N}-\log N}{S_{\log N}\sqrt{2}}\right)$.

The character of the distribution of $\varphi_{\min}(\log N)$ for values $S_{\log N}$ = 0.15 and n = 5, 10, and 100 is indicated in Fig.1.69. The values of the mathematical expectations and the mean-square deviations of this distribution as a function of $S_{\log N}$ and n can be found from the curves presented in Figs.1.70 and 1.71.

The mathematical expectation of the minimum endurance value can be determined by the formula

$$m_{\log N_{\min}}=m_{\log N}-\Delta m_{\log N}.$$

The value of $\Delta m_{\log N}$ is determined as a function of the mean-square deviation $S_{\log N}$ and of the number of tested specimens, from the curve in Fig.1.70.

The mean-square deviation of the minimum endurance value $S_{\log N\min}$ referred to $S_{\log N}$ is given in Fig.1.71.

Thus, if the characteristics of the distribution of endurance of the structure are known, eq.(11.15) can be used for determining the distribution of the minimum endurance values when testing a small number of specimens n. Knowing this distribution, we can determine the probability of failure of a structure at a number of cycles of stress of /173

$$N_s = \frac{N_{min}}{\eta_N}, \tag{11.16}$$

where

η_N = reliability coefficient with respect to the number of cycles;
N_{min} = minimum value of the number of cycles to failure of the structure in tests.

Taking the logarithm of eq.(11.16), we obtain

$$\log N_s = \xi - \log \eta_N, \tag{11.17}$$

where

$$\xi = \log N_{min}.$$

If dynamic tests of full-scale models are carried out at loads equivalent to the loads acting on the structure in question in flight, it can be taken as certain that the distribution of endurance in dynamic tests and under service conditions is identical. A difference in these distributions can arise only from errors in the dynamic tests and from the scale effect in cases in which the volume of the loaded material in the structure is greater than in the specimen. An example would be the case in which a specimen cut out of a blade is loaded in the test only on its midsection. If dynamic tests are carried out at loads differing from those acting in flight, then the characteristics of the distribution of endurance in service substantially differ from those obtained in tests and can be determined only approximately by a conversion based on specific assumptions with respect to the Wöhler curve.

If the distribution of endurance under service conditions φ_{serv} has been determined, then the conditional probability of failure of one arbitrarily taken specimen of a structure in service at the given outcome of dynamic tests ξ_2 /174 can be determined from the expression

$$P_{con} = \int_{-\infty}^{\xi_2 - \log \eta_N} \varphi_{serv}(\xi_1)\, d\xi_1. \tag{11.18}$$

The total probability of failure of this specimen of the structure in service will be equal to the sum of the conditional probabilities multiplied by the absolute possibility of each outcome $\varphi_{min}(\xi_2)d\xi_2$:

$$P = \int_{-\infty}^{\infty} \varphi_{min}(\xi_2) \left[\int_{-\infty}^{\xi_2 - \log \eta_N} \varphi_{serv}(\xi_1)\, d\xi_1 \right] d\xi_2. \tag{11.19}$$

After calculating the value of this integral, we can construct the dependence of the probability of failure of the structure P on the adopted magnitude of the factor of safety with respect to the number of cycles η_N.

If the distribution of endurance in service and in tests is identical

$$m_{\log N_{test}} = m_{\log N_{serv}};\quad S_{\log N_{test}} = S_{\log N_{serv}}$$

then the probability P depends only on two factors: the number of tested specimens n and the ratio of the logarithm of the factor of safety $\log \eta_N$ to the mean-square deviation of the logarithms of the numbers of cycles to failure of the specimens $S_{\log N}$ (Fig.1.72).

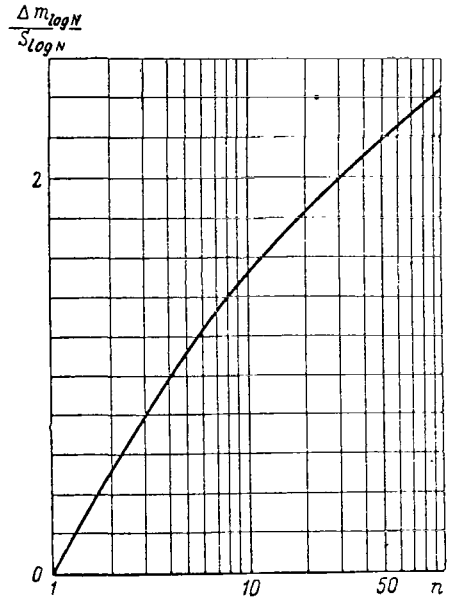

Fig.1.70 Change in Magnitude of Mathematical Expectation of Minimum Endurance Values as a Function of the Number of Tested Specimens.

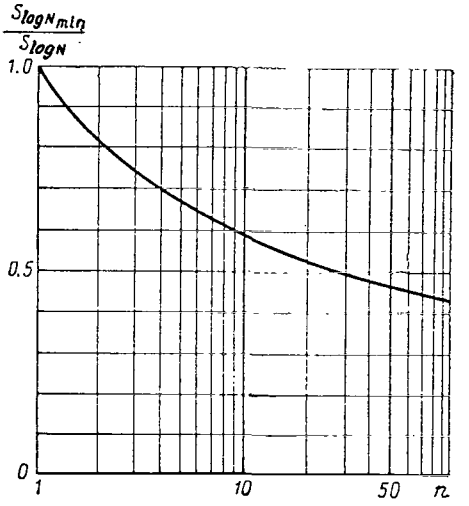

Fig.1.71 Mean-Square Deviations of Minimum Endurance Values as a Function of the Number of Tested Specimens.

Thus, to determine the required safety factor for the number of cycles, we can conduct dynamic tests on n specimens of the structure, determine the mean-square deviation $S_{\log N}$ and N_{min} and, after assigning a certain probability of failure P_{asd}, derive η_N from the curves in Fig.1.72. After this, the safe number of cycles to failure can be determined from eq.(11.12). /175

This approach is possible when only few specimens are tested. The value of $S_{\log N}$ can be taken from the results of other tests of similar structures*.

If we assume beforehand that $S_{\log N} = 0.2$ (this value is close to the minimum mean-square deviations observed for most helicopter units) and assign the probabilities of failure indicated in Table 1.18, then values of the safety fac-

* A similar approach as related to the calculation of airplane structures was proposed by V.L.Raykher.

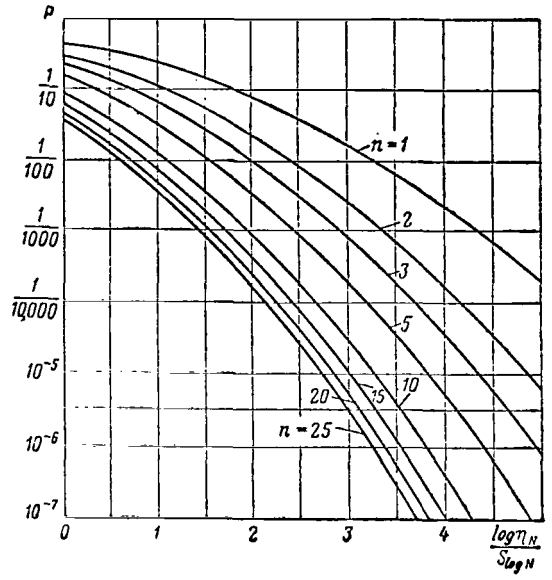

Fig.1.72 Diagram for Selecting the Magnitude of the Safety Factor η_N with Respect to the Number of Cycles of Stress.

tors close to those given in Table 1.16 can be obtained. Usually, the values of $S_{\log N}$ are higher. Therefore, the safety factors obtained by this method are larger than those given in the table (Table 1.16).

The main problem in using the method presented here lies in defining the probability of failure of the structure to be assigned in calculations of service life. Frequently, the probabilities recommended by different sources differ by three or four orders of magnitude [see, for example (Ref.43)]. The values for the probability proposed here (in Table 1.18) were selected with the aim of having them correspond, with more or less reliability, to numbers of cycles smaller than the sensitivity threshold N_0. Therefore, these probabilities should be regarded as certain conditional values pertaining to the normal law of distribution. The actual values are much lower or even equal to zero. /176

9. Determination of $S_{\log N}$ at Given Fiducial Probability

As follows from the preceding Subsection, the logarithm of the factor of safety with respect to the number of cycles $\log \eta_N$ needed for ensuring the given probability of failure is directly proportional to the mean-square deviation in the distribution of the logarithms of the numbers of cycles to failure of the structure $S_{\log N}$. The greater $S_{\log N}$, the greater should be the factor η_N. Therefore, the reliability of determining the service life of a structure depending on the admissibility of numerous adopted assumptions is largely related with the accuracy of determining $S_{\log N}$.

TABLE 1.18

Group of Units of Different Essentiality for Safety	Probability of Failure of Structure
Group I	$\frac{1}{10000}$
Group II	$\frac{1}{1000}$
Group III	$\frac{1}{100}$
Group IV	$\frac{1}{10}$

Usually, 3 - 5 specimens of a full-scale structure are tested to establish its service life. In many cases it is considered sufficient to test only one specimen. There is no doubt that, with such a small number of tested structures, there is no possibility for a sufficiently accurate determination of

$S_{\log N}$. Therefore, it is assumed in the method proposed by A.F.Selikhov (see Subsect.8) that $S_{\log N}$ cannot be determined in all cases. With a small number of tested specimens, we can take $S_{\log N}$ based on the test results of analogous specimens of another structure tested earlier. Such an approach greatly simplifies the process of establishing the service life and proves extremely useful in practice.

A determination of $S_{\log N}$ with sufficient reliability is possible by testing at least ten specimens of the structure. For an estimation of this reliability, one often uses the concept of fiducial probability distribution of $S_{\log N}$.

The fiducial probability β is usually selected such that it is possible to consider confident that the value $S_{\log N}$ lies in the interval:

$$\frac{1}{q}\tilde{S}_{logN} < S_{logN} < q\tilde{S}_{logN},$$

where

$\tilde{S}_{\log N}$ = estimation of $S_{\log N}$ obtained for a limited number of test results;

q = coefficient greater than unity in magnitude.

It follows from the aforesaid that the unknown value of $S_{\log N}$ may lie within the confidence limits, with a probability β. Consequently, this can be equal to $q\tilde{S}_{\log N}$. In this case, the logarithm of the safety factor for the number of cycles $\log \eta_N$ in conformity with the method presented in Subsection 8 increases in proportion to the quantity q, which is the reason for the fact that the calculated value of the service life decreases.

The value of the coefficient q depends on the number of tested specimens and on the adopted value of the fiducial probability β.

Table 1.19 gives the values of the coefficient q and the values of the fiducial probability β corresponding to them, which we have taken from the book of E.S.Wenzel "Theory of Probability".

As follows from Table 1.19, if - for example - a total of 25 specimens is tested and the fiducial probability is not less than 70%, then the experimentally obtained value of $\tilde{S}_{\log N}$ must be increased by a factor of 1.15 when calculating the service life.

In assigning the fiducial probability, it must be borne in mind that the /177
reliability of determining $S_{\log N}$ should not exceed the reliability of determining all other parameters entering into the calculation of service life. This pertains primarily to parameters determining the law of distribution of endurance in the region of small probabilities of failure, such as the threshold q of sensitivity N_0, and to the character of the distribution law itself which only approximately can be taken as logarithmically normal.

Therefore, the fiducial probability β, characterizing the reliability of determining $S_{\log N}$, can be lowered substantially to values at which the coeffi-

cient q will be not much greater than unity.

Based on these considerations, in determining the factors η_N we often assume q = 1 and use the value of $\tilde{S}_{\log N}$ as not being the value corresponding to the upper limits of the confidence interval at sufficiently high β.

10. Dispersion in the Stress Levels for Various Structural Specimens and Reliability Margin with Respect to the Amplitude of Alternating Stresses η_σ

The amplitudes of alternating stresses set up in flight in individual specimens of helicopter parts of identical structure differ considerably.

Actual measurements have shown that, in identical flight regimes, the amplitudes of alternating stresses differ both for the blades of one and the same rotor and for blades of different rotors. This can be attributed to the dispersion of the parameters of series-produced blades because of differences in their size and shape and hence in their weight. Usually, there are deviations from the theoretical contour of the profile and differences in the geometric twist of the blade. Furthermore, when installing the blades on the helicopter and adjusting the coning of the rotor, certain differences arise in the blade setting angle. All this ultimately leads to some difference in the operating conditions of individual blades and, as a consequence, to a dispersion of the amplitudes of alternating stresses set up in identical flight regimes.

TABLE 1.19

Number of Tested Specimens	Values of Fiducial Probability β in % for Different q					
	1.06	1.1	1.15	1.20	1.25	1.3
n=5	14.6	24.1	35.5	46.1	55.6	63.7
n=10	20.8	34	49	62	72.2	79.7
n=25	32.7	51.8	70.6	83.2	90.5	94.4
n=50	45.2	68.2	86	94	97.4	98.8

There is also a difference in flight regime parameters associated with the manner of piloting by individual pilots.

Another difference, which is not smaller but might even be greater, is observed in the stress amplitudes of all other helicopter parts. The dispersion in stress amplitude is especially great in components where alternating loads from individual blades should be equal to zero when added (if the blades are ideally identical), for all harmonics with the exception of harmonics that are multiples of the number of blades. If the blade parameters are different - and this is practically always the case - then the small alternating loads with harmonic frequencies that are multiples of the number of blades in these helicopter units will be supplemented by relatively high loads with other harmonics, having magnitudes proportional to the magnitude of the difference in blade parameters. The scattering of the values of the alternating stresses in such units may be very great. Usually, such units include the following: automatic pitch control, rotor control components, and fuselage parts; in the latter, it is mainly the reduction gear frame that is especially stressed by alternating loads.

To allow for all above factors in calculating the service life, we will introduce the reliability coefficient with respect to the amplitude of alternating stresses η_σ. This coefficient should ensure operational reliability of any structural specimen in a group of helicopters with consideration of the existing scattering in the alternating stress values. /178

Usually, some helicopter is arbitrarily selected for measuring the alternating stresses in a structure. The alternating stresses σ_{meas} obtained in tests with this helicopter are then used for conducting dynamic tests. This means that the tests are made with stresses $\sigma_{test} = \eta_\sigma \sigma_{meas}$. Therefore, the method presented above (see Subsect.8) of determining the reliability margin η_N and a safe life yields results that can be applied only to a specimen of the structure in which stresses equal to σ_{test} are acting. For all other specimens of this structure the service life will be longer if the active stresses $\sigma_{act} < \sigma_{test}$ and shorter if $\sigma_{act} > \sigma_{test}$.

Let us determine the value of the reliability coefficient η_σ from the condition that the probability of failure of the helicopter unit in question P_Σ, with consideration of the existing dispersion in the amplitudes of alternating stresses, is equal to the assigned probability P_{asd}. Usually, this value is taken to be the same as the probability of failure P_0 of the unit in which the alternating stresses σ_{test} adopted in dynamic tests are active.

Thus, if the value of η_N is chosen from the condition that the probability of failure of the specimen with stresses σ_{test} is equal to $P_0 = P_{asd}$, then the probability of failure of other specimens of this structure can be determined by means of the formula

$$P_\sigma = \int_{-\infty}^{\infty} \varphi_{min}(\xi_2) \left[\int_{-\infty}^{\xi_2 - \log \eta_N} \varphi_{serv}(\xi_1)\, d\xi_1 \right] d\xi_2. \qquad (11.20)$$

Here, P_σ is the probability of failure of the helicopter unit in which stresses equal to σ are set up. In this case, the endurance distribution φ_{serv} determined on the basis of dynamic tests for some selected equivalent stress level which enters eq.(11.20) should be recalculated with consideration of the fact that, in different specimens of the structure, different equivalent stresses are set up.

If we assume that the endurance changes in accordance with the law

$$\sigma^m N = \text{const}, \qquad (11.21)$$

then the characteristics of the distribution $\varphi_{serv}(\xi)$ can be set equal to

$$(S_{\log N})_\sigma = S_{\log N_{test}}; \qquad (11.22)$$

$$(m_{\log N})_\sigma = m_{\log N_{test}} + m\,[\log \sigma_{test} - \log \sigma_{act}], \qquad (11.23)$$

where

$(S_{\log N})_\sigma$ = mean-square deviation of distribution of the number of cycle logarithms at stresses σ_{act} differing from those used in the dynamic tests;

$(m_{\log N})_\sigma$ = mathematical expectation of this distribution;

σ_{test} = stresses in the test;

σ_{act} = stresses acting in some helicopter specimen.

Let us assume that the distribution of the acting alternating stress amplitudes in different specimens of a structure can be taken as logarithmically normal. Then the probability of failure of the helicopter unit in question will be equal to /179

$$P_{meas} = \int_{-\infty}^{\infty} P_\sigma \varphi_{\log \sigma_{act}} \, d\log\sigma, \qquad \int_{-\infty}^{\infty} P_\sigma \varphi_{\log \sigma_{act}} \, d\log\sigma, \tag{11.24}$$

where $\varphi_{\log \sigma_{act}}$ is the distribution law of the acting alternating stress amplitudes (Fig.1.73).

Here, it must be borne in mind that the value of σ_{test} adopted for dynamic tests is selected arbitrarily, based on the results of measuring stresses in one randomly chosen helicopter or in several helicopters. Therefore, the probability distribution of failure P_σ for units with different acting stresses will shift along the axis log σ (see Fig.1.73) depending on the adopted value of σ_{test} so that, at $\sigma_{act} = \sigma_{test}$, the probability of failure P_σ would be equal to P_{asd} in view of the fact that the value of η_N was selected from this condition. Hence, it is clear that the value of P_{meas} will depend on the quantity σ_{test}.

Consequently, the probability P_{meas} is a conditional probability for a specific, randomly selected value of σ_{test}. The total probability of failure of a unit, arbitrarily selected from a group of helicopters P_Σ, can be obtained as the sum of conditional probabilities P_{meas} multiplied by the probability of occurrence, in this unit, of stresses which had been taken as the basis for the dynamic tests $\varphi_{\log \sigma_{meas}} d \log \sigma$:

$$P_\Sigma = \int_{-\infty}^{\infty} P_{meas} \varphi_{\log \sigma_{meas}} d\log\sigma = \int_{-\infty}^{\infty} \left[\int_{-\infty}^{\infty} P_\sigma \varphi_{\log \sigma_{act}} \, d\log\sigma \right] \varphi_{\log \sigma_{meas}} d\log\sigma. \tag{11.25}$$

If the stresses are measured in one and the same helicopter, then we can consider that

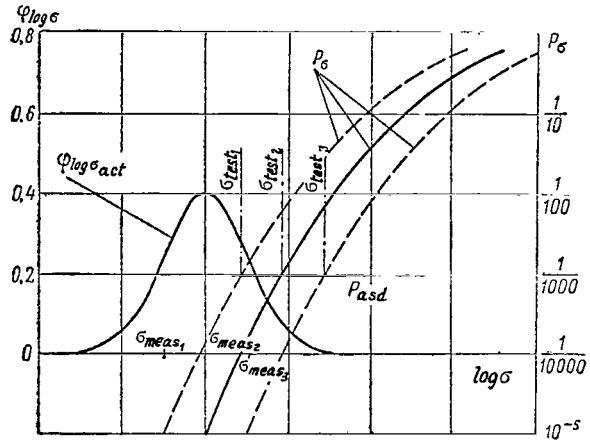

Fig.1.73 Character of the Distribution of $\varphi_{\log\sigma}$ and P_σ for Different $\sigma_{test} = \eta_\sigma\sigma_{meas}$.

$$\varphi_{\log\sigma_{meas}} = \varphi_{\log\sigma_{act}}$$

If the measurement is made on several specimens of a structure /180 and if, in the dynamic tests, the following stresses are assigned:

$$\sigma_{test} = \eta_\sigma\sigma_{meas_{av}},$$

where $\sigma_{meas_{av}}$ is the average amplitude of alternating stresses measured on several specimens of a structure, then the distribution parameters $\varphi_{\log\sigma_{meas}}$ should be determined as the distribution parameters of the average values of alternating stresses

$$\varphi_{\log\sigma_{meas}} = \varphi_{\log\sigma_{av}}.$$

It follows from eq.(11.25) that the total probability of failure P_Σ depends upon the quantity η_σ. Therefore, after assigning $P_\Sigma = P_{asd}$, we can determine the necessary value of η_σ. It is evident that in this case the required value of η_σ depends on the law of alternating stress distribution for different specimens of identical helicopter units $\varphi_{\log\sigma_{act}}$. To determine the characteristics of this distribution law we can use data from different stress analyses which are often performed on the same helicopter units in tests made for different purposes.

It is logical that the dispersion of the average equivalent alternating stresses may differ for different units.

The mean-square deviation in the distribution of alternating stresses for different rotor blades usually lies in the range of

$$S_{\log\sigma} = 0.02 - 0.035.$$

If, as is often done, we assume a normal distribution law of the alternating stress amplitudes, then these values of $S_{\log\sigma}$ will correspond to the values

$$\gamma_\sigma = \frac{S_\sigma}{m_\sigma} = 0.05 - 0.08, \qquad (11.26)$$

where

S_σ = mean-square deviation in the distribution of alternating stress amplitudes for different blades;

m_σ = mathematical expectation of this distribution, i.e., average stress in these blades.

For small γ_σ, we can assume $S_{\log\sigma} = \gamma_\sigma \log e$.

For units whose load depends on the quality of adjustment of the rotor, such as automatic pitch control, reduction gear frame, and others, the coefficient γ_σ is somewhat larger.

It follows from the composition of eq.(11.25) that the total probability of failure P_Σ depends mainly on two parameters:

$$a = \frac{mS_{\log\sigma}}{S_{\log N}};$$

$$b = \frac{\log\eta_\sigma}{S_{\log\sigma}},$$

where m is the exponent of the Wöhler curve.

The total probability of failure P_Σ depends also on the probability of failure P_0 of the structural specimen with stresses σ_{test}, used in the calculation.

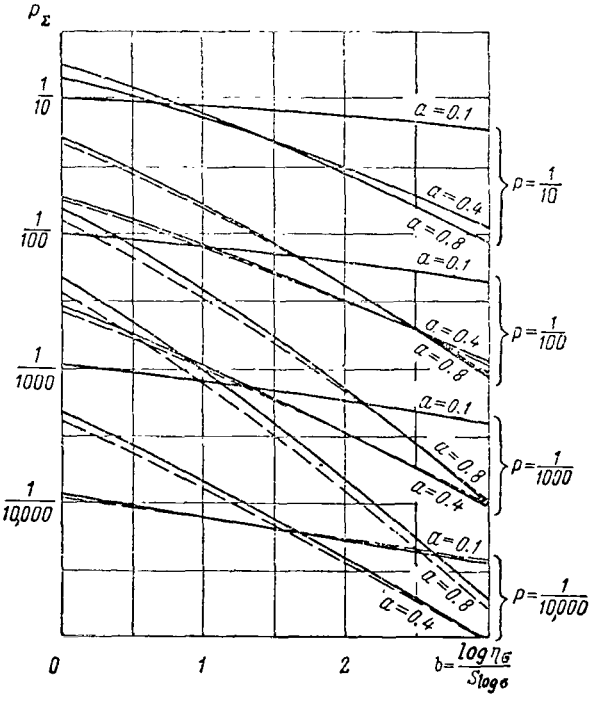

Fig.1.74 Results of Calculating the Probability of Failure with Consideration of Dispersion in the Values of Stresses Acting in Different Specimens of a Structure.

Figure 1.74 shows the calculations of total probability P_Σ for different values of a, b, and P_0 according to eq.(11.25) in the case where the stresses were measured only in one specimen of the helicopter structure. The calculations were carried out also for different values of the number of tested specimens, but it was found that the total probability of failure does not depend appreciably on this number. In Fig.1.74 the broken curves represent n_{spec} = = 5 and the solid curves, n_{spec} = = 20. /181

If it is required that P_Σ = = P_0 = P_{asd}, then we can obtain final graphs from which it is easy to determine the necessary margin η_σ if the values of $S_{\log\sigma}$, $S_{\log N}$, and P_{asd} are known. These graphs are given in Fig.1.75. As in Fig.1.74, the broken curves pertain to the case n_{spec} = 5 and the solid curves, to the case n_{spec} = 20.

As an example, let us find the required margin η_σ for a helicopter blade if it is known that $\gamma_\sigma = 0.08$ ($S_{\log\sigma} = 0.035$), and $S_{\log N} = 0.4$.

First, we determine the value of the coefficient a:

$$a=\frac{mS_{\log\sigma}}{S_{\log N}}=\frac{6\times0.035}{0.4}=0.525.$$

Then, assigning the value $P_\Sigma = 1/1000$, we obtain from the curves in Fig.1.75:

$$b=1.28\ (\ at\ n_{spec}=5);$$

from where

$$\log\eta_\sigma=1.28\times0.035=0.0448,$$

and

$$\eta_\sigma=1.11.$$

If the distribution law φ_σ is unknown, we usually take $\eta_\sigma = 1.2$. This value of η_σ, as already mentioned in Subsection 7, is often used in practical calculations. /182

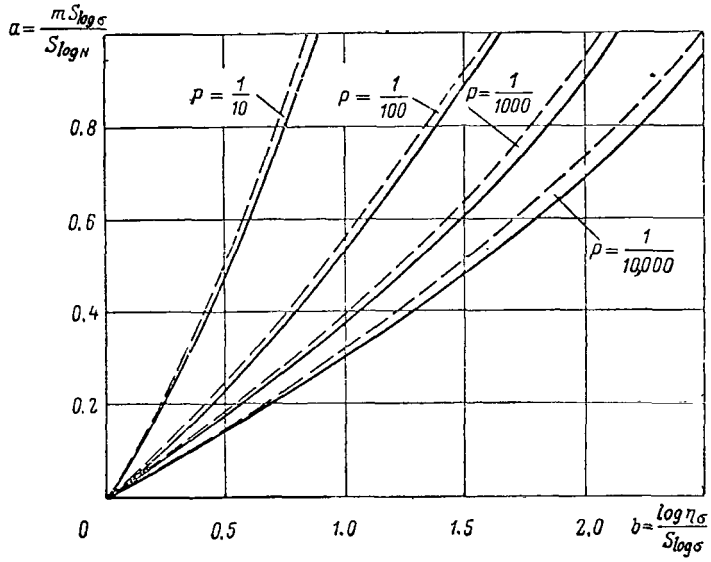

Fig.1.75 Diagram for Selecting the Reliability Margin η_σ.

11. Method of Determining the Reliability Margin η_σ Proposed by A.F.Selikhov

In our presentation, certain methods and arguments differ somewhat from those suggested by A.F.Selikhov, but the basic principle of the approach to

solving the problem is borrowed from that author.

Here, in determining η_σ the method described in Subsection 8 was used except that the dispersion in the amplitudes of stresses acting in flight is taken into account in the characteristics of the endurance distribution.

If, as before, it is assumed that - upon a change in stress amplitude - the endurance under service conditions changes in conformity with the law (11.21), i.e., that

$$\log N_{serv} = \log N_{test} + m(\log \sigma_{test} - \log \sigma_{act}), \tag{11.27}$$

then we can determine the characteristics of the endurance distribution in service with consideration of the dispersion in the amplitudes of acting stresses.

The mathematical expectation of this distribution will be equal to

$$m_1 = m_{\log N test} + m(\log \sigma_{test} - m_{\log \sigma act}), \tag{11.28}$$

where $m_{\log \sigma_{act}}$ is the mathematical expectation of the distribution of stress amplitudes in different specimens of the investigated structure (the average value of the amplitudes of alternating stresses in different specimens of the structure).

If the tests are carried out at stresses of /183

$$\sigma_{test} = \eta_\sigma m_{\sigma_{av}},$$

then, after putting

$$m_{\log \sigma act} \approx \log m_{\sigma_{av}},$$

we obtain

$$m_1 = m_{\log N test} + m \log \eta_\sigma.$$

The mean-square deviation in the logarithms of the numbers of cycles to failure under service conditions can be determined from the formula

$$S_1 = \sqrt{S^2_{\log N} + m^2 S^2_{\log \sigma}}. \tag{11.29}$$

If the dynamic tests are carried out at an amplitude of stresses $\sigma_{test} = \eta_\sigma \sigma_{av}$ (where σ_{av} is the average amplitude measured in flight on different specimens of the structure), then the dispersion of the characteristics of endurance in tests will depend on the dispersion of the acting stresses in different helicopter specimens. The amplitude established in tests is a random quantity depending on the results of stress analysis. As before (see Subsect.8), we are interested in the characteristics of the distribution of the logarithms of the minimum number of cycles to failure.

Let us assume that the values of the minimum number of cycles to failure obey the law

$$\log N_2 = \log N_{\min} + m\,[\log \sigma_{test} - \log(\eta_\sigma \sigma_{av})], \tag{11.30}$$

where

N_2 = minimum number of cycles to failure of a structure, with consideration of the fact that the amplitude of the tests can be established as different, depending upon the results of measuring the average stress amplitude σ_{av};

N_{min} = minimum number of cycles to failure of a structure at a certain fixed value of the stress amplitude in the tests σ_{test}.

Then,

$$m_2 = m_{\log N_{\min}} + m\,(\log \sigma_{test} - \log \eta_\sigma - m \log \sigma_{av}). \tag{11.31}$$

If

$$\sigma_{test} = \eta_\sigma m_{\sigma_{av}},$$

then

$$\log \sigma_{test} = \log \eta_\sigma + \log m_{\sigma_{av}}.$$

We put

$$\log m_{\sigma_{av}} \approx m_{\log \sigma_{av}}.$$

Then, $m_2 = m_{\log N_{min}}$, and the value of the mean-square deviation of the logarithms of the numbers of cycles in tests will be

$$S_2 = \sqrt{S^2_{\log N_{\min}} + m^2 (S_{\log \sigma})^2_{av}}, \tag{11.32}$$

where $(S_{\log \sigma})_{av}$ is the mean-square deviation in the values of the average logarithm of the stress amplitude measured in different specimens.

This value depends on the number of measurements n_{meas}:

$$(S_{\log \sigma})_{av} = \frac{S_{\log \sigma}}{\sqrt{n_{meas}}}. \tag{11.33}$$

For one measurement ($n_{meas} = 1$) /184

$$(S_{\log \sigma})_{av} = S_{\log \sigma}. \tag{11.34}$$

With consideration of eq.(11.33), the mean-square deviation in the endurance distribution in tests can be determined by means of the formula

$$S_2 = \sqrt{S^2_{\log N_{\min}} + \frac{(mS_{\log\sigma})^2}{n_{meas}}}. \tag{11.35}$$

Using the same reasoning as above (see Subsect.8), we arrive at the fact that the probability of failure in this case can be determined by an expression similar to eq.(11.19):

$$P_\Sigma = \int_{-\infty}^{\infty} \varphi_{\min}(\xi_2) \left[\int_{-\infty}^{\xi_2 - \log\eta_N^\Sigma} \varphi_{serv}(\xi_1)\, d\xi_1 \right] d\xi_2. \tag{11.36}$$

If the distribution of the logarithms of the minimum number of cycles to failure in tests can be represented approximately by the normal distribution law, then eq.(11.36) can be rewritten in the form

$$P_\Sigma = \frac{1}{2\pi} \int_{-\infty}^{\infty} \frac{1}{S_2} e^{-\frac{(\xi_2 - m_2)^2}{2S_2^2}} \left[\int_{-\infty}^{\xi_2 - \log\eta N} \frac{1}{S_1} e^{-\frac{(\xi_1 - m_1)^2}{2S_1^2}} d\xi_1 \right] d\xi_2. \tag{11.37}$$

If we introduce new variables

$$\bar{\xi}_1 = \frac{\xi_1 - m_1}{S_1} \text{ and } \bar{\xi}_2 = \frac{\xi_2 - m_2}{S_2}, \tag{11.38}$$

then eq.(11.37) is transformed into

$$P_\Sigma = \frac{1}{2\pi} \int_{-\infty}^{\infty} e^{-\frac{\bar{\xi}_2^2}{2}} \left[\int_{-\infty}^{f(\bar{\xi}_2)} e^{-\frac{\bar{\xi}_1^2}{2}} d\bar{\xi}_1 \right] d\bar{\xi}_2, \tag{11.39}$$

where the upper limit $f(\bar{\xi}_2)$ is determined by the expression

$$f(\bar{\xi}_2) = \frac{S_2}{S_1}\bar{\xi}_2 + \frac{\log\eta_N + (m_1 - m_2)}{S_1}. \tag{11.40}$$

Substituting here the values of m_1 and m_2, we obtain

$$f(\xi_2) = \frac{S_2}{S_1}\xi_2 + \frac{m\log n_\sigma + \log\eta_N + m\log N_{test} - m\log N_{\min}}{S_1}. \tag{11.41}$$

It follows from this expression that the probability of failure P_Σ can be determined for each η_σ, if we know the values of

S_1, S_2, η_N and $\Delta m_{\log_N} = m_{\log N_{test}} - m_{\log N_{min}}$.

We can propose the following method of determining the required margin η_σ: First, construct the dependence of S_2/S_1 on $\frac{m \log \eta_\sigma + \log \eta_N + \Delta m_{\log_N}}{S_1}$ for assigned values of P_Σ (see Fig.1.76). Then, after determining S_1 and S_2 from eqs.(11.29) and (11.35), use Fig.1.76 for determining the assigned value P_{assd} /185

$$\frac{m \log \eta_\sigma + \log \eta_N + \Delta m_{\log_N}}{S_1}, \qquad (11.42)$$

from where, knowing η_N, $\Delta m_{\log N}$ (see Fig.1.70), and S_1, it is easy to determine also η_σ.

The method proposed here is rather simple, although it involves somewhat more complicated computations for determining the service life in comparison with the method proposed in Subsection 10, where the margins η_σ were calculated on the basis of values taken directly from the graph.

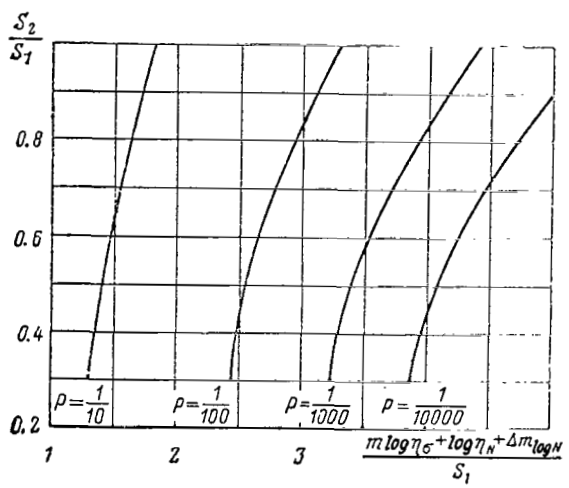

Fig.1.76 Graph for Determining $\frac{m \log \eta_\sigma + \log \eta_N + \Delta m_{\log N}}{S_1}$ as a Function of S_1/S_2, for Different Assigned Probabilities of Failure.

It follows from the above formulas that, under the assumptions adopted here, the margins of reliability η_N and η_σ can be combined into a single criterion $\eta = \eta_N \eta_\sigma^m$ or one reliability margin can be substituted for the other. This is convenient in carrying out calculations and conducting dynamic tests, a fact already mentioned in Subsection 7, but it offers no advantage in selecting the margins η_N and η_σ since their values are determined from different conditions.

12. Example of Calculation of Service Life

As an example, let us calculate the service life for a blade of a heavy helicopter with a tubular steel spar.

In determining the service life of a blade, the calculation is first performed for sections located at different relative radii, after which the service life obtained for the weakest section is established for the entire blade.

Let the weakest section be that at a relative radius $\bar{r} = 0.74$.

We now assume that the results of the dynamic tests of five specimens of the spar at an alternating stress amplitude ± 15 kg/mm^2 are as follows (see Table 1.20):

From tests, we draw the conclusion that the endurance limit σ_w of the specimens Nos.2, 3, 4, and 5 is higher than $\sigma_w = 15$ kg/mm^2. Consequently, the probability P that the endurance limit σ_w is lower than 15 kg/mm^2 can be taken as equal to 0.2. /186

TABLE 1.20

No. of Specimen	Number of Cycles of Stress	Test Results
No.1	9.8×10^6	Specimen failed
No.2	20×10^6	Specimens did not fail
No.3	20×10^6	
No.4	20×10^6	
No.5	20×10^6	

On setting $S_{\log\sigma_w}$ equal to 0.07 (see Subsect.13), it will be found that the endurance limit $\sigma_{w_{5\%}} = 13$ kg/mm^2 corresponds to a 5% probability. This limit will be considered minimum.

The margin for the number of cycles can be taken either on the basis of practical experience by assigning the service life in accordance with Table 1.16 or on the basis of the method of A.F.Selikhov (see Subsect.8). Based on Table 1.16 for Group II (blade equipped with a spar-damage warning device) and n = 5, the reliability margin η_N can be taken as equal to about 2.7.

In the second case, $S_{\log N}$ must be known. It is obvious that merely from the results of tests it is impossible to determine the value of $S_{\log N}$. However, it is possible to assign a certain value to $S_{\log N}$ based on results of tests with similar specimens.

Let us put $S_{\log N} = 0.4$. Then, assigning the value $P_{asd} = 1/1000$ (Group II of units) we obtain $\log \eta_N = 2.3 \cdot S_{\log N}$, i.e., $\eta_N = 8.3$, from Fig.1.72. Thus, the required reliability margin for the number of cycles η_N according to Selikhov's method is substantially greater than that obtainable from service life determinations. In many cases, this difference is partially compensated by introducing the concept of fatigue limit into the calculation and by refining the required reliability margins η_σ.

As mentioned above, in defining the service life with the use of the reliability coefficients selected on the basis of practical experience, the value of η_σ can always be taken as equal to 1.2. However, this coefficient can be refined in conformity with the method proposed in Subsections 10 and 11. For this purpose, more complete data are necessary on the dispersion of the alternating stress amplitude for different specimens of the structure.

Let us assume that the stresses are measured in only one specimen. However, on the basis of experience in measuring similar units of other helicopters it can be assumed that $\gamma_\sigma = 0.08$ and thus $S_{\log\sigma} = 0.035$. Then, by means of the methods

presented in Subsections 10 and 11 we obtain $\eta_\sigma = 1.11$. Nevertheless, we will take $\eta_\sigma = 1.2$.

The minimum value of N_{min} of five tested specimens ($n = 5$) at an alternating stress amplitude of $\sigma = \mp 15$ kg/mm^2 is $N_{min} = 9.8 \times 10^6$ cycles.

The number of cycles corresponding to the minimum fatigue limit is deter- /187
mined from the formula

$$N_{w_{min}} = N_{min}\left(\frac{\sigma_{test}}{\sigma_{w_{min}}}\right)^m = 23\times10^6,$$

while the values of N_i are obtained from the formula

$$N_i = \frac{N_{w_{min}}}{\eta_N}\left(\frac{\sigma_{w_{min}}}{\eta_\sigma \sigma_{\Sigma_i}}\right)^m.$$

In the calculation of service life, we will assume that, in all regimes where the acting stresses are below the minimum value of the fatigue limit, no increase in damage potential for the structure takes place.

We will not calculate the equivalent stresses in individual flight regimes, but will assume them as equal to the maximum measured stress amplitudes. In this case, the value of ε_i will be either zero or unity.

The calculation of equivalent stresses is given in Table 1.21.

If we assume that the endurance obeys the law (11.21) at all alternating stress levels and that there is no fatigue limit (in this case $\varepsilon_i = 1$ in all regimes), then all flight regimes are equivalent in damageability to the regime with a stress amplitude of $\sigma_{eq} = 11.5$ kg/mm^2 acting during the entire service /188
life of the blade. In this case,

$$N_{min} = N_{w_{min}}\left(\frac{13}{1.2\times11.5}\right)^m = 16.2\times10^6;$$

$$N_s = \frac{N_{min}}{\eta_N} = 1.95\times10^6;$$

$$R = \frac{N_s}{60f} = 271\ hrs.$$

If it is assumed that the minimum endurance limit is $\sigma_{w_{min}} = 13$ kg/mm^2, then one regime [see eq.(11.9)] with an amplitude $\sigma_{eq} = 13.6$ kg/mm^2 will be equivalent to all flight regimes. The duration of this regime, as follows from Table 1.21, will be about 23% of the service life of the blade ($\varepsilon = 0.229$).

Then the lifetime itself can be determined in the following manner:

$$N_{\min} = N_{w_{\min}} \left(\frac{13}{\eta_\sigma \sigma_{eq}} \right)^m = 3.86 \times 10^6;$$

$$N_s = \frac{N_{\min}}{\eta_N} = 0.707 \times 10^6;$$

$$R = \frac{N_s}{60 f \varepsilon} = 429 \text{ hrs}.$$

The same results can be obtained from the total damageability without making use of the concept of equivalent stresses [see eq.(11.5)]:

$$N_s = \frac{1}{\sum_i \frac{\alpha_i}{N_i}} = 3.09 \times 10^6;$$

$$R = \frac{N_s}{60 f} = 429 \text{ hrs}.$$

TABLE 1.21

EXAMPLE OF CALCULATION OF BLADE SERVICE LIFE WITH RESPECT TO A SECTION OF RELATIVE RADIUS $\bar{r}$ = 0.74

$\sigma_{w\ \min} = 13$ kg/mm²; $\xi = 0.5$; $n = 5$; $S_{\log N} = 0.4$; $\eta_\sigma = 1.2$;
$\eta_N = 8.3 \left(P_{asd} = \frac{1}{1000} \right)$; $N_{w\ \min} = 23 \times 10^6$

Flight Regime	ε_i	α_i	σ_{x_i}	σ_{y_i}	$\xi = 0.5$; σ_{Σ_i}	$\eta_\sigma \cdot \sigma_{\Sigma_i}$	N_i	$\frac{\alpha_i}{N_i}$
Hovering	0	0.1	6.0	8.8	9.7	11.64	∞	0
Low speeds								
$V = 20$ km/hr	1	0.03	7.2	10.5	11.6	13.92	1.84×10^6	0.016×10^{-6}
$V = 30$ km/hr	1	0.02	10.5	13.2	15.02	18.02	0.39×10^6	0.051×10^{-6}
$V = 60$ km/hr	1	0.05	12.4	12.5	15.05	18.06	0.39×10^6	0.128×10^{-6}
Takeoff	1	0.02	9.5	12.4	14.0	16.8	0.59×10^6	0.034×10^{-6}
Climb	0	0.06	6.0	5.6	6.9	8.28	∞	0
Cruising speed	0	0.55	8.0	9.0	10.5	12.60	∞	0
Maximum speed	1	0.10	8.0	10.5	11.09	13.31	2.4×10^6	0.042×10^{-6}
Gliding	0	0.05	7.5	7.2	8.8	10.56	∞	0
Braking								
1st stage—$\sigma_{\max}$	1	0.002	15.2	18.4	21.11	25.33	0.05×10^6	0.04×10^{-6}
2nd stage—$0.7\ \sigma_{\max}$	1	0.007	10.64	12.88	14.79	17.75	0.43×10^6	0.016×10^{-6}
3rd stage—hovering	0	0.011	6.0	8.8	9.72	11.66	∞	0
		$\varepsilon = 0.229$						$\Sigma\ 0.327 \times 10^{-6}$

These results show that on introduction of the concept of fatigue limit or endurance limit, the service life of a blade will be greater when derived from calculation.

However, it must be borne in mind that the margins with respect to the number of cycles presented in Table 1.16 were introduced into the calculations without assumption of the existence of a fatigue limit. Therefore, they should not be used in calculations with a fatigue limit.

13. Possible Ways of Determining the Minimum Endurance Limit of a Structure

The above example indicates that substantially higher values for the service life of a structure can be obtained when making use of the concept of minimum endurance limit. Therefore, a determination of these values is mandatory in many cases.

A sufficiently accurate determination of the values of $\sigma_{w_{min}}$ from the results of tests is virtually infeasible. Only a highly approximate determination of this value is possible. Even then, an appreciable increase in the number of test specimens is required. Nevertheless, in calculations of service life, even approximate endurance limits will closely approach the calculation results to reality and offer the possibility of developing more competent technical solutions. Therefore, it is always advisable to resort to a determination of endurance limits, using both approximate and simply formal methods of calculation. /189

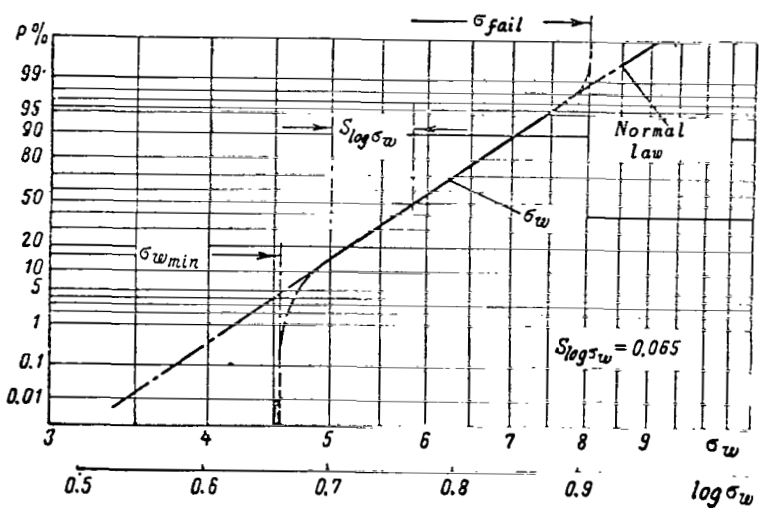

Fig.1.77 Distribution of Endurance Limits.

Primarily, an attempt must be made to define and determine the parameters of the distribution law of endurance limits. Toward this end, fatigue tests must be performed with specimens at several alternating stress levels, located in the region of endurance limit distribution. The tests should be carried out

on the base of a sufficiently large number of cycles. In selecting the test base, it is generally assumed that, for steel specimens, this base can be set somewhat greater than 10^7 cycles, for example 2×10^7 cycles, whereas for duralumin specimens the base must be somewhat higher than 2×10^7 cycles (frequently, a base of 5×10^7 cycles is used).

The probability that the endurance limit is higher than the assigned alternating stress level is defined as the ratio of the number of specimens tested at the given base at no failure $n_{no\text{-}fail}$ to the total number of specimens tested at this and at a lower level of stresses n:

$$P = \frac{n_{no\text{-}fail}}{n}.$$

The resultant distribution of endurance limits can coincide with the normal law only in a small section corresponding to the average values of probability (Fig.1.77). At small probabilities, the distribution of the endurance limits deviates from the normal law and has a certain sensitivity threshold $\sigma_{w_{min}}$. At large probabilities, beginning with some stress σ_{fail}, all specimens fail without having been subject to the assigned base of the test.

The distribution of endurance limits at average probability of failure is best represented by the lognormal distribution law. This can be used also for determining the minimum endurance limit.

Available results of tests on blade specimens show that, for this law, we /190 can take values of $S_{\log \sigma_w}$ equal to about

$$S_{\log \sigma_w} = 0.05 - 0.07,$$

where $S_{\log \sigma_w}$ is the mean-square deviation of the distribution of fatigue limit logarithms.

It is impossible to propose a sufficiently reliable method for determining $\sigma_{w_{min}}$. Thus, we can suggest only a purely formal method which, however, yields sufficiently good results in practice. It can be assumed that the minimum endurance limit coincides with the value of σ_w corresponding to 5% probability of a logarithmically normal distribution law of endurance limits.

If such an approach is used, the values of $\sigma_{w_{min}}$ can be refined by a method in which fatigue tests are carried out at two alternating stress levels, close in amplitude. The test specimens, at least 15 - 20 of them, are divided into two groups.

The first group is tested at maximum alternating stress which supposedly does not exceed the minimum endurance limit; for this reason, it is desirable to prevent any of the specimens from failing at a number of cycles corresponding to the selected test base. The results of testing this group serve to confirm that the minimum endurance limit may actually correspond to their test level.

The second group of specimens is tested at somewhat higher alternating stresses, so that a certain percentage will fail without having operated the rated number of cycles. After determining the probability that the endurance limit is below the amplitude of the second test level and after assigning some value of $S_{\log \sigma_w}$, we calculate the value of σ_w corresponding to the 5% probability. If the test data of the first group do not contradict this result, then the resultant value of $\sigma_{w5\%}$ can be taken as the minimum endurance limit.

Occasionally, it is assumed for greater reliability that the minimum endurance limit corresponds to smaller probability values, say, a probability of 1/100. However, it seems that still lower values of this probability are not advisable.

It should be noted that in many cases an arbitrary concept, which could be called the reduced endurance limit, is used for characterizing the fatigue strength.

The reduced endurance limit is determined by converting the test results, by means of eq.(11.3), to an arbitrary base which often is taken as N_{base} = $= 10^7$ cycles for steel and $N_{base} = 2 \times 10^7$ cycles for duralumin:

$$\sigma_{w_{red}} = \sigma_{test} \sqrt[m]{\frac{N_p}{N_{base}}},$$

where

σ_{test} = alternating stress amplitude in the test;
N_p = number of cycles to failure corresponding to a probability of failure equal to P;
m = exponent of the Wöhler curve, usually taken as m = 6.

If we take N_p corresponding to the probability of failure as equal to 5%, /191 then the value of $\sigma_{w_{red}}$ furnishes an approximate idea as to the magnitude of the minimum endurance limit. The minimum value of the number of cycles to failure of a given structure N_{min} often is substituted for N_p as the characteristic of fatigue strength. We must emphasize that the reduced endurance limit, irrespective of the manner in which it is determined, does not correspond to the concept of endurance limit in the sense in which it is used above, in this Section.

It is also of importance that the distribution of the reduced endurance limits has a mean-square deviation equal to

$$(S_{\log \sigma_w})_{red} = \frac{S_{\log N}}{m},$$

which is almost always greater than the value of $S_{\log \sigma_w}$.

14. Advantages and Disadvantages of Various Approaches in Determining the Necessary Reliability Margins, and Estimation of their Accuracy

The simplest approach, as already shown above (see Subsect.7), is to calculate the service life under application of the coefficients η_N and η_σ taken on the basis of practical experience in defining the service life. These coefficients have been checked on a large number of helicopters and many hundreds of units have successfully lived out the service life thus established. However, it must be borne in mind that the use of the coefficients η_N and η_σ has been confirmed by practice only in combination with some method of calculating the service life which, in particular, differs by the following assumptions:

1. No endurance limit exists, and the Wöhler curve is described by eq.(11.21). Accordingly, the coefficients ϵ and ϵ_1 are taken as equal to unity.
2. In each flight regime, the stress amplitude is considered equal to its maximum measured value in this regime.

However, such an approach to the calculation of service life has substantial shortcomings:

1. In determining the service life, one disregards the difference in the dispersion of the characteristics of endurance which may be dissimilar for units of different design which, furthermore, are dissimilar with respect to the materials used and the manufacturing process. The magnitude of dispersion of stresses acting in different specimens of a given structure is also disregarded.

2. Rejection of the concepts of endurance limit and exclusive use in the calculation of the maximum stress amplitudes in each flight regime lead to incorrect ideas as to the share of damage potential contributed by different flight regimes.

Therefore, an attempt should be made to use improved methods, incorporating the basic principles of the theory of probability. One of the possible variants of this approach is given in Subsections 8, 10, and 11.

It is necessary to point out that this method, in the form in which it is presented here, gives completely satisfactory values of service life rather close to those obtained by the preceding method. Of course, there is some redistribution in the values of the safety factors. The margin η_N is substantially larger whereas the margin η_σ is smaller. Furthermore, the concept of minimum endurance limit should be used in the calculation. Otherwise, the service lives will be underestimated. /192

In applying this method, such large probabilities of failure (equal to 1/1000 or even more) often raise doubt. Actually, this means that one unit out of 1000 should fail during its rated service life. Therefore, we must again emphasize that the indicated probabilities are purely conditional values, corresponding to the normal distribution law of endurance. In reality, in the region of small values of probability of failure, this law deviates from the normal and a sensitivity threshold is observed in the endurance characteristics. Its values lie in the probability region of about 1/100 or fluctuate about this value. Con-

sequently, assignment of a conditional probability of 1/1000 is actually equivalent to the requirement of a very small or even zero probability. Therefore, we cannot agree with those authors who are not afraid to stipulate a probability of the order of 10^{-6} or even 10^{-7}, under application of the normal law of distribution of endurance. There is no sufficiently valid reason for such demands.

Generally, anyone familiar with the above method will object to doing away with refinements of experimentally obtained values of the mean-square deviations $\tilde{S}_{\log N}$, based on the rather high values of fiducial probability accepted in practical applications of the probability theory. If such a refinement is made, the calculation would have to incorporate a two-fold value of $\tilde{S}_{\log N}$ (see Subsect.9), which would lead to an increase in the required margin η_N and thus to a decrease in service life.

In addition to the above considerations (see Subsect.9), another inaccuracy in the proposed method of calculation should be pointed out. Usually, the equivalent stresses acting in different flight regimes are replaced by their maximum values, leading to an underestimation of service life. These two inaccuracies mutually cancel out, and an elimination of one should definitely be accompanied by elimination of the other. In such a case, the values of the service lives obtained by calculation do not change substantially.

There is no doubt that in time, as new experimental data are collected, more extensive refinements will have to be introduced into the method of calculating the service life. Practical experience in operating helicopters and the ever greater number of results of dynamic tests will also furnish an incentive in this direction.

15. Blade Strength Requirements in Design Selection

A helicopter blade operates under conditions severely taxing its strength. During its entire service life, the blade is subject to excessive static and variable loads. This characteristic of the blade operating conditions imposes extremely stringent requirements on its structure and primarily on the fatigue strength of its main element, the spar. Consequently, the blade spar should be made only of materials with high fatigue strength characteristics.

Blade designs with tubular steel spars and pressed duralumin spars are /193
the most common type at present.

Excellent results can be expected when manufacturing spars of various synthetic materials. Blade designs with a glass-laminate spar are already known. However, practical experience operating such blades is still insufficient. For this reason, we will not further discuss the strength aspects of such types.

The most important requirement for blades with steel and duralumin spars is that of maximum elimination of any stress raisers which lower the fatigue strength. The use of bolts and rivets is impermissible in blades. The frame of the blade is fastened to the spar exclusively by glued joints.

Fittings with large stress raisers can be tolerated only in segments with

small alternating stresses, for example, in the blade root close to the hub hinges. In this case, despite the small alternating stresses, the section of the spar near the root joint must be increased by a factor of 3 - 4. Only a very appreciable reduction in alternating stresses will permit the use of fittings with stress raisers.

Fatigue strength is also distinctly lowered by small technological defects which also act as stress raisers. Consequently, in the manufacture of blade spars the process used must be aimed at complete elimination of all apparent defects of the spar.

To eliminate the possibility of some flaws remaining undetected, the spars must be subjected to rigorous inspection under application of all modern methods of nondestructive materials testing.

Below, the strength properties of a blade with steel and duralumin spars will be investigated in greater detail.

16. Strength of a Blade with Tubular Steel Spar

Cold-rolled tubing of high-alloy steels 30KhGSA or 40KhNMA quenched and tempered to a strength of σ_b = 110 - 130 kg/mm^2 is commonly used for the blade spar.

After hot- and cold-rolling, shaping, and quenching, the outer and inner surfaces of the tube are polished. Recently, cold-working of the spars has become a mandatory operation after polishing.

A thus manufactured spar without cold-working may have a minimum endurance limit of the order of $\sigma_{w_{min}}$ = 12 - 13 kg/mm^2 at an average component of the cycle σ_m = 20 - 25 kg/mm^2. However, the strength is reduced greatly if, in manufacturing the spar, various technological defects and miscalculations are permitted. The following can be mentioned as the most dangerous types:

Internal cracks and laps. During hot-rolling, plastic deformation may be accompanied by partial tearing of the material. This usually occurs at a reduction in temperature of the workpiece during rolling and also as result of contamination of the steel by nonmetallic and gas inclusions, the formation of films, high porosity, segregation, and other metallurgical defects. The cracks run into the workpiece at an acute angle, so that it is often difficult to trace the outcropping of the crack on the surface.

On further cold-rolling, the degree of deformation increases and the crack folds over into the wall of the tube at an ever smaller angle to its surface. /194
Usually a series of such internal cracks is observed. They are small, being about 0.1 - 1.0 mm deep and 3 - 10 mm wide.

Laps appear upon cold-rolling on the outer surface. They are usually due to extensive surface roughness after hot-rolling. Subsequent plastic cold-working leads to an uneven flow of the material during which defects known as laps

and seams may form. Laps are also able to form by flow of metal into the gap between the roll grooves and formation of a fin which folds over upon subsequent deformation.

Both defects can be detected by magnaflux inspection of the polished surface. Figure 1.78 shows characteristic internal cracks at the inner surface of a spar. The micrograph was obtained during magnetic inspection. The endurance limit of a tube with seams and laps drops to $\sigma_{w_{min}} = 5 - 7$ kg/mm^2.

Fig.1.78 Cracks on Inner Surface of Steel Spar.

Rolled-in scale on inner surface. After hot-rolling, a layer of scale is left on the tube surface, which has a greater hardness than the metal. Annealing is done after each step in cold-rolling. Although annealing proceeds in an inert atmosphere, thin films of scale are formed on the surface, due to the oxygen content of the metal. If the scale is not completely removed, it will be crushed during the rolling process and forced into the metal, forming so-called rolled-in scale. On the exposed outer surface of the tube, the rolled-in scale is readily eliminated by machining. On the inner surface of the tube whose machining is more complex and possible only by belt-grinding or hydraulic polishing, the rolled-in scale cannot be completely removed. Therefore, small but acute-angled pits of a size not exceeding 0.1 - 0.05 mm and difficult to detect during inspection, may be left even after grinding. The fatigue strength of the surface drops in this case to $\sigma_{w_{min}} = 10 - 12$ kg/mm^2.

Rolled-in scale can be eliminated by turning and grinding the surface of the workpiece after hot-rolling until all scale is removed and by sandblasting after annealing before each operation of cold-rolling.

For a complete elimination of cooling cracks, laps, rolled-in scale, and other surface defects, longitudinal grinding of the outer and inner surfaces of the tube, after final cold-rolling and before shaping, is highly effective.

Reduction of fatigue strength from tube straightening. After quenching and tempering, the spar tubes are bent slightly. Therefore, before assembling the blade, the tubes may need straightening. This sets up residual stresses in the tube material. Usually, limiters are used during the straightening operation, to keep the residual tensile stresses in the tube from exceeding 10 - 20 kg/mm^2. These stresses increase the average component of the cycle and lead to a decrease of 20 - 25% in the endurance limit. Still greater reductions in strength may /195 occur if the straightening is improperly done. To do away with the necessity of straightening, the quenched tubes should be tempered in special devices that eliminate the strains produced on quenching.

In estimating the fatigue strength of spars, special attention must be paid

to the possibility of fretting corrosion. Fretting corrosion is an almost certain attendant phenomenon of cyclic blade stresses and leads to a substantial reduction in fatique strength. This usually occurs at points where there is mating between parts and the spar, if relative microslip is present between the osculating surfaces. Points of clamp installation for attachment of the blade frame are the usual seats of fretting corrosion in steel spars.

Fig.1.79 Incipient Fatigue Failure from Fretting Corrosion.

Figure 1.79 gives a micrograph of a ruptured spar. The root of the fatigue crack coincides with the seat of fretting corrosion.

A marked increase in the dynamic strength of steel spars can be obtained by mechanical work-hardening of their surface, known also as cold-working.

At present, cold-working of spars has become an almost indispensable operation in the fabrication of blades. Three methods of mechanical strengthening have become common in helicopter engineering: the dynamic method of M.I.Kuz'min, the vibratory impact method of S.V.Ochagov, and the shot-peening method. The choice of the method generally depends on the characteristics of the structural component to be strengthened and on the production facilities. When using the dynamic method for strengthening the outer surface of a spar, its inner surface is work-hardened by shot-peening. In developing complicated devices for the vibratory impact method, main emphasis is usually on simultaneous treatment of both inner and outer surfaces of the spar by this method.

An increase in fatigue strength is obtained by older methods of cold-working. The best method, giving the most stable results in treating the outer surface of steel spars, is M.I.Kuz'min's dynamic method.

The increase in fatigue strength due to cold-working is attributed mainly to two causes: The outer surface of a given part which is most sensitive to incipient fatigue failure is rendered smoother (Fig.1.80) and residual compressive stresses are set up in the surface layers which, in conformity with Hay's diagram (see Fig.1.63), leads to an increase in fatigue strength of the surface layer of the part.

Figure 1.81 shows the distribution of internal stresses in the material of a steel spar, obtained by dynamic cold-working and grit-blasting. Grit-blasting sets up almost the same residual stresses as the shot-peening method of cold-working.

The increment in fatigue strength due to cold-working is especially large /196 in the presence of fretting corrosion. Apparently, compressive stresses impede the spread of corrosion into the material. Figure 1.82 shows the results of

testing steel spars with cold-worked and noncold-worked surfaces operating under conditions of onset of fretting corrosion.

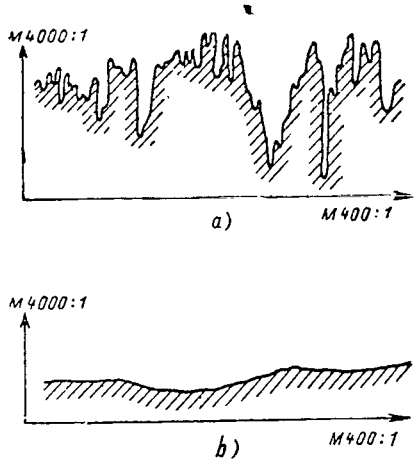

Fig.1.80 Surface Profilogram of Spar Pressed from Aluminum Alloys after Machining (a) and after Cold-Working (b).

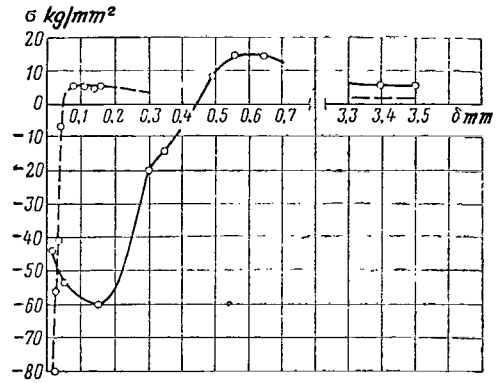

Fig.1.81 Distribution of Internal Stresses from Cold-Working with Respect to Wall Thickness of Tubular Steel Spar.
———Cold-working by the method of M.I.Kuz'min;
– – – –Triple grit-blasting.

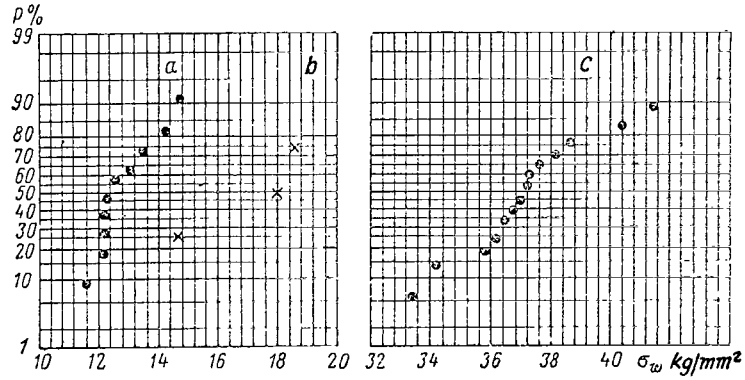

Fig.1.82 Distribution of Reduced Endurance Limits of Tubular Steel Spars under the Effect of Fretting Corrosion.
a - Surface polished and sandblasted; b - Surface polished and sandblasted three times with grit; c - Surface cold-worked by M.I.Kuz'min's method.

The fatigue strength of steel spars can be increased by cold-working by a factor of 1.5 - 2 and, in the presence of fretting corrosion, by a factor of 2.5 - 3.

Cold-working will raise the fatigue limit of a steel spar to values of the order $\sigma_{w_{min}} = 28 - 30$ kg/mm^2 at $\sigma_m = 20 - 25$ kg/mm^2. Thus, cold-working has proved a most effective means of increasing the reliability and service life of blades.

17. Strength of a Blade with Duralumin Spar /197

The most important problem in designing blades of this type is to secure a sufficiently high fatigue strength of the spar. Generally, attachment of the frame to the spar is accomplished by glue and thus creates no substantial stress raisers in the spar. Stress concentrations in spars are due mainly to small defects tolerated in its fabrication.

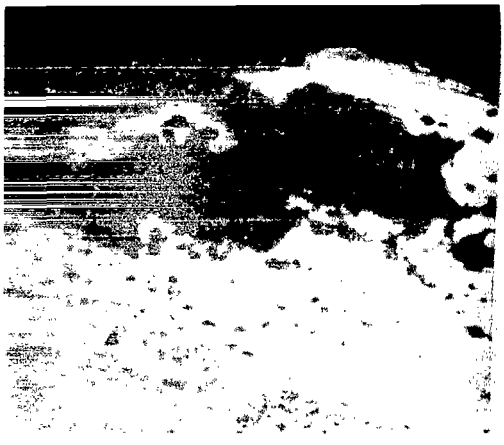

Fig.1.83 Microsection of Spar Wall through Blowhole Formed in Pressing.

The surface finish of a spar plays the main role in reducing its fatigue strength. A milled and sand-blasted spar made of AVT-1 alloy without machining of the inner surface may have an endurance limit of the order of $\sigma_{w_{min}} = 3.8 - 4.2$ kg/mm^2 at an average component of the cycle $\sigma_m = 6$ kg/mm^2.

The fatigue strength of a given spar may be reduced due to defects produced in its pressing and machining.

Frequently, the inside channel of the spar is not machined after pressing. Therefore, pressing defects may remain on the inner surface: adherent metal slugs, longitudinal scratches, blowholes (Fig.1.83), and, finally, coarse-crystalline rings. These defects may reduce the fatigue strength to values of $\sigma_{w_{min}} = 2.5 - 3.0$ kg/mm^2 ($\sigma_m = 6$ kg/mm^2). This suggests to follow the pressing by machining of the surface of blade spars with relatively high stresses.

A substantial reduction in fatigue strength is produced also by nonmetallic and gas inclusions. To eliminate such inclusions, a special melting practice should be used (settling of the metal, teeming from certain levels, filtering through mesh filters, etc.). The best metal is obtained by melting in electric induction furnaces, with holding of the molten metal in electrically heated mixers.

To eliminate the possibility of overlooking nonmetallic and gas inclusions,

each spar should be subjected to careful ultrasonic inspection.

No less important is the elimination of possible corrosion pitting of pressed spars during fabrication (as well as under service conditions). Practical experience has shown that surface and intercrystalline corrosion of a depth to 0.1 - 0.15 mm will greatly lower the endurance limit. Therefore, metals of high corrosion resistance should be used for blade spars, and special measures must be taken in fabrication to protect the spars from corrosion by electroplating after intermediate treatment steps (for example, anodizing).

/198

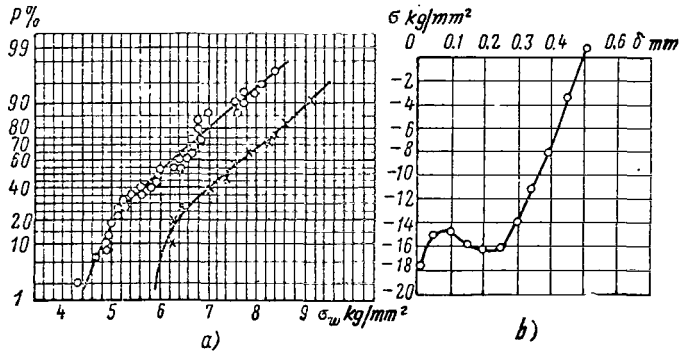

Fig.1.84 Distribution of Reduced Endurance Limits (to a Base of 10^7 Cycles) of Pressed Spars Made of AVT-1 Alloy with Polished (Circles) and Cold-Worked (Crosses) Surfaces (a) and Distribution of Compressive Stresses in the Thickness of the Spar Wall from Cold-Working by S.V.Ochagov's Vibratory Impact Method (b).

A marked increase in fatigue strength of spars made of aluminum alloys can be achieved by cold-working of the spars. Figure 1.84 gives the results of fatigue tests of cold-worked spars compared with spars without cold-working. The distribution of internal stresses set up by cold-working is also shown. The endurance limit of cold-worked spars can be raised to values of $\sigma_{w_{min}} = 5.5$ to 6.0 kg/mm² (σ_m = 6.0 kg/mm²).

It should be noted that the strength of cold-worked duralumin spars is reduced greatly if the spar frame, during the gluing process, is heated to a temperature of about 200°C and higher. This makes it mandatory to control the temperature in the gluing operation.

18. Effect of Service Conditions on Fatigue Strength of Spars

The above method for determining the fatigue strength and service life can be used only if the structure, during actual service, does not suffer mechanical or corrosion damage. Otherwise, the approach to determining the service life must be modified and reduced to a study of the effect of such damage. From this

viewpoint, the structures of all blades should be divided into two types: blades with protected and blades with exposed spars.

In a blade design with tubular steel, the spar is usually completely protected by the frame and cannot be mechanically damaged in service. The greatest risk in such a design is corrosion; therefore, the service life of such blades is determined by the quality of the anticorrosion coatings of the spar.

In blade designs in which the spar forms the contour of the leading edge of the profile, special attention must be paid to its protection from mechanical damage. If such protection is inadequate, the service life is shortened and /199 becomes dependent on the degree of damage of the spar. Usually, a permissible degree of damage is stipulated here and checked during preflight blade inspection.

To estimate the effect of damage of a spar in service, dynamic tests are run on specimens cut out of blades operated for a certain number of hours under various service conditions, followed by establishing a rated service life based on the conditions of endurance of specimens undamaged in service. When the fatigue strength decreases excessively, measures are taken to improve the protection of the spar.

CHAPTER II

/200

HELICOPTER VIBRATIONS

Section 1. Forces Causing Helicopter Vibrations

1. Excitation Frequencies

Since, in forward flight of a helicopter, the rotor blades which are subject to the effect of time-variant aerodynamic forces vibrate both in the plane of rotor thrust and in the plane of rotation, the reaction forces acting on the blade in the hub hinges are also variable in time. Correspondingly, variable forces equal in magnitude to these reaction forces act on the rotor hub.

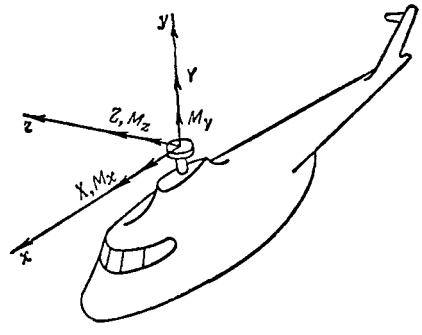

Fig.2.1 Forces and Moments from the Rotor, Acting on a Helicopter.

The variable forces acting on the rotor hub and produced by the vibrating blades can be given in the form of three forces X(t), Y(t), Z(t) and three moments relative to the coordinate axes $M_x(t)$, $M_y(t)$, $M_z(t)$ (Fig.2.1). If the helicopter has an antitorque rotor, the blades of this rotor will cause time-variant forces of the same origin to act on the helicopter; these can also conveniently be given in the form of three variable forces and three moments.

The variable forces from the vibrating rotor blades, acting on the helicopter, are the main source of fuselage vibration.

Fuselage vibrations may also be caused directly by aerodynamic forces acting on the fuselage due to the fluctuating airflow repulsed by the rotors. Thus, the velocity of the flow pushed back by the rotor in the fuselage region increases whenever any of the rotor blades passes above the fuselage. However, numerous calculations and measurements of pressure fluctuations at the fuselage demonstrate that these variable aerodynamic forces are appreciably weaker than the variable forces produced by the vibrating blades and acting on the rotor hub. For example, for the Mi-4 helicopter the variable force acting on the fuselage due to fluctuations of the flow repulsed by the rotor in the most unfavorable flight regime (deceleration before landing) is of the order of ±10 - 15 kgf, whereas the variable forces acting on the rotor hub in different flight regimes are of the order of ±(200 - 600) kgf. Therefore, in analyzing helicopter vi- /201
brations we are primarily interested in variable forces imposed on the rotor hub.

These forces, generally speaking, can be defined as dynamic reactions at forced blade vibrations in flight, for which the calculation methods are presented in Chapter I. Here, it must be emphasized that the variable forces in

such a calculation are determined with considerable inaccuracy. The reason for this lies in the fact that, in calculating blade vibrations, only the lower harmonics of the loads are satisfactorily determined and the calculation errors increase with an increase in the order of the harmonics. Furthermore, as will be shown below, in the calculation of vibrations it is the high harmonics of excitation that are of decisive importance. This is due to the fact that all methods of vibration analysis presented in this Chapter are of a mainly qualitative nature.

An exact calculation of vibrations by means of methods presented in this Chapter is possible only in certain special cases. The most important of these is the designing of a new helicopter fuselage or even of a helicopter of a different configuration (for example, tandem or side-by-side in place of single-rotor) equipped with previously used rotors, for which the variable forces were determined experimentally (for example, by measuring stresses in the rotor shaft or in the reduction gear mount).

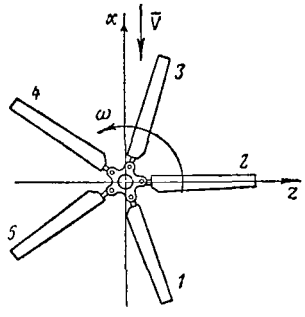

Fig.2.2 Rotor Rotating in an Oncoming Airflow.

It should be noted that the qualitative methods of estimating vibrations permits a number of useful conclusions in designing helicopters and in improving them during flight tests. For example, it is possible to judge the effect on vibrations of the shape of the blade resonance diagram and the fuselage resonance diagram and thus define the direction toward which the design parameters should be changed so as to reduce vibrations, and sometimes even to estimate the degree of reduction in vibration.

To draw certain general conclusions as to the nature of time-variance of the forces $X(t)$, $T(t)$, and $Z(t)$ and of the moments $M_x(t)$, $M_y(t)$, and $M_z(t)$, let us turn to Fig.2.2 which shows a 5-blade rotor uniformly rotating with an angular velocity ω in a relative airflow of constant velocity V. At a certain time t, let the rotor blades occupy the position shown in the sketch and let at this time the force X have a certain value $X(t)$. After a time interval equal to 1/5 of the time of one complete revolution of the rotor, the rotor will turn by 1/5 of this complete revolution. This causes blade No.1 to occupy the position of blade No.2, blade No.2 that of blade No.3, and so on. It is obvious that, in the new position and if all rotor blades are absolutely identical, the entire pattern of flow and hence all forces acting on the blade will be exactly the same as at the initial time t. In particular, the value of the force X will be the same. It is evident that the situation is repeated with the next turn of the rotor by 1/5 of a complete revolution. Consequently, the function $X(t)$ is a periodic function of time of a period equal to 1/5 the time of one complete rotor revolution. Figure 2.3 shows one of the possible slopes of the curve of the dependence $X = X(t)$.

Thus, the force X will vary in time with an angular frequency 5ω, whereas the variable forces acting on the rotor blade will change with a frequency ω (once per rotor revolution).

Like any periodic function, the function X(t) can be expanded in a Fourier series. This will cause the lower harmonic in the expansion to be the harmonic 5ω, so that the expansion will have the form /202

$$X(t)=X_0+X_{a_1}\cos 5\omega t+X_{b_1}\sin 5\omega t+X_{a_2}\cos 10\omega t+X_{b_2}\sin 10\omega t+$$
$$+X_{a_3}\cos 15\omega t+X_{b_3}\sin 15\omega t+\ldots,$$

i.e., the fundamental frequency p = 5ω, while the multiple frequencies are 2p = = 10ω, 3p = 15ω, 4p = 20ω, etc.

Obviously, exactly the same conclusions can be drawn with respect to the functions Y(t), Z(t), $M_x(t)$, $M_y(t)$, and $M_z(t)$.

In general, for a rotor with a number of blades equal to z, all forces and moments acting on the helicopter periodically change in time, with the frequency of the so-called fundamental harmonic of the rotor p = zω. The expansion of these forces and moments in a Fourier series has the form

$$\left.\begin{aligned} X(t)&=X_0+X_{a_1}\cos pt+X_{b_1}\sin pt+X_{a_2}\cos 2pt+\\ &+X_{b_2}\sin 2pt+X_{a_3}\cos 3pt+X_{b_3}\sin 3pt+\ldots;\\ M_x(t)&=M_{x_0}+M^x_{a_1}\cos pt+M^x_{b_1}\sin pt+M^x_{a_2}\cos 2pt+\\ &+M^x_{b_2}\sin 2pt+M^x_{a_3}\cos 3pt+M^x_{b_3}\sin 3pt+\ldots, \end{aligned}\right\} \qquad (1.1)$$

where

$$p=z\omega. \qquad (1.2)$$

Thus, in a helicopter with a number of blades z, excitation of vibrations is possible only with frequencies zω, 2zω, 3zω, etc. We note that this conclusion is valid also for fluctuating aerodynamic forces generated by the flow repulsed by the rotor and acting directly on the fuselage.

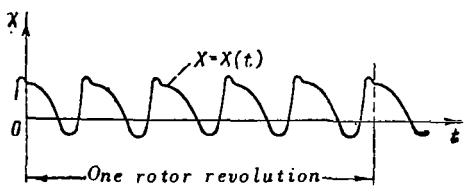

Fig.2.3 Possible Shape of the Dependence of the Longitudinal Force on Time.

If, in addition, the helicopter is equipped with an antitorque rotor having $z_{a.r}$ blades and rotating with an angular velocity $\omega_{a.r}$, then the fuselage will be acted upon also by exciting forces containing harmonics $p_{a.r}=z_{a.r}\omega_{a.r}$, $2p_{a.r}$, $3p_{a.r}$ etc.

All these conclusions are valid only if the rotor blades are perfectly identical. If this condition is not met, low excitation frequencies ω, 2ω, 3ω, etc. might appear. However, many experimental data - results of vibration and stress analyses of structural fuselage members of various helicopters - show that the content of lower harmonics is always so insignificant that they can be disregarded in helicopter vibration analysis as well as in strength estimates of structural fuselage parts. This indicates that the state of the art in manufacture and the demands imposed on the blade structure result in sufficiently small deviations

of individual blade quality.

We note that all above arguments are fully applicable to investigations of variable forces acting on the swashplate of the automatic pitch control and produced by the rotor blades. Despite the fact that the moment of the forces acting on the blade relative to the axial hinge (hinge moment) varies in time with a fundamental frequency ω, the resultant forces and moments acting on the swashplate vary in time with a fundamental frequency $z\omega$. Therefore, the variable forces acting in the collective and cyclic pitch control loops vary with a /203
fundamental frequency $p = z\omega$ and also contain the harmonics 2p, 3p, 4p, etc. In addition, lower excitation harmonics can appear only at deviations in individual blade properties.

2. Dependence of the Frequency Spectrum of Exciting Forces on the Harmonic Content of Blade Vibrations

Above, on the basis of very general considerations, we have demonstrated that variable forces and moments X, Y, Z, M_x, M_y, and M_z produced by the vibrating blades and acting on the rotor hub vary in time with the frequency of the fundamental harmonic $z\omega$ of the rotor and also contain its multiple harmonics $2z\omega$, $3z\omega$, etc., whereas the rotor blades and hence the forces generated by each blade and acting on the hub perform vibrations with the fundamental frequency ω and contain multiple harmonics 2ω, 3ω, 4ω, etc. which comprises also the harmonics $z\omega$, $2z\omega$, etc. This suggests that certain harmonic components of the variable forces set up by each blade and impressed on the hub are neutralized at the hub while others are summed. We will prove that this is actually so. Let us refer to Fig.2.4 which gives a schematic sketch of a hub with hinged blades.

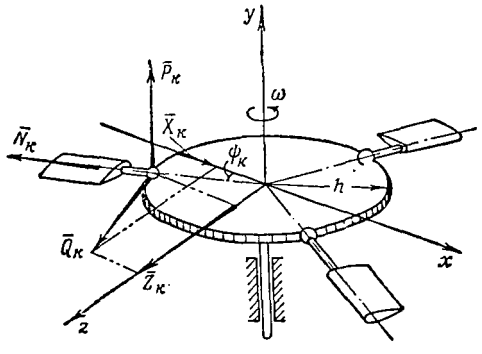

Fig.2.4 Polygon of Forces Generated by the Blade and Impressed on the Rotor Hub.

The force impressed on the hub from the k-th blade can be resolved into three components: N_k directed along the blade radius, P_k parallel to the axis of the rotor shaft, and Q_k perpendicular to both.

Each of these components is a periodic function of time with a fundamental frequency ω. It is obvious that, in a steady-flight regime, the functions $N_k(t)$, $P_k(t)$, and $Q_k(t)$ are identical for all blades but shifted in phase for each blade relative to the adjacent one by some quantity corresponding to the time of rotor turn through an angle $2\pi/z$. This justifies writing the expansion of these functions in Fourier series in the form

$$P_k = P_0 + P_{a_1}\cos(\omega t + \varphi_k) + P_{b_1}\sin(\omega t + \varphi_k) +$$

$$+P_{a_2}\cos 2(\omega t+\varphi_k)+P_{b_2}\sin 2(\omega t+\varphi_k)+\ldots+$$
$$+P_{a_n}\cos n(\omega t+\varphi_k)+P_{b_n}\sin n(\omega t+\varphi_k)+\ldots, \tag{1.3}$$

where

$$\varphi_k=\frac{2\pi}{z}k \quad (k=1, 2, 3\ldots z),$$

or, more concisely,

$$P_k=P_0+\sum_{n=1}^{\infty}[P_{a_n}\cos n(\omega t+\varphi_k)+P_{b_n}\sin n(\omega t+\varphi_k)]. \tag{1.4}$$

In like manner, we have /204

$$Q_k=Q_0+\sum_{n=1}^{\infty}[Q_{a_n}\cos n(\omega t+\varphi_k)+Q_{b_n}\sin n(\omega t+\varphi_k)]; \tag{1.5}$$

$$N_k=N_0+\sum_{n=1}^{\infty}[N_{a_n}\cos n(\omega t+\varphi_k)+N_{b_n}\sin n(\omega t+\varphi_k)]. \tag{1.6}$$

Let us now formulate the following problem: Knowing the values of the coefficients of expansion in Fourier series of the functions $P_k(t)$, $Q_k(t)$, and $N_k(t)$, or, in other words, knowing the harmonic components of the forces P_k, Q_k, N_k, we find the variable forces X, Y, Z and the moments M_x, M_y, M_z (more exactly their harmonic components) from which we can plot the dependence of the vibration-inducing forces on various harmonic components of the forces produced by an individual blade and acting on the hub.

Summing the forces generated by each blade and acting on the hub, we obtain the following formulas:

$$Y=\sum_{k=1}^{z}P_k; \tag{1.7}$$

$$\left.\begin{aligned} X&=\sum_{k=1}^{z}[Q_k\sin\psi_k-N_k\cos\psi_k];\\ Z&=\sum_{k=1}^{z}[Q_k\cos\psi_k+N_k\sin\psi_k];\end{aligned}\right\} \tag{1.8}$$

$$M_y=\sum_{k=1}^{z}Q_kh; \tag{1.9}$$

$$\left.\begin{aligned} M_x&=-\sum_{k=1}^{z}P_kh\sin\psi_k;\\ M_z&=-\sum_{k=1}^{z}P_kh\cos\psi_k,\end{aligned}\right\} \tag{1.10}$$

where

ψ_k = azimuthal angle of the k-th blade:

$$\psi_k = \omega t + \varphi_k = \omega t + \frac{2\pi}{z} k; \tag{1.11}$$

h = distance between axis of rotation and matched flapping and drag hinges.

If the hub has unmatched hinges, then we must take $h = l_{v.h}$ in eq.(1.9) and $h = l_{h.h}$ in eq.(1.10).

Let us examine in detail eq.(1.7) for determining the variable force Y. Substituting into it eq.(1.3) for the force P_k, it becomes necessary to calculate the sums in the form

$$\sum_{k=1}^{z} \cos n(\omega t + \varphi_k) \text{ and } \sum_{k=1}^{z} \sin n(\omega t + \varphi_k),$$

where n are integers (n = 1, 2, 3, ...).

We will show that the trigonometric sums of such a form have the following noteworthy property: For any n not a multiple of the number of blades z, both /205 sums are equal to zero for any t; when n is a multiple of z, i.e., if n = sz (s = 1, 2, 3, ...), then

$$\left.\begin{aligned} \sum_{k=1}^{z} \cos sz(\omega t + \varphi_k) &= z\cos(sz\omega t); \\ \sum_{k=1}^{z} \sin sz(\omega t + \varphi_k) &= z\sin(sz\omega t). \end{aligned}\right\} \tag{1.12}$$

For example, for a rotor with five blades (z = 5)

$$\sum_{k=1}^{5} \cos(\omega t + \varphi_k) = \sum_{k=1}^{5} \cos 2(\omega t + \varphi_k) =$$
$$= \sum_{k=1}^{5} \cos 3(\omega t + \varphi_k) = \sum_{k=1}^{5} \cos 4(\omega t + \varphi_k) = 0$$

for any value of t, but

$$\sum_{k=1}^{5} \cos 5(\omega t + \varphi_k) = 5\cos(5\omega t).$$

Furthermore,

$$\sum_{k=1}^{5} \cos 6(\omega t + \varphi_k) = \sum_{k=1}^{5} \cos 7(\omega t + \varphi_k) =$$

$$= \sum_{k=1}^{5} \cos 8(\omega t + \varphi_k) = \sum_{k=1}^{5} \cos 9(\omega t + \varphi_k) = 0,$$

but

$$\sum_{k=1}^{5} \cos 10(\omega t + \varphi_k) = 5\cos(10\omega t), \text{ etc.}$$

We can prove the validity of eqs.(1.12) by different methods. For this, let us use the convenient method proposed by R.A.Mikheyev based on the application of the well-known Euler formula expressing the relationship between trigonometric functions and exponential functions with an imaginary argument. We will prove the validity of only the first equation in the system (1.12). We have:

$$\cos n\psi_k = \frac{1}{2}\left(e^{in\psi_k} + e^{-in\psi_k}\right); \quad \left(\psi_k = \omega t + \frac{2\pi}{z}k\right).$$

Therefore,

$$\sum_{k=1}^{z} \cos n\psi_k = \frac{1}{2}\sum_{k=1}^{z}\left[e^{in\psi_k} + e^{-in\psi_k}\right] =$$

$$= \frac{1}{2}\left[e^{in\omega t}\sum_{k=1}^{z} e^{in\frac{2\pi}{z}k} + e^{-in\omega t}\sum_{k=1}^{z} e^{-in\frac{2\pi}{z}k}\right].$$

Let us separately check the sum

$$\sum_{k=1}^{z} e^{in\frac{2\pi}{z}k} = \left(e^{in\frac{2\pi}{z}}\right) + \left(e^{in\frac{2\pi}{z}}\right)^2 + \left(e^{in\frac{2\pi}{z}}\right)^3 + \ldots + \left(e^{in\frac{2\pi}{z}}\right)^z.$$

This is a geometric progression with the denominator $e^{in\frac{2\pi}{z}}$. /206

Using the well-known formula for the sum of a geometric progression, we obtain

$$\sum_{k=1}^{z} e^{in\frac{2\pi}{z}k} = \frac{e^{i2\pi\frac{n}{z}}\left(1 - e^{i2\pi n}\right)}{1 - e^{i2\pi\frac{n}{z}}}.$$

Since n is an integer, the numerator of this expression is always equal to zero, so that $e^{i2\pi n} = 1$ ($n = 1, 2, 3, \ldots$).

The denominator of this expression can vanish only if $\left(\frac{n}{z}\right)$ is an integer, i.e., if n is a multiple of the number of blades z. Thus, this sum is equal to zero for any n with the exception of those n that are multiples of the number z. In the latter case, the value of the sum becomes indeterminate $\left(\frac{0}{0}\right)$. This in-

determinacy can be evaluated by the well-known L'Hospital rule. Let n vary continuously, approaching some value sz (s is any integer; s = 1, 2, 3, ...). Differentiating the numerator and denominator with respect to n and passing to the limit n → sz, we have

$$\sum_{k=1}^{z} e^{in\frac{2\pi}{z}k} = \lim_{n\to sz} e^{i2\pi\frac{n}{z}} \lim_{n\to sz} \frac{-i2\pi e^{i2\pi n}}{\left(\frac{-i2\pi}{z}\right) e^{i2\pi\frac{n}{z}}} = z.$$

We can also show exactly that

$$\sum_{k=1}^{z} e^{-in\frac{2\pi}{z}k} = \begin{cases} 0, & \text{if } n \text{ is not a multiple of } z; \\ z, & \text{if } n = sz, \text{ where } s = 1, 2, 3... \end{cases}$$

As a result, we arrive at the conclusion that if n is not a multiple of z, then

$$\sum_{k=1}^{z} \cos n\psi_k = 0.$$

If n is a multiple of z (n = sz; s = 1, 2, 3, ...), then

$$\sum_{k=1}^{z} \cos n\psi_k = \frac{z}{2}\left(e^{in\omega t} + e^{-in\omega t}\right) = z\cos n\omega t = z\cos(sz\omega t).$$

In like manner, we can prove the validity of the second equation of the system (1.12).

The indicated property of trigonometric sums is conveniently written in the form

$$\left.\begin{aligned} \sum_{k=1}^{z} \cos n\psi_k &= \begin{cases} 0, & \text{if } n \text{ is not a multiple of } z; \\ z\cos n\omega t, & \text{if } n = sz;\ s = 1, 2, 3...; \end{cases} \\ \sum_{k=1}^{z} \sin n\psi_k &= \begin{cases} 0, & \text{if } n \text{ is not a multiple of } z; \\ z\sin n\omega t, & \text{if } n = sz;\ s = 1, 2, 3... \end{cases} \end{aligned}\right\} \qquad (1.13)$$

Let us now return to the expression for the force Y from eq.(1.7), into which we substitute the value of the force P_k from eq.(1.4): /207

$$Y = \sum_{k=1}^{z} [P_0 + P_{a_1}\cos\psi_k + P_{b_1}\sin\psi_k + P_{a_2}\cos 2\psi_k + P_{b_2}\sin 2\psi_k + \ldots + P_{a_n}\cos n\psi_k + P_{b_n}\sin n\psi_k + \ldots]$$

On the basis of the established property of trigonometric sums [eq.(1.13)] it can be stated that, upon summation of different harmonics in this expression, all harmonics that are not a multiple of the number of blades z will disappear. The harmonics that are a multiple of z are summed in conformity with eqs.(1.13), so that we finally obtain

$$Y = zP_0 + zP_{a_z}\cos z\omega t + zP_{bz}\sin z\omega t + zP_{a_{(2z)}}\cos 2z\omega t + zP_{b_{(2z)}}\sin 2z\omega t + \ldots \qquad (1.14)$$

Thus, all harmonic components of the force $P_k(t)$ that are not a multiple of the number of blades are neutralized at the rotor hub and do not cause vibrations of the helicopter fuselage. As a result, the variable force Y changes in time with the fundamental harmonic $p = z\omega$ of the rotor, and also contains multiple harmonics 2p, 3p, etc. This completely confirms the basic conclusion of the preceding Subsection, and yields additional information exactly defining the harmonic components of the force P_k that are dangerous from the aspect of vibrations.

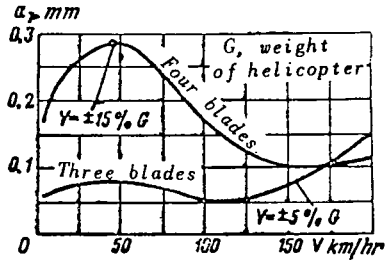

Fig.2.5 Amplitude of Vibrations in Cockpit of Single-Rotor Helicopter as a Function of Flying Speed.

Let us examine an example for illustration purposes. We assume that, for some rotor, there is resonance of the second overtone of blade vibration in the flapping plane with the fifth harmonic of the rotor (5ω). In this case the harmonic component corresponding to the fifth harmonic (P_{a5} and P_{b5}) will be large in the expansion of the force P_k for such a rotor.

If the rotor has five blades, the above type of resonance will lead to appreciable vibrations of the helicopter.

If the rotor has four blades, this resonance will in no way manifest itself in vibrations of the helicopter, since the harmonic components of the force P_k corresponding to this resonance will be neutralized at the hub. As will be shown later, the variable moments M_x and M_z at the hub can be appreciable; however, for all practical purposes the helicopter vibrations are determined mainly by the variable forces X, Y, Z. Occasionally, it is erroneously assumed that the vibrations of a given helicopter are smaller, the larger the number of rotor blades. However, it is evident in this example that in reality the matter is not so simple and that in this case a reduction in the number of blades actually will lead to a reduction in vibration.

Let us examine another example: Figure 2.5 shows the results of experimental vibration measurements in the cockpit of a single-rotor helicopter which was tested with two rotors: three- and four-blade types. The rotors had completely identical blades and differed only in the hubs. The curves depict the dependence of the amplitude a_y of vertical vibrations in the cockpit on the flying speed V for both rotors.

As shown by calculations of these rotors, the rotor blade had a resonance /208

of the second overtone of vibrations in the flapping plane with the fourth harmonic of the rotor at the operating rpm. As a result, the vibrations of the helicopter with a four-blade rotor, over the greater portion of the speed range, were appreciably higher (at V = 40 - 50 km/hr, by a factor of more than 3) than the vibrations of a helicopter with the three-blade rotor. However, at a high flying speed the vibrations of the helicopter with a four-blade rotor were smaller than those of the helicopter with a three-blade rotor. This is explained by the fact that, at low flying speed, a large harmonic component of aerodynamic forces exists, corresponding to the fourth harmonic and caused by the large nonuniformity of the induced velocity field of the rotor at a low flying speed. With an increase in flying speed there occurs an equalization of the velocity field of the flow passing through the rotor (see Chapt.I, Sect.8); correspondingly, the excitation of blade vibrations with respect to the fourth harmonic decreases rapidly, whereas the third harmonic does not decrease as rapidly with an increase in speed or may not decrease at all. The relatively large magnitude of the fourth harmonic in the induced velocity field at low flying speed apparently is a phenomenon common to all rotors.

Let us now return to a determination of other forces and moments acting on the helicopter. Equation (1.9) for the moment M_y is completely analogous to eq.(1.7).

Repeating the reasoning used in deriving eq.(1.14) for the force Y, we obtain the following expression:

$$M_y = zh\,[Q_0 + Q_{a_z}\cos z\omega t + Q_{b_z}\sin z\omega t + \\ + Q_{a_{(2z)}}\cos 2z\omega t + Q_{b_{(2z)}}\sin 2z\omega t + \ldots]. \tag{1.15}$$

The variable moment M_y is dangerous not only from the aspect of helicopter vibrations (it will be shown in Sect.3, Subsect.1 that this moment causes only lateral fuselage vibrations). This moment is one of the sources of torsional vibrations in the transmission system of a helicopter.

As we see from eq.(1.15), the variable portion of this moment is determined exclusively by the harmonic components of the force Q(t) which are multiples to the number of blades.

Let us now turn to the first equation of the system (1.8). Substituting into it the expressions for $Q_k(t)$ and $N_k(t)$ [eqs.(1.5) and (1.6)], we obtain

$$X = \sum_{k=1}^{z}(Q_0\sin\psi_k - N_0\cos\psi_k) + \sum_{k=1}^{z}[Q_{a_1}\cos\psi_k + Q_{b_1}\sin\psi_k]\sin\psi_k - \\ - \sum_{k=1}^{z}[N_{a_1}\cos\psi_k + N_{b_1}\sin\psi_k]\cos\psi_k + \ldots + \sum_{k=1}^{z}[Q_{a_n}\cos n\psi_k + \\ + Q_{b_n}\sin n\psi_k]\sin\psi_k - \sum_{k=1}^{z}[N_{a_n}\cos n\psi_k + N_{b_n}\sin n\psi_k]\cos\psi_k + \ldots$$

The first addend of this sum is equal to zero, in conformity with eqs.(1.13) since

$$\sum_{k=1}^{z}[Q_0\sin\psi_k - N_0\cos\psi_k] = Q_0\sum_{k=1}^{z}\sin\psi_k - N_0\sum_{k=1}^{z}\cos\psi_k = 0.$$

To calculate the remaining addends let us examine the expression

$$X_{Q_n} = \sum_{k=1}^{z}[Q_{a_n}\cos n\psi_k + Q_{b_n}\sin n\psi_k]\sin\psi_k,$$

which represents the component of the force X caused by the n-th harmonic of the force Q. /209

Here, we encounter sums of the form $\sum_{k=1}^{z}\cos n\psi_k\sin\psi_k$ and $\sum_{k=1}^{z}\sin n\psi_k\sin\psi_k$. These sums are also easily calculated by means of eq.(1.13). Actually,

$$\sum_{k=1}^{z}\cos n\psi_k\sin\psi_k = \frac{1}{2}\sum_{k=1}^{z}\sin(n+1)\psi_k - \frac{1}{2}\sum_{k=1}^{z}\sin(n-1)\psi_k;$$

$$\sum_{k=1}^{z}\sin n\psi_k\sin\psi_k = -\frac{1}{2}\sum_{k=1}^{z}\cos(n+1)\psi_k + \frac{1}{2}\sum_{k=1}^{z}\cos(n-1)\psi_k.$$

On the basis of eqs.(1.13) we can assert that these sums will be nonzero only if one of the numbers (n + 1) or (n - 1) is a multiple of the number of blades. Let (n + 1) = sz (s = 1, 2, 3, ...) and thus n = sz - 1. Then,

$$\sum_{k=1}^{z}\cos n\psi_k\sin\psi_k = \frac{z}{2}\sin(sz\omega t);$$

$$\sum_{k=1}^{z}\sin n\psi_k\sin\psi_k = -\frac{z}{2}\cos(sz\omega t).$$

Furthermore, if (n - 1) = sz; n = sz + 1, then

$$\sum_{k=1}^{z}\cos n\psi_k\sin\psi_k = -\frac{z}{2}\sin(sz\omega t);$$

$$\sum_{k=1}^{z}\sin n\psi_k\sin\psi_k = \frac{z}{2}\cos(sz\omega t).$$

As a result, we obtain the following expression for the component of the force X which is obtained from all harmonic components of the force Q:

$$X_Q = z\left\{\frac{Q_{a\,(z-1)} - Q_{a\,(z+1)}}{2}\sin z\omega t - \frac{-Q_{b\,(z-1)} + Q_{b\,(z+1)}}{2}\cos z\omega t + \right.$$
$$\left. + \frac{Q_{a\,(2z-1)} - Q_{a\,(2z+1)}}{2}\sin 2z\omega t + \frac{-Q_{b\,(2z-1)} + Q_{b\,(2z+1)}}{2}\cos 2z\omega t + \ldots\right\}. \quad (1.16)$$

For the portion of the force X caused by harmonic components of the force N(t), we obtain in like manner the expression of the form

$$X_N = z\left\{-\frac{N_{a\,(z-1)} + N_{a\,(z+1)}}{2}\cos z\omega t + \frac{N_{b\,(z-1)} + N_{b\,(z+1)}}{2}\sin z\omega t - \right.$$
$$\left. - \frac{N_{a\,(2z-1)} + N_{a\,(2z+1)}}{2}\cos 2z\omega t - \frac{N_{b\,(2z-1)} + N_{b\,(2z+1)}}{2}\sin 2z\omega t + \ldots\right\}. \quad (1.17)$$

The force X can be determined by the formula

$$X = X_Q + X_N.$$

If the expression for the force X(t) is written in the form of eq.(1.1), /210 the following formulas for its harmonic components are obtained:

$$\left.\begin{aligned} X_{a_1} &= \frac{z}{2}[Q_{b\,(z+1)} - Q_{b\,(z-1)} - N_{a\,(z+1)} - N_{a\,(z-1)}]; \\ X_{b_1} &= \frac{z}{2}[Q_{a\,(z-1)} - Q_{a\,(z+1)} - N_{b\,(z+1)} - N_{b\,(z-1)}]. \end{aligned}\right\} \quad (1.18)$$

The components corresponding to harmonics that are multiples of the fundamental harmonic X_{a2}, X_{b2}, etc. are obtained from these same formulas, if we replace the index z by the indices 2z, 3z, etc.

Thus, the variable part of the force X(t) is determined by the harmonic components of the forces Q(t) and N(t) which are combinatory with respect to the fundamental harmonic of the rotor (z - 1; z + 1) or to its multiple harmonics (2z - 1; 2z + 1), etc.

For example, for a rotor with three blades (z = 3), the fundamental harmonic of the force X (frequency 3ωt) will be determined by the second and fourth harmonics of the forces Q(t) and N(t), the second harmonic of the force (frequency 6ωt) will be determined by the fifth and seventh harmonics of forces Q(t) and N(t), and so on.

Completely analogous formulas are obtained for harmonic components of the force Z(t)

$$\left.\begin{aligned} Z_{a_1} &= \frac{z}{2}[Q_{a\,(z+1)} + Q_{a\,(z-1)} + N_{b\,(z+1)} - N_{b\,(z-1)}]; \\ Z_{b_1} &= \frac{z}{2}[Q_{b\,(z+1)} + Q_{b\,(z-1)} + N_{a\,(z-1)} - N_{a\,(z+1)}]. \end{aligned}\right\} \quad (1.19)$$

Just as in eqs.(1.18), to obtain the multiple harmonics Z_{a2}, Z_{b2}, Z_{a3}, Z_{b3} the index z in these formulas must be substituted respectively by the indices 2z, 3z, etc.

In like manner, the expressions for the harmonic components of the moments M_x and M_z are obtained from eqs.(1.10):

$$\left.\begin{aligned} M^x_{a_1} &= \frac{zh}{2}\left[P_{b\,(z-1)} - P_{b\,(z+1)}\right]; \\ M^x_{b_1} &= \frac{zh}{2}\left[P_{a\,(z+1)} - P_{a\,(z-1)}\right]; \end{aligned}\right\} \tag{1.20}$$

$$\left.\begin{aligned} M^z_{a_1} &= \frac{zh}{2}\left[-P_{a\,(z+1)} - P_{a\,(z-1)}\right]; \\ M^z_{b_1} &= \frac{zh}{2}\left[-P_{b\,(z+1)} - P_{b\,(z-1)}\right]. \end{aligned}\right\} \tag{1.21}$$

Let us also mention the following fact which occasionally might facilitate a qualitative vibration analysis. If the variable force in the rotor plane (X or Z) or the moment (M_x, M_z) are determined by some harmonic component of the force generated by the blade, then we obtain a vector of constant length uniformly rotating in the plane of the rotor with an angular velocity $z\omega$ (or $sz\omega$). The direction of rotation is opposite to that of the rotor if this vector is obtained from the harmonic component z + 1 (or sz + 1), and equidirectional with the rotation of the rotor if this vector is obtained from the harmonic component z - 1 (or sz - 1).

For instance, let the rotor have five blades (z = 5) and let us look at /211 the vector of the moment at the hub, with components M_x and M_z obtained from the harmonic component (z - 1):

$$P = P_{a_4}\cos 4\omega t + P_{b_4}\sin 4\omega t.$$

Then [eqs.(1.20) and (1.21)],

$$M_x = \frac{zh}{2}\left[P_{b_4}\cos 5\omega t - P_{a_4}\sin 5\omega t\right];$$

$$M_z = \frac{zh}{2}\left[-P_{b_4}\sin 5\omega t - P_{a_4}\cos 5\omega t\right].$$

As indicated by these formulas, the vector

$$\overline{M} = \overline{M}_x + \overline{M}_z$$

represents a vector of constant length

$$M = \frac{zh}{2}\sqrt{P^2_{a_4} + P^2_{b_4}},$$

uniformly rotating in the plane of the rotor with an angular velocity 5ω in a direction coinciding with the direction of rotor rotation.

Thus, the above analysis shows that a rotor is a sort of filter which, out of all harmonic components of the forces on vibrating blades, transmits to the fuselage only certain ones corresponding to the fundamental harmonic of the rotor $z\omega$, to its composite harmonics $(z - 1)\omega$ and $(z + 1)\omega$, harmonics that are multiples of the fundamental harmonic $2z\omega$, $3z\omega$, etc., and to composite harmonics $(2z - 1)\omega$, $(2z + 1)\omega$, $(3z - 1)\omega$, $(3z + 1)\omega$, etc.

As a rule, the lower harmonics $z\omega$, $(z + 1)\omega$, and $(z - 1)\omega$ represent the greatest danger both from the aspect of the vibration level and from the aspect of dynamic strength of the fuselage members.

Of the harmonics which are a consequence of blade vibrations in the flapping plane (force $\bar{P}_k$, see Fig.2.4), the harmonic $z\omega$ (and multiples of it) lead to the appearance of a vertical variable force on the rotor, whereas the harmonics $(z - 1)$ and $(z + 1)$ (and also $2z - 1$, $2z + 1$, etc.) lead to the appearance of variable moments at the hub relative to the axes Ox and Oz.

Of the harmonics which are a consequence of blade vibrations in the plane of rotation (forces $\bar{Q}_k$ and $\bar{N}_k$, see Fig.2.4), the harmonic $z\omega$ (and multiples of it) lead to the appearance of a variable twisting moment on the rotor shaft, whereas the harmonics $(z - 1)\omega$ and $(z + 1)\omega$, and also $(2z - 1, 2z + 1$, etc.), lead to the appearance of variable forces (longitudinal and lateral) in the plane of rotation of the rotor.

We note in conclusion that, upon summation of the forces generated by the blades and acting on the swashplate of the pitch control, we obtain exactly the same formulas for calculating the harmonic components of the vertical force Y and the moments M_x and M_z applied to the swashplate. In this case, eqs.(1.14), (1.20), and (1.21) can be used directly, understanding by the force

$$P_k(t) = P_0 + \sum_{n=1}^{\infty} (P_{a_n} \cos n\psi_k + P_{b_n} \sin n\psi_k)$$

the force acting in the trimmer of the k-th blade (hinge moment divided by the corresponding arm), and understanding by the quantity h the radius of the swashplate of the pitch control.

Thus, knowing the harmonic content of the hinge moment, it is not difficult to calculate the variable forces acting in the collective and cyclic pitch control loops.

Section 2. Flexural Vibrations of the Fuselage as an Elastic Beam /212

If the variable forces imparted to the fuselage by the rotors are known, then calculation of vibrations at different points of the fuselage can be carried out by conventional methods of calculating the forced vibrations of an elastic beam of variable cross section. Of course, the fuselage of a real helicopter

can be regarded as a thin flexurally elastic beam.

In reality, the transverse dimensions of a fuselage cannot be considered small in comparison with the longitudinal dimensions. Furthermore, the fuselage of a helicopter of single-rotor configuration may have "discontinuities" in the region of the tail boom, pronounced reduction in rigidity over the length, and other peculiarities. These special features and their consideration in vibration analysis are discussed in Section 3. Here, we will describe methods of vibration analysis of an elastic beam, since these form the basis for further discussion. In this Section, we will also investigate vibrations of a system consisting of two elastic beams forming a "cross". A fuselage with a wing is reduced to such a system.

1. Calculation of Forced Vibrations of an Elastic Beam by the Method of Expansion in Natural Modes

Let a time-variant load q, distributed over the beam length and varying in accordance with the harmonic law

$$q(x, t)=q(x)\cos pt \tag{2.1}$$

be applied to a flexurally elastic ideal beam (Fig.2.6) without damping, which is in a free state under the effect of a balanced system of time-invariant forces (the force of rotor thrust balances the force of gravity).

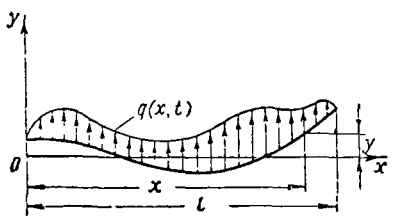

Fig.2.6 Diagram of a Free Elastic Beam under Application of a Distributed Load.

The equation of lateral flexural vibrations of such a beam has the form

$$(EIy'')''+m\ddot{y}=q(x, t). \tag{2.2}$$

This equation in partial derivatives was derived in Subsection 10, Section 1, Chapter I for an elastic beam in a centrifugal force field. In their absence ($N \equiv 0$), the expression takes the form of eq.(2.2).

The problem is to find the motion of the beam, i.e., to find the function $y = y(x, t)$ which satisfies eq.(2.2) and the boundary conditions which, in the case of a beam with free ends, have the form

$$\left.\begin{aligned} &\text{at } x=0;\ M=EIy''=0;\ Q=(EIy'')'=0;\\ &\text{at } x=l;\ M=EIy''=0;\ Q=(EIy'')'=0. \end{aligned}\right\} \tag{2.3}$$

The functions $y(x, t)$ satisfying the homogeneous equation (without the right-hand side)

$$(EIy'')''+m\ddot{y}=0 \tag{2.4}$$

and the boundary conditions (2.3) correspond to the natural vibrations of the beam. The solution of eq.(2.4) is sought in the form

$$y(x, t)=\bar{y}(x)\cos pt. \tag{2.5}$$

This expression, after substitution into eq.(2.4), leads to an ordinary differential equation with the parameter p for determining the function $\bar{y}(x)$: /213

$$(EI\bar{y}')''-p^2m\bar{y}=0. \tag{2.6}$$

The last equation has solutions different from zero only at certain values of the parameter p: $p = p_0$; $p = p_1$; $p = p_2$; $p = p_3$, etc. To each value of $p = p_k$ ($k = 0, 1, 2, 3, \ldots$) there corresponds a certain function $\bar{y}_k(x)$, which satisfies eq.(2.6) at $p = p_k$, so that

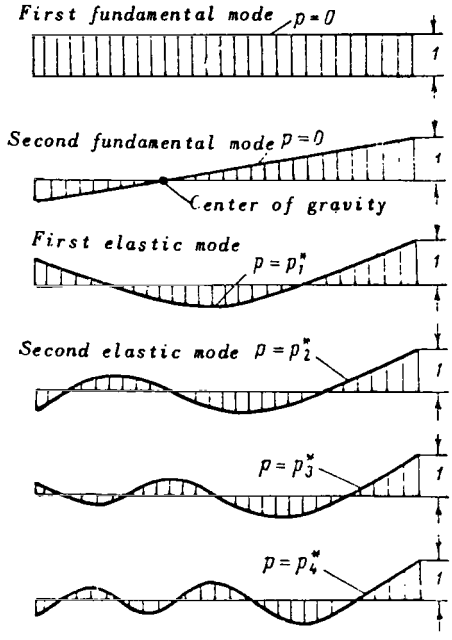

Fig.2.7 Characteristic Natural Vibration Modes of a Fuselage as a Free Beam. (p_1^*, p_2^*, etc. are the vibration frequencies of the first, second, etc. elastic overtones; in general we can assume: $p_0 = 0$; $p_1 = 0$, $p_2 = p_1^*$; $p_3 = p_2^*$, etc.).

$$(EI\bar{y}_k')''-p_k^2m\bar{y}_k=0; \quad (k=1, 2, 3,\ldots). \tag{2.7}$$

The orders of p_k ($k = 0, 1, 2, 3, \ldots$) are called the natural frequencies of the beam, while the functions $\bar{y}_k(x)$ are designated as the corresponding natural vibration modes.

The motion of the beam according to the law

$$y(x, t)=a_k\bar{y}_k(x)\cos p_kt, \tag{2.8}$$

where a_k is a constant, is called the natural vibration of the beam with respect to the k-th overtone.

The general solution of the homogeneous equation (2.4) has the form

$$y(x, t)=\sum_k a_k\bar{y}_k(x)\cos(p_kt+\varphi_k), \tag{2.9}$$

where a_k and φ_k are arbitrary constants.

Thus, the natural vibrations of a beam represent motion produced as a result of the superposition of vibrations of different overtones.

The methods of finding the natural frequencies p_k and the corresponding modes $\bar{y}_k(x)$ for a beam with a given law of variation in rigidity EI(x) and a linear mass m(x) are presented in Section 2 of Chapter I.

Figure 2.7 shows the characteristic modes of natural vibrations of a free beam. The two modes correspond to vibrations of a beam as a solid body and have natural frequencies equal to zero. The first of these modes corresponds to forward motions of the beam, and the second to angular displacement of the beam relative to its center of gravity.

All formulas derived in this Section are equally suitable for calculating the vibrations of an elastic beam with any clamping conditions at its ends. However, when these formulas are used for vibrations of a free beam and particularly of a fuselage, it must be remembered that the number of the frequencies p_k and of the modes $\bar{y}_k(x)$ of natural vibrations must include the two lower modes which correspond to fundamental frequencies. Thus, in all formulas it is necessary to set $p_0 = 0$ and $p_1 = 0$ and to take into account that the corresponding /214 normed modes have the form

$$\bar{y}_0(x) = 1;$$
$$\bar{y}_1(x) = \frac{x - x_c}{l - x_c},$$

where x_c is the coordinate of the center of gravity of the beam.

If the above modes are not taken into account in calculations of fuselage vibrations, the vibration analysis will not include vibrations of the fuselage as a solid body, which will lead to appreciable errors in the vibration magnitude.

Let us study here the problem of forced vibrations of a beam subjected to a "purely" harmonic load [see eq.(2.1)]. In this case, eq.(2.2) takes the form

$$(EIy'')'' + m\ddot{y} = q(x)\cos pt. \tag{2.10}$$

Let us first seek the particular solution of this equation corresponding to steady forced vibrations of the beam with a frequency p in the form

$$y = \bar{y}(x)\cos pt. \tag{2.11}$$

Substituting this expression into eq.(2.10), we arrive at an ordinary differential equation for determining the function $\bar{y}(x)$ which, of course, is known as the mode of forced vibrations:

$$(EI\bar{y}'')'' - p^2 m\bar{y} = q(x). \tag{2.12}$$

Let us then seek the solution of this equation in the form of an expansion in natural modes:

$$\bar{y} = \sum_k c_k \bar{y}_k(x). \tag{2.13}$$

If, in this sum, we take a limited number of terms, then, in determining the values of the coefficients c_k, we can obtain only the approximate solutions of eq.(2.12). However, it is possible to prove that in the method of determin-

ing the coefficients c_k given below, the approximate solution with a rather large number of terms in the series (2.13) can differ from the exact solution as much as desired.

To find the coefficients c_k, we substitute eq.(2.13) into eq.(2.12) and, after multiplying both sides of eq.(2.12) by $\bar{y}_n(x)$, we integrate them from 0 to l. This will yield the equation

$$\sum_k c_k \int_0^l (EI\bar{y}_k'')''\bar{y}_n dx - p^2 \sum_k c_k \int_0^l m\bar{y}_k\bar{y}_n dx = \int_0^l q\bar{y}_n dx. \tag{2.14}$$

The integrals in the first term on the left-hand side of this equation can be simplified by using integration by parts:

$$\int_0^l (EI\bar{y}_k'')''\bar{y}_n dx = \int_0^l \bar{y}_n d(EI\bar{y}_k'') = [\bar{y}_n(EI\bar{y}_k'')']\Big|_0^l - \int_0^l \bar{y}_n'(EI\bar{y}_k'')' dx,$$

but

$$[\bar{y}_n(EI\bar{y}_k'')']\Big|_0^l = 0,$$

since the functions $\bar{y}_k(x)$ satisfies the boundary conditions (2.3).

Furthermore, /215

$$\int_0^l \bar{y}_n'(EI\bar{y}_k'')' dx = \int_0^l \bar{y}_n' d(EI\bar{y}_k'') = [\bar{y}_n'(EI\bar{y}_k'')]\Big|_0^l - \int_0^l EI\bar{y}_n''\bar{y}_k'' dx.$$

By virtue of the conditions (2.3), we have

$$[\bar{y}_n'(EI\bar{y}_k'')]\Big|_0^l = 0,$$

so that, as a result, we obtain

$$\int_0^l (EI\bar{y}_k'')''\bar{y}_n dx = \int_0^l EI\bar{y}_n''\bar{y}_k'' dx. \tag{2.15}$$

Since all functions $\bar{y}_k(x)$ ($k = 1, 2, 3, \ldots$) satisfy eq.(2.7), we can write

$$(EI\bar{y}_k'')'' - p_k^2 m\bar{y}_k = 0;$$
$$(EI\bar{y}_n'')'' - p_n^2 m\bar{y}_n = 0.$$

Multiplying the first equation by $\bar{y}_n$ and the second by $\bar{y}_k$, we then subtract one from the other and integrate the obtained expression from 0 to l. This yields

$$\int_0^l (EI\bar{y}_k'')''\bar{y}_n dx - \int_0^l (EI\bar{y}_n'')''\bar{y}_k dx = (p_k^2 - p_n^2)\int_0^l m\bar{y}_n\bar{y}_k dx.$$

However, the left-hand side of this equation is equal to zero by virtue of the condition (2.15). Therefore, if only $p_k \neq p_n$, then

$$\int_0^l m\bar{y}_n\bar{y}_k dx = 0; \quad (n \neq k). \tag{2.16}$$

This is the so-called condition of orthogonality of the natural vibration modes (see also Chapt.I, Sect.2, Subsect.3).

Furthermore, multiplying both sides of eq.(2.7) by $\bar{y}_n$ and integrating from 0 to l, we obtain

$$\int_0^l (EI\bar{y}_k'')''\bar{y}_n dx = p_k^2 \int_0^l m\bar{y}_k\bar{y}_n dx.$$

Hence, we can conclude that if $n \neq k$, then

$$\int_0^l (EI\bar{y}_k'')''\bar{y}_n dx = \int_0^l EI\bar{y}_n''\bar{y}_k'' dx = 0. \tag{2.17}$$

If $n = k$, we obtain an expression for the frequency p_n of the n-th overtone of vibrations in terms of its mode $\bar{y}_n(x)$:

$$p_n^2 = \frac{\int_0^l EI\bar{y}_n''^2 dx}{\int_0^l m\bar{y}_n^2 dx}. \tag{2.18}$$

This is the well-known Rayleigh formula.

On the basis of conditions (2.16) and (2.17) we can assert that, in eq.(2.14), all terms for which $k \neq n$ vanish. Taking this into account and making use of eq.(2.15), we rewrite eq.(2.14) in the form /216

$$c_n \int_0^l EI\bar{y}_n''^2 dx - c_n p^2 \int_0^l m\bar{y}_n^2 dx = \int_0^l q\bar{y}_n dx.$$

Dividing both sides of the last equation by $\int_0^l m\bar{y}_n^2 dx$, solving it relative to c_n, and using Rayleigh's formula [eq.(2.18)], we find

$$c_n = \frac{1}{p_n^2 - p^2} \cdot \frac{\int_0^l q\bar{y}_n dx}{\int_0^l m\bar{y}_n^2 dx}. \tag{2.19}$$

We then introduce the notations:

$$A_n = \int_0^l q\bar{y}_n dx; \tag{2.20}$$

$$K_n = \int_0^l m\bar{y}_n^2 dx. \tag{2.21}$$

The quantity A_n represents the work of the exciting load q(x) at the mode of the n-th overtone of vibrations, while the quantity k_n denotes the largest (during the period) value of the kinetic energy of the given overtone of vibrations referred to the quantity p_n^2. Thus,

$$c_n = \frac{1}{p_n^2 - p^2} \frac{A_n}{K_n}. \tag{2.22}$$

Taking into account eqs.(2.13) and (2.11), we obtain the following solution of equation (2.10):

$$y(x, t) = \left[\sum_k \frac{1}{p_k^2 - p^2} \frac{A_k}{K_k} \bar{y}_k(x)\right] \cos pt. \tag{2.23}$$

From this expression, we can draw certain important conclusions.

First, it is obvious that if the frequency of variation of the exciting load p approaches one of the frequencies p_k of natural vibrations, then the vibration amplitude at any point of the beam increases without bounds. This is the phenomenon of resonance of an exciting load with the k-th overtone of natural blade vibrations. Since we do not consider here the effect of damping forces (this will be done later on), the vibration amplitude in resonance is unlimited.

Furthermore, if the quantity p is close to the frequency p_n of the n-th overtone of vibrations, the term with the number n in the sum (2.23) becomes appreciably larger than the other terms. Therefore, we can assume approximately that, in the vicinity of resonance ($p = p_n$), we have

$$y(x, t) = \frac{1}{p_n^2 - p^2} \frac{A_n}{K_n} \bar{y}_n(x) \cos pt = c_n \bar{y}_n(x) \cos pt,$$

meaning that, in the vicinity of resonance with some overtone of natural vibrations the mode of forced vibrations differs little from the mode of vibrations of the given overtone.

Finally, when the value of p changes from an amount somewhat smaller than /217 p_n to an amount somewhat larger than p_n, the quantity in the brackets of formula (2.23) changes sign. Therefore, if we construct a graph for the dependence of the amplitude $\bar{y}_0$ of some point of the beam on the excitation frequency p [for a constant q(x)], this graph will have the shape shown in Fig.2.8. The curve of the graph has infinite discontinuities at the points $p = p_1$, $p = p_2$, $p = p_3$, etc.

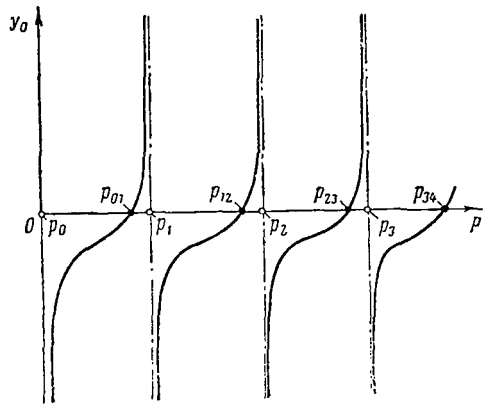

Fig.2.8 Dependence of Vibration Amplitude of any Fuselage Point on the Excitation Frequency.

2. Dynamic Rigidity of a Beam. Resonance and Antiresonance

In the preceding Subsection, we discussed the case of forced vibrations of a beam subjected to an exciting force distributed over its length, which varies in time by the harmonic law (2.1); the derived formulas remain in force for any law of variation in load over the beam length, i.e., for any form of the function q(x). Therefore, it is not difficult to derive, from these expressions, formulas for determining the forced vibrations of a beam caused by a concentrated exciting force

$$F = F_0 \cos pt, \tag{2.24}$$

applied at a certain point $x = x_0$ (Fig.2.9).

In fact, let the load q(x) be applied to a beam over only a small segment of length Δx in the vicinity of the point $x = x_0$. In this case, eqs.(2.22), (2.20), and (2.21) remain valid, but in eq.(2.20) the corresponding integral must not be taken over the entire length of the beam l but only over a segment Δx, i.e.,

$$A_n = \int_0^l q\bar{y}_n dx = \int_{\Delta x} q\bar{y}_n dx.$$

At a small value of Δx, this integral can be approximately replaced by the quantity

$$\int_{\Delta x} q\bar{y}_n dx = F_0 \bar{y}_n(x_0), \tag{2.25}$$

where

$$F_0 = \int_{\Delta x} q dx. \tag{2.26}$$

Equation (2.25) becomes exact at an infinitely small Δx, i.e., in the case of a concentrated exciting force.

Thus, we arrive at the following conclusions: If the vibrations of a beam are caused by a concentrated force [eq.(2.24)] applied at the point $x = x_0$, then the motion of the beam is described as before by eq.(2.23) in which the quantity A_k is determined by the formula /218

$$A_k = F_0 \bar{y}_k(x_0), \tag{2.27}$$

i.e., the quantity A_k represents the work done by the exciting load "at the mode of the k-th overtone of vibrations".

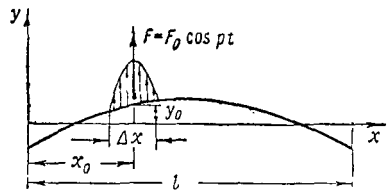

Fig.2.9 For Analyzing Forced Vibrations of a Free Beam due to a Concentrated Force.

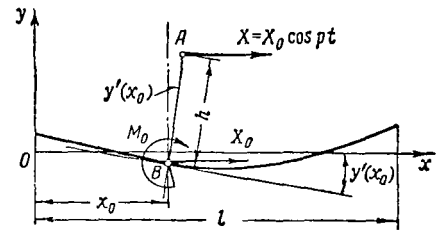

Fig.2.10 Diagram of the Action of a Longitudinal Force Produced by the Rotor and Exerted on an Elastic Fuselage.

We note that this method of defining the forced vibrations holds also if the vibrations are caused by a concentrated bending moment varying by a harmonic law

$$M = M_0 \cos pt, \tag{2.28}$$

applied at the point $x = x_0$. In this case, the quantity A_k should be determined by the formula

$$A_k = M_0 \bar{y}_k'(x_0), \tag{2.29}$$

where $\bar{y}_k'(x_0)$ is the angle of rotation of the elastic line at the point $x = x_0$ corresponding to the mode of the k-th overtone.

If the beam vibrations are caused by a longitudinal force

$$X = X_0 \cos pt, \tag{2.30}$$

applied to some arm h (Fig.2.10), all of the derived formulas remain valid since, in this case, the force X_0 can be transferred from the point A to the corresponding point B of the beam, during which process the couple with a moment equal to $M_0 = X_0 h$ has been added.

The longitudinal variable force applied at the point B is able to cause only longitudinal (axial) vibrations of the beam, whereas lateral vibrations of the beam due to the harmonic moment M_0 are determined in the manner indicated above.

In examining lateral forced vibrations of a beam produced by a concentrated force $F = F_0 \cos pt$, it is convenient to introduce the concept of dynamic rigidity of the beam at the point of application of the force $x = x_0$.

Let the dynamic rigidity $D(p)$ of the beam at the point $x = x_0$ be represented as the ratio of the highest value (amplitude) of the exciting force F_0 to the amplitude $\bar{y}_0 = \bar{y}(x_0)$ of the forced vibrations of the beam at the point of application of force, such that

$$D(p) = \frac{F_0}{\bar{y}_0}. \tag{2.31}$$

We have in mind that, on a variation in force in accordance with the harmonic law $F = F_0 \cos pt$, the point of application of this force will execute steady forced vibrations according to the law $y = \bar{y}_0 \cos pt$.

Thus, the dynamic rigidity of a beam is a function of the vibration frequency p and is considered positive if the force and displacement vary in time "in phase" and negative if the force and displacement vary in "antiphase".

The vibration amplitude of the point of application of the force $x = x_0$ can be determined from eq.(2.23): /219

$$\bar{y}_0 = \sum_k \frac{1}{p_k^2 - p^2} \frac{A_k}{K_k} \bar{y}_k(x_0). \tag{2.32}$$

If we plot the graph of the variation of $\bar{y}_0$ with respect to the frequency p at a constant value of F_0, a curve analogous to that shown in Fig.2.8 will be obtained. Therefore, if we construct the graph of the dependence of the dynamic rigidity $D(p)$ at the given point of the beam as a function of the vibration frequency, this graph will have the form shown in Fig.2.11.

The dynamic rigidity $D(p)$ vanishes at the resonances $p = p_1$, $p = p_2$, etc. and becomes infinite at all values of the frequency p ($p = p_{12}$, $p = p_{23}$, $p = p_{34}$, etc.) at which the vibration amplitude of the point of application of force vanishes. These values of the frequency p are known as antiresonance frequencies and are equal to the frequencies of the corresponding overtones of natural vibrations of the beam with a hinged support at the point of application of force F.

Actually, let us imagine that at the point of application of force F the beam has a hinged support (the beam is not crosscut at this point) so that this point of the beam remains stationary during vibration. Such a beam has its own natural vibration frequencies and modes. In the presence of natural beam vibra-

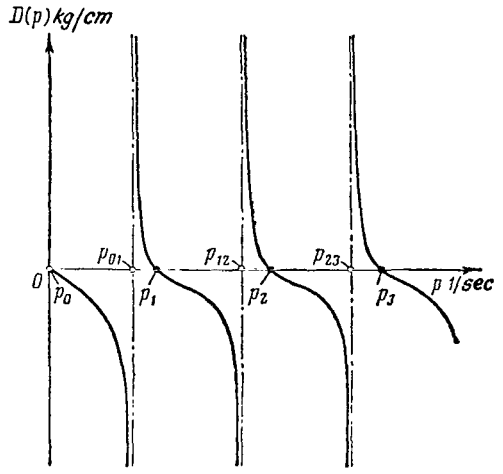

Fig.2.11 Graph of Dynamic Rigidity.

tions of a certain overtone, a dynamic reaction will arise at the support $x = x_0$ which varies in time according to a harmonic law with the frequency of this overtone. The amplitude (highest value) of this reaction force will depend on the amplitude (of some point, for example, the end) of natural vibrations of the beam, which may have any magnitude (depending upon the initial conditions). Therefore, we can always select a beam vibration amplitude such that the reaction force amplitude has a prescribed value F_0. If we now imagine the support as removed but still continue to apply, to the beam at this point, the force F varying by a harmonic law with the same frequency, then the free beam will continue to vibrate with respect to the same mode with the same amplitude. However, these vibrations can be regarded as forced vibrations of a free beam under the effect of the exciting force F. With such forced vibrations, the point of application of the exciting force is stationary so that the dynamic rigidity of the beam corresponding to this regime is infinite. This is known as antiresonance.

In the graph of the dynamic rigidity (Fig.2.11), the points of resonance $D(p) = 0$ and antiresonance $D(p) = \infty$ alternate. It can be demonstrated that this is always so for an elastic beam.

Thus, at a certain excitation frequency, the point of application of the exciting force becomes arrested, and the node of the forced vibration will be formed at this point. This phenomenon is called antiresonance. The frequency of each antiresonance is always located between two adjacent natural vibration frequencies of a free beam.

The phenomenon of antiresonance in "pure form" can occur only in ideal /220
oscillatory systems without damping. In the presence of damping, the vibration amplitude of the point of application of the force in antiresonance does not vanish. This amplitude will be lower, the smaller the damping [see, for example, the paper by Den-Gartog (Ref.19) on a dynamic vibration damper).

3. Application of the Method of Dynamic Rigidity to the Vibration Analysis of Side-by-Side Helicopters

The concept of dynamic rigidity is rather convenient in calculating oscillatory systems that can be divided into two or more components, making it easy to define their vibrations individually.

Let us examine a vibratory system consisting of two crossed elastic beams 1 and 2, shown in Fig.2.12. A fuselage with an elastic wing, characteristic for

helicopters of side-by-side configuration, represents such a system.

It is necessary to calculate the forced vibrations of this system caused by a variable force F, varying according to a harmonic law and applied at the coupling point A of the beams 1 and 2 (the method of calculation will be indicated below for the case in which the exciting forces are applied at any point). Using the method presented in Subsections 1 and 2, it is possible to calculate, for each of the beams, the forced vibrations produced by certain forces F_1 and F_2 applied to each of these beams at the point A. In so doing, we can find the dynamic rigidity of each of the beams at the point A. Let these dynamic rigidities be $D_1(p)$ and $D_2(p)$.

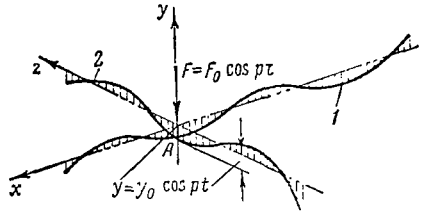

Fig.2.12 Diagram of Vibratory System of Two Crossed Beams.

It is easy to show that the dynamic rigidity D(p) of the entire system will be equal to the sum of the dynamic rigidities of both beams:

$$D(p)=D_1(p)+D_2(p). \tag{2.33}$$

Actually, the force $F = F_0 \cos pt$ acting on the system as a whole will be equal to the sum of the forces $F_1 = F_{01} \cos pt$ and $F_2 = F_{02} \cos pt$ acting on each of the beams. However,

$$F_{01}=D_1(p)\bar{y}_0;$$
$$F_{02}=D_2(p)\bar{y}_0,$$

where $\bar{y}_0$ is the vibration amplitude of the point A, identical for both beams.

Consequently,

$$F_0=F_{01}+F_{02}=[D_1(p)+D_2(p)]\bar{y}_0=D(p)\bar{y}_0.$$

Thus, the dynamic rigidity of the system is easily found by means of eq.(2.33) if the dynamic rigidities of the beams 1 and 2 are known. The graph of the dynamic rigidity D(p) can be obtained by simple addition of the ordinates of the graphs $D_1(p)$ and $D_2(p)$. The values of the frequency p at which D(p) = 0 will give the values of the natural frequencies of the system of two beams. This yields a convenient method for determining the natural frequencies of the system. Since these frequencies are the roots of the equation

$$D(p)=D_1(p)+D_2(p)=0,$$

they can be found from the condition /221

$$D_1(p)=-D_2(p). \tag{2.34}$$

The last equation is easy to solve graphically by superposition of the graphs of $D_1(p)$ and $-D_2(p)$, as is shown in Fig.2.13. The abscissas p_1, p_2, etc. of the points of intersection of the graphs $D_1(p)$ and $-D_2(p)$ give the values of the natural frequencies of the system.

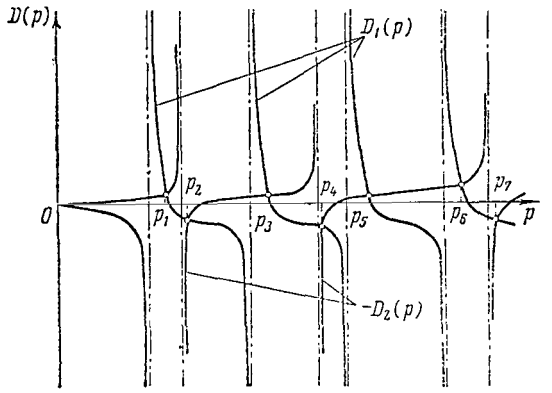

Fig.2.13 For Determining the Natural Frequencies of the System by the Method of Dynamic Rigidities.

With this method of calculation, the natural vibration modes of the system are simultaneously determined. The natural vibration mode of the system, corresponding to some frequency p_k ($k = 1, 2, \ldots$), will consist of the forced vibration modes of each of the beams at this frequency, due to the forces F_{01} and F_{02}. Since, at natural frequencies,

$$F_0 = F_{01} + F_{02} = 0,$$

it follows that

$$F_{01} = -F_{02},$$

i.e., the force F_{01} applied to the beam 1 is equal in magnitude and opposite in sign to the force F_{02} applied to the beam 2.

The natural vibration modes of this system can be normed by selecting an appropriate scale. For example, it is possible to select a scale such that the vibration mode of the beam 1 has an amplitude equal to unity at its tip ($x = l$). In this case, the corresponding scale of the vibration mode of the beam 2 should be selected from the condition of a vibration amplitude identical with the beam 1 at the coupling point.

Having the normed natural vibration modes of the system available, its forced vibrations can be calculated from harmonic forces applied at any point, by the method of expansion in normal modes in the same manner as in the case of an isolated beam. Here, the vibrations of both beams are sought in the form

$$y(x, t) = \sum_k c_k \bar{y}_k(x), \tag{2.35}$$

where $\bar{y}_k(x)$ is the vibration mode of a given beam corresponding to the normed mode of the k-th overtone of vibrations of the system (simultaneous vibrations of both beams).

The coefficients c_k are determined in the conventional manner from eq.(2.22):

$$c_k = \frac{1}{p_k^2 - p^2} \frac{A_k}{K_k}, \tag{2.36}$$

where p_k is the frequency of simultaneous vibrations of the k-th overtone of the system.

The coefficients A_k and K_k are determined by means of the following formulas:

$$A_k = F_0 \bar{y}_k(x_0). \qquad (k = 1, 2, 3, \ldots) \tag{2.37}$$

This coefficient represents the work done by the exciting load at the mode of the k-th overtone of natural vibrations of the system. The quantity $\bar{y}_k(x_0)$ represents the amplitude of the normed vibration mode of the k-th overtone of the system at the point of application of force, regardless to which beam the excitation is applied [here, $\bar{y}_k(x_0)$ is taken with a "plus" sign if the direction of the force and the deflection coincide, and with a "minus" sign if the direction of the force and deflection do not coincide]: /222

$$K_k = \underset{\text{for 1st beam}}{\int m\bar{y}_k^2 dx} + \underset{\text{for 2nd beam}}{\int m\bar{y}_k^2 dx}. \tag{2.38}$$

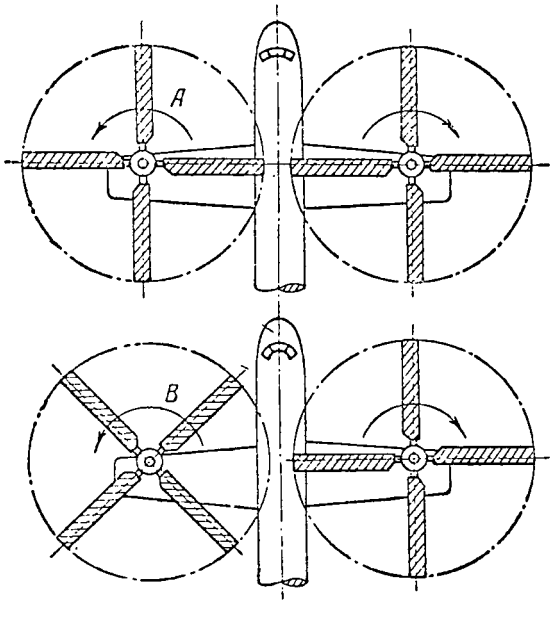

Fig.2.14 For Analysis of Vibrations of Side-by-Side Helicopter.

If vibrations of the system are excited by several harmonic forces applied to different points instead of by a single force, then the forced vibrations are found by adding the vibrations caused by each of the forces separately.

Here, we should briefly mention one of the peculiarities of excitation by rotors of helicopters of multirotor configuration. Depending on the kinematic connection of the rotors (over the transmission system), it may happen that variable exciting forces produced by different rotors vary in time in phase or in antiphase. For example, if the rotors of a side-by-side helicopter are so coupled that the blades of both rotors simultaneously occupy analogous positions (for example, extreme forward position as shown in the diagram A of Fig.2.14), the forces exerted on both rotors simultaneously attain maximum and minimum values - they will vary in phase. If the rotors are coupled as shown in the diagram B, then the exciting loads from both rotors vary in antiphase. In case A, the exciting loads from both rotors will cause only symmetric modes of simultaneous vibrations of the fuselage-wing system whereas, in case B, only skew-symmetric modes occur (Fig.2.15). Since, in the case of skew-symmetric vibrations, there are no vertical vibrations of the fuselage points for helicopters of side-by-side configuration, it is desirable to

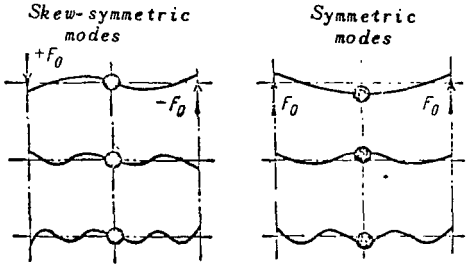

Fig.2.15 Natural Vibration Modes of a Wing-Fuselage System in a Side-by-Side Helicopter.

connect the rotors as shown in the diagram B (Fig.2.14). Analogous consideration can be made with respect to tandem helicopters.

Of course, in solving the problem of the most suitable mutual arrangement of /223 rotors it is also necessary to consider the specific values of natural frequencies of various overtones of the fuselage and to examine, along with fuselage vibrations in the plane of symmetry, lateral vibrations; this will be discussed further in Section 3.

4. Method of Auxiliary Mass

To determine the dynamic stiffness by the method proposed in Subsection 2, results from a natural vibration analysis of the fuselage are required. In this case, the amplitude of forced vibration of the point of application of force, needed for determining the dynamic stiffness, is determined by means of eq.(2.32) as an expansion in natural modes. However, whenever it is possible to program the calculation of natural frequencies on a digital computer so that this calculation will take little time, we can recommend the so-called method of auxiliary mass for determining the dynamic stiffness of the fuselage at a given point. In this method, the natural fuselage frequency is calculated under attachment of an auxiliary mass Δm to the point at which the dynamic stiffness is to be determined. The calculation is performed for different values of Δm, and its results are used for plotting the graph $\Delta m(p)$ of the dependence of Δm on the natural frequencies of different overtones.

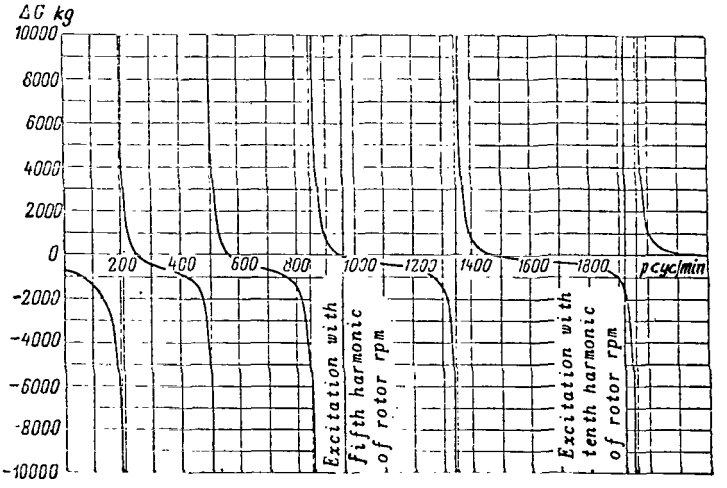

Fig.2.16 Typical Dependence of Auxiliary Mass of an Elastic Fuselage (or Dynamic Stiffness) at the Point of Rotor Attachment on the Excitation Frequency.

Figure 2.16 gives an example of such a graph for a single-rotor helicopter. In this diagram, the weight of the extra mass $\Delta G = g\Delta m$ is laid off on the ordinate.

It is easy to show that this graph, to some degree, can completely replace the graph D(p) in Fig.2.11. In fact, for natural vibrations of a beam with an auxiliary mass Δm at a frequency p, the beam will be loaded by the corresponding additional force of inertia whose amplitude is

$$F_0 = \Delta m p^2 y_0, \tag{2.39}$$

where y_0 is the vibration amplitude at the point of attachment of the auxiliary mass.

The force of inertia F_0 at the instant of maximum deflection from the equilibrium position is directed toward the same side as the deflection y_0. A spring attached to a beam with a stiffness $|c| = |\Delta m p^2|$, producing a force proportional to the deflection y_0 and directed opposite to this deflection, corresponds to negative values of Δm. /224

Of course, exactly the same vibrations of the beam can be obtained without an auxiliary mass, but these are forced vibrations produced by the action of a harmonic force of the same amplitude $\bar{F}_0$ and varying with the same frequency p.

The dynamic stiffness of the beam is determined by means of the formula

$$D(p) = \frac{F_0}{y_0}.$$

Comparing this expression with eq.(2.39), we find

$$D(p) = p^2 \Delta m(p). \tag{2.40}$$

On the basis of this formula, it is easy to construct the graph of the dependence D(p), since we have the dependence $\Delta m(p)$ at our disposal. However, this need not be done and the graph $\Delta m(p)$ or $\Delta G(p)$ can be used directly. For example, to determine the natural fuselage frequencies of a side-by-side configuration, we can locate the point of intersection of the graphs $\Delta G_1(p)$ and $-\Delta G_2(p)$ instead of the points of intersection on the graph $D_1(p)$ and $-D_2(p)$ (see Fig.2.13).

5. Effect of Damping Forces. Vibrations at Resonance

The theory presented above and the resultant methods of calculation are based on the assumption that the beam is perfectly elastic and that damping forces are absent. As for any other oscillatory system, a vibration analysis of a beam far from resonance need not take the damping forces into account; this does not lead to large errors.

However, a vibration analysis of a beam close to resonance or actually in

resonance requires allowance for the damping forces, since the vibration amplitude at resonance is determined exclusively by the presence of damping and since, if absence of damping is assumed, the amplitude at resonance becomes unbounded.

Damping forces during vibrations of an elastic beam are generated mainly as a consequence of friction between structural elements of the beam during its deformations and also as a consequence of so-called internal friction in the beam material which, for a composite beam, is generally negligible in comparison with the friction between structural elements (Ref.16).

The equation of flexural vibrations of a beam in the presence of damping can be derived by assuming that the bending moment M in the beam section is proportional to its curvature $\frac{\partial^2 y}{\partial x^2}$ (in accordance with Hooke's law) and to the time rate of change of curvature, so that we can write

$$M = EI\frac{\partial^2 y}{\partial x^2} + \eta\frac{\partial}{\partial t}\left(EI\frac{\partial^2 y}{\partial x^2}\right), \tag{2.41}$$

where η is some coefficient characterizing the damping properties of the beam at a given cross section, which is assumed to be a given function of the x-coordinate.

Using the known relationship: /225

$$\frac{\partial^2 M}{\partial x^2} = q^*(x, t),$$

where $q^*(x, t)$ is the intensity of the lateral load applied to the beam, and taking into account that this load, during vibration, is composed of the external exciting load $q(x, t)$ and the load due to inertia forces, so that

$$q^*(x, t) = q(x, t) - m\frac{\partial^2 y}{\partial t^2},$$

then eq.(2.41) will yield the following partial differential equation describing lateral vibrations of a beam with damping:

$$\frac{\partial^2}{\partial x^2}\left(EI\frac{\partial^2 y}{\partial x^2}\right) + \eta\frac{\partial^3}{\partial t\,\partial x^2}\left(EI\frac{\partial^2 y}{\partial x^2}\right) + m\frac{\partial^2 y}{\partial t^2} = q(x, t). \tag{2.42}$$

This equation differs from eq.(2.2) only by the presence of a term with a factor η; if $\eta = 0$, it will coincide with eq.(2.2).

If $q(x, t) = 0$, we obtain an equation describing the natural vibration of a beam in the presence of damping:

$$\frac{\partial^2}{\partial x^2}\left(EI\frac{\partial^2 y}{\partial x^2}\right)+\eta\frac{\partial^3}{\partial t\,\partial x^2}\left(EI\frac{\partial^2 y}{\partial x^2}\right)+m\frac{\partial^2 y}{\partial t^2}=0. \tag{2.43}$$

The exact solution of this equation is rather complex. However, at relatively weak damping, a simple approximate solution can be used. Such an approximate solution of this equation, corresponding to natural vibrations of a beam with respect to the k-th overtone, can be found by assuming

$$y=\bar{y}_k(x)\,e^{\lambda_k t}, \tag{2.44}$$

where $\bar{y}_k(x)$ is the natural vibration mode of the k-th overtone of the beam in the absence of damping.

Substituting this solution into eq.(2.43), canceling the factor $e^{\lambda k t}$, multiplying by $\bar{y}_k(x)$, integrating the equation within the interval 0 to l, and taking eqs.(2.17) and (2.18) into account, we obtain the following equation for determining λ_k:

$$\lambda_k^2+2n_k\lambda_k+p_k^2=0, \tag{2.45}$$

where

$$2n_k=\frac{1}{K_k}\int_0^l \eta EI\bar{y}_k''^2\,dx \tag{2.46}$$

The roots of this equation will be

$$\lambda_k=-n_k\pm ip_k^*, \tag{2.47}$$

where

$$p_k^*=\sqrt{p_k^2-n_k^2}. \tag{2.48}$$

Accordingly, we can write eq.(2.44) in the form

$$y=\bar{y}_k(x)\,e^{-n_k t}\cos(p_k^* t+\varphi), \tag{2.49}$$

i.e., the quantity n_k represents the damping coefficient of vibrations of the k-th overtone while p_k^* represents the natural frequency of the k-th overtone in the presence of damping.

We can show that such an approximate solution of eq.(2.43) will differ less from the exact solution the smaller - in comparison with unity - the dimensionless coefficient of damping of the k-th overtone determinable by the formula /226

$$\bar{n}_k=\frac{n_k}{p_k}. \tag{2.50}$$

This coefficient is one of the most important characteristics of vibrations of the given overtone and can be determined experimentally, either by analysis of the oscillogram of damped vibrations of the given overtone or by applying the

results of measuring the forced vibration amplitude of the beam under the effect of a vibrator (to be discussed below).

For a conventional fuselage (riveted fuselage with duralumin skin) the damping coefficients $\overline{n}_k$ of different overtones are located within limits of 0.02 to 0.05. These are rather small values of the damping coefficient, in whose presence the vibration frequency of the k-th overtone can be considered equal to the frequency calculated without consideration of damping, since $p_k^* = p_k \sqrt{1 - \overline{n}_k^2}$. This correction is insignificant for the indicated values of $\overline{n}_k$.

In calculating forced vibrations of a beam with damping, described by eq.(2.42), it is preferable - in view of the weak damping - to use an approximate method based on the fact that damping is completely disregarded far from resonance whereas, close to resonance, an approximate solution is obtained on the assumption that the natural vibration mode near resonance of the k-th overtone, just as in the case of absence of damping, is close to the natural vibration mode of the given overtone.

In the presence of damping, the equation of forced vibrations of a beam under the effect of a harmonic load

$$q(x, t) = q(x) \cos pt \tag{2.51}$$

is conveniently written in the complex form

$$\frac{\partial^2}{\partial x^2}\left(EI \frac{\partial^2 y}{\partial x^2}\right) + \eta \frac{\partial^3}{\partial x^2 \partial t}\left(EI \frac{\partial^2 y}{\partial x^2}\right) + m \frac{\partial^2 y}{\partial t^2} = q(x) e^{ipt}. \tag{2.52}$$

Since the real part of the right-hand side of this equation coincides with eq.(2.51), the actual motion of the beam is described, in view of the linearity of the solution, by the real part of the complex solution of eq.(2.52). Close to resonance with the k-th overtone of natural vibrations, the solution of this equation in conformity with the above considerations is best sought in the form

$$y(x, t) = c_k \overline{y}_k(x) e^{ipt}, \tag{2.53}$$

where $\overline{y}_k(x)$, as usual, is the mode of the k-th overtone of vibrations in the absence of damping.

Let us substitute this expression into eq.(2.52). We then multiply both sides of eq.(2.52) by $\overline{y}_k(x)$ and integrate from 0 to l. Transforming the obtained integrals and taking eqs.(2.17) and (2.18) as well as eq.(2.46) into account, we obtain the following equation for determining the coefficient c_k:

$$c_k(p_k^2 + i2n_k p - p^2) = \frac{A_k}{K_k},$$

where A_k and K_k are as usual determined from eqs.(2.20) and (2.21). Hence,

$$c_k = \frac{1}{p_k^2 - p^2 + i2n_k p} \cdot \frac{A_k}{K_k}. \qquad (2.54)$$

The modulus of the complex quantity c_k determines the vibration amplitude: /227

$$|c_k| = \frac{1}{\sqrt{(p_k^2 - p^2)^2 + 4n_k^2 p^2}} \cdot \frac{A_k}{K_k}, \qquad (2.55)$$

while the argument c_k

$$\arg c_k = \tan^{-1}\left(\frac{2n_k}{p^2 - p_k^2}\right) \qquad (2.56)$$

determines the phase of the forced vibrations with respect to the exciting load [eq.(2.51)]. In the presence of resonance, the value of c_k [see eq.(2.54)] becomes purely imaginary:

$$c_k = -i\frac{A_k}{2n_k p K_k} \quad (at \quad p = p_k).$$

This means that, at resonance, the phase angle between the exciting load and the vibrations of the beam is equal to $\pi/2$. In this case, as is readily verified by direct substitution into the equation, the vibrations will take place in accordance with the law

$$y(x, t) = \bar{c}_k \bar{y}_k(x) \sin pt, \qquad (2.57)$$

where

$$\bar{c}_k = \frac{A_k}{2\bar{n}_k p_k^2 K_k}. \qquad (2.58)$$

Thus, the vibration amplitude at resonance is completely determined by the value $\bar{n}_k$ of the dimensionless coefficient of damping of the k-th overtone. This can be used for an experimental determination of $\bar{n}_k$. If vibrations of the beam are excited by means of a vibrator, i.e., by a given concentrated force $F = F_0 \cos pt$ applied at a certain point $x = x_0$, and if the vibration amplitude $\bar{y}_0$ at resonance ($p = p_k$) is measured at the point of application of force, it becomes easy to find the quantity $\bar{n}_k$. Here A_k will be determined by eq.(2.27) and the quantity y_0, by the formula

$$y_0 = \bar{c}_k \bar{y}_k(x_0).$$

Therefore, taking account of eq.(2.58), we find

$$\bar{n}_k = \frac{1}{2} \frac{F_0 [\bar{y}_k(x_0)]^2}{y_0 p_k^2 K_k}$$

or

$$\bar{n}_k = \frac{1}{2} \frac{F_0}{m_k p_k^2 y_0}, \qquad (2.59)$$

where the quantity m_k, which we can call the mass of the k-th overtone reduced to the point $x = x_0$, is determined by the formula

$$m_k = \int_0^l m\tilde{y}_k^2 dx. \tag{2.60}$$

Here,

$$\tilde{y}_k = \frac{\bar{y}_k(x)}{\bar{y}_k(x_0)}. \tag{2.61}$$

The value of the reduced mass m_k is determined with sufficient accuracy by calculation, but it can also be determined experimentally by measuring the natural vibration mode of the beam at resonance with the k-th overtone.

When desiring to make a pre-estimate of the amplitude at resonance for a fuselage still on the drawing board and not yet given over to manufacture, it is possible to use eq.(2.58), using for $\bar{n}_k$ the values known from some other fuselage of similar design, since the values of $\bar{n}_k$ for similar designs differ little. /228

Section 3. Vibration Analysis with Consideration of Fuselage Characteristics

1. Fuselage Characteristics. Lateral and Vertical Vibrations

In the preceding Section, methods were proposed for calculating the vibrations of a fuselage as an elastic beam (or as a system of two crossed beams for a side-by-side configuration) for which the dimensions of the cross sections were small in comparison with the length. In many cases, such a method of calculation gives completely satisfactory results. However, in some cases when the fuselage of the helicopter has characteristics that differ greatly from those of the model of an elastic beam, more complicated calculation systems are involved. The fuselage designs of various types of helicopters (single-rotor, side-by-side configurations, tandem configuration) vary widely. Therefore, it would be difficult to give any generally applicable method of calculation which would permit a sufficiently accurate analysis of fuselage vibrations generated by certain forces.

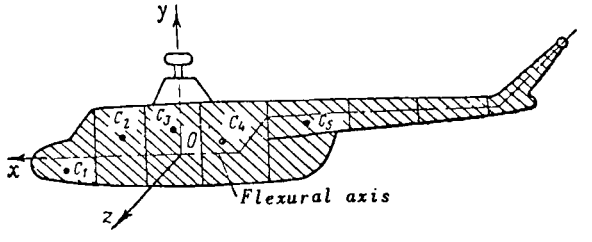

Fig.2.17 For Reducing the Vibration Problem of an Elastic Fuselage to the Vibration Problem of an Elastic Beam.

Each new fuselage design may necessitate substantial changes in the method of calculation of vibrations. This problem might become rather complicated. However, in all cases the method of calculation should be based on general principles of the theory of vibrations of elastic systems. The design engineer who

has the function of making vibration analyses of new configurations for helicopter prototypes should be so versed in these general methods as to be able to modify each computational system to fit each new problem. Therefore, the material in this Chapter is presented in a manner to demonstrate the essence of the most important methods used in vibration analysis. For example, the method of expansion in natural modes, the method of dynamic rigidity, the concept of resonance and antiresonance are not only applicable to an elastic beam or to a system of two crossed beams but also to any other more complicated vibratory system. These methods were presented in their application to a beam since, on the one hand, it is easiest to demonstrate them for this example and, on the other hand, the method of calculating vibrations of a beam is often applicable to fuselage vibration analyses without modification.

To illustrate certain characteristics of a real fuselage, let us turn to Fig.2.17 which schematically shows the fuselage of a single-rotor helicopter. This fuselage is characterized by the fact that its flexural axis is a broken line, that the centers of gravity of the fuselage compartments do not lie on the flexural axis, and that each fuselage compartment is a body all of whose measurements are of the same order so that, in calculating vibrations, not only the /229 mass of the compartment but also its moments of inertia relative to all three axes must be taken into consideration. Calculations show that, in determining the lower harmonic of flexural vibrations of such a fuselage both in the plane xOy (vertical vibrations) and in the plane xOz (lateral vibrations), we can obtain completely satisfactory results if we conceive the fuselage as a thin elastic beam with a rectilinear axis.

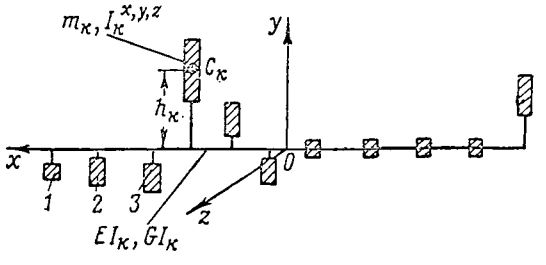

Fig.2.18 Design Model for Vibration Analysis of an Elastic Fuselage.

If, in the vibration analysis, we limit ourselves to a study of vibrations of the fuselage as a solid body and take into account only the lower elastic mode (the first three modes in Fig.2.7), the calculation of vibrations of a fuselage as a thin beam with a rectilinear axis gives satisfactory results. However, if the second elastic mode has a frequency close to the frequency of the fundamental harmonic of the rotor $z\omega$ (and this is often the case), this type of calculation may lead to certain errors. In vibration analyses of the cockpit (at the fuselage nose) the error may be insignificant while the vibration amplitudes in the region of the tail boom may differ greatly from the real values. To increase the accuracy of the calculations the vibrations must be determined with consideration of a large number of elastic overtones (second and third). However, a sufficiently accurate determination of the second elastic mode now involves a complication of the calculation model.

An appreciable refinement of the calculated results can be obtained by using the design model shown in Fig.2.18. The fuselage here is replaced by an elastic beam with a rectilinear axis, to which individual loads 1, 2, 3, etc. are attached. The center of gravity of each load is at a certain distance $h_к$ from

the beam axis. For each load, we assign its mass m_k and moments of inertia I_x and I_z with respect to axes parallel to the axes Ox and Oz and passing through the center of gravity of the load. For each segment of the elastic beam between the loads k and k + 1, we prescribe the flexural rigidities EI_k^z and EI_k^y in both planes xOz and xOy and the torsional rigidity GI_k.

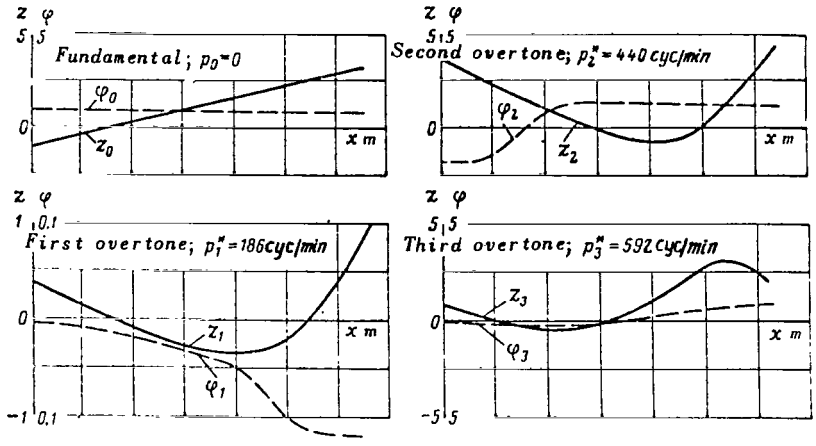

Fig.2.19 Natural Vibration Modes of an Elastic Fuselage of a Single-Rotor Helicopter in the Plane of Symmetry.

For this design model, the lateral vibrations (in the plane xOz) represent simultaneous flexural and torsional (binary) vibrations. The frequencies and modes of the natural binary vibrations of such a system can be calculated by the method proposed in Section 6 of Chapter I (see Fig.1.19) as applied to a rotor blade. In this case, it must be assumed that the centrifugal force N = 0, that the rigidity of the control lines $c_{con} = 0$, as well as that $EIy''(0) = 0$ and $(EI'')' \Big|_{x=0}^{=0}$. This corresponds to the fact that the left end of the beam is not clamped. The quantity $x_{c.g}$ in the blade calculation must be substituted by the values of staggers h_k.

In calculating the forced lateral vibrations of this system, the method of expansion in natural modes (binary) can be used. In this case, all formulas of Section 2 of this Chapter are applicable in which the quantity A_k means the work done by the exciting load at the normed mode of a given harmonic and the quantity K_k represents the kinetic energy of a given harmonic referred to the square of its frequency p_k^2. Figure 2.19 shows the characteristic modes of natural, /230 lateral binary vibrations of a single-rotor helicopter.

The calculation method and model given in Fig.2.18 can be used for an analysis of vertical binary vibrations of the wing of a side-by-side helicopter with wing-tip engine pods (Fig.2.20). If the centers of gravity of the pods have a large offset h, the vibration analysis of such a wing cannot take only isolated flexural vibrations in a vertical plane into consideration but must allow also for simultaneous binary vibrations. A calculation of synchronous vibrations of

the fuselage-wing system in this case requires the method of dynamic stiffness.

The design model best simulating an actual helicopter fuselage obviously is that shown in Fig.2.21. Here, the flexural axis of the beam is given as a certain discontinuous line. The angle of inclination of the k-th segment of this offset line is denoted as the angle α_k. Such a design model satisfactorily reflects the properties of any fuselage having a plane of symmetry xOy. For a fuselage with such a plane of symmetry, a separate calculation can be made of the vertical flexural vibrations (or vibrations in the plane of symmetry) and the lateral binary vibrations.

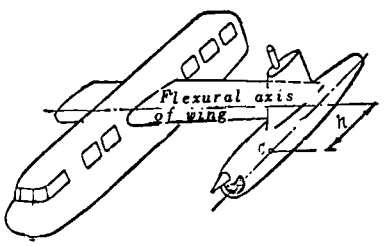

Fig.2.20 Diagram of Engine Pod with Large Offset.

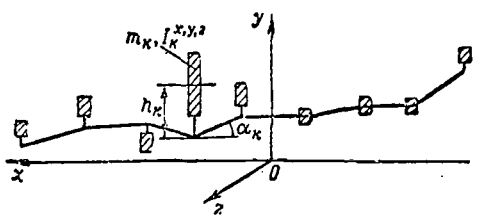

Fig.2.21 Design Model for Calculating Vibrations of an Elastic Fuselage with a Discontinuous Flexural Axis.

In calculating the vertical vibrations for each load, three degrees of freedom must be taken into consideration: /231

displacement of the center of gravity of the load along the axis Ox;
displacement of the center of gravity of the load along the axis Oy;
rotation of the load relative to the axis Oz.

In calculating the lateral binary vibrations for each load, three degrees of freedom must again be taken into account:

displacement of the center of gravity of the load along the axis Oz;
rotation about the axis Ox;
rotation about the axis Oy.

Calculation of vertical vibrations of such a system is discussed in the Subsection below. We will also illustrate application of the so-called methods of residues for vibration analysis, which often is rather convenient to use.

The calculation of lateral vibrations of such a system is not discussed here since, for calculating lateral binary vibrations, rather satisfactory results can be obtained by using the design model shown in Fig.2.18. It should be noted that, for the system shown in Fig.2.21, the calculation of lateral binary vibrations could also be carried out by the method of residues.

2. Calculation of Fuselage Vibrations in the Plane of Symmetry by the Method of Residues

Let a two-dimensional elastic system, depicted in Fig.2.21, execute steady forced vibrations in its own plane xoy under the effect of a harmonic exciting load consisting of forces and moments

$$\left.\begin{aligned} P_{kx} &= P^0_{kx}\cos pt;\\ P_{ky} &= P^0_{ky}\cos pt;\\ M_k &= M^0_k\cos pt, \end{aligned}\right\} \qquad (3.1)$$

applied to each load (Fig.2.22).

During steady vibration, all points of the system will execute harmonic vibrations with an excitation frequency p so that, if we denote by $\bar{x}$, $\bar{y}$, and ϑ respectively the displacements of the center of gravity c of the load along the axes Ox and Oy and the angle of rotation of the load relative to its center of gravity, then we can express the k-th load by

$$\left.\begin{aligned} \bar{x} &= \bar{x}_k\cos pt;\\ \bar{y} &= \bar{y}_k\cos pt;\\ \vartheta &= \vartheta_k\cos pt. \end{aligned}\right\} \quad (k=1, 2, 3, \ldots \qquad (3.2)$$

Let us then establish the relations connecting the forces applied to the loads with the deformation of the beam segments. We will consider the forces and deformations only for the position of the system corresponding to the maximum deviation from the position of equilibrium (i.e., we will study only amplitudes of forces and deformations). We then construct the equations of equilibrium for the k-th load (Fig.2.23). To the load, the following are applied:

external forces P^0_{kx}, P^0_{ky}, M^0_k (applied at point A);

inertia forces of the load $m_k p^2\bar{x}_k$; $m_k p^2\bar{y}_k$; $I_k p^2\vartheta_k$ (applied at point C);

forces acting on the load from the segment of the beam to the left of it: X_{k-1}, Y_{k-1}, M'_{k-1};

forces acting on the load from the beam segment to the right of it: X_k, Y_k, M_k. /232

The equations of equilibrium of the load are written in the form

$$X_k = X_{k-1} + m_k p^2\bar{x}_k + P^0_{kx}; \qquad (3.3)$$

$$Y_k = Y_{k-1} + m_k p^2\bar{y}_k + P^0_{ky}; \qquad (3.4)$$

$$M_k = M'_{k-1} + m_k\bar{x}_k h_k p^2 - \vartheta_k I_k p^2 + P^0_{kx}e_k - M^0_k. \qquad (3.5)$$

The positive directions of forces and displacements are indicated in Figs.2.22, 2.23, and 2.24. The quantity I_k represents the distance from the point of application of the external exciting forces P^0_{kx} to the point of attach-

ment of the load to the elastic beam.

From the condition of equilibrium of a section of the beam (Fig.2.24) we have

$$M'_k = M_k + Y_k l_k \cos\alpha_k - X_k l_k \sin\alpha_k. \tag{3.6}$$

To study the deformations, let us turn to Fig.2.24 which shows the k-th section of an elastic beam $A_k B_k$ in a position of equilibrium and the same section in a displaced position $A'_k B'_k$. Let the quantities x_k, y_k, x_{k+1} and y_{k+1} be the displacement of the point A_k and B_k (ends of the section), and let ϑ_k and ϑ_{k+1} be the angles of rotation of a tangent to the elastic axis on the left and right ends. Furthermore, let δ_k be the deflection of the beam at the k-th section, i.e., the displacement of the right end of the beam (point B_k) in a direction perpendicular $A_k B_k$ relative to the tangent to the elastic axis at the left end (point A_k). Then we can write

$$\left.\begin{aligned} x_{k+1} &= x_k - (\delta_k + \vartheta_k l_k)\sin\alpha_k; \\ y_{k+1} &= y_k + (\delta_k + \vartheta_k l_k)\cos\alpha_k, \end{aligned}\right\} \tag{3.7}$$

where l_k and α_k are, respectively, the length and angle of inclination of the k-th section of the beam (Fig.2.24).

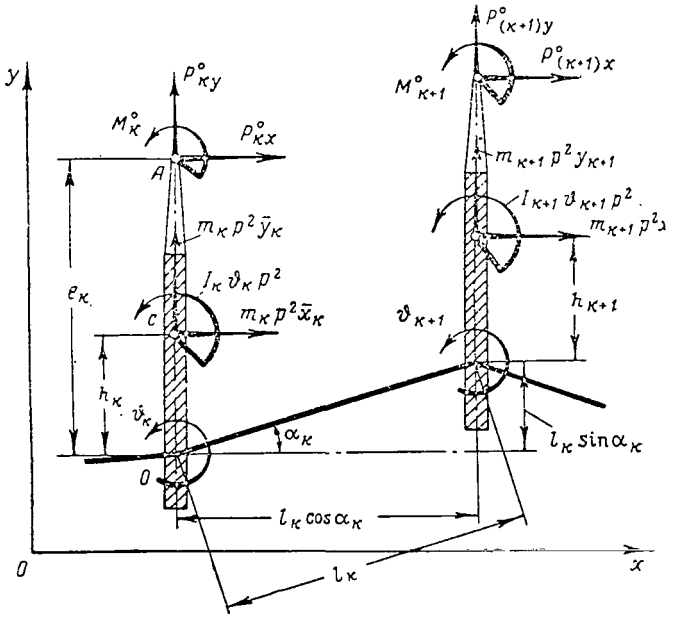

Fig.2.22 Polygon of Forces Acting on a Section of the Elastic Fuselage Model.

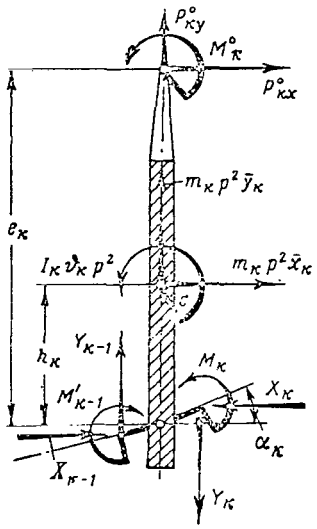

Fig.2.23 Polygon of Forces Applied to k-th Element of an Elastic Fuselage Model.

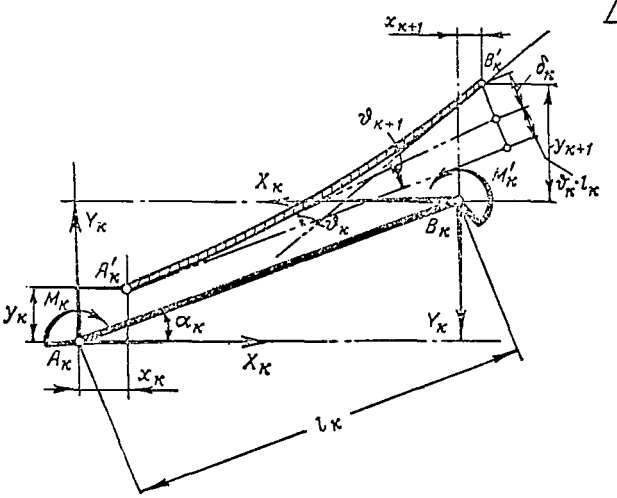

Fig.2.24 Polygon of Forces Applied to a Section of an Elastic Fuselage Model.

Applying the usual methods of strength of materials, we find the following equations correlating the forces and deformations:

$$\delta_k = \frac{l_k^2}{EI_k}\left[\frac{1}{3}M_k + \frac{1}{6}M_k'\right]; \tag{3.8}$$

$$\vartheta_{k+1} = \vartheta_k + \Delta\vartheta_k; \tag{3.9}$$

$$\Delta\vartheta_k = \frac{l_k}{2EI_k}[M_k + M_k']. \tag{3.10}$$

The displacements of the beam points x_k and y_k are related with the center-of-gravity displacements of the loads by the evident formulas

$$\left.\begin{aligned}\bar{y}_k &= y_k;\\ \bar{x}_k &= x_k - \vartheta_k h_k.\end{aligned}\right\} \tag{3.11}$$

The recurrence formulas (3.3), (3.4), (3.5), and (3.7), together with eqs.(3.8), (3.9), (3.10), and (3.11) and if the forces and displacements of the k-th load are known, make it possible to determine the forces and displacements of the (k+1)-th load. Using these formulas, we can solve the problem by the "chain method", as follows: After assigning the amplitudes $x_0 y_0$ and ϑ_0 at the left end of the beam, it becomes possible to determine, successively passing from section to section, the amplitudes and forces at the extreme right end of the beam, expressing them in terms of the quantities x_0, y_0, ϑ_0. If the beam has n loads, we can thus determine the quantities X_n, Y_n, and M_n at the right

end or the "residual". However, since the right end of the beam is free, the "residual" should be equal to zero, i.e., at the right end of the beam the conditions

$$X_n = Y_n = M_n = 0$$

should be satisfied.

These conditions represent a system of three equations for determining the unknowns x_0, y_0, ϑ_0, in terms of which we had already expressed the vibration amplitudes and the forces on all loads of the beam.

This method of calculating the forced vibrations of a system (Fig.2.21) is completely analogous to the well-known method of "residues" (Tolle method), /234 used for calculating torsional vibrations of multidisk systems (Ref.20). A similar method is used for calculating flexural vibrations of elastic beams. In the American and English literature such a method is known as Myklestad's method (Ref.33, 34). This method permits: 1) finding the curve of dynamic stiffness (Fig.2.11) of a system at any point and in any direction by calculating vibrations at different values of p; 2) finding the natural vibration frequencies and modes of a system from an analysis of the forced vibrations of the system close to resonance, when the forced vibration amplitudes increase without bounds.

This method is especially convenient when using electronic computers, without which it is presently impossible to conduct dynamic calculation in the necessary volume.

For a practical application of this method it is convenient to express the forces and displacements at the k-th section in terms of the values of x_0, y_0, and to give ϑ_0 in the form

$$\left.\begin{aligned} x_k &= A_k^x + B_k^x x_0 + C_k^x y_0 + D_k^x \vartheta_0; \\ y_k &= A_k^y + B_k^y x_0 + C_k^y y_0 + D_k^y \vartheta_0; \\ \vartheta_k &= A_k^\vartheta + B_k^\vartheta x_0 + C_k^\vartheta y_0 + D_k^\vartheta \vartheta_0; \\ X_k &= A_k^X + B_k^X x_0 + C_k^X y_0 + D_k^X \vartheta_0; \\ Y_k &= A_k^Y + B_k^Y x_0 + C_k^Y y_0 + D_k^Y \cdot \vartheta_0; \\ M_k &= A_k^M + B_k^M x_0 + C_k^M y_0 + D_k^M \vartheta_0, \end{aligned}\right\} \qquad (3.12)$$

where A_k^x, B_k^x, etc. are coefficients.

When calculating by the "chain" method, the values of these coefficients of the k-th section must be used for determining their values for the (k+1)-th section. Using recurrence formulas for forces and displacements, it is easy to construct recurrence formulas for the corresponding coefficients. The following formulas are obtained in this manner:

For the coefficients A_k^ϑ, B_k^ϑ, C_k^ϑ, and D_k^ϑ, we have

$$A_k^{\vartheta} = A_{k-1}^{\vartheta} + \frac{l_{k-1}}{EI_{k-1}} A_{k-1}^{M} + \frac{l_{k-1}^2 \cos \alpha_{k-1}}{2EI_{k-1}} A_{k-1}^{Y} - \frac{l_{k-1}^2 \sin \alpha_{k-1}}{2EI_{k-1}} A_{k-1}^{X}. \qquad (3.13)$$

For the quantities B_k^{ϑ}, C_k^{ϑ}, and D_k^{ϑ}, analogous formulas are obtained by replacing the quantities A by B, C, and D, respectively. This pertains also to the following formulas [eqs.(3.14) and (3.15)].

For the coefficients A_k^x, B_k^x, C_k^x and D_k^x:

$$A_{k+1}^x = A_k^x - \frac{l_k^2 \sin \alpha_k}{2EI_k} A_k^M - \frac{l_k^3 \sin \alpha_k \cos \alpha_k}{6EI_k} A_k^Y + \\ + \frac{l_k^3 \sin^2 \alpha_k}{6EI_k} A_k^X - l_k \sin \alpha_k A_k^{\vartheta}. \qquad (3.14)$$

For the coefficients A_k^y, B_k^y, C_k^y and D_k^y:

$$A_{k+1}^y = A_k^y + \frac{l_k^2 \cos \alpha_k}{2EI_k} A_k^M + \frac{l_k^3 \cos^2 \alpha_k}{6EI_k} A_k^Y - \\ - \frac{l_k^3 \cos \alpha_k \sin \alpha_k}{6EI_k} A_k^X + l_k \cos \alpha_k A_k^{\vartheta}. \qquad (3.15)$$

/235

For the coefficients A_k^X, B_k^X, C_k^X and D_k^X:

$$A_k^X = A_{k-1}^X + m_k p^2 A_k^X - m_k p^2 h_k A_k^{\vartheta} + P_{kx}^0; \qquad (3.16)$$

$$\left.\begin{aligned} B_k^X &= B_{k-1}^X + m_k p^2 A_k^x - m_k p^2 h_k B_k^{\vartheta}; \\ C_k^X &= C_{k-1}^X + m_k p^2 C_k^x - m_k p^2 h_k C_k^{\vartheta}; \\ D_k^X &= D_{k-1}^X + m_k p^2 D_k^x - m_k p^2 h_k D_k^{\vartheta}. \end{aligned}\right\} \qquad (3.17)$$

For the coefficients A_k^Y, B_k^Y, C_k^Y and D_k^Y:

$$A_k^Y = A_{k-1}^Y + m_k p^2 A_k^Y + P_{ky}^0; \qquad (3.18)$$

$$\left.\begin{aligned} B_k^Y &= B_{k-1}^Y + m_k p^2 B_k^y; \\ C_k^Y &= C_{k-1}^Y + m_k p^2 C_k^y; \\ D_k^Y &= D_{k-1}^Y + m_k p^2 D_k^y. \end{aligned}\right\} \qquad (3.19)$$

Finally, for the coefficients A_k^M, B_k^M, C_k^M and D_k^M:

$$A_k^M = A_{k-1}^M + A_{k-1}^Y l_{k-1} \cos \alpha_{k-1} - A_{k-1}^X l_{k-1} \sin \alpha_{k-1} + m_k h_k p^2 A_k^x - \\ - p^2 (m_k h_k^2 + I_k) A_k^{\vartheta} - M_k^0 + P_{kx}^0 e_k; \qquad (3.20)$$

$$B_k^M = B_{k-1}^M + B_{k-1}^Y l_{k-1} \cos \alpha_{k-1} - B_{k-1}^X l_{k-1} \sin \alpha_{k-1} + \\ + m_k h_k p^2 B_k^X - p^2 (m_k h_k^2 + I_k) B_k^{\vartheta}. \qquad (3.21)$$

The formulas for C_k^M and D_k^M are obtained from the last equation on replacing the quantities B by the quantities C and D, respectively.

The derived formulas permit determining the values of the coefficients at the next section from their known values in the previous section. Thus, moving from section to section or from station to station from left to right, the values of the coefficients at the right end of the beam are determined. On the right (free) end (k = n), the conditions

$$\left.\begin{aligned} X_n &= A_n^X + B_n^X x_0 + C_n^X y_0 + D_n^X \vartheta_0 = 0; \\ Y_n &= A_n^Y + B_n^Y x_0 + C_n^Y y_0 + D_n^Y \vartheta_0 = 0; \\ M_n &= A_n^M + B_n^M x_0 + C_n^M y_0 + D_n^M \vartheta_0 = 0 \end{aligned}\right\} \quad (3.22)$$

should be satisfied.

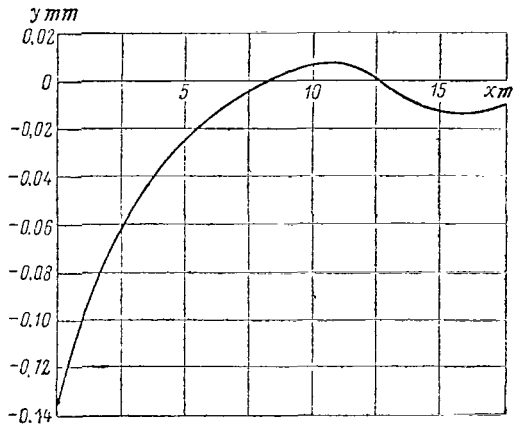

Fig.2.25 Forced Vibration Mode of an Elastic Fuselage of a Single-Rotor Helicopter Obtained by the Method of Residues.

Solving this system, we find the values of x_0, y_0, and ϑ_0 of interest here:

$$\left.\begin{aligned} x_0 &= \frac{\Delta_{x_0}}{\Delta}; \\ y_0 &= \frac{\Delta_{y_0}}{\Delta}; \\ \vartheta_0 &= \frac{\Delta_{\vartheta}}{\Delta}, \end{aligned}\right\} \quad (3.23)$$

where

Δ = determinant of the system (3.22);

Δx_0, Δy_0, $\Delta \vartheta$ = determinants obtained from the determinant Δ by replacing the corresponding column by the free terms of the equations.

Knowing the quantities x_0, y_0, and ϑ_0 permits finding, by means of eqs.(3.12), the displacements and forces acting in each cross section of the beam.

Figure 2.25 shows the mode of forced vibrations of a single-rotor helicopter, determined by the indicated method. The vibration mode in this case should be represented by three graphs: $x_k(x)$, $y_k(x)$, and $\vartheta_k(x)$. /236

Table 2.1 gives the initial data for the performed calculation.

The forced vibrations were calculated from the following forces applied to the rotor hub (load No.3):

$$P_{3x}^0 = 0.05G; \quad P_{3y}^0 = 0.03G; \quad M_3^0 = 0,$$

where G is the helicopter weight.

Table 2.1

No. of Station	0	1	2	3	4	5	6	7	8	9	10
x_k (m)	0	1.7	3.45	5.1	7.2	9.1	12.4	13.7	15.1	16.7	18.2
G_k (kg)	30	1471	1692	3584	3599	259	24	24	22	92	153
I_k (kg/m·sec²)	0.10	37.65	63.0	260.5	286.7	4.62	0.19	0.10	0.05	0.077	0.185
h_k (m)	−0.15	−0.024	−0.025	0.778	0.316	−0.15	0	0	0	0	0
I_k (m⁴)	0.00155	0.0066	0.0068	0.207	0.0015	0.00042	0.00028	0.00017	0.00013	1.0	—
a_k^0	0	0	0	0	21	0	0	0	0	43	—

One of the virtues of this method of calculation is that, for calculating forced vibrations it is not necessary to perform a preliminary calculation of the natural vibration frequencies and modes of the system. Furthermore, in such a calculation for different values of frequencies p, it is possible to construct a graph of the dynamic stiffness of the system D(p) at any point and also to find all natural vibration frequencies and modes. Figure 2.26 presents the results of the calculation of the graph of dynamic stiffness for the same system, given in Table 2.1 for forced P^0_{ky}. The values of p_k for which D(p) = 0 give the natural vibration frequencies of the system, while the mode of forced vibrations at a value of p close to any of the natural vibration frequencies p_k (k = 1, 2, 3, ...) gives, with any desired degree of accuracy, the natural vibration mode of this overtone. The modes of the first three harmonics for the examined system obtained in this manner are shown in Fig.2.27.

/237

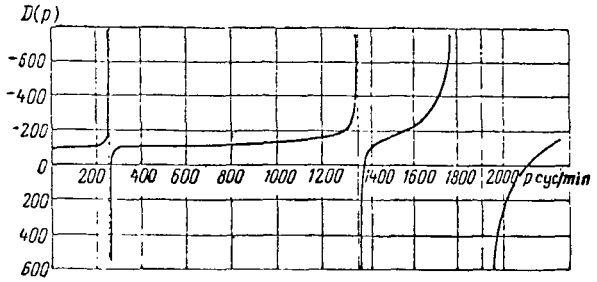

Fig.2.26 Curve of Dynamic Fuselage Stiffness, Obtained by the Method of Residues.

We note in conclusion that the method of "residues" presented here requires performing the calculation with a very high accuracy (at least four or five significant digits). This makes the above method unsuitable in practice for a keyboard calculator. However, as already indicated, vibration calculations in the required volume can generally be performed only on high-speed computers for which the indicated accuracy is common.

/238

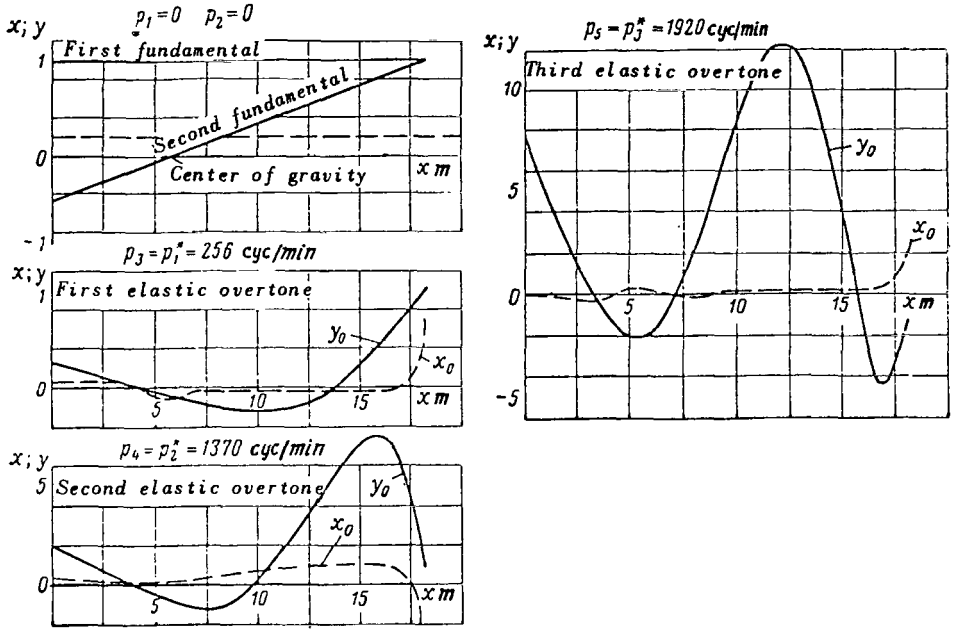

Fig 2.27 Natural Vibration Modes of the Three Lower Overtones of a Single-Rotor Helicopter Fuselage, Obtained by the Method of Residues.

3. Consideration of the Effect of Shearing Deformation

All above-described methods of vibration analysis for a fuselage were based on the use of conventional relationships of the strength of materials for bending of a thin beam. These relations take into account only tensile and compressive deformation of the fibers of the beam material and disregard shear deformation. Furthermore, a consideration of these strains introduces certain corrections into the calculation results, which are rather insignificant for the first harmonic of vibrations (decrease in frequency by 5 - 6%), somewhat greater for the second harmonic (decrease in frequency by 10 - 15%), still greater for the third harmonic (20 - 30%), and so on. Therefore, if a vibration analysis requires consideration of high harmonics, the vibration should be calculated with consideration of shear strains caused by tangential stresses in the fuselage skin. This can be performed in the following manner: If the calculation is carried out for a model of the type shown in Fig.2.21, then all formulas of the "residue" method can be used, with the exception of eq.(3.8) which, in this case, must be written in the form

$$\delta_k = \frac{l_k^2}{EI_k}\left(\frac{1}{3}M_k + \frac{1}{6}M_k'\right) + \delta_k', \qquad (3.24)$$

where δ_k' is the additional deflection of the k-th station due to the shear force Q_k

$$Q_k = X_k \sin\alpha_k - Y_k \cos\alpha_k. \tag{3.25}$$

This additional deflection δ_k' can be determined by means of the following formula [see, for example (Ref.21)]:

$$\delta_k' = \frac{Q_k l_k}{G F_k} \varkappa. \tag{3.26}$$

Here, F_k is the cross-sectional area of the fuselage at the k-th station, while $\varkappa$ is some dimensionless coefficient determined by the formula

$$\varkappa = \frac{F_k}{I_k^2} \int_F \frac{S_k^2(z)\,dz}{2\delta(z)}, \tag{3.27}$$

where

I_k = moment of inertia of the cross section relative to the neutral axis;

$S_k(z)$ = static moment relative to the neutral axis of a part of the cross section located above a straight line parallel to the neutral axis and at a distance z from it;

$\delta(z)$ = thickness of the fuselage skin at a distance z from the neutral axis.

The integral in eq.(3.27) is taken over the entire cross section F of the fuselage.

In conformity with the correction in eq.(3.8), corrections must be intro- /239
duced into the recurrence formulas for the coefficients A_k^X, A_k^Y, A_k^ϑ, etc.

Section 4. Combined Vibrations of the System Fuselage-Rotor

1. Vibrations of the System Fuselage-Rotor

The methods of calculating vibrations of elastic blades presented in Chapter I assume that the blade is hinged to the hub which, in turn, is attached to a stationary support. Actually, the hub is attached to an elastic fuselage and forces are created during blade vibration that cause the hub to move so that, in reality, the deflection at the hinge of the hub during blade vibrations is not equal to zero but to the corresponding deflection of the fuselage.

Results of flight tests have shown in many cases that calculations of the natural vibration frequencies of blades performed without consideration of the elasticity of the fuselage may result in substantial errors. In this connection, M.L.Mil' has formulated and stated the problem of calculating combined vibrations of the system fuselage-rotor as a single oscillatory system. The basic results of investigations carried out in this direction are given below.

The frequencies and modes of natural combined vibrations of the system fuselage-rotor can be found by using the method of dynamic stiffness, whose essence is presented in Subsections 2, 3, and 4 of Section 2.

However, performance of such calculations involves a large volume of computational work. This pertains specifically to determinations of the lateral natural vibration frequencies of the system fuselage-rotor, when the dynamic stiffness of the rotor in the plane of rotation is to be determined. Furthermore, calculations show that the relation between fuselage and blade vibrations generally is weak and that the natural vibration frequencies of the system fuselage-rotor can always be divided into two groups such that the frequencies of the first group are quite close to the natural frequencies of the isolated fuselage, in whose calculation the blade mass is considered as concentrated at the rotor center, whereas the frequencies of the second group are sufficiently close to the natural blade frequencies calculated on the assumption that the blades are attached to a perfectly rigid and infinitely heavy fuselage.

When the hub attachment to the fuselage is insufficiently rigid (elastic rotor shaft, elastic reduction-gear frame, gear case), it may happen that some of the frequencies of vibrations of the second group noticeably change in comparison with blade frequencies calculated by the usual method.

Therefore, the natural vibration frequencies of the first group can usually be determined by means of methods presented in this Chapter as fuselage frequencies, disregarding elasticity of the blades. An exception are special cases where, for example, the rotors are attached to light and elastic wings on a helicopter of side-by-side configuration. In such cases, the frequencies of combined oscillations of the system fuselage-rotor must be calculated with the above-described method of dynamic stiffness.

As regards the natural blade vibration frequencies, it is apparently always necessary to estimate the possible variation of some of these frequencies due to local elasticity of the rotor attachment to the fuselage.

Thus, to allow for the correlation of fuselage and blade vibrations, it /240
suffices in practice to estimate only the change in natural blade frequencies caused by local elasticity of the rotor attachment.

In the next Subsection, we will present a method for such a calculation to determine the natural blade vibrations in the plane of rotation, with consideration of the flexural elasticity of the rotor shaft. This case is the most important in practice.

To the elasticity of the rotor shaft one can always add the elasticity of other elements of the rotor attachment (gear frame, gear case, etc.). Here we will give certain important fundamental considerations, from which it will become obvious that only some of the natural blade vibration frequencies are able to change as a result of elasticity of the rotor attachment.

In Section 1 of this Chapter it was shown that not all harmonic components of forces generated by vibrating blades "pass" to the fuselage, since many are neutralized at the rotor hub casing.

For instance, during blade vibrations of a five-blade rotor in the flapping plane, the first four harmonic components of forces transferred to the hub from the blades (ω, 2ω, 3ω, 4ω) are neutralized at the hub and only the fifth harmonic component is transmitted to the fuselage.

Hence it is obvious that, in calculating forced blade vibrations due to forces corresponding to the harmonics ω, 2ω, 3ω, and 4ω, we must examine the natural blade vibration modes and frequencies (with the method of expansion in natural modes), calculated for ordinary boundary conditions when the blade is assumed to be hinged to a stationary hub.

When dealing with forced vibrations of the fifth harmonic, the presence of combined vibrations of blade and fuselage must be taken into consideration.

The physical meaning of this phenomenon is that the natural vibration modes of a rotor with elastic blades can be divided into two groups:

1) rotor vibration modes at which the forces from individual blades are neutralized at the hub casing;
2) rotor vibration modes at which the forces from individual blades are summed at the hub casing and are transmitted to the fuselage.

Figure 2.28, as a typical example, shows two such vibration modes for a rotor with four blades since the picture is clearest for such a rotor. Both vibration modes A and B correspond to the vibration frequency p_1 of a single-mode overtone of an isolated blade in the flapping plane and differ only by the phase distribution of the vibrations with respect to individual blades. The vibration mode A corresponds to a situation where pairs of opposite blades vibrate in opposite phase. In this case, the forces p_1, p_2, p_3 and p_4 acting on the rotor hub mutually cancel out at each instant of time and are not transmitted to the fuselage. The vibration mode B corresponds to the situation where all four blades vibrate in phase. In this case the forces p_1, p_2, p_3 and p_4 are summed at the hub and generate a force acting on the fuselage and varying in time with a frequency p_1.

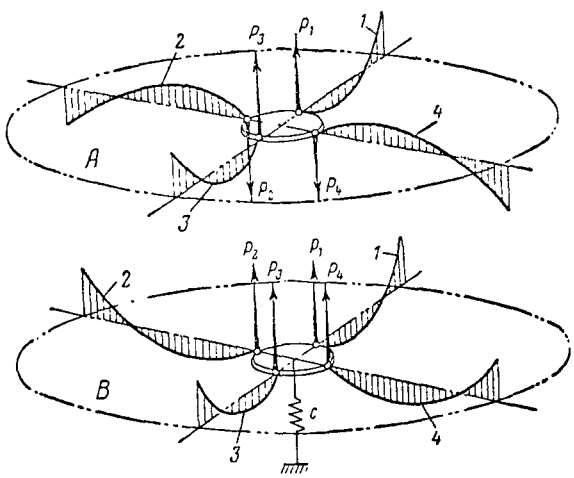

Fig.2.28 Vibration Modes of a Rotor with Elastic Blades.

If the rotor hub is attached to a perfectly rigid support, then the frequencies of both vibration modes A and B of the rotor are identical and equal to the frequency p_1 or to the natural vibrations of the first harmonic of an isolated blade with a hinged butt. If the hub is attached to some elastic base with a vertical rigidity c, the frequency of the vibration mode A will not change and remains equal /241 to p_1, whereas the frequency of the modes B will decrease and that the more the lower the rigidity c.

It can be demonstrated that the modes of the two indicated types exist for a rotor with any number of blades z. These vibration modes can be characterized by a formula. For example, all vibration modes of the z-bladed rotor corresponding to the k-th overtone of vibrations of an isolated blade are characterized by the following law of blade vibration:

$$y_n(x, t) = \bar{y}_k(x) \cos s\psi_n \cos p_k t, \tag{4.1}$$

where

$y_n(x, t)$ = deviation of a point with the coordinate x, belonging to the n-th blade;

$\cos s\psi_n$ = characteristic of the law of vibration phase distribution for individual blades, i.e., of the vibration mode of the rotor as a whole;

s = any integer that can be called the order of a given rotor vibration mode (s = 1, 2, 3, ..., z).

The quantities ψ_n are determined by the formula

$$\psi_n = \frac{2\pi}{z} n.$$

On the basis of eq.(1.13) in Section 1, it is easy to show that the vibration modes of the orders s = 1, 2, 3, ..., z - 1 correspond to a situation in which the forces generated by individual blades are equalized at the hub and that only the mode of the order s = z corresponds to a situation where the forces from individual blades are summed and transmitted to the fuselage.

The modes A and B presented in Fig.2.28 are modes of the second and fourth order for a four-blade rotor. It is obvious from the aforesaid that the natural vibration frequencies of a rotor, corresponding to vibration modes of all orders with the exception of s = z, do not depend upon the elasticity of the hub attachment and that only the frequencies corresponding to the rotor vibration mode of the order s = z depend on this elasticity.

We can further show that all harmonics of forces that excite blade vibrations in the flapping plane, with the exception of the "transient" harmonics $z\omega$, $2z\omega$, $3z\omega$, etc. will excite only those rotor vibration modes at which the forces produced by the blades are neutralized at the hub and that only the harmonic /242
components of the exciting forces corresponding to the "transient" harmonics will excite rotor vibration modes at which the blade-generated forces are summed and transmitted to the hub.

Hence, we can draw a useful practical conclusion: If we construct an ordinary resonance diagram of the blade (see Fig.1.6 of Chapt.I) in the flapping plane, calculated without consideration of elasticity of the rotor attachment to the fuselage, then the resonances with all of the harmonics, except for resonances with the harmonics $z\omega$, $2z\omega$, etc., correspond to reality. The resonances with the harmonics $z\omega$, $2z\omega$, etc., must be investigated additionally, taking into account the elasticity of the rotor hub attachment and refining the values of the corresponding natural frequencies.

However, it should be mentioned that, in studies of blade vibrations in the flapping plane, it is generally possible to disregard the elasticity of hub attachment for such harmonics since the rigidity of the hub attachment in a vertical direction is usually large and has little influence on the natural blade vibration frequencies (except for the case of rotor attachment of a side-by-side helicopter to light and flexible wings).

In studying the resonance diagram of a blade in the plane of rotation the effect of elasticity of the rotor hub attachment to the fuselage must be taken into consideration. All above considerations hold also for blade vibrations in the plane of rotation, with the only difference that in this case the "transient" harmonics are the harmonics $(z-1)\omega$, $(z+1)\omega$, $(2z-1)\omega$, $(2z+1)\omega$, etc. Furthermore, at resonance with the harmonics $z\omega$, $2z\omega$, etc. in the plane of rotation, allowance must be made for the combination of rotor vibrations with torsional vibrations of the transmission system (the pertaining calculations can also be carried out on the basis of the method of dynamic stiffness).

2. Calculation of the Natural Rotor Blade Vibrations in the Plane of Rotation, with Consideration of Elasticity of the Rotor Shaft and Attachment to the Fuselage

Let us examine the problem of natural blade vibrations of a rotor mounted to a flexurally elastic shaft (Fig.2.29). Let the rigidity of the shaft with respect to the force P applied to the shaft at the hub center and lying in the plane of rotation of the rotor be equal to c_0. Consequently, the force P and the resultant displacement δ of the shaft end are correlated by

$$P = c_0\delta. \tag{4.2}$$

In this case, it is immaterial whether the displacement δ is produced by bending of the shaft itself or is due to the elasticity of its attachment to the fuselage.

Let us discuss only the case when the given rigidity is identical in all directions in the plane xOz, i.e., when the elastic support to which the rotor is attached is isotropic. In reality this is not so, but the rigidities of attachment in the directions of the Ox and Oz axes generally differ little so that the support can be assumed as isotropic, understanding by the quantity c_0 the arithmetic mean of the rigidities c_x and c_z:

$$c_0 = \frac{c_x + c_z}{2}. \tag{4.3}$$

Calculation of natural vibrations of a rotor on an elastic base can be performed by the method of dynamic stiffness.

First, we introduce the concept of dynamic stiffness of a blade in the plane of rotation. Let a flexurally elastic blade in the central centrifugal force field be attached at the root by a hinge such that the hinge is able to move /243 freely in a direction perpendicular to the axis of the undeformed blade (see Fig.2.30).

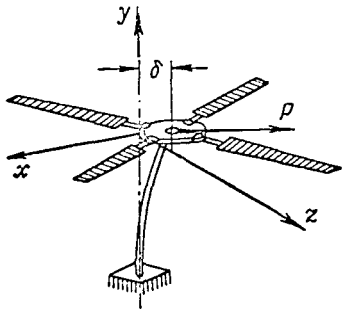

Fig.2.29 Diagram of Rotor on Elastic Shaft.

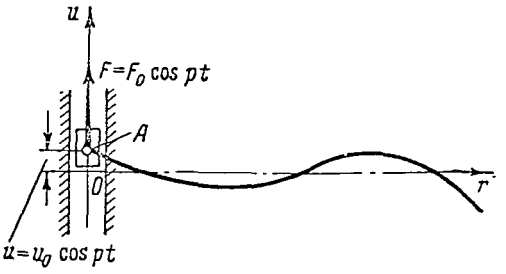

Fig.2.30 Diagram for Calculation of Forced Blade Vibrations to Determine Dynamic Rotor Stiffness.

Furthermore, let the blade execute steady forced vibrations under the effect of a lateral exciting harmonic force

$$F=F_0\cos pt,$$

applied to the hinge A. In this case, the point A of the application of force will also execute vibrations according to the law

$$u=u_0\cos pt.$$

We will call the quantity

$$D_b(p)=\frac{F_0}{u_0}, \tag{4.4}$$

the dynamic stiffness of the blade.

The dynamic blade stiffness can be determined either by the method given in Subsection 2 of Section 2 or by the method of auxiliary mass (Sect.2, Subsect.4). In so doing we must take into account that the blade moves in a centrifugal force field so that it is no longer a question of solving an equation of the type of eq.(2.2), as had been done in calculating the fuselage, but of solving the equation of blade vibration in the plane of rotation (see Chapt.I, Sect.1, Subsect.11), which has the form

$$(EIu'')''-(Nu')'+m\ddot{u}-\omega^2u=q(r,t). \tag{4.5}$$

Here, N is the centrifugal force in the blade section at a radius r.

When using the method of auxiliary mass, the natural blade vibration frequencies and modes must be calculated in the plane of rotation in the presence of an attachment according to the scheme depicted in Fig.2.30, with a different value for the auxiliary mass Δm_b at the point A, using the method presented in Chapter I, Section 2, Subsection 5.

From the results of such a calculation we can construct the graph of $\Delta m_b = f(p)$. An example of such a graph is shown in Fig.2.32. The points of infinite discontinuities of the function f(p) give the natural frequencies of the blade with a fixed hinge at the point A, i.e., the natural frequencies of a blade for the case of an infinitely large rigidity of the rotor shaft. The points at which $\Delta m_b = 0$ yield the natural frequencies of a blade attached freely according to the scheme depicted in Fig.2.30.

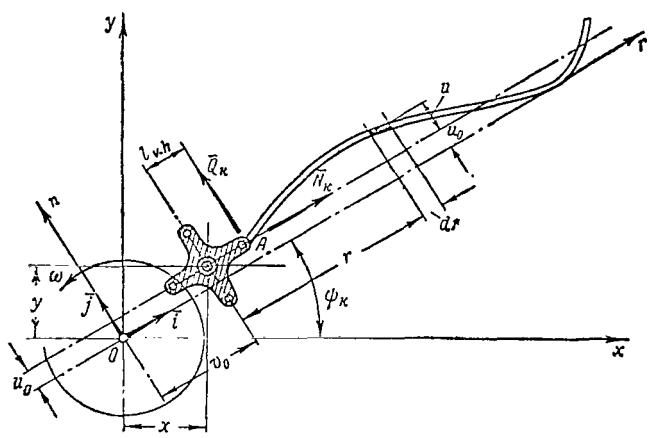

Fig.2.31 For Calculation of Dynamic Stiffness of a Rotor with Elastic Blades.

The magnitude of the dynamic blade stiffness corresponding to this value of p can be determined from the formula /244

$$D_b(p) = (p^2 + \omega^2)\,\Delta m_b(p). \qquad (4.5a)$$

The additional term $\omega^2 \Delta m_b(p)$ in this formula is due to the centrifugal force component of mass Δm_b directed along the normal to the blade.

We will show further that the dynamic stiffness of the rotor as a whole can be found if the dynamic stiffness of the blade is known. Let us turn to Fig.2.31 which gives the planform of a rotor hub with vertical hinges and the k-th elastic blade. Let xOy be a coordinate system rotating together with the rotor with an angular velocity ω. Furthermore, let the center of the hub execute prescribed harmonic vibrations in the plane of rotation in obedience to the law

$$\left.\begin{aligned} x &= x_0 \cos pt; \\ y &= y_0 \sin pt. \end{aligned}\right\} \qquad (4.6)$$

Such vibrations of the hub cause vibrations of the elastic blades in the plane of rotation, reducing the problem to finding the forces exerted by the vibrating blades on the hub during its motion.

Let us choose an auxiliary rectangular coordinate system rotating together with the rotor nOr, for which the Or-axis is parallel to a straight line passing through the center of the hub and through the drag hinge A of the k-th blade. The Or-axis makes a certain angle ψ_k with the Ox-axis. We denote by u_0 and v_0 the coordinates of the hub center in the system nOr. Then, obviously,

$$\begin{aligned} u_0 &= -x \sin \psi_k + y \cos \psi_k; \\ v_0 &= x \cos \psi_k + y \sin \psi_k. \end{aligned}$$

During vibrations of the hub in accordance with the law (4.6), the coordinates u_0 and v_0 will vary in time in obedience to the law

$$\left.\begin{aligned} u_0 &= (-x_0 \sin\psi_k)\cos pt + (y_0 \cos\psi_k)\sin pt; \\ v_0 &= (x_0 \cos\psi_k)\cos pt + (y_0 \sin\psi_k)\sin pt. \end{aligned}\right\} \tag{4.7}$$

Furthermore, let u denote the deflection of the point of the elastic blade axis at a radius r from a straight line passing through the drag hinge A of the blade and running parallel to the Or-axis. During vibrations of the blade, the quantity u is a function of the radius r and the time t such that u = = u(r, t). /245

Let $\bar{w}$ be the vector of the total acceleration of a point of radius r of the elastic blade axis. Then,

$$\bar{w} = \bar{w}_{rel} + \bar{w}_{tr} + \bar{w}_{Cor},$$

where

$\bar{w}_{rel}$ = vector of relative acceleration of a point due to motion in a moving coordinate system nOr;
$\bar{w}_{tr}$ = vector of translational acceleration due to motion of a point together with the coordinate system nOr;
$\bar{w}_{Cor}$ = vector of Coriolis acceleration.

We then introduce the unit vectors $\bar{i}$ and $\bar{j}$, directed along the axes r and n, respectively. Then, we can write

$$\begin{aligned} \bar{w}_{rel} &= \bar{i}(\ddot{v}_0) + \bar{j}(\ddot{u}_0 + \ddot{u}); \\ \bar{w}_{tr} &= \bar{i}[-\omega^2(r + v_0)] + \bar{j}[-\omega^2(u_0 + u)]; \\ \bar{w}_{Cor} &= \bar{i}[-2\omega(\dot{u}_0 + \dot{u})] + \bar{j}[(2\omega\dot{v}_0]. \end{aligned}$$

If we denote by w_n and w_r the projections of the vector of total acceleration onto the axes On and Or, the following expressions are obtained:

$$\left.\begin{aligned} w_n &= (\ddot{u}_0 - \omega^2 u_0) + (\ddot{u} - \omega^2 u) + 2\omega\dot{v}_0; \\ w_r &= (\ddot{v}_0 - \omega^2 v_0) - \omega^2 r - 2\omega\dot{u}_0 - 2\omega\dot{u}. \end{aligned}\right\} \tag{4.8}$$

The equation of equilibrium in the centrifugal force field has the form

$$(EIu'')'' - (Nu')' = q, \tag{4.9}$$

where q is the intensity of the lateral load applied to a beam.

During blade vibrations, the lateral load due to inertia forces can be written in the form

$$q(r, t) = -mw_n = -m[(\ddot{u}_0 - \omega^2 u_0) + (\ddot{u} - \omega^2 u) + 2\omega\dot{v}_0],$$

where m is the linear mass of the blade [m = m(r)].

Substituting this expression into eq.(4.9), we obtain the following partial differential equation for determining the function u(r, t):

$$(EIu'')'' - (Nu')' + m\ddot{u} - \omega^2 u = q^*(r, t), \tag{4.10}$$

where

$$q^*(r,t) = -m[\ddot{u}_0 - \omega^2 u_0 + 2\omega\dot{v}_0]. \tag{4.11}$$

If the motion of the center of the hub is given by eqs.(4.7), then the load $q^*(r, t)$ will be a known function of time.

The unknown function u(r, t) should satisfy eq.(4.10) as well as the boundary conditions

$$\left.\begin{aligned} u(0, t) = u''(0, t) = 0; \\ u''(R,t) = (EIu'')'|_{r=R} = 0. \end{aligned}\right\} \tag{4.12}$$

Differentiating eqs.(4.7) and substituting them into eq.(4.11) will yield

$$q^*(r, t) = mA_k \cos pt + mB_k \sin pt, \tag{4.13}$$

where the constants A_k and B_k are determined by the formulas

$$\left.\begin{aligned} A_k = -[(p^2 + \omega^2)x_0 + 2\omega p y_0] \sin\psi_k; \\ B_k = [(p^2 + \omega^2) y_0 + 2\omega p x_0] \cos\psi_k. \end{aligned}\right\} \tag{4.14}$$

The solution of eq.(4.10), corresponding to steady forced vibrations due to a load [see eq.(4.13)], is sought in the form /246

$$u(r, t) = \bar{u}(r)[A_k \cos pt + B_k \sin pt]. \tag{4.15}$$

Substituting this expression into eq.(4.10) with the right-hand side for q^* from eq.(4.13), we find that the function $\bar{u}(r)$ should satisfy the ordinary differential equation

$$(EI\bar{u}'')'' - (N\bar{u}')' - (p^2 + \omega^2)m\bar{u} = m, \tag{4.16}$$

as well as the boundary conditions

$$\left.\begin{aligned} \bar{u}(0) = \bar{u}''(0) = 0; \\ \bar{u}''(R) = (EI\bar{u}'')'|_{r=R} = 0. \end{aligned}\right\} \tag{4.17}$$

We note further that, in calculating blade vibrations excited by vibration of the hinge A according to the scheme depicted in Fig.2.30, it is necessary to solve an equation of the form

$$(EIu'')'' - (Nu')' - m\ddot{u} - \omega^2 u = 0,$$

where u is the total displacement of a point of the elastic blade axis of radius r. In this case, the function u(r, t) should satisfy the conditions

$$\left.\begin{aligned} u(0, t) &= u_0 \cos pt; \\ u''(0, t) &= 0. \end{aligned}\right\}$$

$$\left.\begin{aligned} u''(R, t) &= 0; \\ (EIu'')'|_{r=R} &= 0. \end{aligned}\right\}$$

Seeking the solution of this equation in the form

$$u = [u_0 + \bar{u}(r)] \cos pt,$$

we arrive at the conclusion that the function $\bar{u}(r)$ should satisfy the equation

$$(EI\bar{u}'')'' - (N\bar{u}')' - (p^2 + \omega^2)\, m\bar{u} = (p^2 + \omega^2)\, mu_0,$$

which differs from eq.(4.16) only by the constant $u_0(p^2 + \omega^2)$. The boundary conditions for the function $\bar{u}(r)$ in this case fully coincides with eqs.(4.17).

Thus, during blade vibrations according to the scheme shown in Fig.2.30, the function $\bar{u}(r)$ is the same as in the problem of interest here [see eqs.(4.16) and (4.17)] if we select the amplitude u_0 such that the condition

$$u_0(p^2 + \omega^2) = 1 \tag{4.18}$$

is satisfied.

Physically, this means that the mode of forced blade vibrations in the problem of interest here coincides with the mode of blade vibrations excited according to the scheme in Fig.2.30. On the basis of this result, an important formula is derived. For this, we note that during vibrations of a blade attached according to the scheme shown in Fig.2.30 and excited by the force $F = F_0 \cos pt$, the sum of the projections of all lateral inertia forces applied to the blade /247 should be balanced by the force F. Hence, we find

$$F_0 = \Delta m_b(p)(p^2 + \omega^2) u_0 = -(p^2 + \omega^2) \int_{l_{v.h}}^{R} m(u_0 + \bar{u})\, dr =$$

$$= -(p^2 + \omega^2) u_0 m_b - (p^2 + \omega^2) \int_{l_{v.h}}^{R} m\bar{u}\, dr,$$

where m_b is the blade mass up to the drag hinge

$$\left(m_b = \int_{l_{v.h}}^{R} m\,dr\right).$$

On satisfying condition (4.18), we obtain the formula

$$\int_{l_{v.h}}^{R} m\,\bar{u}\,dr = -\frac{\Delta m_b + m_b}{p^2+\omega^2}, \tag{4.19}$$

meaning that the integral with respect to the blade of the function $m\bar{u}$ [where $\bar{u}$ is the solution of eq.(4.16)] is expressed in terms of dynamic blade stiffness or, which comes to the same, in terms of the auxiliary mass $\Delta m_b(p)$.

It is now easy to obtain expressions for the forces exerted on the hub by the vibrating blades. We denote by Q_k and N_k, respectively, the projections onto the On- and Or-axes of a force exerted by the k-th blade k on the drag hinge of the hub. Then,

$$\left.\begin{aligned} Q_k &= -\int_{l_{v.h}}^{R} mw_r\,dr = -\int_{l_{v.h}}^{R} m(\ddot{u}-\omega^2 u)\,dr - \\ &\quad -(\ddot{u}_0-\omega^2 u_0+2\omega\dot{v}_0)\,m_b; \\ N_k &= -\int_{l_{v.h}}^{R} mw_r\,dr = -m_b(\ddot{v}_0-\omega^2 v_0-2\dot{u}_0\omega)+ \\ &\quad +\omega^2\int_{l_{v.h}}^{R} mr\,dr+2\omega\int_{l_{v.h}}^{R} mu\,dr. \end{aligned}\right\} \tag{4.20}$$

Substituting here eqs.(4.15), (4.7), (4.14) and taking into account eq.(4.19), we find

$$\begin{aligned} Q_k &= \Delta m_b\{[(p^2+\omega^2)x_0+2\omega p y_0]\sin\psi_k\cos pt - \\ &\quad -[(p^2+\omega^2)y_0+2\omega p x_0]\cos\psi_k\sin pt\}; \end{aligned} \tag{4.21}$$

$$\begin{aligned} N_k &= N_0+\left[m_b(p^2+\omega^2)x_0-\Delta m_b 2p\omega y_0-\frac{\Delta m_b+m_b}{(p^2+\omega^2)}4p^2\omega^2 x_0\right]\cos\psi_k\cos pt+ \\ &\quad +\left[m_b(p^2+\omega^2)y_0-\Delta m_b 2p\omega x_0-\frac{\Delta m_b+m_b}{p^2+\omega^2}4p^2\omega^2 y_0\right]\sin\psi_k\sin pt, \end{aligned} \tag{4.22}$$

where $N_0 = \omega^2\int_{l_{v.h}}^{R} mr\,dr$ is the centrifugal force exerted by the blade on the drag hinge.

Denoting by X and Y the forces exerted on the hub by the vibrating blades,

we derive the formulas: /248

$$X=\sum_{k=1}^{z}(-Q_k\sin\psi_k+N_k\cos\psi_k);$$

$$Y=\sum_{k=1}^{z}(Q_k\cos\psi_k+N_k\sin\psi_k).$$

Substituting here eqs.(4.21) and (4.22) and taking into account the properties of the trigonometric sums described in Subsection 2, Section 1 of this Chapter [eqs.(1.13)], we arrive at the following expressions:

$$X=\left\{-\frac{z}{2}\Delta m_b[(p^2+\omega^2)x_0+2\omega p y_0]+\frac{n}{2}\left[m_b(p^2+\omega^2)x_0-\right.\right.$$
$$\left.\left.-\Delta m_b 2p\omega y_0-\frac{\Delta m_b+m_b}{p^2+\omega^2}\cdot 4p^2\omega^2 x_0\right]\right\}\cos pt; \tag{4.23}$$

$$Y=\left\{-\frac{z}{2}\Delta m_b[(p^2+\omega^2)y_0+2\omega p x_0]+\right.$$
$$\left.+\frac{z}{2}\left[m_b(p^2+\omega^2)y_0-\Delta m 2p\omega x_0-\frac{\Delta m_b+m_b}{p^2+\omega^2}\cdot 4p^2\omega^2 y_0\right]\right\}\sin pt. \tag{4.24}$$

On the other hand, we can construct the equations of motion of the hub of a rotor on an elastic shaft, which have the form

$$m_{hub}(\ddot{x}-\omega^2 x-2\omega\dot{y})+c_0 x=X;$$
$$m_{hub}(\ddot{y}-\omega^2 y+2\omega\dot{x})+c_0 y=Y,$$

where

m_{hub} = mass of the hub casing;
c_0 = shaft rigidity.

If the motion of the hub takes place in obedience to the law (4.6), the last equations will yield

$$X=\{m_{hub}[-(p^2+\omega^2)x_0-2\omega p y_0]+c_0 x_0\}\cos pt;$$
$$Y=\{m_{hub}[-(p^2+\omega^2)y_0-2\omega p x_0]+c_0 y_0\}\sin pt.$$

If we equate these expressions to eqs.(4.23) and (4.24), we obtain a system of two linear homogeneous equations for determining the amplitudes x_0 and y_0:

$$\left.\begin{aligned}Ax_0+By_0=0;\\ Bx_0+Ay_0=0,\end{aligned}\right\} \tag{4.25}$$

where

$$A=(p^2+\omega^2)\left[\frac{z}{2}(m_b-\Delta m_b)+m_{hub}\right]-2z\frac{\Delta m_b+m_b}{(p^2+\omega^2)}\,p^2\omega^2-c_0; \tag{4.26}$$

$$B=2\omega p\,[m_{hub}-z\Delta m_b]. \tag{4.27}$$

Equating to zero the determinant of this system, we obtain the characteristic equation for determining the natural frequencies p:

$$\begin{vmatrix} A & B \\ B & A \end{vmatrix}=A^2-B^2=0, \tag{4.28}$$

whence

$$A=\pm B.$$

In the case A = -B [as is apparent from eq.(4.25)], $x_0 = y_0$. This corresponds to rotation of the hub center in the direction of rotation of the rotor [see eq.(4.6)]. /249

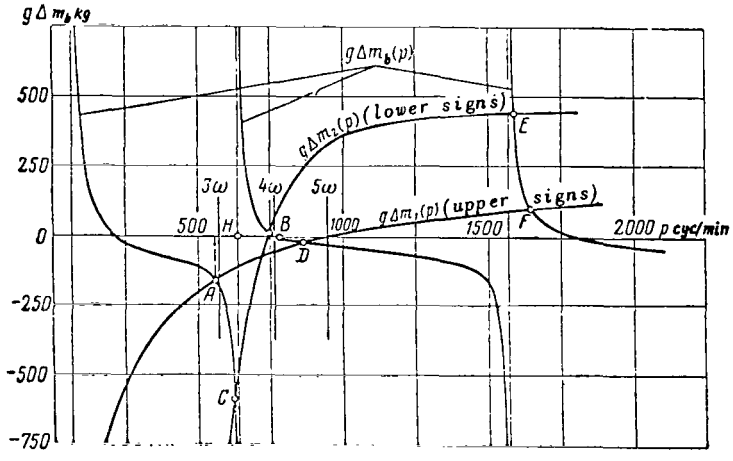

Fig.2.32 Determination of Vibration Frequencies of a Rotor on an Elastic Shaft, by the Dynamic Stiffness Method.

In the case A = B we have $x_0 = -y_0$, which corresponds to rotation of the rotor center opposite to the rotation of the rotor.

The characteristic equations (4.28) can be solved with respect to the quantity $\Delta m_b(p)$. This yields the following equation:

$$\Delta m_b(p)=\frac{(p^2+\omega^2)\left(\frac{z}{2}m_b+m_{hub}\right)-c_0-\frac{2zp^2\omega^2}{p^2+\omega^2}\cdot m_b\mp 2\omega p m_{hub}}{\frac{z}{2}\cdot(p^2+\omega^2)+\frac{2zp^2\omega^2}{p^2+\omega^2}\pm 2n\omega p}. \tag{4.29}$$

This equation can be solved graphically by superimposing, on the curve of the auxiliary blade mass $\Delta m_b = \Delta m_b(p)$, two curves corresponding to the right-hand side of this expression in which we take either the upper signs (minus sign in the numerator and plus sign in the denominator) or the lower signs. The first of these quantities will be denoted by $\Delta m_1(p)$ and the second, by $\Delta m_2(p)$.

The abscissas of the intersection points of the curve $\Delta m_1(p)$ with the graph of auxiliary blade mass $\Delta m_b(p)$ yield the natural vibration frequencies of a rotor on an elastic shaft, corresponding to vibration modes in which the center of the hub rotates in the direction of rotation of the rotor, with an angular velocity p relative to the coordinate system xOy fixed to the rotor and hence with an angular velocity $p + \omega$ relative to the body-fixed coordinate system (helicopter body). Obviously, such modes can be excited only by the harmonics $(z - 1)\omega$, $(2z - 1)\omega$, etc. The abscissas of the intersection points of the curves $\Delta m_2(p)$ and $\Delta m_b(p)$ yield the natural vibration frequencies of a rotor on an elastic shaft in which the hub center rotates in a direction opposite to that of the rotor. Such vibration modes can be excited only by the harmonics $(z + 1)\omega$, $(2z + 1)\omega$, etc.

Figure 2.32 gives the graphs for the curves $\Delta m_b(p)$, $\Delta m_1(p)$, and $\Delta m_2(p)$, constructed for the following initial data: $c_0 = 500$ kg/mm; $m_{hub} = 38$ kg·cm^2/m; $m_b = 15$ kg·sec^2/m; $\omega_0 = 190$ rpm; $z = 5$. These graphs show appreciable differences between the natural frequencies of a rotor on an elastic shaft and the natural frequencies of an isolated blade. For example, the point H of an infinite discontinuity of the curve $\Delta m_b(p)$ corresponds to the frequency of a single-node overtone of natural vibrations of an isolated blade of the given rotor (with a stationary hub). In this case, $p = p_1 = 640$ cycles/min. Here, Fig.2.33 shows the vibration mode of this overtone. /250

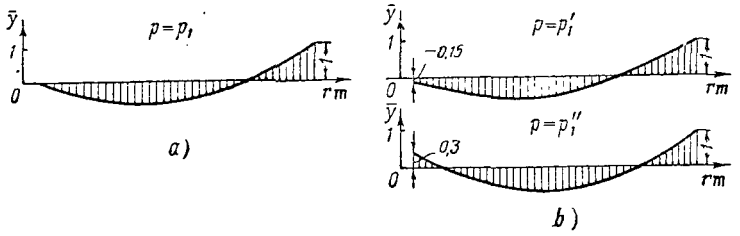

Fig.2.33 Modes of Blade Vibrations.
a - Mode of blade vibrations without consideration of shaft elasticity; b - Modes of blade vibrations with consideration of blade elasticity.

In addition to this natural frequency, a rotor on an elastic shaft also has vibration frequencies corresponding to the points A, B, C and D of the intercepts of the curves $\Delta m_1(p)$ and $\Delta m_2(p)$ with the curve $\Delta m_b(p)$. Here, vibrations of modes corresponding to the points A and D can be excited only by the harmonics $(z - 1)\omega$, $(2z - 1)\omega$, etc. (in this case, 4ω and 9ω etc.). Vibrations corresponding to the points C and B can be excited only by the harmonics $(z + 1)\omega$, $(2z + 1)\omega$, etc. (in this case, 6ω, 11ω, etc.).

These resonance curves were plotted for a helicopter which first had been equipped with a four-blade rotor; however, later the rotor hub had to be modified and the rotor was designed as a five-blade type so as to eliminate the severe resonance of the blade with the harmonic 3ω in the plane of rotation (point A).

Figure 2.33 gives the natural blade vibration modes in the plane of rotation, with consideration of shaft elasticity corresponding to the points A ($p_1' =$ = 560 cycles/min) and B($p_1'' = 761$ cycles/min).

In conclusion, we should mention that the above method for determining the natural frequencies of a blade in the plane of rotation with consideration of shaft elasticity is one of the most complex examples of using the method of dynamic stiffness; this was the main reason for describing it here in some detail. As regards finding the natural blade vibrations in the flapping plane with consideration of elasticity of the hub attachment and of the blade vibration frequencies in the plane of rotation with consideration of torsional elasticity of the transmission system (which are excited by the harmonics $z\omega$, $2z\omega$, $3z\omega$, etc.), the calculations involved are much simpler and can be carried out in full on the basis of the principles set forth in Section 2.

CHAPTER III

/251

GROUND RESONANCE

Ground resonance usually is to mean spontaneous vibrations (build-up) of a helicopter on the ground with increasing amplitude. This phenomenon was first noticed after a drag hinge permitting the blade to move in the plane of rotation of the rotor was introduced into the design of the rotor hub.

In the history of helicopter engineering there were quite a few cases where a helicopter was destroyed by vibrations of this type. Attempts to eliminate ground resonance on a full-scale helicopter sometimes required extensive modifications of the helicopter design. This forced design engineers to work on the development of the theory of ground resonance and reliable methods of its calculation, which would permit selecting the characteristics of the structural members determining the stability margin of the helicopter on the ground.

At present there is a theory of ground resonance which explains all the most important features of this phenomenon and permits calculating the design characteristics on which depends ground resonance. This theory arose as a result of numerous theoretical and experimental investigations of ground resonance carried out both in the Soviet Union and abroad. Of the Soviet works on the theory of ground resonance we must point out first the works of B.Ya.Zherebtsov and A.I.Pozhalostin.

Investigations of ground resonance have shown that the physical essence of this phenomenon involves the following: During natural vibrations of the rotor blades in the plane of rotation (relative to the drag hinges), which can arise from any impetus (wind gust, rough landing, etc.), inertia forces appear in the plane of rotation of the rotor. Being transmitted to the helicopter fuselage, they cause its vibrations on the elastic landing gear. The forces swinging the helicopter vary with a definite frequency depending upon the natural frequency of the blade in the plane of rotation and the angular velocity of rotation of the rotor. A helicopter is most easily swung when the frequency of change of the exciting forces is close to the frequency of natural vibrations of the helicopter on an elastic landing gear. Simultaneously with vibrations of the helicopter body, forces arise which swing the helicopter in the plane of rotation. The presence of this bilateral couple between vibrations of the helicopter and blades results in the helicopter becoming unstable at a certain angular velocity of rotor rotation, i.e., the helicopter vibrations once begun (as a consequence of some impetus) are not damped but increased.

The basic means of combatting ground resonance are:

1) The installation of special dampers on the drag hinges of the rotor blades which damp the blade vibrations in the plane of rotation.

2) The introduction of special damping elements in the design of the /252

shock absorber strut or the proper selection of the characteristics of hydraulic resistance of the shock absorber struts in forward and reverse strokes, and also the characteristics of rigidity of the shock absorber struts and pneumatic tires.

The proper selection of the characteristics of the blade dampers and the characteristics of the rigidity and damping of the landing gear is the main purpose of calculating a helicopter for ground resonance.

The theory of ground resonance which will be presented below holds true only for rotors with a number of blades $n \geq 3$.

The theory of ground resonance of a two-blade rotor has a number of special features and is appreciably more complex (Ref.36).

Section 1. Stability of Rotor on Elastic Base

1. Statement of Problem and Equations of Motion

The most important features of ground resonance of a helicopter can be obtained from an examination of the motion of some idealized mechanical system, which we will call a "rotor on an elastic base". Such a system is schematically shown in Fig.3.1. The shaft of the rotor with heavy and perfectly rigid blades (3), attached to the rotor hub by means of the drag hinges (4), rotates in supports rigidly connected with some heavy casing (body) (1) which is elastically mounted to a stationary base (2) and has only one degree of freedom, namely forward displacement along the axis Ox parallel to the plane of rotation of the rotor. Upon displacement of the body (1) along the Ox-axis, an elastic restoring force is generated by the spring c and a damping force by the damper k. Let us assume the elastic and damping characteristics of the base to be linear, i.e., that the force X acting on the casing (1) during its displacement x(t) is expressed by the formula

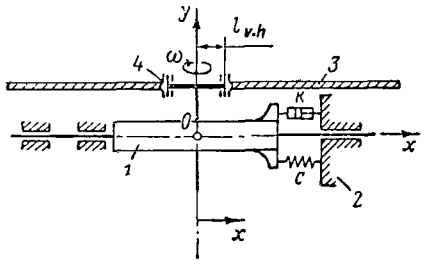

Fig.3.1 Diagram of Rotor on Elastic Base.
1 - Casing; 2 - Base; 3 - Blade; 4 - Hinge.

$$X = -cx - \kappa \frac{dx}{dt}, \tag{1.1}$$

where

c = coefficient of stiffness of the spring (spring constant);
k = damping coefficient.

We will call the quantities c and k the coefficients of stiffness and damping of the elastic base. If m_0 is the mass of the casing (1) and P_x is the projection onto the Ox-axis of the force exerted on the casing by the rotor, then the equation of motion of the casing can be written in the form

$$m_0\ddot{x}+\kappa\dot{x}+cx=P_x. \tag{1.2}$$

Here and below, the dots denote differentiation with respect to time.

Furthermore, we will assume that the rotor rotates uniformly with an angular velocity ω in vacuum, i.e., we will neglect the aerodynamic forces. The theory of ground resonance disregarding aerodynamic forces agrees rather well with experiment. Thus, only inertia forces arising during blade vibrations in the plane of rotation are taken into account.

To construct the equations of motion of the blade, let us turn to Figs.3.1 and 3.2. /253

Let us select a stationary rectangular coordinate system Oxyz. The axis Oy is directed along the axis of the rotor shaft, at a position of the casing (1) corresponding to static equilibrium. The direction of the Ox-axis is taken such that the only possible displacement of the casing is directed along the Ox-axis.

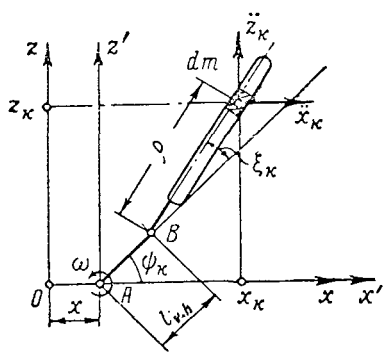

Fig.3.2 For Derivation of Equations of Motion.

As usual, let x be the displacement of the axis of the rotor shaft together with the casing along the Ox-axis (Fig.3.2). Furthermore, let ψ_k be the azimuthal angle of the k-th rotor blade reckoning from the positive direction of the Ox-axis.

The angles ψ_k of different rotor blades are determined by means of the formula

$$\psi_k=\omega t+\frac{2\pi}{n}k, \tag{1.3}$$

where n is the number of rotor blades; k = 1, 2, ..., n.

We denote by $l_{v.h}$ the distance AB (Fig.3.2) from the axis of rotation A to the axis of the vertical or drag hinge B, and by ξ_k the angle of deflection of the k-th blade during its rotation relative to the drag hinge, taking ξ_k as positive when the blade is deflected in the direction of rotation of the rotor.

Then, the coordinates x_k and z_k of the element of the k-th blade with a mass dm at a distance ρ from the axis of the drag hinge are expressed by the following formulas:

$$\left.\begin{aligned} x_k&=x+l_{v.h}\cos\psi_k+\varrho\cos(\psi_k+\xi_k);\\ z_k&=l_{v.h}\sin\psi_k+\varrho\sin(\psi_k+\xi_k). \end{aligned}\right\} \tag{1.4}$$

Differentiating these expressions twice with respect to time, we obtain formulas for determining the components of the acceleration of the blade element:

$$\ddot{x}_k = \ddot{x} - \omega^2 l_{v.h} \cos\psi_k - \varrho(\omega + \dot{\xi}_k)^2 \cos(\psi_k + \xi_k) + \ddot{\xi}_k \varrho \sin(\psi_k + \xi_k);$$
$$\ddot{z}_k = -\omega^2 l_{v.h} \sin\psi_k - \varrho(\omega + \dot{\xi}_k)^2 \sin(\psi_k + \xi_k) + \ddot{\xi}_k \varrho \cos(\psi_k + \xi_k).$$

In deriving the equations of small blade vibrations relative to the drag hinge we must, as usual, limit ourselves to small quantities of the first order. Therefore, we can assume that

$$(\omega + \dot{\xi}_k)^2 \approx \omega^2 + 2\omega\dot{\xi}_k.$$

Thus, with an accuracy to small quantities of the second order, the formulas for the accelerations $\ddot{x}_k$ and $\ddot{y}_k$ can be written in the form

$$\left.\begin{aligned} \ddot{x}_k &= \ddot{x} - \omega^2 l_{v.h} \cos\psi_k - \varrho(\omega^2 + 2\omega\dot{\xi}_k)\cos(\psi_k + \xi_k) + \ddot{\xi}_k \varrho \sin(\psi_k + \xi_k); \\ \ddot{z}_k &= -\omega^2 l_{v.h} \sin\psi_k - \varrho(\omega^2 + 2\omega\dot{\xi}_k)\sin(\psi_k + \xi_k) + \ddot{\xi}_k \varrho \cos(\psi_k + \xi_k). \end{aligned}\right\} \quad (1.5)$$

When the system moves in a vacuum, the rotor blades at each instant of time t are loaded only by inertia forces. The elementary inertia forces acting on a blade element are expressed by the formulas:

$$\left.\begin{aligned} dX_k &= -dm_k \ddot{x}_k; \\ dZ_k &= -dm_k \ddot{z}_k. \end{aligned}\right\} \quad (1.6)$$

In the drag hinges of the rotor hub, let there be linear elastic and damp- /254
ing devices which, during rotation of the blade relative to the drag hinge, load it by the moment

$$M = -c_b \xi_k - \kappa_b \dot{\xi}_k, \quad (1.7)$$

directed toward the side opposite to the positive direction ξ_k. We will call c_b and k_b, respectively, the coefficients of elasticity and damping of the blade.

At each instant of time, the moment from the inertia forces applied to the blade relative to the drag hinge should be balanced by the moment M. Therefore, we can write

$$\int_l [\ddot{x}_k \varrho \sin(\psi_k + \xi_k) - \ddot{z}_k \varrho \cos(\psi_k + \xi_k)]\, dm = c_b \xi_k + \kappa_b \dot{\xi}_k,$$

where integration is carried out over the blade length l.

The equation of motion of the k-th blade is derived from the last expression and from eqs.(1.5) after simple transformations. Since we are interested in the equations of small blade vibrations, we can limit ourselves to terms of the first order of smallness relative to the quantities x, $\dot{x}$, ξ_k, and $\dot{\xi}_k$, after discarding terms containing squares and products of these quantities. Then, we can put

$$\cos\xi_k \approx 1;$$

$$\sin \xi_k \approx \xi_k;$$

$$\sin(\psi_k + \xi_k) \approx \sin \psi_k + \xi_k \cos \psi_k;$$

$$\cos(\psi_k + \xi_k) \approx \cos \psi_k - \xi_k \sin \psi_k.$$

After such simplifications, the equation of small vibrations of the k-th blade will take the following form:

$$\ddot{\xi}_k + 2n_b \dot{\xi}_k + (p_{b_0}^2 + \nu_0^2 \omega^2)\xi_k = \frac{\nu_0^2}{l_{v.h}} \ddot{x} \sin \psi_k. \tag{1.8}$$

Here, the following notations are used:

$n_b = \dfrac{k_b}{2I_{v.h}}$ = relative damping coefficient of the blade;

$p_{b_0}^2 = \dfrac{c_b}{I_{v.h}}$ = natural frequency of a nonrotating blade (at $\omega = 0$) relative to the drag hinge;

ν_0 = dimensionless blade parameter determined by the formula:

$$\nu_0 = \sqrt{\frac{l_{v.h}\, S_{v.h}}{I_{v.h}}}, \tag{1.9}$$

where

$S_{v.h} = \int_l \rho \, dm$ = static blade moment relative to the drag hinge;

$I_{v.h} = \int_l \rho^2 dm$ = moment of inertia of the blade relative to the drag hinge.

The right-hand side of eq.(1.8) represents the moment due to inertia forces acting on the blade, generated by the rotor shaft displacement (x). When the shaft is stationary, at $\ddot{x} = 0$, eq.(1.8) describes the natural blade vibrations of a uniformly rotating rotor in the plane of rotation.

The general solution of eq.(1.8) without the right-hand side has the form /255

$$\xi_k = \xi_{k_0} e^{n_b t} \cos(p_b t + \varphi_k),$$

where ξ_{k_0} and φ_k are arbitrary constants, while the quantity p_b is determined by the formula

$$p_b = \sqrt{p_{b_0}^2 + \nu_0^2 \omega^2 - n_b^2}$$

and represents the angular frequency of natural blade vibrations in the plane of rotation.

Furthermore, it is necessary to determine the force P_x exerted on the casing

by the rotor. The force P_x represents the resultant of the inertia forces of vibrating blades and, on the basis of the well-known theorem of motion of the center of inertia (center of gravity) of a mechanical system, can be determined as the product of the mass of the blade system and the component of acceleration of the common center of gravity of the blade system along the axis ox.

Let us derive formulas for determining the coordinates of the common center of gravity of the blade system.

Let x_{k_c} and z_{k_c} be the coordinates of the center of gravity of the k-th blade. Then, the coordinates x_c and z_c of the center of gravity of the blade system can be calculated by means of the expressions:

$$\left.\begin{aligned} x_c &= \frac{1}{n}\sum_{k=1}^{n} x_{k_c}; \\ z_c &= \frac{1}{n}\sum_{k=1}^{n} z_{k_c}. \end{aligned}\right\} \tag{1.10}$$

Furthermore, let ρ_c be the distance of the center of gravity of the blade from the axis of the drag hinge. Then, in conformity with eqs.(1.4), the coordinates x_c, z_c can be determined as

$$\begin{aligned} x_{k_c} &= x + l_{v.h}\cos\psi_k + \varrho_c\cos(\psi_k + \xi_k); \\ z_{k_c} &= l_{v.h}\sin\psi_k + \varrho_c\sin(\psi_k + \xi_k). \end{aligned}$$

Substituting these expressions into eq.(1.10) and considering that, for $n \geq 3$ [see Chapt.II, Sect.1, Subsect.2, eq.(1.13)],

$$\left.\begin{aligned} \sum_{k=1}^{n}\cos\psi_k &= 0; \\ \sum_{k=1}^{n}\sin\psi_k &= 0, \end{aligned}\right\} \tag{1.11}$$

we obtain the following simple expressions for the coordinates of the common center of gravity of the blade system:

$$\left.\begin{aligned} x_c &= -\frac{\varrho_c}{n}\sum_{k=1}^{n}\xi_k\sin\psi_k + x; \\ z_c &= \frac{\varrho_c}{n}\sum_{k=1}^{n}\xi_k\cos\psi_k. \end{aligned}\right\} \tag{1.12}$$

The force P_x acting on the elastic base can be determined from the formula

$$P_x = -nm_b\ddot{x}_c.$$

Twice differentiating the first equation of the system (1.12), we obtain /256

$$P_x = -nm_b\ddot{x} + S_{v.h}\sum_{k=1}^{n}[(\ddot{\xi}_k - \omega^2\xi_k)\sin\psi_k + 2\omega\dot{\xi}_k\cos\psi_k].$$

Substituting this expression into eq.(1.2) will finally yield the following equation of motion of the casing:

$$(m_0 + nm_b)\ddot{x} + \kappa\dot{x} + ex = S_{v.h}\sum_{k=1}^{n}[(\ddot{\xi}_k - \omega^2\xi_k)\sin\psi_k + 2\omega\dot{\xi}_k\cos\psi_k].$$

This equation is conveniently written in the form

$$\ddot{x} + 2n_0\dot{x} + p_0^2x = \frac{S_{v.h}}{M}\sum_{k=1}^{n}[(\ddot{\xi}_k - \omega^2\xi_k)\sin\psi_k + 2\omega\dot{\xi}_k\cos\psi_k],$$

where the quantity

$$M = m_0 + nm_b \tag{1.13}$$

represents the total mass of the system, while n_0 is the relative damping coefficient of the elastic base, determined by the formula

$$n_0 = \frac{\kappa}{2M}, \tag{1.14}$$

and the quantity p_0 represents the angular frequency of natural vibrations of a rigid rotor (without drag hinges) on an elastic base and is determined by the formula

$$p_0^2 = \frac{c}{M}. \tag{1.15}$$

We will now write the system of equations of motion of a rotor on an elastic base, consisting of the equations of motion of the blades [eq.(1.8)] and the equation of motion of the casing of the base:

$$\left.\begin{aligned}\ddot{\xi}_k + 2n_b\dot{\xi} + (p_{b_0}^2 + \nu_0^2\omega^2)\xi_k &= \frac{\nu_0^2}{l_{v.h}}\ddot{x}\sin\psi_k;\\ \ddot{x} + 2n_0\dot{x} + p_0^2x &= \frac{S_{v.h}}{M}\sum_{k=1}^{n}[(\ddot{\xi}_k - \omega^2\xi_k)\sin\psi_k + 2\omega\dot{\xi}_k\cos\psi_k],\end{aligned}\right\} \tag{1.16}$$

where k = 1, 2, ..., n.

Thus, the equations of small vibrations of a rotor on an elastic base represent a homogeneous system of (n + 1) linear differential equations with periodic coefficients for determining (n + 1) unknown functions $x(t)$, $\xi_k(t)$ (where k = = 1, 2, ..., n).

2. Stability Analysis and Basic Results

Investigations conducted by Coleman (Ref.35) and B.Ya.Zherebtsov showed that, for a rotor with a number of blades $n \geq 3$, this system of equations can be reduced to a system of linear equations with constant coefficients, if we replace $\xi_k(t)$ by new variables $x_c(t)$ and $z_c(t)$ representing the coordinates of the center of gravity of the blade system. In the case of a two-blade rotor, eqs.(1.16) cannot be reduced to equations with constants. An investigation of the stability of motion of a two-blade rotor on an elastic base is quite complex. Its presentation can be found elsewhere (Ref.36). B.Ya.Zherebtsov studied also the case of a two-blade rotor on an isotropic elastic support when the /257 casing of this support had two degrees of freedom - in direction of the Ox- and Oz-axes (see Fig.3.2) - and the stiffness of the base in both directions was identical. In this exceptional case, the problem is easily reduced to a system of equations with constants.

Here, we will investigate the stability of a rotor with a number of blades $n \geq 3$, which is of the greatest practical value.

In order to obtain the equations of motion with constant coefficients, we will transform eqs.(1.16) to the new variables $x(t)$, $\eta(t)$, $\zeta(t)$ related with the previous formulas:

$$\left.\begin{aligned} \eta &= \sum_{k=1}^{n} \xi_k \sin \psi_k; \\ \zeta &= \sum_{k=1}^{n} \xi_k \cos \psi_k. \end{aligned}\right\} \tag{1.17}$$

The new quantities η and ζ, as is apparent from eqs.(1.12), are equal - with an accuracy to within the constant factor ρ_c/n - to the coordinates of the center of gravity of the blade system in a moving coordinate system x'Az' whose axes are parallel to the Ox- and Oz-axes of the fixed system, while the origin of the coordinates A coincides with the center of the rotor (see Fig.3.2).

To derive the equations of motion in the new variables, all equations of motion of the blades [the first equation of the system (1.16)] must first be multiplied by $\cos \psi_k$ followed by addition of their left- and right-hand sides from k = 1 to k = n; multiplication is then performed by $\sin \psi_k$ again followed by addition. Here, it must be noted that, for a rotor with a number of blades $n \geq 3$, we have by virtue of eqs.(1.13) of Chapter II:

$$\left.\sum_{k=1}^{n} \sin \psi_k \cos \psi_k = 0;\right\} \tag{1.18}$$

$$\sum_{k=1}^{n} \sin^2 \psi_k = \frac{n}{2}.$$

Furthermore,

$$\left.\begin{aligned}
&\sum_{k=1}^{n} \dot{\xi}_k \sin \psi_k = \dot{\eta} - \omega\zeta;\\
&\sum_{k=1}^{n} \dot{\xi}_k \cos \psi_k = \dot{\zeta} + \omega\eta;\\
&\sum_{k=1}^{n} \ddot{\xi}_k \sin \psi_k = \ddot{\eta} - 2\omega\dot{\zeta} - \omega^2\eta;\\
&\sum_{k=1}^{n} \ddot{\xi}_k \cos \psi_k = \ddot{\zeta} + 2\omega\dot{\eta} - \omega^2\zeta.
\end{aligned}\right\} \qquad (1.19)$$

The last formulas are obtained by successive differentiation of eqs.(1.17).

This results in the following system of equations:

$$\left.\begin{aligned}
&\ddot{x} + 2n_0\dot{x} + p_0^2 x - \frac{S_{v.h}}{M}\ddot{\eta} = 0;\\
&\ddot{\eta} + 2n_b\dot{\eta} - [\omega^2(1-\nu_0^2) - p_{b_0}^2]\eta - 2\omega\dot{\zeta} - 2n_b\omega\zeta -\\
&\quad - \frac{n}{2}\cdot\frac{S_{v.h}}{I_{v.h}}\ddot{x} = 0;\\
&\ddot{\zeta} + 2n_b\dot{\zeta} - [\omega^2(1-\nu_0^2) - p_{b_0}^2]\zeta + 2\omega\dot{\eta} + 2n_b\omega\eta = 0.
\end{aligned}\right\} \qquad (1.20)$$

/258

Thus, we obtain a homogeneous system of three linear differential equations of the second order with constant coefficients relative to three unknown functions $x(t)$, $\eta(t)$, and $\zeta(t)$.

Now, the stability analysis of the system can be carried out in the conventional manner.

Let us put

$$\begin{aligned}
x &= x_0 e^{\lambda t};\\
\eta &= \eta_0 e^{\lambda t};\\
\zeta &= \zeta_0 e^{\lambda t},
\end{aligned}$$

where x_0, η_0, and ζ_0 are certain constants.

Substituting these expressions into eqs.(1.20), we obtain a system of three algebraic linear homogeneous equations for determining the quantities x_0, η_0, and ζ_0. Equating the determinant of this system to zero, we obtain the characteristic equation for determining λ. On expanding this equation in powers of λ, we obtain

$$\lambda^6 + a\lambda^5 + b\lambda^4 + c\lambda^2 + e\lambda + f = 0, \qquad (1.21)$$

Here and below, we introduce the following notations:

$$\left.\begin{aligned}\bar{\lambda}&=\frac{\lambda}{p_0};\\ \bar{\omega}&=\frac{\omega}{p_0};\\ \bar{p}_{b_0}&=\frac{p_{b_0}}{p_0}.\end{aligned}\right\} \tag{1.22}$$

$$\left.\begin{aligned}a&=A_0;\\ b&=B_0+B_1\bar{\omega}^2;\\ c&=C_0+C_1\bar{\omega}^2;\\ d&=D_0+D_1\bar{\omega}^2+D_2\bar{\omega}^4;\\ e&=E_0+E_1\bar{\omega}^2+E_2\bar{\omega}^4;\\ f&=F_0+F_1\bar{\omega}^2+F_2\bar{\omega}^4.\end{aligned}\right\} \tag{1.23}$$

$$\left.\begin{aligned}A_0&=\frac{2}{1-\varepsilon}\left[\bar{n}_0+\bar{n}_b(2-\varepsilon)\right];\\ B_0&=\frac{1}{1-\varepsilon}\left[1+8\bar{n}_0\bar{n}_b+4\bar{n}_b^2+\bar{p}_{b_0}^2(2-\varepsilon)\right];\\ B_1&=\frac{1}{1-\varepsilon}\left[4-(2-\varepsilon)(1-\nu_0^2)\right];\\ C_0&=\frac{4}{1-\varepsilon}\left[\bar{n}_b+2\bar{n}_0\bar{n}_b^2+(\bar{n}_0+\bar{n}_b)\,\bar{p}_{b_0}^2\right];\\ C_1&=\frac{4}{1-\varepsilon}\left[\bar{n}_0+\bar{n}_b\right](1+\nu_0^2);\\ D_0&=\frac{1}{1-\varepsilon}\left[4\bar{n}_b^2+\bar{p}_{b_0}^4+2(1+4\bar{n}_0\bar{n}_b)\,\bar{p}_{b_0}^2\right];\\ D_1&=\frac{2}{1-\varepsilon}\left[2\bar{n}_b^2+(1+\nu_0^2)(1+4\bar{n}_0\bar{n}_b)-\bar{p}_{b_0}^2(1-\nu_0^2)\right];\\ D_2&=\frac{(1-\nu_0^2)^2}{1-\varepsilon};\\ E_0&=\frac{2}{1-\varepsilon}(2\bar{n}_b\bar{p}_{b_0}^2+\bar{n}_0\bar{p}_{b_0}^4);\\ E_1&=\frac{2}{1-\varepsilon}\left[4\bar{n}_0\bar{n}_b^2+2\bar{n}_b(1+\nu_0^2)-2\bar{p}_{b_0}^2\bar{n}_0(1-\nu_0^2)\right];\\ E_2&=\frac{2\bar{n}_0(1-\nu_0^2)^2}{1-\varepsilon};\\ F_0&=\frac{\bar{p}_{b_0}^4}{1-\varepsilon};\\ F_1&=\frac{1}{1-\varepsilon}\left[4\bar{n}_b^2-2\bar{p}_{b_0}^2(1-\nu_0^2)\right];\\ F_2&=\frac{(1-\nu_0^2)^2}{1-\varepsilon}.\end{aligned}\right\} \tag{1.24}$$

/259

The dimensionless coefficients of damping $\bar{n}_0$ (of an elastic base) and $\bar{n}_b$ (blade) are determined by means of

$$\left.\begin{aligned}\bar{n}_0 &= \frac{n_0}{p_0},\\ \bar{n}_b &= \frac{n_b}{p_0}.\end{aligned}\right\} \tag{1.25}$$

The dimensionless coefficient ε is obtained from the formula:

$$\varepsilon = \frac{n}{2}\,\frac{S_{v.h}^2}{I_{v.h}\,M}. \tag{1.26}$$

It is easy to explain the mechanical meaning of this important coefficient. The quantities $S_{v.h}$ and $I_{v.h}$ can be written in the form

$$\begin{aligned}S_{v.h} &= m_b\varrho_c;\\ I_{v.h} &= m_b\varrho_i^2.\end{aligned}$$

where $\rho_i = \sqrt{\frac{I_{v.h}}{m_b}}$ is the radius of inertia of the blade relative to the drag hinge. Therefore, eq.(1.26) can be rewritten as

$$\varepsilon = \frac{1}{2}\,\frac{nm_b}{m_0 + nm_b}\left(\frac{\varrho_c}{\varrho_i}\right)^2. \tag{1.27}$$

The quantity ρ_c/ρ_i depends upon the law of mass distribution over the blade length and, for different blades, lies within the narrow limits of $\rho_c/\rho_i \approx$ $\approx 0.8 - 0.9$.

Consequently, it can be assumed in first approximation that the quantity ε is proportional to the ratio of the total blade mass to the total system mass (mass of the elastic base casing plus mass of the blades) and thus can be called the relative rotor mass.

A detailed analysis of the characteristic equation shows that only oscillatory instability is possible in the system while aperiodic instability is impossible (Ref.35). The boundaries of the zones of oscillatory instability (corresponding values of $\bar{\omega}$) can be found in the following manner: At the boundary of the zone of instability there are purely harmonic (not damped and not increasing) vibrations, which furnishes a purely imaginary value of one of the roots of the characteristic equation (1.21). Setting, in this equation, $\bar{\lambda} = i\bar{p}$ (where $\bar{p}$ is a real quantity) and equating to zero the real and imaginary parts, we obtain the following equations: /260

$$\left.\begin{aligned}a\bar{p}^4 - c\bar{p}^2 + e &= 0;\\ \bar{p}^6 - b\bar{p}^4 + d\bar{p}^2 - f &= 0.\end{aligned}\right\} \tag{1.28}$$

Since the coefficients a, b, c, d, e, and f are known functions of $\bar{\omega}$ [see eqs.(1.23) and (1.24)], we can regard eqs.(1.28) as a system of two equations with two unknowns $\bar{p}$ and $\bar{\omega}$. The values of $\bar{\omega}$ and $\bar{p}$, being the solution of the system (1.28), represent the dimensionless angular velocity $\bar{\omega}$ of rotor rotation at which harmonic vibrations of the system are possible, and the corresponding dimensionless angular vibration frequency $\bar{p}$.

We can solve the system (1.28) by making use of the fact that the first equation of the system (1.28) is biquadratic with respect to $\bar{p}$. Prescribing different values of $\bar{\omega}$, we can determine $\bar{p}$ from this equation followed by calculation of the value of a certain quantity $D(\bar{\omega})$ equal to the left-hand side of the second equation of the system (1.28) at this value of $\bar{p}$:

$$D(\bar{\omega}) = \bar{p}^6 - b\bar{p}^4 + d\bar{p}^2 - f. \tag{1.29}$$

From the results of this calculation, a curve for the dependence of D on $\bar{\omega}$ can be plotted. The values of $\bar{\omega}$ at which D vanishes will also be the boundaries of the instability zone. We can demonstrate that the values of $\bar{\omega}$, at which $D > 0$, correspond to steady motion of the system while the values of $\bar{\omega}$, at which $D < 0$, correspond to unsteady motion.

Calculation of the unstable range is quite laborious and, for all practical purposes, can be performed only on digital computers. Figures 3.3 - 3.12 show certain results of such calculations carried out by engineer V.G.Pashkin on the digital computer "Strela". The graphs permit determining the stability boundaries and the damping margins.

The stability of the system is determined in general by the following five parameters: ν_0, ϵ, $\bar{p}_{b_0}$, $\bar{n}_0$, $\bar{n}_b$. The graphs are plotted for the two most frequently encountered values $\nu_0 = 0.25$ and $\nu_0 = 0.3$. Here, the value of $\bar{p}_{b_0} = 0$, i.e., for a rotor with drag hinge dampers, is examined. Elastic elements are absent. The effect of elastic elements will be discussed later in the text. For each of the values of ν_0 there is a series of graphs corresponding to different values of ϵ. The abscissa of each graph gives the values of the dimensionless angular velocity $\bar{\omega}$ corresponding to the boundaries of the instability zone, while the ordinate gives the dimenionless coefficient $\bar{n}_b$ of blade damping at which the instability zone is obtained. The graphs are constructed for different values $\bar{n}_0$ of the dimensionless damping coefficient of an elastic base.

As shown by these graphs, the width of the instability zone substantially depends upon the damping coefficients $\bar{n}_b$ and $\bar{n}_0$. On an increase in damping $\bar{n}_b$ (at fixed $\bar{n}_0$) the unstable range narrows and, at a certain critical value $\bar{n}_b^*$, contracts into a point. At a value $\bar{n}_b > \bar{n}_b^*$, the instability zone is absent at all values of $\bar{\omega}$. For example, at $\epsilon = 0.02$, $\nu_0 = 0.25$ (see Fig.3.3), if $\bar{n}_0 = 0.06$, the instability zone contracts to a point as soon as $\bar{n}_b = 0.128$; at $\bar{n}_b > 0.128$, the system is stable for any $\bar{\omega}$ (in this case, $\bar{n}_b^* = 0.128$).

The ratio $\delta = \dfrac{\bar{n}_b}{\bar{n}_b^*}$, whenever it is greater than unity, is conveniently called the damping margin. /266

The value of $\bar{\omega}$ at which the instability zone contracts to a point is called

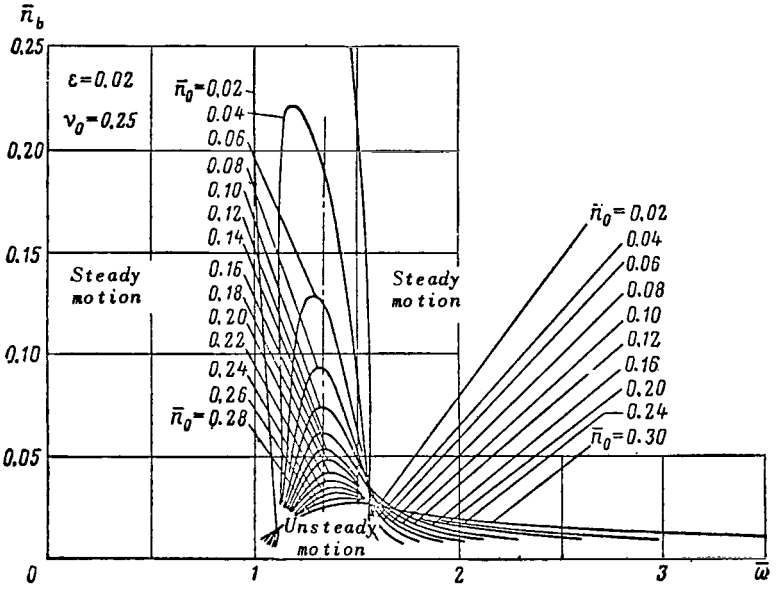

Fig.3.3 Graphs for Determining Instability Boundaries ($\varepsilon = 0.02$; $\nu_0 = 0.25$).

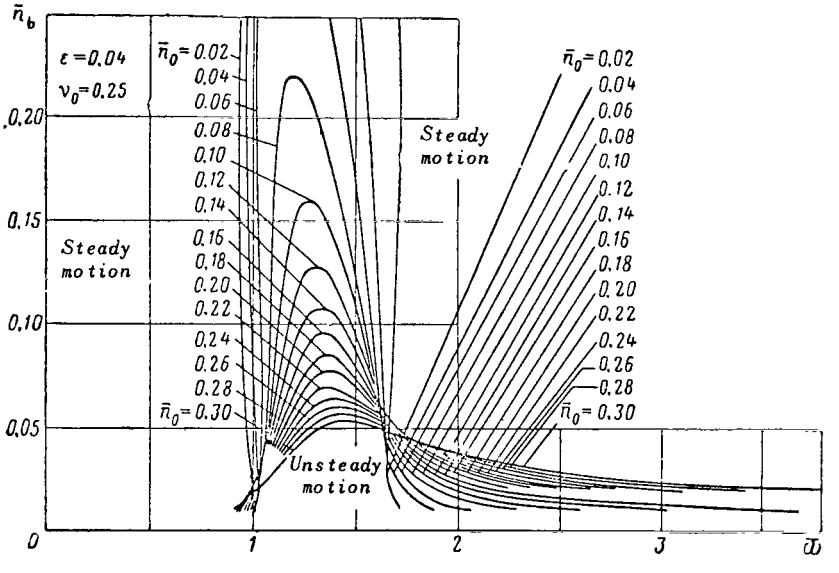

Fig.3.4 Graphs for Determining Instability Boundaries ($\varepsilon = 0.04$; $\nu_0 = 0.25$).

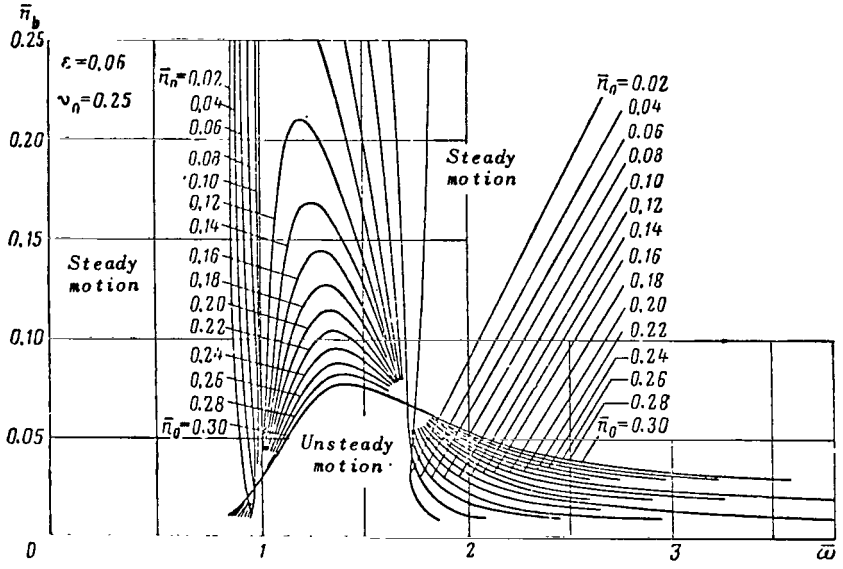

Fig.3.5 Graphs for Determining Instability Boundaries (ε = 0.06; ν_0 = 0.25).

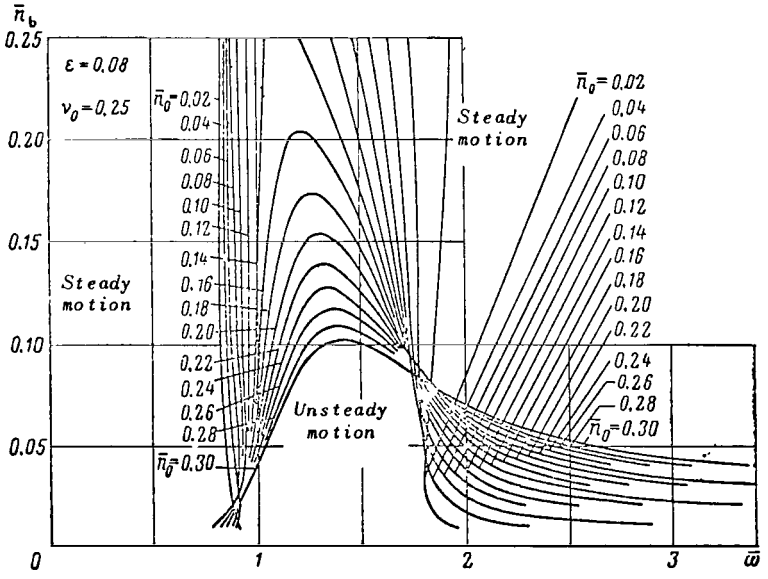

Fig.3.6 Graphs for Determining Instability Boundaries (ε = 0.08; ν_0 = 0.25).

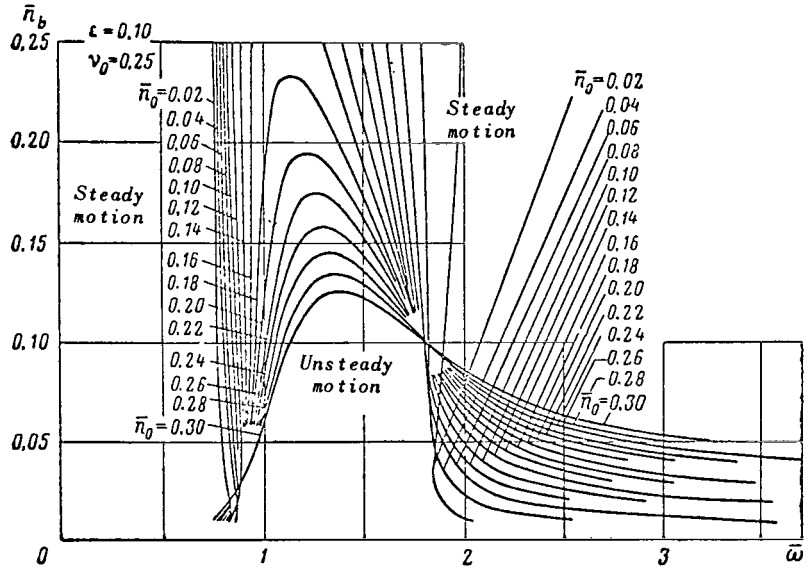

Fig.3.7 Graphs for Determining Instability Boundaries (ε = 0.10; ν_0 = 0.25).

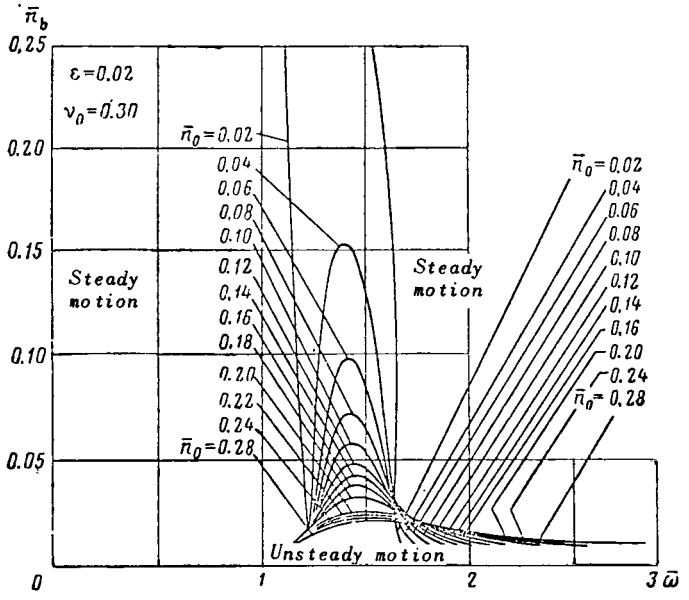

Fig.3.8 Graphs for Determining Instability Boundaries (ε = 0.02; ν_0 = 0.30).

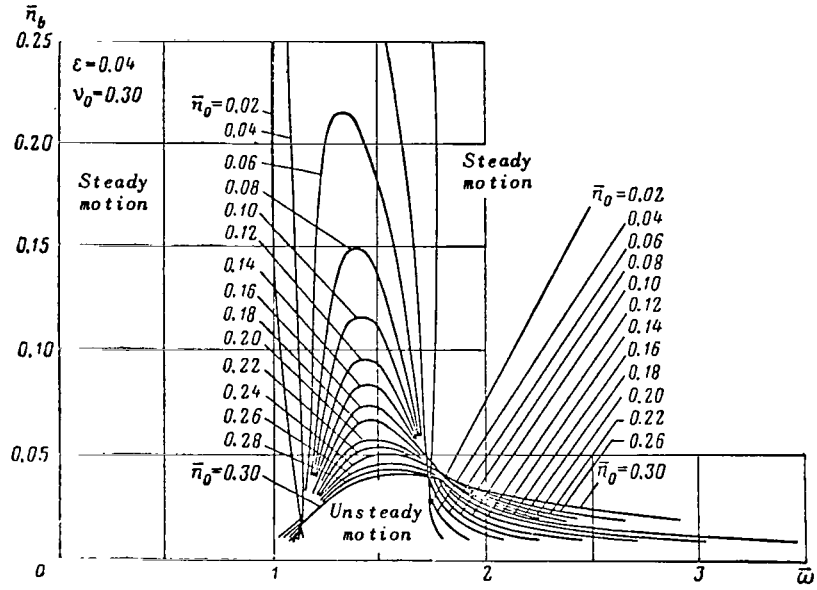

Fig.3.9 Graphs for Determining Instability Boundaries ($\varepsilon = 0.04$; $\nu_0 = 0.30$).

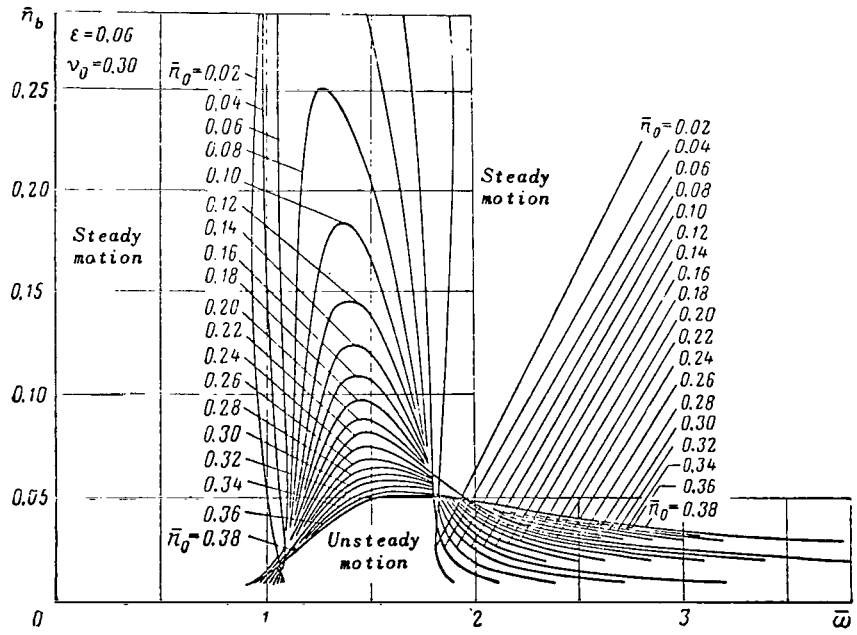

Fig.3.10 Graphs for Determining Instability Boundaries ($\varepsilon = 0.06$; $\nu_0 = 0.30$).

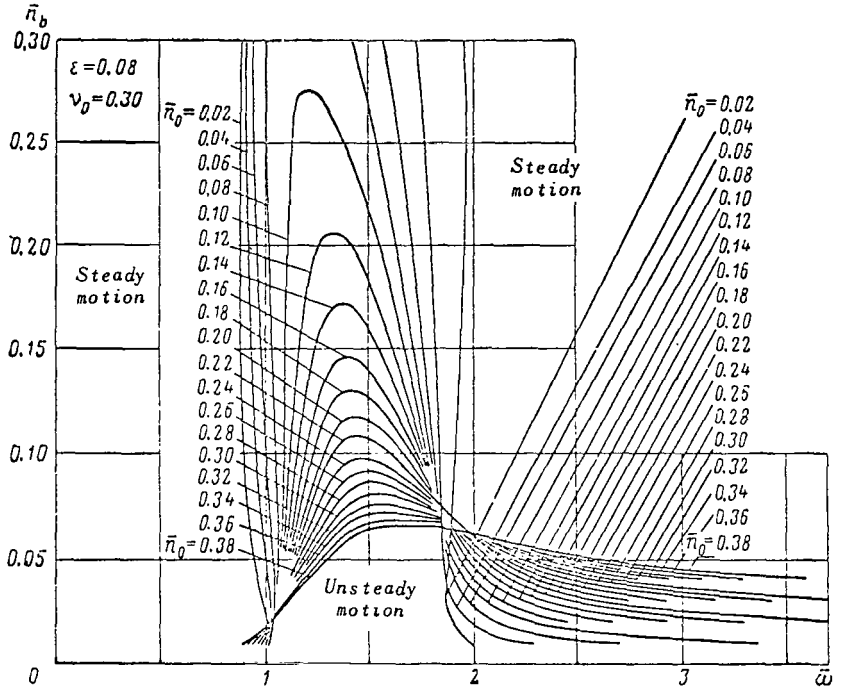

Fig.3.11 Graphs for Determining Instability Boundaries ($\varepsilon = 0.08$; $\nu_0 = 0.30$).

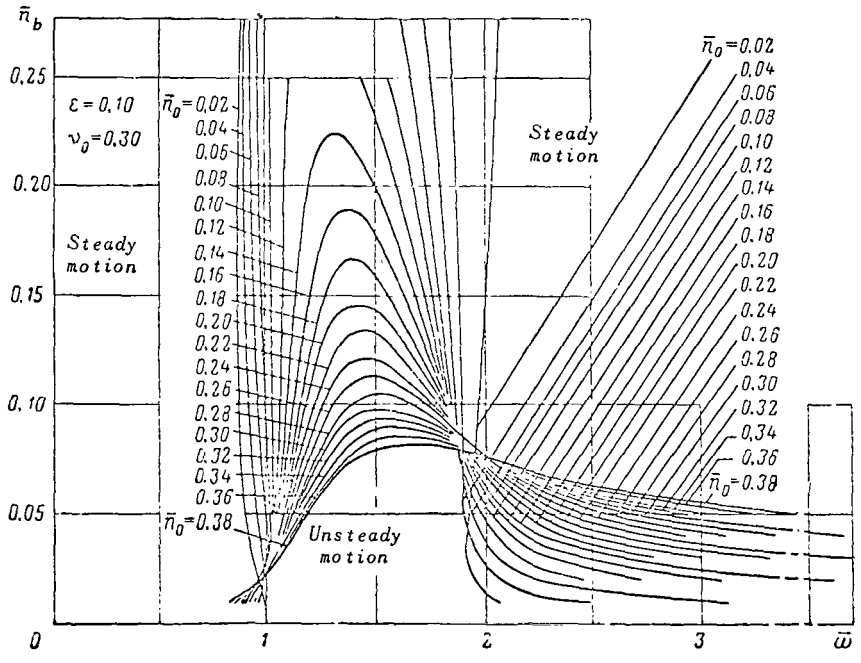

Fig.3.12 Graphs for Determining Instability Boundaries ($\varepsilon = 0.10$; $\nu_0 = 0.30$).

the critical value and can be calculated by means of the approximate formula:

$$\bar{\omega}_{cr} = \frac{1}{1 - \nu_0}.$$

Below, we will give a physically clear elucidation of this formula.

It should be noted that an increase in the quantity $\bar{n}_b$ does not always lead to an improvement of stability. At low values of $\bar{n}_0$ (this can be traced from the graphs), an increase in $\bar{n}_b$ may even lead to a small displacement of the lower boundary of the instability zone toward smaller values of $\bar{\omega}$. This might result in the appearance of instability at values of $\bar{\omega}$ for which the motion was steady at smaller $\bar{n}_b$.

An increase in damping $\bar{n}_0$ of the elastic base at moderate values of $\bar{n}_b$ also leads to an improvement of stability; however, at very low values of $\bar{n}_b$ an increase in $\bar{n}_0$ may lead to a rightward shift of the upper boundary of the instability zone and thus to a broadening of the zone itself.

An analysis of the graphs permits the following important conclusion: Whenever the quantities $\bar{n}_b$ and $\bar{n}_0$ are of the same order of magnitude and differ to one or the other side by not more than a factor of 2 - 3, any increase in damping $\bar{n}_b$ or $\bar{n}_0$ will result only in an increase of stability. At such values of $\bar{n}_b$ and $\bar{n}_0$, the greatest required damping occurs approximately at

$$\bar{\omega} = \bar{\omega}_{cr} = \frac{1}{1 - \nu_0}.$$

For this quite important practical case, B.Ya.Zherebtsov's simple approximate formula* can be derived, which shows that the damping margin is proportional to the product of the quantities $\bar{n}_b$ and $\bar{n}_0$. This formula yields the values of the product $\bar{n}_b\bar{n}_0$ at which the instability zone contracts to a point:

$$\bar{n}_b\bar{n}_0 = \frac{\varepsilon(1 - \nu_0)}{8\nu_0}. \tag{1.30}$$

This approximate formula holds only at $\bar{p}_{b_0} = 0$; its validity can be traced from the graphs. At $\bar{p}_{b_0} \neq 0$, we can use another approximate formula:

$$\bar{n}_b\bar{n}_0 = \frac{\varepsilon(1 - \nu_0)}{8 \cdot \nu_0}\Delta, \tag{1.31}$$

where the dimensionless quantity Δ is determined from the formula

---

* This formula will be derived in Section 3. Equation (1.31) will also be constructed there.

$$\Delta = \frac{1+\nu_0}{\nu_0 + \sqrt{1+\bar{p}_{b_0}^2\left(\frac{1-\nu_0^2}{\nu_0^2}\right)}}. \qquad (1.32)$$

Figure 3.13 shows the dependence of Δ on $\bar{p}_{b_0}$, for $\nu_0 = 0.25$. The graph indicates that the required damping can be substantially reduced by introducing an elastic element in the drag hinge of the rotor. An improvement in stability of the system by an increase in $\bar{p}_{b_0}$ is illustrated also by the series of graphs in Fig.3.14. /267

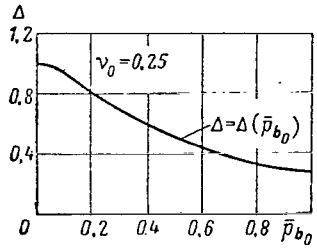

Fig.3.13 Effect of Elasticity of the Drag Hinge on Required Damping.

However, when introducing an elastic element into the design of the drag hinge or when introducing so-called elastic interblade couplings, it is necessary to recall that the bending moment acting on the blade root in flight is generated both by the damper and by the elastic element in the drag hinge. Therefore, upon increasing the rigidity of the elastic element (on increasing $\bar{p}_{b_0}$) the moment exerted on the blade by the elastic element (or interblade couplings) will increase simultaneously with a decrease in the required moment produced by the damper. The optimal value of $\bar{p}_{b_0}$ should be considered that value at which the bending moment acting on the blade in flight will be minimum, at constant damping margin with respect to ground resonance. This optimal value of $\bar{p}_{b_0}$ depends on $\bar{n}_0$ and should be separately selected for each helicopter. For more details, see Section 6.

3. Physical Picture of Rotor Behavior in the Presence of Ground Resonance

To elucidate the physical picture of rotor behavior in the presence of ground resonance, let us examine the following problem:

Let the casing of the elastic base (Fig.3.1) execute harmonic vibrations according to the prescribed law: /268

$$x = x_0 \sin pt, \qquad (1.33)$$

where x_0 and p are the vibration amplitude and frequency of the casing.

Let us examine forced blade vibrations during such movement of the casing. The equation of motion (1.8) of the k-th rotor blade will take the following form in this case:

$$\ddot{\xi}_k + 2n_b\dot{\xi}_k + (p_{b_0}^2 + \nu_0^2\omega^2)\xi_k = \\ = -\frac{\nu_0^2}{I_{y.h}} p^2 x_0 \sin pt \sin\psi_k. \qquad (1.34)$$

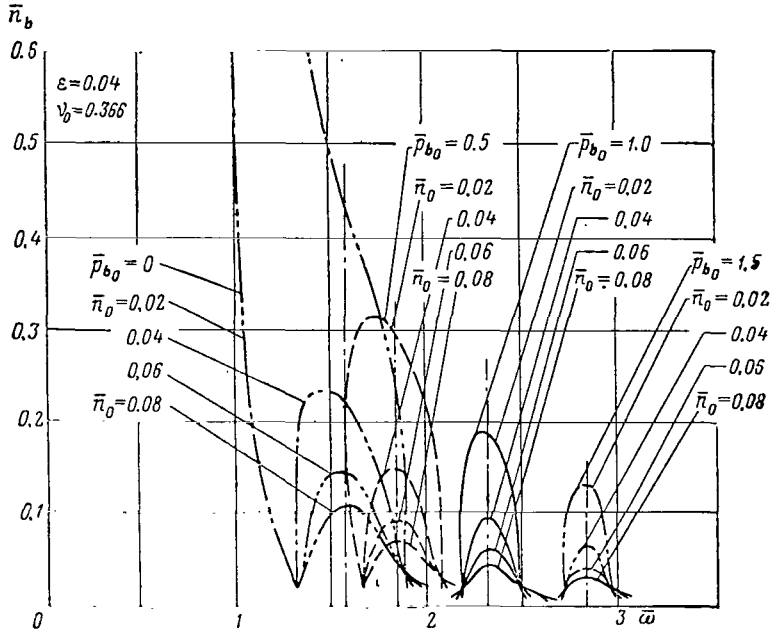

Fig.3.14 Graphs Illustrating the Effect of Elasticity of the Drag Hinge ($\varepsilon = 0.04$; $\nu_0 = 0.366$).

Considering that $\psi_k = \omega t + \frac{2\pi}{n} k$ ($k = 1, 2, \ldots, n$) and representing the right-hand side of this equation as two harmonics, we can write the equation in the form

$$\ddot{\xi}_k + 2n_b\dot{\xi}_k + (p_{b_0}^2 + \nu_0^2\omega^2)\xi_k = \\ = -\frac{\nu_0^2}{2I_{v.h}} p^2 x_0 \left\{\cos\left[(\omega - p)t + \frac{2\pi}{n} k\right] - \cos\left[(\omega + p)t + \frac{2\pi}{n} k\right]\right\}. \quad (1.35)$$

This is the conventional equation of forced vibrations of a system with one degree of freedom.

The right-hand side of eq.(1.35) represents the exciting force which, in this case, consists of two components, each of which represents a load varying by a simple harmonic law with a frequency equal to (ω - p) or (ω + p), respectively. By virtue of the linearity of eq.(1.35), the blade vibrations due to each of these loads can be examined independently. The forced (steady) vibrations of the blade will take place in obedience to the law:

$$\xi_k(t) = \xi_1 \cos[(\omega + p)t + \varphi_1] + \xi_2 \cos[(\omega + p)t + \varphi_2], \quad (1.36)$$

where ξ_1, ξ_2, φ_1, φ_2, are certain constants that are readily determined from eq.(1.35).

Thus, during vibrations of the casing of the elastic base according to a simple harmonic law with a frequency p, the rotor blades will execute forced vibrations with two combined frequencies ($\omega + p$) and ($\omega - p$) depending upon the angular velocity ω of rotor rotation.

The most intense blade vibrations occur at resonance, when one of the excitation frequencies ($p + \omega$) or ($p - \omega$) is close to the natural vibration frequency of the blade $p_b = \sqrt{p_{b_0}^2 + \nu_0^2\omega^2}$.

Let us first examine the case of resonance when

$$\sqrt{p_{b_0}^2 + \nu_0^2\omega^2} = |p - \omega|. \tag{1.37}$$

In this case, the quantity ξ_1 in eq.(1.36) will be appreciably greater than the quantity ξ_2, so that we can neglect the second term in eq.(1.36). With this simplification and with the condition (1.37), the law of motion of the blade will have the form

$$\xi_k = \xi_0 \sin\left[(p-\omega)t - \frac{2\pi}{n}k\right], \tag{1.38}$$

where

$$\xi_0 = \frac{\nu_0^2 p^2}{4 l_{v.h}\, n_b (\omega - p)}\, x_0. \tag{1.39}$$

Let us next calculate the force P_x exerted on the casing of the elastic base by the inertia of the rotor blades vibrating in this mode. For this, let us find the displacement of the center of gravity of the blade system by means of eq.(1.12). Substituting into these formulas eq.(1.38) for ξ_k and taking into account that /269

$$\sum_{k=1}^{n} \cos\left[(2\omega - p)t + \frac{4\pi}{n}k\right] = 0$$

and

$$\sum_{k=1}^{n} \sin\left[(2\omega - p)t + \frac{4\pi}{n}k\right] = 0,$$

easy transformations will yield the following law of motion of the center of gravity of the blade system:

$$\left.\begin{aligned} x_c &= x + \frac{Q_c}{2}\xi_0 \cos pt; \\ z_c &= \frac{Q_c}{2}\xi_0 \sin pt. \end{aligned}\right\} \tag{1.40}$$

If we take into account that the coordinates of the center of gravity in

the coordinate system $x'Az'$ referring to the casing are expressed by the formulas $x'_c = x_c - x$ and $z'_c = z_c$, then the center of gravity of the system of blades in this coordinate system moves in accordance with the law:

$$\left.\begin{aligned} x'_c &= \frac{1}{2}\varrho_c\xi_0\cos pt; \\ z'_c &= \frac{1}{2}\varrho_c\xi_0\sin pt. \end{aligned}\right\} \qquad (1.41)$$

Thus, at resonance when the equality (1.37) is satisfied, the center of gravity of the blade system describes, in the coordinate system fixed with respect to the casing, a circle of radius $\frac{1}{2}\rho_c\xi_0$. In this case, the angular velocity of its rotation with respect to this circle is equal to the frequency p of the given vibrations of the casing.

Let us then determine the force P_x acting on the casing, by means of the formula $P_x = -nm_b\ddot{x}_c$. Here, we obtain the following expression:

$$P_x = +nm_bp^2\left[x_0 + \frac{\varrho_c}{2}\xi_0\right]\cos pt.$$

Substituting here the expression for ξ_0 from eq.(1.39), we obtain

$$P_x = nm_bp^2\left[1 + \frac{\varrho_c}{8}\frac{v_0^2p^2}{l_{v.h}\,n_b(\omega - p)}\right]x_0\cos pt. \qquad (1.42)$$

Thus, during vibrations of the casing by the harmonic law [eq.(1.33)] and under the condition of blade resonance [eq.(1.37)], the force exerted on the casing by the vibrating blades varies in time by a harmonic law with the same frequency p, with a vibration phase $\pi/2$ (with respect to the vibrations of the casing) and is proportional to the azimuth x_0 of the vibrations of the casing.

Equation (1.42) can also be represented in the form

$$P_x = -nm_b\ddot{x} + nm_bp^2\,\frac{\varrho_c}{8}\cdot\frac{v_0^2p^2}{l_{v.h}\cdot n_b(\omega - p)}x_0\cos pt.$$

On deriving the equation of the casing (1.2) under the effect of the force P_x given by such an expression, we obtain /270

$$m_0x + 2\kappa\dot{x} + c\dot{x} = -nm_b\ddot{x} + nm_bp^2\,\frac{\varrho_c}{8}\,\frac{v_0^2p^2}{l_{v.h}\,n_b(\omega - p)}x_0\cos pt.$$

Using our previously adopted notations, this equation can be written as

$$\ddot{x}+2n_0\dot{x}+p_0^2x=\frac{nm_bp^2}{m_0+nm_b}\,\frac{Q_c}{8}\cdot\frac{v_0^2p^2}{l_{v.h}\,n_b(\omega-p)}x_0\cos pt. \tag{1.43}$$

If it were possible to find the parameters of the system at which the law of motion of the casing [eq.(1.33)] satisfies this equation, this would mean that, at such system parameters, purely harmonic motion (undamped vibrations) with a frequency p would be possible. Substituting eq.(1.33) into eq.(1.43), it is easy to demonstrate that this is obtained when the following two conditions are satisfied:

$$\left.\begin{aligned} &p=p_0;\\ &\bar{n}_0\bar{n}_b=\frac{\varepsilon p_0}{8(\omega-p_0)}. \end{aligned}\right\} \tag{1.44}$$

Furthermore, it should be recalled that eq.(1.43) was derived from the condition of blade resonance, i.e., under the condition (1.37) which, taking $p_0 = p$ into account, can be written in the form

$$\sqrt{p_{b_0}^2+v_0^2\omega^2}=|p_0-\omega|. \tag{1.45}$$

From this equation, one can determine the value of the critical angular velocity ω_{cr} of rotor rotation at which undamped vibrations in the system are possible.

Equation (1.44) gives the value of the product $\bar{n}_0\bar{n}_b$ at which undamped vibrations are possible; then, as now is obvious, this formula together with the condition (1.45) will yield the approximate formula (1.31).

Thus, undamped vibrations are possible only at a value of ω at which two resonances occur simultaneously: resonance of the blade [condition (1.45)] and resonance of the elastic base $p = p_0$. At such a value of ω and on satisfying the condition (1.44), the natural vibrations of the rotor on an elastic base can be sustained by a variable exciting force generated by the vibrating blades, which here are in a state of resonance.

A study of eq.(1.35) shows that blade resonance is possible in two cases, namely: when one of the combined frequencies $(p + \omega)$ or $(p - \omega)$ coincides with the natural frequency of blade vibrations, i.e.,

$$p_b=|p-\omega|$$

and when

$$p_b=|p+\omega|.$$

Of these two cases, we examined only the first. For the second case, all derived formulas are obtained in the same manner except that, in all expressions, the quantity ω is replaced by the quantity $-\omega$, including also in eqs.(1.44). This expression shows that, at $p_b = |p + \omega|$, undamped vibrations are possible

only if $\bar{n}_0\bar{n}_b < 0$, meaning that in this case one of the quantities $\bar{n}_0$ and $\bar{n}_b$ should be negative. Consequently, ground resonance is possible only at $p_b = |p - \omega|$ and impossible at $p_b = |p + \omega|$.

Let us next peruse the resonance diagram (Fig.3.15). This diagram gives /271 the curve of the natural blade frequency p_b as a function of the angular velocity ω, with superposition of the straight lines $p = p_0 + \omega$ and $p = |p_0 - \omega|$. The diagram is plotted for the case of $p_{b_0} < p_0$.

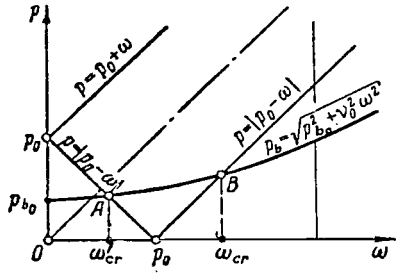

Fig.3.15 Resonance Diagram.

As we see from the diagram, there are two values of ω at which the condition $p_b = |p_0 - \omega|$, corresponding to the points A and B, is satisfied. For the point A, we have the condition $p_b = p_0 - \omega$ and, for the point B, the condition $p_b = \omega - p_0$.

Thus, in the first case $\omega < p_0$ and in the second, $\omega > p_0$. Turning to the second condition of the system (1.44), we see that it can be satisfied (at positive values of $\bar{n}_0$ and $\bar{n}_b$) only for $\omega > p_0$. Consequently, of the two possible values of ω at which blade resonance is possible, only one ($\omega > p_0$) can correspond to undamped vibrations of the system.

Let us determine this value of ω and call it (ω_{cr}) critical. Solving eq.(1.45) relative to ω and discarding one of the obtained values ($\omega < p_0$), we find

$$\omega_{cr} = p_0 \frac{1 + \sqrt{\nu_0^2 + \bar{p}_{b_0}^2(1 - \nu_0^2)}}{1 - \nu_0^2}. \qquad (1.46)$$

At $\bar{p}_{b_0} = 0$ we obtain the formula

$$\omega_{cr} = \frac{p_0}{1 - \nu_0}. \qquad (1.47)$$

Substituting the value of ω_{cr} from eq.(1.46) into the second condition of the system (1.44), we find

$$\bar{n}_0\bar{n}_b = \frac{\varepsilon(1 - \nu_0)}{8\nu_0}\Delta,$$

where

$$\Delta = \frac{1 + \nu_0}{\nu_0 + \sqrt{1 + \bar{p}_{b_0}^2\left(\frac{1 - \nu_0^2}{\nu_0^2}\right)}}.$$

These formulas exactly coincide with the approximate equations (1.31) and (1.32).

The reasonings set forth here, together with the stability analysis given in Section 2, permit to state: The condition $\bar{n}_0 \bar{n}_b > \frac{\varepsilon(1-\nu_0)}{8\nu_0}\Delta$ always provides stability at the critical angular velocity of rotor rotation determined by eq.(1.46). However, as indicated in the analysis of the graphs in Figs.3.3 to 3.12, this condition holds only when the quantities $\bar{n}_b$ and $\bar{n}_0$ are of the same order of magnitude. This means that ensurance of stability at $\omega = \omega_{cr}$ does not definitely ensure stability at any ω.

4. Rotor on an Isotropic Elastic Base

The theory of stability of a rotor on an elastic base presented in this Section holds only if the number of rotor blades $n \geq 3$ and if the elastic base has only one degree of freedom, namely motion along the Ox-axis (Fig.3.2). /272

However, an analogous stability theory can be constructed also for the more general case where the elastic base has two degrees of freedom: displacement along the axes Ox and Oz. A stability analysis for this more complex system is rather cumbersome. On the other hand, in practical application one can almost always use the formulas for the case of an elastic base with one degree of freedom. Thus, this can be done whenever the natural longitudinal and lateral vibration frequencies of the helicopter on an elastic landing gear (see Sect.5) are far apart.

It is of interest to give a few simple results, obtained in the stability theory for a rotor on an elastic support with two degrees of freedom in the special case of a so-called isotropic elastic support when the stiffness and damping of the elastic attachment of the casing to the base are identical in both directions (Ox and Oz). In this case, the elastic and damping properties of the base are identical in all directions parallel to the plane xOz. Therefore, such a base or support is called isotropic.

Let the stiffness and damping of the isotropic base, identical in directions of the Ox- and Oz-axes, be characterized respectively by the coefficients c and k, so that the forces P_x and P_z applied to the base are related with the corresponding displacements x and z by the formulas

$$\left.\begin{aligned} P_x &= -cx - \kappa \frac{dx}{dt}; \\ P_z &= -cz - \kappa \frac{dz}{dt}. \end{aligned}\right\} \qquad (1.48)$$

It is found that, in this case, there can also be instability of the rotor on an elastic base. Here the unstable range is close to the same value of $\omega = \omega_{cr}$ as before:

$$\omega_{cr} = p_0 \frac{1 + \sqrt{\nu_0^2 + \bar{p}_{b_0}^2(1-\nu_0^2)}}{1-\nu_0^2}. \tag{1.49}$$

At $\bar{p}_{b_0} = 0$, just as before, we obtain a simpler formula:

$$\omega_{cr} = \frac{p_0}{1-\nu_0}. \tag{1.50}$$

In this case, the quantities p_0, $\bar{p}_{b_0}$, and ν_0 are determined, as usual, by the formulas:

$$\left.\begin{aligned} p_0 &= \sqrt{\frac{c}{M}}; \\ p_{b_0} &= \sqrt{\frac{c_b}{I_{v.h}}}; \\ \nu_0 &= \sqrt{\frac{I_{v.h}\, S_{v.h}}{I_{v.h}}}. \end{aligned}\right\} \tag{1.51}$$

Analogous formulas are obtained for determining the required damping, but the required damping in this case is greater by a factor of 2.

The formula for the required damping at which the instability zone contracts to a point, has the form /273

$$\bar{n}_0 \bar{n}_b = \frac{\varepsilon(1-\nu_0)}{4\nu_0}\Delta. \tag{1.52}$$

The quantities ε and Δ are determined, as before, by eqs.(1.26) and (1.32).

Section 2. Lateral Vibrations of a Single-Rotor Helicopter

1. Preliminary Comments

In calculating the vibrations of a helicopter on an elastic landing gear we can regard the fuselage as a perfectly solid body attached to a stationary base (ground) by means of a system of elastic elements.

The calculation of ground resonance of a helicopter, as will be shown below, can be reduced to the calculation of a rotor on an elastic base, examined in Section 1. The initial data for such a calculation (characteristics of the elastic base) are derived from a preliminary calculation of natural vibrations of a rigid fuselage on an elastic landing gear.

A helicopter regarded as a solid body on an elastic landing gear has six

degrees of freedom. However, since the fuselage, as a rule, has a plane of symmetry, the longitudinal and lateral natural vibrations of the helicopter can be examined independently of each other.

For a single-rotor helicopter with an elongated fuselage, the lateral vibrations are generally calculated from the viewpoint of ground resonance. In the presence of longitudinal vibrations, the damping margin for eliminating ground resonance is appreciably greater. Therefore, to calculate ground resonance of a single-rotor helicopter it suffices to examine only lateral vibrations (see also Sect.5).

When examining the lateral vibrations, we must take into account three degrees of freedom:

1) lateral displacement of the center of gravity of the helicopter;
2) rotation of the helicopter about the longitudinal axis (rolling);
3) rotation of the helicopter about the vertical axis (yawing).

Generally speaking, the helicopter vibrations corresponding to these three degrees of freedom cannot be regarded as independent. For example, on lateral displacement of the center of gravity of a helicopter, forces are generated that cause rolling, etc.

However, in a single-rotor helicopter for which the longitudinal fuselage dimensions are relatively large in comparison with its lateral dimensions (this need not be the case, e.g., for helicopters of coaxial and side-by-side configurations), the yawing vibrations are weakly related with lateral vibrations of the helicopter and with its rotation about the longitudinal axis. Therefore, in first approximation, the yawing vibrations for a single-rotor helicopter can be regarded as independent. Furthermore, during yawing vibrations of a helicopter the displacements of the center of the rotor in the plane of rotation are relatively small (in comparison with lateral vibrations) so that, as a rule, yawing vibrations for a single-rotor helicopter are not dangerous so far as ground resonance is concerned. As we will see later (Sect.5), such vibrations are dangerous for helicopters of fore-and-aft and side-by-side configurations.

Thus, in studying the lateral vibrations of a single-rotor helicopter it is sufficient, in first approximation, to consider the fuselage as a body with two degrees of freedom:

1) lateral displacement of the center of gravity of the helicopter;
2) rotation of the helicopter about the longitudinal axis (rolling).

With such simplifications, the problem of natural lateral vibrations of /274
a helicopter can be reduced to the problem of natural vibrations of a two-dimensional solid body elastically attached in its own plane (Fig.3.16).

2. Lateral and Angular Stiffness of Landing Gear. Flexural Center

Let a rigid body A, simulating a helicopter fuselage, be mounted to a stationary base by means of a system of springs (Fig.3.16). We select a fixed coordinate system yc_0z, directing the axis c_0y along the axis of symmetry of the

body and the axis $c_0 z$ along the axis of the horizontal springs c_z'.

If, to the body A, a force P_z parallel to the axis $c_0 z$ at a distance y from the point c_0 is applied, then the deformations of the springs will cause the body A to be displaced in its own plane so that its axis of symmetry will come to occupy a certain position $c_0'y'$. Let us denote by φ the angle of rotation of the axis of symmetry of the body (angle of roll) and by z the displacement of the point c_0 (segment c_0c_0').

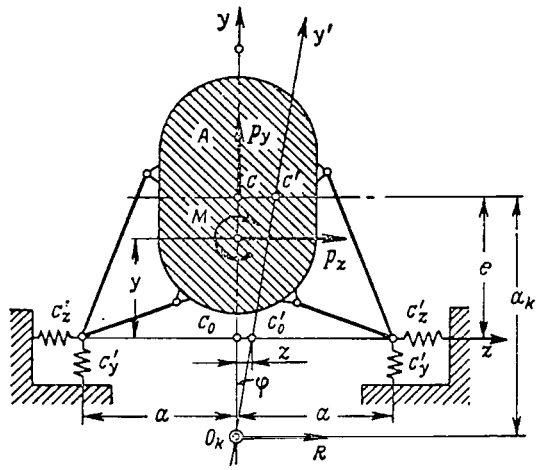

Fig.3.16 Diagram of Elastic Mounting of Helicopter.

Let the springs have linear characteristics. Then, as is known, a point of application of force is always found on the axis $c_0 y$ (or a value of y) at which the angular displacement φ of the body will be equal to zero, meaning that, upon application of the force P_z at this point, the body will undergo purely forward displacement ($\varphi = 0$). We will call such a point the flexural center of the shock absorber system.

If, to the body A, a couple with a moment M is applied, then the body will undergo only angular displacement - turning about the flexural center.

It is easy to see that, for the simplest shock absorber system, as it is shown in Fig.3.16, the center of gravity will be located at the point c_0. The position of the center of gravity of the shock absorber system is conveniently characterized by the magnitude of the distance e from the center of gravity c of the body to the center of gravity c_0.

If, to the body, a force P_y directed along the axis of symmetry $c_0 y$ is applied, then the body will undergo only forward displacement y along the axis $c_0 y$. Since the characteristics of all elastic elements of a shock absorber system are linear, the forces P_z, P_y and the moment M of the couple are linearly related with the corresponding displacements y, z, and φ of the body A.

Let this relation be expressed by the formulas:

$$P_y = c_y y; \tag{2.1}$$

$$P_z = c_z z; \tag{2.2}$$

$$M = c_\varphi \varphi. \tag{2.3}$$

We will call the quantities c_y, c_z, and c_φ, respectively, the coefficients of vertical, lateral, and angular stiffness of the shock absorber system.

The elastic properties of the shock absorber leg are fully determined by four parameters: position of the flexural center (e) and coefficients of stiffness c_y, c_z, and c_φ.

For the simplest shock absorber system depicted in Fig.3.16, the coefficients of stiffness of the shock absorption can be determined by means of the formulas: /275

$$\left.\begin{aligned} c_y &= 2c'_y; \\ c_z &= 2c'_z; \\ c_\varphi &= 2c'_y a^2, \end{aligned}\right\} \qquad (2.4)$$

where

c'_y and c'_z = coefficients of stiffness of the vertical and horizontal springs;

2a = distance between the axes of the vertical springs (wheel track).

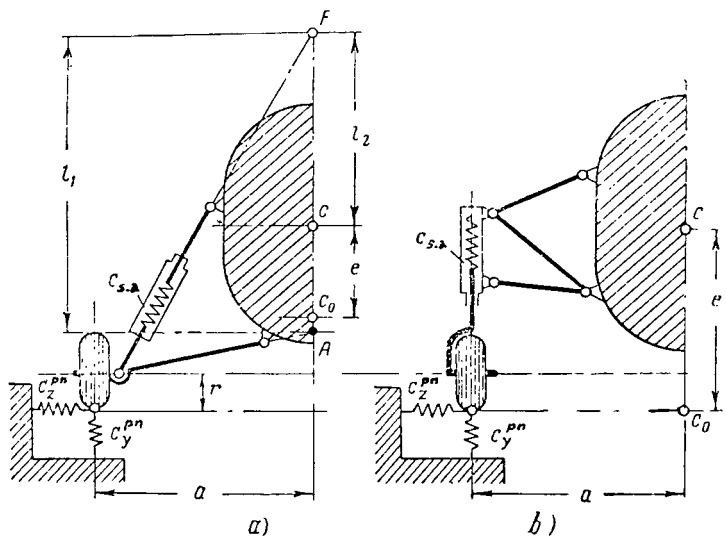

Fig.3.17 Various Landing Gear Configurations.
a - Pyramidal; b - With vertical struts.

The types of helicopter landing gears are mainly of two variants:

1) pyramidal landing gear;
2) landing gear with vertical struts.

The elastic shock absorber systems corresponding to these two types of landing gear are depicted in Fig.3.17, a and b.

The pneumatic tires in this scheme can be considered perfectly rigid, and their elasticity can be simulated by special springs with stiffnesses c_y^{pn} and

c_z^{pn}, equal, respectively, to the vertical and lateral stiffness of the pneumatic tire.

The coefficient of vertical stiffness of the tire can be determined from the diagram of static tire compression, which is always available in the catalog of wheels and represents the ratio of the magnitude of the force compressing the tire toward the rim surface to the magnitude of the corresponding tire compression. The lateral stiffness of the tire, if there are no data available, can also be determined experimentally. The magnitude of lateral stiffness of the tire must also be known for calculations of shimmy. Therefore, if shimmy has been calculated for a given wheel, the magnitude of the lateral stiffness will be known. For an approximate determination of lateral stiffness of a tire we can also use Table 3.1.

TABLE 3.1

Type of Pneumatic Tire	c_z^{pn}/c_y^{pn}
Arched	0.7—0.9
Semi-balloon	0.4—0.64
High-pressure	0.3—0.4

The shock absorber strut of the landing gear in Fig.3.17,a and b is also replaced by a certain spring of stiffness $c_{s.a}$. In reality, the shock strut of the landing gear is a nonlinear elastic element, and its characteristic is determined by the diagram of static compression of the strut which gives the force P acting on the strut as a function of the stroke s of the strut. /276

In calculating small vibrations, the strut can be replaced by an equivalent linear elastic element (spring) whose stiffness is determined by the formula:

$$c_{s.a} = \frac{dP}{ds}\Big|_{s=s_{st}}, \tag{2.5}$$

where s_{st} is the standing compression of the shock absorber.

In a landing gear system with vertical struts (Fig.3.17,b) the flexural center of shock absorption is always situated at the point c_0 on the ground surface. The coefficients of stiffness of such a landing gear are determined by eqs.(2.4) where c_z' and c_y' are equal, respectively, to

$$\left.\begin{aligned} c_z' &= c_z^{pn}; \\ c_y' &= \frac{c_{s.a} \cdot c_y^{pn}}{c_{s.a} + c_y^{pn}}. \end{aligned}\right\} \tag{2.6}$$

For a pyramidal landing gear (Fig.3.41,a), the flexural center is always above the ground surface, and its position must be calculated by special formulas which we will give below.

The pyramidal landing gear is a special version of a more complex landing gear system developed by the British Bristol Aeroplane Co. (Ref.39) and depicted

(schematically) in Fig.3.18. This landing gear system differs from the pyramidal landing gear by the presence of a rocker AB and a special horizontal spring of stiffness c_{sp}. In this system, the height of the position of the flexural center c_0 (i.e., the quantity e) can be varied by selecting a certain spring constant c_{sp}. In particular, by choosing a certain value of c_{sp} it is possible to obtain a position at which the flexural center of the shock absorber system coincides with the center of gravity of the helicopter. In this case, as will be seen later, there is no coupling between the rolling vibrations and the lateral vibrations of the helicopter, which permits obtaining good helicopter characteristics with respect to ground resonance (see Sect.4, Subsect.3).

For the landing gear system depicted in Fig.3.18, we can write the following formulas which can be derived easily by the usual methods of structural mechanics:

$$c_\varphi = \frac{1}{\left(\frac{1}{2c_y^{pn}a^2}\right)+\left(\frac{1}{2c_{s.a}l^2}\right)+\left(\frac{1}{c_{sp}l_1^2}\right)}; \tag{2.7}$$

$$c_z = \frac{1}{\frac{1}{c_{sp}}\left(\frac{l_2^*}{l_1}\right)^2+\frac{1}{2c_{s.a}}\left(\frac{l_1-l_2^*}{l}\right)^2+\frac{1}{2c_y^{pn}}\left(\frac{h_0-l_2^*}{a}\right)^2+\frac{1}{2c_z^{pn}}}; \tag{2.8}$$

$$e = \frac{c_\varphi}{2}\left(\frac{l_1}{c_{s.a}l_2^2}+\frac{h_0}{c_y^{pn}a^2}\right)-l_2; \tag{2.9}$$

/277

$$l_2^* = e+l_2 = \frac{c_\varphi}{2}\left(\frac{l_1}{c_{s.a}l^2}+\frac{h_0}{c_y^{pn}a^2}\right), \tag{2.10}$$

where

h_0 = distance between ground surface and the point F of intersection of the axes of the shock struts (see Fig.3.18);
l = distance between shock absorber axis and the point A;
l_1 = distance between the points F and A;
l_2 = distance between the point F and helicopter center of gravity.

As a special case, the derived formulas contain the formulas for calculating the pyramidal landing gear (see Fig.3.17,a). To obtain formulas of the pyramidal landing gear, it is necessary to set $c_{sp} = \infty$ in eqs.(2.7) and (2.8).

3. Natural Lateral Vibrations of a Helicopter

Let us now turn to Fig.3.16. In studying the lateral vibrations, let us use, for the body A, two degrees of freedom corresponding to the coordinates φ and z. We will impose an additional limitation on the motion of the body A: We will stipulate that the point O_k belonging to the body A at a distance a_k from the center of gravity of the body remains stationary. Then, the body A will have one degree of freedom - rotation about the point O_k. The equation of natural vibrations of the body A, attached in this manner, will have the form

$$I_{o_k}\ddot{\varphi}+c_{o_k}\varphi = 0, \tag{2.11}$$

where

I_{O_k} = moment of inertia of the body relative to the point O_k:

$$I_{O_k} = I_c + ma_k^2; \tag{2.12}$$

I_c = moment of inertia of the body relative to the center of gravity;
m = mass of the body.

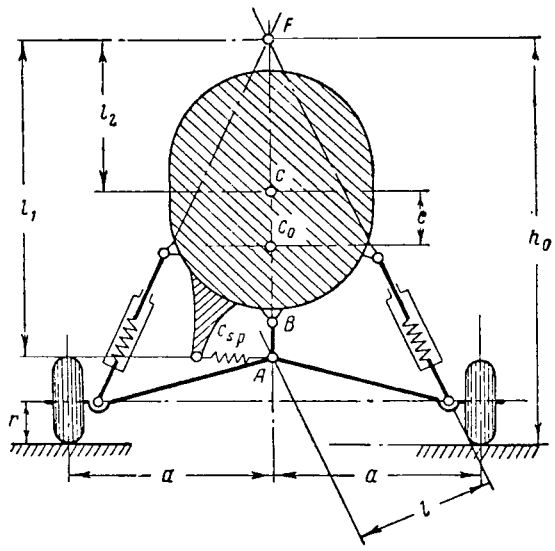

Fig.3.18 Landing Gear Scheme of the Bristol 192 Helicopter.

The coefficient c_{O_k} represents the angular stiffness of the shock absorber system upon rotation of the body A relative to the point O_k. The quantity c_{O_k} is readily determined if the position of the flexural center c_0 of the shock absorber and its angular stiffness c_φ and lateral stiffness c_z are known. /278

Upon rotation of the body through an angle φ relative to the point O_k, the flexural center is displaced by the amount

$$z = \varphi(a_k - e). \tag{2.13}$$

In this case, a force $P_z = c_z z$ directed to the left and a couple of moment $M = c_\varphi \varphi$ directed counterclockwise will be applied to the body at the flexural center. The moment of these forces relative to the point O_k is

$$M = P_z(a_k - e) + c_\varphi \varphi = [c_\varphi + c_z(a_k - e)^2]\varphi.$$

Hence, we obtain the following formula for the angular stiffness c_{O_k}:

$$c_{O_k} = c_\varphi + c_z(a_k - e)^2. \tag{2.14}$$

The natural vibration frequency of the body with the fixed point O_k is

$$p_k = \frac{c_{O_k}}{I_{O_k}},$$

or

$$p_k = \frac{c_\varphi + c_z(a_k - e)^2}{I_c + ma_k^2}. \tag{2.15}$$

During vibrations of the system at the point O_k, a reaction force R arises which will depend on the position of the point O_k. If we could select a point of attachment O_k (a value of a_k) for which R = 0, this would mean that such a point O_k is the natural vibration node of a free system with a movable point O_k, and the corresponding frequency p_k is the natural vibration frequency of a free system.

The reaction force R is readily determined: During vibration, the body A is loaded by the inertia force F_{in} applied at the center of gravity and parallel to the axis O_z,

$$F_{in} = -m\ddot{z}_c = -m\ddot{\varphi}a_k,$$

and also by the couple of inertia forces. The forces exerted by the shock absorption on the body are also reduced to the horizontal force

$$P_z = c_z z = c_z \varphi (a_k - e)$$

and to the couple. Therefore, projecting all forces acting on the body onto the axis $c_0 z$, we obtain

$$R = P_z + F_{in}.$$

If

$$\varphi = \varphi_0 \cos p_k t,$$

then

$$R = [c_z (a_k - e) - m p_k^2 a_k] \varphi_0 \cos p_k t.$$

Equating this expression to zero yields

$$c_z (a_k - e) - m p_k^2 a_k = 0.$$

From this, we obtain the following formula relating the natural frequency /279 of the system with the position a_k of the vibration node:

$$a_k = \frac{e}{1 - \left(\frac{p_k}{p_z}\right)^2}, \tag{2.16}$$

where

$$p_z^2 = \frac{c_z}{m}. \tag{2.17}$$

Excluding the quantity p_k from eqs.(2.15) and (2.16), we obtain a quadratic equation for determining the quantity a_k. This quadratic equation always has two real roots a_1 and a_2, which correspond to the two natural vibration overtones of the system. For each overtone, we obtain a certain natural vibration frequency p_k which, at a known a_k, can be determined from eqs.(2.16) or (2.15).

To determine the natural vibration frequencies p_k and the corresponding

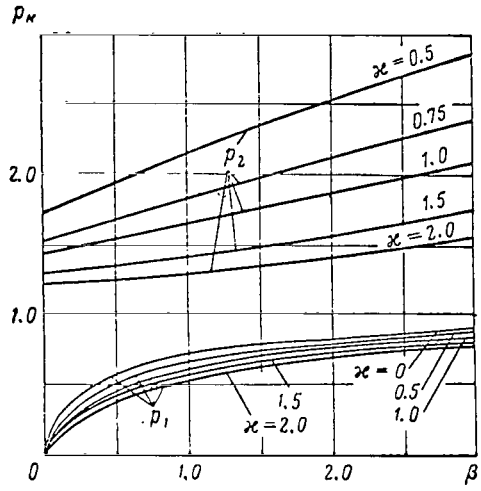

Fig.3.19 Graphs for Determining the Natural Helicopter Frequencies.

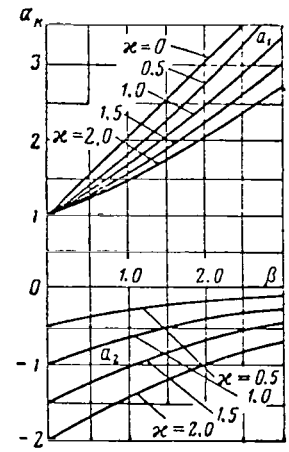

Fig.3.20 Graphs for Determining the Position of Vibration Nodes.

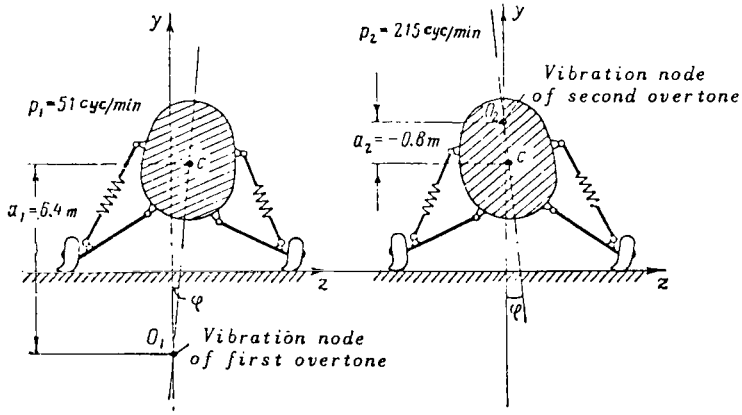

Fig.3.21 Characteristic Vibration Modes of the First and Second Overtones.

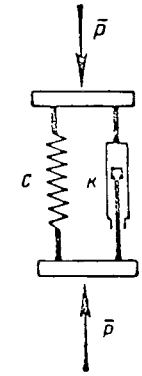

Fig.3.22 Diagram of a Linear Elastic Element with Damping.

quantities a_k, it is convenient to reduce all formulas to a dimensionless form, introducing the notations:

$$\bar{a}_k = \frac{a_k}{e}; \tag{2.18}$$

$$\bar{p}_k = \frac{p_k}{p_z}; \tag{2.19}$$

$$\varkappa = \frac{I_c}{me^2}; \tag{2.20}$$

$$\beta = \frac{c_\varphi}{c_z e^2}. \tag{2.21}$$

The final formulas for determining a_k (k = 1, 2) and $\bar{p}_k$ (k = 1, 2) can be written, in such notations, in the form

$$\bar{a}_{1,2} = \gamma^2 \pm \sqrt{\gamma^2 + \varkappa}, \tag{2.22}$$

where

$$\gamma = \frac{1 + \beta - \varkappa}{2}; \tag{2.23}$$

$$\bar{p}_k = \sqrt{1 - \frac{1}{\bar{a}_k}}; \quad (\text{at} \quad k = 1, 2). \tag{2.24}$$

For convenience of calculating the positions of the natural vibration nodes of the first and second harmonics and the corresponding vibration frequencies, Figs.3.19 and 3.20 show graphs calculated by means of eqs.(2.22), (2.23), and (2.24).

The lower of the frequencies p_1 and p_2 will be called the frequency of the first vibration overtone while the higher frequency will be that of the second overtone. The vibration node of the first overtone is always below the center of gravity of the helicopter ($\bar{a}_1 > 0$) while the vibration node of the second overtone is always above the center of gravity ($a_2 < 0$).

Figure 3.21 shows the characteristic vibration modes of the first and second harmonics for a single-rotor helicopter with a pyramidal landing gear.

4. Determination of Damping Coefficients

The damping of vibrations (i.e., absorption of energy during vibrations) is generally small and can be neglected in determinations of the natural frequencies and positions of the nodes (as was done in Subsect.3).

Damping of vibrations takes place mainly in the shock struts of the land- /281
ing gear. Damping in pneumatic tires can be disregarded in first approximation.

Let us examine the system depicted in Fig.3.16. Let certain linear elastic elements with damping be installed in place of the springs. Such an element is schematically shown in Fig.3.22. Let the force P acting on this element and its

displacement s (stroke of the element) be connected by the relation

$$P = cs + k\frac{ds}{dt}. \tag{2.25}$$

We will call the quantities c and k, respectively, the coefficients of stiffness and damping of the elastic element.

We will denote the coefficients of stiffness and damping of the elastic elements in the system shown in Fig.3.16 by c'_z, c'_y, k'_z, and k'_y, respectively*. The equation of vibrations of the body A relative to the node can be written analogously to eq.(2.11) in the form

$$I_{O_k}\ddot{\varphi} + k_{O_k}\dot{\varphi} + c_{O_k}\varphi = 0, \tag{2.26}$$

where the quantities I_{O_k} and c_{O_k} are determined from eqs.(2.12) and (2.14) and the quantity k_{O_k}, by the formula

$$k_{O_k} = 2k'_y a^2 + 2k'_z (a_k - e)^2. \tag{2.27}$$

We will call this quantity the angular coefficient of damping of the shock absorber system upon rotation of the body relative to the vibration node O_k.

Equation (2.26) can be written in the form

$$\ddot{\varphi} + 2n_k\dot{\varphi} + p_k^2\varphi = 0, \tag{2.28}$$

where p_k (k = 1, 2) is the frequency of the k-th vibration overtone, while the damping coefficient n_k is determined by the formula

$$n_k = \frac{k_{O_k}}{2I_{O_k}}. \tag{2.29}$$

The natural vibrations of the k-th overtone of the helicopter can be described approximately by the law:

$$\varphi = \varphi_0 e^{-n_k t}\cos(p_k t + \psi), \tag{2.30}$$

where

φ_0 = initial angle of deflection;
ψ = phase angle.

The natural vibration frequency p_k can be taken as approximately equal to the natural vibration frequency of the k-th overtone, calculated without con-

---

* The manner of determining the coefficient k'_z and k'_y will be shown in Subsection 5 of this Section, and also in Subsections 1 and 2 of Section 3.

sideration of damping.

In order to calculate the quantities k'_y and k'_z for a specific landing gear system (see Fig.3.17,a and b) it is necessary to determine first the effect of the system formed by the shock strut and the tire.

5. Combined Action of the System Shock Strut-Pneumatic Tire

We will discuss here a landing gear system with vertical struts (see Fig.3.17,b). The tire-oleo combination represents two springs with stiffnesses $c_{s.a}$ and c^y_{pn} connected in sequence.

Let us examine the work done by such a system for the case in which the shock absorber has damping. Such a system is shown in Fig.3.23. Let the shock absorber have a linear characteristic analogous to eq.(2.25): /282

$$P_{s.a} = c_{s.a}\, s_{s.a} + k_{s.a} \frac{ds_{s.a}}{dt}. \tag{2.31}$$

After deriving the equations of motion of the tire-oleo system, it is easy to show that, with the given harmonic law of variation of its total stroke s with a frequency p, the force P acting on the shock absorber is expressed by the formula

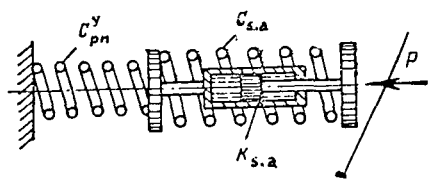

Fig.3.23 Schematic Diagram of Tire-Oleo System.

$$P = c_{eq}\, s + k_{eq} \frac{ds}{dt}, \tag{2.32}$$

where s_{eq} and k_{eq} are the characteristics of some equivalently linear shock absorber of the conventional type (Fig.3.22) and can be determined by means of the formulas:

$$c_{eq} = c^y_{pn} \frac{\left(c^y_{pn} + c_{s.a}\right) c_{s.a} + k^2_{s.a}\, p^2}{\left(c^y_{pn} + c_{s.a}\right)^2 + k^2_{s.a}\, p^2}; \tag{2.33}$$

$$k_{eq} = k_{s.a} \frac{\left(c^y_{pn}\right)^2}{\left(c^y_{pn} + c_{s.a}\right)^2 + k^2_{s.a} p^2}. \tag{2.34}$$

Thus, in vibration analysis a landing gear system with vertical struts (see Fig.3.17,b) can be replaced by the system shown in Fig.3.16, in which the characteristics of elasticity and damping of vertical springs are selected according to eqs.(2.33) and (2.34). At $k_{s.a} = 0$, eq.(2.33) yields a value of c_{eq} equal to the value of c'_y obtained by the second equation of the system (2.6). Consequently, in the presence of damping, eq.(2.6) - generally speaking - does not hold. However, for an approximate calculation of natural frequencies we can use eq.(2.6) for determining c'_y, since the value of c_{eq} determined by eq.(2.33)

is close to the value of c_y' found from eq.(2.6). After determining the natural frequency p, the value of c_y' can be refined by eq.(2.33), followed by refinement of the calculation of the frequency p.

For an exact calculation of the natural frequencies we can use the method of successive approximations (in practice, the above correction equivalent to the first approximation is sufficient) or else the following method: Prescribing the values of c_y' in the interval

$$\frac{c_{s.a}\, c_{pn}^{y}}{c_{s.a}+c_{pn}^{y}} < c_y' < c_y^{pn},$$

we find the natural frequencies and then, from eq.(2.33), we find for the given $c_{eq} = c_y'$ the corresponding value of $k_{s.a}$. As a result of this calculation, the graph of the natural vibration frequencies of the system can be plotted as a function of $k_{s.a}$. Calculations show that the natural vibration frequencies and modes depend little on the quantity $k_{s.a}$. Therefore, in practical application it is sufficient to carry out the above-described approximate calculation with a subsequent single refinement of the frequencies.

To calculate the damping coefficient n_k [eq.(2.29)] we can set, neglecting the tire damping, in eqs.(2.27): /283

$$k_z'=0 \quad k_y'=k_{eq}.$$

For a pyramidal landing gear, the damping of vibrations can be calculated approximately by the same method; however, in calculating k_{eq}, the quantities $c_{s.a}$ and $k_{s.a}$ in eq.(2.34) must be substituted by the values of the so-called stiffness and damping of the shock absorber reduced to the tire $c_{s.a}^{red}$ and $k_{s.a}^{red}$, determined by means of the formulas:

$$\left.\begin{aligned} c_{s.a}^{red} &= c_{s.a}\left(\frac{l}{a}\right)^2; \\ k_{s.a}^{red} &= k_{s.a}\left(\frac{l}{a}\right)^2, \end{aligned}\right\} \qquad (2.35)$$

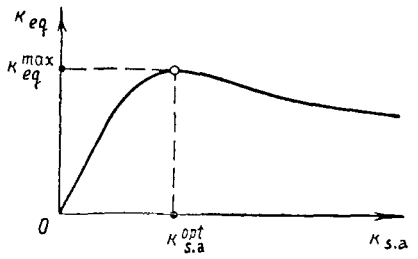

Fig.3.24 Equivalent Damping as a Function of Shock Absorber Damping.

where l is the distance between the shock absorber axis and the point A (see Figs.3.18 and 3.17,a) of the intersection of the axes of the lower inclined struts.

Let us discuss in more detail the dependence of the equivalent damping coefficient k_{eq} of the tire-oleo system on the quantity $k_{s.a}$. Figure 3.24 gives the graph of this dependence. As indicated there, the quantity k_{eq} increases with increasing $k_{s.a}$ only up to a certain value $k_{s.a} = k_{s.a}^{opt}$ at which maximum damping k_{eq}^{max} is attained. Upon further increase in $k_{s.a}$, the damping of the tire-oleo system decreases.

From eq.(2.34) it is easy to obtain the expression for the optimal value of $k_{s.a}^{opt}$:

$$k_{s.a}^{opt} = \frac{c_{pn}^{y} + c_{s.a}}{p}. \tag{2.36}$$

For this value of $k_{s.a}$, eqs.(2.33) and (2.34) give the corresponding values of c_{eq}^{0} and k_{eq}^{max}:

$$c_{eq}^{0} = \frac{1}{2} c_{pn}^{y} \left(1 + \frac{c_{s.a}}{c_{s.a} + c_{pn}^{y}}\right); \tag{2.37}$$

$$k_{eq}^{max} = \frac{1}{2} \cdot \frac{c_{pn}^{y}}{p} \cdot \frac{1}{\left(1 + \frac{c_{s.a}}{c_{pn}^{y}}\right)}. \tag{2.38}$$

We see from the last formula that the maximum obtainable value of k_{eq}^{max} is greater the smaller the ratio $\frac{c_{s.a}}{c_{pn}^{y}}$ and the larger c_{pn}^{y}. Therefore, from the viewpoint of damping of lateral helicopter vibrations, the tire should be as rigid as possible and the shock absorber should be as little rigid as possible. At improper selection of the landing gear characteristics (greater relative stiffness of the shock absorber $\frac{c_{s.a}}{c_{pn}^{y}}$) it may happen that ground resonance is impossible to eliminate no matter how far the shock absorber damping is increased.

6. Reduction of the Problem to Calculation of a Rotor on an Elastic Base

/284

After calculating the natural vibrations of the helicopter on the ground, i.e., after determining frequencies, position of the vibration nodes, and damping coefficients for both natural vibration overtones, it becomes possible to calculate ground resonance in first approximation by reducing the problem to calculation of a rotor on an elastic base.

It would be possible to carry out an exact calculation of ground resonance by deriving the equations of motion of the rotor blades and of the helicopter body in a manner similar to that used in Section 1 for a rotor on an elastic base. Then, the order of the characteristic equation would be higher the more degrees of freedom of the helicopter on an elastic landing gear are taken into account. However it would be necessary in each case to perform cumbersome calculations.

An approximate calculation based on reducing the problem to a rotor on a flexible support permits using established data obtained for a rotor on an elas-

tic base. The accuracy of such a calculation is adequate for practical application.

The essence of such an approximate calculation is as follows: An individual calculation of ground resonance is carried out for each natural vibration harmonic of the helicopter on the ground; in this, the helicopter casing is considered as a body with one degree of freedom - rotation about the corresponding vibration node.

The equation of motion of a helicopter with a fixed vibration node has the form

$$I_{O_k}\ddot{\varphi}+k_{O_k}\dot{\varphi}+c_{O_k}\varphi=P(h+a_k). \tag{2.39}$$

The right-hand side of this equation represents the moment of the force P due to the vibrating rotor blades relative to the vibration node of the harmonic in question. The quantity h is the distance from the plane of the rotor to the center of gravity of the helicopter.

We then introduce a new variable $x = \varphi(h + a_k)$ representing the degree of displacement of the rotor center. Equation (2.39) can now be rewritten in a form analogous to the equation of motion [eq.(1.2)] of an elastic base:

$$m^k_{eq}\ddot{x}+k^k_{eq}\dot{x}+c^k_{eq}x=P, \tag{2.40}$$

where the quantities m^k_{eq}, k^k_{eq}, c^k_{eq} represent the mass, damping, and stiffness of the equivalent elastic base and are calculated by means of the formulas:

$$m^k_{eq}=\frac{I_{O_k}}{(a_k+h)^2}=\frac{I_c+ma_k^2}{(a_k+h)^2}; \tag{2.41}$$

$$k^k_{eq}=\frac{k_{O_k}}{(a_k+h)^2}; \tag{2.42}$$

$$c^k_{eq}=\frac{c_{O_k}}{(a_k+h)^2}. \tag{2.43}$$

Thus, the problem reduces to the calculation of a rotor on an equivalent elastic base whose characteristic is determined from eqs.(2.41), (2.42), and (2.43).

It is easy to demonstrate that, for calculating ground resonance by means of the formulas given in Section 1, we require only three characteristics of the elastic base $m_o = m_{eq}$, $n_o = n_k$ [see eq.(2.29)], and $p_o = p_k$, which are obtained from calculations of the natural lateral vibrations of the helicopter.

Thus, for each natural vibration overtone of the helicopter on an elastic /285
landing gear, we carry out an approximate calculation of ground resonance by means of the formulas derived for a rotor on a flexible support (Sect.1). In such a calculation, we can determine the boundaries of the instability zones and

the magnitudes of the damping coefficients of the blade and landing gear, which are required for eliminating instability with respect to each vibration overtone.

7. Analysis of the Results of Ground Resonance Calculations

The results of ground resonance calculations are conveniently represented as a diagram of safe rpm. Figure 3.25 shows such a diagram for the Mi-4 helicopter. The abscissa gives the rotor rpm while the ordinate shows the rotor thrust T.

The vibration frequencies of the helicopter on the ground are calculated in two variants:

1) shock struts of the landing gear operative;
2) shock struts inoperative.

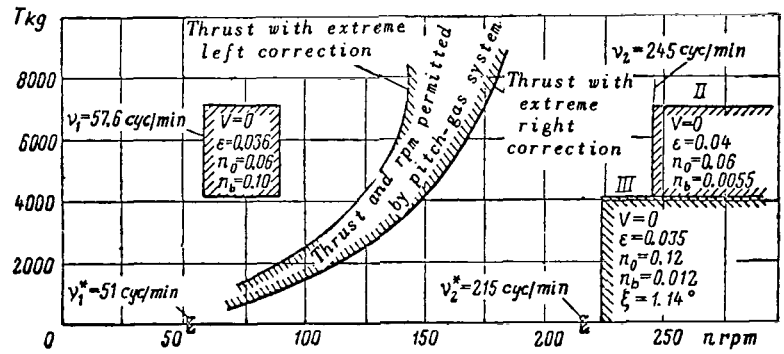

Fig.3.25 Diagram of Safe Revolutions for the Mi-4 Helicopter.

ν_1 - Frequency of first vibration overtone with struts inoperative; ν_2 - Frequency of second vibration overtone with struts inoperative; ν_1^* and ν_2^* - Frequency of first and second overtones with struts operative.

This must be done since the shock struts of the landing gear operate only when the compressive force of the strut is greater than the so-called force of pretightening of the shock absorber. Therefore, at a certain (critical) value of thrust $T = T_{cr}$ of the rotor, the force compressing the strut becomes less than the force of pretightening of the shock absorber and the strut ceases to operate. At $T > T_{cr}$, the shock absorber struts behave as rigid rods, and the helicopter is able to rock only as a consequence of elasticity of the tires which are virtually devoid of damping. The unstable range of the helicopter with inoperative struts is usually impossible to eliminate and is always present in the diagram of safe rpm (this range is hatched in Fig.3.25).

The boundaries of the instability zones and the zone of possible values of rotor thrust T and rpm n permitted by the rotor and engine control systems

(system pitch-gas) are plotted in the diagram of safe rpm. If none of the possible combinations of the values of T and n come to lie outside the boundaries of the unstable range, stability of the helicopter is ensured. In this case, it is always desirable (for greater details, see Sect.6) to have a certain stability margin, i.e., sufficient distances in the diagram between the boundaries of the unstable range and the boundaries of the possible T and n values.

For a single-rotor helicopter with conventional landing-gear design /286
(pyramidal landing gear or gear with vertical struts; see Fig.3.17,a and b), the frequency of the first vibration overtone generally is below the operating rpm of the rotor (Fig.3.25), whereas the frequency of the second overtone usually is above this rpm. Therefore, selection of the damping coefficients must ensure absence of an instability zone of the first vibration overtone with the struts operative. Here, a reliable damping margin is required. The stability margin with respect to the second vibration overtone can be ensured in practice only "with respect to rotor rpm" and can be characterized by a certain quantity η:

$$\eta = \frac{n_1}{n_{max}}, \qquad (2.46)$$

where

n_{max} = maximum possible rotor rpm;
n_1 = rpm corresponding to the lower boundary of the instability zone of the second overtone.

Section 3. Characteristics of Damping of Landing Gear and Blade. Influence on Ground Resonance

1. Determination of the Damping Coefficient of the Landing Gear Shock Absorber

In calculating the natural frequencies of a helicopter we assumed that the shock absorbers of the landing gear have linear characteristics. Actually, the characteristics of the shock strut of a landing gear are nonlinear as a rule. However, for calculating small helicopter vibrations (as usually done in the theory of nonlinear vibrations) the nonlinear shock absorber can be replaced by some equivalent linear shock absorber, for which the coefficients of stiffness and damping depend on the vibration frequency and amplitude. For an approximate determination of the stiffness of an equivalent linear shock absorber we have proposed eq.(2.5). To determine the coefficient of damping k of an equivalent linear shock absorber, we can suggest another simple formula. This formula can be derived if we consider as equivalent a linear shock absorber which, per vibration period, absorbs the same energy as a real shock absorber at the same vibration frequency and amplitude.

The most common designs of shock struts of a given landing gear absorb energy because of friction in the packing glands and of the hydraulic resistance set up when the hydraulic fluid is forced through small orifices.

If we assume the force of hydraulic resistance in such a shock strut as pro-

portional to the square of velocity, then the dependence of the force of resistance P of the strut on the rate $\frac{ds}{dt}$ of its compression can be expressed as

$$P=\begin{cases}+\left[P_0+\sigma_1\left(\frac{ds}{dt}\right)^2\right] & at \quad \frac{ds}{dt}>0;\\ -\left[P_0+\sigma_2\left(\frac{ds}{dt}\right)^2\right] & at \quad \frac{ds}{dt}<0,\end{cases} \tag{3.1}$$

where P_0 is the force of friction in the gland, while σ_1 and σ_2 are the coefficients of hydraulic resistance of the strut in the forward and return strokes.

Let the rod of the shock absorber execute vibrations according to the law $s = s_0 \sin pt$ and, consequently, $\dot{s} = \frac{ds}{dt} = ps_0 \cos pt$.

Let us then calculate the energy absorbed by the shock absorber under these conditions during one oscillatory period. This energy is determined by means of the formula /287

$$A=\int_0^T P(t)\dot{s}(t)\,dt; \quad \left(T=\frac{2\pi}{p}\right).$$

On calculating this integral for the case in which the function P(t) is given by eqs.(3.1), we obtain

$$A=4P_0s_0+\frac{8}{3}\sigma p^2 s_0^3,$$

where

$$\sigma=\frac{\sigma_1+\sigma_2}{2}. \tag{3.3}$$

The damper with linear damping $\left(P = k\frac{ds}{dt}\right)$, under the same conditions, absorbs the energy $A_1 = \pi k p s_0$ during one oscillatory period.

A comparison of the expressions for A and A_1 yields the following formula for determining the coefficient of an equivalent linear damper:

$$k_{eq}=\frac{4}{\pi}\left(\frac{P_0}{ps_0}+\frac{2}{3}\sigma ps_0\right). \tag{3.4}$$

Thus, in a real shock absorber strut, the quantity k_{eq} depends on the amplitude s_0 and on the vibration frequency p, a fact that must be taken into consideration in calculating helicopter vibrations.

Figure 3.26 shows the quantity k_{eq} as a function of the vibration amplitude s_0. On an increase in vibration amplitude, the quantity k_{eq} decreases, reaches a minimum value k_{eq}^{min} at a certain amplitude s_0^* and, upon a further increase in amplitude, rises again.

An analysis of eq.(3.4) readily yields the following formulas for determining the minimum value k_{eq}^{min} and the corresponding vibration amplitude s_0^* of the rod:

$$k_{eq}^{min} = \frac{8}{\pi}\sqrt{\frac{2}{3}\sigma P_0}; \tag{3.5}$$

$$s_0^* = \frac{1}{p}\sqrt{\frac{3}{2}\frac{P_0}{\sigma}}. \tag{3.6}$$

We see from eq.(3.5) that the minimum damping of the shock absorber does not depend on the vibration frequency and amplitude. For a rough estimate of the damping capability of the shock absorber system of the landing gear it is convenient to use eq.(3.5) and to assume, in calculating the tire-oleo system, that $k_{s.a} = k_{eq}^{min}$. Here, it is also useful to determine the quantity s_0^* by means of eq.(3.6).

Whenever there is an occasion to make damping tests on full-scale shock struts, it is suggested to perform such tests since the proposed formulas yield only approximate damping characteristics.

Damping tests can be carried out by one of two methods:

1) determination of the dependence of the force of hydraulic resistance on the rate of travel of the rod;
2) determination of the energy absorbed by the shock absorber in the presence of harmonic vibrations of the rod.

When conducting tests by either of these methods, the air (or nitrogen) should be drained from the shock strut, since only the damping forces are to be determined in the test. /288

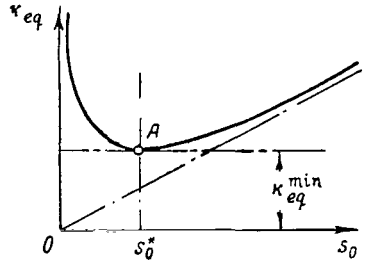

Fig.3.26 Vibration Amplitude Dependence of Equivalent Damping for Shock Absorber with Dry Friction and Quadratic Hydraulic Resistance.

The test procedure by the first method consists in measuring the steady rate of travel of the rod of the shock absorber under the effect of a constant load at various values.

In the second method of testing, harmonic vibrations are imparted to the rod of the shock absorber on a special rig with a rotating eccentric. The variable axial force in the shock absorber is measured at different values of the vibration amplitude and frequency (revolutions of the eccentric) of the rod.

For a landing gear with vertical struts

(Fig.3.17,b), direct tests of the tire-oleo system should be carried out. It is desirable to make such tests also for a pyramidal landing gear (see Fig.3.17,a). Here, the shock absorber connected in sequence with the tire can be tested in the same manner as that used for a landing gear with vertical struts except that a special tire identical with that used on the helicopter is selected, whose stiffness is greater by a factor of n than that of the tire corresponding to a pyramidal landing gear. The value of n is calculated by means of the formula

$$n=\left(\frac{P_{s.a}}{P''_{pn}}\right)^2,$$

where $P_{s.a}$ is the force in the shock absorber under the vertical force P^{y}_{pn} on the tire.

2. Effect of Locking of the Shock Absorber as a Consequence of Frictional Resistance of the Gland and Self-Excited Vibrations of the Helicopter

The force of friction P_0 in the packing (glands) of the shock absorber for all practical purposes is independent of the rate of motion of the rod [eq.(3.1)]. Therefore, the effect of friction in the gland is analogous to the effect of so-called dry (or Coulomb) friction.

This leads to the effect that, in the presence of small vibrations at a variable force $P < P_0$, the shock absorber does not operate and behaves like a rigid rod. Therefore, at a sufficiently small vibration amplitude of the helicopter the shock absorbers are inoperative and only the tires, which are virtually deprived of damping, act as elastic components of the landing gear system.

If the angular velocity of rotor rotation lies within the instability zone of the helicopter with inoperative shock absorbers, the position of equilibrium of the helicopter, generally speaking, will always be unstable and small helicopter vibrations of increasing amplitude are sure to arise. Upon an increase in amplitude of the vibrations, the variable force in the shock absorber also increases. At a certain vibration amplitude a^*, the force P in the shock absorber becomes equal to P_0. At large vibration amplitudes of $a > a^*$ the force $P > P_0$, and (if $T < T_{cr}$) the shock absorbers begin to operate.

If the shock absorption damping is properly selected, self-excited vibrations with a certain constant small amplitude a, greater than a^*, are generated in the system.

Thus, for any helicopter within the unstable range with the struts inoperative, there will always be self-excited vibrations caused by the effect of dry friction in the landing gear shock absorbers. /289

Such self-excited vibrations should never be confused with ground resonance in the conventional meaning of the term. Self-excited vibrations are safe and may arise even when the margin for ground resonance (at large displacements) is sufficiently great.

In the most common designs of shock absorbers (oleo-pneumatic struts), the friction in the gland is relatively great so that, in calculating the amplitude of such self-excited vibrations, only the damping caused by this fraction need be allowed for and the forces of hydraulic resistance in the shock absorber can be neglected. With such an approximate calculation, the amplitude of self-excited vibrations can only be greater than the actual amplitude.

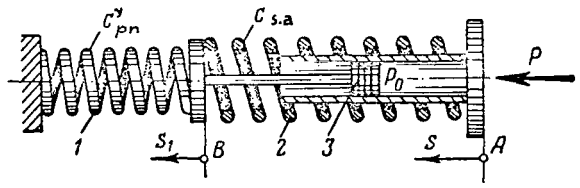

Fig.3.27 Diagram of In-Series Connection of Tire and Shock Absorber with Dry Friction.
1 and 2 - Springs; 3 - Piston.

To estimate the amplitude of self-excited vibrations, we can derive certain simple formulas.

Let us examine a system consisting of two springs (1) and (2) connected in series, one of which with a stiffness c^y_{pn} simulates the tire and the other with a stiffness $c_{s.a}$, the shock absorber (Fig.3.27). Some element [piston (3)] with dry friction characterized by the force P_0 is connected in parallel with the spring (2).

Under the effect of a force P(t) varying in time according to a certain law, let the system execute vibrations such that the point A whose displacement we denote by s will execute the harmonic vibrations

$$s = s_0 \cos pt. \tag{3.7}$$

If the amplitude s_0 is small, the spring (2) does not work and the spring (1) will suffer a deformation $s_1 = s$ varying in accordance with the harmonic law (3.7). In this case, the force P also varies in obedience to the harmonic law

$$P = c^y_{pn} \cdot s_0 \cos pt.$$

However, the work done by the system will be of this type only if $P_{max} < P_0$ and thus if $s_0 < \frac{P_0}{c^y_{pn}}$. As soon as $s_0 > \frac{P_0}{c^y_{pn}}$, the spring (2) starts moving. Here, there are certain time intervals when the spring (2) operates [sliding in the element (3)] and time intervals when the spring does not operate.

Let $\delta = s - s_1$ be the deformation of the spring (2), which we will consider as positive if the spring (2) is compressed. Then, the dependence of the compressing force P on the quantity δ can be written in the form

$$P = \begin{cases} c_{s.a}\delta + P_0, & \text{at} \quad \dot{\delta} > 0; \\ c_{s.a}\delta - P_0, & \text{at} \quad \dot{\delta} < 0. \end{cases} \tag{3.8}$$

In the presence of oscillatory motion, the dependence $P = P(\delta)$ has the form of a hysteresis loop (Fig.3.28).

When the quantity δ reaches a maximum value of a and remains constant after this (δ = a), force P can take any value in the interval $c_{s.a}a - P \leq P \leq c_{s.a}a + P_0$. /290

The relation $\delta(t)$ for time intervals corresponding to sliding ($\dot{\delta} \neq 0$) can be determined from the equation

$$c^y_{pn}(s_0 \cos pt - \delta) = c_{s.a}\delta \pm P_0,$$

which expresses the equality of forces on both elements (1) and (2).

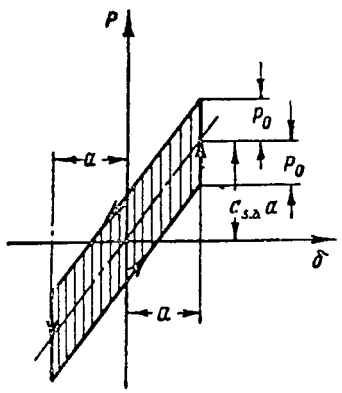

Fig.3.28 Hysteresis Loop for Shock Absorber with Dry Friction.

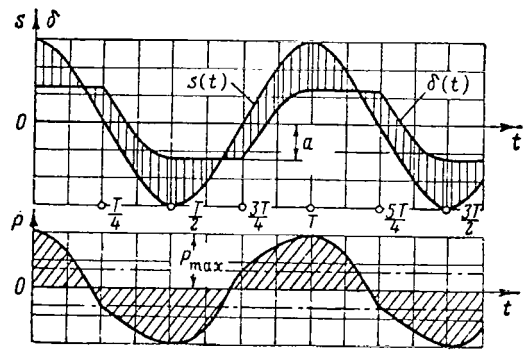

Fig.3.29 Law of Time Rate of Change of Forces and Displacements in Shock Absorber.

From this equation, we find $\delta(t)$ for the sliding sections:

$$\delta(t) = \frac{c^y_{pn} s_0}{c^y_{pn} + c_{s.a}} \cos pt \pm \frac{P_0}{c^y_{pn} + c_{s.a}}.$$

For sections where sliding is absent, we have $\delta = \pm a$.

Figure 3.29 gives graphs of the time rate of change of the quantities s(t), $\delta(t)$, and P(t) for the case $c_{s.a} = c^y_{pn}$ and $s_0 = 2\frac{P_0}{c^y_{pn}}$. The magnitude of the vibration amplitude a of the shock absorber rod can be found from the expression for $\delta(t)$, if we set there cos pt = 1. This will yield

$$a = \frac{c^y_{pn} s_0 - P_0}{c^y_{pn} + c_{s.a}}. \qquad (3.9)$$

The work done by the frictional force during vibrations can be determined from the formula

$$A_{P_0}=4P_0a.$$

Let us compare the system shown in Fig.3.27 with some equivalent linear shock absorber which, at an amplitude of the rod s_0, absorbs the same work and has the same value of maximum force P_{max}.

Equating the expression for work done by the linear shock absorber ($A = \pi k_{eq} p s_0^2$) to the work done by the frictional force A_{P_0}, we obtain the following expression for the damping coefficient k_{eq} of an equivalent linear shock absorber: /291

$$k_{eq}=\frac{4}{\pi}\frac{(c_{pn}^{y})^2}{p\left(c_{pn}^{y}+c_{s.a}\right)}\eta, \tag{3.10}$$

where η is some dimensionless coefficient depending on the vibration amplitude s_0 and determined by the formula

$$\eta=\frac{1}{\bar{s}_0}-\frac{1}{\bar{s}^2}\quad (\text{if } \bar{s}_0>1). \tag{3.11}$$

$$\bar{s}_0=s_0\frac{c_{pn}^{y}}{P_0}. \tag{3.12}$$

The expression for stiffness c_{eq} of an equivalent linear shock absorber is obtained on comparing the value of the maximum force for the linear ($P_{max} = c_{eq} s_0$) and nonlinear [$P_{max} = c_{pn}^{y}(s_0 - a)$] shock absorbers:

$$c_{eq}=c_{pn}^{y}\cdot\frac{\frac{c_{s.a}}{c_{pn}^{y}}+\frac{P_0}{c_{pn}^{y}\cdot s_0}}{\frac{c_{s.a}}{c_{pn}^{y}}+1}. \tag{3.13}$$

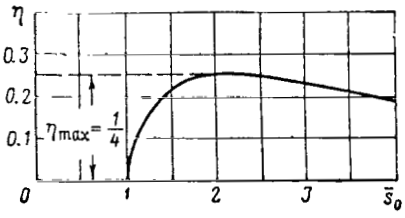

Fig.3.30 Dimensionless Damping Coefficient η as a Function of the Relative Vibration Amplitude $\bar{s}_0$.

Figure 3.30 shows the dependence of the quantity η on the dimensionless vibration amplitude $\bar{s}_0$. The quantity η reaches a maximum value $\eta_{max} = \frac{1}{4}$ at $\bar{s}_0 = 2$. At $\bar{s}_0 > 2$, the damping drops with an increase in vibration amplitude.

The maximum value of $k_{eq} = k_{eq}^{max}$ is equal to

$$k_{eq}^{max}=\frac{1}{\pi}\frac{(c_{pn}^{y})^2}{p\left(c_{pn}^{y}+c_{s.a}\right)}. \tag{3.14}$$

A comparison of this value with the value of k_{eq}^{max} obtained for the linear tire-oleo system [see eq.(2.38)] shows that the shock absorber with dry friction in a system with a pneumatic tire produces, under the same conditions, a maximum damping lower by a factor of $\pi/2$ than the linear shock absorber.

Thus, the amplitude of self-excited helicopter vibrations caused by friction in the packing of the shock absorbers can be found from the condition (3.10):

$$k^{req} = k_{eq} = \frac{4}{\pi} \frac{(c_{pn}^{y})^2}{p\left(c_{pn}^{y} + c_{s.a}\right)} \eta,$$

where k^{req} is the damping required for elimination of ground resonance.

From this equation, we determined the corresponding value of η and then, from the graph in Fig.3.30, the corresponding value of s_0.

3. Characteristics of Blade Dampers and their Analysis /292

In our presentation of methods for calculating ground resonance, we proposed that the drag hinge dampers have linear characteristics, i.e., that the moment of the damper M is proportional to the angular velocity $\dot{\xi}$ of rotation of the blade relative to the drag hinge: $M = k_b \dot{\xi}$.

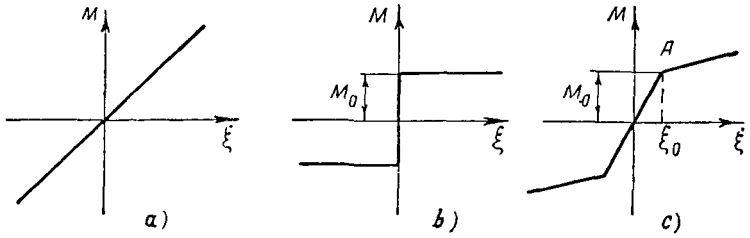

Fig.3.31 Typical Characteristics of Blade Dampers.
a - Linear dampers; b - Friction dampers;
c - Stepped damper.

Actually, the characteristics of blade dampers are nonlinear as a rule. Two types of dampers are predominantly used:

1) hydraulic dampers;
2) friction dampers.

Hydraulic dampers may have different characteristics depending upon design. In particular, a hydraulic damper can be linear (so-called laminar damper, characteristic a in Fig.3.31). However, linear dampers are used extremely rarely, since they have serious shortcomings.

One of the shortcomings is the great sensitivity of linear dampers to tem-

perature, which is explained by the fact that damping in such dampers is proportional to the viscosity of the hydraulic fluid which is greatly dependent upon temperature.

Another shortcoming of linear dampers is that the moment of such a damper is proportional to the blade vibration frequency. Actually, if a blade executes harmonic vibrations relative to the drag hinge $\xi = \xi_0 \sin \nu t$, then the moment of the linear damper varies in accordance with the law $M = k_b\dot{\xi} = \nu k_b \xi_0 \cos \nu t$.

This causes the linear dampers, during forward flight of a helicopter, to load the root portion of the blade with large bending moments, since the blade vibration frequency in flight is by a factor of about 4 greater than at ground resonance.

This drawback is largely absent in the most widely used hydraulic dampers with a stepped characteristic (see Fig.3.31,c) and also in friction dampers (see Fig.3.31,b). The point A on the characteristic curve of the stepped damper corresponds to the instant of opening of special valves.

The characteristic of a friction damper (see Fig.3.31,b) can be regarded as a particular case of a stepped characteristic.

To calculate ground resonance of a helicopter with nonlinear blade dampers, the latter can be replaced by some "equivalent" linear dampers whose coefficient of damping depends upon the amplitude and frequency of blade vibrations. The coefficient k_{eq} of such an equivalent linear damper can be determined from the condition of absorption by this damper of the same energy per oscillatory period, at a given harmonic vibration amplitude and frequency, as is absorbed under /293 the same conditions by a nonlinear damper. For a friction damper, we have

$$k_{eq} = \frac{4}{\pi} \frac{M_0}{\nu \xi_0}, \tag{3.15}$$

where

M_0 = tightening moment of the damper (see Fig.3.31,b);
ξ_0 = amplitude of blade vibrations;
ν = frequency of blade vibrations.

From the same formula, we can determine approximately the value of k_{eq} for hydraulic dampers with a stepped characteristic, if the latter is close to the characteristic of the friction damper.

In the general case, the quantity k_{eq} can be determined from the known characteristic $M(\dot{\xi})$ of a nonlinear damper by means of the formula

$$k_{eq}(\xi_0, \nu) = \frac{1}{\pi \nu \xi_0^2} \int_0^T M(\dot{\xi})\, d\xi \tag{3.16}$$

at

$$\xi = \xi_0 \sin \nu t \text{ and } T = \frac{2\pi}{\nu}.$$

For a manufactured damper, the quantity k_{eq} can be determined also experimentally in special laboratory tests. In such tests, harmonic vibrations are imparted to the rod of the damper and the magnitudes of the damper moment are recorded on an oscillogram.

The main shortcoming of dampers with a stepped characteristic and, in particular, of friction dampers is the presence of a so-called excitation threshold for helicopters equipped with dampers of this type. A helicopter which is stable at small vibration amplitudes may become unstable at large vibration amplitudes exceeding the excitation threshold.

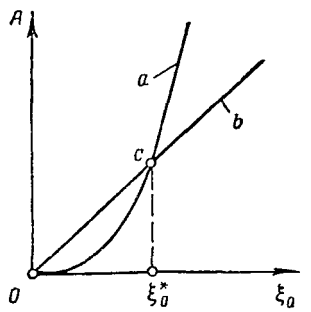

Fig.3.32 Work Absorbed per Oscillatory Period as a Function of Amplitude, for a Damper with Dry Friction and a Damper with Linear Characteristic.

Let us examine this phenomenon for the example of a friction damper. Figure 3.32 shows the dependence of the work A absorbed during one oscillatory period by friction dampers (curve a) and linear (curve b) dampers on the blade vibration amplitude ξ_0 (at constant vibration frequency). For the friction damper, the graph A (ξ_0) is represented by a straight line, whereas for the linear damper it forms a parabola. As result of calculating the ground resonance, let the value k_b^{req} of the required damping of the blade be determined for the case of a linear damper; then, the curve a in Fig.3.32 corresponds to this value of k_b whereas the curve b corresponds to the available damping of the friction damper actually lashed-up to the helicopter.

Let these curves intersect at a certain point c, corresponding to the amplitude ξ_0^*. Then, during blade vibrations with an amplitude $\xi_0 < \xi_0^*$, the damping provided by the friction damper will be greater than required, whereas during blade vibrations with an amplitude $\xi_0 > \xi_0^*$, the damping will be inadequate. The vibration amplitude ξ_0^* also represents the excitation threshold. The value of ξ_0^* can be determined from eq.(3.15):

$$\xi_0^* = \frac{4}{\pi} \frac{M_0}{\nu k_b^{req}}.$$

Thus, if the helicopter suffers some perturbation (shock) which sets up vibrations (both of the helicopter and of the blade) then, if the blade vibration amplitude is less than ξ_0^*, the motion will be stable and the vibrations will die out. If the perturbation is sufficiently great ($\xi_0 > \xi_0^*$), then increasing helicopter vibrations will occur. /294

The presence of an excitation threshold for helicopters with blade dampers of stepped characteristics is a serious shortcoming.

There are quite a few cases known where a helicopter that has been in service for a long time underwent ground resonance as the result of some severe shock, usually as a result of a rough landing with only one wheel of the main landing gear making contact with the ground.

This main shortcoming of nonlinear dampers can be completely eliminated only by using dampers that provide considerable damping at low blade vibration frequencies (ground resonance) and slight damping at a vibration frequency equal to the rotor rpm (and higher). In particular, such a damper can be linear. Figure 3.33 shows the diagram of a linear damper of this type. The damper consists of an elastic element of stiffness c and of the damper proper with a coefficient k, connected in series.

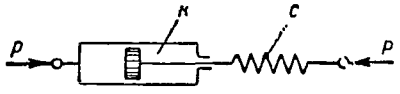

Fig.3.33 Diagram of Element in which the Elastic Element and Damper are Connected in Series.

The characteristics k and c of this damper can be selected such that, after ensuring adequate damping at ground resonance, there are small bending moments on the blade in forward flight of the helicopter (see Sect.6). For the calculation, such an element can be replaced by some equivalent element of stiffness c_{eq} and a damping coefficient k_{eq} determined by means of the formulas

$$\left.\begin{aligned} c_{eq} &= c\,\frac{1}{1+\left(\frac{c}{kp}\right)^2}; \\ k_{eq} &= k\,\frac{1}{1+\left(\frac{kp}{c}\right)^2}. \end{aligned}\right\} \qquad (3.17)$$

These formulas are obtained in the same manner as eqs.(2.33) and (2.34).

4. Effect of Flapping Motion of Rotor on Ground Resonance

As already stated, the commonly used blade dampers are nonlinear. The main feature of any nonlinear damper is that, if the motion of the blade consists of two harmonic components, the damping of one of these components will depend on the amplitude and frequency of the other harmonic component, whereas a linear damper absorbs the energy of each of the harmonic components regardless of the magnitude of the other.

This feature of nonlinear dampers explains the following important phenomenon which has long been noted in helicopter tests: When a helicopter is operating on the ground, ground resonance may be caused by smooth deflection of the cyclic pitch control stick from the neutral position. If the stick is then returned rapidly to the neutral position, the vibrations die out. This phenomenon is utilized in experimental tests of helicopters for ground resonance. The /295
phenomenon is analogous to the effect of flapping on the occurrence of flutter. Let us examine the mechanism of this phenomenon for the case of a friction damper (see Fig.3.31,b).

Let us first attack the following abstract problem: Let some body A slide with a velocity $\bar{V}$ along some plate B (see Fig.3.34) which is executing harmonic vibrations in a horizontal direction according to the law $y = y_0 \sin \omega t$.

The body A is forced against the vibrating plate B by a certain normal force N. We will assume that the friction between the surface of the body A and the plate B corresponds to the ideal law of dry friction, i.e., the force of friction is constant in magnitude and equal to $P_0 = \mu N$ where μ is the coefficient of sliding friction.

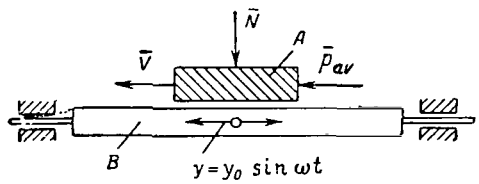

Fig.3.34 Diagram of Body Motion along a Plate Vibrating in a Horizontal Direction.

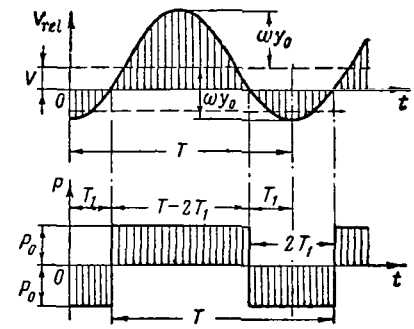

Fig.3.35 Law of Time Rate of Change in Relative Velocity and Force of Friction during Uniform Motion of the Body along a Vibrating Plate.

The direction of the friction force depends upon the direction of the relative velocity of the body A in comparison with the plate B.

Let us assume the friction force P applied to the plate as positive when directed opposite to the absolute velocity of the body A, i.e., to the right. The displacement y of the plate B will be considered as positive when directed to the left. Then the law of friction can be written as

$$P = \begin{cases} +P_0 & at \quad V > \dot{y}; \\ -P_0 & at \quad V < \dot{y}. \end{cases}$$

For the relative velocity of motion of the plate, we have the expression

$$V_{rel} = V - \dot{y} = V - \omega y_0 \cos \omega t.$$

Figure 3.35 gives the graph of this dependence. The relative velocity as a function of time is depicted by a cosine curve shifted by an amount V along the ordinate.

The graph indicates that, at $V < \omega y_0$, during one oscillatory period T the time interval $(T - 2T_1)$ during which V_{rel} is positive is greater than the time interval $2T_1$ during which V_{rel} is negative. Below this graph, we show a corresponding graph of the time dependence of the friction force P. During one oscillatory period, the friction force for a certain time interval $2T_1$ is directed

to the left (negative), while during the time interval $(T - 2T_1)$ it is directed to the right, opposite to the direction of motion.

Thus, during motion of the body A (see Fig.3.34) along a vibrating plate B, the friction force periodically varies its direction only if $V < \omega y_0$. In this case, the friction force for the greater part of time is directed opposite to the motion so that, on the average, the friction offers resistance to the motion of the body A.

For a uniform motion of the body A to the left, we must apply to it a time-variant force which, at each instant of time, would balance the friction force. Let us calculate the average value P_{av} of this force during the period, understanding by this a constant force which, during one oscillatory period, does the same work in absolute displacement of the body A as the actual force of friction. If the mass of the body A is infinitely great and if vibrations of the body A can be neglected and if, in addition, its motion on the vibrating plate can be assumed as uniform, then the force P_{av} will represent the actual force needed for a uniform motion of the body A. /296

The work done by the average force per oscillatory period of the plate will then be equal to

$$A_{av} = P_{av} VT.$$

The work done by the friction force during one period will be equal to

$$A_{fr} = P_0 V[T - 2T_1] - P_0 V[2T_1] = P_0 V[T - 4T_1].$$

Equating these two values of work A_{fr} and A_{av}, we obtain the following expression for the average motive force:

$$P_{av} = P_0\left[1 - 4\frac{T_1}{T}\right].$$

To determine the value of $\frac{T_1}{T}$ we note that

$$\cos \omega T_1 = \frac{V}{\omega y_0}.$$

Hence, taking into account that $T = \frac{2\pi}{\omega}$, we obtain

$$\frac{T_1}{T} = \frac{1}{2\pi} \cos^{-1}\left(\frac{V}{\omega y_0}\right).$$

Consequently,

$$P_{av} = P_0\left[1 - \frac{2}{\pi} \cos^{-1}\left(\frac{V}{\omega y_0}\right)\right].$$

The obtained expression holds if and only if $V < \omega y_0$. At $V > \omega y_0$, the friction force will not change either magnitude or sign, remaining equal to P_0. Taking into account the aforesaid and introducing the dimensionless average force $\bar{P}_{av} = \frac{P_{av}}{P_0}$, we obtain the following expression for the latter:

$$\bar{P}_{av} = \frac{P_{av}}{P} = \begin{cases} 1 - \frac{2}{\pi} \cos^{-1}\left(\frac{V}{\omega y_0}\right), & \text{if} \quad V < \omega y_0; \\ 1, & \text{if} \quad V > \omega y_0. \end{cases} \tag{3.18}$$

Figure 3.36 gives the graphs of the dependence of $\bar{P}_{av}$ on the dimensionless velocity $\bar{V} = \frac{V}{\omega y_0}$.

At a low relative velocity $\bar{V}$ of the plate, we can use a simplified linear dependence $\bar{P}_{av}(\bar{V})$ which is obtained if, in the expansion of $\cos^{-1}\bar{V}$ in a power series in $\bar{V}$, we limit ourselves to the first two terms. In this case, we have

$$\bar{P}_{av} = \frac{2}{\pi} \frac{V}{\omega y_0}.$$

Thus, during slow motion of a body over a rapidly vibrating plate, the /297
average force of friction can be considered approximately proportional to the first power of the velocity

$$P_{av} = k_{eq} V, \tag{3.19}$$

where the proportionality factor is

$$k_{eq} = \frac{2}{\pi} \frac{P_0}{\omega y_0}. \tag{3.20}$$

The above statements indicate that, under the examined conditions, dry friction is in a sense equivalent to linear viscous friction, the equivalent damping coefficient being inversely proportional to the vibration frequency and amplitude of the plate. This important fact was first noted by Heinrich (Ref.41) and checked experimentally by A.A.Krasovskiy (Ref.14).

It is obvious that, during slow harmonic vibrations of the body A over a rapidly vibrating plate B, it is also possible to approximately calculate the damping of these vibrations, making use of eqs.(3.19) and (3.20).

Thus, if in an element with dry friction the relative motion of the rubbing surfaces represents the sum of two harmonic vibrations, one low-frequency and the other high-frequency, then the damping of the low-frequency vibrations can be calculated approximately by using eqs.(3.19) and (3.20), understanding by ω and y_0 the frequency and amplitude, respectively, of the other (high-frequency) harmonic component.

Let us now return to an examination of blade vibrations of a helicopter equipped with a friction damper lashed to the drag hinge. Upon deflection of the pitch stick during operation of the helicopter on the ground, blade flapping relative to the flapping hinges takes place. As is known, the blade flapping angle β will then vary in time according to the harmonic law:

$$\beta = a_0 - a_1 \cos \omega t - b_1 \sin \omega t,$$

where

a_0 = coning angle;
a_1 and b_1 = flapping coefficients.

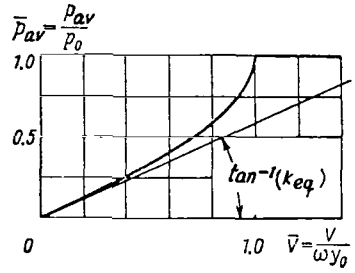

Fig.3.36 Relative Average Friction Force as a Function of the Dimensionless Velocity of the Body over a Vibrating Plate.

During blade flapping, Coriolis forces arise which cause blade vibrations relative to the drag hinge. The amplitude of the first harmonic ξ_1 of blade vibration relative to the drag hinge can be determined from the well-known formula (Ref.48)

$$\xi_1 = \frac{a_0 \sqrt{a_1^2 + b_1^2}}{1 - \nu_0^2}. \qquad (3.21)$$

As already explained in Sections 1 and 3, during ground resonance (in the case $p_{b_0} = 0$) the blades vibrate with a frequency $\nu_0 \omega$ ($\nu_0 \approx 0.25$), i.e., with a frequency about four times lower than the frequency of forced blade vibrations caused by flapping. Therefore, in conformity with the foregoing statements, the damping moment acting on the blade at ground resonance can be calculated approximately by means of the formula /298

$$M = k_{eq} \dot{\xi}, \qquad (3.22)$$

where

$$k_{eq} = \frac{2}{\pi} \frac{M_0}{\omega \xi_1}. \qquad (3.23)$$

The quantity M_0 represents the tightening moment of the friction damper (see Fig.3.31,b).

Thus, forced vibrations in the plane of rotation of a blade with a friction damper, caused by flapping of the blade in the thrust plane, lead to an effect equivalent to the introduction of a linear damper in the drag hinge whose damping coefficient [eq.(3.23)] is inversely proportional to the amplitude ξ_1 of the forced blade vibrations relative to the drag hinge. Therefore, all statements on the excitation threshold of a helicopter with friction dampers (Subsect.3) hold only when there is no blade flapping. This usually occurs when the rotor is operating at low rpm. Consequently, the excitation threshold must be estimated for ground resonance in terms of the first overtone. Equation (3.23) should be used for estimating ground resonance in the presence of rotor flapping (at the operating rotor rpm). This is especially important when calculating ground reso-

nance of a helicopter during the ground run, which will be taken up in Section 4.

Section 4. Ground Resonance of a Helicopter during Ground Run

In presenting methods of calculation for natural lateral vibrations of a helicopter on the ground (Sect.2), it was assumed that there was no wobbling of the pneumatic tire on the ground surface.

When a tire wobbles its lateral stiffness diminishes, while the vertical stiffness remains unchanged. A decrease in lateral stiffness of the tire during such rocking and a certain additional damping during lateral displacements of the wobbling tire can be determined on the basis of the existing theory of shimmy of castoring wheels. A method of such a calculation is given in this Section.

Any decrease in lateral stiffness of the tire on wobbling (decrease in the quantity c_z^{pn}, see Fig.3.17) leads to a decrease in the natural vibration frequencies of the first and second overtones and thus to a reduction of the boundaries of the corresponding unstable range. As indicated above (Sect.2, Subsect.7), for a single-rotor helicopter the instability zone, corresponding to the second vibration overtone, is above the operating rpm of the rotor, and the margin with respect to rotor rotations is sometimes no more than 30%. A reduction of the unstable range during tire wobbling may be of the order of 20 - 30%. Therefore, it might happen that a helicopter, which is stable when operating in situ, becomes unstable during the ground run. In this case, we can speak of a critical ground speed of the helicopter at which motion becomes unstable.

1. Stiffness and Damping of a Wobbling Tire

Let us examine a tire uniformly rolling along the ground (Fig.3.37). Let the wheel execute lateral vibrations in obedience to a harmonic law, such that the axis of rotation of the wheel remains at all times parallel to its initial position and the distance from the axis to the ground remains constant.

We will select a stationary rectangular coordinate system z0s lying on /299
the ground surface, with the Oz-axis being parallel to the wheel axis. Let the lateral displacement z of the diametral plane of the wheel vary in time in accordance with the harmonic law*:

$$z = z_0 e^{i\omega t}, \tag{4.1}$$

where

z_0 = vibration amplitude;
ω = angular vibration frequency.

Let us then determine the lateral force P_z exerted on the tire by the ground during its motion.

---

* We have in mind that the actual displacement is the real part of the indicated complex expression. The use of complex expressions in deriving basic formulas permits an appreciable simplification of the calculations.

Let λ be the lateral deformation of the tire, i.e., the distance between the diametral wheel plane and the point of the tire which forms the center of the contact area before lateral deformation. Then, the lateral force P_z will be equal to

$$P_z = c_z^{pn}\lambda, \tag{4.2}$$

where c_z^{pn} is the lateral stiffness of the tire in the absence of wobbling.

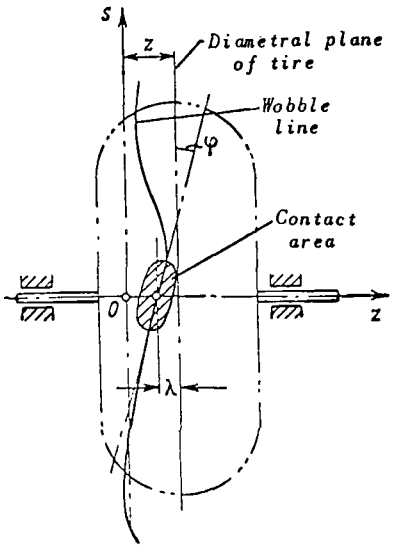

Fig.3.37 Planview of Contact Surface and Line of Tire Wobbling.
φ - Angular deformation of tire; λ - Lateral deformation of tire ("tilt").

Furthermore, let s be the path of the tire reckoned from the line of wobbling and φ the angular deformation of the tire, i.e., the angle between the line of intersection of the diametral wheel plane with the ground surface and the tangent to the material line belonging to the tire surface and representing the line of intersection of the diametral wheel plane with the undeformed tire surface.

The quantities z, λ, and φ are related by the so-called conditions of wobbling which, in conformity with M.V.Keldysh's hypothesis (Ref.15), have the form

$$\left.\begin{aligned} \frac{dz}{ds} &= \varphi + \frac{d\lambda}{ds}; \\ \frac{d\varphi}{ds} &= \alpha\lambda - \beta\varphi. \end{aligned}\right\} \tag{4.3}$$

Here, α and β are certain constants for a given tire, which can be found by conventional methods.

Changing to derivatives with respect to time t and taking into account that s = Vt (where V is the velocity of the tire in the direction of the Os-axis), we obtain

$$\left.\begin{aligned} \frac{dz}{dt} &= V\varphi + \frac{d\lambda}{dt}; \\ \frac{d\varphi}{dt} &= V(\alpha\lambda - \beta\varphi). \end{aligned}\right\} \tag{4.4}$$

Putting

and

$$\left.\begin{aligned} \lambda &= \lambda_0 e^{i\omega t} \\ \varphi &= \varphi_0 e^{i\omega t} \end{aligned}\right\} \tag{4.5}$$

and taking into account eq.(4.1), we obtain from eqs.(4.4) the following expressions for determining the constants λ_0 and φ_0: /300

$$V\varphi_0 + i\omega\lambda_0 = i\omega z_0;$$
$$(i\omega + \beta V)\varphi_0 - \alpha V\lambda_0 = 0.$$

Hence,

$$\lambda_0 = \frac{i\omega z_0}{i\omega + \dfrac{\alpha V^2}{i\omega + \beta V}}. \tag{4.6}$$

Substituting the found value of λ_0 into the first equation of the system (4.5) and then into eq.(4.2), we obtain the following expression for the force P_z exerted on the tire by the ground:

$$P_z = P_0 e^{i\omega t}, \tag{4.7}$$

where

$$P_0 = \frac{i\omega c_z^{pn}}{i\omega + \dfrac{\alpha V^2}{i\omega + \beta V}} z_0.$$

We will designate the complex quantity

$$D(\omega) = \frac{P_0}{z_0} = c_z^{pn} \frac{i\omega}{i\omega + \dfrac{\alpha V^2}{i\omega + \beta V}} \tag{4.8}$$

the lateral complex dynamic tire stiffness in the presence of lateral harmonic vibrations of the wheel.

The modulus of the complex dynamic stiffness represents the ratio of the amplitude P_0 of the lateral force to the vibration amplitude z_0 of the diametral plane of the wheel. The argument of the complex quantity $D(\omega)$ represents the vibration phase of the force P_z with respect to vibrations z of the wheel.

Furthermore, let us examine some linear elastic element with damping (see Fig.3.22). The force P acting on this element and its deformation s (stroke of the element) are connected by the relation [eq.(2.25)]

$$P = cs + k\frac{ds}{dt}.$$

Let us introduce the concept of complex dynamic stiffness of such an element and establish its connectivity with the coefficients c and k of its stiffness and damping.

Let the displacement s of the elastic element vary in time according to the

harmonic law $s = s_0 e^{i\omega t}$. Then the force acting on this element will vary also by the harmonic law:

$$P = (c + i\omega k) s_0 e^{i\omega t}$$

or

$$P = P_0 e^{i\omega t},$$

where

$$P_0 = (c + i\omega k) s_0.$$

We designate the quantity

$$D(\omega) = c + i\omega k \tag{4.9}$$

the complex dynamic stiffness of an elastic element with damping. As shown by eq.(4.9), the real part of the complex quantity $D(\omega)$ represents the stiffness coefficient c of a spring, while the imaginary part represents the damping coef- /301 ficient k of the element multiplied by ω.

To calculate the natural vibrations of a helicopter on the ground in conformity with the scheme depicted in Fig.3.16, the characteristics of elasticity and damping of the elements c_z' and c_y' must be properly chosen.

It is obvious that, to calculate vibrations of a helicopter during ground run, it is sufficient to select the horizontal elastic elements (c_z^{pn} in Fig.3.17) such that their complex dynamic stiffness will be equal to the complex lateral stiffness of the tire in wobbling. The coefficients of stiffness and damping of the thus selected "equivalent" elastic element can be determined, respectively, as the real and imaginary parts of the complex quantity $D(\omega)$ which is expressed by eq.(4.8).

Separating the real and imaginary parts in eq.(4.8), we obtain

$$c_{eq} = c_z^{pn} \frac{\left(1 - \frac{\alpha V^2}{\omega^2}\right) + \frac{\beta^2 V^2}{\omega^2}}{\left(1 - \frac{\alpha V^2}{\omega^2}\right)^2 + \frac{\beta^2 V^2}{\omega^2}}; \tag{4.10}$$

$$k_{eq} = \frac{c_z^{pn}}{\omega} \frac{\left(\frac{\beta V}{\omega}\right)\left(\frac{\alpha V^2}{\omega^2}\right)}{\left(1 - \frac{\alpha V^2}{\omega^2}\right)^2 + \frac{\beta^2 V^2}{\omega^2}}. \tag{4.11}$$

The resultant formulas are comparatively complex and require knowledge of the tire constants α and β.

The formulas for determining c_{eq} and k_{eq} can be greatly simplified if we replace M.V.Keldysh's conditions of wobbling by the so-called "tilt" hypothesis, according to which the lateral deformation of the tire λ ("tilt") is connected

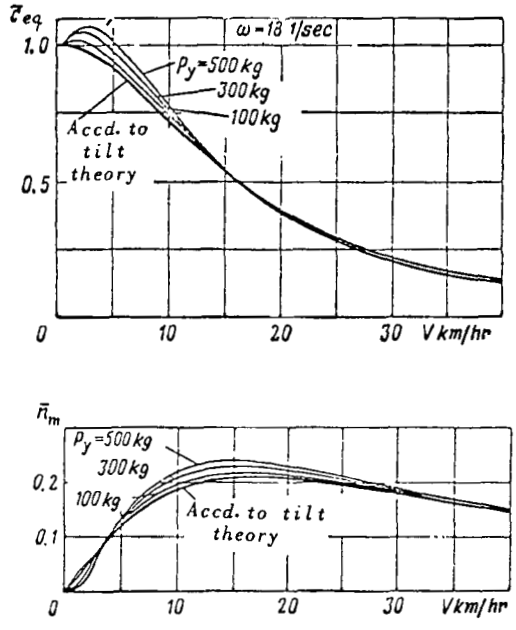

Fig.3.38 Relative Lateral Stiffness and Lateral Damping of Tire as a Function of Helicopter Ground Speed $\left(\omega = 18\ \frac{1}{\text{sec}}\right)$.

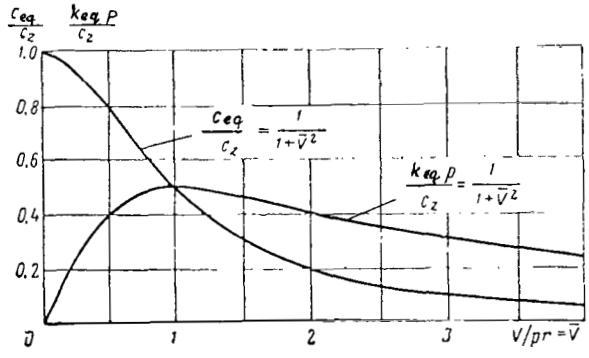

Fig.3.39 Relative Lateral Stiffness and Lateral Damping of Tire as a Function of Dimensionless Helicopter Ground Speed.

with the angular deformation of the tire φ by the simple relation

$$\lambda = \eta\varphi, \qquad (4.12)$$

where $\eta = \frac{\beta}{\alpha}$ is the so-called "tilt" coefficient.

As shown in a paper by M.V. Keldysh (Ref.15), this coefficient is approximately equal to the radius r of the undeformed tire

$$\eta = \frac{\beta}{\alpha} \approx r \qquad (4.13)$$

(r being the distance between the tire axis and the ground in the absence of compression).

In this hypothesis, the first condition of the system (4.4) yields

$$\frac{dz}{dt} = \frac{V}{\eta}\lambda + \frac{d\lambda}{dt}.$$

Putting, as before,

$$z = z_0 e^{i\omega t};$$
$$\lambda = \lambda_0 e^{i\omega t};$$
$$P = P_0 e^{i\omega t},$$

we obtain

$$D(\omega) = \frac{P_0}{z_0} = c_z^{pn}\frac{1 + i\left(\frac{V}{\omega\eta}\right)}{1 + \left(\frac{V}{\omega\eta}\right)^2}. \qquad (4.14)$$

On separating the real and imaginary parts in this expression, we obtain the following expressions for the stiffness and damping coefficients of an equivalent elastic element: /303

$$c_{eq} = c_z^{pn}\frac{1}{1 + \left(\frac{V}{\eta\omega}\right)^2}; \qquad (4.15)$$

$$k_{eq} = \frac{c_z^{pn}}{\omega} \frac{\left(\frac{V}{\eta\omega}\right)}{1+\left(\frac{V}{\eta\omega}\right)^2}. \qquad (4.16)$$

The simplified formulas (4.15) and (4.16) are more convenient for practical calculations and do not require knowledge of the tire constants α and β. The accuracy of the approximate formulas is fully sufficient for practical purposes. This is demonstrated by the comparison graphs in Fig.3.38, which were obtained from calculations of the main landing gear wheels of the Mi-1 helicopter (ω = $= 18 \frac{1}{\text{sec}}$ corresponds to the frequency of the second overtone of vibrations), using Keldysh's theory and the tilt theory.

Thus, in calculations of natural helicopter vibrations during ground run it is expedient to use eqs.(4.15) and (4.16). In this case, the quantity ω in these equations must be substituted by the frequency p of the lateral helicopter vibrations. Figure 3.39 presents graphs of the dependence of the dimensionless lateral stiffness $\left(\frac{c_{eq}}{c_z^{pn}}\right) = \bar{c}_{eq}$ and damping $\left(\frac{k_{eq}p}{c_z^{pn}}\right)$ on the dimensionless relative velocity $\bar{V} = \frac{V}{p\eta} = \frac{V}{pr}$. As we see from the graph, the lateral stiffness of the tire largely depends on the helicopter speed. At $\bar{V} = 3$ (which, for the tire of the Mi-1 helicopter at $p = 18 \frac{1}{\text{sec}}$ is about 50 km/hr), the lateral tire stiffness is by a factor of 10 less than that of a stationary tire.

2. Calculation of Ground Resonance and Results

The calculation of ground resonance during ground run can be performed in the conventional manner (Sect.2), except that the values of lateral tire stiffness c_z^{pn}, when calculating the natural vibrations, should be replaced by the values of c_{eq} derived from eq.(4.15); when determining the coefficients of damping of the natural vibrations (Sect.2, Subsect.4), the additional damping of the horizontal elastic elements (see Fig.3.17) should be taken into account in conformity with eq.(4.16). In this case, the values of ω in eqs.(4.15) and (4.16) must be substituted by the values of the frequency p of the corresponding vibration overtone of the helicopter. Such a calculation method is completely justified since, at the boundaries of the instability zones, there are purely harmonic (undamped) vibrations, and eqs.(4.15) and (4.16) are derived precisely for the case of harmonic lateral tire vibrations. The purpose of calculating ground resonance is to find these boundaries of the unstable range.

When using the formula

$$c_{eq} = c_z^{pn} \frac{1}{1 + \left(\frac{V}{rp}\right)^2} \qquad (4.17)$$

in the calculation of natural helicopter vibration frequencies, a difficulty is encountered connected with the fact that, to find the natural vibration frequency p the value of c_{eq} must be known which, in turn, depends upon p. Therefore, the calculation of natural vibrations (determination of p) should be carried out by assigning different values to c_{eq} in the interval $0 < c_{eq} < c_z^{pn}$, and then, after determining p, deriving the corresponding value of the ground run speed from eq.(4.17). Here, for determining this speed we have the formula

/304

$$V = rp \sqrt{\frac{c_z^{pn}}{c_{eq}} - 1}. \qquad (4.18)$$

Based on such a calculation, it is possible to construct the graph of the dependence of the instability zone boundaries on the ground run speed V. Here, Fig.3.40 gives the results of a calculation of this type for the Mi-1 helicopter. The graph shows the lower boundary of the instability zone corresponding to the second vibration overtone as a function of the ground run speed V.

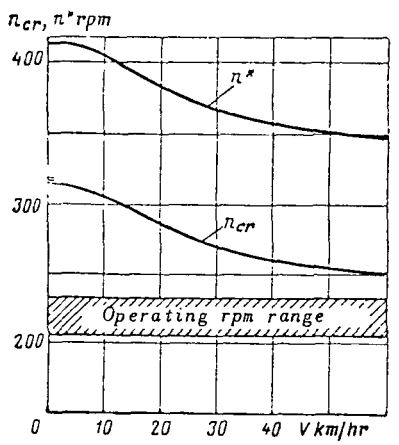

Fig.3.40 Lower Instability Zone Boundary as a Function of Ground Run, for the Mi-1 Helicopter.
n_{cr} - Critical revolutions corresponding to onset of self-excited vibrations;
n^* - Revolutions corresponding to the instability zone center.

As indicated by the graph, the critical revolutions n_{cr} of the rotor corresponding to the onset of ground resonance appreciably decrease with an increase in helicopter speed. If for a stationary parked helicopter the rpm margin is 36%, this margin will decrease to 8% at a ground run speed of 60 km/hr.

It is important to note that, upon an increase in speed V, the graph of n_{cr} approaches some asymptote. This has the following physical meaning:

Upon an increase in V, the lateral stiffness of the tire determined by the quantity C_{eq} [eq.(4.17)] decreases without bounds, approaching zero. In this case, the natural vibration frequencies of the first and second overtones decrease, with the frequency p of the first overtone approaching zero and the frequency of the second overtone tending to the value

$$p_0 = \sqrt{\frac{2c' ya^2}{I_c}}. \qquad (4.19)$$

The quantity p_0 represents the natural lateral vibration frequency of the helicopter in the absence of lateral tire stiffness.

The vibration mode of the helicopter corresponding to this frequency represents the rotation of the helicopter body about the principal longitudinal axis of inertia. The corresponding vibration node (see Sect.2, Subsect.3) coincides with the center of gravity of the helicopter.

A situation of this type might occur for a helicopter standing still or moving over a smooth surface of ice, where it can be assumed that there is no friction between tire and ground (here, also $c_z^{pn} = 0$).

This results in the possibility of a simplified (estimate) calculation of ground resonance during the ground run, when the natural vibration frequency /305 is determined from eq.(4.19). Here, for the mass of the equivalent elastic base (Sect.2, Subsect.6) we have the formula

$$m_{eq} = \frac{I_c}{h^2}. \tag{4.20}$$

For the damping coefficient of the helicopter we have

$$\bar{n}_0 = \frac{k_{eq} H^2}{I_c p_0} + \frac{k'_y a^2}{I_c p_0}, \tag{4.21}$$

where H is the distance from the ground surface to the center of gravity of the helicopter.

The quantity k_{eq} is determined by means of the formula

$$k_{eq} = \frac{c_z^{pn}}{p_0} \frac{\left(\frac{V}{r p_0}\right)}{1 + \left(\frac{V}{r p_0}\right)^2}. \tag{4.22}$$

The quantity k'_y is the damping coefficient of the vertical elastic elements (see Fig.3.16), which depends on the damping properties of the shock struts of the landing gear and is determined in the same manner as that used in Section 2, Subsection 5.

Such an approximate calculation for a helicopter having an unstable range located above the operating rpm produces a small error "in the safety factor".

3. Ground Resonance on Breaking Contact of the Tires with the Ground

All above methods of calculating ground resonance presumed linearity of the tire characteristics. However, in reality the tire characteristic (even approx-

imately) can be considered linear only in situations in which the tire, during its deformation, remains in contact with the ground surface. In general, the characteristic curve of the tire has a slope as shown in Fig.3.41.

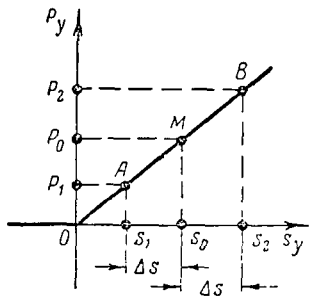

Fig.3.41 Nonlinear Dependence of the Force Exerted by the Ground on the Tire on the Vertical Displacement of the Wheel Axis.

If P_y is the force exerted by the ground on the tire and s_y is the corresponding displacement, the characteristic of the tire has the form

$$P_y = \begin{cases} c_y s_y & at \quad s_y > 0; \\ 0 & at \quad s_y < 0. \end{cases}$$

If the investigation covers only small vibrations of a helicopter near a position of equilibrium corresponding to the given rotor thrust T at which $P_y = P_0$ and $s_y = s_0$, so that the point of the state of the tire during vibrations comes to lie on a certain segment AB wholly within the linear portion of the characteristic, then all calculation methods based on linearity of the tire characteristic are valid (for such small vibrations).

However, at large vibration amplitudes it may happen that the point on the diagram depicting the state of the tire is beyond the limits of linearity of the characteristic. Obviously, this will be the case whenever the amplitude of displacement Δs is greater than the amplitude of static compression s_0. The extent of static compression s_0, just as the force P_0, /306 depends on the rotor thrust and decreases with increasing rotor thrust T, approaching the magnitude of the helicopter weight G. If $T < G$, the tire is forced against the ground; however, the helicopter vibration amplitude at which the tires begin to break contact with the ground is smaller the closer the quantity T approaches the value $T = G$. Therefore, breaking contact of the tires on takeoff and landing is most readily achieved when the rotor thrust is less than the helicopter weight but still sufficiently high.

Calculation of helicopter vibrations on breaking contact with the ground is rather complicated. However, without actually performing such calculations, certain valuable but qualitative conclusions can be drawn. Actually, during vibrations on breaking contact of the tires, the helicopter represents a nonlinear oscillatory system with backlash. It is known that the natural vibration frequency of a system with backlash depends on the vibration amplitude and on the magnitude of backlash; the greater the backlash (at a given amplitude), the smaller the frequency of natural vibrations. This is physically understandable, since the presence of backlash is equivalent to a decrease in the average (during one oscillatory period) stiffness of the elastic element.

Consequently, during helicopter vibrations on breaking contact with the ground the natural vibration frequencies decrease, accompanied by a reduction in the extent of the unstable range. Therefore, if the instability zone corresponding to the second vibration overtone is higher than the operating rpm of the rotor, then the rpm margin up to the lower boundary of the instability zone de-

creases during vibrations on lift-off, and it may happen that, at a sufficiently large vibration amplitude, the lower boundary of the instability zone "descends" to the operating rpm.

Thus, a helicopter which, in the presence of small vibrations, has an instability zone located above the operating rpm will be stable only at small vibration amplitudes not exceeding a certain critical amplitude a^{cr}, which can be designated as the excitation threshold at vibrations on lift-off.

It is obvious from the above statements that the magnitude of the excitation threshold is smaller, the weaker the forces forcing the tire against the ground, i.e., the more closely the rotor thrust approaches the helicopter weight. Thus, the most dangerous situation occurs at the instant of lift-off of the helicopter and immediately after landing. Consequently, on occurrence of vibrations during takeoff or landing the rotor thrust must be reduced immediately. This causes the shock struts to operate, inhibiting vibration of bouncing.

It is important to note that vibrations on lift-off are dangerous only if the unstable range is above the operating rpm of the rotor. From this viewpoint, the landing gear configuration proposed by the Bristol Company (see Fig.3.18) is of interest. As indicated above (Sect.2, Subsect.2), it is possible in this landing gear configuration to cause the flexural center of the shock absorber system to coincide with the center of gravity of the helicopter by choosing the stiffness of a special spring c_{sp} if the landing characteristics of the gear are otherwise satisfactory. Here the lateral forward vibrations of the helicopter and the angular vibrations about the principal longitudinal axis of inertia of the fuselage become independent.

Calculations show that in this case the frequency of lateral forward vibrations is approximately the same (somewhat lower) as the frequency of the first vibration overtone of a helicopter with a landing gear of conventional configuration, whereas the angular vibration frequency may be appreciably reduced in comparison with the frequency of the second overtone for conventional landing gears (in this case, it can even be made equal to the frequency of the first overtone).

Thus, the use of a landing gear of the "Bristol" type permits obtaining /307
a rather low frequency of the second vibration overtone so that the corresponding unstable range will come to lie below the rotor operating rpm. Ground resonance on breaking contact with the ground cannot occur in such a helicopter.

Section 5. Ground Resonance of Helicopters of Other Configurations

1. General Comments

As indicated above (Sect.2, Subsect.1), a calculation of natural vibrations of a helicopter on the ground must be based on the problem of vibrations of a solid body (disregarding fuselage elasticity) on an elastic base. A solid body on an elastic base has six degrees of freedom. Accordingly there are six natural vibration overtones for such a system, each corresponding to a certain vibration frequency and mode. For a single-rotor helicopter with a slender fuselage, we were able to consider only lateral vibrations and to disregard yawing oscillations (Sect.2, Subsect.1).

For a helicopter for which the moments of inertia of the fuselage relative to the three principal axes of inertia are magnitudes of the same order, such a simplification is impermissible. However, if there is a plane of symmetry of the fuselage, then the longitudinal and lateral vibrations can be considered as independent. In this case, the calculation of lateral vibrations must take three degrees of freedom into consideration:

1) lateral displacement;
2) angle of roll;
3) angle of yaw.

A calculation of vibrations in the plane of symmetry (longitudinal vibrations) must also allow for three degrees of freedom:

1) longitudinal displacement;
2) vertical displacement;
3) angle of pitch.

From the viewpoint of ground resonance, both lateral and longitudinal vibrations are dangerous.

Below, we will give methods of calculating the natural vibrations of a helicopter which take into account all of the above-indicated degrees of freedom.

It should be noted that these methods are applicable also to a single-rotor helicopter and permit obtaining results more accurate than the results of an approximate calculation by the method presented in Section 2.

We will also describe a method of calculating ground resonance in air, caused by elasticity of the fuselage.

2. Calculation of Lateral Natural Vibrations with Consideration of Three Degrees of Freedom

Figure 3.42 shows a helicopter on an elastic landing gear. Let us choose a rectangular fixed coordinate system cxyz with its origin at the center of gravity c of the helicopter. The cx-axis is directed forward (in the plane of symmetry of the fuselage) parallel to the surface of the ground, the cy-axis is directed upward, and the cz-axis is directed to the right, viewed in direction of the cx-axis. Let z be the displacement of the center of gravity of the helicopter in direction of the cz-axis, and let φ_x and φ_y be the angles of rotation of the fuselage relative to the cx- and cy-axes (φ_x being the angle of roll and φ_y the angle of yaw).

The equations of lateral vibrations of the helicopter can be written in the form /308

$$\left.\begin{aligned} I_x\ddot{\varphi}_x - I_{xy}\ddot{\varphi}_y &= M_x; \\ I_y\ddot{\varphi}_y - I_{xy}\ddot{\varphi}_x &= M_y; \\ m\ddot{z} &= Z, \end{aligned}\right\} \qquad (5.1)$$

where

m = mass of the helicopter;

I_x and I_y = moments of inertia of the fuselage relative to the cx- and cy-axes;

I_{xy} = corresponding centrifugal moment of inertia;

M_x and M_y = moments of external forces acting on the fuselage relative to the cx- and cy-axes;

Z = projection of the external forces acting on the fuselage at the cz-axis.

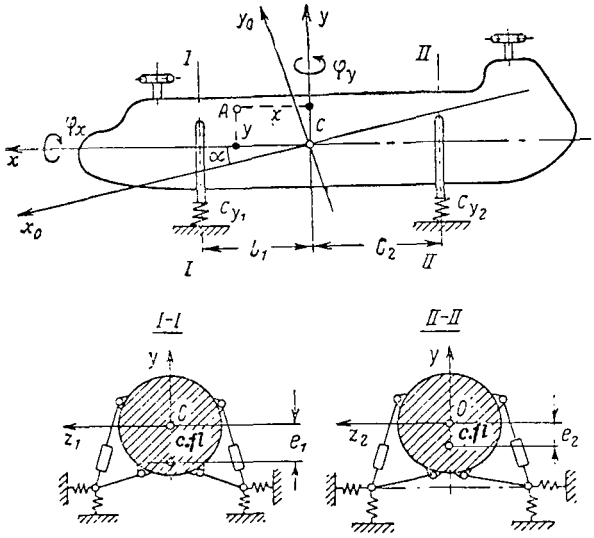

Fig.3.42 Scheme of Helicopter on an Elastic Landing Gear.

Let us first study vibrations in the absence of damping. In this case, the quantities M_x, M_y and Z in the presence of small natural helicopter vibrations relative to the position of equilibrium can be linearly expressed in terms of the displacements z, φ_x, and φ_y. We can then write the expressions for displacements of the flexural centers of shock absorption (c.fl) in the cross sections I-I and II-II of the fuselage (Fig.3.42) corresponding to the fore and aft landing gear in terms of the quantities z, φ_x, φ_y:

1) fore landing gear:

$$z_1 = z - \varphi_y l_1 - \varphi_x e_1;$$

2) aft landing gear:

$$z_2 = z + \varphi_y l_2 - \varphi_x e_2,$$

where

l_1 and l_2 = distances of the planes of the fore and aft landing gears from the center of gravity c;

e_1 and e_2 = distances from the cx-axis to the flexural centers of the fore and aft landing gears.

Knowing the displacement of the flexural center of the fuselage cross section z in the plane of the given landing gear and the rotation of this cross section relative to the flexural center (which for both cross sections will be /308 equal to φ_x), we can determine the elastic forces and moments acting on the fuselage in this cross section in the same manner as before (Sect.2, Subsect.2) for a plane body on a flexible support. Determining then the quantities M_x, M_y, and Z, we obtain the following expressions:

$$\left.\begin{aligned} M_x &= -c_{\varphi_x}\varphi_x - c_{el}\varphi_y + c_e z + Gz; \\ M_y &= -c_{\varphi_y}\varphi_y - c_{el}\varphi_x + c_l z; \\ Z &= -c_z z + c_e\varphi_x + c_l\varphi_y, \end{aligned}\right\} \qquad (5.2)$$

where the corresponding stiffness coefficients are determined by the formulas

$$\left.\begin{aligned} c_z &= c_{z_1} + c_{z_2}; \\ c_{\varphi_x} &= c_{\varphi_1} + c_{\varphi_2} + c_{z_1}e_1^2 + c_{z_2}e_2^2; \\ c_{\varphi_y} &= c_{z_1}l_1^2 + c_{z_2}l_2^2; \\ c_e &= c_{z_1}e_1 + c_{z_2}e_2; \\ c_l &= c_{z_1}l_1 - c_{z_2}l_2; \\ c_{el} &= c_{z_1}e_1l_1 - c_{z_2}e_2l_2. \end{aligned}\right\} \qquad (5.3)$$

The quantities c_{z_1}, c_{z_2}, c_{φ_1}, and c_{φ_2} represent the coefficients of lateral and angular stiffness of the fore and aft landing gears.

The first equation of the system (5.2) also contains the term Gz representing the moment of the force of the helicopter weight G relative to the cx-axis, generated during the lateral displacement z.

Substituting eqs.(5.2) into eqs.(5.1), we finally obtain the following equations of small lateral helicopter vibrations:

$$\left.\begin{aligned} I_x\ddot{\varphi}_x - I_{xy}\ddot{\varphi}_y &= (G + c_e)z - c_{\varphi_x}\varphi_x - c_{el}\varphi_y; \\ I_y\ddot{\varphi}_y - I_{xy}\ddot{\varphi}_x &= c_l z - c_{el}\varphi_x - c_{\varphi_y}\varphi_y; \\ m\ddot{z} &= -c_z z + c_e\varphi_x + c_l\varphi_y. \end{aligned}\right\} \qquad (5.4)$$

Seeking the solution of this system in the form

$$z = z_0 \cos pt;$$
$$\varphi_x = \varphi_x^\circ \cos pt;$$
$$\varphi_y = \varphi_y^\circ \cos pt,$$

where z_0, φ_x°, φ_y°, and p are constants, we arrive at the following system of linear algebraic equations for determining these constants:

$$\left.\begin{aligned} &(c_z - mp^2) z_0 - c_e \varphi_x^\circ - c_l \varphi_y^\circ = 0; \\ &-(G + c_e) z_0 + (c_{\varphi_x} - I_x p^2) \varphi_x^\circ + (c_{el} + I_{xy} p^2) \varphi_y^\circ = 0; \\ &-c_l z_0 + (c_{el} + I_{xy} p^2) \varphi_x^\circ + (c_{\varphi_y} - I_y p^2) \varphi_y^\circ = 0. \end{aligned}\right\} \qquad (5.5)$$

Equating to zero the determinant of this system

$$\begin{vmatrix} (c_z - mp^2); & -c_e; & -c_l \\ -(G + c_e); & (c_{\varphi_x} - I_x p^2); & (c_{el} + I_{xy} p^2) \\ -c_l; & (c_{el} + I_{xy} p^2); & (c_{\varphi_y} - I_y p^2) \end{vmatrix} = 0$$

and performing simple transformations, we obtain the following characteristic /310 equation for determining the natural lateral vibration frequencies p of the helicopter:

$$Ap^6 + Bp^4 + Cp^2 + D = 0, \qquad (5.6)$$

where

$$\left.\begin{aligned} &A = h_x h_y - 1; \\ &B = p_z^2 + p_{\varphi_x}^2 + p_{\varphi_y}^2 - h_x h_y p_z^2 + 2h_y p_{xy}^2; \\ &C = p_{xy}^2 p_{yx}^2 - p_{\varphi_y}^2 p_{\varphi_x}^2 + p_{zy}^2 p_{yz}^2 - p_z^2 (p_{\varphi_y}^2 + p_{\varphi_x}^2) + \\ &\quad + p_{zx}^2 (p_{xz}^2 + p_G^2) + (2p_{zy}^2 p_{xz}^2 - 2p_z^2 p_{xy}^2 + p_{zy}^2 p_G^2) h_y; \\ &D = p_z^2 p_{\varphi_x}^2 p_{\varphi_y}^2 + 2p_{zx}^2 p_{yz}^2 p_{xy}^2 + p_{zy}^2 p_{yx}^2 p_G^2 - \\ &\quad - p_{zy}^2 p_{yz}^2 p_{\varphi_x}^2 - p_z^2 p_{xy}^2 p_{yx}^2 - p_{zx}^2 p_{\varphi_y}^2 p_G^2 - p_{zx}^2 p_{xz}^2 p_{\varphi_y}^2; \end{aligned}\right\} \qquad (5.7)$$

$h_x = \frac{I_{xy}}{I_x}$; $h_y = \frac{I_{xy}}{I_y}$ are dimensionless coefficients.

The partial frequencies p_z, p_{φ_x}, p_{φ_y} and the quantities p_{xy}^2, p_{yz}^2, etc. are obtained by means of the formulas

$$\left.\begin{aligned} &p_z^2 = \frac{c_z}{m}; \quad p_{\varphi_x}^2 = \frac{c_{\varphi_x}}{I_x}; \quad p_{\varphi_y}^2 = \frac{c_{\varphi_y}}{I_y}; \\ &p_{xy}^2 = \frac{c_{el}}{I_x}; \quad p_{yx}^2 = \frac{c_{el}}{I_y}; \\ &p_{zy}^2 = \frac{c_l}{m}; \quad p_{yz}^2 = \frac{c_l}{I_x}; \end{aligned}\right\} \qquad (5.8)$$

$$p_{zx}^2=\frac{c_e}{m};\quad p_{xz}^2=\frac{c_e}{I_x};$$
$$p_G^2=\frac{G}{I_x}.$$

Equation (5.6) is an equation of the third power with respect to the quantity p^2. It can be demonstrated that its roots p_k^2 (k = 1, 2, 3) are always real and positive. Therefore, one of the possible methods of finding the natural vibration frequencies p_k is the graphic method in which we construct the graph of the left-side of this equation, which is regarded as a function of the quantity p. The points of intersection of this graph with the abscissa give the values of the natural frequencies (Fig.3.43).

Let us number the natural vibration frequencies of the system in increasing order: $p_1 < p_2 < p_3$. Let us call the quantities p_1, p_2, p_3, the frequencies of the first, second, and third overtones of the helicopter natural lateral vibrations. Each natural vibration frequency corresponds to a certain vibration mode characterized by a certain correlation of the amplitudes z_0, φ_x^0, φ_y^0, which can be found for a given p_k (k = 1, 2, 3) from eqs.(5.5) if we substitute there p_k for the quantity p. This will yield the expression

$$(\bar{\varphi}_x^0)_k=\left(\frac{\varphi_x^0}{z_0}\right)_k=\frac{(c_z-mp_k^2)(c_{\varphi_y}-I_yp_k^2)-c_l^2}{(c_{\varphi_y}-I_yp_k^2)c_e-(c_{el}+I_{xy}p_k^2)c_l};$$
$$(\bar{\varphi}_y^0)_k=\left(\frac{\varphi_y^0}{z_0}\right)_k=\frac{(c_z-mp_k^2)(c_{el}+I_{xy}p_k^2)-c_lc_e}{(c_{el}+I_{xy}p_k^2)c_l-(c_{\varphi_y}-I_yp_k^2)c_e}, \qquad (5.9)$$

where k = 1, 2, 3.

It is easy to show that the vibration mode of a given overtone is characterized by a certain straight line lying in the plane of symmetry of the fuselage xcy and representing the locus of the points (belonging to the fuselage) remaining stationary during vibrations of this overtone. /311

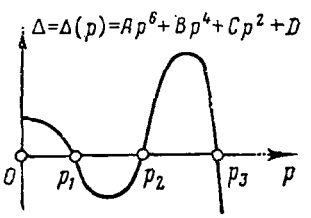

Fig.3.43 Character of the Graph Δ = Δ(p) for Determination of the Natural Vibration Frequencies of a Helicopter on an Elastic Landing Gear.

In fact, the displacement z_A of a certain fuselage point A lying in the plane xcy and having the coordinates x and y (see Fig.3.42) can obviously be determined by the formula

$$z_A=z+\varphi_x y-\varphi_y x.$$

In the presence of vibrations of the k-th overtone, we have

$$z=z_0\cos p_kt;$$
$$\varphi_x=\varphi_x^0\cos p_kt;$$
$$\varphi_y=\varphi_y^0\cos p_kt.$$

Hence,

$$z_A = (z_0 + \varphi^\circ_x y - \varphi^\circ_y x)\cos p_k t =$$
$$= z_0 [1 + (\bar{\varphi}^\circ_x)_k y - (\bar{\varphi}^\circ_y)_k x]\cos p_k t.$$

Therefore, the condition

$$1 + (\bar{\varphi}^\circ_x)_k y - (\bar{\varphi}^\circ_y)_k x = 0 \qquad (5.10)$$

represents the equation of the locus of the points in the plane xcy, whose vibration amplitudes are equal to zero during vibrations of the k-th overtone. However, this is an equation of some straight line.

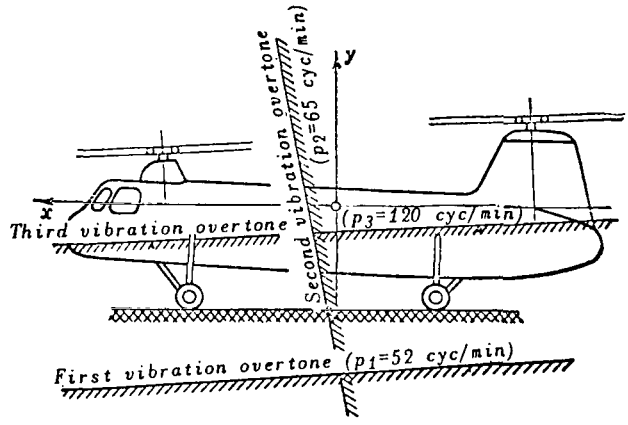

Fig.3.44 Characteristic Arrangement of the Nodal Lines of Vibrations of the First, Second, and Third Overtones.

Thus, the vibration mode of the k-th overtone can be characterized by the position of some straight line in the plane xcy. This straight line will be designated here as the line of the nodes of the k-th overtone of lateral vibrations. The equation of the nodal line [eq.(5.10)] is easily derived by means of eq.(5.9) for a given value of p_k.

The results of natural lateral vibration analyses of a helicopter are conveniently represented as a sketch giving a side view of the helicopter and the nodal lines of all three vibration overtones, with an indication of the corresponding frequencies (Fig.3.44).

The approximate calculation method for natural lateral vibrations given in Section 2 and based on the assumption of independence of yawing vibrations, /312 can be obtained as a particular case of the equations derived here.

If the cx- and cy-axes are the principal axes of inertia ($I_{xy} = 0$) and if the conditions

$$c_l = c_{z_1} l_1 - c_{z_2} l_2 = 0;$$
$$c_{el} = c_{z_1} e_1 l_1 - c_{z_2} e_2 l_2 = 0,$$

are satisfied, then eqs.(5.4) are resolved into two independent systems of equations:

$$\left.\begin{aligned} I_x \ddot{\varphi}_x &= (G - c_e) z - c_{\varphi_x} \varphi_x; \\ m\ddot{z} &= -c_z z + c_e \varphi_x; \end{aligned}\right\} \qquad (5.10')$$

$$I_y\ddot{\varphi}_y = -c_\varphi\varphi_x. \qquad (5.10'')$$

Equation (5.10″) determines the independent yawing vibrations, while the system of equations (5.10′) determines the lateral vibrations corresponding to the physical picture presented in Section 2 (in this case, two of the nodal lines are parallel to the cx-axis, and the third coincides with the cy-axis).

For a real helicopter, the conditions $c_l = c_{el} = 0$ and $I_{xy} = 0$ are never accurately satisfied. However, for helicopters with an elongated fuselage, if the angle α between the principal axis of inertia cx_0 and the cx-axis is low (see Fig.3.42) and the moment of inertia I_x is small in comparison with the two others (I_y and I_z), the results of the "exact" and approximate calculations may agree with an accuracy sufficient for practical purposes.

To determine the damping coefficients of natural vibrations, one can use an approximate method analogous to that presented in Section 2 (Subsect.4) for a system with two degrees of freedom. For each natural vibration overtone, we then determine the damping coefficient on the assumption that in the presence of damping the vibrations of this overtone represent also angular vibrations about the nodal line of this overtone. In this case, just as before (Sect.2, Subsect.4), the equation of natural angular vibrations of the helicopter about the nodal line can be written in the form

$$I_k\ddot{\varphi} + k_{\varphi_k}\dot{\varphi} + c_{\varphi_k}\varphi = 0, \qquad (5.11)$$

where

I_k = moment of inertia of the helicopter relative to the nodal line of the k-th overtone;

$c_{\varphi_k} = p_k^2 I_k$ = angular stiffness of the shock absorber system during rotation relative to the nodal line of the k-th overtone;

k_{φ_k} = corresponding damping coefficient.

The moment of inertia of the helicopter relative to the nodal line can be determined by means of the formula:

$$I_k = mh_k^2 + I_x\cos^2\gamma_k + I_y\sin^2\gamma_k + I_{xy}\sin 2\gamma_k, \qquad (5.12)$$

where

h_k = distance from the center of gravity of the helicopter to the nodal line;

γ_k = angle made by the nodal line with the cx-axis (Fig.3.44).

The quantities h_k and γ_k are determined from the formulas

$$\tan\gamma_k = -\frac{(\mathring{\varphi}_y)_k}{(\mathring{\varphi}_x)_k}; \qquad (5.13)$$

$$h_k = \frac{1}{\sqrt{(\mathring{\varphi}_x)_k^2 + (\mathring{\varphi}_y)_k^2}}. \qquad (5.14)$$

The coefficient of angular damping k_{φ_k} is determined from the expression /313

$$k_{\varphi_k} = 2k'_{z_1}d_{1k}^2 + 2k_{z_2}d_{2k}^2 + 2(k'_{y_1}a_1^2 + k'_{y_2}a_2^2)\cos^2\gamma_k, \qquad (5.15)$$

where

d_{1k} and d_{2k} = distances between the nodal lines (Fig.3.45) and the lines connecting the point of contact with the ground of the tires of the fore and aft landing gears;

a_1 and a_2 = wheel tracks of the fore and aft landing gears (Fig.3.16);

k'_{z_1}, k'_{z_2}, k'_{y_1}, and k'_{y_2} = damping coefficients of the lateral and vertical springs (see Fig.3.16) of the fore and aft landing gear, having the same meaning as in Section 2 (Subsect.4).

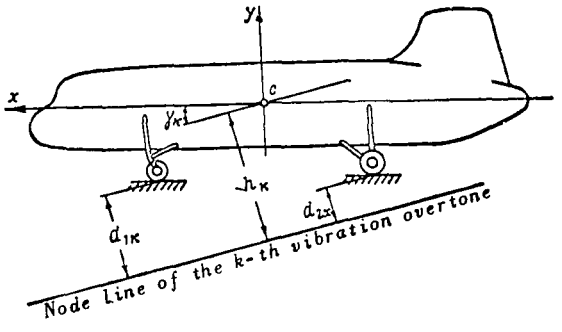

Fig.3.45 For Basic Correlations during Vibrations of a Helicopter Relative to the Nodal Line of the k-th Vibration Overtone.

After determining the quantity k_{φ_k}, we can derive the dimensionless coefficient of damping of the k-th overtone:

$$\bar{n}_k = \frac{k_{\varphi_k}}{2I_k p_k}. \qquad (5.16)$$

3. Calculation of Natural Helicopter Vibrations in the Plane of Symmetry (Longitudinal Vibrations)

Let us turn to Fig.3.46. The problem of helicopter vibrations in the plane of symmetry reduces to an investigation of oscillations of a clamped plane elastic solid body in its own plane (xOy). The vertical springs with a stiffness coefficient c_{y_1} and c_{y_2} simulate the vertical rigidity of the fore and aft landing gears, while the horizontal springs c_{x_1} and c_{x_2} simulate the fore and aft landing gears in the direction of the Ox-axis. If the tires of the landing gears are not braked, then c_{x_1} and $c_{x_2} = 0$. In the case of braked tires, the elasticity of the landing gear in the direction of the Ox-axis is composed of the elasticity of the tire and the elasticity of the tire suspension system (for example, flexural elasticity of the landing gear struts, etc.). For approximate calculations, the longitudinal stiffness of one tire c_x^{pn} can be taken as equal to $c_x^{pn} \approx 1.5\, c_y^{pn}$.

Let the point M (Fig.3.46) with the coordinates e_x and e_y represent the flexural center of the shock absorber system at longitudinal vibrations. The quantity e_y is the distance of the center of gravity of the helicopter from the ground surface, while the quantity e_x is determined from the expression

$$e_x = \frac{c_{y_1}l_1 - c_{y_2}l_2}{c_{y_1} + c_{y_2}}. \qquad (5.17)$$

Let x and y represent displacements of the center of gravity of the heli- /314
copter in the direction of the Ox- and Oy-axes, and let φ_z be the angle of rotation of the fuselage relative to the Oz-axis. Then, the equations of small vibrations of the helicopter in the plane xOy in the absence of damping have the form

$$\left.\begin{aligned} m\ddot{x} &= -c_x x + c_x e_y \varphi_z; \\ m\ddot{y} &= -c_y y - c_y e_x \varphi_z; \\ I_z\ddot{\varphi}_z &= -(c_\varphi + c_x e_y^2 + c_y e_x^2)\varphi_z + c_x e_y x - c_y e_x y + Gx, \end{aligned}\right\} \tag{5.18}$$

where

$$\left.\begin{aligned} c_x &= c_{x_1} + c_{x_2}; \\ c_y &= c_{y_1} + c_{y_2}; \\ c_\varphi &= c_{y_1}(l_1 - e_x)^2 + c_{y_2}(l_2 + e_x)^2. \end{aligned}\right\} \tag{5.19}$$

Let us introduce the following notations:

$$\left.\begin{aligned} c_0 &= c_x e_y^2 + c_y e_x^2 + c_\varphi; \\ p_x^2 &= \frac{c_x}{m}; \quad p_y^2 = \frac{c_y}{m}; \quad p_\varphi^2 = \frac{c_0}{I_z}; \\ \varrho &= \frac{I_z}{m}; \quad \bar{e}_x = \frac{e_x}{\varrho}; \quad \bar{e}_y = \frac{e_y}{\varrho}; \quad \bar{e}_y^* = \bar{e}_y\left(1 + \frac{G}{c_y e_x}\right). \end{aligned}\right\} \tag{5.20}$$

Let us also substitute φ_z by the new variable

$$s = \varrho\varphi_z. \tag{5.21}$$

Equations (5.18) can then be written in the form

$$\left.\begin{aligned} \ddot{x} &= -p_x^2 x + p_x^2 \bar{e}_y s; \\ \ddot{y} &= -p_y^2 y - p_y^2 \bar{e}_x s; \\ \ddot{s} &= -p_\varphi^2 s + p_x^2 \bar{e}_y^* x - p_y^2 \bar{e}_x y. \end{aligned}\right\} \tag{5.22}$$

Seeking the solution of this system of equations in the form

$$x = x_0 \cos pt; \quad y = y_0 \cos pt; \quad s = s_0 \cos pt, \tag{5.23}$$

we arrive at the following system of linear homogeneous algebraic equations for determining the quantities x_0, y_0, and s_0:

$$\left.\begin{aligned} (p_x^2 - p^2)x_0 - p_x^2 \bar{e}_y s_0 &= 0; \\ (p_y^2 - p^2)y_0 + p_y^2 \bar{e}_x s_0 &= 0; \\ -p_x^2 \bar{e}_y^* x_0 + p_y^2 \bar{e}_x y_0 + (p_\varphi^2 - p^2)s_0 &= 0. \end{aligned}\right\} \tag{5.24}$$

Equating the determinant of this system to zero /315

$$\Delta=\begin{vmatrix} p_x^2-p^2; & 0; & -p_x^2\bar{e}_y \\ 0; & p_y^2-p^2; & p_y^2\bar{e}_x \\ -p_x^2\bar{e}_y^*; & p_y^2\bar{e}; & p_\varphi^2-p^2 \end{vmatrix}=0,$$

we obtain the following characteristic equation for determining the natural vibration frequencies p:

$$p^6+ap^4+bp^2+c=0, \tag{5.25}$$

where

$$\left.\begin{aligned} a&=p_x^2+p_y^2+p_\varphi^2; \\ b&=p_x^4\bar{e}_y\bar{e}_y^*+p_y^4\bar{e}_x^2-p_x^2p_y^2-p_y^2p_\varphi^2-p_\varphi^2p_x^2; \\ c&=-p_y^2p_x^2(p_x^2\bar{e}_y\bar{e}_y^*+p_y^2\bar{e}_x^2). \end{aligned}\right\} \tag{5.26}$$

This equation has three real roots p^2 which can be found graphically by constructing the graph of the function $\Delta = \Delta(p) = p^6 + ap^4 + bp^2 + c$, similar to that indicated in Section 5 (Subsect.2) for eq.(5.6) (see Fig.3.43). Let us then arrange the roots of the eq.(5.25) in ascending order $p_1 < p_2 < p_3$ and designate by the quantities p_1, p_2, and p_3 the frequencies of the first, second, and third natural vibration overtones of the helicopter in the plane of symmetry, or longitudinal vibrations. To each longitudinal vibration overtone there corresponds its own vibration mode of the helicopter, which is conveniently characterized by the position of the corresponding vibration node O_k (here k = 1, 2, 3) in the plane xOy, i.e., the fuselage points that remain stationary during vibrations of this overtone. The coordinates of the vibration node x_k and y_k can be found in the following manner: The vibration amplitude a_x and a_y of any fuselage point with the coordinates x_k and y_k in directions of the Ox- and Oy-axes are determined by the obvious formulas

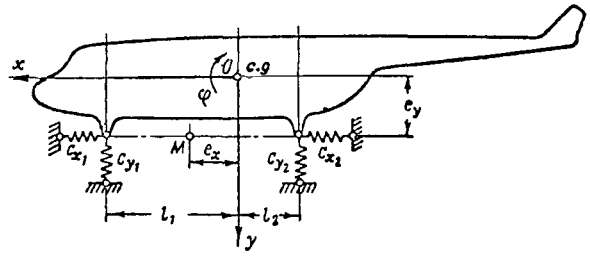

Fig.3.46 Scheme of Helicopter on an Elastic Landing Gear, for Calculating Vibrations in the Plane of Symmetry.

$$\left.\begin{aligned} a_x&=x_0-\varphi_0y_k; \\ a_y&=y_0+\varphi_0x_k, \end{aligned}\right.$$

where $\varphi_0 = s_0\rho$ is the angular vibration amplitude of the helicopter.

The coordinates x_k and y_k are determined from the conditions $a_x = 0$ and $a_y = 0$, such that

$$x_k = -\frac{y_0}{\varphi_0} = -\frac{y_0}{s_0}\varrho;$$

$$y_k = \frac{x_0}{\varphi_0} = \frac{x_0}{s_0}\varrho.$$

The values of the ratio $\frac{y_0}{s_0}$ and $\frac{x_0}{s_0}$ can be found from the first two equations of the system (5.24), if the vibration frequency p is known. For vibrations of the k-th overtone, we obtain

$$\left(\frac{x_0}{s_0}\right)_k = \frac{p_x^2 e_y}{p_x^2 - p_k^2};$$

$$\left(\frac{y_0}{s_0}\right)_k = -\frac{p_y^2 e_x}{p_y^2 - p_k^2}.$$

Hence, we obtain the following formulas for determining the coordinates of the vibration node: /316

$$\left.\begin{aligned} x_k &= \frac{e_x}{1-\left(\frac{p_k}{p_y}\right)^2}; \\ y_k &= \frac{e_y}{1-\left(\frac{p_k}{p_x}\right)^2}. \end{aligned}\right\} \qquad (5.27)$$

We will give two possibilities for a simplified calculation of natural helicopter vibrations in the plane of symmetry.

When the flexural center of shock absorption M (see Fig.3.46) lies on the Oy-axis ($e_x = 0$), the equations of motion (5.18) are simplified and take the form

$$m\ddot{y} = -c_y y; \qquad (5.28)$$

$$\left.\begin{aligned} m\ddot{x} &= -c_x x + c_x e_y \varphi_z; \\ I_z\ddot{\varphi}_z &= -c_0\varphi_z + (c_x e_y + G)x. \end{aligned}\right\} \qquad (5.29)$$

Equation (5.28) describes vertical forward vibrations of the helicopter, which are not of interest from the viewpoint of ground resonance.

Equations (5.29) express longitudinal vibrations of the helicopter, which in this case can be regarded as a system with two degrees of freedom x and φ_z. Such a system is mechanically equivalent to the system discussed in Section 2

(Subsect.3) and depicted in Fig.3.16. Therefore, in calculating the natural frequencies of a helicopter, it is here possible (neglecting the moment due to the force of the weight G) to use the graphs in Figs.3.19 and 3.20 as well as eqs.(2.22), (2.23), and (2.24), putting there

$$\varkappa = \frac{I_z}{me_y^2}; \tag{5.30}$$

$$\beta = \frac{c_{\varphi_z}}{c_x e_y^2} = \frac{c_{y_1} l_1^2 + c_{y_2} l_2^2}{c_x e_y^2}. \tag{5.31}$$

The quantity $\bar{a}_k = \frac{y_k}{e_y}$ will represent the relative distance between the vibration node of the k-th overtone (which here comes to lie on the Oy-axis) and the center of gravity of the helicopter.

For a real helicopter, the quantity e_x is generally not equal to zero, but usually is small in comparison with the quantity $l_1 + l_2$. In most cases, an approximate calculation in which we set $e_x = 0$ will give natural vibration values close to those obtained by an exact calculation and can be successfully used as a preliminary calculation whenever one wishes to obtain results quickly, without the need for greater accuracy.

When calculations of longitudinal vibrations are carried out in the presence of unbraked tires ($c_x = 0$), the equations of motion (5.18) again are resolved into two independent systems:

$$m\ddot{x} = 0;$$
$$m\ddot{y} = -c_y y - c_y e_x \varphi_z;$$
$$I_z \ddot{\varphi}_z = -c_0 \varphi_z + Gx - c_y e_x y.$$

In this case, we can assume $x = 0$ during vibrations since there is no projection of the external forces onto the Ox-axis. One of the natural frequencies of the system is equal to zero and corresponds to uniform motion of the center of gravity of the helicopter along the Ox-axis. The two other natural vibration frequencies, as in the preceding case, can be found from the graphs in Figs.3.19 and 3.20 or from eqs.(2.22), (2.23), and (2.24) in which we must put /317

$$\varkappa = \frac{I_z}{me_x^2}; \tag{5.32}$$

$$\beta = \frac{c_{y_1}(l_1 - e_x)^2 + c_{y_2}(l_2 + e_x)^2}{c_y e_x^2}. \tag{5.33}$$

The values of $a_k = \frac{x_k}{e_x}$ represent the relative distances between the center of gravity of the helicopter and the vibration nodes which, in this case, lie on the Ox-axis.

Finally, when there is no tire braking but $e_x = 0$, the simplest formulas for natural frequencies in the plane of symmetry are obtained:

$$p_1 = 0;$$

$$p_2 = p_y = \sqrt{\frac{c_y}{m}};$$

$$p_3 = p_\varphi = \sqrt{\frac{c_{y_1} l_1^2 + c_{y_2} l_2^2}{I_z}}.$$

To determine the damping coefficients of natural longitudinal vibrations we can again use an approximate method based on the assumption that, in the presence of damping forces, the vibrations of the given overtone are angular vibrations relative to the nodal line of the given overtone which, in this case, represents a straight line parallel to the Oz-axis and intersecting the plane xOy at a point with the coordinates x_k and y_k [see eqs.(5.27)]. The equation of vibrations of this overtone can be rewritten in the form of eq.(5.11), except that the quantity I_k is found from the formula

$$I_k = I_z + m(x_k^2 + y_k^2). \tag{5.34}$$

In determining the damping coefficient k_{φ_k} there is no need to allow for damping of the longitudinal elastic elements c_{x_1} and c_{x_2} (see Fig.3.46) so that only damping of the vertical elastic elements with stiffnesses c'_{y_1} and c'_{y_2} of the fore and aft landing gears must be considered (see Fig.3.16).

The corresponding damping coefficients k'_{y_1} and k'_{y_2} are determined as indicated in Section 2 (Subsects.4 and 5).

By calculating the moment from the damping forces relative to the nodal line, we obtain the following expression for determining the quantity k_{φ_k}:

$$k_{\varphi_k} = 2[k'_{y_1}(l_1 - x_k)^2 + k'_{y_2}(l_2 + x_k)^2]. \tag{5.35}$$

The dimensionless damping coefficient $\bar{n}_k$ of the given vibration overtone is determined by the formula

$$\bar{n}_k = \frac{k_{\varphi_k}}{2I_k p_k^2}. \tag{5.36}$$

4. Reduction of the Problem to Calculation of a Rotor on an Elastic Base

/318

After determining the natural vibration frequencies and modes of the helicopter on an elastic landing gear, the calculation of ground resonance can be

reduced to the calculation of a rotor on a flexible support, as presented in Section 1.

The method of calculation based on reducing the problem to a rotor on a flexible support is an approximate method and analogous to that given in Section 2 (Subsect.6) for a single-rotor helicopter.

The essence of the approximate method is as follows: A separate calculation of ground resonance is performed for each natural vibration overtone; here, the helicopter fuselage is regarded as a solid body with one degree of freedom, namely rotation about the nodal line of the given overtone. Of course, such an approximate method holds only for the case in which the natural vibration frequencies of different overtones are sufficiently "far" from each other.

When there are two "close" natural vibration frequencies, certain corrections must be introduced into the calculation. The method of refining the calculation will be presented below.

Thus, for calculating ground resonance, the helicopter vibrations with respect to each overtone are separately considered as angular vibrations of the fuselage about some fixed straight line: nodal line of the given overtone.

It can be demonstrated that, with such a simplification, the equations of motion of the system reduce to a system of equations analogous to the system (1.16) (Sect.1). In this case, all formulas of Section 1 remain in force and we can use the graphs for determining the instability fringe (see Figs.3.3 to 3.12); however, here the quantity $\overline{n}_0$ is to mean a dimensionless damping coefficient $\overline{n}_k$ of the given vibration overtone determinable from eqs.(5.16) or (5.36) (Sect.5, Subsects.2 and 3), while the quantity ε is to mean the quantity ε_k calculated for the given overtone by the formula

$$\varepsilon_k = \varepsilon_{1k} + \varepsilon_{2k} + \ldots + \varepsilon_{sk} = \sum_{i=1}^{s} \varepsilon_{ik}, \tag{5.37}$$

where

i = 1, 2, ..., s;

s = number of rotors, with each of the quantities ε_{ik} determined by the formula

$$\varepsilon_{ik} = \left(\frac{n}{2} \frac{S^2_{v.h}\, l^2_k}{I_{v.h}\, I_k} \right)_i, \tag{5.38}$$

Here,

I_k = moment of inertia of the fuselage (with the rotor masses concentrated at the center) relative to the nodal line of the k-th overtone [see eqs.(5.12) and (5.34)];

l_k = distance between the center of the given i-th rotor and the nodal line of the k-th overtone if lateral vibrations are considered, or the distance between the nodal line of the k-th overtone and the plane of rotation of the given rotor if longitudinal vibrations of

the helicopter are considered;

n = number of blades of a given rotor;

$S_{v.h}$ and $I_{v.h}$ = static moment and moment of inertia of the rotor blade relative to the drag (vertical) hinge.

The rotors can be different; however, the above method is valid only if all rotors have identical angular velocities of rotation and identical values of the parameter ν_0 [see eq.(1.9)].

As indicated above, the approximate calculation method presented here /319
holds only if the vibration frequencies of different overtones are sufficiently "far apart". It can be demonstrated that, if there are two close natural lateral (or longitudinal) vibration frequencies - for example, p_n and p_m - then the calculation of the boundaries of the instability zones can be performed for one overtone - for example, p_m - but is refined by substituting a certain quantity $\bar{n}_{eq}$ for $\bar{n}_m$ (for a given overtone, where $\bar{n}_{eq} < \bar{n}_m$), which is determined by the formula

$$\bar{n}_{eq} = \bar{n}_m \frac{1}{1 + \frac{\bar{n}_m}{\bar{n}_n} \frac{I_m}{I_n}}. \qquad (5.39)$$

This formula is derived for the case of $p_n = p_m$, i.e., when the natural vibration frequencies of the two overtones in question coincide exactly. If $p_n \neq p_m$, then eq.(5.39) yields an understated value of $\bar{n}_{eq}$.

If there are two close natural vibration frequencies p_n and p_m, with one of them - for example, p_n - being the frequency of the n-th overtone of lateral vibrations and the other, p_m, being the frequency of the m-th overtone of longitudinal vibrations, then, generally speaking, a rotor on a flexible support with two degrees of freedom must be considered (see Sect.1, Subsect.4). In this case, it is possible to approximately estimate (within the safety factor) the required damping by eq.(1.52), for a rotor on an isotropic flexible support, substituting into it the quantities $\bar{n}_0$ and ϵ for that of the two examined overtones for which the value of the ratio $\frac{\bar{n}_k}{\epsilon_k}$ is smaller.

It should be noted that such a calculation is required only in the rather rare case in which, for both examined overtones, not only the values of the frequencies p_n and p_m but also the values of $\frac{\bar{n}_n}{\epsilon_n}$ and $\frac{\bar{n}_m}{\epsilon_m}$ are close. If the quantity $\frac{\bar{n}_k}{\epsilon_k}$ for one of the overtones is larger by a factor of 2.5 - 3 than for the other - for example, $\frac{\bar{n}_n}{\epsilon_n} = 3 \cdot \frac{\bar{n}_m}{\epsilon_m}$ - then we can disregard vibrations of the n-th overtone, and examine only vibrations of the m-th overtone (as independent).

5. Self-Excited Vibrations in Flight of a Helicopter with an Elastic Fuselage

Self-excited vibrations of the ground resonance type are also possible in

helicopter flight. The fuselage of a real helicopter is an elastic system which has its own natural vibration frequencies and modes. If the vibration mode of any overtone of an elastic fuselage is such that the center of the rotor (or centers of the rotors) during vibrations of this overtone is displaced in the plane of rotation of the rotor, then ground resonance is possible and the fuselage will execute vibrations with the mode of this overtone.

The natural vibration frequencies of an elastic fuselage are usually high in comparison with the vibration frequencies of a helicopter with shock absorption of the landing gear, and only one or two low natural vibration harmonics are dangerous from the viewpoint of the possibility of self-excited vibrations.

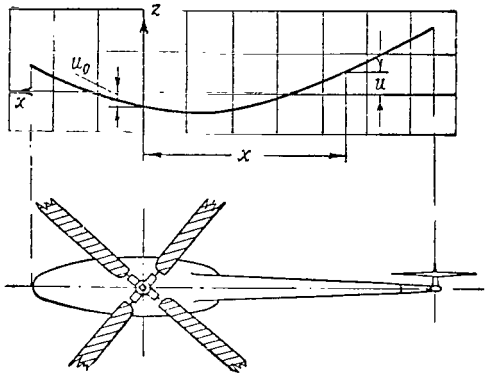

Fig.3.47 Mode of First Vibration Overtone of an Elastic Helicopter Fuselage.

The lower natural vibration frequencies of the fuselage usually correspond to its flexural vibrations.

Figure 3.47 shows the vibration mode of the first partial of bending of the fuselage of a Mi-4 helicopter in the horizontal plane. The vibration mode is given as a curve of the elastic line u = u(x) (u being the vibration amplitude of the point with the coordinate x). /320

The natural flexural vibration frequencies and modes of a fuselage can be found by conventional methods used for elastic beams of variable cross section (see, for example, Chapter II of this volume) or can be determined experimentally (if a full-scale helicopter is available).

If the frequency p_0 and mode u(x) of any flexural vibration overtone of the fuselage are known, the calculation of self-excited vibrations with the mode of this partial can be reduced to the calculation of a rotor on an elastic base, using the formulas in Section 1 or the graphs in Figs.3.3 - 3.12. In this case, the quantity ε should be determined by means of the formula

$$\varepsilon=\varepsilon_1+\varepsilon_2+\ldots\varepsilon_s=\sum_{i=1}^{s}\varepsilon_i, \tag{5.40}$$

where s is the number of rotors.

The quantities ε_i (i = 1, 2, ..., s) are determined from

$$\varepsilon_i=\frac{n}{2}\,\frac{S_{v.h}^2}{I_{v.h}\,m_{eq}^{(i)}}; \tag{5.41}$$

$$m_{eq}^{(i)}=\int \varrho\,[\bar{u}_i(x)]^2\,dx, \tag{5.42}$$

where

$$\bar{u}_i(x) = \frac{u(x)}{u(x_i)};$$

x_i = coordinate of the center of the i-th rotor;
ρ = linear mass of the fuselage (with the integral taken over the entire fuselage length).

The quantity $\bar{u}_i(x)$ represents the vibration amplitude at the point with the coordinate x, referred to the vibration amplitude of the center of the i-th rotor. The quantity m_{eq} is the maximum value of kinetic energy of the fuselage during vibrations with respect to the mode of the given overtone, with the vibration amplitude at the center of the i-th rotor being equal to unity, referred to the quantity p_i^2.

The quantity $\bar{n}_0$ should then be equal to the dimensionless coefficient of damping of the given vibration overtone of the fuselage. It is determined exclusively by hysteresis losses in the fuselage design and usually amounts to 0.02 - 0.05.

Such a comparatively low value of $\bar{n}_0$ does not permit eliminating ground resonance in flight by means of a blade damper, and flight safety of the helicopter can be ensured only at sufficient rpm margins up to the lower fringe of instability. Consequently, self-excited /321 vibrations in the air are dangerous only for helicopters with comparatively low natural vibration frequencies of the elastic fuselage. For example, for the Mi-4 helicopter the rpm margin up to the lower boundary of instability corresponding to the first vibration overtone of the fuselage (see Fig.3.47) is 28%.

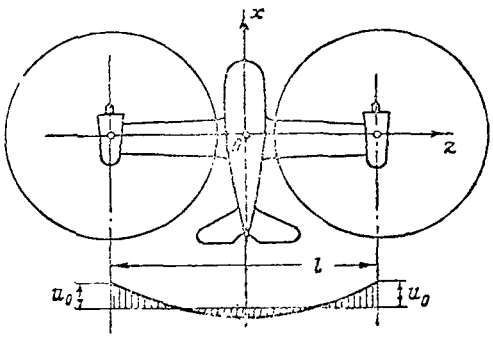

Fig.3.48 Mode of Lower Vibration Overtone of a Side-by-Side Helicopter, Most Dangerous from the Viewpoint of Ground Resonance.

Ground resonance in the air constitutes the greatest danger for helicopters of side-by-side configuration with a long elastic wing (Fig.3.48). The danger of self-excited vibrations for such helicopters is aggravated by the fact that the rotor centers coincide with the antinodes of the corresponding vibration harmonic, which yields comparatively small values m_{eq} [eq.(5.42)] and, consequently, relatively wide instability zones.

Section 6. Selection of Basic Parameters of Landing Gear and Blade Dampers. Design Recommendations

As indicated by the general theory of stability of a rotor on an elastic

base, the stability margin, generally speaking, can be increased by increasing the degree of blade vibration damping as well as the fuselage vibration damping, i.e., by increasing the damping capacity of the landing gear.

However, the possibilities of increasing these types of damping are quite limited in practice, since both the blade damper and the landing gear have a number of other functions not related with ground resonance.

The blade damper works in forward flight of the helicopter and loads the blade root with a variable bending moment which is greater the greater the degree of its damping. The mechanical strength of the root portions of the blade and hub, and consequently their weight, is determined mainly by the presence of a damper.

An extreme increase of the degree of damping of the landing gear without the use of special devices leads to an increase in shock absorber stiffness and hence to an increase in the dynamic loads during landing of the craft.

These aspects of the work of blade dampers and of the landing gear must be considered in designing a helicopter. It frequently is impossible to provide a sufficient margin with respect to ground resonance without using special devices, either in the blade damper or in the landing gear system.

For helicopters of single-rotor and fore-and-aft configuration, ground resonance during the ground run may prove the most dangerous. Therefore, this is conveniently considered to be the design case for selecting the parameters of blade and landing gear damping. For simplicity, we can consider that the helicopter oscillates about the horizontal axis going through its center of gravity, which is a sufficiently valid assumption at high taxiing speed(Sect.4,Subsect.2). As shown above, we derived very simple calculation formulas [eqs.(4.18)-(4.21)] for this case and were able to determine the required characteristics of land- /322
ing gear and blade damper by the simplest method. However, after having selected the parameters for landing gear and blade dampers, a complete calculation of ground resonance for all possible cases is required, including ground resonance during the ground run, followed by plotting a diagram of safe rpm (see Fig.3.25). If necessary, the selected characteristics of the landing gear and hub can then be corrected.

1. Selection of Blade Damper Characteristics

The main characteristic of the work of a blade damper is the fact that the natural blade frequency (characteristic frequency for ground resonance) is always by a factor of about 3 - 4 lower than the frequency of forced blade vibrations in forward flight.

In fact, in flight a blade executes forced vibrations relative to the flapping and drag hinges with a frequency ω equal to the rotor rpm whereas the natural blade vibration frequency is $p_b = \nu_0\omega$. Usually, $\nu_0 = 0.25 - 0.3$; in any case, the angular velocity ω of rotor rotation at ground resonance cannot be greater than the angular velocity of rotor rotation in flight.

This characteristic explains, in particular, the unsuitability of using dampers with a linear characteristic (Sect.3, Subsect.3) in view of the fact that a linear damper, at constant vibration amplitude, will generate a moment proportional to the vibration frequency.

The simplest dampers producing a moment independent of the vibration frequency are friction dampers and hydraulic dampers with stepped characteristic, where this characteristic should be as close as possible to the characteristic of the friction damper (see Fig.3.31,b). A stepped hydraulic damper of this type is suitable for heavy helicopters since it is lighter in weight than a similar friction damper, the gain in weight of the damper increasing with an increase in its power.

When using ordinary dampers, the moment M_0 of the damper is selected from blade strength considerations, while its damping coefficient is determined from eq.(3.23). Here, the damping margin for ground resonance can be ensured only by proper selection of the landing gear characteristics. When this is impossible, special designs of blade dampers might be needed, which would produce large blade damping at low vibration frequencies (characteristic for ground resonance) and small blade damping at vibration frequencies corresponding to helicopter flight. One of the simplest types of such a damper is one connected in series with an elastic element (see Fig.3.33). Figure 3.49 shows one of the possible design versions of such a damper. Let us designate this type of damper a "spring damper"*.

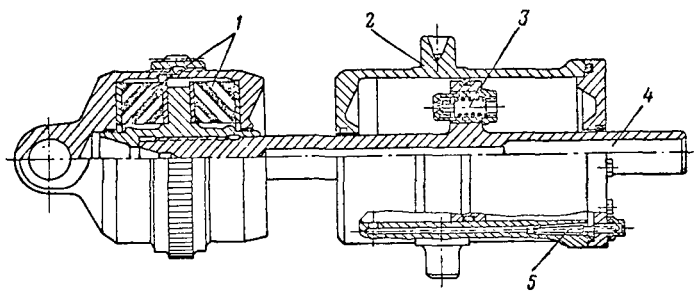

Fig.3.49 Damper with Series-Connected Elastic Element.
1 - Elastic elements (rubber); 2 - Casing; 3 - Safety valve; 4 - Rod; 5 - Adjusting needle.

To estimate the advantages of a spring damper, we will compare it with a conventional friction damper. Let the helicopter undergo ground resonance during the ground run so that the center of the instability zone coincides with the operating rpm of the rotor. Furthermore, let the maximum moment in flight, permissible with respect to strength considerations of the blade, be equal to M_0.

* The design of a spring blade damper for eliminating ground resonance was proposed by engineers O.P.Bakhov, L.N.Grodko, I.V.Kurova, and M.A.Leykand (Patent No. 184142).

Then the equivalent damping coefficient with a friction damper is determined by the following formula (3.23): /323

$$k_{eq}^{frict} = \frac{2}{\pi} \cdot \frac{M_0}{\omega \xi_1},$$

where ξ_1 is the amplitude of the first harmonic of blade vibrations in the plane of rotation.

When using a spring damper, the corresponding equivalent damping coefficient is determined from eq.(3.17)

$$k_{eq}^{spring} = k \frac{1}{1 + \left(\frac{k p_b}{c}\right)^2},$$

where p_b is the frequency of blade vibrations at ground resonance, which can be considered equal to the product $\nu_0 \omega$.

$$p_b = \nu_0 \omega.$$

The moment produced by the spring damper in flight can be determined by means of the formula

$$M = c_{eq} \xi + k_{eq} \frac{d\xi}{dt},$$

which, in the presence of harmonic blade vibrations with a frequency ω, gives the following value of the amplitude of the moment M [see eqs.(3.17)]:

$$M = \frac{k \omega \xi_1}{\sqrt{1 + \left(\frac{k\omega}{c}\right)^2}}. \qquad (6.1)$$

Let us now pose the following question: If we select the values of c and k for a spring damper such that it produces in flight the same moment M_0 as the friction damper, then what is the maximum value of k_{eq}^{spring} obtainable by varying the quantities c and k? Here, we will consider that the amplitude of blade vibrations with respect to the first harmonic ξ_1 in flight and during the ground run of the helicopter is the same.

The relative increase in damping when using a spring damper is conveniently characterized by the quantity /324

$$\psi = \frac{k_{eq}^{spring}}{k_{eq}^{frict}} = \frac{\pi}{2} \frac{\omega \xi_1}{M_0} \frac{k}{1 + \left(\frac{k p_b}{c}\right)^2}. \qquad (6.2)$$

Substituting in this formula $p_b = \nu_0\omega$ and taking into account the condition $M = M_0$, we obtain

$$\psi = \frac{\pi}{2} \cdot \frac{\sqrt{1+\bar{k}^2}}{1+\nu_0^2\bar{k}^2}, \tag{6.3}$$

where the dimensionless quantity is

$$\bar{k} = \frac{k\omega}{c}. \tag{6.4}$$

Thus, the relative advantage gained from using the spring damper depends exclusively upon selecting the value of $\bar{k}$. Figure 3.50 gives a graph of the dependence $\psi(\bar{k})$ for the case $\nu_0 = 0.25$. As we see from this graph, an increase in $\bar{k}$ causes the quantity ψ to increase first and then to decrease, attaining a maximum $\psi = \psi_{max}$ at a certain value $\bar{k} = \bar{k}_{opt}$ which we will call optimal.

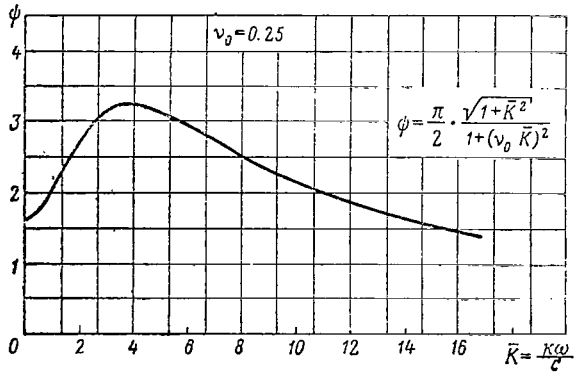

Fig.3.50 Dependence $\psi = f(\bar{k})$ for $\nu_0 = 0.25$.

Equating to zero the derivative $\frac{d\psi}{dk}$, we find

$$\bar{k}_{opt} = \frac{\sqrt{1-2\nu_0^2}}{\nu_0}; \tag{6.5}$$

$$\psi_{max} = \frac{\pi}{2} \frac{1}{\nu_0\sqrt{1-\nu_0^2}}. \tag{6.6}$$

At $\nu_0 = 0.25$, we obtain $\bar{k}_{opt} = 3.74$, $\psi_{max} = 3.24$.

Thus, the use of a spring damper permits increasing the damping at ground resonance by a factor of more than 3, while keeping the moment loading the blade in flight constant.

However, this does not exhaust the advantage of a spring damper as compared to a customary damper. In fact, a spring damper gives "elasticity" in the drag hinge (c_{eq}), and the presence of such elasticity, as is shown in Section 1, Subsection 2, reduces the extent of the necessary damping [see eq.(1.31) and the graph in Fig.3.13]. /325

Calculations show that with consideration of all above statements, the damping margin at ground resonance can be increased by a factor of 5 - 6 while keeping unchanged the moment acting on the blade in flight.

2. Rotor with Interblade Elastic Elements and Dampers

So far we discussed only the case where the elastic element and damper in the drag hinge are lashed up between the blade and the hub casing so that the moment acting on the blade depends exclusively on the motion of the given blade and is independent of the motion of the other blades. Occasionally, hub designs with so-called interblade coupling are used. The diagram of such a hub is shown in Fig.3.51. Let us assume that each such interblade element has a certain stiffness c and a damping characterized by the coefficient k, so that the force P acting on such an element is connected with the variation of its length s by the relation

$$P = cs + k\frac{ds}{dt}.$$

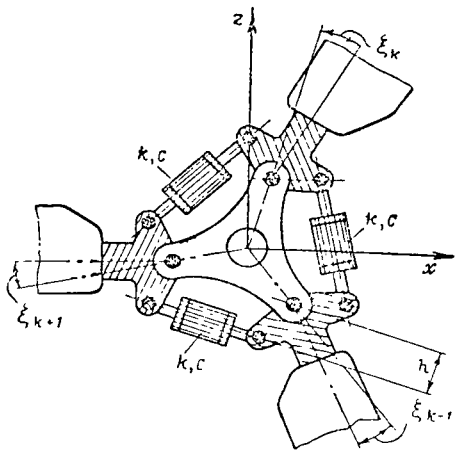

Fig.3.51 Diagram of Rotor Hub with Interblade Coupling.

In this case, the moment exerted on a given (k-th) blade by the interblade elements will depend not only on the motion of this blade characterized by the angle $\xi_k(t)$ but also on the motions of the two adjacent blades $\xi_{k-1}(t)$ and $\xi_{k+1}(t)$.

At small vibrations of the blades relative to the drag hinges, the moment acting on the k-th blade will be expressed by the formula

$$M = c_0(\xi_k - \xi_{k-1}) + c_0(\xi_k - \xi_{k+1}) + k_0(\dot{\xi}_k - \dot{\xi}_{k-1}) + k_0(\dot{\xi}_k - \dot{\xi}_{k+1}),$$

whence

$$\left.\begin{aligned} c_0 &= ch^2; \\ k_0 &= kh^2, \end{aligned}\right\} \qquad (6.7)$$

where h is the arm of the interblade element (see Fig.3.51).

Therefore, the equations of motion of blades in this case have the following form [compare with eq.(1.8)]:

$$\begin{aligned} I_{v.h}\ddot{\xi}_k + k_0(\dot{\xi}_k - \dot{\xi}_{k-1}) + k_0(\dot{\xi}_k - \dot{\xi}_{k+1}) + \\ + c_0(\xi_k - \xi_{k-1}) + c_0(\xi_k - \xi_{k+1}) + \\ + I_{v.h}S_{v.h}\cdot\omega^2\xi_k = \frac{v_0^2 I_{v.h}}{a}\ddot{x}\sin\psi_k, \end{aligned} \qquad (6.8)$$

where

$$k = 1, 2, 3, \ldots n.$$

If the rotor shaft vibrates harmonically /326

$$x = x_0 \cos pt,$$

we can find the forced vibrations of the blades. The right-hand sides of eqs.(6.8) in this case have the form

$$x_0 \frac{v_0^2 p^2}{2l_{v.h}} I_{v.h} \left\{ \sin\left[(p-\omega)t + \frac{2\pi}{n} k\right] + \sin\left[(p+\omega)t + \frac{2\pi}{n} k\right] \right\}.$$

Equations (6.8) then permit a solution of the form

$$\xi_k(t) = \xi_{01} \sin\left[(p-\omega)t - \frac{2\pi}{n} \cdot k\right] + \xi_{02} \sin\left[(p+\omega)t + \frac{2\pi}{n} \cdot k\right].$$

Let us calculate the elastic moment exerted on the k-th blade by the inter-blade elastic elements during blade vibrations with respect to some one of these harmonics - for example, the harmonic $(p - \omega) = p_b$. We have

$$M_{el} = c_0(\xi_k - \xi_{k-1}) + c_0(\xi_k - \xi_{k+1}) = c_0(2\xi_k - \xi_{k-1} - \xi_{k+1}).$$

Moreover,

$$\xi_k = \xi_{01} \sin\left(p_b t - \frac{2\pi}{n} k\right) = \xi_{01} \sin \varphi_k;$$

$$\xi_{k-1} = \xi_{01} \sin\left[p_b t - \frac{2\pi}{n}(k-1)\right] = \xi_{01} \sin\left(\varphi_k + \frac{2\pi}{n}\right);$$

$$\xi_{k+1} = \xi_{01} \sin\left[p_b t - \frac{2\pi}{n}(k+1)\right] = \xi_{01} \sin\left(\varphi_k - \frac{2\pi}{n}\right),$$

where

$$\varphi_k = p_b t - \frac{2\pi}{n} k.$$

Using these expressions, we obtain

$$M_{el} = c_0 \xi_0 \left\{ 2 \sin \varphi_k - \sin\left(\varphi_k - \frac{2\pi}{n}\right) - \sin\left(\varphi_k + \frac{2\pi}{n}\right) \right\}.$$

Taking into account that

$$\sin\left(\varphi_k + \frac{2\pi}{n}\right) = \sin \varphi_k \cos \frac{2\pi}{n} + \cos \varphi_k \sin \frac{2\pi}{n};$$

$$\sin\left(\varphi_k - \frac{2\pi}{n}\right) = \sin \varphi_k \cos \frac{2\pi}{n} - \cos \varphi_k \sin \frac{2\pi}{n},$$

we finally obtain the following expression:

$$M_{el} = 2c_0\left[1-\cos\frac{2\pi}{n}\right]\xi_0\sin\varphi_k =$$
$$= 2c_0\left[1-\cos\frac{2\pi}{n}\right]\xi_0\sin\left[p_b t - \frac{2\pi}{n}\cdot k\right].$$

In the case of ordinary elastic elements of angular stiffness c_{eq} located between the blade and hub casing, we would have

$$M_{el} = c_{eq}\,\xi_0\sin\left[p_k t - \frac{2\pi}{n}\cdot k\right].$$

Thus, the interblade elastic elements for the given blade are equivalent to one ordinary elastic element of stiffness

$$c_{eq} = 2c_0\left[1-\cos\frac{2\pi}{n}\right]. \qquad (6.9)$$

We can also establish exactly that the interblade dampers for the given /327
blade are equivalent to one ordinary damper lashed up between the blade and hub casing and having a damping coefficient

$$k_{eq} = 2k_0\left[1-\cos\frac{2\pi}{n}\right]. \qquad (6.10)$$

Consequently, calculation of ground resonance of a helicopter with elastic interblade coupling and dampers can be carried out by conventional formulas, taking the coefficient of the damper as equal to k_{eq} and the stiffness coefficient in the drag hinge as equal to c_{eq}.

TABLE 3.2

Number of Blades	2	3	4	5	6
$\frac{c_{eq}}{c_0} = \frac{k_{eq}}{k_0}$	4	3.73	2	1.382	1

Table 3.2 presents the values of the quantity

$$\frac{c_{eq}}{c_0} = \frac{k_{eq}}{k_0} = 2\left(1-\cos\frac{2\pi}{n}\right) \qquad (6.11)$$

for rotors with a different number of blades.

One of the shortcomings of a rotor with interblade dampers lies in the fact that, during simultaneously deflections of the blades relative to the drag hinges (all to one side and by the same angle) which might occur in transition flight regimes and during run-up of the rotor, such dampers do not operate.

In existing hub designs, this drawback is sometimes eliminated by using composite designs in which the elastic elements are made in the form of interblade couplings while the dampers are made separately for each blade, i.e., are mounted between blade and hub casing.

3. Selection of Stiffness and Damping Characteristics for Landing Gears*

After choosing the characteristics of the blade dampers, the basic parameters of the landing gear can be selected. For helicopters of the usual single-rotor and fore-and-aft configurations the wheel track 2a (see Fig.3.17) should be selected such that the natural vibration frequency p_{pn} of the helicopter during the ground run (rotation about the longitudinal axis going through the center of gravity) with inoperative struts (only the tires are operative) is approximately 20% higher than the operating rpm of the rotor. This is given by the condition (4.19):

$$p_{pn}=1.2\omega_{op}=\sqrt{\frac{2c_{pn}^{y}a^{2}}{I_c}}.$$

If the landing gear is of the four-wheel type, the quantity $2c_y^{pn}a^2$ in the above formula must be replaced by the quantity $c_{\varphi_x} = c_{\varphi_1} = c_{\varphi_2}$ [see eq.(5.3)].

Since the tires are selected in terms of a standing load, the quantity c_{pn}^{y} in the given formula can be considered as known; therefore, it will yield the corresponding value of a.

The stiffness of the shock absorbers and their damping can be selected by assuming that the center of the instability zone during the ground run (during vibrations with operative struts) coincides with the operating rpm of the rotor. Such an approach issues from the following considerations: If the stiffness /328
of the shock absorbers is selected such that the unstable range during the ground run is greater than the operating rpm, ground resonance might occur at the instant of becoming airborne (see Sect.4, Subsect.3) since, during vibrations of the helicopter on lift-off of the tires, the instability zone can "descend" to the operating rpm. It is usually impossible to make the instability zone lower than the operating rpm (with the exception of the landing gear of the Bristol system whose design, however, is rather complex) since this would require an unfeasibly low stiffness of the shock absorbers. On the other hand, if the instability zone is located directly at the operating rpm and the damping margin is sufficient, no ground resonance on breaking contact with the ground can occur since, during lift-off of the tires, the instability zone will be lower than the operating rpm. This was checked in numerous calculations and programming on an electronic computer of ground resonance on tire lift-off, performed by engineer Yu.A.Myagkov.

For simplicity, let us assume that the landing gear is equipped with vertical shock absorber struts (see Fig.3.17,b). As shown in Section 2, Subsection 5, the maximum damping of the tire-oleo system obtainable in choosing the optimal damping of the shock absorber depends on the ratio $\frac{c_{s.a}}{c_{pn}^{y}}$. Making use of

* The method of selecting the landing gear parameters proposed here was developed by engineer Yu.A.Myagkov.

eqs.(2.37) and (2.38) and considering that, during the ground run,

$$\bar{n}_0 = \frac{k_{eq}^{max} a^2}{I_c p_\varphi}; \quad p_\varphi = \sqrt{\frac{2c_{eq}a^2}{I_c}},$$

we can obtain the following formula which determines the maximum possible coefficient of available helicopter damping during the ground run:

$$[\bar{n}_0]_{max}^{avail} = \frac{0.25}{\sqrt{\varkappa(1+\varkappa)}}, \tag{6.12}$$

where

$$\varkappa = \frac{c_{s.a}}{c_{pn}^{y}}. \tag{6.13}$$

This means that the maximum possible damping coefficient which can be obtained during the ground run by varying the quantity $k_{s.a}$ depends exclusively on the ratio $\frac{c_{s.a}}{c_{pn}^{y}}$. Therefore, knowing the damping required for the elimination of ground resonance, it is easy to determine the necessary stiffness of the shock absorber $c_{s.a}$. If the blade damping is known, the required damping $\bar{n}_0$ can be determined by eq.(1.31)

$$[\bar{n}_0]_{req} = \frac{\varepsilon(1-\nu_0)}{8\nu_0 \bar{n}_b^{pn}} \bar{p}^* \Delta, \tag{6.14}$$

where $\bar{n}_b^{pn}$ is the damping coefficient of the blade $\bar{n}_b$ referred to the natural vibration frequency p_{pn} of the helicopter during the ground run with inoperative struts (using only the tires):

$$\left.\begin{aligned} \bar{n}_b^{pn} &= \frac{n_b}{p_{pn}}; \\ p_{pn} &= \sqrt{\frac{2c_y^{pn}a^2}{I_c}}; \end{aligned}\right\} \tag{6.15}$$

$\bar{p}^*$ is the natural vibration frequency of a helicopter with operative struts at optimal damping, referred to the quantity p_{pn}: /329

$$\bar{p}^* = \frac{p^*}{p_{pn}} = \sqrt{\frac{2\varkappa}{1+2\varkappa}}. \tag{6.16}$$

It is required to provide a damping margin of

$$\eta = \frac{[\bar{n}_0]_{max}^{avail}}{[\bar{n}_n]_{req}}. \tag{6.17}$$

Using eqs.(6.12), (6.14), and (6.16), we obtain

$$\eta=\frac{0.25}{\sqrt{\varkappa(1+\varkappa)}}\,\frac{8\nu_0\overline{n}_b^{pn}}{\varepsilon(1-\nu_0)}\sqrt{\frac{1+2\varkappa}{2\varkappa}}\cdot\frac{1}{\Delta}.$$

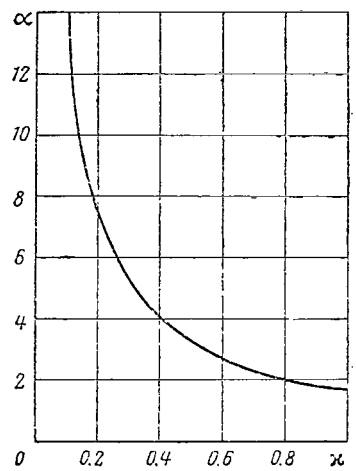

Fig.3.52 Graph of the Dependence of the Coefficient α on $\varkappa$.

This relationship can be rewritten in the following manner:

$$\frac{\varepsilon(1-\nu_0)}{\nu_0}\,\frac{\eta}{\overline{n}_b^{pn}}\Delta=\alpha, \tag{6.18}$$

where

$$\alpha=\sqrt{\frac{2(1+2\varkappa)}{\varkappa^2(1+\varkappa)}}. \tag{6.19}$$

After selecting the blade and tire characteristics and designating the necessary damping margin η, the left-hand side of eq.(6.18) is known. Knowing the quantity α, it is easy to find the quantity $\varkappa$ from eq.(6.19) and then the necessary stiffness $c_{s.a}$ of the shock absorber. For convenience of determining $\varkappa$, Fig.3.52 gives the graph of the dependence $\alpha(\varkappa)$.

To select the stiffness $c_{s.a}$ by the indicated method, we can take $\eta = 1$ since the "kinematic" damping of the tire during the ground run is disregarded in the formulas [see eq.(4.21)]. The actual damping margin η with consideration of this additional damping should be at least 1.5 - 2*.

After the stiffness of the shock absorber is found, its optimal damping coefficient can be determined by eq.(2.36), namely

$$k_{s.a}^{opt}=\frac{c''_{pn}+c_{s.a}}{p^*}, \tag{6.20}$$

where

$$p^*=p_{pn}\overline{p}^*=p_{pn}\sqrt{\frac{2\varkappa}{1+2\varkappa}}. \tag{6.21}$$

Since, in reality, the characteristic of the shock absorber damping is generally nonlinear (Sect.3, Subsect.1), we must understand by the quantity $k_{s.a}^{opt}$ the damping coefficient of an equivalent linear shock absorber.

* It should be recalled here that the case without kinematic damping is obtained during vibrations of a helicopter on ice, when there is no friction between tire and ground (see Sect.4, Subsect.2).

4. Certain Recommendations for Landing Gear Design /330

One of the basic difficulties in designing a landing gear is the complexity of providing the necessary damping of the shock strut. If the size of the orifices through which the hydraulic fluid passes when the shock absorber is operative is selected from the condition of ground resonance, then, as a rule, the work of the shock absorber during landing will be unsatisfactory (the forces will be too great when making contact with the ground). If this size is selected from the conditions of landing, then we obtain too small a damping during helicopter lateral vibrations, which is completely insufficient for avoiding ground resonance.

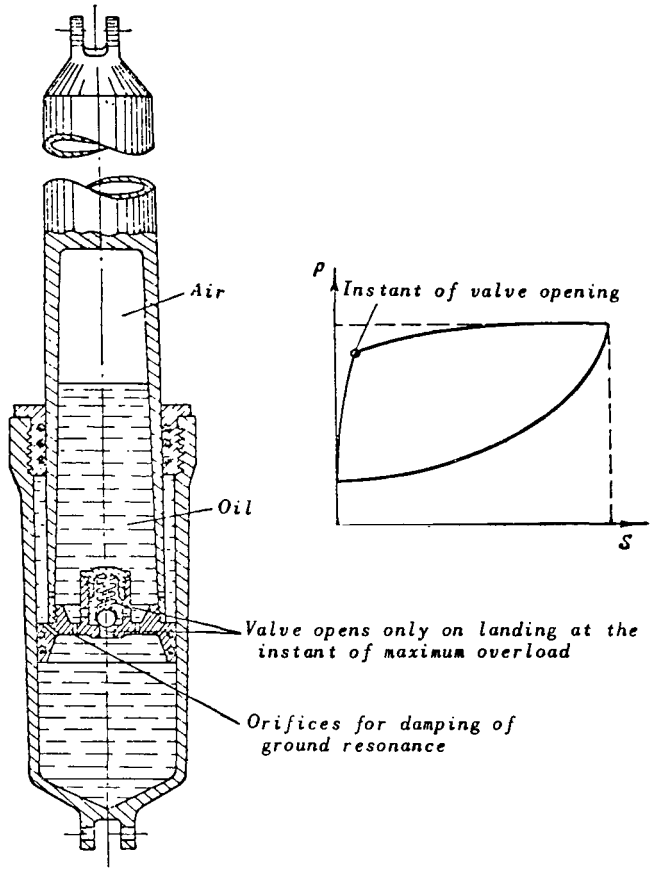

Fig.3.53 Shock Strut with Valve.

This difficulty can be overcome by two methods (Ref.18):

1) increase in damping on the backstroke of the shock absorber;
2) installation of special valves in the design of the shock absorber.

The first of these methods is the simplest and involves the following: The size of the orifices through which the hydraulic fluid is forced during the forward stroke of the shock absorber (compression) is selected from the landing conditions, while the size of the orifices through which the hydraulic fluid passes during the return stroke of the shock absorber (extension) is selected from the ground resonance conditions. This is possible because of the fact that, during helicopter vibrations, one of the shock struts (right or left) executes a backstroke at each instant of time. Therefore, /331 generally speaking, the necessary damping coefficient of the helicopter at ground resonance can be secured only by damping in the backstroke of the shock absorbers.

However, damping in the backstroke can be increased only within certain limits. An extreme increase of damping in the backstroke (very small orifices) leads to a very slow "emergence" of the shock absorber struts from a compressed state after touchdown. Therefore, in heavy rolled landing on rough ground when

the first touchdown may be followed by further impacts, such a method of increasing the damping might be unacceptable.

The second method does not have this shortcoming and involves the following: A special spring valve is placed in the shock absorber, which opens only when the compressive force in the shock absorber exceeds (at touchdown) a certain critical value $P^{cr}_{s.a}$. At $P_{s.a} < P^{sp}_{s.a}$, those orifices whose size had been selected from conditions of ground resonance will be operative while at $P_{s.a} > P^{sp}_{s.a}$ the orifices of larger diameter whose size had been based on conditions of limiting the landing overload become operative. Figure 3.53 shows a design scheme and a diagram of dynamic compression of such a shock absorber.

Another important factor to be allowed for in designing a landing gear is the inevitable presence in any shock absorber of prestressing forces (Sect.2, Subsect.7), i.e., forces in whose presence the shock absorber begins to operate. For a helicopter landing gear, it is desirable to have the smallest possible preloading forces P_0 since, at high rotor thrust, the forces P on the landing gear decrease and since, at $P < P_0$, the shock absorbers do not operate. In this case, ground resonance may develop with inoperative shock absorbers on elastic tires which are virtually without damping. For helicopter landing gears, the strut characteristics must be chosen such that the prestressing force will not be more than 10% of the standing load on the shock absorber at zero rotor thrust.

CHAPTER IV /332

THEORETICAL PRINCIPLES OF CALCULATING BEARINGS OF MAIN HELICOPTER COMPONENTS

The service life of the main components of a helicopter depends in many respects upon the performance of their bearing assemblies, which means that considerable attention must be paid to problems of the theory of calculating antifriction bearings in helicopter engineering.

As known, the life expectancy of general-purpose antifriction bearings may vary within wide limits owing to various factors of a metallurgical and technological nature. In this respect, the necessary reliability of bearing assemblies in general machine construction is achieved by introducing suitable safety factors, i.e., some overestimate of design loads. It is logical that, in this case, the requirement for accuracy of calculation of bearings can be reduced substantially. Of course, for aircraft components, where an increase in reliability should be attained by improving the design without increasing the size and weight of the bearing assemblies, such a procedure is unacceptable. This is all the more so since aircraft bearings are manufactured from high-quality materials, have high precision, and are subjected to very strict inspection in production, as result of which the dispersion of their service life is noticeably reduced. Aircraft bearings, including those used in helicopters, should be calculated as accurately as possible with consideration of the peculiarities of their loading and service.

In recent years, thanks to studies by Soviet and foreign researchers, considerable advances have been made in practical calculation methods for antifriction bearings; nevertheless, these are by no means always sufficiently accurate. This is especially true of bearings working under complex combinations of external loads and vibrations with small amplitudes; these are the cases of greatest interest for helicopter engineering. The lack of reliable calculation methods for antifriction bearings working under the above-indicated conditions, handicaps the design of reducing gears, pitch controls, and hubs of the main and tail rotors of helicopters. We can cite many examples where these vitally important components failed prematurely due to the failure of improperly selected bearings.

In this Chapter, we will attempt to report the results of theoretical and experimental investigations which had the purpose of refining the calculation methods for bearings of helicopter components. As shown in practical use, the methods of calculation given below permit a fuller utilization of the load-carrying capacity of the bearings. Such methods, in designing bearing assemblies, /333 have frequently made it possible to create sufficiently compact and light structures capable of operating reliably for protracted periods of time at relatively high loads.

Section 1. Equations of Static Equilibrium of Radial and Radial-Thrust Ball Bearings under Combined Load

The relations used in the calculation of bearings are based on results of investigations of the distribution of external loads over the rolling bodies.

We will construct equations from which we can derive the pressure on the balls in the general case of loading of radial and radial-thrust ball bearings.

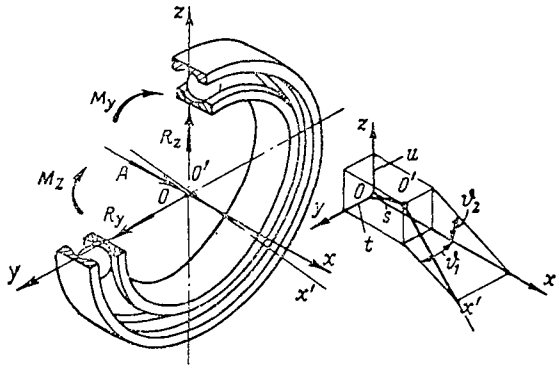

Fig.4.1 Scheme of Displacements of Inner Race of Bearing under an Arbitrary External Load.

Let a single-row ball bearing, after landing, have a radial play 2Δ on the shaft and in the housing at an established operating temperature regime of the assembly.

Let us take a rectangular coordinate system xyz with its origin at the center O of the outer race. The x-axis is directed along the axis of rotation of this race (see Fig.4.1).

Upon applying an arbitrary external load to the bearing, the center of the inner race is shifted to a point O′ with coordinates s, t, and u, while its axis of rotation x′ is deflected relative to the x-axis through some angle ϑ whose projections onto the planes xOy and xOz are equal to ϑ_1 and ϑ_2, respectively (Fig.4.1).

Let us assume that the ball whose center O_{ba} lies in the plane P1 which, together with the plane xOz, makes the angle ψ is acted upon by normal forces P_ψ identical in magnitude and directed along a common straight line passing through the centers O_{out} and O_{in} of the cross sections of the raceways of the outer and inner races and the point O_{ba} (Fig.4.2). As is common in the theory of antifriction bearings, we will disregard any displacement of the center of the contact area of the ball with the inner race from the plane P1 as well as the tangential forces arising at the points of contact of the ball with the races.

According to the well-known Hertz formula, we have

$$P_\psi = B\delta_\psi^{3/2}. \tag{1.1}$$

Here, δ_ψ is the convergence of the raceways of the races in the direction $O_{out}O_{in}$ due to elastic deformations at the contact zones.

For ball bearings with the usual internal geometry, we can put /334

$$B = \nu B_0 \frac{d_{ba}^2}{g^{3/2}}, \tag{1.2}$$

where

ν = factor depending on the relation between the radii r_{out} and r_{in} of the raceways of the outer and inner races and the diameter of the ball d_{ba};

$g = r_{out} + r_{in} - d_{ba}$ = distance between the points O_{out} and O_{in} at the moment of contact of the ball with the races (when $\delta_\psi = 0$).

If the diameter d_{ba} is expressed in millimeters and the forces in kilograms, then at a modulus of elasticity $E = 2.08 \times 10^6$ kg/cm^2, of the material of the races and balls, the coefficient B_0 is equal to 62.

The factor ν has values indicated in Table 4.1.

TABLE 4.1

$r_{out\,(in)}/d_{ba}$	0.510	0.515	0.520
ν	0.63	1.00	1.39

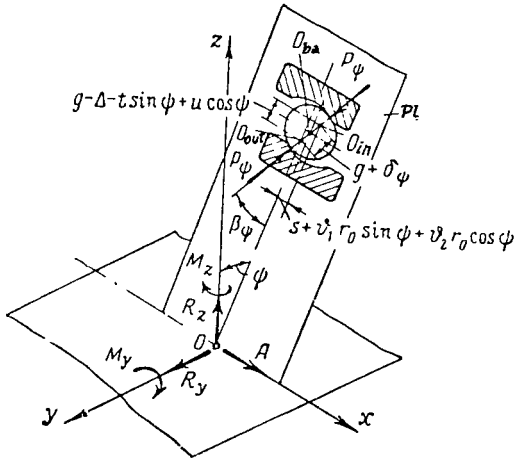

Fig.4.2 Polygon of Forces Acting on the Ball.

It follows from the conditions of static equilibrium of the bearing elements that the external forces and moments applied to the inner race can be written as (see Fig.4.2)

$$\left.\begin{aligned} A &= \sum P_\psi \sin\beta_\psi; \\ R_y &= -\sum P_\psi \cos\beta_\psi \sin\psi; \\ R_z &= \sum P_\psi \cos\beta_\psi \cos\psi; \\ M_y &= r_0 \sum P_\psi \sin\beta_\psi \cos\psi; \\ M_z &= r_0 \sum P_\psi \sin\beta_\psi \sin\psi. \end{aligned}\right\} \qquad (1.3)$$

Here,

β_ψ = angle of contact between ball and races;

r_0 = radius at which the centers of the balls are located. The sign Σ extends over all loaded balls.

Let us assume that the races have a perfectly regular geometric shape which does not change when a load is applied. In this case, to determine the convergence of the raceways δ_ψ and the angle of contact β_ψ we can use the formulas

$$\delta_\psi = [(s + \vartheta_1 r_0 \sin\psi + \vartheta_2 r_0 \cos\psi)^2 + (g - \Delta - t\sin\psi + u\cos\psi)^2]^{1/2} - g; \quad (1.4)$$

$$\beta_\psi = \tan^{-1} \frac{s + \vartheta_1 r_0 \sin\psi + \vartheta_2 r_0 \cos\psi}{g - \Delta - t\sin\psi + u\cos\psi}. \quad (1.5)$$

Having expressed, in eqs.(1.4) and (1.5), all linear quantities in fractions of the distance g, we can rewrite them in the form /335

$$\bar{\delta}_\psi = [(\bar{s} + \bar{\varepsilon}_1 \sin\psi + \bar{\varepsilon}_2 \cos\psi)^2 + (\cos\beta_0 - \bar{t}\sin\psi + \bar{u}\cos\psi)^2]^{1/2} - 1; \quad (1.6)$$

$$\beta_\psi = \tan^{-1} \frac{\bar{s} + \bar{\varepsilon}_1 \sin\psi + \bar{\varepsilon}_2 \cos\psi}{\cos\beta_0 - \bar{t}\sin\psi + \bar{u}\cos\psi}, \quad (1.7)$$

where $\beta_0 = \cos^{-1} \frac{g - \Delta}{g}$ is the so-called initial angle of contact (angle of contact in purely axial displacement of the races due to the operating radial play 2Δ).

In eqs.(1.6) and (1.7), the terms $\bar{\varepsilon}_1$ and $\bar{\varepsilon}_2$ denote the quantities $\vartheta_1 \frac{r_0}{g}$ and $\vartheta_2 \frac{r_0}{g}$.

It should be borne in mind that the operative axial play of the bearing s_0 is connected with the angle β_0 by the following relation:

$$2s_0 = 2g\sin\beta_0$$

or, changing to relative quantities,

$$2\bar{s}_0 = 2\sin\beta_0. \quad (1.8)$$

The relative quantities are denoted everywhere by the same letters as the absolute quantities but with vinculi.

These equations describe the conditions of static equilibrium of radial and radial-thrust ball bearings under any combinations of external loads. They permit finding all parameters characterizing the distribution of forces between individual balls. However, it should be remembered that, due to the complexity of the correlations between the quantities δ_ψ and β_ψ and the relative displacement of the races, practical application of these equations involves a large calculation volume. In engineering calculations these are usually replaced by various approximate correlations. One of the most convenient variants of such correlations, with a sufficiently high accuracy, is described below.

An analysis of the operating conditions of bearing assemblies of various types shows that, in most cases, the resultant radial force $R = (R_y^2 + R_z^2)^{1/2}$ and the resultant moment $M = M_y^2 + M_z^2)^{1/2}$ absorbed by the bearing act in one and the same plane. In conformity with this, by laying out the plane of the coordinates xOz such that it coincides with the plane of action of the external loads applied to the bearing, we can write

$$\left.\begin{aligned} R_y &= 0; \\ R_z &= R; \\ M_y &= M; \\ M_z &= 0. \end{aligned}\right\} \tag{1.9}$$

As shown by calculations, the load distribution depends little on the angular arrangement of the set of balls. Taking this into account, we can assume that the balls are arranged symmetrically with respect to the plane xOz. Under this condition, we have

$$\left.\begin{aligned} \bar{t} &= 0; \\ \bar{\varepsilon}_1 &= 0; \\ \bar{\varepsilon}_2 &= \bar{\varepsilon} = \vartheta \frac{r_0}{g}. \end{aligned}\right\} \tag{1.10}$$

Keeping in mind the equalities (1.10), we then expand eq.(1.6) in a Maclaurin series in the neighborhood of $\bar{u} = 0$ and $\bar{\varepsilon}_2 = \bar{\varepsilon} = 0$. Limiting ourselves to linear terms we obtain, after easy transformations, /336

$$\bar{\delta}_\psi = \bar{\delta} + (\bar{u}\cos\beta + \bar{\varepsilon}\sin\beta)\cos\psi. \tag{1.11}$$

In the equality (1.11), we have

$$\bar{\delta} = (\bar{s}^2 + \cos^2\beta_0)^{1/2} - 1 \tag{1.12}$$

and

$$\beta = \tan^{-1}\left(\frac{\bar{s}}{\cos\beta_0}\right). \tag{1.13}$$

The quantities $\bar{\delta}$ and β are none other than the relative convergence of the raceways and the angle of contact in the cross section $\psi = 90^\circ$.

As follows from eq.(1.7),

$$\left.\begin{aligned} \sin\beta_\psi &= \frac{\bar{s} + \bar{\varepsilon}_1\sin\psi + \bar{\varepsilon}_2\cos\psi}{[(\bar{s} + \bar{\varepsilon}_1\sin\psi + \bar{\varepsilon}_2\cos\psi)^2 + (\cos\beta_0 - \bar{t}\sin\psi + \bar{u}\cos\psi)^2]^{1/2}}; \\ \cos\beta_\psi &= \frac{\cos\beta_0 - \bar{t}\sin\psi + \bar{u}\cos\psi}{[(\bar{s} + \bar{\varepsilon}_1\sin\psi + \bar{\varepsilon}_2\cos\psi)^2 + (\cos\beta_0 - \bar{t}\sin\psi + \bar{u}\cos\psi)^2]^{1/2}}. \end{aligned}\right\} \tag{1.14}$$

Treating the equalities (1.14) in the same manner as eq.(1.6), discarding all nonlinear terms, and making appropriate transformations, we obtain

$$\left.\begin{aligned} \sin\beta_\psi &= \sin\beta\left[1 - \frac{\cos^2\beta}{\cos\beta_0}(\bar{u} - \bar{\varepsilon}\cot\beta)\cos\psi\right]; \\ \cos\beta_\psi &= \cos\beta\left[1 + \frac{\sin^2\beta}{\cos\beta_0}(\bar{u} - \bar{\varepsilon}\cot\beta)\cos\psi\right]. \end{aligned}\right\} \tag{1.15}$$

Having put

$$\frac{\bar{u}\cos\beta+\bar{\varepsilon}\sin\beta}{\bar{\delta}}=\lambda, \tag{1.16}$$

we can represent eqs.(1.11) and (1.15) in the form

$$\bar{\delta}_\psi=\bar{\delta}(1+\lambda\cos\psi); \tag{1.17}$$

$$\left.\begin{aligned}\sin\beta_\psi&=\sin\beta\left[1-\frac{\cos\beta}{\cos\beta_0}\left(\lambda\bar{\delta}-\frac{\bar{\varepsilon}}{\sin\beta}\right)\cos\psi\right];\\ \cos\beta_\psi&=\cos\beta\left[1+\frac{\cos\beta}{\cos\beta_0}\tan^2\beta\left(\lambda\bar{\delta}-\frac{\bar{\varepsilon}}{\sin\beta}\right)\cos\psi\right].\end{aligned}\right\} \tag{1.18}$$

The quantity $\bar{\delta}$ determining the pressure on the ball whose center lies in the plane xOy can be expressed in terms of the angles β and β_0:

$$\bar{\delta}=\frac{\cos\beta_0}{\cos\beta}-1. \tag{1.19}$$

The loading zone of the bearing, as is known, can be found from the condition that $\bar{\delta}_\psi = 0$ at its boundaries.

Setting $\bar{\delta}_\psi = 0$ in the equality (1.17), we obtain the following expression established at the boundaries of the loading zone:

$$\psi'_{i_0}{}''=\cos^{-1}\left(-\frac{1}{\lambda}\right). \tag{1.20}$$

The relative convergence of the raceways of the races $\bar{\delta}_\psi$ attains a maximum $\bar{\delta}_0$ at the center of the loading zone, which is situated in the cross section $\psi = \psi_0 = 0$, if $\bar{u}\cos\beta + \bar{\varepsilon}\sin\beta = \bar{\delta}\lambda \geq 0$, and in the cross section $\psi = \psi_0 = 180^\circ$, if $\bar{u}\cos\beta + \bar{\varepsilon}\sin\beta = \bar{\delta}\lambda < 0$ (Fig.4.3). /337

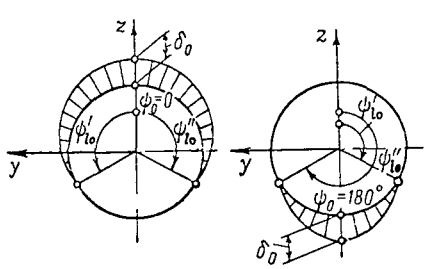

Fig.4.3 Loading Zone of Bearing.

In the case $\psi_0 = 0$, $0 < \psi''_{i_0} \leq 180^\circ$ and $\psi'_{i_0} = -\psi''_{i_0}$, and in the case $\psi_0 = 180^\circ$, $180^\circ < \psi''_{i_0} \leq 360^\circ$ and $\psi'_{i_0} = 360^\circ - \psi''_{i_0}$.

It is understandable that eq.(1.20) holds only if the parameter λ exceeds unity in absolute magnitude. If $|\lambda| \leq 1$, then the loading zone will be 360°, i.e., all balls will carry a load in the bearing; in this case, the quantity $\bar{\delta}$ is always positive and the sign of λ coincides with the sign of $\cos\psi_0$. The latter means that, for bearings in which all balls are loaded $0 \leq \lambda \leq 1$ at $\psi_0 = 0$, and $-1 \leq \lambda \leq 0$ at $\psi_0 = 180^\circ$.

Having taken $\psi = \psi_0$ in the equality (1.17), we find

$$\bar{\delta}_0 = \bar{\delta}(1 + \lambda \cos \psi_0). \tag{1.21}$$

By means of eq.(1.2), (1.17), and (1.21), recalling that $\bar{\delta}_\psi = \frac{\delta_\psi}{g}$, we can reduce eq.(1.1) to the form

$$P_\psi = B_0 z d_{ba}^2 \bar{\delta}_0^{3/2} \left(\frac{1 + \lambda \cos \psi}{1 + \lambda \cos \psi_0} \right)^{3/2}. \tag{1.22}$$

Equations (1.19) and (1.21) show that in the case $\lambda = \infty$, i.e., at a 180° loading zone $\bar{\delta} = 0$ so that $\beta = \beta_0$ is independent of the loading level.

Let us introduce into the examination the sum

$$J_k = \frac{1}{z(1 + \lambda \cos \psi_0)^{3/2}} \sum (1 + \lambda \cos \psi)^{3/2} \cos^{k-1} \psi, \tag{1.23}$$

where

$$k = 1, 2, 3.$$

Here, as in all preceding equalities, the angle ψ can assume only the discrete values that determine the angular position of the loaded balls.

Let us next transform eqs.(1.3) by means of the obtained expression.

After substituting in these equations P_ψ, $\sin \beta_\psi$, and $\cos \beta_\psi$ by their values from eqs.(1.22) and (1.18) in conformity with the equalities (1.9) and (1.23) and taking eq.(1.21) into account, we obtain

$$\left.\begin{aligned}
&\frac{A}{z v d_{ba}^2} = B_0 \bar{\delta}_0^{3/2} \sin \beta J_1 \times \\
&\quad \times \left[1 - \frac{\cos \beta}{\cos \beta_0} \left(\frac{\lambda \bar{\delta}_0}{1 + \lambda \cos \psi_0} - \frac{\bar{\varepsilon}}{\sin \beta} \right) \frac{J_2}{J_1} \right]; \\
&\frac{R}{z v d_{ba}^2} = B_0 \bar{\delta}_0^{3/2} \cos \beta J_2 \times \\
&\quad \times \left[1 + \frac{\cos \beta}{\cos \beta_0} \tan^2 \beta \left(\frac{\lambda \bar{\delta}_0}{1 + \lambda \cos \psi_0} - \frac{\bar{\varepsilon}}{\sin \beta} \right) \frac{J_3}{J_2} \right]; \\
&\frac{M}{r_0 z v d_{ba}^2} = B_0 \bar{\delta}_0^{3/2} \sin \beta J_2 \times \\
&\quad \times \left[1 - \frac{\cos \beta}{\cos \beta_0} \left(\frac{\lambda \bar{\delta}_0}{1 + \lambda \cos \psi_0} - \frac{\bar{\varepsilon}}{\sin \beta} \right) \frac{J_3}{J_2} \right].
\end{aligned}\right\} \tag{1.24}$$

Equations (1.19) and (1.21) yield the following expression for the angle β:

$$\cos\beta = \frac{\cos\beta_0}{1 + \frac{\bar{\delta}_0}{1+\lambda}}. \tag{1.25}$$

The equalities (1.24) and (1.25) constitute relations which, in engineering calculations, can replace the "exact" equations of static equilibrium of radial and radial-thrust ball bearings. As shown by actual investigations, the error produced by this substitution in the end results usually does not exceed a few percent.

When changing the number of balls, the sums (1.23) vary only slightly. This permits expressing them in terms of the integrals

$$j_k = \frac{1}{2\pi(1+\lambda\cos\psi_0)^{3/2}} \int_{\psi'_{l0}}^{\psi''_{l0}} (1+\lambda\cos\psi_0\cos\psi)^{3/2}\cos^{k-1}\psi\, d\psi, \tag{1.26}$$

which are a function of the product $\lambda\cos\psi_0$. Here, k = 1, 2, 3.

It is easy to demonstrate that, with the usual number of balls, we have

$$J_k \approx \cos^{k-1}\psi_0 j_k. \tag{1.27}$$

The values of the integrals j_k are given in Table 4.2.

Table 4.2

$\lambda\cos\psi_0$	j_1	j_2	j_3	w	$\lambda\cos\psi_0$	j_1	j_2	j_3	w
0	1.000	0.000	0.500	1.000	3.33	0.323	0.247	0.210	0.612
0.1	0.868	0.065	0.435	0.879	5	0.309	0.242	0.207	0.605
0.2	0.766	0.114	0.385	0.804	10	0.294	0.236	0.203	0.596
0.3	0.686	0.151	0.346	0.757	20	0.286	0.233	0.201	0.59
0.4	0.622	0.180	0.316	0.726	$\pm\infty$	0.279	0.229	0.199	0.587
0.5	0.570	0.202	0.292	0.705	—20	0.271	0.225	0.197	0.583
0.6	0.528	0.220	0.273	0.690	—10	0.262	0.221	0.194	0.578
0.7	0.494	0.233	0.258	0.678	—5	0.247	0.212	0.188	0.567
0.8	0.466	0.243	0.246	0.670	—3.33	0.229	0.201	0.181	0.556
0.9	0.443	0.250	0.237	0.663	—2.5	0.211	0.189	0.172	0.543
1	0.425	0.255	0.231	0.657	—2	0.192	0.175	0.162	0.528
1.111	0.409	0.257	0.226	0.651	—1.667	0.171	0.159	0.149	0.512
1.25	0.395	0.258	0.223	0.645	—1.429	0.147	0.140	0.133	0.488
1.429	0.380	0.258	0.220	0.639	—1.25	0.120	0.116	0.112	0.459
1.667	0.366	0.256	0.218	0.633	—1.111	0.084	0.083	0.080	0.414
2	0.352	0.254	0.215	0.626	—1	0.000	0.000	0.000	0.000
2.5	0.338	0.251	0.212	0.619					

Section 2. Calculation of Radial and Radial-Thrust Ball Bearings under Combined Loads, for Absence of Misalignment of the Races

1. Pressure on Balls

If the distance between the bearings is large in comparison with the diametral dimensions of the bearings and if all components of the bearing assembly have a high rigidity, then, in calculations of the pressures on the rolling bodies, we can disregard the misalignment of the races under load and take into account only their displacements in radial and axial directions.

Let us introduce the quantities $\bar{\delta}_0$ and λ into eq.(1.22) which determines the pressures on the balls in radial and radial-thrust ball bearings.

Equations (1.24) and (1.25) which connect these quantities with the external loads applied to the bearing, in the absence of misalignment of the races, i.e., in the case $\vartheta = 0$, can be represented in the form

$$\left.\begin{aligned} \frac{A}{z\nu d_{ba}^2} &= B_0\bar{\delta}_0^{3/2}\sin\beta j_1\left(1-\frac{\cos\beta}{\cos\beta_0}\frac{\lambda\bar{\delta}_0}{1+\lambda}\frac{j_2}{j_1}\right);\\ \frac{R}{z\nu d_{ba}^2} &= B_0\bar{\delta}_0^{3/2}\cos\beta j_2\left(1+\frac{\cos\beta}{\cos\beta_0}\tan^2\beta\,\frac{\lambda\bar{\delta}_0}{1+\lambda}\frac{j_3}{j_2}\right); \end{aligned}\right\} \tag{2.1}$$

$$\cos\beta = \frac{\cos\beta_0}{1+\frac{\bar{\delta}_0}{1+\lambda}}. \tag{2.2}$$

We will not write out the expression for the moment since, at $\vartheta = 0$, it does not play an independent role and is not used in the calculation.

We will assume, for convenience, that the direction of the z-axis coincides with the direction of the radial load R. Under this condition, the radial displacement u is positive, and hence the angle ψ_0 is equal to zero. This fact is taken into account both in eqs.(2.1) and (2.2) and in all subsequent relations.

It should be noted that the case $\vartheta = 0$ is fundamental in the theory of antifriction bearings. Usually, when no special stipulations are made as to design and characteristics of loading a bearing assembly, this is the case applicable. Basic investigations (Refs.22, 23, 29, and 42) have been carried out to refine the calculation of antifriction bearings working under combined loads.

The static load capacity of a bearing is characterized by the magnitude of maximum pressure on the rolling body.

According to eq.(1.22) the maximum pressure on the ball is

$$P_0 = B_0\nu d_{ba}^2\bar{\delta}_0^{3/2}. \tag{2.3}$$

For protracted static loads on a nonrotating bearing, the maximum bearing

stress σ_{max} on the track of the inner race caused by this pressure should not exceed 40,000 kg/cm^2. If the static loads acting on a nonrotating bearing create greater contact stresses, then noticeable traces of residual deformations, in the form of depressions made by the balls, will appear on the track.

The indicated permissible value of σ_{max} is selected from the condition that the extent of residual deformation (permanent set) of the track is not more than one micron per centimeter of the ball's diameter. In this case, the smoothness of the bearing rotation is not disturbed and the bearing capacity is not lessened. /340

In the relations required to calculate the life expectancy of bearings, the quantity

$$P_{eq}=\left(\frac{1}{2\pi}\int_{\psi'_{lo}}^{\psi''_{lo}} P_{\psi}^{m}\,d\psi\right)^{1/m}, \tag{2.4}$$

appears, where m is the exponent of the load in the life expectancy formulas.

By means of the equalities (1.22) and (2.3), we reduce the expression (2.4) to the form

$$P_{eq}=wP_0. \tag{2.5}$$

The coefficient w here is equal to

$$w=\left[\frac{1}{2\pi(1+\lambda\cos\psi_0)^{3/2m}}\int_{\psi'_{lo}}^{\psi''_{lo}}(1+\lambda\cos\psi_0\cos\psi)^{3/2m}\,d\psi\right]^{1/m}. \tag{2.6}$$

We note that the quantity P_{eq} is the constant pressure P_{ψ} = const, at which the probability of fatigue failure of the rotating race under the given service conditions is the same as for the actual distribution of forces between the balls. This justifies denoting it as the equivalent pressure on the ball for a rotating race.

It should be borne in mind that, in some cases, it is impossible to relate the quantity P_{eq} to the entire length of the track as is done in eq.(2.4), but only to the loaded zone $\psi''_{lo}-\psi'_{lo}$.

At m = 3.33, as is adopted in Soviet practice,

$$w=\left\{\frac{1}{\pi(1+\lambda\cos\psi_0)^5}\left[\frac{\psi''_{lo}-\varphi'_{lo}}{2}\left(1+5\lambda^2+\frac{15}{8}\lambda^4\right)-\right.\right. \tag{2.7}$$

$$\left.\left.-\tan\psi''_{lo}\left(\frac{137}{60}+\frac{607}{120}\lambda^2+\frac{8}{15}\lambda^4\right)\right]\right\}^{0,3}.$$

For practical application of eqs.(2.6) and (2.7) it must be remembered that, for the selected direction of the z-axis, the angle ψ_0 is equal to zero. The angles ψ''_{i_0} and ψ'_{i_0} in eq.(2.7) are taken in radians. The values of the coefficient w found by this formula are given in Table 4.2, together with the values of the integrals j_k.

The pressures P_0 and P_{eq} at the given external loads R and A can be calculated in two ways.

The first consists in calculating these quantities by means of eqs.(2.3) and (2.5), making use of the values of $\bar{\delta}_0$ and λ obtained from a direct solution of eqs.(2.1) and (2.2).

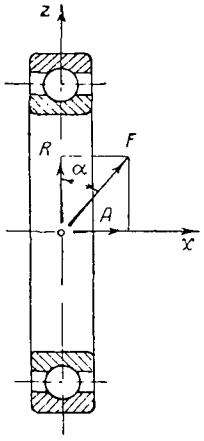

Fig.4.4 Resultant of Force Applied to Bearing.

Since eqs.(2.1) and (2.2) have a complex structure, it is logical that this procedure encounters great difficulties. These are still large, even when the problem is solved approximately.

The second way, more acceptable for practical use in determining the pressures P_0 and P_{eq} is based on the following considerations:

If the angle of contact of all balls is the same /341
$\beta_\psi = \beta = \text{const}$, then

$$\left.\begin{aligned} \frac{A}{z v d_{ba}^2} &= B_0 \bar{\delta}_0^{3/2} \sin\beta j_1; \\ \frac{R}{z v d_{ba}^2} &= B_0 \bar{\delta}_0^{3/2} \cos\beta j_2. \end{aligned}\right\} \qquad (2.8)$$

The relations (2.8) differ from eqs.(2.1) in that they do not contain terms allowing for the variation in angle of contact as a function of the position of the ball relative to the plane x0z.

For a 180° loading zone, when half of the balls are operative in the bearing, we have $\lambda = \pm\infty$ so that $\beta = \beta_0$, $j_1 = 0.279$, $j_2 = 0.229$ and $w = 0.587$.

For the given case, eqs.(2.8) yield

$$\frac{A}{R} = \frac{j_1}{j_2}\tan\beta = 1.217\tan\beta_0, \qquad (2.9)$$

such that

$$\left.\begin{aligned} P_0 &= \frac{R}{z\cos\beta j_2} = 4.37\frac{R}{z\cos\beta_0}; \\ P_{eq} &= wP_0 = 2.57\frac{R}{z\cos\beta_0}. \end{aligned}\right\} \qquad (2.10)$$

TABLE 4.3

/342

$\frac{F}{z\nu d_{b\Delta}^2}$ \ α	0°	10°	20°	30°	40°	50°	60°	70°	80°	90°
				Values of the coefficient k_o						
				$\beta_0 = 0$						
0.02	1.000	0.889	1.070	1.210	1.308	1.380	1.422	1.428	1.398	1.308
0.04	1.000	0.890	0.966	1.091	1.146	1.196	1.212	1.192	1.152	1.080
0.07	1.000	0.880	0.924	1.014	1.078	1.116	1.116	1.094	1.050	0.976
0.11	1.000	0.920	0.880	0.958	1.010	1.034	1.030	1.000	0.950	0.874
0.14	1.000	0.926	0.873	0.933	0.974	0.994	0.984	0.952	0.906	0.826
0.21	1.000	0.936	0.858	0.898	0.930	0.938	0.916	0.880	0.830	0.750
0.35	1.000	0.948	0.858	0.858	0.876	0.872	0.850	0.804	0.746	0.667
0.53	1.000	0.956	0.874	0.836	0.842	0.828	0.798	0.750	0.686	0.602
0.70	1.000	0.961	0.882	0.824	0.822	0.802	0.748	0.718	0.648	0.566
1.00	1.000	0.967	0.893	0.818	0.800	0.774	0.734	0.678	0.602	0.526
				$\beta_0 = 12°$						
0.02	1.399	1.171	0.839	0.897	0.963	0.999	1.005	0.992	0.937	0.877
0.04	1.249	1.109	0.842	0.875	0.933	0.959	0.956	0.938	0.883	0.808
0.07	1.184	1.077	0.847	0.858	0.902	0.918	0.914	0.879	0.824	0.752
0.11	1.136	1.046	0.853	0.841	0.871	0.881	0.870	0.831	0.777	0.705
0.14	1.114	1.034	0.860	0.831	0.859	0.862	0.847	0.809	0.754	0.681
0.21	1.086	1.018	0.870	0.816	0.833	0.833	0.809	0.771	0.713	0.636
0.35	1.056	1.008	0.889	0.803	0.806	0.799	0.781	0.721	0.655	0.579
0.53	1.038	1.002	0.899	0.802	0.789	0.772	0.734	0.688	0.623	0.538
0.70	1.028	0.995	0.908	0.810	0.778	0.754	0.715	0.665	0.601	0.514
1.00	1.020	0.983	0.912	0.813	0.761	0.734	0.694	0.636	0.567	0.479
				$\beta_0 = 18°$						
0.02	1.628	1.476	1.001	0.785	0.804	0.813	0.804	0.770	0.718	0.647
0.04	1.453	1.338	0.981	0.818	0.797	0.799	0.789	0.759	0.697	0.625
0.07	1.327	1.238	0.961	0.786	0.780	0.782	0.766	0.727	0.672	0.597
0.11	1.252	1.172	0.951	0.781	0.777	0.770	0.749	0.707	0.649	0.572
0.14	1.217	1.140	0.948	0.782	0.771	0.761	0.741	0.696	0.637	0.560
0.21	1.169	1.108	0.941	0.784	0.763	0.749	0.719	0.675	0.612	0.534
0.35	1.108	1.058	0.932	0.789	0.748	0.730	0.694	0.646	0.582	0.496
0.53	1.073	1.027	0.924	0.789	0.739	0.717	0.671	0.618	0.554	0.466
0.70	1.056	1.018	0.926	0.797	0.736	0.707	0.661	0.604	0.536	0.455
1.00	1.035	1.008	0.915	0.806	0.732	0.682	0.647	0.590	0.518	0.429

TABLE 4.3 (cont'd)

$\frac{F}{z\nu d_{ba}^2}$ \ α	0°	10°	20°	30°	40°	50°	60°	70°	80°	90°
					$\beta_0 = 26°$					
0.02	1.914	1.815	1.478	0.872	0.692	0.667	0.641	0.594	0.530	0.454
0.04	1.609	1.528	1.321	0.865	0.692	0.665	0.635	0.587	0.523	0.447
0.07	1.483	1.415	1.218	0.858	0.692	0.661	0.629	0.577	0.514	0.440
0.11	1.389	1.326	1.150	0.850	0.692	0.656	0.621	0.566	0.504	0.431
0.14	1.336	1.279	1.119	0.847	0.692	0.655	0.618	0.560	0.500	0.424
0.21	1.249	1.204	1.069	0.845	0.692	0.650	0.611	0.551	0.492	0.413
0.35	1.175	1.125	1.011	0.837	0.693	0.647	0.600	0.544	0.480	0.398
0.53	1.121	1.078	0.975	0.828	0.696	0.642	0.593	0.535	0.466	0.383
0.70	1.087	1.051	0.955	0.826	0.698	0.639	0.589	0.527	0.455	0.373
1.00	1.051	1.016	0.932	0.819	0.701	0.632	0.580	0.515	0.440	0.358
					$\beta_0 = 36°$					
0.02	2.171	2.051	1.823	1.426	0.795	0.580	0.507	0.455	0.388	0.310
0.04	1.815	1.756	1.574	1.242	0.777	0.575	0.507	0.453	0.388	0.307
0.07	1.629	1.567	1.403	1.132	0.757	0.574	0.514	0.453	0.385	0.304
0.11	1.496	1.425	1.272	1.052	0.746	0.578	0.514	0.451	0.380	0.299
0.14	1.445	1.359	1.205	1.011	0.742	0.578	0.514	0.449	0.379	0.299
0.21	1.343	1.262	1.144	0.970	0.736	0.578	0.510	0.449	0.375	0.299
0.35	1.207	1.156	1.060	0.913	0.724	0.578	0.510	0.445	0.370	0.291
0.53	1.129	1.086	0.999	0.870	0.714	0.578	0.509	0.444	0.364	0.285
0.70	1.098	1.053	0.967	0.848	0.707	0.578	0.506	0.440	0.364	0.283
1.00	1.053	1.006	0.925	0.821	0.696	0.578	0.502	0.434	0.356	0.275
					Values of the coefficient k					
					$\beta_0 = 0°$					
0.02	1.000	0.995	1.297	1.520	1.710	1.882	2.030	2.150	2.230	2.270
0.04	1.000	0.962	1.150	1.350	1.502	1.655	1.758	1.825	1.870	1.900
0.07	1.000	0.950	1.055	1.212	1.355	1.475	1.540	1.608	1.680	1.710
0.11	1.000	0.968	1.005	1.130	1.232	1.325	1.400	1.452	1.477	1.490
0.14	1.000	0.966	0.985	1.093	1.190	1.275	1.330	1.375	1.395	1.408
0.21	1.000	0.963	0.952	1.045	1.120	1.175	1.225	1.260	1.275	1.283
0.35	1.000	0.970	0.937	0.979	1.041	1.082	1.107	1.122	1.133	1.140
0.53	1.000	0.972	0.934	0.944	0.986	1.015	1.025	1.032	1.030	1.029
0.70	1.000	0.977	0.934	0.928	0.952	0.973	0.976	0.972	0.968	0.966
1.00	1.000	0.982	0.935	0.907	0.919	0.926	0.922	0.905	0.896	0.890
					$\beta_0 = 12°$					
0.02	1.237	1.090	0.929	1.039	1.190	1.301	1.384	1.438	1.480	1.489
0.04	1.125	1.051	0.919	0.991	1.142	1.235	1.299	1.333	1.369	1.377
0.07	1.093	1.034	0.913	0.979	1.082	1.159	1.213	1.257	1.270	1.280
0.11	1.065	1.014	0.913	0.963	1.040	1.100	1.146	1.181	1.188	1.197

TABLE 4.3 (cont'd)

$\frac{F}{z\nu d_{ba}^2}$ \ α	0°	10°	20°	30°	40°	50°	60°	70°	80°	90°
0.14	1.053	1.006	0.914	0.951	1.017	1.071	1.111	1.136	1.149	1.152
0.21	1.037	0.999	0.916	0.921	0.981	1.022	1.051	1.057	1.082	1.077
0.35	1.017	0.994	0.923	0.897	0.937	0.959	0.983	0.986	0.991	0.989
0.53	1.010	0.988	0.929	0.885	0.911	0.927	0.931	0.925	0.918	0.917
0.70	1.006	0.982	0.931	0.883	0.891	0.897	0.892	0.885	0.877	0.869
1.00	1.001	0.976	0.933	0.873	0.870	0.864	0.851	0.834	0.826	0.812
	$\beta_0 = 18°$									
0.02	1.336	1.260	0.972	0.879	0.944	1.003	1.048	1.070	1.091	1.102
0.04	1.231	1.175	0.962	0.873	0.931	0.979	1.008	1.036	1.056	1.062
0.07	1.170	1.115	0.952	0.866	0.915	0.957	0.981	0.999	1.017	1.013
0.11	1.125	1.077	0.941	0.860	0.899	0.933	0.957	0.965	0.973	0.965
0.14	1.104	1.057	0.937	0.856	0.889	0.920	0.942	0.944	0.951	0.942
0.21	1.067	1.033	0.932	0.856	0.872	0.894	0.906	0.906	0.913	0.906
0.35	1.041	1.011	0.935	0.856	0.856	0.865	0.865	0.865	0.858	0.856
0.53	1.024	0.996	0.934	0.856	0.837	0.846	0.836	0.825	0.810	0.808
0.70	1.013	0.986	0.932	0.856	0.830	0.830	0.818	0.799	0.780	0.780
1.00	0.999	0.974	0.929	0.856	0.819	0.806	0.789	0.770	0.751	0.737
	$\beta_0 = 26°$									
0.02	1.451	1.411	1.227	0.863	0.775	0.778	0.782	0.778	0.775	0.767
0.04	1.285	1.249	1.132	0.863	0.773	0.776	0.773	0.772	0.767	0.759
0.07	1.215	1.195	1.078	0.859	0.772	0.769	0.764	0.761	0.754	0.747
0.11	1.182	1.159	1.034	0.856	0.769	0.762	0.754	0.749	0.741	0.732
0.14	1.150	1.120	1.011	0.854	0.768	0.758	0.749	0.741	0.732	0.722
0.21	1.096	1.071	0.980	0.850	0.766	0.755	0.741	0.729	0.719	0.705
0.35	1.043	1.021	0.959	0.847	0.764	0.746	0.728	0.707	0.692	0.678
0.53	1.016	0.992	0.936	0.841	0.764	0.737	0.714	0.690	0.668	0.652
0.70	1.005	0.971	0.923	0.836	0.764	0.732	0.705	0.678	0.652	0.634
1.00	0.989	0.953	0.905	0.836	0.764	0.728	0.701	0.658	0.634	0.615
	$\beta_0 = 36°$									
0.02	1.525	1.480	1.363	1.149	0.778	0.643	0.603	0.566	0.540	0.526
0.04	1.367	1.333	1.124	1.060	0.769	0.639	0.603	0.566	0.536	0.525
0.07	1.269	1.233	1.141	0.990	0.756	0.638	0.600	0.564	0.534	0.521
0.11	1.195	1.157	1.076	0.942	0.748	0.637	0.599	0.558	0.531	0.518
0.14	1.157	1.120	1.045	0.922	0.746	0.638	0.599	0.557	0.527	0.514
0.21	1.098	1.066	0.996	0.888	0.744	0.639	0.597	0.554	0.520	0.508
0.35	1.035	1.012	0.946	0.858	0.736	0.639	0.592	0.550	0.511	0.498
0.53	0.993	0.970	0.910	0.832	0.728	0.639	0.589	0.544	0.502	0.491
0.70	0.970	0.946	0.890	0.815	0.723	0.639	0.585	0.540	0.500	0.485
1.00	0.945	0.914	0.863	0.798	0.718	0.639	0.582	0.534	0.493	0.473

Equations (2.10) are known in the theory of antifriction bearings as "Stribeck formulas".

For the case $\frac{A}{R} \neq 1.217 \tan \beta_0$ the pressures P_0 and P_{eq} can be represented as

$$\left.\begin{aligned} P_0 &= 4.37 \frac{\kappa_0 F}{z \cos \beta_0}; \\ P_{eq} &= 2.57 \frac{\kappa F}{z \cos \beta_0}, \end{aligned}\right\} \qquad (2.11)$$

where $F = (R^2 + A^2)^{1/2}$ is the resultant load on the bearing (Fig.4.4).

This same form of notation can also be retained when taking account of the variability of the angle β_ψ.

After substituting the values of P_0 and P_{eq} from the equalities (2.3) and (2.5) into eq.(2.11), we obtain

$$\left.\begin{aligned} \kappa_0 &= \frac{B_0 \bar{\delta}_0^{3/2} \cos \beta_0}{4.37 \frac{F}{z \nu d_{ba}^2}}; \\ \kappa &= \frac{w}{0.587} \kappa_0. \end{aligned}\right\} \qquad (2.12)$$

The coefficients k_0 and k are unique reduction coefficients referred to the resultant load F. It is essential that they can be found from eqs.(2.1) and (2.2) by different indirect methods which preclude the need for direct solution of these equations.

The values of the coefficients k_0 and k for bearings with initial angles of contact $\beta_0 = 0$, 12, 18, and 36°, obtained from eqs.(2.1) and (2.2) by the graphoanalytic method (Ref.30), are given in Table 4.3.

Introduction of the tabulated reduction coefficients k_0 and k greatly facilitates finding the pressures P_0 and P_{eq}, permitting the use, for this purpose, of rather simple and convenient formulas [eqs.(2.11)]. /345

The coefficients k_0 and k are given in Table 4.3 as a function of the quantity $\frac{F}{z\nu d_{ba}^2}$, which characterizes the level of the load received by the bearing, and of the angle $\alpha = \tan^{-1} \frac{A}{R}$, which determines the direction of the resultant F*.

---

* In calculating the quantities $\frac{F}{z\nu d_{ba}^2}$ and also $\frac{R}{z\nu d_{ba}^2}$ as well as $\frac{A}{z\nu d_{ba}^2}$, the diameter d_{ba} is always expressed in millimeters.

2. Reduced Loads

Let us denote by Q the radial force which, in combination with the axial force $A = 1.217 \tan \beta_0 Q$ at a constant contact angle between balls and races $\beta_\psi = \beta_0 = \text{const}$, creates the same equivalent pressure P_{eq} as the actual combination of external loads applied to the bearing.

The force Q is commonly called the "reduced dynamic load".

Along with the concept of reduced dynamic load, the concept of "reduced static load" is widely used in the theory of antifriction bearings. By reduced static load we mean the radial force Q_0 which, under the indicated conditions, exerts a maximum pressure on the ball P_0 equal to the actual pressure.

The replacement of actual loads by reduced loads, determined as indicated above, permits using data from catalogs and handbooks of radially loaded bearings, when calculating bearings operating under combined loads.

A comparison of the equalities (2.10) and (2.11) shows that

$$\left.\begin{aligned} Q &= \kappa F; \\ Q_0 &= \kappa_0 F. \end{aligned}\right\} \qquad (2.13)$$

In other countries, and recently also in domestic use, a formula of the following type is often used to determine the reduced loads:

$$Q = xR + yA.$$

Different sources give different values of the reduction coefficients x and y, so that the reduced loads calculated for one and the same case may differ substantially.

Since all calculation methods for radial and radial-thrust ball bearings under combined loads, used in practice, are based on the same initial equations [eqs.(1.1) - (1.7)] and basically differ only by the assumptions used for simplifying their solution, one of the principal criteria of the quality of one or another calculation method is the closeness of the reduced loads calculated on its basis to the "exact" value of these loads obtained from the indicated equations.

Figure 4.5 gives a comparison of the reduced loads determined by means of the coefficients of Table 4.3 with the reduced loads found as the result of the "exact" solution of eqs.(1.1) to (1.7). The same diagram shows the reduced /346
loads calculated by the method of the International Standards Organization (ISO*) recently adopted in other countries and calculated by the method of M.P.Belyanchikov (Ref.24) which is now being recommended for the calculation of general-purpose bearings.

---

* Draft of recommendations for calculating dynamic load-carrying capacity of ball and roller bearings, ISO, No.278, 1960.

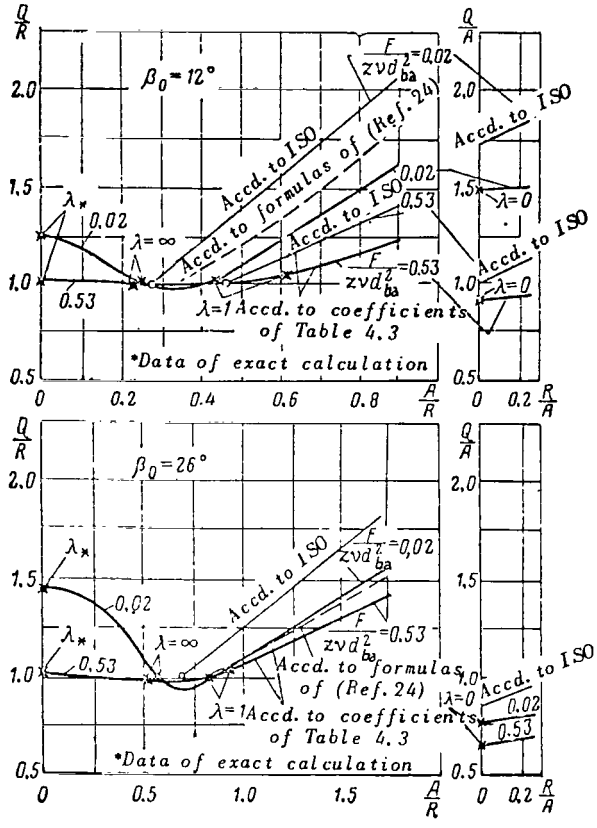

Fig.4.5 Comparison of Various Methods for Calculating Reduced Loads on a Bearing.

As we see from Fig.4.5, the reduced loads obtained by using the data of Table 4.3 are closest to their "exact" values.

Use of the ISO method, under certain conditions will overestimate the reduced loads by 20 - 30% which is naturally impermissible for bearing assemblies of aircraft components.

Sufficiently accurate values of the reduced loads are obtained with the method developed by M.P.Belyanchikov for calculating radial-thrust ball bearings with contact angles of $\beta_0 \geq 26°$. However, at smaller contact angles, the accuracy of the method decreases steeply. For instance, in the case of contact angles of $\beta_0 = 12 - 18°$, the error in the reduced load may go as high as 40%. For contact angles less than 12°, this method is generally unacceptable.

3. Statistical Theory of Dynamic Load-Carrying Capacity /347

In calculations of life expectancy we generally use the principles of the statistical theory of fatigue of metals, which assumes that failure of the material under the effect of alternating loads is a random process of accumulation of fatigue cracks having various probabilistic characteristics. Such an approach to the problem of life expectancy is highly useful for any machine component operating under alternating stresses, including antifrictions bearings which fail as a consequence of fatigue chipping of the tracks or rolling body.

Statistical representations, underlying modern methods of determining the service life of antifriction bearings, were developed mainly by Weibull (Ref.43) and Lundberg and Palmgren (Ref.44). Investigations by Harris (Ref.45) and others were devoted to the development of these representations for small probabilities of failure.

The basic principles of the statistical theory of the dynamic load capacity of roller bearings can be formulated in the following manner:

Let q_{b_e} be the probability that the bearing, rotating at an rpm of n, works h hours without signs of fatigue.

On the basis of the theorem of mathematical statistics for the product of independent events, disregarding the probability of failure of the roller by virtue of its smallness in comparison with the probability of failure of the tracks, we can write

$$q_{be} = q_{rot}\, q_{st}, \tag{2.14}$$

where q_{rot} and q_{st} are the corresponding probabilities characterizing the reliability of the rotating and stationary races.

Taking into account the characteristics of the state of stress under the effect of contact loads and the character of the primary fatigue microcracks formed in roller bearings, Lundberg and Palmgren introduced the following distribution determining the probability F_Δ of the appearance of traces of fatigue on a portion of the track of length ΔL after N rollers loaded by a constant force P have rolled along it:

$$F_\Delta = 1 - \exp\left(-H_1 \frac{\tau_0^{m_1} N^l}{z_0^{m_2}} \Delta V\right). \tag{2.15}$$

Here,

H_1 = coefficient depending upon material properties, surface finish, and precision of manufacture;
τ_0 = maximum tangential stress acting in areas parallel to the surface of the area of contact strain;
z_0 = depth at which this stress arises;
ΔV = stressed volume.

At $m_2 = 0$, which might occur when the probability of failure introduced by each element of volume does not depend upon its location relative to the surface, the distribution (2.15) changes to the customary Weibull distribution.

The stress τ_0 and the depth z_0 can be expressed, respectively, by the maximum bearing stress σ_0 at the center of the area of contact strain and the semiminor axis b of this area:

$$\left.\begin{aligned} \tau_0 &= \alpha_\tau \sigma_0; \\ z_0 &= \alpha_z b. \end{aligned}\right\} \tag{2.16}$$

The stressed volume ΔV, in first approximation, can be taken as equal to /348

$$\Delta V = 2az_0 \Delta L, \tag{2.17}$$

where a is the semimajor axis of the area of contact strain.

As follows from the theory of contact stresses and strains, for radial and radial-thrust ball bearings,

$$\left.\begin{aligned}
\sigma_0 &= \frac{4100}{\mu\nu}\left(4 \pm \frac{2}{\frac{1}{\eta} \mp 1} - \frac{1}{\theta}\right)^{\frac{2}{3}} P^{\frac{1}{3}} d_{ba}^{-\frac{2}{3}};\\
a &= 0.0108\,\mu\left(4 \pm \frac{2}{\frac{1}{\eta} \mp 1} - \frac{1}{\theta}\right)^{-\frac{1}{3}} P^{\frac{1}{3}} d_{ba}^{\frac{1}{3}};\\
b &= 0.0108\nu\left(4 \pm \frac{2}{\frac{1}{\eta} \mp 1} - \frac{1}{\theta}\right)^{-\frac{1}{3}} P^{\frac{1}{3}} d_{ba}^{\frac{1}{3}}.
\end{aligned}\right\} \qquad (2.18)$$

In the equalities (2.18) the following notations are adopted:

$$\eta = \frac{d_{ba}\cos\beta_0}{2r_0} \text{ and } \theta = \frac{r_{in\,(out)}}{d_{ba}}.$$

The coefficients H_1, α_T, and α_z, strictly speaking, are not constants; however, for all practical purposes this can be disregarded since the limits within which their values vary (depending on the ratio b/a) are quite negligible.

It is easy to prove that

$$\Delta L = \frac{1}{2} d_{ba}\cos\beta_0 \left(\frac{1}{\eta} \mp 1\right)\Delta\psi, \qquad (2.19)$$

where $\Delta\psi$ is the central angle corresponding to the examined portion of the track.

By means of the equalities (2.16) - (2.19) we can reduce eq.(2.15) to the form

$$F_\Delta = 1 - \exp\left(-H_2\cos\beta_0 \frac{P^{ml}N^l}{d_{ba}^{mlc}} \frac{\Delta\psi}{2\pi}\right). \qquad (2.20)$$

The number of balls contacting each portion of the track during h hours of work of the bearing will be

$$N = 30znh(1 \pm \eta). \qquad (2.21)$$

Substituting this value into eq.(2.20), we finally obtain

$$F_\Delta = 1 - \exp\left[-H_3 z^l \cos\beta_0 (nh)^l \frac{P^{ml}}{d_{ba}^{mlc}} \frac{\Delta\psi}{2\pi}\right]. \qquad (2.22)$$

The exponents m and c are expressed in terms of the exponents m_1, m_2, and l in the following manner:

$$\left.\begin{aligned} m &= \frac{m_1 + 2 - m_2}{3l}; \\ c &= \frac{2m_1 + m_2 - 5}{m_1 + 2 - m_2} l. \end{aligned}\right\} \qquad (2.23)$$

According to the data of foreign bearing manufacturers, which are generalized in the recommendations of the ISO, m = 3 and c = 1.8 (at $d_{ba} < 25$ mm). /349

The portion of the track of the stationary race located at the azimuth ψ when the balls roll along it, is loaded each time by the same force P_ψ. Setting, in conformity with this, $P = P_\psi$ in eq.(2.22), we obtain for this portion

$$F_\Delta = 1 - \exp\left[-H_3 z^l \cos\beta_0 (nh)^l \frac{P_\psi^{ml}}{d_{ba}^{mlc}} \frac{\Delta\psi}{2\pi} \right]. \qquad (2.24)$$

It follows from eq.(2.24) that the probability q_{st}, characterizing the reliability of the stationary race as a whole, is equal to

$$q_{st} = \Pi(1 - F_{\Delta j}) = \exp\left[-H_3 z^l \cos\beta_0 (nh)^l \frac{P_{eq.o}^{ml}}{d_{ba}^{mlc}} \right], \qquad (2.25)$$

where

$$P_{eq.o} = \left(\frac{1}{2\pi} \int_{\psi_{lo}'}^{\psi_{lo}''} P_\psi^{ml} d\psi \right)^{\frac{1}{ml}}.$$

During a sufficiently long time interval, each element of the track of the rotating race will contact the balls at practically all azimuths.

Accounting for this fact and considering the hypothesis of linear summation of damageability to be valid, eq.(2.22) will yield for each portion of the track of the rotating race

$$F_\Delta = 1 - \exp\left[-H_3 z^l \cos\beta_0 (nh)^l \frac{P_{eq}^{ml}}{d_{ba}^{mlc}} \frac{\Delta\psi}{2\pi} \right]. \qquad (2.26)$$

Here, $P_{eq} = \left(\frac{1}{2\pi} \int_{\psi_{lo}'}^{\psi_{lo}''} P^m d\psi \right)^{\frac{1}{m}}$ is the same equivalent pressure discussed in Subsection 1.

The probability q_{rot} characterizing the reliability of the entire rotating race in conformity with eq.(2.26) will then be

$$q_{rot} = \Pi(1 - F_{\Delta j}) = \exp\left[-H_3 z^l \cos\beta_0 (nh)^l \frac{P_{eq}^{ml}}{d_{ba}^{mlc}} \right]. \qquad (2.27)$$

The coefficient H_3, figuring in the above equalities, can be represented as the product of a certain constant H_4 and the quantity

$$H_0=\frac{(1\pm\eta)^l\left(\frac{1}{\eta}\mp 1\right)}{(\mu\nu)^{m_1-1}\nu^{m_2}}\left(4\pm\frac{2}{\frac{1}{\eta}\mp 1}-\frac{1}{\theta}\right)^{\frac{2m_1+m_2-2}{3}}, \tag{2.28}$$

which is a function of η and θ, i.e., parameters characterizing the interior geometry of the bearing.

Let us assume that the inner race rotates. For this, eqs.(2.14), (2.25), and (2.27) will yield

$$\begin{aligned}\ln\frac{1}{q_{be}}&=\ln\frac{1}{q_{rot}}+\ln\frac{1}{q_{st}}=\\&=H_4\left[H_{in}+\left(\frac{P_{eq.o}}{P_{eq}}\right)^{ml}H_{out}\right]z^l\cos^3\beta_0(nh)^l\frac{P_{eq}^{ml}}{d_{ba}^{mlc}}.\end{aligned} \tag{2.29}$$

The indices "in" and "out" (eq.o = equivalent, outer) as well as the upper and lower signs in eqs.(2.18), (2.19), (2.21), and (2.28), pertain, respectively, to the inner and outer races of the bearing. /350

At $\eta = 0.2$, $\theta = 0.52$ and $\lambda = \infty$, let

$$H_{in}+\left(\frac{P_{eq.o}}{P_{eq}}\right)^{ml}H_{out}=H_5.$$

Furthermore, let us introduce the quantities C_0 and f_q over the formulas

$$C_0=f'f''d_{ba}^{c}z^{\left(1-\frac{1}{m}\right)}, \tag{2.30}$$

where

$$f'=\frac{1}{2.57}\left[\frac{1}{H_4H_5}\ln\frac{1}{0.9}\right]^{\frac{1}{ml}}$$

and

$$\begin{aligned}f''&=\left[\frac{H_5}{H_{in}+\left(\frac{P_{eq.o}}{P_{eq}}\right)^{ml}H_{out}}\right]^{\frac{1}{ml}};\\f_q&=\left[\frac{\log\frac{1}{q_{be}}}{\ln\frac{1}{0.9}}\right]^{\frac{1}{l}}.\end{aligned} \tag{2.31}$$

Using eqs.(2.30) and (2.31), we transform eq.(2.29) such that

$$0.39z\cos\beta_0 P_{eq}(nh)^{\frac{1}{m}} = C_0(\cos\beta_0)^{\left(1-\frac{1}{ml}\right)} f_q^{\frac{1}{m}}. \tag{2.32}$$

Having expressed here P_{eq} in terms of the equivalent dynamic load Q, we obtain

$$Q(nh)^{\frac{1}{m}} = Cf_q^{\frac{1}{m}}, \tag{2.33}$$

where

$$C = C_0(\cos\beta_0)^{\left(1-\frac{1}{ml}\right)}.$$

In like manner, we can examine the case where the outer race rotates.

Combining the formulas of life expectancy for rotation of the inner and outer races and introducing the coefficients k_b and k_t which take into account the effect of the type of load and temperature regime of the bearing on the load-carrying capacity, we finally have

$$\kappa_b\kappa_t\kappa_\kappa Q(nh)^{\frac{1}{m}} = Cf_q^{\frac{1}{m}}. \tag{2.34}$$

Here $k_k = 1$ if the inner race rotates, and

$$\kappa_k = \left[\frac{H_{in} + \left(\frac{P_{eq.o}}{P_{eq}}\right)^{ml} H_{out}}{H_{out} + \left(\frac{P_{eq.o}}{P_{eq}}\right)^{ml} H_{in}}\right]^{\frac{1}{ml}}, \tag{2.35}$$

if the outer race rotates.

In the specific numerical calculations of radial and radial-thrust ball bearings on the basis of tabulated coefficients k_0 and k, the values of the kine- /351

TABLE 4.4

η	0.05	0.10	0.20	0.30	0.40
f''	0.77	0.92	1	0.93	0.81

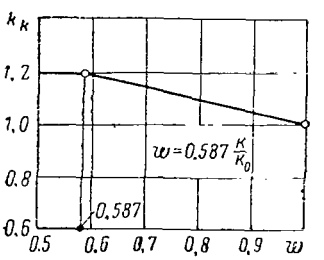

Fig.4.6 Kinematic Coefficient k_k.

matic coefficient k_k can be determined approximately as a function of the quantity $w = 0.587 \frac{k}{k_o}$ from the graph in Fig.4.6.

In other countries, calculations of the coefficients of utilization C_o and C usually take the coefficient f′ as equal to 150 - 200.

Calculations show that, at a given θ, the coefficient f″ depends mainly on η. At m = 3, C = 1.8, and t = 1.11 which corresponds to the ISO recommendations, this coefficient has the values indicated in Table 4.4.

For general-purpose bearings, the life expectancy h_{10} at which the probability of failure is equal to 10%, is considered to be the rated life.

Since we have at q = 0.9 a value of f_q = 1, it follows that

$$\kappa_b \kappa_t \kappa_\kappa Q (n h_{10})^{\frac{1}{m}} = C. \tag{2.36}$$

Comparing the equalities (2.34) and (2.36), we find

$$\frac{h}{h_{10}} = f_q. \tag{2.37}$$

It follows from eqs.(2.37) and (2.31) that the average life expectancy of roller bearings is determined from the expression

$$\frac{h_{av}}{h_{10}} = \frac{\Gamma\left(1 + \frac{1}{t}\right)}{\left(\log \frac{1}{0.9}\right)^{\frac{1}{t}}}, \tag{2.38}$$

where Γ is the gamma function of the argument $\left(1 + \frac{1}{t}\right)$.

The ratio of the median life expectancy h_{50}, corresponding to the reliability q = 0.5, to the rated life h_{10} will then be

$$\frac{h_{50}}{h_{10}} = \left(\frac{\ln \frac{1}{0.5}}{\ln \frac{1}{0.9}}\right)^{\frac{1}{t}}. \tag{2.39}$$

Equations (2.38) and (2.39) show that the main parameters characterizing the dispersion of the life expectancy of roller bearings is the exponent t.

In most cases, the ratio $\frac{h_{50}}{h_{10}}$ varies within limits from 4.08 to 5. At

$\frac{h_{50}}{h_{10}} = 4.08$, $t = 1.34$ and $\frac{h_{av}}{h_{10}} = 4.95$. At $\frac{h_{50}}{h_{10}} = 5$, $t = 1.17$ and $\frac{h_{av}}{h_{10}} = 6.5$.

As experimental investigations indicate, these relationships satisfactorily describe the dispersion of life expectancy at $q_{be} \leq 0.9$. Noticeable deviations are observed in the region of small probabilities of failure. These deviations can be taken into account if, for this region, eq.(2.37) is replaced by the following: /352

$$\frac{h - h_0}{h_{10} - h_0} = f_q. \tag{2.40}$$

Here, h_0 is some threshold of life expectancy, prior to which the probability of failure is equal to zero.

Since we have $f_q \approx [10(1 - q_{be})]^{1/t}$ at $q_{be} < 0.9$, eq.(2.40) can finally be written in the form

$$\frac{h}{h_{10}} = \left(1 - \frac{h_0}{h_{10}}\right)[10(1 - q_{be})]^{\frac{1}{t}} + \frac{h_0}{h_{10}}. \tag{2.41}$$

According to Harris' data (Ref.45), the ratio for ball bearings is $\frac{h_0}{h_{10}} \approx$ ≈ 0.045. This means that, to ensure 100% reliability, a rated life margin of the order of 22 is required which corresponds to a load margin of 2.8.

The basic principles of the static theory of dynamic load capacity of radial and radial-thrust ball bearings have been presented above. The corresponding static theories of dynamic load capacity can be developed in a similar fashion for bearings of other types.

The main results of static representations of the life expectancy of roller bearings have been applied both in foreign and domestic practice. However, it should be borne in mind here that some of the fundamental relations used in preparing our own catalogs and manuals have a form differing from that in other countries. For example, our coefficients of utilization C_0 and C are not calculated from eqs.(2.30) and (2.33) but are taken as equal to

$$\left.\begin{aligned} C_0 &= f\frac{d_{ba}^2}{1 + 0.02d_{ba}} z^{\left(1 - \frac{1}{m}\right)}; \\ C &= C_0 \cos\beta_0. \end{aligned}\right\} \tag{2.42}$$

For general-purpose bearings, $f = 65$. We recall that, in Soviet practice, the exponent m is considered as equal to 3.33.

The life expectancy of two-row bearings as well as of roller bearings consisting of several identical bearings which can be regarded as one multirow bearing, is determined by the expression

$$0.39\,\kappa_b\kappa_t z\cos\beta_0 P_{eq_j}(nh_{10})^{\frac{1}{m}} = C. \tag{2.43}$$

The equivalent pressure entering here is

$$P_{eq_j} = \left[\sum_{j=1}^{i}(\kappa_{\kappa_j}P_{eq})^{ml}\right]^{\frac{1}{ml}}, \tag{2.44}$$

where P_{eq_j} and k_{k_j} are the equivalent load and kinematic coefficient for the j-th bearings.

Equations (2.43) and (2.44) follow directly from the relations given above for individual bearings.

If all bearings are loaded identically, then

$$P_{eq_j} = i^{\frac{1}{ml}}\kappa_\kappa P_{eq}. \tag{2.45}$$

As shown by an analysis of the values of the coefficients f" in Table 4.4, /353 the performance of roller bearings largely depends upon η. In eqs.(2.42) this important fact is not taken into account, which is their essential shortcoming.

As is known, for high-precision aircraft bearings manufactured from particularly high-grade metal, the coefficients of utilization have much larger values than those obtained from eq.(2.42) for f = 65.

Therefore, using the data of machinery catalogs and handbooks for calculations of aircraft structures, it can be expected that, in reality, the rated life h_{10} will not correspond to the 10% probability of failure but will be appreciably smaller in value. With this approach to a determination of the service life of bearing assemblies of aircraft components, this life expectancy is often identified with the required lifetime. In practice, this is achieved by replacing h_{10} in eqs.(2.36) and (2.43) by h, understanding by h the life expectancy at which the level of reliability of bearings for aircraft components is ensured.

4. Effect of Axial Load on Bearing Performance

Let us discuss the manner in which an axial load affects the performance of radial and radial-thrust ball bearings.

Figures 4.7 and 4.8 show typical graphs of the relation $\frac{Q}{R} = f\left(\frac{A}{R}\right)$ for $\frac{R}{zvd_{ba}^2}$ = const, plotted from data of calculations performed in compiling the tables of the coefficients k_0 and k.

As we see from these graphs, for each load level there is a range of values of $\frac{A}{R}$ in which $\frac{Q}{R} < 1$. Its boundaries are given in Table 4.5.

TABLE 4.5

$\frac{R}{z\nu d_{ba}^2}$	Values of A/R at Different Contact Angles β_o deg.				
	0	12	18	26	36
0.02	0—0.15	0.26—0.38	0.39—0.56	0.56—0.82	0.84—1.20
0.11	0—0.28	0.25—0.45	0.37—0.60	0.55—0.84	0.76—1.21
0.35	0—0.37	0.22—0.47	0.35—0.63	0.47—0.85	0.38—1.21
1.00	0—0.43	0.04—0.49	0.00—0.65	0.00—0.86	0.00—1.22

At values of $\frac{A}{R}$ as indicated in Table 4.5, the axial load not only will not reduce the load capacity of the bearing but even increase it somewhat. It is true that this increase is insignificant, since the possible decrease of the reduced dynamic load is several percent.

In radial-thrust ball bearings, the balls are acted upon by Coriolis forces which tend to make them rotate about axes perpendicular to the contact surfaces. Friction forces arising at the points of contact with the races prevent such "spinning" of the balls. If there is an unloaded zone in the bearing, then /355 this zone contains no friction forces that would prevent "spinning" of the balls, and the balls begin to slide relative to the raceways of the races; at high rates of rotation, this will lead to overheating and rapid wear of the bearings. It is logical that, in designing high-speed bearing assemblies with radial-thrust ball bearings, it is always necessary to have all balls share the load. In practice, this is achieved either by installing the bearings at suitable contact angles or with some auxiliary axial load produced by preloading.

The magnitude of the loading zone depends on the correlation between axial and radial loads applied to the bearing. The greater the ratio A/R, the larger this zone. As indicated earlier, at $\psi_o = 0$ the loading zone is 360° if $0 \leq \lambda \leq 1$. The value $\lambda = 0$ corresponds to the case of axial loading of the bearing in which the pressures on the balls are identical. The value $\lambda = 1$ determines the minimum magnitude of the ratio A/R at which all balls are loaded. This, in particular, follows from eq.(1.22) which shows that, in the case $\psi_o = 0$ and $\lambda = 1$, the force absorbed by the ball located at the azimuth $\psi_o = 180^\circ$ vanishes.

Taking into account that, at $\lambda = 1$, we have $j_1 = 0.425$, $j_2 = 0.225$, and $j_3 = 0.231$, we find from eqs.(2.1) and (2.2) that

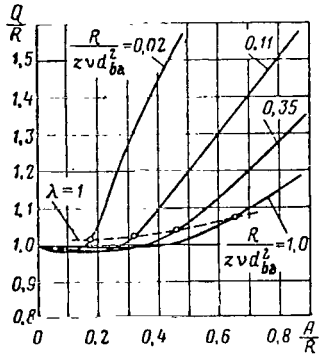

Fig.4.7 Graphs of the Relation $\frac{Q}{R} = f\left(\frac{A}{R}\right)$ at Certain Constant Values of $\frac{R}{z\nu d_{ba}^2}$ and $\beta_0 = 0$

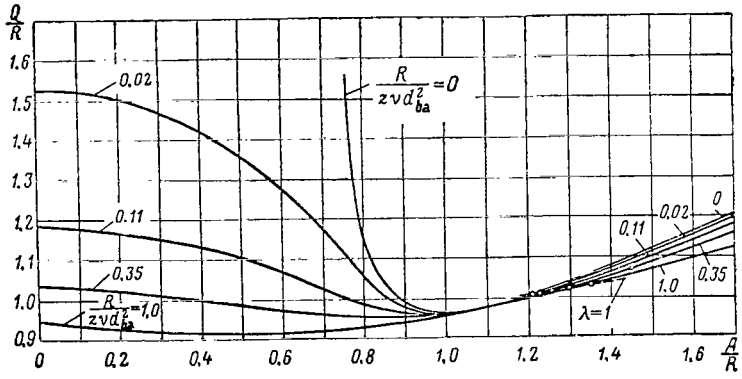

Fig.4.8 Graphs of the Relation $\frac{Q}{R} = f\left(\frac{A}{R}\right)$ at Certain Constant Values of $\frac{R}{z\nu d_{ba}^2}$ and $\beta_0 = 36°$.

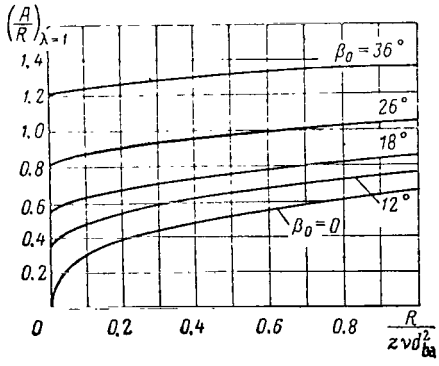

Fig.4.9 Dependence of the Ratio $\left(\frac{A}{R}\right)_{\lambda=1}$ on Load Level.

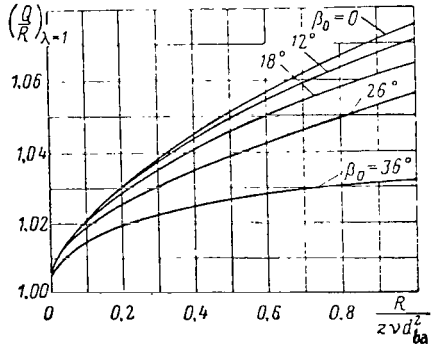

Fig.4.10 Dependence of the Ratio $\left(\frac{Q}{R}\right)_{\lambda=1}$ on Load Level.

$$\frac{A}{R_{(\lambda-1)}} = 1.666 \frac{\left(\sin^2\beta_0 + \bar{\delta}_0 + \frac{\bar{\delta}_0^2}{4}\right)^{1/2}}{\cos\beta_0} \frac{1 - 0.6\frac{\bar{\delta}_0}{2+\bar{\delta}_0}}{1 + 0.905\frac{\sin^2\beta_0 + \bar{\delta}_0 + \frac{\bar{\delta}_0^2}{4}}{\cos^2\beta_0}\frac{\bar{\delta}_0}{2+\bar{\delta}_0}}, \quad (2.46)$$

where the radial load R is determined by the expression

$$\frac{R}{z\nu d_{ba}^2} = 0.51 B_0 \cos\beta_0 \frac{\bar{\delta}_0^{3/2}}{2+\bar{\delta}_0}\left(1 + 0.905\frac{\sin^2\beta_0 + \bar{\delta}_0 + \frac{\bar{\delta}_0^2}{4}}{\cos^2\beta_0}\frac{\bar{\delta}_0}{2+\bar{\delta}_0}\right), \quad (2.47)$$

while the ratio is

$$\left(\frac{Q}{R}\right)_{\lambda-1} = 0.5025 \cdot \frac{2+\bar{\delta}_0}{1 + 0.905\frac{\bar{\delta}_0}{2+\bar{\delta}_0}\frac{\sin^2\beta_0 + \bar{\delta}_0 + \frac{\bar{\delta}_0^2}{4}}{\cos^2\beta_0}}. \quad (2.48)$$

As we see from the equalities (2.46), (2.47), and (2.48), the values of $\left(\frac{A}{R}\right)_{\lambda=1}$ and $\left(\frac{Q}{R}\right)_{\lambda=1}$ depend on the initial contact angle as well as on the level of the load received by the bearing.

For the most frequently encountered initial contact angles β_0 = 0, 12, 18, 26, and 36°, we plotted in Figs.4.9 and 4.10 on the basis of eqs.(2.46), (2.47), and (2.48) curves determining the values $\left(\frac{A}{R}\right)_{\lambda=1}$ and $\left(\frac{Q}{R}\right)_{\lambda=1}$ as a function of $\frac{R}{z\nu d_{ba}^2}$.

For small loads,

$$\left(\frac{A}{R}\right)_{\lambda-1} \approx 1.67\tan\beta_0 \text{ and } \left(\frac{Q}{R}\right)_{\lambda-1} \approx 1.$$

With an increase in load, the quantities $\left(\frac{A}{R}\right)_{\lambda=1}$ and $\left(\frac{Q}{R}\right)_{\lambda=1}$ will also in- /356

crease. For instance, for the angle β_0 = 18° at $\frac{R}{z\nu d_{ba}^2}$ = 1, we have

$$\left(\frac{A}{R}\right)_{\lambda-1} = 2.6\tan\beta_0 \text{ and } \left(\frac{Q}{R}\right)_{\lambda-1} = 1.064.$$

As shown above, in the case of a constant contact angle between balls and

races for a loading zone of 180° and a parameter $\lambda = \pm\infty$, the ratio $\frac{A}{R} = 1.217 \tan \beta_0$.

The values of the ratio $\left(\frac{A}{R}\right)_{\lambda=\infty}$ with consideration of the variation in contact angle as a function of the position of the ball relative to the plane xOz can be found from the curves in Fig.4.11. Figure 4.12 shows curves by means of which the corresponding values of the ratio $\left(\frac{Q}{R}\right)_{\lambda=\infty}$ can be determined.

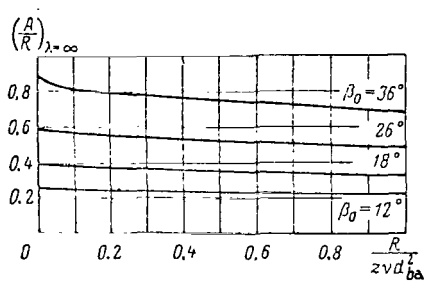

Fig.4.11 Dependence of the Ratio $\left(\frac{A}{R}\right)_{\lambda=\infty}$ on the Load Level.

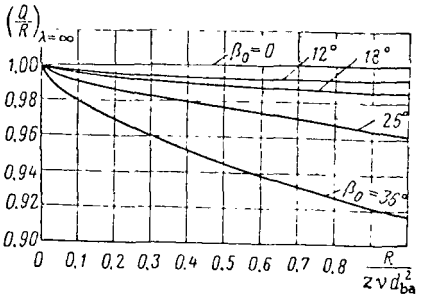

Fig.4.12 Dependence of the Ratio $\left(\frac{Q}{R}\right)_{\lambda=\infty}$ on the Load Level.

The graphs in Figs.4.11 and 4.12 are constructed by means of the formulas

$$\left.\begin{aligned}\left(\frac{A}{R}\right)_{\lambda=\infty} &= 1.217\tan\beta_0 \cdot \frac{1-0.822\bar{\delta}_0}{1+0.868\tan^2\beta_0\bar{\delta}_0};\\ \left(\frac{R}{z\nu d_{ba}^2}\right)_{\lambda=\infty} &= 0.229 B_0 \bar{\delta}_0^{3/2}\cos\beta_0(1+0.868\tan^2\beta_0\bar{\delta}_0);\\ \left(\frac{Q}{R}\right)_{\lambda=\infty} &= \frac{1}{1+0.868\tan^2\beta_0\bar{\delta}_0},\end{aligned}\right\} \qquad (2.49)$$

which follow from eqs.(2.1) and from the equalities (2.12) and (2.13).

These data permit estimating the effect of the axial load on the load capacity of radial and radial-thrust ball bearings. With their aid, one can establish the optimal axial preloading with which the bearings should be mounted in the assembly and select the most rational values of the initial contact angle β_0 for different combinations of radial and axial loads.

5. Approximate Solutions of Equations (2.1) and (2.2)

It should be recalled that the angle β_0 is determined by the radial clearance 2Δ present in the bearing after fitting to the shaft and in the housing at an established operating temperature of the component, and also by the actual /357

distance g between the centers O_0 and O_i of the cross sections of the raceways of the races [see Fig.4.2 and eq.(1.7)].

Because of the effect of shaft-fitting tolerances, nonuniformity of heating of individual elements of the assembly, and possible difference in the values of the coefficients of linear expansion of the shaft and housing, the clearance 2Δ may differ substantially from the initial radial clearance in a self-contained bearing. Deviations of the radii of the raceways and ball diameter may have a noticeable effect on the magnitude of the distance g. In this connection, when calculating highly loaded radial and radial-thrust ball bearings the angle β_0 cannot always be replaced by the rated initial contact angle indicated in a catalog. This fact must not be disregarded in designing vital bearing assemblies of helicopter units and of other aircraft.

The values of the coefficient k_0 and k for radial and radial-thrust ball bearings with initial contact angles β_0 differing from standard can be obtained by interpolation of the data presented in Table 4.3. At the same time, a number of cases exist in which it is more convenient not to resort to this method but to solve the problems in the calculation of such bearings by a direct determination of the quantities $\bar{\delta}_0$ and λ from eqs.(2.1) and (2.2), using the following approximate methods.

If $\frac{A}{R} \geq \left(\frac{A}{R}\right)_{\lambda=1}$, i.e., if all bearings share the load, the integrals can be found from the expressions

$$\left.\begin{aligned} j_1(1+\lambda)^{3/2} &= 1+\frac{3}{16}\lambda^2; \\ j_2(1+\lambda)^{3/2} &= \frac{3}{4}\lambda\left(1-\frac{1}{32}\lambda^2\right); \\ j_3(1+\lambda)^{3/2} &= \frac{1}{2}\left(1+\frac{9}{32}\lambda^2\right). \end{aligned}\right\} \qquad (2.50)$$

The right-hand sides of the equalities (2.50) represent the first terms of power series in which the products $j_k(1+\lambda)^{3/2}$ have been expanded for $\psi_0 = 0$ and $0 \leq \lambda \leq 1$. In view of the rapid convergence of these series in the indicated region, the terms containing the parameter λ in a power higher than the third are discarded here.

Solving eqs.(2.1) and (2.2) with consideration of the equalities (2.50), successive approximations will yield the working formulas

$$\bar{\delta}_0 = \left(\frac{\bar{A}}{D_3}\right)^{2/3} \frac{\left[1+\left(\frac{\bar{A}}{1.41\,D_3}\right)^{1/2}\right]^{2/3}}{\left[\sin^2\beta_0+2\left(\frac{\bar{A}}{1.41\,D_3}\right)^{1/2}\right]^{1/3}}\left(1+D_2\,\frac{1+\frac{3}{16}D_2^2}{1-\frac{1}{32}D_2^2}\right); \qquad (2.51)$$

$$\lambda = D_2 \frac{1 + \frac{3}{16} D_2^2}{1 - \frac{1}{32} D_2^2}, \tag{2.52}$$

where

$$\overline{A} = \frac{A}{B_0 z v d_{ba}^2}.$$

The coefficients D_1, D_2, D_3 are correspondingly equal to /358

$$\left.\begin{aligned} D_1 &= \overline{A}^{2/3} \frac{\left[1 + \left(\frac{\overline{A}}{1.41}\right)^{1/2}\right]^{2/3}}{\left[\sin^2 \beta_0 + 2\left(\frac{\overline{A}}{1.41}\right)^{1/2}\right]^{1/3}}; \\ D_2 &= \frac{4}{3} \cdot \frac{R}{A} \frac{(\sin^2 \beta_0 + 2D_1)^{1/2}}{\cos \beta_0 \left(1 + \frac{2}{3} \frac{\sin^2 \beta_0 + 2D_1}{\cos^2 \beta_0} \frac{D_1}{1 + D_1}\right)}; \\ D_3 &= \left(1 + \frac{3}{16} D_2^2\right)\left(1 - \frac{3}{4} D_2^2 \cdot \frac{1 - \frac{1}{32} D_2^2}{1 + \frac{3}{16} D_2^2} \cdot \frac{D_1}{1 + D_1}\right). \end{aligned}\right\} \tag{2.53}$$

If $\frac{A}{R} \geq \left(\frac{A}{R}\right)_{\lambda=1}$, the formula for the maximum pressure on the balls can be represented in the form

$$P_0 = \overline{\kappa}_0^{(A)} \frac{A}{z}. \tag{2.54}$$

It follows from eqs.(2.3) and (2.51) that the coefficient $\overline{k}_0^{(A)}$ in eq.(2.54) can be equated to

$$\overline{\kappa}_0^{(A)} = \frac{\left(1 + D_2 \frac{1 + \frac{3}{16} D_2^2}{1 - \frac{1}{32} D_2^2}\right)^{3/2} \left[1 + \left(\frac{\overline{A}}{1.41 D_3}\right)^{1/2}\right]}{D_3 \left[\sin^2 \beta_0 + 2\left(\frac{\overline{A}}{1.41 D_3}\right)^{1/2}\right]^{1/2}}. \tag{2.55}$$

It is obvious that, in the examined case, the reduced loads Q_0 and Q can be expressed in the following manner:

$$\left.\begin{aligned} Q_0 &= 0.229 \overline{\kappa}_0^{(A)} \cos \beta_0 A; \\ Q &= 0.390 w \overline{\kappa}_0^{(A)} \cos \beta_0 A. \end{aligned}\right\} \tag{2.56}$$

A comparison of the equalities (2.56) and (2.13) yields, for the given case,

$$\left.\begin{aligned}\kappa_0 &= 0.229\bar{\kappa}_0^{(A)}\cos\beta_0\sin\alpha;\\ \kappa &= 0.390\omega\bar{\kappa}_0^{(A)}\cos\beta_0\sin\alpha.\end{aligned}\right\} \qquad (2.57)$$

If the radial load is R = 0 then, in conformity with the equalities (2.53), we have $D_2 = 0$ and $D_3 = 1$. Substituting these values into eq.(2.55), we obtain the following for the case of purely axial loading:

$$\bar{\kappa}_0^{(A)} = \bar{\kappa}_{00}^{(A)} = \frac{1+\left(\frac{\bar{A}}{1.41}\right)^{1/2}}{\left[\sin^2\beta_0 + 2\left(\frac{\bar{A}}{1.41}\right)^{1/2}\right]^{1/2}}. \qquad (2.58)$$

Figure 4.13 gives graphs of the dependence $\bar{k}_{00}^{(A)} = \bar{k}_{00}^{(A)}(\bar{A})$, obtained from the initial equations of static equilibrium of radial and radial-thrust ball bearings without simplifying assumptions. There, the sign "×" denotes the values of the coefficient $\bar{k}_{00}^{(A)}$ calculated by eq.(2.58), furnishing graphic proof of its completely satisfactory accuracy. /359

The described method of determining the quantities $\bar{\delta}_0$ and λ can be used only when there are no unloaded balls in the bearing.

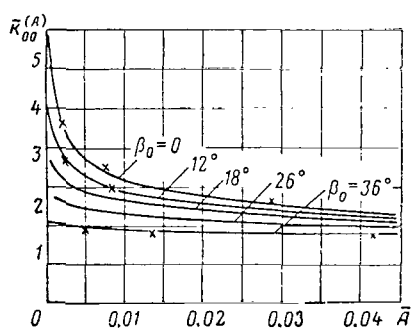

Fig.4.13 Graphs of the Dependence $\bar{k}_{00}^{(A)} = \bar{k}_{00}^{(A)}(\bar{A})$.

Now let the loading zone be less than 360°. For a loading zone less than 360°, the quantity λ can vary within limits from ∞ to 1 and from $-\infty$ to some negative value λ_* corresponding to the case where the bearing absorbs a purely radial load. In the absence of an axial load, the center of the contact area "slides" to the middle of the raceway and the angle β vanishes. If, in eq.(1.19), the angle β is equated to zero and at radial loading of the bearing, we obviously have

$$\bar{\delta} = \cos\beta_0 - 1. \qquad (2.59)$$

Let us introduce the notations

$$\left.\begin{aligned}E_1 &= \frac{1}{(1+\lambda)j_2^{2/3}}; & E_2 &= \frac{\lambda}{1+\lambda}\cdot\frac{j_3}{j_2^{5/3}};\\ E_3 &= \frac{j_1}{j_2}; & E_4 &= \lambda\cdot\frac{j_2}{j_1}.\end{aligned}\right\} \qquad (2.60)$$

The values of E as a function of λ are given in Table 4.6.

At $\bar{\delta} = \cos\beta_0 - 1$ and $\beta = 0$, the second equation of the system (2.1) can be

represented as

$$\bar{R}^{2/3} = \frac{\cos\beta_0 - 1}{E_1}, \tag{2.61}$$

where

$$\bar{R} = \frac{R}{B_0 z v d_{ba}^2}.$$

We recall that, in conformity with the accepted direction of the z-axis, /360 the angle $\psi_0 = 0$ and thus $\lambda \cos\psi_0 = \lambda$ and $\bar{\delta}_0 = \bar{\delta}(1 + \lambda)$.

TABLE 4.6

$\frac{1}{\lambda}$	E_1	E_2	E_3	E_4	$\frac{1}{\lambda}$	E_1	E_2	E_3	E_4
1	1.244	1.125	1.666	0.600	—0.1	—0.304	2.670	1.185	—8.441
0.9	1.173	1.149	1.594	0.697	—0.2	—0.704	3.126	1.164	—4.296
0.8	1.097	1.187	1.532	0.816	—0.3	—1.248	3.146	1.139	—2.927
0.7	1.017	1.242	1.476	0.968	—0.4	—2.021	4.597	1.115	—2.243
0.6	0.930	1.317	1.430	1.166	—0.5	—3.191	5.899	1.093	—1.829
0.5	0.831	1.409	1.386	1.443	—0.6	—5.111	7.998	1.075	—1.550
0.4	0.717	1.522	1.346	1.857	—0.7	—8.663	11.74	1.051	—1.360
0.3	0.586	1.662	1.309	2.546	—0.8	—16.91	20.23	1.032	—1.210
0.2	0.429	1.836	1.277	3.915	—0.9	—47.49	52.48	1.015	—1.094
0.1	0.238	2.055	1.247	8.021	—1	—∞	∞	1	—1
0	0	2.321	1.217	∞					

It follows from the equality (2.62) that λ_* should satisfy the condition

$$E_1(\lambda_*) = \frac{\cos\beta_0 - 1}{\bar{R}^{2/3}}. \tag{2.62}$$

To solve eqs.(2.1) and (2.2) in the case of $\frac{A}{R} < \left(\frac{A}{R}\right)_{\lambda=1}$, we proceed in the following manner: Assuming the parameter λ as known, iteration of the second equation of the system (2.1) will furnish the quantity $\bar{\delta} = \frac{\bar{\delta}_0}{1 + \lambda}$. Replacing the trigonometric functions of the angle β by the corresponding values from eq.(2.2), we take the following as an approximate value of $\bar{\delta}$:

$$\bar{\delta} = G_1^{2/3} E_1 \left(\frac{\bar{R}}{\cos\beta_0}\right)^{2/3}, \tag{2.63}$$

where

$$G_1 = \frac{1 + E_1\left(\frac{\bar{R}}{\cos\beta_0}\right)^{2/3}}{1 + E_2\left(\frac{\bar{R}}{\cos\beta_0}\right)^{2/3} \cdot \frac{\sin^2\beta_0 + 2E_1\left(\frac{\bar{R}}{\cos\beta_0}\right)^{2/3} + E_1^2\left(\frac{\bar{R}}{\cos\beta_0}\right)^{4/3}}{\cos^2\beta_0\left[1 + E_1\left(\frac{\bar{R}}{\cos\beta_0}\right)^{2/3}\right]}}. \tag{2.64}$$

It should be borne in mind that, since eq.(2.63) is approximate, the value of $\bar{\delta}$ determined from this expression for $\lambda = \lambda_*$ will differ somewhat from the value corresponding to eq.(2.59).

Furthermore, from eqs.(2.1) we have

$$\frac{A}{R} = \frac{E_3}{\cos\beta_0} \frac{(\sin^2\beta_0 + 2\bar{\delta} + \bar{\delta}^2)^{1/2}}{1 + \frac{\sin^2\beta_0 + 2\bar{\delta} + \bar{\delta}^2}{\cos^2\beta_0} \cdot \frac{E_2}{E_1} \cdot \frac{\bar{\delta}}{1+\bar{\delta}}} \left(1 - E_4 \frac{\bar{\delta}}{1+\bar{\delta}}\right). \tag{2.65}$$

Prescribing λ, we then use eqs.(2.63) and (2.65) for plotting the graph of the dependence $\frac{A}{R} = F(\lambda)$ (Fig.4.14). From this graph, knowing the ratio $\frac{A}{R}$, we find the value of λ which constitutes an approximate solution of eqs.(2.1) and (2.2). Using the obtained value of λ, we calculate by eq.(2.63) the actual value of $\bar{\delta}$ and then find $\bar{\delta}_0$ from it.

As shown by numerical calculations, the accuracy of eqs.(2.63) and (2.65), just as of eqs.(2.51) and (2.52), is completely sufficient for engineering applications. The deviations of the values of $\bar{\delta}_0$ and λ calculated by the indicated formulas from the corresponding "exact" values determined by eqs.(2.1) and (2.2) for initial contact angles of $\beta_0 \leq 45^\circ$ are usually no more than 3 - 4%.

On the basis of eq.(2.63), we can write

$$P_0 = B_0 \nu d_{ba}^2 (1+\lambda)^{3/2} G_1 E_1^{3/2} \frac{\bar{R}}{\cos\beta_0}. \tag{2.66}$$

Recalling that $E_1 = \frac{1}{(1+\lambda) j_2^{3/2}}$ and $\bar{R} = \frac{R}{B_0 z \nu d_{ba}^2}$, we find the following /361 for the case $\frac{A}{R} < \left(\frac{A}{R}\right)_{\lambda=1}$:

$$P_0 = \kappa_0^{(R)} \frac{R}{z\cos\beta_0}. \tag{2.67}$$

Here,

$$\kappa_0^{(R)} = \frac{G_1}{j_2}. \tag{2.68}$$

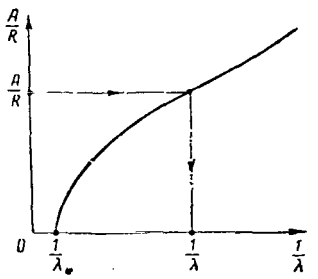

Fig.4.14 Auxiliary Graph for Approximate Solution of Eqs.(2.1) for a Loading Zone less than 360°.

A comparison of the equalities (2.11) and (2.67) readily shows that the coefficient k_0 in this case can be expressed as

$$\kappa_0 = 0.229\kappa_0^{(R)} \cos\alpha.$$

Accordingly,

$$\kappa = 0.390\omega\kappa_0^{(R)} \cos\alpha.$$

6. Relative Displacements of Races

For certain ultra-precision high-speed bearing assemblies, a proper determination of the relative displacements of the bearing races under load is of importance. When combined loads are absorbed by radial and radial-thrust ball bearings, this problem is solved in the following manner:

Equations (1.13) and (1.16), in the absence of mutual misalignment of the races $\left(\bar{\epsilon} = \vartheta \frac{r_0}{g} = 0\right)$, indicate that

$$\left.\begin{aligned} \bar{s} &= \tan\beta \cos\beta_0; \\ \bar{u} &= \frac{\lambda\bar{\delta}}{\cos\beta}. \end{aligned}\right\} \tag{2.69}$$

On the basis of eq.(1.19), we find

$$\left.\begin{aligned} \bar{s} &= \left(\sin^2\beta_0 + 2\bar{\delta} + \bar{\delta}^2\right)^{1/2}; \\ \bar{u} &= \frac{\lambda\bar{\delta}(1+\bar{\delta})}{\cos\beta_0}. \end{aligned}\right\} \tag{2.70}$$

Let $\frac{A}{R} \geq \left(\frac{A}{R}\right)_{\lambda=1}$. Under this condition, disregarding the quantity $\bar{\delta}^2$ owing to its smallness in the equalities (2.42), the following expressions are obtained from eqs.(2.51) and (2.52) for the relative displacements $\bar{s}$ and $\bar{u}$:

$$\left.\begin{aligned} \bar{s} &= \left\{\sin^2\beta_0 + 2\left(\frac{\bar{A}}{D_3}\right)^{2/3} \frac{\left[1+\left(\frac{\bar{A}}{1.41D_3}\right)^{1/2}\right]^{2/3}}{\left[\sin^2\beta_0 + 2\left(\frac{\bar{A}}{1.41D_3}\right)^{1/2}\right]^{1/3}}\right\}^{1/2}; \\ \bar{u} &= \frac{D_2}{\cos\beta_0} \cdot \frac{1+\frac{3}{16}D_2^2}{1-\frac{1}{32}D_2^2} \left(\frac{\bar{A}}{D_3}\right)^{2/3} \frac{\left[1+\left(\frac{\bar{A}}{1.41D_3}\right)^{1/2}\right]^{2/3}}{\left[\sin^2\beta_0 + 2\left(\frac{\bar{A}}{1.41D_3}\right)^{1/2}\right]^{1/3}}. \end{aligned}\right\} \tag{2.71}$$

It is easy to define the variation in the displacements $\bar{s}$ and $\bar{u}$ with any change in the ratios of radial and axial loads on the example of a 36207 bearing, for which the curves $\bar{u} = \bar{u}\left(\frac{R}{zvd_{ba}^2}\right)$ and $\bar{s} = \bar{s}\left(\frac{R}{zvd_{ba}^2}\right)$ are plotted by means of eqs.(2.71) in Fig.4.15 for a constant value of the axial load $\left(\frac{A}{zvd_{ba}^2} = 0.53\right)$. For comparison, the sign "×" indicates the exact values of displacements $\bar{s}$ and $\bar{u}$ calculated by eqs.(1.3), (1.6), and (1.7) for the cases $\lambda = 0$ and $\lambda = 1$, which determine the limits of applicability of eqs.(2.71). /362

As follows from the presented data, the equation of moments does not enter into the system of equations by means of which we investigate the distribution of the load in radial and radial-thrust ball bearings operating without misalignment of the races. Therefore, the assumption of the effect of the radial force and moment in one plane, which was used in deriving eqs.(1.24), introduces no additional limitations that would narrow the range of applicability of the aforementioned method of calculating such bearings.

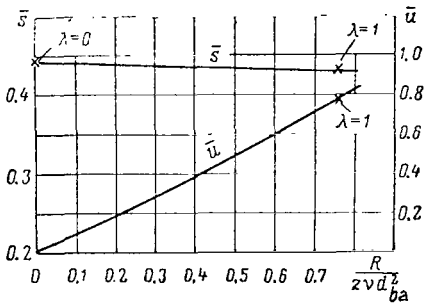

Fig.4.15 Curves of $\bar{u} = \bar{u}\left(\frac{R}{zvd_{ba}^2}\right)$ and $\bar{s} = \bar{s}\left(\frac{R}{zvd_{ba}^2}\right)$ at a Constant Value of the Axial Load.

Until now, we had assumed the radial and axial loads acting on the bearing as given.

The radial loads on bearings are found from the equations of equilibrium of the shaft to which they are fitted.

At large distances between the individual supports, a determination of such loads is not difficult since, in this case, they depend little on the moments absorbed by the bearings so that these can be disregarded in the calculation.

Often, considerable difficulties are encountered in calculating axial loads. Strictly speaking, the axial load can be considered as known only in the case in which the bearing in question absorbs the entire axial force applied to the shaft, as takes place in bearing assemblies with one bearing fixed in an axial direction.

Of course, if the equations of equilibrium of the shaft are not sufficient for finding the loads acting on its supports, it is impossible to make a separate calculation of bearings mounted on separate supports. In such cases, the pressures on the balls can be determined only by solving the equations of equilibrium of the shaft simultaneously with the equations of static equilibrium of all bearings fitted to this shaft.

Section 3. Certain Problems in Calculating Radial-Thrust Ball Bearings with Consideration of Misalignment of their Races under Load

1. Basic Relationships

In a number of helicopter units, narrowly spaced radial-thrust ball bearings absorb combined loads in which the moment plays an appreciable if not the main role. It is understandable that, in determining the parameters characterizing the performance of such bearings, it is impermissible to disregard the misalignment of the races as had been done in the preceding Section; this greatly complicates their calculation. /363

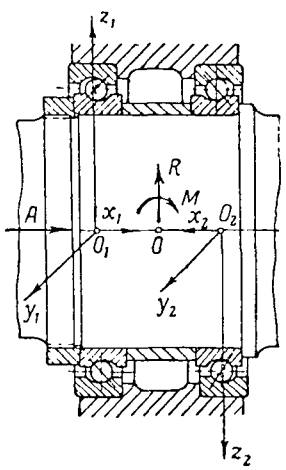

Fig.4.16 Diagram of Loading of Two Ball Bearings by Radial and Axial Forces and Moment.

The absence of reliable methods for calculating radial-thrust ball bearings receiving appreciable moments at close spacing of the supports interferes with the design of numerous bearing assemblies, in particular the assembly of the pitch control swashplate which is one of the most stressed and vital elements of a helicopter.

Let us examine certain problems in the calculation of radial-thrust ball bearings, with consideration of misalignment of their races under load. The results obtained in solving these problems yield answers to the basic questions arising in the designing of bearing assemblies for helicopter units which have to absorb large moments.

Let the bearing assembly, consisting of two radial-thrust ball bearings, absorb a combined load in the form of a radial force R applied in the middle between the supports, an axial force A, and a moment M (Fig.4.16). It is assumed that the force R and the moment M act in one and the same plane.

Let us assign the index 1 to that bearing of a given assembly for which the pressures on the balls caused by the action of the force R and the moment M are cumulative. All quantities pertaining to this bearing will be written with this index. The index 2 is given to the second bearing in this assembly and to all quantities pertaining to it.

Let us direct the axes of the coordinates for the bearings 1 and 2 as shown in Fig.4.16. It is obvious that, in the coordinate system $x_1 y_1 z_1$, the force R and the moment M always have positive values whereas the axial force A can be either positive or negative.

The conditions of equilibrium of the shaft to which the bearings are mounted reduce to the following system of equations:

$$\left.\begin{aligned} A &= A_1 - A_2; \\ R &= R_1 - R_2; \\ M &= M_1 + M_2 + R_1\frac{L}{2} + R_2\frac{L}{2}, \end{aligned}\right\} \qquad (3.1)$$

where L is the distance between supports.

Since the moments M_1 and M_2 at small distances between the supports are not only commensurable with the moments $R_1 \frac{L}{2}$ and $R_2 \frac{L}{2}$ but may even appreciably exceed them, eqs.(3.1) should be solved simultaneously with the equations of static equilibrium of the bearings 1 and 2.

We assume that, in the loaded assembly, the center of the stack of inner races is displaced in the direction of action of the forces A and R by distances s and u and that the common axis of rotation of these races is turned in the direction of action of the moment M through an angle ϑ. The angle ϑ is the angle of misalignment (obliquity) for the bearing 1 and for the bearing 2. /364

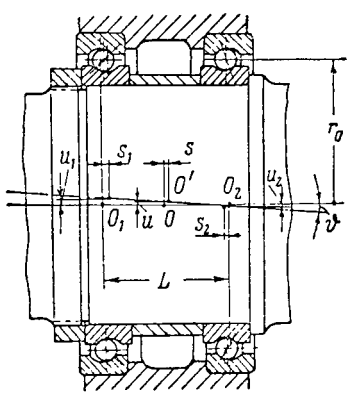

Fig.4.17 Diagram of Displacements of Inner Races of Bearings under the Effect of an Arbitrary External Load.

The relative displacements* determining the position of the centers of the inner races of the bearings 1 and 2 in the coordinate systems $x_1y_1z_1$ and $x_2y_2z_2$, according to Fig.4.17 are equal to

$$\left.\begin{aligned} \bar{s}_1 &= \sin\beta_0 + \bar{\Delta}_{pr} + \bar{s}; \\ \bar{u}_1 &= \bar{u} + \zeta\bar{\varepsilon}; \\ \bar{s}_2 &= \sin\beta_0 + \bar{\Delta}_{pr} - \bar{s}; \\ \bar{u}_2 &= -\bar{u} + \zeta\bar{\varepsilon}. \end{aligned}\right\} \qquad (3.2)$$

Here,

Δ_{pr} = half of the axial preloading with which the bearings are installed;

$\zeta = \frac{L}{2r_0}$ = ratio of the interbearing distance to diameter at which balls are located; $\bar{\varepsilon} = \vartheta\, r_0/g$.

After writing the equalities (1.16) for both bearings and substituting eqs.(3.2) into them, easy transformations will give

* All relative quantities, as before, are expressed in fractions of the distance $g = r_{out} + r_{in} - d_{ba}$.

$$\left.\begin{aligned}
\bar{u} &= \frac{1}{2\left(\frac{\tan\beta_1+\tan\beta_2}{2}+\zeta\right)}\cdot\left[\frac{(\tan\beta_2+\zeta)\lambda_1\bar{\delta}_1}{\cos\beta_1}-\frac{(\tan\beta_1+\zeta)\lambda_2\bar{\delta}_2}{\cos\beta_2}\right];\\
\bar{\varepsilon} &= \frac{1}{2\left(\frac{\tan\beta_1+\tan\beta_2}{2}+\zeta\right)}\cdot\left[\frac{\lambda_1\bar{\delta}_1}{\cos\beta_1}+\frac{\lambda_2\bar{\delta}_2}{\cos\beta_2}\right].
\end{aligned}\right\} \qquad (3.3)$$

In bearing assemblies of the type in question, we generally use radial-thrust ball bearings with large initial contact angles, for which the relative displacements $\bar{\delta}_1$ and $\bar{\delta}_2$ rarely exceed $0.25\sin^2\beta_0$. For the indicated values of $\bar{\delta}_1$ and $\bar{\delta}_2$, the equalities (3.3) can be replaced by the following approximate relations:

$$\left.\begin{aligned}
\bar{u} &= \frac{1}{2\cos\beta_0}(\lambda_1\bar{\delta}_1-\lambda_2\bar{\delta}_2);\\
\bar{\varepsilon} &= \frac{1}{2\cos\beta_0(\tan\beta_0+\zeta)}(\lambda_1\bar{\delta}_1+\lambda_2\bar{\delta}_2).
\end{aligned}\right\} \qquad (3.4)$$

For the selected direction of the axes of the coordinates, the angle ψ_0 determining the position of the most loaded ball in the bearing 1 is always equal to zero. The angle ψ_{02} characterizing the position of the most loaded ball in the bearing 2, depending upon the ratio of the radial force R to the moment M, may have either a value of zero (for the prevailing moment) or may be equal to 180° (for the prevailing radial load).

Bearing in mind the latter circumstance, it becomes possible by means of /365
the equalities (1.24), (1.25), (1.21), (1.27), and (3.4), taking the comments made on the order of the quantities $\bar{\delta}_1$ and $\bar{\delta}_2$ into account, to represent the forces and moments taken by the bearings 1 and 2 as follows:

$$\left.\begin{aligned}
\frac{A_1}{z\nu d_{ba}^2} &= B_0\bar{\delta}_{01}^{3/2}\sin\beta_0 j_{11}\left(1+b_{11}\cdot\frac{\bar{\delta}_{01}}{1+\lambda_1}+c_{11}\cdot\frac{\bar{\delta}_{02}}{1+\lambda_2\cos\psi_{02}}\right);\\
\frac{R_1}{z\nu d_{ba}^2} &= B_0\bar{\delta}_{01}^{3/2}\cos\beta_0 j_{21}\left(1-b_{21}\tan^2\beta_0\cdot\frac{\bar{\delta}_{01}}{1+\lambda_1}-c_{21}\tan^2\beta_0\cdot\frac{\bar{\delta}_{02}}{1+\lambda_2\cos\psi_{02}}\right);\\
\frac{M_1}{r_0 z\nu d_{ba}^2} &= B_0\bar{\delta}_{01}^{3/2}\sin\beta_0 j_{21}\left(1+b_{21}\cdot\frac{\bar{\delta}_{01}}{1+\lambda_1}+c_{21}\frac{\bar{\delta}_{02}}{1+\lambda_2\cos\psi_{02}}\right);\\
\frac{A_2}{z\nu d_{ba}^2} &= B_0\bar{\delta}_{02}^{3/2}\sin\beta_0 j_{12}\left(1+b_{12}\cdot\frac{\bar{\delta}_{02}}{1+\lambda_2\cos\psi_{02}}+c_{12}\cdot\frac{\bar{\delta}_{01}}{1+\lambda_1}\right);\\
\frac{R_2}{z\nu d_{ba}^2} &= B_0\bar{\delta}_{02}^{3/2}\cos\beta_0 j_{22}\left(1-b_{22}\tan^2\beta_0\cdot\frac{\bar{\delta}_{02}}{1+\lambda_2\cos\psi_{02}}-\right.\\
&\qquad\left.-c_{22}\tan^2\beta_0\cdot\frac{\bar{\delta}_{01}}{1+\lambda_1}\right)\cos\psi_{02};\\
\frac{M_2}{r_0 z\nu d_{ba}^2} &= B_0\bar{\delta}_{02}^{3/2}\sin\beta_0 j_{22}\left(1+b_{22}\cdot\frac{\bar{\delta}_{02}}{1+\lambda_2\cos\psi_{02}}+c_{22}\frac{\bar{\delta}_{01}}{1+\lambda_1}\right)\cos\psi_{02}.
\end{aligned}\right\} \qquad (3.5)$$

The following notations are adopted in eqs.(3.5)

$$
\left.
\begin{aligned}
b_{11} &= \cot^2\beta_0 + \frac{j_{21}}{j_{11}}\left[\frac{1}{\sin 2\beta_0\,(\tan\beta_0+\zeta)} - 1\right]\lambda_1;\\
c_{11} &= \frac{j_{21}}{j_{11}}\cdot\frac{\lambda_2}{\sin 2\beta_0\,(\tan\beta_0+\zeta)};\\
b_{21} &= \cot^2\beta_0 + \frac{j_{31}}{j_{21}}\left[\frac{1}{\sin 2\beta_0\,(\tan\beta_0+\zeta)} - 1\right]\lambda_1;\\
c_{21} &= \frac{j_{31}}{j_{21}}\cdot\frac{\lambda_2}{\sin 2\beta_0\,(\tan\beta_0+\zeta)};\\
b_{12} &= \cot^2\beta_0 + \frac{j_{22}}{j_{12}}\left[\frac{1}{\sin 2\beta_0\,(\tan\beta_0+\zeta)} - 1\right]\lambda_2\cos\psi_{02};\\
c_{12} &= \frac{j_{22}}{j_{12}}\cdot\frac{\lambda_1}{\sin 2\beta_0\,(\tan\beta_0+\zeta)}\cdot\cos\psi_{02};\\
b_{22} &= \cot^2\beta_0 + \frac{j_{32}}{j_{22}}\left[\frac{1}{\sin 2\beta_0\,(\tan\beta_0+\zeta)} - 1\right]\lambda_2\cos\psi_{02};\\
c_{22} &= \frac{j_{32}}{j_{22}}\left[\frac{\lambda_1}{\sin 2\beta_0\,(\tan\beta_0+\zeta)}\cdot\cos\psi_{02}\right].
\end{aligned}
\right\} \qquad (3.6)
$$

As follows from eqs.(3.2) and (1.13), we have

$$\tan\beta_1 + \tan\beta_2 = \frac{\bar{s}_1 + \bar{s}_2}{\cos\beta_0} = 2\tan\beta_0 + \frac{2\bar{\Delta}_{pr}}{\cos\beta_0}.$$

Since, at $\bar{\delta} \le 0.25\sin^2\beta_0$, we can put approximately $\tan\beta = \tan\beta + \dfrac{\bar{\delta}}{\sin\beta_0\cos\beta_0}$ the last expression will yield

$$\bar{\delta}_1 + \bar{\delta}_2 = 2\bar{\Delta}_{pr}\sin\beta_0.$$

Using the equality (1.21), we finally have /366

$$\frac{\bar{\delta}_{01}}{1+\lambda_1} + \frac{\bar{\delta}_{02}}{1+\lambda_2\cos\psi_{02}} = 2\bar{\Delta}_{pr}\sin\beta_0. \qquad (3.7)$$

The relations (3.5), (3.6), and (3.7) together with eqs.(3.1) make it possible to determine all parameters characterizing the performance of radial-thrust ball bearings for closely spaced supports, when misalignment of the races under load cannot be disregarded. As shown by numerical calculations, the accuracy of these relations obtained on the assumption that the quantities $\bar{\delta}_1$ and $\bar{\delta}_2$ do not exceed $0.25\sin^2\beta_0$ at initial contact angles of $\beta_0 \ge 26^\circ$, with which we usually deal in bearing assemblies intended for absorbing large moments, is sufficient.

We will next analyze the basic calculation cases encountered when designing bearing assemblies of this type for helicopter units.

2. Case of "Pure" Moment

If a bearing assembly consisting of two identical radial-thrust ball bearings absorbs a "pure" moment (Fig.4.18), then by virtue of the identical loads on both bearings we must have $R_1 = R_2$, $A_1 = A_2$, and $M_1 = M_2$. It is logical that, in this case, $\psi_{02} = \psi_{01} = 0$, $\lambda_1 = \lambda_2$, and $\bar{\delta}_{01} = \bar{\delta}_{02}$.

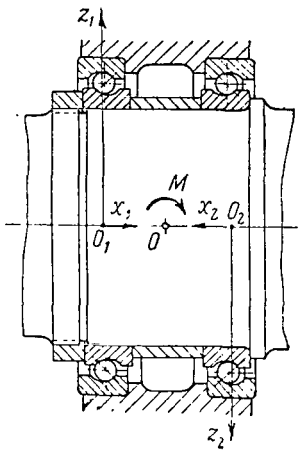

Fig.4.18 Diagram of Loading of Two Ball Bearings by a "Pure" Moment.

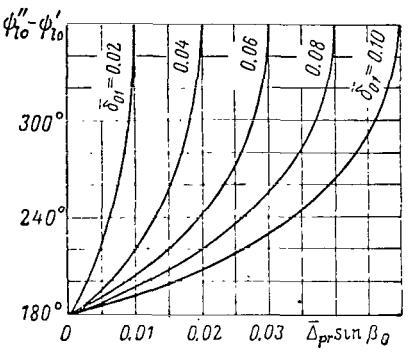

Fig.4.19 Effect of Preloading on the Loading Zone.

As indicated in eq.(3.7), at $\psi_{02} = 0$, $\lambda_1 = \lambda_2$, and $\bar{\delta}_{01} = \bar{\delta}_{02}$, we have

$$\frac{\bar{\delta}_{01}}{1+\lambda_1} = \sin\beta_0 \bar{\Delta}_{pr}. \tag{3.8}$$

Consequently, under the effect of a "pure" moment,

$$\lambda_1 = \frac{\bar{\delta}_{01}}{\sin\beta_0 \bar{\Delta}_{pr}} - 1. \tag{3.9}$$

It is understandable that the ratio $\dfrac{\bar{\delta}_{01}}{\sin\beta_0\bar{\Delta}_{pr}}$ should always be greater than unity. This becomes obvious when taking into account that the product $\sin\beta_0\bar{\Delta}_{pr}$ represents the relative convergence of the raceways caused by the preloading, i.e., the relative approach of the raceways present before applying /367 an external load to the assembly.

Equation (3.9) determines the loading zone as a function of the level of the load and the preloading. This relation, in particular, shows that, to have all balls share the load, the bearing should be mounted with a relative preloading $2\bar{\Lambda}_{pr} \geq \dfrac{\bar{\delta}_{01}}{\sin\beta_0}$.

The effect of the preloading on the loading zone is shown in Fig.4.19.

Frequently, the preload is not given as a relative axial displacement $2\bar{\Delta}_{pr}$ but as a corresponding axial load A_{pr}, determined by the expression

$$A_{pr}=zB_0\nu d_{ba}^2\bar{\Delta}_{pr}^{3/2}\sin^{5/2}\beta_0\left(1+\frac{\cos^2\beta_0}{\sin\beta_0}\cdot\bar{\Delta}_{pr}\right). \tag{3.10}$$

Since, under the effect of a "pure" moment, we have $R_1 = R_2$ and $A_1 = A_2$, the first two equations of the system (3.1) are identically satisfied. The third equation of the system, for the case of a "pure" moment, can be transformed by means of eqs.(3.5), (3.6), and (3.7) in the following manner:

$$\frac{M}{r_0 z\nu d_{ba}^2}=2B_0\bar{\delta}_{01}^{3/2}\sin\beta_0(1+\zeta\cot\beta_0)j_{21}\times$$
$$\times\left[1+\cot^2\beta_0\cdot\frac{1-\zeta\tan\beta_0}{1+\zeta\cot\beta_0}\left(1+\frac{j_{31}}{j_{21}}\frac{1-\zeta\tan\beta_0}{1+\zeta\cot\beta_0}\cdot\lambda_1\right)\frac{\bar{\delta}_{01}}{1+\lambda_1}\right]. \tag{3.11}$$

Using eqs.(2.3), (2.5), (3.9), and (3.11), it is easy to construct the graphs of the relations $\frac{P_{01}}{\nu d_{ba}^2}=F_0\left(\frac{M}{r_0 z\nu d_{ba}^2}\right)$ and $\frac{P_{eq1}}{\nu d_{ba}^2}=F_{eq}\left(\frac{M}{r_0 z\nu d_{ba}^2}\right)$, from which we can find the maximum and equivalent pressures on the balls. The curves shown in Fig.4.20 can serve as a typical example of such graphs. They were obtained on the assumption that $\beta_0 = 36^\circ$, $\zeta = 0$, and $\bar{\Delta}_{pr}\sin\beta_0 = 0.01$.

Let us now represent the maximum pressure on the ball P_{01} in the form

$$P_{01}=\frac{\kappa_0^{(M)}M}{2j_{21_{\lambda=\infty}}r_0 z\sin\beta_0(1+\zeta\cot\beta_0)}=\frac{4.37\kappa_0^{(M)}M}{2r_0 z\sin\beta_0(1+\zeta\cot\beta_0)}. \tag{3.12}$$

Accordingly, we put

$$P_{eq1}=wP_{01}=\frac{2.57\kappa^{(M)}M}{2r_0 z\sin\beta_0(1+\zeta\cot\beta_0)}, \tag{3.13}$$

where $k^{(M)}=\frac{w}{0.587}\cdot k_0^{(M)}$.

It is necessary to note that under the effect of the "pure" moment, $P_{02} = P_{01}$ and $P_{eq\,2} = P_{eq\,1}$.

It is easy to demonstrate that the coefficient is

$$\kappa_0^{(M)}=\frac{j_{21_{\lambda=\infty}}}{j_{21}\left[1+\cot^2\beta_0\cdot\frac{1-\zeta\tan\beta_0}{1+\zeta\cot\beta_0}\left(1+\frac{j_{31}}{j_{21}}\frac{1-\zeta\tan\beta_0}{1+\zeta\cot\beta_0}\cdot\lambda_1\right)\frac{\bar{\delta}_{01}}{1+\lambda_1}\right]}. \tag{3.14}$$

At zero preloading when $\lambda_1 = \infty$ according to eq.(3.9), we obtain from eq.(3.14) /368

$$\kappa_0^{(M)} = \frac{1}{1 + 0.868\left(\frac{1-\zeta\tan\beta_0}{\tan\beta_0+\zeta}\right)^2 \bar{\delta}_{01}}. \qquad (3.15)$$

The values of the coefficient $k_0^{(M)}$ corresponding to eq.(3.15) can be determined from the graphs in Fig.4.21. Here, the abscissa gives the quantity $\bar{M} = \frac{1}{z\nu d_{ba}^2 \sin\beta_0(1+\zeta\cot\beta_0)} \frac{M}{r_0}$. The quantity $\rho = \left|\frac{1-\zeta\tan\beta_0}{\tan\beta_0+\zeta}\right|$ is taken as a parameter.

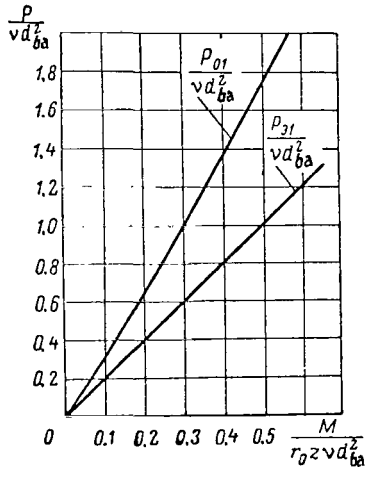

Fig.4.20 Values of $\frac{P_{01}}{\nu d_{ba}^2}$ and $\frac{P_{eq\,1}}{\nu d_{ba}^2}$ as a Function of $\frac{M}{r_0 z\nu d_{ba}^2}$ for $\beta_0 = 36^\circ$.

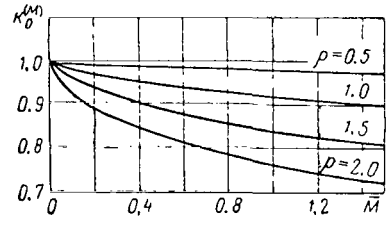

Fig.4.21 Values of the Coefficient $k_0^{(M)}$ as a Function of the Parameters ρ and $\bar{M}$.

The graphs in Figs.4.22 and 4.23 show the mode of variation in the coefficients $k_0^{(M)}$ and $k^{(M)}$ as a function of preloading when $\beta_0 = 36^\circ$ and $\zeta = 0$. The curves indicate that the preloading should be selected such that the parameter λ_1 lies within the limits of 1 to 1.25. At such a selection of the preloading, the coefficient $k_0^{(M)}$ and hence the maximum pressure on the ball drop by 10 - 12%. In this case, the coefficient $k^{(M)}$ and, together with it, the equivalent pressure on the ball will keep approximately the same magnitude as in the case without preloading. Analogous conclusions can be drawn from a study of other combinations of the quantities β_0 and ζ.

It is extremely important to estimate the effect of preloading on the angu-

lar stiffness of the bearing assembly. This is easily done by means of the second equation of the system (3.4) which, for the case of a "pure" moment, can be represented in the form

$$\bar{\varepsilon} = \frac{\bar{\delta}_{01}}{\cos\beta_0 (tan\beta_0 + \zeta)} \frac{\lambda_1}{1+\lambda_1}. \qquad (3.16)$$

Equation (3.16) shows that a change from $\lambda_1 = \infty$ to $\lambda_1 = 1 - 1.25$ leads to a decrease in misalignment of the races of the bearings by a factor of 2.2 to 2.

It is obvious from the aforesaid that, in installing radial-thrust ball bearings with an optimal preloading corresponding to values of the parameter λ_1 from 1 to 1.25, the service conditions of the bearing assemblies loaded by a moment improve noticeably. /369

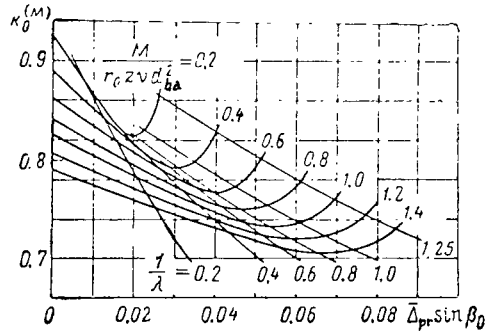

Fig.4.22 Values of the Coefficient $k_0^{(M)}$ versus Preloading for Certain Constant Values of $\frac{M}{r_0 z \nu d_{ba}^2}$.

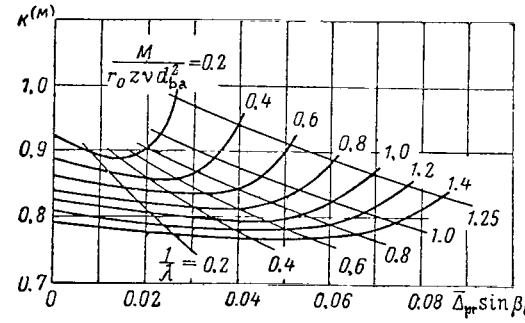

Fig.4.23 Values of the Coefficient $k^{(M)}$ versus Preloading for Certain Constant Values of $\frac{M}{r_0 z \nu d_{ba}^2}$.

The preloading at which the parameter $\lambda_1 = 1$ to 1.25, in practical calculations, can be computed from the approximate formula

$$\bar{\Delta}_{pr} = \frac{1}{(2-2.25)\sin\beta_0} \left\{ \frac{(1.96-1.94)\bar{M}}{1 + H[(1.96-1.94)\bar{M}]^{2/3}} \right\}^{2/3}, \qquad (3.17)$$

where

$$H = \frac{1}{2-2.25} cot^2\beta_0 \frac{1-\zeta tan\beta_0}{1+\zeta cot\beta_0} \left[1 + (0.905-1.08) \frac{1-\zeta tan\beta_0}{1+\zeta cot\beta_0} \right].$$

In this case, the quantities P_{01} and $P_{eq\,1}$ are respectively equal to

$$\left.\begin{aligned} P_{01} &= \frac{(3.92-3.88)M}{2r_0 z \sin\beta_0 (1+\zeta cot\beta_0)\{1 + H[(1.96-1.94)\bar{M}]^{2/3}\}}; \\ P_{eq1} &= (0.657-0.645) P_{01}. \end{aligned}\right\} \qquad (3.18)$$

3. Simultaneous Action of Moment and Axial Force

In the presence of simultaneous action of moment and axial force (Fig.4.24), the loading conditions of the bearings 1 and 2 are dissimilar, which greatly complicates the calculations for determining the ball pressures. To find the quantities P_{01}, $P_{eq\,1}$, P_{02}, and $P_{eq\,2}$, a number of auxiliary graphs must be constructed. The sequence of plotting such graphs is easily understood from the following example:

Let the initial contact angle be $\beta_0 = 36^\circ$. For simplicity, let us assume that the relative preloading is $\bar{\Delta}_{pr} = 0$ and the relative base $\zeta = 0$, i.e., let us study the case directly related to calculations of the bearings of the pitch control swashplate, for which these assumptions are sufficiently valid.

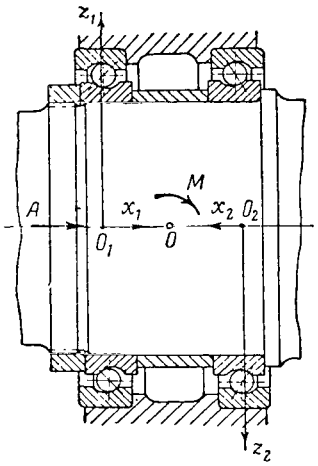

Fig.4.24 Diagram of Loading Two Ball Bearings by Moment and Axial Force.

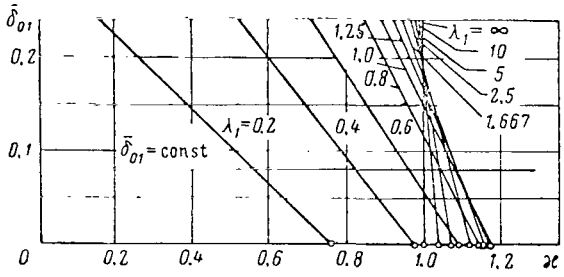

Fig.4.25 Typical Graph of $\bar{\delta}_{01} = \bar{\delta}_{01}(\kappa, \lambda)$ for $R = R_1 - R_2 = 0$.

According to eqs.(3.5) for a radial load of $R = R_1 = R_2 = 0$, the quantities $\bar{\delta}_{01}$, $\bar{\delta}_{02}$, λ_1, and λ_2 are correlated by the following relations:

$$j_{21} - \left(\frac{\bar{\delta}_{02}}{\bar{\delta}_{01}}\right)^{3/2} j_{22} = \tan^2\beta_0 \left[j_{21} b_{21} - \left(\frac{\bar{\delta}_{02}}{\bar{\delta}_{01}}\right)^{3/2} j_{22} c_{22} \right] \frac{\bar{\delta}_{01}}{1+\lambda_1} + \\ + \tan^2\beta_0 \left[j_{21} c_{21} - \left(\frac{\bar{\delta}_{02}}{\bar{\delta}_{01}}\right)^{3/2} j_{22} b_{22} \right] \frac{\bar{\delta}_{02}}{1+\lambda_2}. \tag{3.19}$$

In the equality (3.19), as in all subsequent relations, we have taken into account that - during the simultaneous action of moment and axial force - we have $\psi_{02} = \psi_{01} = 0$, just as in the case of action of a "pure" moment.

From eq.(3.7) at zero preloading we obtain

$$\frac{\bar{\delta}_{01}}{1+\lambda_1}+\frac{\bar{\delta}_{02}}{1+\lambda_2}=0. \tag{3.20}$$

From this follows

$$\lambda_2=-\left[\frac{\bar{\delta}_{02}}{\bar{\delta}_{01}}(1+\lambda_1)+1\right]. \tag{3.21}$$

Henceforth, the ratio $\frac{\bar{\delta}_{02}}{\bar{\delta}_{01}}$ will be denoted everywhere by $\varkappa$.

Making use of the equalities (3.6), (3.19), (3.20), and (3.21), let us plot the curves $\bar{\delta}_{01} = \bar{\delta}_{01}(\varkappa, \lambda_1)$ satisfying the condition $R = R_1 - R_2 = 0$ (Fig.4.25). Intersecting the obtained curves by lines $\bar{\delta}_{01}$ = const, we find the values of $\varkappa$ /371 corresponding to the selected values of $\bar{\delta}_{01}$ for the given values of λ_1 (from ∞ to 0). Furthermore, taking λ_1 as a parameter, we can use eqs.(3.1), (3.5), and the preceding equalities for calculating the quantities $\frac{A}{z\nu d_{ba}^2}$, $\frac{M}{r_0 z\nu d_{ba}^2}$, and the ratios $\frac{P_{02}}{P_{01}} = \varkappa^{3/2}$ and $\frac{P_{eq\,2}}{P_{eq\,1}} = \varkappa^{3/2}\frac{w_2}{w_1}$.

The results of the calculations are presented graphically, as is done in Figs.4.26 - 4.28. Figure 4.26, from the given values of $\frac{A}{z\nu d_{ba}^2}$ and $\frac{M}{r_0 z\nu d_{ba}^2}$, permits determining the quantities $\bar{\delta}_{01}$ and λ_1; when these are known it becomes easy to calculate the maximum and equivalent pressures P_{01} and $P_{eq\,1}$. From Figs.4.27 and 4.28, we find the ratios $\frac{P_{02}}{P_{01}}$ and $\frac{P_{eq\,2}}{P_{eq\,1}}$ and then calculate the maximum and equivalent pressures P_{02} and $P_{eq\,2}$.

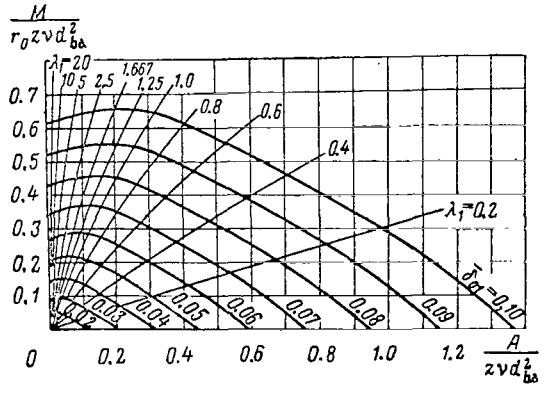

Fig.4.26 Dependence of $\frac{M}{r_0 z\nu d_{ba}^2}$ on $\frac{A}{z\nu d_{ba}^2}$, for Certain Constant Values of $\bar{\delta}_{01}$ and λ_1.

The case $\bar{\Delta}_{pr} = 0$ and $\zeta = 0$ was analyzed above. For arbitrary values of these quantities and also for other initial contact angles β_0, determination of the pressures P_{01}, $P_{eq\,1}$, P_{02}, and $P_{eq\,2}$ is made in the same manner as in the example under study. It should be remembered that, in the presence of preloading, the quantity $\bar{\delta}_{01}$ cannot be less than $\sin\beta_0\bar{\Delta}_{pr}$.

We should note that the case of $\bar{\Delta}_{pr} = 0$ and $\zeta = 0$ is characteristic not only for bearings of the pitch control but also for many large-diameter roller bearings used in rotary devices of modern machines and mechanisms.

It is obvious from the presented material that, for the prevailing moment when $\lambda_1 > 1$, the bearing 2 is usually the most loaded, although at first glance the service conditions of the bearing 1, toward which the axial load A is directed, seem more severe.

The presented method of calculating radial-thrust ball bearings under the combined action of moment and axial force requires a large volume of calculations and constructions. Therefore, its use is warranted only in special studies having the purpose of determining the peculiarities of the load distribution in /372
bearing assemblies with closely spaced supports, and also for plotting auxiliary graphs for calculating individual standard structures. If such graphs have not been constructed beforehand, the engineering calculations should use the simplified procedure based on critical relations obtained for the case of small loads, when the forces are distributed between the balls in the most unfavorable manner.

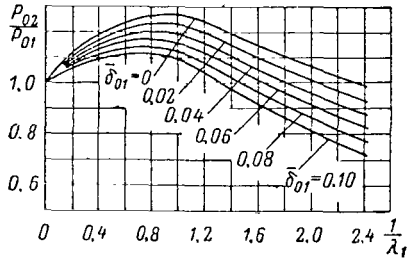

Fig.4.27 Dependence of the Ratio $\frac{P_{02}}{P_{01}}$ on $\frac{1}{\lambda_1}$, for Certain Constant Values of $\bar{\delta}_{01}$.

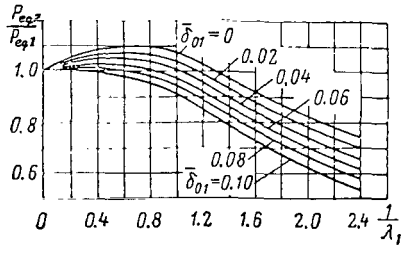

Fig.4.28 Dependence of the Ratio $\frac{P_{eq\,2}}{P_{eq\,1}}$ on $\frac{1}{\lambda_1}$, for Certain Constant Values of $\bar{\delta}_{01}$.

4. Limit Dependences on Small Loads

In the presence of small loads, it can be assumed that the contact angles of all balls are approximately identical and equal to β_0.

After discarding in eqs.(3.5) all terms that allow for the variation in contact angles and substituting the quantities $\bar{\delta}_{01}$ and $\bar{\delta}_{02}$ by the maximum pressures on the balls P_{01} and P_{02}, which is more convenient for small loads, we have

$$\left.\begin{aligned} R_1 &= zP_{01}\cos\beta_0 j_{21};\\ A_1 &= zP_{01}\sin\beta_0 j_{11};\\ M_1 &= r_0 zP_{01}\sin\beta_0 j_{21};\\ R_2 &= zP_{02}\cos\beta_0 j_{22};\\ A_2 &= zP_{02}\sin\beta_0 j_{12};\\ M_2 &= r_0 zP_{02}\sin\beta_0 j_{22}. \end{aligned}\right\} \qquad (3.22)$$

Substituting the dependences (3.22) into eqs.(3.1), we obtain

$$\left.\begin{aligned} R &= zP_{01}\cos\beta_0(j_{21}-\varkappa^{3/2}j_{22}\cos\psi_{02});\\ A &= zP_{01}\sin\beta_0(j_{11}-\varkappa^{3/2}j_{12});\\ M &= r_0zP_{01}\sin\beta_0(1+\zeta\cot\beta_0)(j_{21}+\varkappa^{3/2}j_{22}\cos\psi_{02}), \end{aligned}\right\} \tag{3.23}$$

where, as before, $\varkappa = \dfrac{\bar{\delta}_{02}}{\bar{\delta}_{01}} = \left(\dfrac{P_{02}}{P_{01}}\right)^{2/3}$.

Since in this case the angle ψ_{02} need not be equal to zero, the equality (3.7), under consideration of this circumstance, will yield

$$\lambda_2\cos\psi_{02} = -\left[1+\frac{\varkappa(1+\lambda_1)}{1-(1+\lambda_1)\dfrac{2\bar{\Delta}_{pr}\sin\beta_0}{\bar{\delta}_{01}}}\right]. \tag{3.24}$$

Let us examine the system of equations /373

$$\left.\begin{aligned} \frac{j_{21}+\varkappa^{3/2}j_{22}}{j_{11}-\varkappa^{3/2}j_{12}} &= \tau;\\ \frac{j_{21}-\varkappa^{3/2}j_{22}}{j_{21}+\varkappa^{3/2}j_{22}} &= \upsilon;\\ \lambda_2\cos\psi_{02} &= -[\varkappa(1+\lambda_1)+1. \end{aligned}\right\} \tag{3.25}$$

It is easy to demonstrate that the values of λ_1, λ_2, and $\varkappa$ for zero preloading, satisfying equations (3.25), also satisfy eqs.(3.23) and (3.24), if we set

$$\frac{r_0R(1+\zeta\cot\beta_0)\tan\beta_0}{M} \leqslant 1:$$

$$\left.\begin{aligned} \tau &= \frac{M}{r_0A(1+\zeta\cot\beta_0)};\\ \upsilon &= \frac{r_0R(1+\zeta\cot\beta_0)\tan\beta_0}{M}; \end{aligned}\right\} \tag{3.26}$$

and $\dfrac{r_0R(1+\zeta\cot\beta_0)\tan\beta_0}{M} \geqslant 1$:

$$\left.\begin{aligned} \tau &= \frac{R}{A}\tan\beta_0;\\ \upsilon &= \frac{M}{r_0R(1+\zeta\cot\beta_0)\tan\beta_0}. \end{aligned}\right\} \tag{3.27}$$

It must be recalled that, in the first case, the angle ψ_{02} is equal to zero and in the second, to 180°.

If the axial force plays the major role in the external load, then the pressures on the balls are usually written in the form

$$\left.\begin{aligned} P_{01} &= \frac{\kappa_{01}^{(A)} A}{z \sin \beta_0}; \\ P_{eq1} &= \frac{\kappa_1^{(A)} A}{z \sin \beta_0}; \\ P_{02} &= \frac{\kappa_{02}^{(A)} A}{z \sin \beta_0}; \\ P_{eq2} &= \frac{\kappa_2^{(A)} A}{z \sin \beta_0}. \end{aligned}\right\} \qquad (3.28)$$

If the moment predominates, it is generally acceptable to use the form of notation given earlier:

$$\left.\begin{aligned} P_{01} &= \frac{4.37 \kappa_{01}^{(M)} M}{2 r_0 z \sin \beta_0 (1 + \zeta \cot \beta_0)}; \\ P_{eq1} &= \frac{2.57 \kappa_1^{(M)} M}{2 r_0 z \sin \beta_0 (1 + \zeta \cot \beta_0)}; \\ P_{02} &= \frac{4.37 \kappa_{02}^{(M)} M}{2 r_0 z \sin \beta_0 (1 + \zeta \cot \beta_0)}; \\ P_{eq2} &= \frac{2.57 \kappa_2^{(M)} M}{2 r_0 z \sin \beta_0 (1 + \zeta \cot \beta_0)}. \end{aligned}\right\} \qquad (3.29)$$

According to eqs.(3.23), we have /374

$$\left.\begin{aligned} \kappa_{01}^{(M)} &= \frac{2}{4{,}37 (j_{21} + \varkappa^{3/2} j_{22} \cos \psi_{02})}; \\ \kappa_{02}^{(M)} &= \varkappa^{3/2} \kappa_{01}^{(M)}; \\ \kappa_{01}^{(A)} &= \frac{1}{j_{11} - \varkappa^{3/2} j_{12}}; \\ \kappa_{02}^{(A)} &= \varkappa^{3/2} \kappa_{01}^{(A)}. \end{aligned}\right\} \qquad (3.30)$$

As regards the coefficients $k_1^{(M)}$, $k_1^{(A)}$, $k_2^{(M)}$, and $k_2^{(A)}$, these are equal to

$$\kappa_1^{(M)} = \frac{w_1}{0.587} \kappa_{01}^{(M)}; \quad \kappa_1^{(A)} = w_1 \kappa_{01}^{(A)}; \quad \kappa_2^{(M)} = \frac{w_2}{0.587} \kappa_{02}^{(M)}; \quad \kappa_{02}^{(A)} = w_2 \kappa_{02}^{(A)}.$$

It should be noted that, between the coefficients $k_0^{(A)}$ and $k_0^{(M)}$, there exists the following relation:

$$\kappa_0^{(A)} = \frac{4.37}{2} \kappa_0^{(M)} \frac{M}{r_0 A (1 + \zeta \cot \beta_0)}. \qquad (3.31)$$

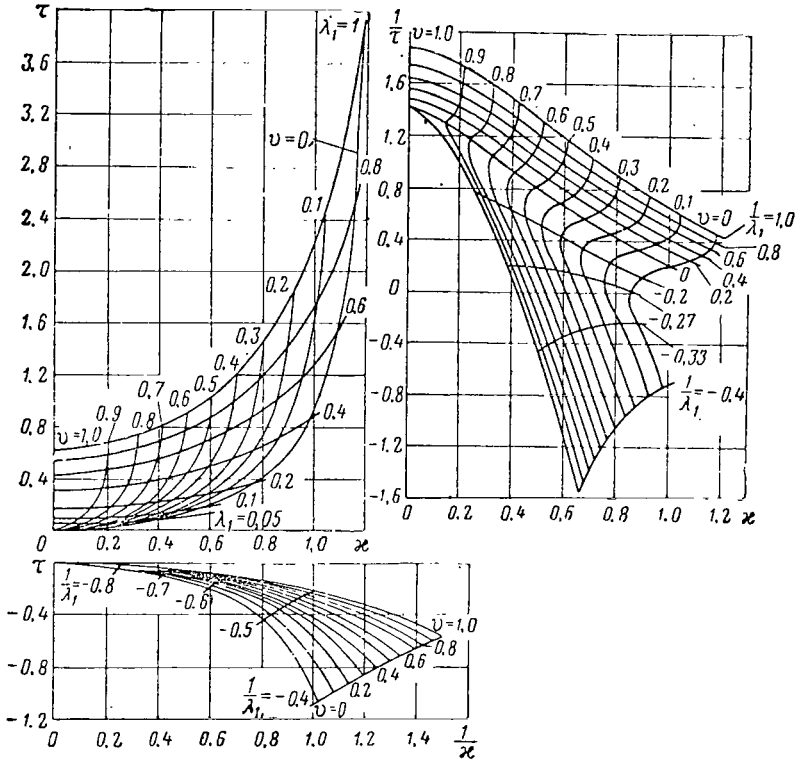

Fig.4.29 Nomograms for Approximate Calculations of Bearings Loaded by Axial and Radial Forces and Moments.

The solution of the system (3.25) can be represented in the form of graphs shown in Fig.4.29. From these graphs, knowing τ and v, it is easy to find the values of $\varkappa$ and λ_1, from which we calculate the product $\lambda_2 \cos\psi_{02}$ and then calculate the coefficients $k_{01}^{(A)}$, $k_1^{(A)}$, $k_{02}^{(A)}$, $k_2^{(A)}$, or $k_{01}^{(M)}$, $k_1^{(M)}$, $k_{02}^{(M)}$, $k_2^{(M)}$. After this, it is not particularly difficult to determine the pressures on the balls. /375

The graphs in Fig.4.29 are interesting in that neither the angle β nor ζ figures in them. Thus, we have arrived at a rather convenient approximate method of calculating radial-thrust ball bearings with large initial contact angles in the most common case of their loading. The preloading, as already demonstrated by a study of bearing assemblies loaded by a "pure" moment, mainly has an effect on the stiffness of the system but leaves the calculated values of the maximum and equivalent ball pressures practically unchanged. Thus, the presented approximate method of determining these quantities, based on the assumption that the preloading is equal to zero, can be used for solving a rather wide range of problems associated with the calculation of radial-thrust ball bearings with large initial contact angles installed in bearing assemblies with closely spaced supports and absorbing an arbitrary combined load. In simpler loading cases, when examining the critical distribution of forces between balls corresponding to small loads, it is relatively easy to allow for the preloading if necessary.

Let the assembly be loaded only by the moment and the axial force. In the absence of a radial load, as follows from eqs.(3.23), we have $j_{z1} - \nu^{3/2} j_{z2} \cos \psi_{o2} = 0$. Making use of this relation, we reduce the expressions for the coefficients $k^{(M)}$ and $k^{(A)}$ to the form

$$\left.\begin{aligned} \kappa_{01}^{(M)} &= \frac{1}{4.37 j_{21}}; \quad \kappa_{01}^{(A)} = \frac{\tau}{2 j_{21}}; \\ \kappa_{02}^{(M)} &= \frac{1}{4.37 j_{22}}; \quad \kappa_{02}^{(A)} = \frac{\tau}{2 j_{22}}; \\ \kappa_{1}^{(M)} &= \frac{w_1}{2.57 j_{21}}; \quad \kappa_{1}^{(A)} = \frac{\tau w_1}{2 j_{21}}; \\ \kappa_{2}^{(M)} &= \frac{w_2}{2.57 j_{22}}; \quad \kappa_{2}^{(A)} = \frac{\tau w_2}{2 j_{22}}. \end{aligned}\right\} \qquad (3.32)$$

Equations (3.32) are valid also in the presence of preloading.

The coefficients $k_{01}^{(M)}$, $k_{02}^{(M)}$, $k_1^{(M)}$, and $k_2^{(M)}$ determined from eqs.(3.32) for zero preloading can be found from the graphs in Figs.4.30 and 4.31. Since, at small values of the ratio $\frac{1}{\tau}$, the coefficients $k_0^{(M)}$ and $k^{(M)}$ for the bearing 2 are substantially greater than for the bearing 1, the question naturally arises whether we can equate their values by proper selection of the preloading. Without dwelling on the transformations related with the solution of this problem, since they are sufficiently obvious from the foregoing, we will directly give the the final solution. Figure 4.33 presents curves giving the values of the ratio $\frac{\bar{\Delta}_{pr} \sin \beta_o}{\bar{\delta}_{o1}}$ at which identity of the static and dynamic loads of the bearings 1 and 2, i.e., equality of the coefficients $k_{01}^{(M)}$ and $k_{02}^{(M)}$ or $k_1^{(M)}$ and $k_2^{(M)}$, can be theoretically secured. The values of these adjusted coefficients are shown in Figs.4.30 and 4.31 as broken lines.

For assemblies which should have high rigidity, it is desirable that all balls in both bearings be loaded. This problem is also easily solved by proper choice of the preloading. Since, under the combined action of moment and axial force, the loading zone in the bearing 1 is always greater than in the bearing 2, the condition of complete loading of the balls of both bearings is the inequality $\lambda_2 \geq 1$. The values of the coefficient $k_{01}^{(M)}$, $k_{02}^{(M)}$, $k_1^{(M)}$, and $k_2^{(M)}$ and the ratio $\frac{\bar{\Delta}_{pr} \sin \beta_o}{\bar{\delta}_{o1}}$, corresponding to the case $\lambda_2 = 1$, are also given in Figs.4.31 and 4.32. Figure 4.33 shows that, with a preloading which ensures loading of all balls of both bearings, the angular stiffness of the assembly increases by a factor of more than 2, which causes the maximum and equivalent pressures on the balls to increase by about 10 - 15%. /376

The limit dependences obtained for the case of small loads are rather convenient for practical calculations, since they substantially lessen the laboriousness of determining the pressures on the balls. It must only be remembered

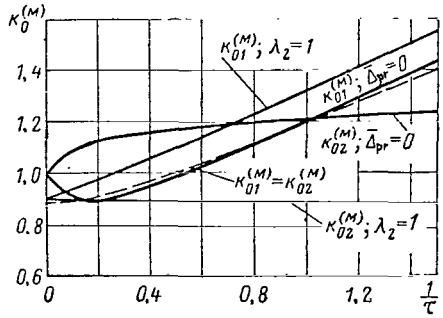

Fig.4.30 Values of the Coefficient $k_0^{(M)} = k_0^{(M)}\left(\frac{1}{\tau}\right)$ for the Case of Simultaneous Action of Moment and Axial Force.

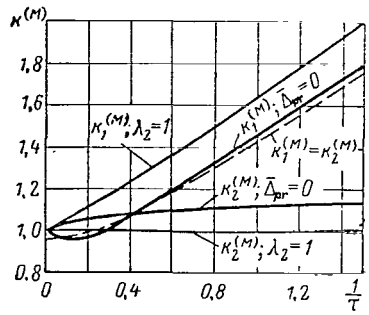

Fig.4.31 Values of the Coefficient $k^{(M)} = k^{(M)}\left(\frac{1}{\tau}\right)$ for the Case of Simultaneous Action of Moment and Axial Force.

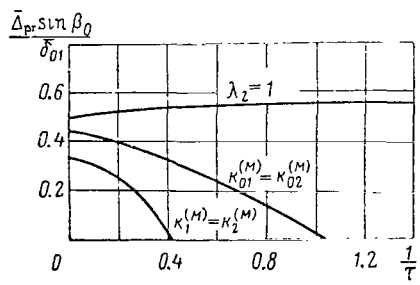

Fig.4.32 Values of Preloading for Ensuring the Conditions $k_1^{(M)} = k_2^{(M)}$, $k_{01}^{(M)} = k_{02}^{(M)}$ and $\lambda_2 = 1$.

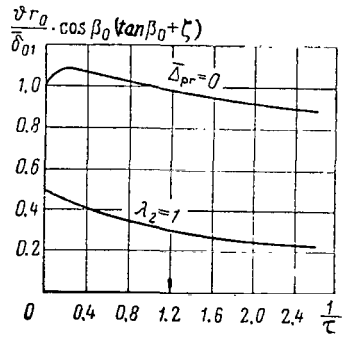

Fig.4.33 Effect of Preloading (Condition $\lambda_2 = 1$) on Angular Stiffness of the Assembly.

that the use of these limit dependences leads to a certain overestimation of the rated ball pressures. For contact stresses of the order of 20,000 kg/cm^2, /377 this amounts to 15 - 25% for the angle $\beta_0 = 26^\circ$ and to 2 - 17% for the angle $\beta_0 = 60^\circ$. Allowing for this fact in calculating the rated loads of a given bearing assembly with the use of the above critical dependences, the values of the safety factor can be reduced considerably.

On the basis of the dependences presented above, we can determine the pressures on the balls of eccentrically loaded double-row thrust ball bearings. Here we must remember that for an initial contact angle of $\beta_0 = 90^\circ$ at $\bar{\Delta}_{pr} = 0$, eqs.(3.32) yield the "exact" values of the coefficients entering eqs.(3.28) and (3.29). We note that in this case the quantity τ represents the relative eccentricity $\frac{e}{r_0}$ (Fig.4.34).

If a single-row thrust ball bearing takes an eccentrically applied axial force, then

$$\left.\begin{aligned} P_0 &= \kappa_0^{(A)} \cdot \frac{A}{z}; \\ P_{eq} &= \kappa^{(A)} \frac{A}{z}, \\ \kappa_0^{(A)} &= \frac{1}{j_1}, \quad \kappa^{(A)} = \frac{w}{j_1}. \end{aligned}\right\} \qquad (3.33)$$

where

The values of the coefficients $k_0^{(A)}$ and $k^{(A)}$ are found from the curves plotted in Fig.4.35. These curves are obtained from the values of λ corresponding to the equation $\frac{j_2}{j_1} = \tau$ which, in turn, is obtained directly from the conditions of static equilibrium

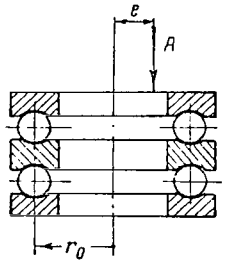

Fig.4.34 Double-Row Thrust Ball Bearing Loaded by Axial Force and Moment (Eccentrically Applied Axial Force).

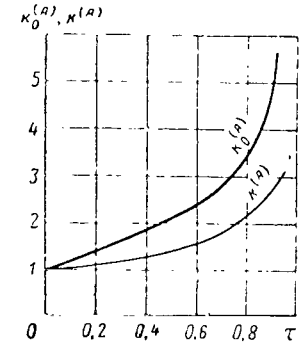

Fig.4.35 Values of the Coefficient $k_0^{(A)}$ and $k^{(A)}$ as a Function of τ.

5. Distribution of Load between Rows of Balls of Double-Row Radial-Thrust Ball Bearings

Radial-thrust ball bearings with initial contact angles of 26 and 36°, having a small preloading, are widely used in helicopter components designed for taking simultaneously acting radial and axial loads (Fig.4.36).

We will attempt to establish the manner in which the load is distributed over the rows of balls of such bearings, working under conditions precluding the possibility of a noticeable misalignment of their races.

Keeping in mind that a small preloading has little effect on the ball pressures, we will use the limit dependences given in the preceding Subsection /378

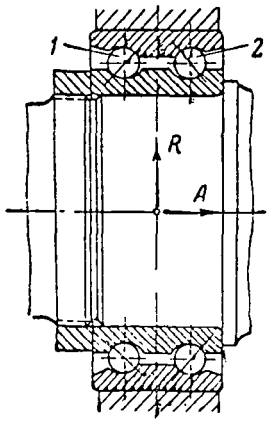

Fig.4.36 Double-Row Radial-Thrust Ball Bearing Loaded by Radial and Axial Forces.

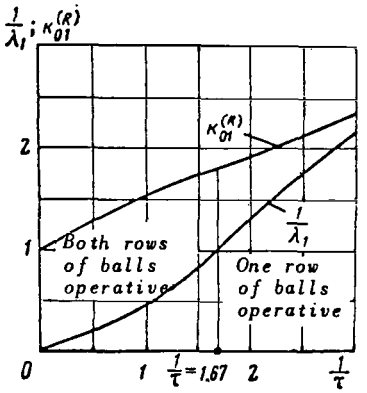

Fig.4.37 Values of λ_1 and of the Coefficients $k_{01}^{(R)}$ as a Function of $\frac{1}{\tau}$.

for an approximate solution of the problem.

Setting $\bar{\epsilon} = 0$ and $\bar{\Delta}_{pr} = 0$ in the equalities (3.4) and (3.7) and recalling that $\bar{\delta}_1 = \frac{\bar{\delta}_{01}}{1+\lambda_1}$ and $\bar{\delta}_2 = \frac{\bar{\delta}_{02}}{1+\lambda_2 \cos\psi_{02}}$, we find $\lambda_2 = \lambda_1$. The index "1" is given to the row of balls toward which the axial force is directed. Since, if the bearing is loaded by radial and axial forces, the angle will be $\psi_{02} = 180^\circ$ and thus $\cos\psi_{02} = -1$, so that eqs.(3.23) will yield, for the case under study,

$$\varkappa = \frac{\lambda_1 - 1}{\lambda_1 + 1}; \tag{3.34}$$

$$\left.\begin{aligned} A &= zP_{01}\sin\beta_0\left[j_{11} - \left(\frac{\lambda_1-1}{\lambda_1+1}\right)^{3/2} j_{12}\right]; \\ R &= zP_{01}\cos\beta_0\left[j_{21} + \left(\frac{\lambda_1-1}{\lambda_1+1}\right)^{3/2} j_{22}\right]. \end{aligned}\right\} \tag{3.35}$$

The dependences determining the pressures P_{01} and P_{02} for double-row radial-thrust ball bearings can be written in the following manner:

$$\left.\begin{aligned} P_{01} &= \frac{4{,}37}{z\cos\beta_0}\,\frac{\kappa_{01}^{(R)} R}{2}; \\ P_{02} &= \left(\frac{\lambda_1-1}{\lambda_1+1}\right)^{3/2} P_{01}, \end{aligned}\right\} \tag{3.36}$$

where

$$\kappa_{01}^{(R)} = \frac{2}{4.37\left[j_{21} + \left(\frac{\lambda_1-1}{\lambda_1+1}\right)^{3/2} j_{22}\right]}.$$

The equivalent pressures for both rows of balls are, respectively, equal /379 to

$$\left.\begin{aligned} P_{eq1} &= w_1 P_{01}, \\ P_{eq2} &= w_2 P_{02}. \end{aligned}\right\} \qquad (3.37)$$

The values of the parameter λ_1 and of the coefficient $k_{01}^{(R)}$ as a function of the quantity $\frac{l}{\tau} = \frac{A}{R} \cot \beta_0$ can be found from the graphs in Fig.4.37.

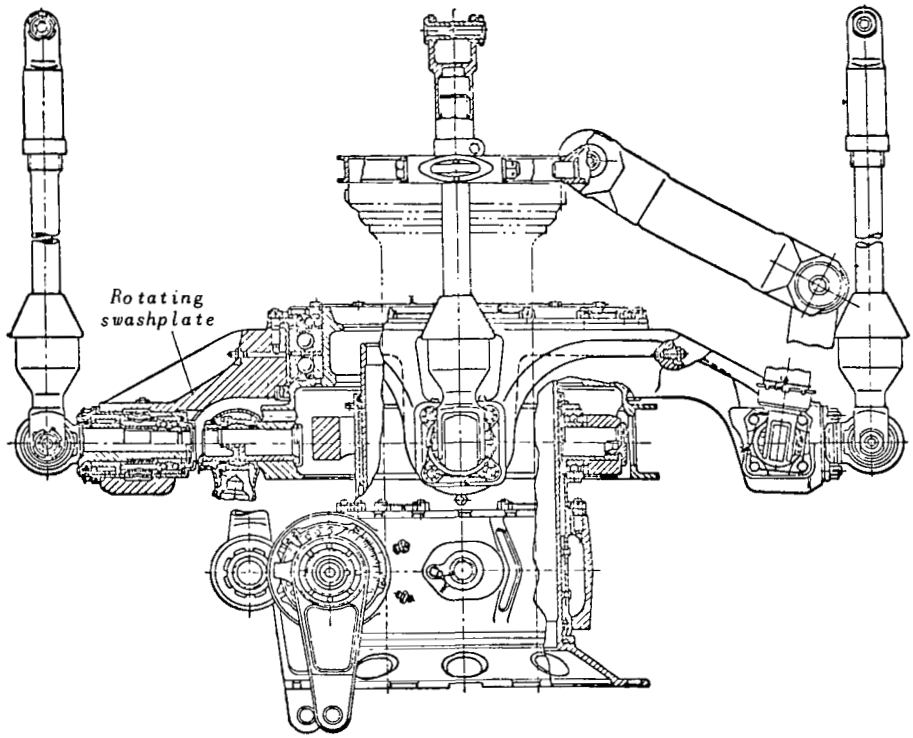

Fig.4.38 Pitch Control of Helicopter Rotor.

As shown by calculations, the first row is always more loaded. For $\frac{l}{\tau} \geq$ $\geq$ 1.67 at $\lambda_1 \leq 1$, this row carries the entire load applied to the bearing. We note that, for $\tau = 0.6$, the ratio $\frac{A}{R} = 1.67 \tan \beta_0$.

In the presence of predominantly axial loads, when one row of balls is operative, more accurate results are obtained by using the dependences in Section 2 for calculating double-row radial-thrust ball bearings of all types, including those examined in this Subsection.

6. Examples of Calculation

Example 1. Let us determine the rated life of the bearings of the swash-plate of the pitch control (Fig.4.38) loaded by the moments M = 150 kg·m and rotating at 240 rpm. The bearings have the following parameters: $\beta_0 = 36^\circ$, $d_{ba} = 9.525$ mm, $z = 42$, $r_0 = 79$ mm.

Relative base $\zeta = 0.1$, preloading $\Delta_{pr} = 0$. /380

Since the bearing has zero preloading, the coefficients $k_0^{(M)}$ and $k^{(M)}$ needed for calculating the loads on the balls are determined by means of Fig.4.21.

We then calculate the quantities

$$\varrho = \left| \frac{1 - \zeta \tan\beta_0}{\tan\beta_0 + \zeta} \right| = \left| \frac{1 - 0.1 \times 0.726}{0.726 + 0.1} \right| = 1.12;$$

$$\overline{M} = \frac{1}{z\nu d_{ba}^2 \sin\beta_0 (1 + \zeta \cot\beta_0)} \cdot \frac{M}{r_0} =$$

$$= \frac{1}{42 \times 1 \times 9.525^2 \times 0.588 (1 + 0.1 \times 1.376)} \cdot \frac{150}{0.079} = 0.744.$$

Since $\frac{r_{in\,(out)}}{d_{ba}} = 0.515$, the coefficient ν is taken as equal to unity.

According to Fig.4.21, the value $k_0^{(M)} = 0.912$ corresponds to the obtained values of ϱ and $\overline{M}$.

Thus, the maximum pressures on the balls in both bearings will be

$$P_{01} = P_{02} = \frac{4.37 \kappa_0^{(M)} M}{2 r_0 z \sin\beta_0 (1 + \zeta \cot\beta_0)} =$$

$$= \frac{4.37 \times 0.912 \times 150}{2 \times 0.079 \times 42 \times 0.588 (1 + 0.1 \times 1.376)} = 134.7 \text{ kg.}$$

In the examined case, $\lambda_1 = \lambda_2 = \infty$. Consequently,

$$P_{eq1} = P_{eq2} = w_{\lambda=\infty} P_{01} = 0.587 \times 134.7 = 79.1 \text{ kg.}$$

The equivalent pressure $P_{eq\,1,2}$, determining the life expectancy of the assembly, can be found from eq.(2.44). Taking into consideration that, at $\lambda_1 = \lambda_2 = \infty$, $k_{k1} = k_{k2} = 1.2$ (see Fig.4.5), this equation will yield

$$P_{eq\,2} = 2^{\frac{1}{3.33\iota}} \kappa_{k1} P_{eq\,1} = 1.21 \times 1.2 \times 79.1 = 114.8 \text{ kg.}$$

Here, we assume that $\iota = \frac{10}{9}$.

For bearings with the indicated dimensions, according to eq.(2.42) the coefficient of utilization will be

$$C = 65 \times z^{0.7} \times \frac{d_{ba}^2}{1 + 0.02 d_{ba}} = 65 \times 42^{0.7} \times \frac{9.525^2}{1 + 0.02 \times 9.525} = 67\,794.$$

As a result of stand tests, for bearings of the pitch control cam plate the product of the coefficients $k_b k_t k_M = 1.1$.

In conformity with this, eq.(2.43), considering that $h = h_{10}$, will furnish

$$(nh)^{0.3} = \frac{C}{0.39 \times \kappa_b \kappa_t \kappa_M z P_{eq\text{-}A} \cos \beta_0} = \frac{67{,}794}{0.39 \times 1.1 \times 42 \times 114.8 \times 0.809} = 40.5.$$

Hence,

$$nh = 228\,370 \text{ and } h = \frac{228{,}370}{240} \approx 950 \text{ hrs}.$$

Example 2. Let us calculate the maximum and equivalent pressures on balls in bearings examined in example 1 when they absorb a moment of M = 60 kg·m and an axial force of A = 500 kgf.

Since the relative base ζ is small, Figs.4.26 - 4.28 will be used for determining the indicated pressures. /381

From the quantities

$$\frac{M}{r_0 z \nu d_{ba}^2} = \frac{60}{0.079 \times 42 \times 1 \times 9.525^2} = 0.1993 \text{ kg/mm}^2$$

and from

$$\frac{A}{z \nu d_{ba}^2} = \frac{500}{42 \times 1 \times 9.525^2} = 0.1312 \text{ kg/mm}^2$$

by means of Fig.4.26 we find $\bar{\delta}_{01} = 0.055$ and $\lambda_1 = 0.7$.

Furthermore, let us calculate P_{01} and P_{eq1}. Since $\lambda_1 = 0.7$ corresponds to the value w = 0.678, then according to eqs.(2.2) and (2.6) we have

$$P_{01} = B_0 \nu d_{ba}^2 \bar{\delta}_0^{3/2} = 62 \times 1 \times 9.525^2 \times 0.055^{3/2} = 72.5 \text{ kg};$$
$$P_{eq1} = w P_{01} = 49.2 \text{ kg}.$$

From the graphs in Figs.4.27 and 4.28 we find the values of P_{eq2}/P_{eq1} and P_{02}/P_{01}. Using these values, we obtain

$$P_{02} = 1.085 P_{01} = 78.7 \text{ kg};$$
$$P_{eq2} = 0.875 P_{eq1} = 43 \text{ kg}.$$

Section 4. Calculation of Tapered Roller Bearings under Combined Loads

1. Calculation of Single-Row Tapered Roller Bearings

Methods were presented above for calculating radial and radial-thrust ball bearings absorbing combined loads. Let us now examine the peculiarities of calculating tapered roller bearings working under conditions of a complex load.

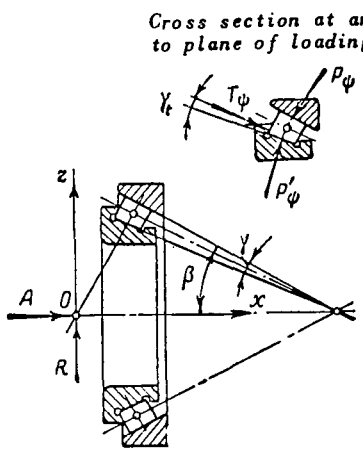

Fig.4.39 Diagram of Loading of Tapered Roller Bearing by Radial and Axial Forces.

First, let us give the solution of the problem of determining the forces acting on the rollers of a single-row tapered roller bearing at given values of the radial and axial loads applied to it (Fig.4.39).

The normal forces P_ψ and P'_ψ exerted on the roller by the outer and inner races are correlated by the relation

$$P'_\psi = \frac{\cos(\gamma - \gamma_t)}{\cos\gamma_t} P_\psi. \qquad (4.1)$$

For the usual values of the angles γ and γ_t, we can consider for all practical purposes that

$$P'_\psi = P_\psi. \qquad (4.2)$$

In conformity with the Hertz theory, it is possible to set, for the case of linear contact and with sufficient accuracy,

$$P_\psi = B\delta_\psi, \qquad (4.3)$$

where δ_ψ is the convergence of the races in the cross section located at an angle ψ to the loading plane.

/382

In the absence of misalignment of the races under load, the convergence δ_ψ is determined by the expression

$$\delta_\psi = s\sin\beta + u\cos\beta\cos\psi. \qquad (4.4)$$

Here,

u and s = radial and axial displacements of the inner race relative to the outer race, reckoned from the position at which the clearances in the bearing are selected;

β = angle of taper of the outer race.

Having put

$$\frac{u}{s}\cot\beta = \lambda, \qquad (4.5)$$

we obtain from eqs.(4.3) and (4.4)

$$P_\psi = B\, s \sin\beta (1+\lambda\cos\psi). \tag{4.6}$$

If the direction of the radial load coincides with the positive direction of the z-axis ($R > 0$), then the displacement will be $u > 0$. In this case, the center of the loading zone lies in the cross section $\psi = \psi_0 = 0$. If the radial load acts in the opposite direction ($R < 0$), then the displacement will be $u < 0$, in which case the center of the loading zone is situated in the cross section $\psi = \psi_0 = 180^\circ$.

According to eq.(4.6), the maximum value of the force P_ψ is equal to

$$P_0 = B\, s \sin\beta (1+\lambda\cos\psi_0). \tag{4.7}$$

Using the equality (4.7), we finally have

$$P_\psi = \frac{P_0}{1+\lambda\cos\psi_0}(1+\lambda\cos\psi). \tag{4.8}$$

As follows from the conditions of static equilibrium,

$$\left.\begin{aligned} R &= \frac{P_0}{1+\lambda\cos\psi_0}\cos\beta\sum(1+\lambda\cos\psi)\cos\psi; \\ A &= \frac{P_0}{1+\lambda\cos\psi_0}\sin\beta\sum(1+\lambda\cos\psi). \end{aligned}\right\} \tag{4.9}$$

For the usual number of rollers, eqs.(4.9) can be replaced by the relations

$$\left.\begin{aligned} R &= P_0 z\cos\beta j_2\cos\psi_0; \\ A &= P_0 z\sin\beta j_1. \end{aligned}\right\} \tag{4.10}$$

Here,

$$\left.\begin{aligned} j_1 &= \frac{1}{2\pi(1+\lambda\cos\psi_0)}\int_{\psi'_{lo}}^{\psi''_{lo}}(1+\lambda\cos\psi_0\cos\psi)\,d\psi = \\ &= \frac{1}{2\pi(1+\lambda\cos\psi_0)}\left[(\psi''_{lo}-\psi'_{lo})+2\lambda\cos\psi_0\sin\psi''_{lo}\right]; \\ j_2 &= \frac{1}{2\pi(1+\lambda\cos\psi_0)}\int_{\psi'_{lo}}^{\psi''_{lo}}(1+\lambda\cos\psi_0\cos\psi)\cos\psi\,d\psi = \\ &= \frac{1}{2\pi(1+\lambda\cos\psi_0)}\left\{2\sin\psi''_{lo}+\frac{\lambda\cos\psi_0}{2}\left[(\psi''_{lo}-\psi'_{lo})+\sin 2\psi''_{lo}\right]\right\}. \end{aligned}\right\} \tag{4.11}$$

The boundaries of the loading zone ψ''_{lo} and ψ'_{lo} are determined in the same manner as for the radial and radial-thrust ball bearings [see eq.(1.20) and the explanation to it]. /383

Equation (4.10) will yield, if for simplicity we set $R > 0$ and thus $\psi_0 = 0$,

$$P_0 = \frac{1}{j_2}\frac{R}{z\cos\beta}. \tag{4.12}$$

The equivalent pressure P_{eq} for a tapered roller bearing can be represented in the form

$$P_{eq} = wP_0, \tag{4.13}$$

where

$$w = \frac{1}{1+\lambda\cos\psi_0}\left[\frac{1}{2\pi}\int_{\psi'_{lo}}^{\psi''_{lo}}(1+\lambda\cos\psi_0\cos\psi)^{3.33}d\psi\right]^{0.3}.$$

The values of the quantities j_1, j_2, and w as a function of $\lambda\cos\psi_0$ are given in Table 4.7.

TABLE 4.7

$\lambda\cos\psi_0$	j_1	j_2	w	$\lambda\cos\psi_0$	j_1	j_2	w
0	1	0.5	1	2.000	0.405	0.268	0.698
0.1	0.909	0.454	0.913	2.500	0.389	0.267	0.692
0.2	0.833	0.417	0.853	3.333	0.371	0.264	0.686
0.3	0.769	0.385	0.806	5.000	0.354	0.261	0.679
0.4	0.714	0.357	0.773	10.000	0.336	0.256	0.670
0.5	0.667	0.333	0.751	$\pm\infty$	0.318	0.250	0.660
0.6	0.625	0.312	0.738	—10.000	0.300	0.242	0.648
0.7	0.588	0.294	0.729	—5.000	0.281	0.234	0.634
0.8	0.555	0.278	0.725	—3.333	0.261	0.222	0.617
0.9	0.526	0.263	0.722	—2.500	0.240	0.210	0.598
1.0	0.500	0.250	0.720	—2.000	0.218	0.196	0.575
1.111	0.479	0.258	0.718	—1.667	0.194	0.178	0.548
1.250	0.460	0.264	0.714	—1.428	0.167	0.156	0.518
1.428	0.440	0.266	0.708	—1.250	0.136	0.130	0.484
1.667	0.424	0.268	0.704	—1.000	0.000	0.000	0.000

Calculation for tapered roller bearings, just as for radial-thrust ball bearings, is usually carried out by means of reduced static and dynamic loads. These loads are found from the condition that

$$\left.\begin{aligned} P_0 &= \frac{1}{j_{2\lambda=\infty}} \frac{Q_0}{z\cos\beta} = 4\frac{Q_0}{z\cos\beta}; \\ P_{eq} &= \frac{w_{\lambda=\infty}}{j_{2\lambda=\infty}} \frac{Q}{z\cos\beta} = 2.64\frac{Q}{z\cos\beta}. \end{aligned}\right\} \qquad (4.14)$$

A comparison of the equalities (4.14) with eqs.(4.12) and (4.13) yields /384

$$\left.\begin{aligned} Q_0 &= \kappa_0^{(R)} R; \\ R &= \kappa^{(R)} R, \end{aligned}\right\} \qquad (4.15)$$

where

$$\left.\begin{aligned} \kappa_0^{(R)} &= \frac{j_{2\lambda=\infty}}{j_2} = \frac{0.25}{j_2}; \\ \kappa^{(R)} &= \frac{w}{w_{\lambda=\infty}} \kappa_0^{(R)} = \frac{0.38w}{j_2}. \end{aligned}\right\} \qquad (4.16)$$

In conformity with eqs.(4.10), the values of the parameter λ needed for determining the coefficients $k_0^{(R)}$ and $k^{(R)}$ should satisfy the condition

$$\frac{j_2}{j_1} = \frac{R}{A}\tan\beta = \tau. \qquad (4.17)$$

Since we have $\frac{j_1}{j_2} = 0.5$ at $\lambda = 1$, the value of τ should not exceed 0.5 for all rollers in a single-row tapered roller bearing to be loaded.

At $\tau \geq 0.5$, the values of the coefficients $k_0^{(R)}$ and $k^{(R)}$ can be determined from the graphs in Fig.4.40. These graphs were plotted on the basis of the equalities (4.16) and (4.17).

If $\tau \leq 0.5$ and thus $\lambda \leq 1$, the expressions for the integrals j_1 and j_2 take the form

$$\left.\begin{aligned} j_1 &= \frac{1}{1+\lambda}; \\ j_2 &= \frac{1}{2}\frac{\lambda}{1+\lambda}. \end{aligned}\right\} \qquad (4.18)$$

From eqs.(4.17) and (4.18), we find

$$\left.\begin{aligned} \lambda &= 2\tau; \\ \frac{1}{j_2} &= 2 + \frac{1}{\tau}. \end{aligned}\right\} \qquad (4.19)$$

Thus, for $\tau \leq 0.5$ when all rollers share the load, we have

$$\left.\begin{aligned} \kappa_0^{(R)} &= \frac{0.25}{j_2} = 0.5 + \frac{0.25}{\tau}; \\ \kappa^{(R)} &= \frac{w}{w_{\lambda=\infty}} \kappa_0^{(R)} = 0{,}76w + 0.38\,\frac{w}{\tau}. \end{aligned}\right\} \qquad (4.20)$$

As follows from the equality (4.20), for all loaded rollers,

$$Q_0 = 0.5R + 0.25A \cot \beta; \qquad (4.21)$$

$$Q = 0.76wR + 0.38wA \cot \beta. \qquad (4.22)$$

The values of w as a function of τ are conveniently determined from the curves shown in Fig.4.41.

These relations furnish an answer to all basic problems arising in calculating tapered roller bearings that take combined loads, provided the misalignment of their races can be neglected.

/385

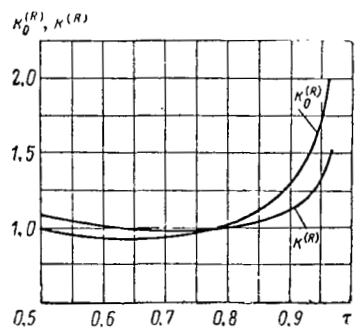

Fig.4.40 Values of the Coefficients $k_0^{(R)}$ and $k^{(R)}$ as a Function of τ.

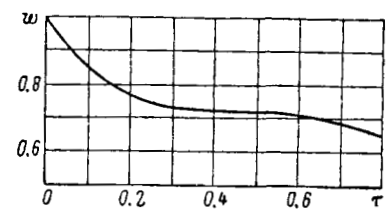

Fig.4.41 Values of w as a Function of τ.

As shown by Fig.4.40, in the region τ = 0.6 - 0.8 the curves of $k_0^{(R)} = k_0^{(R)}(\tau)$ and $k^{(R)} = k^{(R)}(\tau)$ have a rather well-defined minimum. This indicates that proper choice of the contact angle β, for a given combination of radial and axial loads, will ensure maximum and equivalent pressures on the rollers having a minimum value. The optimal contact angles at which the conditions $P_0 = P_0^{min}$ and $P_{eq} = P_{eq}^{min}$ are satisfied are determined from the graphs in Fig.4.42. These graphs were plotted on the basis of investigations of the relations $\frac{zP_0}{R} = F_0\left(\frac{A}{R}\right)$ and $\frac{zP_{eq}}{R} = F\left(\frac{A}{R}\right)$, for a number of contact angles in the range from 0 to 30°.

2. Remarks on Calculation of Bearing Assemblies of Two Tapered Roller Bearings

If a bearing assembly consisting of two tapered roller bearings is loaded by a moment acting in combination with radial and axial forces (Fig.4.43), the following system of equations can be used for its calculation:

$$\left.\begin{aligned} R &= zP_{01}\cos\beta\,(j_{21}-\varkappa j_{22}\cos\psi_{02});\\ A &= zP_{01}\sin\beta\,(j_{11}-\varkappa j_{12});\\ M &= r_0 zP_{01}\sin\beta\,(1+\zeta\cot\beta)\,(j_{21}+\varkappa j_{22}\cos\psi_{02});\\ \lambda_2\cos\psi_{02} &= -\left[1+\frac{\varkappa\,(1+\lambda_1)}{1-(1+\lambda_1)\dfrac{2\Delta_{pr}\sin\beta}{\delta_{01}}}\right], \end{aligned}\right\} \qquad (4.23)$$

which is analogous to the system of equations (3.23) and (3.24) describing the conditions of static equilibrium of bearing assemblies with two radial-thrust ball bearings, on the assumption that the contact angles of all balls are identical and equal to the initial angle.

It should be noted that eqs.(4.23) are "exact" since, in tapered roller bearings, the contact angles are actually constant and do not change under load; these equations are valid in both absence or presence of misalignment of the races.

In eqs.(4.23) the quantity $\varkappa$ is used in place of the quantity $\varkappa^{3/2}$. This is explained by the fact that, for tapered roller bearings, we have $\frac{P_{02}}{P_{01}} = \frac{\delta_{02}}{\delta_{01}} = \varkappa$.

In the case of zero preloading, the values of λ_1 and $\varkappa$ satisfying eqs.(4.23) are found from the graphs in Fig.4.44. The quantities τ and v here have the same meaning as for the radial-thrust ball bearings [see eqs.(3.26) and (3.27)]. /386

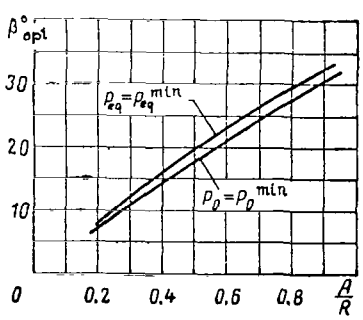

Fig.4.42 Values of the Optimal Contact Angle as a Function of the Ratio A/R.

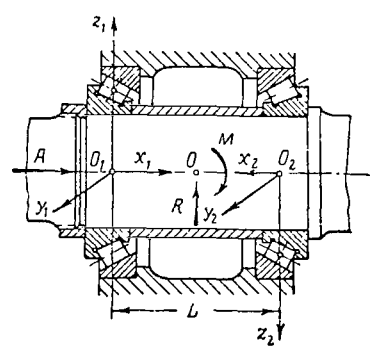

Fig.4.43 Diagram of Loading of Two Tapered Roller Bearings by Radial and Axial Forces and Moments.

From the found values of λ_1 and $\varkappa$, we then calculate the quantity $\lambda_2 \cos \psi_{02}$.

The maximum and equivalent pressures on the rollers in the bearings 1 and 2 are determined from the expressions

$$\left.\begin{aligned} P_{01} &= \frac{2\kappa_{01}^{(M)} M}{r_0 z \sin\beta (1+\zeta \cot\beta)} = \frac{\kappa_{01}^{(A)} A}{z \sin\beta}; \\ P_{02} &= \frac{2\kappa_{02}^{(M)} M}{r_0 z \sin\beta (1+\zeta \cot\beta)} = \frac{\kappa_{02}^{(A)} A}{z \sin\beta}; \\ P_{eq1} &= \frac{1.32\kappa_1^{(M)} M}{r_0 z \sin\beta (1+\zeta \cot\beta)} = \frac{\kappa_1^{(A)} A}{z \sin\beta}; \\ P_{eq2} &= \frac{1.32\kappa_2^{(M)} M}{r_0 z \sin\beta (1+\zeta \cot\beta)} = \frac{\kappa_2^{(A)} A}{z \sin\beta}. \end{aligned}\right\} \qquad (4.24)$$

Here,

$$\left.\begin{aligned} &\kappa_{01}^{(M)} = \frac{1}{2(j_{21} + \varkappa j_{22} \cos\psi_{02})}; \quad \kappa_{02}^{(M)} = \varkappa \kappa_{01}^{(M)}; \\ &\kappa_{01}^{(A)} = \frac{1}{j_{11} - \varkappa j_{12}}; \quad \kappa_{02}^{(A)} = \varkappa \kappa_{01}^{(A)}; \\ &\kappa_1^{(M)} = \frac{w_1}{0.66} \kappa_{01}^{(M)}; \quad \kappa_2^{(M)} = \frac{w_2}{0.66} \kappa_{02}^{(M)}; \\ &\kappa_1^{(A)} = w_1 \kappa_{01}^{(A)}; \quad \kappa_2^{(A)} = w_2 \kappa_{02}^{(A)}. \end{aligned}\right\} \qquad (4.25)$$

Setting $\beta = 90^\circ$ in the system (4.23), we arrive at the following equations describing the conditions of static equilibrium of double-row thrust roller bearings:

$$\left.\begin{aligned} A &= z P_{01} (j_{11} - \varkappa j_{12}); \\ M &= r_0 z P_{01} (j_{21} + \varkappa j_{22}). \end{aligned}\right\} \qquad (4.26)$$

The methods of solving eqs.(4.26) are obvious from the preceding; consequently, we need not further discuss these here.

If we assume $\varkappa = 0$ in eqs.(4.26) they will take the form /388

$$\left.\begin{aligned} A &= z P_0 j_1; \\ M &= r_0 z P_0 j_2. \end{aligned}\right\} \qquad (4.27)$$

Equations (4.27) characterize the load distribution in single-row thrust roller bearings.

The values of the maximum $P_0 = k_0^{(A)} \frac{A}{z}$ and the equivalent $P_{eq} = k^{(A)} \frac{A}{z}$

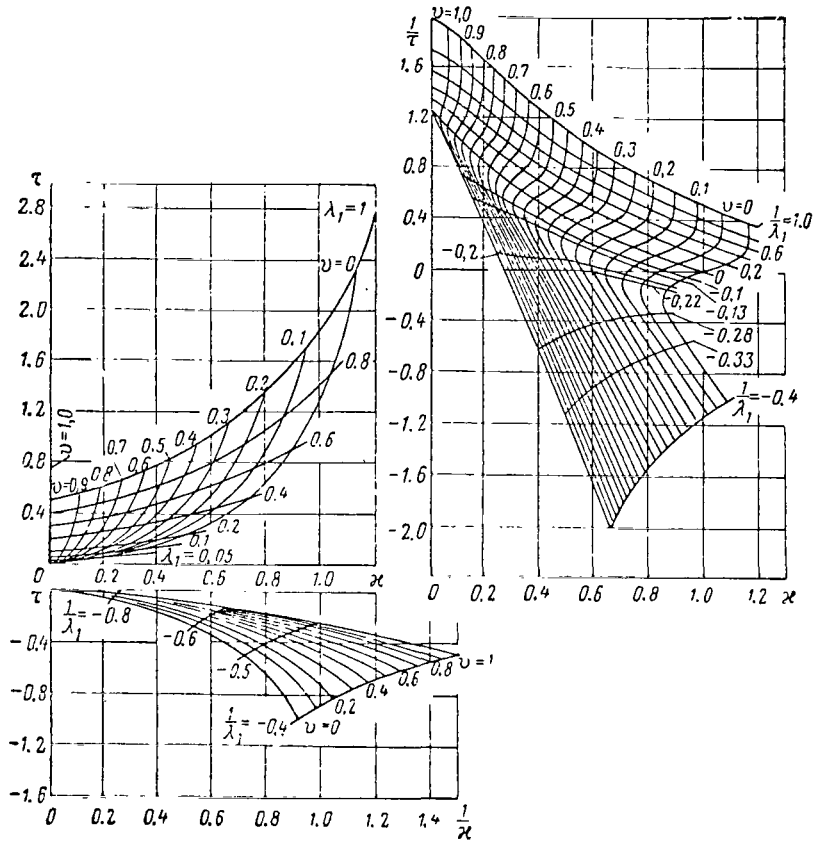

Fig.4.44 Nomograms for Calculating Bearings Loaded by Radial and Axial Forces and Moments.

pressures on the roller satisfying eqs.(4.27) are conveniently found by means of the curves $k_0^{(A)} = k_0^{(A)}(\tau)$ and $k^{(A)} = k^{(A)}(\tau)$ given in Fig.4.45.

At $\lambda \leq 1$, when all rollers are loaded in the bearing, the integrals j_1 and j_2 are determined from eqs.(4.18).

It is easy to demonstrate that in this case which takes place when $\tau = \frac{M}{r_0 A} \leq 0.5$, we have

$$\left.\begin{aligned} \lambda &= 2\tau; \\ \kappa_0^{(A)} &= \frac{1}{j_1} = 1 + \lambda = 1 + 2\tau. \end{aligned}\right\} \qquad (4.28)$$

Section 5. Calculation of Vibrating Bearings

In designing helicopters, the proper selection of bearings for the hubs of

the main and tail rotors presents appreciable difficulties. These bearings, as is known, operate under specific conditions of vibration. They do not fail because of contact fatigue but as a consequence of local wear of the race tracks, which has come to be known as "false brinelling". It is understandable that the usual calculation methods for such bearings are inapplicable.

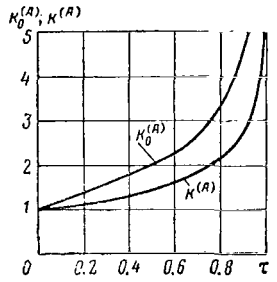

Fig.4.45 Values of the Coefficients $k_0^{(A)}$ and $k^{(A)}$ as a Function of τ.

The properties of the lubricant have a substantial effect on the performance of vibrating bearings. Practice has shown that reliable operation of many Soviet bearing assemblies for helicopters is possible only when using special oils and lubricants. Therefore, in helicopter engineering special attention must be paid to problems of selecting the lubricants for antifriction bearings. This primarily pertains to bearings for the axial (feathering) hinges of the hubs of the main and tail rotors, which absorb appreciable axial loads generated by the centrifugal forces of the blades.

The complexity of calculating the bearings of hubs of the main and tail rotors lies in the fact that the relatively low rigidity of their basic components, especially on heavy helicopters, may lead to noticeable deformation of the races, which is difficult to take into account when determining the forces acting on the rolling bodies. So far it has been impossible to develop general calculation methods that would allow for the effect of all factors determining the load capacity of bearings in the hubs of the main and tail rotors. However, available experimental data permit certain recommendations as to the selection of permissible loads and determination of the life expectancy of the most common types of bearings used in these complex and vital units. This is the same for calculations of the bearings in the hinges of the pitch control and control mechanisms of helicopters which, just as the hub bearings, operate /389 under vibrations. Here, it is merely necessary to take into account that the loads absorbed by most of these bearings have a dynamic character.

1. Characteristics of the Mechanism of Wear of Antifriction Bearings under Vibration Conditions

Let us examine the characteristics of the mechanism of wear of antifriction bearings in the presence of vibrations.

At small vibration amplitudes, when contact of the rolling body with the races takes place only at some spots on the tracks, dents from the balls or grooves from the rollers will form in the bearing which, as their surfaces chip, change to deep pitting (Fig.4.46). Failure of the rolling bodies in most cases begins only after appreciable damage to the races.

An analysis of test results shows that, in the presence of vibration, the wear of bearings is largely determined by oxidation processes and special lubrication conditions in the zones of contact of the rolling bodies with the races.

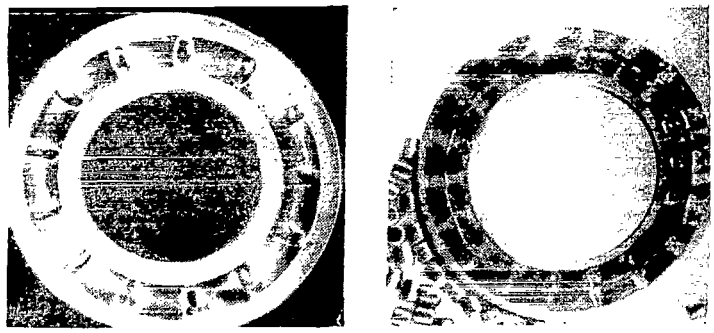

Fig.4.46 Races of Thrust Ball and Roller Bearings after Extended Service in the Presence of Vibrations of Small Amplitude.

In the contact zones there is intense fretting corrosion. The oxidation products of iron formed in this case mix with the lubricant and produce a unique polishing compound which causes rapid wear of the tracks. The rolling motion of the rolling bodies creates lubrication "barriers" ahead of the contact area, while jets of lubricant aft of this area tend to fill the space behind the moving body (Fig.4.47). If the lubricant is too stiff and does not have time to fill this space immediately, the portion of the track directly adjacent to the contact area is coated only by a thin film of lubricant. Naturally, at the instant of change in direction, the rolling body will pass this poorly lubricated portion sooner than the lubricant will be able to reach it. This causes the appearance of pressure peaks leading to acceleration of wear at the periphery of the contact area between rolling elements and races, where the change in direction takes place. At very low vibration amplitudes, when the contact areas in the extreme position of the rolling body overlap, disturbance of the lubricant layer may be constant. In this case, the pressure peaks increase even more and the life expectancy of the bearings decreases noticeably. An increase in mobility of the lubricant will improve the service conditions of vibrating bearings. Nevertheless, even when using highly fluid oils, the service conditions of such bearings substantially differ from those of bearings rotating in a single direction. /390

It is obvious from the aforesaid that, in bearing assemblies operating in the presence of vibration, oils rather than grease should be used in all cases where this is possible relative to design considerations. When grease is used, the load capacity of vibrating bearings drops steeply.

2. Lubrication of Highly Loaded Vibrating Bearings in the Presence of Small Vibration Amplitudes

Since the properties of the lubricant have a considerable effect on the life expectancy of vibrating bearings, one can discuss the permissible loads for such bearings only in conjunction with the lubricants used.

Helicopter bearings subject to vibrations can be divided into two basic groups:

1) Bearings in the hubs of the main and tail rotors, pitch controls, and certain control elements operating at vibration amplitudes up to 10°. For these bearings, the total number of vibrations between two major overhauls, during which they are replaced, usually amounts to less than 10 million.
2) Bearings of the control mechanisms which execute a limited number of vibrations (up to 100,000) with amplitudes of more than 20°. We stipulate that no overlap of adjacent contact areas exists in this case.

Practice has shown that bearings of the second group will operate satisfactorily on high-quality greases. This is due to the fact that appreciable grooving by the rolling bodies can be permitted on the tracks of such bearings, since their performance is usually limited to the magnitude of the permissible moment of friction.

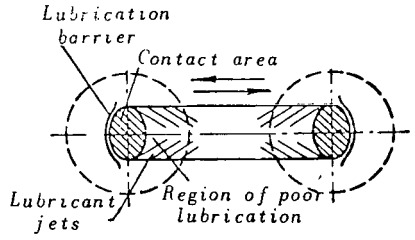

Fig.4.47 Diagram of Lubrication in the Presence of Vibration.

In bearings of the pitch control and control elements belonging to the first group, the use of grease results in a noticeable drop in load-carrying capacity; however, because of design considerations this is an unavoidable evil and the insufficient lubricating quality of the grease must be compensated by some reduction of the permissible loads. Since the permissible wear of the tracks of the hub bearings of the main and tail rotors is not great, prolonged operation at high contact stresses is possible only if oils with a certain complex of physicochemical properties are used.

The life expectancy of vibrating bearings depends largely on the quality of the seal of the bearing units. In the presence of faulty seals that permit penetration of atmospheric oxygen into the assemblies and also at small lubricant volume and large air volume, the life expectancy of vibrating bearings decreases noticeably. A rather effective means for increasing the service life of bearings subject to vibrations is pressure feed of the lubricant and, especially, use of oil circulation which continuously supplies fresh unoxidized oil /391 to the contact zones and carries off products of wear.

Let us discuss in greater detail the problems of selecting oils for the hubs of the main and tail rotors, since these problems are vital for helicopter engineering.

Oils for the feathering hinges of the main and tail rotor hubs. As shown in numerous experiments, the bearings of the feathering hinges, which absorb rather large axial loads due to the centrifugal forces of the blades, are especially sensitive to the physicochemical properties of the lubricant. The oils for such assemblies, whose service life usually determines the overall lifetime of the main and tail rotor hubs, should meet the following basic requirements:

First, the oils should not cause a step-up in the oxidative processes taking place in the contact zones.
Second, the oils should retain high fluidity in the entire operating temperature range and should provide sufficient oil-film strength over the whole of the contact area.

The permissible viscosity level of the oil is limited also by the permissible magnitude of the friction moment of the feathering hinge. Based on our experience with operating the Mi-1 and Mi-4 helicopters, we can stipulate that - at minimum operating temperature - the kinematic viscosity should not exceed 90,000 centistokes. Tests show that, in this case, there is no noticeable increase in the moment of friction and no decrease in service life of the bearings due to decreased fluidity of the oil. It should be noted that MS-14 oil which works satisfactorily in the feathering hinges of the main rotor hubs of the Mi-1 and Mi-4 helicopters at temperatures as low as -25°C, reaches the indicated kinematic viscosity at a temperature of -20°C.

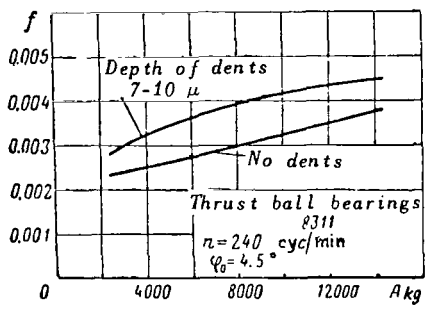

Fig.4.48 Friction Coefficient of Thrust Ball Bearings as a Function of Brinelling Mark Depth in Races.

By virtue of the specific operating conditions of vibrating bearings, selection of the oils and greases for these units should be based exclusively on test results during vibration. The standard procedure of testing oils and greases on a four-ball tester is completely unsuitable here. The lubricating quality of oils and greases for feathering hinges of main and tail rotor hubs is preferably checked in thrust ball bearings, since they operate at higher contact stresses. Experiments show that lubricating materials with optimum performance in such bearings are also best for vibrating bearings of other types, including thrust bearings with "slewed" rollers which are presently used with success in the main rotor hubs of all series-produced Soviet helicopters, and also for multi-row radial-thrust ball bearings used in the main and tail rotor hubs of a number of helicopters in other countries. Since the load in thrust ball bearings is distributed uniformly over the balls, each contacting region of the track during vibration can be regarded as an independent test object.

An essential factor in testing oils and greases for bearings of feathering hinges of main and tail rotor hubs is a proper evaluation of the condition of the tracks. Even at very moderate contact stresses, brinelling marks made by the balls appear on the track after brief operating periods. If the appearance of such dents, regardless of their depth, is considered as a sign of incipient failure of the bearing, then bearings which otherwise might still operate reliably for a long time must be rejected. The curves in Fig.4.48 indicate the manner in which the depth of the dent affects the friction coefficient of a thrust ball bearing. At a brinelling depth of 7 - 10 μ, the friction coefficient increases by 30 - 40%. An increase in friction coefficient within such limits is usually not perceptible in service. Therefore, the condition of thrust ball bearings at a depth of the dent up to 10 μ should be rated as "satisfactory". /392

Such a brinelling depth can be permitted also in radial-thrust ball bearings.

Tests have established that the MS-20 oil is one of the best for vibrating bearings. In conformity with this, this oil can be adopted as a standard for estimating the lubricating properties of oils and greases intended for service in the feathering hinges of main and tail rotor hubs. The results of testing thrust ball bearings running on MS-20 oil are given in Fig.4.49 as a curve of the life expectancy $\sigma = \sigma(nh)$ establishing the relation between the contact stress σ and the product nh of the number of vibrations per minute and duration of operation in hours. The tests were carried out at a vibration amplitude of the revolving race of $\varphi_0 = 4.5^\circ$, frequency of n = 240 cycle/min, and oil-bath temperature of 20 - 40°C.

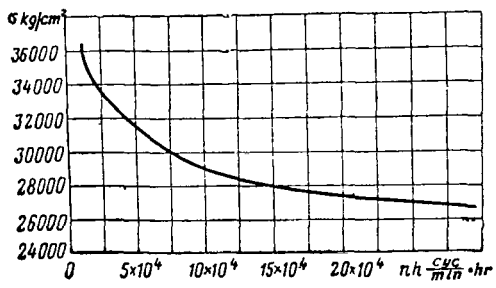

Fig.4.49 Curve of Life Expectancy $\sigma = \sigma(nh)$ for Thrust Ball Bearings.

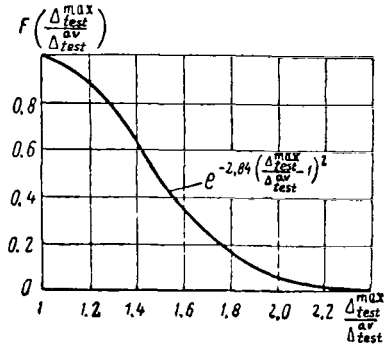

Fig.4.50 Curve of Distribution of the Ratio $\frac{\Delta_{test}^{max}}{\Delta_{test}^{av}}$.

For the values of the contact stresses determined by the curve of life expectancy plotted in Fig.4.49, 98% of the brinelling marks on the tracks have a depth not exceeding 10 μ.

It should be noted that a definite statistical relation exists between the maximum Δ_t^{max} and average Δ_t^{av} depth of the dents. This relation is established by the experimental curve of the distribution $F\left(\frac{\Delta_t^{max}}{\Delta_{test}^{av}}\right)$ of the ratio $\frac{\Delta_t^{max}}{\Delta_{test}^{av}}$, which, as is seen in Fig.4.50, is close to the Maxwellian distribution often encountered in engineering.

An analysis of the life expectancy curve in Fig.4.49 permits proposing /393 the following regime of accelerated selection tests of oils and greases for the feathering hinges of the main rotor hubs: duration 100 hrs, number of vibrations 240/min, vibration amplitude 4.5°, contact stresses 34,000 kg/cm². This regime permits comparing the lubricating properties of the tested oil with those of the MS-20 oil.

One must remember that, with an increase in testing time, the role played by oxidative processes in the contact zones increases in importance. Neverthe-

less, preselection tests of oils and greases for feathering hinge bearings can be carried out by the above accelerated program, since accelerated tests frequently permit the immediate rejection of many samples.

Under conditions of vibrations, the MS-20 oil possesses excellent lubricity. However, it can be used only in summer. During the winter, the MS-20 oil is usually replaced by MS-14 oil whose lubricating properties are also completely satisfactory. Since the MS-14 oil solidifies at a temperature of -30°C, it cannot be used at lower temperatures, which greatly interferes with wintertime operation of helicopters. Replacement of the MS-14 oil by general-purpose oils with low pour points does not yield favorable results. Tests have shown that the feathering hinges of main rotor hubs fail rapidly when operating on ordinary low-congealing oils, just as when operating on greases. This problem must be discussed in some detail, since the regularity of this result has long been disputed by certain specialists in the field of lubricants, which has handicapped solution of the problem of lubricating the feathering hinges of main rotor hubs at low temperatures.

Experiments have established that oils used for the feathering hinges of main and tail rotor hubs, at a temperature of 100°C, should have a kinematic viscosity of not less than 9 - 10 cst. Increased wear of tracks as well as chipping and destruction of the rolling bodies are observed when working with low-viscosity oils.

Low pour point oils of high viscosity in the positive temperature range generally consist of a low-viscosity mineral or synthetic base and a high-polymer thickening agent. In most cases, the thickeners and the base itself have low lubricating properties. Therefore, special antiwear additives containing sulfur, chlorine, phosphorus, or certain combinations of these chemically active elements are added to such oils. In zones of high contact temperatures, the additives react with the surface of the metal, forming films of sulfides, chlorides, and phosphides of iron which prevent a direct contact of the rubbing bodies and thus reduce wear.

According to data obtained with the standard four-ball test device, the lubricating properties of low pour point thickened oils with antiwear additives by far exceed the lubrication properties of the MS-20 and MS-14 oils. Nevertheless, they are completely unsuitable for working under vibration conditions. This is due to the fact that, under the effect of antiwear additives, oxidative processes are stepped up in the contact zones; these play a decisive role in the mechanism of wear of vibrating bearings. Here one must also consider that most high-polymer compounds used in oils of low pour point readily decompose under mechanical action, with the formation of polymers of lower molecular weight. Decomposition of the thickening agent leads to a decrease in viscosity of the oil. In bearing assemblies working in the presence of vibrations, the average decomposition of the oil usually is negligible. However, since only small /394
volumes of oil directly adjacent to the rolling bodies are subject to the mechanical action, local decomposition with a consequent drop in viscosity in the contact zones may reach appreciable magnitudes and lead to noticeable loss of strength of the oil film.

Contradictory results are often obtained when testing oils with antiwear

additives. This shows that testing of such oils should be carried out on a sufficiently large number of samples and that their lubricating properties cannot be judged by solitary favorable results.

It follows from the aforesaid that the oils for feathering hinges of main and tail rotor hubs should contain no antiwear additives or degrading thickeners. This explains the unsatisfactory service of such assemblies with any of the conventional low pour point oils, in whose development the above facts were not taken into account.

Guided by the above data on the performance of lubricating materials under conditions of vibration, the All-Union Research Institute for Petroleum and Gas Conversion and Production of Synthetic Liquid Fuel (VNII NP) has proposed the low pour point oil VNII NP-25 for the feathering hinge of main and tail rotor hubs (Ref.28).

The oil VNII NP-25 contains a low-viscosity petroleum fraction with a pour point of -67°C and a high-viscosity thickener distinguished by extremely high mechanical and thermal stability. Under the effect of high temperatures of friction, the petroleum fraction in the contact zones may evaporate; however, contact of the rolling bodies with the races cannot take place because of the presence of a film of the thickener which has relatively high adhesive properties. The high thermal and mechanical stability of the thickener and the oxidation inhibitor only negligibly changes the properties of the oil VNII NP-25 during service.

The basic properties of the oil VNII NP-25 are given in Table 4.8.

TABLE 4.8

Pour Point, °C	Kinematic Viscosity, cst		Lubricating Capacity on Four-Ball Tester (d_{ba} = 19 mm)		Extent of Corrosion in Pinkevich Device (at a Temperature of + 70°C for 50 hrs)		
	at +100° C	at −35° C	Critical Load P_{cr}, kg	Width of Wear Spot, mm	Steel 30KhGSA	Alloy BrAZhMts 10-3-1.5	Brass LS-59
−56	10.2	23 660	64	0.85	+0.11	+0,26	+0,24

As the test results indicate, the oil VNII NP-25 is close to the MS-20 oil with respect to lubricating properties during vibration.

Bearings of all types working on the oil VNII NP-25 show little wear both at positive and negative temperatures.

An improvement in the lubricating properties of oils may constitute an important factor promoting a pronounced increase in the lifetime of main and tail rotor hubs of helicopters. Therefore, studies in this direction will acquire an

ever greater scope. In such investigations, consideration should be given to /395 the above-described characteristics of the mechanism of wear and lubrication conditions of highly loaded vibrating bearings.

Oils for needle bearings of flapping and drag hinges. These bearings, as a rule, are less loaded than the bearings of feathering hinges, so that they are not as sensitive to the properties of the lubricant. The selection of lubricating materials for needle bearings of the flapping and drag hinges of rotor hubs is facilitated by the fact that solidification of the lubricant when the rotor is inoperative leads to no unfavorable consequences. In the flapping and drag hinges (if they are present) of tail rotors, the lubricant cannot be permitted to solidify since increased moments of friction in these assemblies may result in shaking of the helicopter.

At present, "hypoid" lubricants are used in the flapping and drag hinges of the main and tail rotor hubs of Soviet helicopters. Practical experience with helicopter operation has shown that hypoid oils, despite their content of free sulfur at ordinary specific pressures, ensure a sufficiently long life for vibrating needle bearings. Hypoid lubricants, just as other oils with antiwear additives, are unsuitable for feathering hinges.

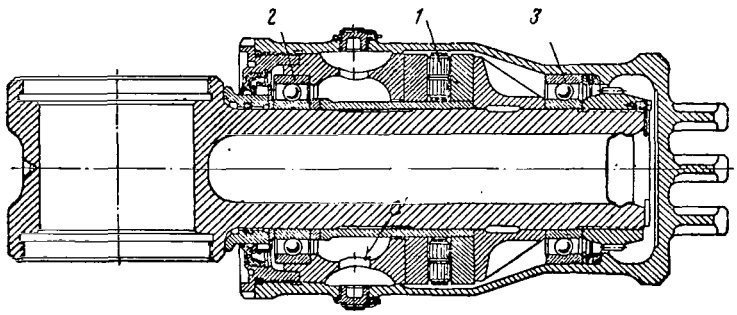

Fig.4.51 Feathering Hinge of Rotor Hub.

Hypoid oil has high tackiness and hence provides the necessary lubrication for contacting elements even if the hubs are not completely tight. The replacement of hypoid oil by greases (which is sometimes resorted to in tail rotors of helicopters operating at especially low temperatures) greatly shortens the service life of needle bearings in flapping and drag hinges.

3. Calculation of Hub Bearings in Main and Tail Rotors

Bearings of feathering hinges. Figure 4.51 shows a typical design of feathering hinges for the main rotor hubs of Soviet helicopters.

In calculations of bearings for the feathering hinges of rotor hubs, it is common to take into account the centrifugal force of the blade N and the moment in the plane of rotation M_d created by the damper.

In feathering hinges manufactured according to the scheme shown in Fig.4.51, the centrifugal force of the blade is absorbed by the thrust bearing (1). The moment of the damper is absorbed in part by the same bearing and in part by the radial bearings (2) and (3).

The loads on the radial bearings (2) and (3) in flight are comparatively small; consequently, they are usually selected from static considerations based on the weight moment of the blade transmitted to them when the helicopter is /396
standing, the rotor is not rotating, and the blades abut the coning stops. As shown in practical use, the loads on the radial bearings of feathering hinges due to the weight moment of the blade may go as high as 100 - 110% of their static load capacity catalog rating.

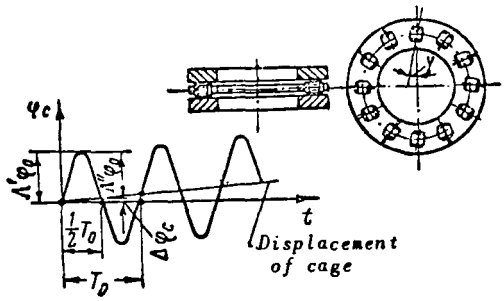

Fig.4.52 Thrust Bearing with Slewed Rollers; Recording of Motion of the Bearing Cage during Vibration.

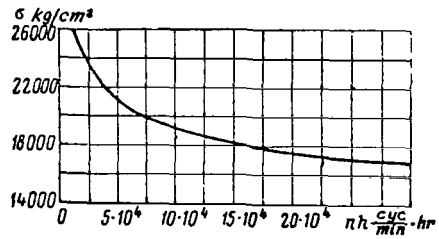

Fig.4.53 Curve of Life Expectancy $\sigma = \sigma(nh)$ for Thrust Bearings with Slewed Rollers.

The life expectancy of thrust bearings of feathering hinges is calculated on the basis of the experimental relation $\sigma = \sigma(nh)$ obtained from tests with the proper types of bearings under vibration conditions at purely axial load. For thrust ball bearings, the curve of life expectancy $\sigma = \sigma(nh)$ is plotted in Fig.4.49.

As mentioned before, thrust bearings with slewed rollers are being used in the feathering hinges of rotor hubs of all series-produced Soviet helicopters. The basic diagram of such bearings is shown in Fig.4.52. Thanks to arrangement of the seats of the cage at an angle to the radial direction in bearings of this type, the cage not only vibrates together with the revolving race but also shifts continuously, although very slowly, in the same direction. This continuous displacement of the cage prevents "brinelling" of the race tracks and leads to a substantial increase of the load-carrying capacity of the bearing.

Tests have established that the life expectancy of thrust bearings with slewed rollers largely depends on the rate of displacement of the retainer. This rate is commonly characterized by the time T_c, during which the cage turns through an angle of 360°. The optimal values of the time T_c for the vibration amplitudes and frequencies at which the thrust bearings of feathering hinges operate are 40 - 80 min. When $T_c > 80$ min, the probability of failure of the bearing due to spalling of the metal on the rollers increases. Despite continu-

ous displacement of the cage, the same surface areas of the rollers are in contact with the races. Therefore, failure of thrust bearings with slewed rollers begins in most cases with damage to the rollers. It should be mentioned that, at T_c = 2.5 to 6 hrs, the durability of the rollers drops by a factor of about 2. When T_c < 40 min, friction losses and wear of the tracks increase noticeably.

The curve of life expectancy $\sigma = \sigma(nh)$ for thrust bearings with slewed rollers having an optimal radial displacement of the cage of T_c = 40 - 80 min is shown in Fig.4.53. This curve has been plotted from test results with several batches of such bearings and MS-20 oil at an amplitude of the revolving race /397 $\varphi_0 = 4.5^\circ$ and a frequency n = 240 cyc/min, i.e., under conditions analogous to the test conditions whose results were used in constructing the relation $\sigma = \sigma(nh)$ in Fig.4.49.

Bench tests and operating experience indicate that the curves of life expectancy plotted in Figs.4.49 and 4.53 can be used for determining the rated service life of rotor hub thrust bearings for all operating conditions these units encounter under real conditions.

As we see from Figs.4.49 and 4.53, the equation of the life expectancy curves $\sigma = \sigma(nh)$ for vibrating bearings has the same form as for bearings rotating in one direction:

$$\sigma^{m^*}(nh) = \text{const}, \tag{5.1}$$

where we have $m^* = 10$ for the case of point contact and $m^* = 6.66$ for the case of linear contact.

Let us take for the base the product nh = 120,000, which corresponds approximately to a 500-hour operating life of helicopters of the Mi-1 type. At nh = 120,000 the permissible contact stresses are 29,000 kg/cm^2 for thrust ball bearings and 18,800 kg/cm^2 for thrust bearings with slewed rollers. Let A_0 denote the axial force which, in a bearing with uniform distribution of forces over the rolling bodies, sets up contact stresses equal to those permissible at nh = 120,000. Then, in conformity with eq.(3.1) the permissible force on the ball will be

$$P_0 = \frac{A_0}{z}\left(\frac{120\,000}{nh}\right)^{0,3}. \tag{5.2}$$

Here we have taken into account that for ball bearings the contact stresses are proportional to the cube root and for roller bearings, to the square root of the load.

Special experiments have established that the moment which must be taken into account in calculating the service life of a thrust bearing for feathering hinges is about 25 - 50% of the moment of the damper, depending on the design features of the assembly and on the clearances. Here the calculation is performed in terms of the instantaneous maximum pressure on the rolling body, meaning that the moment acting on the thrust bearing of the feathering hinge is arbitrarily considered as constant in magnitude and direction.

The maximum pressure on the rolling body of a thrust bearing, loaded by an axial force and moment, can be represented in the form

$$P_0 = \kappa_0^{(A)} \frac{A}{z}.$$

Comparing this equality with eq.(5.2), we obtain the following expression for determining the rated service life of thrust bearings of feathering hinges for rotor hubs:

$$\left(\frac{nh}{120\,000}\right)^{0.3} = \frac{A_0}{\kappa_0^{(A)} N}. \tag{5.3}$$

As follows from Sections 3 and 4, the coefficient $k_0^{(A)}$ depends on the relative eccentricity of application of the axial force, which in this case is equal to

$$\tau = (0.25 - 0.5)\frac{M_d}{r_0 N}. \tag{5.4}$$

For the usual correlations between the moment of the damper and the centrifugal force, τ does not exceed 0.1; therefore, all rolling elements are always loaded in the thrust bearings of feathering hinges*. /398

For thrust roller bearings in which all rollers share the load, we have

$$\kappa_0^{(A)} = 1 + 2\tau. \tag{5.5}$$

For small values of τ, the coefficients $k_0^{(A)}$ for thrust ball and roller bearings practically coincide. This permits use of eq.(5.5) even for calculations of thrust ball bearings.

From eqs.(5.4) and (5.5), we finally find

$$\kappa_0^{(A)} = 1 + (0.5 - 1)\frac{M_d}{r_0 N}. \tag{5.6}$$

It should be noted that the calculation of radial-thrust bearings of different types intended for service in feathering hinges of main and tail rotor hubs can also be performed by means of eqs.(5.3) and (5.5) if the permissible axial loads A_0 corresponding to the value nh = 120,000 are predetermined for these bearings. Here it is assumed that the moments acting on the bearings are known from calculations or experiments.

It must be remembered that the values of A_0 which were not obtained from

* It is known that the relative eccentricity at which unloaded rolling elements occur is 0.5 for thrust roller bearings and 0.6 for thrust ball bearings.

the complete curve of life expectancy $\sigma = \sigma(nh)$ relative to a certain probability of failure of the bearings but from a recomputation based on results of experiments carried out at some value of nh for an insufficiently large number of test specimens, may be incorrect; apparently, this is associated with an appreciable dispersion of the life expectancy, which is difficult to elicit at a single load level.

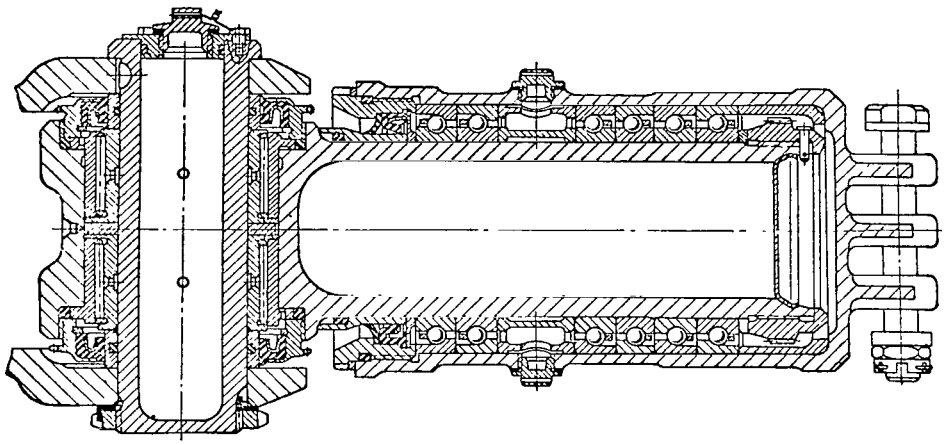

Fig.4.54 Feathering Hinge of Rotor Hub, on Multi-Row Radial-Thrust Bearing.

Multi-row radial-thrust ball bearings with contact angles of $\beta_o = 45^\circ$ and a reduced ratio of track radius to ball diameter are being successfully used in the feathering hinges of main and tail rotor hubs of certain helicopters (see Fig.4.54). This ratio is usually equal to 0.515 in antifriction bearings. In /399 the mentioned multi-row bearings it has been reduced to 0.510, which leads to a decrease in contact stresses by about 7% and thus to an increase in the rated service life of the bearings by a factor of 2. It is logical that such a way of increasing the load-carrying capacity of radial-thrust ball bearings is useful mainly for the case of vibrations, since a reduction in the ratio of track radius to ball diameter increases the length of the area of contact strain due to which the friction losses increase noticeably. Test results indicate that, in the case of high-quality manufacture ensuring a sufficiently uniform distribution of the external load over the bearings of the assembly, the permissible contact stresses on whose basis the axial force must be calculated are here 24,000 kg/cm^2 for multi-row radial-thrust ball bearings.

Available data on the permissible contact stresses in radial-thrust roller bearings for service under vibration conditions are still insufficiently verified.

The above values of permissible contact stresses pertain to cases of the service of feathering hinges in main and tail rotor hubs with oils not inferior in lubricating properties to the oils MS-20 and MS-14. If this requirement is not met, these values must be reduced accordingly.

The permissible contact stresses are noticeably affected by the size of the rolling elements so that, when using large bearings, a certain correction should be introduced for the scale factor. As shown by test results, the values of the permissible stresses given above can be considered binding for bearings with balls up to 25 mm in diameter and rollers up to 15 mm in diameter. On changing from rollers with a diameter of 15 mm to rollers with a diameter of 24 mm, the permissible contact stresses for thrust bearings with slewed rollers drop by about 10%.

Needle Bearings of Flapping and Drag Hinges. In most rotor hubs, needle bearings are used for the flapping and drag hinges.

The performance of needle bearings is usually estimated in terms of the magnitude of specific pressure per unit area of projection of the track of the inner race.

In calculations of needle bearings for drag hinges it is generally assumed that the load is uniformly distributed over the length of the needles (see Fig.4.55,a). In conformity with this, the specific pressure for bearings is taken as equal to

$$q=\frac{N}{Dl_{\Sigma}}, \tag{5.7}$$

where

D = diameter of the track of the inner race;
l_{Σ} = total working length of the needles.

Needle bearings for flapping hinges, in addition to the centrifugal force of the blade N, take a certain moment M (Fig.4.55,b) whose constant component M_a is determined with sufficient accuracy by the expression

$$M_a=\left(\frac{M_{rot}}{z_{rot}}-Na\right)\frac{l_2}{l_{v.h}}. \tag{5.8}$$

Here,

M_{rot} = torque of the rotor;
z_{rot} = number of blades of the rotor;
a = "drift" of the middle of the flapping hinge from the axis of rotation; /400
l_2 = distance between flapping and vertical hinges;
$l_{v.h}$ = "offset" of drag hinge.

The variable component M_v of the moment M, when calculating needle bearings of the flapping hinges of rotor hubs, is disregarded since it has little effect on their life expectancy. It is customary to assume that the load in flapping hinges manufactured in conformity with the scheme in Fig.4.55,b is distributed over the length of the bearings according to the trapezoidal rule. In this case, the loaded state of the bearings is characterized by the specific pressures q_1 and q_2 on the outer edges of the races caused by the combined action of the

force N and the moment M_a. These pressures are calculated by means of the formula

$$q_{1,2}=\frac{N}{Dl_\Sigma}\pm 6\frac{M_a}{DB^2\left[1-\left(1-\frac{l_\Sigma}{B}\right)^3\right]}, \tag{5.9}$$

where B is the working width of the bearing assembly.

Substituting into eq.(5.9) the value of M_a, we reduce it to the form

$$q_{1,2}=\frac{N}{Dl_\Sigma}\left[1\pm 6\frac{\frac{M_{rot}}{z_{rot}N}-a}{B}\cdot\frac{\frac{l_2}{l_{v.h}}\cdot\frac{l_\Sigma}{B}}{1-\left(1-\frac{l_\Sigma}{B}\right)^3}\right]. \tag{5.10}$$

As design data indicate, proper choice of the "drift" a permits approaching the specific pressures q_1 and q_2 sufficiently close to the average specific pressure $q_0=\frac{N}{Dl_\Sigma}$ in the basic powered flight regimes. We note that the "drift" of the middle of the flapping hinge from the axis of rotation by a distance a is equivalent to rotation of this hinge through an angle $\xi_{h.h}=\tan^{-1}\frac{a}{l_{v.h}}$ (see Fig.4.55).

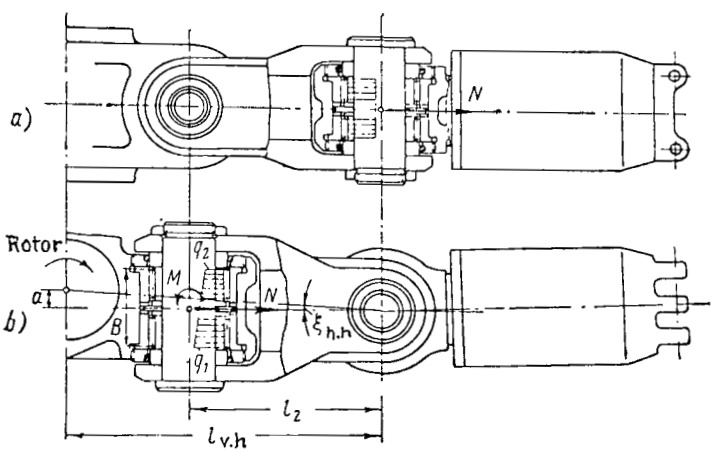

Fig.4.55 For Calculation of Needle Bearings of Flapping and Drag Hinges of Rotor Hubs.

According to eq.(5.10), the specific pressures q_1 and q_2 depend on the centrifugal force N and on the torque M_{rot}. Therefore, these can be regarded as certain functions of the rotor rpm and power. After using eq.(5.10) for plot- /401

ting the graphs of $q_1 = q_1(N_{rot})$ and q_2 and $q_2(N_{rot})$ for the most characteristic rotor rpm, as is done in Fig.4.56, it becomes easy to determine the values of the specific pressures q_1 and q_2 in the main flight regimes of a helicopter and also to estimate the correctness of selection of the "drift" a and, if necessary, to introduce suitable corrections into the rotor hub design.

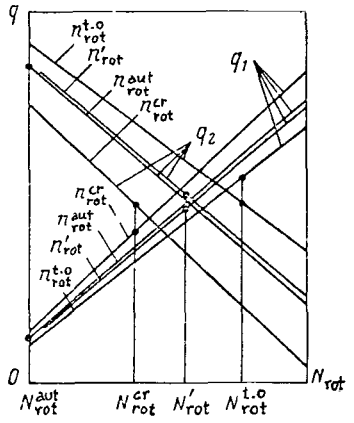

Fig.4.56 Specific Pressures q_1 and q_2 as a Function of Rotor Rpm and Power.
n^{cr}_{rot}, N^{cr}_{rot} = rotor rpm and power in cruising regime; n'_{rot}, N'_{rot} = = rotor rpm and power at cruising speed; $n^{t.o}_{rot}$, $N^{t.o}_{rot}$ = rotor rpm and power in takeoff regime; n^{aut}_{rot}, N^{aut}_{rot} = rotor rpm and power in autorotation regime.

If the flapping hinges are made in the form of two independent supports whose spacing L substantially exceeds the diameter of the track D (Fig.4.57), it can be assumed that, within each support, the specific pressures in the bearings are constant.

In this case, the rated specific pressures determining the life expectancy of the needle bearings in the flapping hinges are equal to

$$q_{1,2} = \frac{N}{Dl_{\Sigma}}\left[1 \pm \frac{2\left(\frac{M_{rot}}{z_{rot}N} - a\right)}{L}\frac{l_2}{l_{v.h}}\right], \qquad (5.11)$$

where l_{Σ} is the total length of the needles in both bearings.

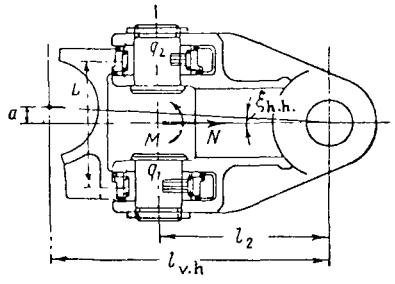

Fig.4.57 For Calculation of Widely Spaced Needle Bearings of Flapping Hinges.

When using hypoid lubricants, the permissible specific pressures in well-sealed needle bearings corresponding to a life expectancy of 1000 hrs at 240 cyc/min are at least 350 kg/cm^2 for the flapping hinges and 400 kg/cm^2 for the drag hinges. The relatively small value of the permissible specific pressures in flapping hinge bearings can be explained in part by the fact that they work at vibration amplitudes of 2 to 6°, whereas the vibration amplitude of the drag hinge bearings usually does not exceed 1°. Although this contradicts established opinions, practical use has shown that, at vibration amplitudes to 1°, the life expectancy of needle bearings is higher than at amplitudes of 2 - 6°. The fact that, due to deformation of the parts under load, the actual specific pressures on the edges of the needle bearings of flapping hinges may at times exceed the rated pressures possibly plays a definite role here.

Many years of actual service experience confirm that, in selecting the /402

size of needle bearings for the flapping and drag hinges of rotor hubs of light and medium helicopters, the above-indicated values of permissible specific pressures can be used as a reliable guide. For heavy helicopters whose units generally have a relatively lower rigidity, these figures can be used as guide only

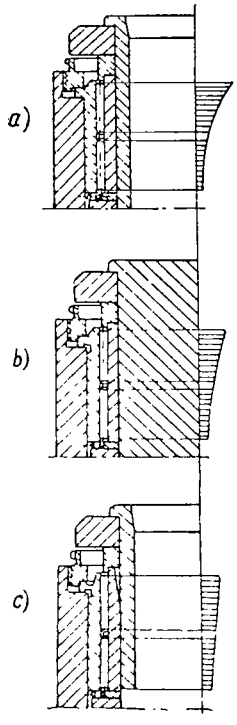

Fig.4.58 Effect of Stiffness of Pin and Flexibility of Races on the Distribution of Specific Pressures over the Length of Needle Bearings in a Flapping Hinge.
a - Initial version; b - Effect of pin of increased stiffness; c - Effect of "flexible" ends of bearing races.

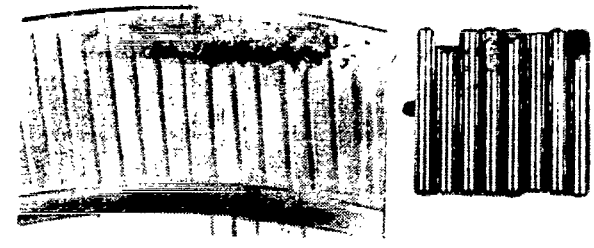

Fig.4.59 Failure of Needle Bearing due to Insufficient Rigidity of the Structure.

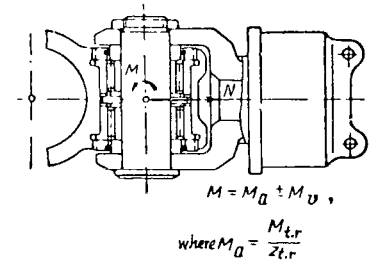

Fig.4.60 For Calculation of Needle Bearings in Tail Rotor Hubs.

if special measures are taken to ensure a uniform load distribution in the drag hinge bearings and if the diagram of the load distribution in the flapping hinges approximates a trapezoidal diagram (see Fig.4.55,b). As a rule, a satisfactory load distribution over the length of needle bearings for flapping and drag hinges can be obtained by properly choosing the stiffness of rings and pins and also by suitably raising the flexibility of the ends of the races. This is shown specifically in Fig.4.58 which contains experimental diagrams of the variation in distance between the generatrices of the outer and inner races, for

three design versions of the flapping hinge in the rotor hub of a heavy helicopter. It should be noted that inadequate mechanical strength of the rings and pins in flapping and drag hinges may not only result in local increases of the depth of brinelling marks at the edges of the tracks but also in spalling of large portions of their surface and sometimes even in breakage of the needles (Fig.4.59).

Calculation of needle bearings for flapping hinges of tail rotor hubs /403
(Fig.4.60) is appreciably more difficult than calculation of needle bearings for flapping hinges of main rotor hubs, since they generally absorb a rather large alternating moment which cannot be disregarded in estimating their performance. This moment is created by alternating aerodynamic and inertia (Coriolis) forces acting on the blades of the tail rotor in the plane of rotation. In rough calculations, the loaded state of needle bearings in tail rotor flapping hinges is usually characterized by the instantaneous maximum specific pressure set up on the edge of the track. On the assumption that the load is distributed over the length of the bearings in accordance with the trapezoidal rule, this pressure is equal to

$$q=\frac{N}{Dl_{\Sigma}}\left[1+6\frac{\frac{M_{t.r}}{z_{t.r}}+M_{v}}{BN}\frac{\frac{l_{\Sigma}}{B}}{1-\left(1-\frac{l_{\Sigma}}{B}\right)^{3}}\right], \qquad (5.12)$$

where

$M_{t.r}$ = torque of tail rotor;
$z_{t.r}$ = blade number of tail rotor;
M_{v} = amplitude of variable moment loading the flapping hinge.

The values of the specific pressure q calculated from eq.(5.12) for tail rotors of light and medium helicopters at cruising speed should not exceed 300 - 350 kg/cm^2. When hypoid lubricants are used in the flapping hinges, it can be expected that the life expectancy of the bearings will be at least 1000 hrs.

Finally, the life expectancy of needle bearings for flapping and drag hinges of main and tail rotor hubs is determined from tests of such units on special rigs.

4. Calculation of Bearings for the Pitch Control and Control Mechanisms

The permissible loads on the bearings of the pitch-control hinges and their connecting control elements generally are determined by experiment. For this, endurance tests are performed on special rather complex installations which permit simulating all types of forces acting on the pitch control in flight.

The loads on the pitch control are of a dynamic nature. This is especially clear from the oscillograph in Fig.4.61, for the blade hinge moment M_h and the forces P_{long} and P_{lat} in the longitudinal and lateral control rods connecting

the corresponding rockers of the pitch control with the hydraulic boosters.

It is logical that, with such a complex character of loading, any recommendations as to the design of bearings for pitch control hinges will of necessity be only conditional. Nevertheless, certain suggestions might guide the designer in problems of the selection of bearings for these vital units; in this respect, we will briefly discuss these.

/404

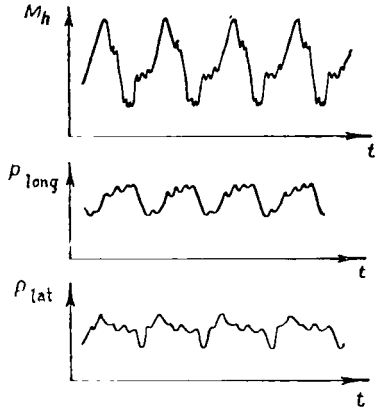

Fig.4.61 Oscillograms for Blade Hinge Moment and Forces in Longitudinal and Lateral Control Rods.

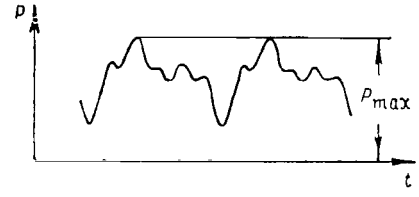

Fig.4.62 Load on Bearings of Pitch Control Hinges.

If we take into consideration that, in conventional rotor designs, only the absolute magnitude of the blade hinge moment changes and that the correlation between the amplitudes and phases of its individual harmonics remains constant, then the selection of bearings for such hinges of the pitch control based on the same design configuration can proceed from the maximum value of the absorbed load P_{max} (Fig.4.62).

For pitch controls close in design to the pitch controls of Mi-1 and Mi-4 helicopters (see Fig.4.38) with all-metal rotor blades of rectangular planform and using greases of the type TsIATIM-201, the permissible load P_{perm}^{max} can be determined from Table 4.9. This table was compiled from results of stand tests with consideration of practical experience in operating pitch controls.

The values of the permissible loads P_{perm}^{max} given in the Table for a rotor rpm of 240 correspond to a life expectancy of 1000 - 1200 hrs. For other rpm, the life expectancy is found from the expression /405

$$h \approx \frac{240{,}000}{n}, \qquad (5.13)$$

where n is the rated rotor rpm.

TABLE 4.9

Site of Installation	Permissible Values P_{perm}^{max} (kg) for Various Bearings					
	Ball, Radial, Radial-Thrust, and Thrust	Ball, Spherical	Roller, Spherical	Roller, Radial-Thrust, and Thrust	Needle	Hinge of Type ShS
Hinges of swashplate, turn rod, and levers of blade	$0.8\ Q_{st}$				$2\ Dl$	
Bearings of universal joint	Q_{st}		$0.8\ Q_{st}$			
Bearings of rockers of longitudinal and lateral controls	Q_{st}	Q_{st}		$0.8\ Q_{st}$	$2\ Dl$	
Bearings of longitudinal and lateral control rods connecting the rockers with outer race of Cardan joint						Db
Bearings of collective pitch lever	Q_{st}	Q_{st}		$0.8\ Q_{st}$	$2\ Dl$	

Q_{st} = permissible static load on a nonrotating bearing, given in catalogs and manuals;
D = diameter of inner race track of needle bearing or spheres of hinged bearing, in mm;
b = width of outer race of hinged bearing, in mm;
l = working length of the needles, in mm.

If the nature of the loads differs from that of the pitch controls of the Mi-1 and Mi-4 helicopters with all-metal rotor blades, then the permissible values P_{perm}^{max} should be refined as a result of appropriate stand and service tests.

Above, we have examined vibrating bearings that execute a large number of vibrations (more than 10^7) during the rated service life.

The permissible loads on the bearings of the control mechanism of aircraft, for which the total number of vibrations does not exceed 100,000 and the vibration amplitude is equal to 20° and more, should be determined - according to VNIPP - by the following experimental formula*:

$$R_{perm} = \alpha_{perm} z d_b^2. \qquad (5.14)$$

The values of the coefficient α_{perm} for certain types of bearings operating on greases at vibration numbers 25,000 and 100,000 are given in Table 4.10.

* It is assumed that the contact areas of adjacent rolling elements do not overlap.

TABLE 4.10

Type of Bearing	Designation of Bearing	Inside Diameter of Bearing, mm	Value of Coefficient α_{perm}	
			At 25000 Vibrations	At 100000 Vibrations
Ball, radial	7000100 100 200	*to* 50	5	2
	900000	*to* 9	5	2
		above 9	4	1.6
	980000	*to* 9	5	2
		above 9	4	1.6
	981000	*to* 9	2.5	2
		above 9	2	1.6
Ball, spherical	1000	*to* 10	4	2.8
	1200	*to* 50	4	2.8
	1300 971000	*to* 50	4.7	3.3

Section 6. Theory and Selection of Basic Parameters of Thrust Bearings with "Slewed" Rollers /406

As indicated in previous Sections, thrust bearings with cylindrical rollers arranged at an angle to the radial direction are being used with success in the feathering hinges of rotor hubs of Soviet helicopters. The high load-carrying capacity of such bearings, known as thrust bearings with "slewed" rollers, is explained by the fact that the cage, during vibrations, not only vibrates together with the revolving race but also shifts continuously in one direction. The time of rotation of the cage T_c through an angle of 360°, characterizing the rate of this displacement, is determined by a number of factors. It is dependent on the coefficient of sliding friction between roller and races, vibration amplitude and frequency of the revolving race, and on a number of geometric parameters of which the angles of slope of the cage seats play a major role. It is logical that these angles should be selected such that the time T_c will be within optimal limits ensuring a long life expectancy of the rollers at acceptable wear of the tracks. A theory is presented below by means of which this problem can be solved.

1. Determination of the Time T_c

In thrust bearings with slewed rollers, the ratio of angular velocity of the cage to angular velocity of the revolving race $\Lambda = \frac{\omega_c}{\omega}$ depends upon the direction of rotation. This causes a continuous displacement of the cage, which is observed in such bearings during vibration.

The values of the ratio Λ corresponding to counterclockwise and clockwise rotation of the bearing are found in the following manner:

The forces of sliding friction arising at the points of contact of the roller with the races are reduced to the resultant forces F_{1y}, F_{1x}, F_{2y}, F_{2x}, and the moments M_{1z}, M_{2z} (Fig.4.63). At a constant coefficient of sliding friction μ between rollers and races, the magnitudes of these forces and moments can be calculated with sufficient accuracy by the formulas

$$\left.\begin{aligned}
F_{1y} &= \mu P\left(B_{10} + \mu\frac{d_r}{2l}B_{11}\frac{y_1}{l}\right);\\
F_{1x} &= \mu P\left(\mu\frac{d_r}{2l}A_{10} + A_{11}\frac{y_1}{l}\right);\\
F_{2y} &= \mu P\left(B_{10} - \mu\frac{d_r}{2l}B_{11}\frac{y_2}{l}\right);\\
F_{2x} &= \mu P\left(-\mu\frac{d_r}{2l}A_{10} + A_{11}\frac{y_2}{l}\right);\\
M_{1z} &= \mu Pl\left[C_{10} + \mu\frac{d_r}{2l}C_{11}\frac{y_1}{l} + C_{13}\left(\frac{y_1}{l}\right)^2\right];\\
M_{2z} &= \mu Pl\left[C_{10} - \mu\frac{d_r}{2l}C_{11}\frac{y_2}{l} + C_{13}\left(\frac{y_2}{l}\right)^2\right].
\end{aligned}\right\} \qquad (6.1)$$

Here,

P = force absorbed by the roller in question;
y_1 and y_2 = coordinates of the contact points at which there is no sliding in a direction perpendicular to the roller axis;
d_r = diameter of the roller;
l = working length of the roller.

In deriving eqs.(6.1), it was assumed that the normal loads q_1 and q_2 are distributed over the roller length according to the law /407

$$\left.\begin{aligned}
q_1 &= \frac{P}{l}\left(1 - K\frac{y}{l}\right);\\
q_2 &= \frac{P}{l}\left(1 + K\frac{y}{l}\right),
\end{aligned}\right\} \qquad (6.2)$$

where

$$K = 6\frac{F_{1y} + F_{2y}}{P}\frac{d_r}{2l}.$$

Such a distribution of normal loads is due to the action of the moment $\left(F_{1y} + F_{2y}\right)\frac{d_r}{2}$ which tends to turn the roller about the axis $O_r x$. Since the usual load concentration at the edges of the roller has little effect on the time T_c, we will disregard it to simplify the calculations. In view of the smallness of the friction force $\mu_c(F_{1x} - F_{2x})$ we consider that

$$\int q_1 dy = \int q_2 dy = P.$$

The coefficients entering eqs.(6.1) are determined by the equalities

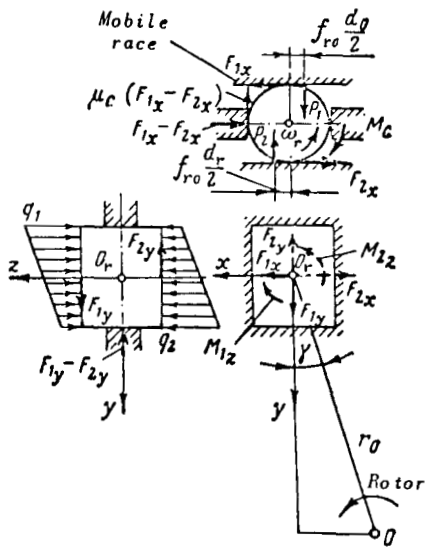

Fig.4.63 Forces and Moments Acting on "Slewed" Rollers.

$$\left.\begin{aligned}
A_{11} &= \frac{1}{\left(\frac{1}{4}+\frac{1}{p^2}\right)^{1/2}};\\
B_{10} &= \frac{1}{p}\ln\frac{\frac{1}{2}+\left(\frac{1}{4}+\frac{1}{p^2}\right)^{1/2}}{-\frac{1}{2}+\left(\frac{1}{4}+\frac{1}{p^2}\right)^{1/2}};\\
C_{10} &= \frac{1}{2}\left(\frac{B_{10}}{p}-\frac{1}{A_{11}}\right);\\
A_{10} &= 6B_{10}\left(\frac{1}{A_{11}}-\frac{B_{10}}{p}\right);\\
B_{11} &= 12B_{10}\left(\frac{A_{11}}{p}-B_{10}\right);\\
C_{11} &= \frac{B_{11}}{p};\\
C_{13} &= \frac{A_{11}^3}{8},
\end{aligned}\right\} \qquad (6.3)$$

where

$$p = \frac{l}{r_0 \sin\gamma}.$$

From the kinematic relations and the equations of moments relative to the axis $O_r y$, we can obtain the following expressions*: /408

$$\left.\begin{aligned}
\frac{y_1}{l} &= \frac{\frac{f}{\mu} \pm \mu\mu_c \frac{d_r}{2l} A_{10}}{A_{11}} -\\
&-\left[(1 \pm \mu_c)\left(\frac{r_0\cos\gamma}{l} - \frac{\frac{f}{\mu} \pm \mu\mu_c \frac{d_r}{2l} A_{10}}{A_{11}}\right)\right](2\Lambda - 1);
\end{aligned}\right\} \qquad (6.4)$$

* It is assumed that the quantity $\mu_c(2\Lambda - 1)$ can be neglected for unity. The inertia moment of the roller is disregarded.

$$\frac{y_2}{l}=\frac{\frac{f}{\mu}\pm\mu\mu_c\frac{d_r}{2l}A_{10}}{A_{11}}+$$
$$+\left[(1\mp\mu_c)\left(\frac{r_0\cos\gamma}{l}-\frac{\frac{f}{\mu}\pm\mu\mu_c\frac{d_r}{2l}A_{10}}{A_{11}}\right)\right](2\Lambda-1).$$

In these expressions,

$$f=f_{r0}+\frac{M_r}{Pd_r},$$

where

f_{r0} = coefficient of rolling friction;
M_r = moment taking into account the friction at the ends of the roller and the friction against the lubricant;
μ_c = coefficient of friction between the rollers and cage.

The upper signs refer to the case of $F_{1x} - F_{2x} > 0$, while the lower signs indicate the case of $F_{1x} - F_{2x} < 0$.

The angle of slope γ is considered positive if the roller can be placed in a radial position by turning about the point O_r counterclockwise. Under this condition, the directions indicated in Fig.4.63 correspond to positive values of the forces calculated by eqs.(6.1). The signs of the angles of slope of the rollers and the direction of rotation are determined when viewing the roller from the side of the movable race.

A roller with an angle of slope γ generates the following moment, relative to the axis of rotation of the cage:

$$M=(F_{1x}-F_{2x})r_0\cos\gamma+(F_{1y}-F_{2y})r_0\sin\gamma-(M_{1z}-M_{2z}).$$

As shown by calculations, the resistance to rolling and the friction of the roller against the cage and lubricant have practically no effect on the magnitude of this moment. In conformity with this, taking $f = \mu_c = 0$ into account and considering that in real designs the angle is $\gamma < 6^\circ$ and hence $\cos\gamma \approx 1$, the last equality, by means of eqs.(6.1), (6.3), and (6.4), can be transformed such that

$$M=\mu Pr_0\overline{M}, \qquad (6.5)$$

where

$$\overline{M}=2\mu\frac{d_r}{2l}\cdot A_{10}-2A_{11}\frac{r_0}{l}(2\Lambda-1).$$

Table 4.11 gives the values of the coefficients A_{10} and A_{11} as a function of the quantity l/p.

TABLE 4.11

	Values of the Coefficients A_{10} and A_{11} at 1/p										
	0	0.05	0.10	0.15	0.20	0.25	0.30	0.35	0.40	0.45	0.50
A_{10}	0	0.87702	1.28664	1.50479	1.60798	1.63952	1.62687	1.58789	1.53409	1.47287	1.40889
A_{11}	2	1.99008	1.96117	1.91565	1.85695	1.78885	1.71498	1.63846	1.56173	1.48659	1.41421

In the case of negative values of p, the coefficients A_{10} and A_{11} can be determined by means of the relation

$$\left.\begin{aligned} A_{10}(-p) &= -A_{10}(p) \\ &\text{and} \\ A_{11}(-p) &= A_{11}(p). \end{aligned}\right\} \tag{6.6}$$

These relations follow directly from eqs.(6.3).

At small vibration amplitudes, when the inertia forces can be disregarded, the equation of motion of the cage of the bearing with "slewed" rollers reduces to the condition

$$M_{sl} - M_{fr} = 0. \tag{6.7}$$

Here,

$M_{sl} = \Sigma M$ = total moment of the sliding friction forces exerted on the rollers by the bearing races;

M_{fr} = moment of friction.

Let us assume that the cage has z seats, in each of which are s rollers. The angles of slope of the cage seats, at an average radius r_c are denoted in terms of γ_{c_i}, and the angles of slope of the rollers in terms of γ_{i_k}. The subscript i denotes the number of the cage seat, while the subscript k indicates the position of the roller in it. Usually, in each seat there are two rollers. The load on a roller with a working length l_{i_k} is equal to

$$P_{l_k} = \frac{N}{z} \cdot \frac{l_{i_k}}{l_\Sigma}, \tag{6.8}$$

where

l_Σ = total working length of the rollers in one seat;

N = axial force applied to the bearing.

A change in direction of rotation of the bearing is equivalent to a change in signs of the angles of slope of the rollers. Bearing in mind this fact, we obtain the following expression from eqs.(6.5), (6.6), and (6.8):

$$M_{sl}=2\mu N r_c \frac{r_c}{z l_{\Sigma}}\left[\pm\mu \frac{d_r}{2r_c}\sum_{i=1}^{z}\sum_{i=1}^{s}\frac{r_{i_k}}{r_c}A_{10}(p_{i_k})-\right.$$

$$\left.-(2\Lambda-1)\sum_{i=1}^{z}\sum_{k=1}^{s}\frac{r_{i_k}^2}{r_c^2}A_{11}\left(p_{i_k}\right)\right], \qquad (6.9)$$

where $A_{10}(p_{i_k})$ and $A_{11}(p_{i_k})$ are the values of the coefficients A_{10} and A_{11} for

$$p=p_{i_k}=\frac{l_{i_k}}{r_{i_k}\sin\gamma_{i_k}}.$$

For definitiveness, we will consider that the signs of the angles of slope of the rollers are given for the case of counterclockwise rotation of the bearing. After substituting eq.(6.9) into eq.(6.7), we obtain: /410

for counterclockwise rotation:

$$\Lambda=\Lambda'=\frac{1}{2}+\frac{1}{2}\frac{\mu\frac{d_r}{2r_c}\sum_{i=1}^{z}\sum_{k=1}^{s}\frac{r_{i_k}}{r_c}\cdot A_{10}(p_{i_k})-\frac{1}{2}\frac{zl_{\Sigma}'}{r_c}\cdot\frac{M_{fr}}{\mu N r_c}}{\sum_{i=1}^{z}\sum_{k=1}^{s}\frac{r_{i_k}^2}{r_c^2}A_{11}\left(p_{i_k}\right)}; \qquad (6.10)$$

for clockwise rotation:

$$\Lambda=\Lambda''=\frac{1}{2}-\frac{1}{2}\frac{\mu\frac{d_r}{2r_c}\sum_{i=1}^{z}\sum_{k=1}^{s}\frac{r_{i_k}}{r_c}A_{10}(p_{i_k})+\frac{1}{2}\frac{zl_{\Sigma}}{r_c}\frac{M_{fr}}{\mu N r_c}}{\sum_{i=1}^{z}\sum_{k=1}^{s}\frac{r_{i_k}^2}{r_c^2}A_{11}\left(p_{i_k}\right)}. \qquad (6.11)$$

Knowing the quantities Λ' and Λ'', it is easy to calculate the time T_c. From Fig.4.52 it follows that, during each half-period of vibrations, the cage is displaced by an angle $\Delta\varphi_c = (\Lambda' - \Lambda'')\varphi_0$. Consequently, the time of rotation of the cage through an angle of 360° will be

$$T_c=\frac{360}{2|\Lambda'-\Lambda''|\varphi_0 n},$$

where $n = \frac{1}{T_0}$ is the number of vibrations of the revolving race per minute.

Since the moment of friction M_{fr} of the cage should be independent of the direction of rotation, we will have, in conformity with the above correlations,

$$T_c = \frac{180}{\varphi_0 n \mu} \frac{2r_c}{d_r} \frac{\sum_{i=1}^{z} \sum_{k=1}^{s} \frac{r_{i_k}^2}{r_c^2} A_{11}(p_{i_k})}{\left| \sum_{i=1}^{z} \sum_{k=1}^{s} \frac{r_{i_k}}{r_c} A_{10}(p_{i_k}) \right|}. \qquad (6.12)$$

TABLE 4.12

Time T_c (min) at Oil Temperature (°C)		
+(20–30)	–(30–40)	–(45–55)
63	54	58

Oil VNII NP-25 (ν = 10 centistokes at t = +100°C and ν = 50,000 centistokes at t = -40°C)

Equation (6.12) is the main formula for the theory of a thrust bearing with a "slewed" roller. It follows specifically that friction of the cage does not affect the time T_c. This important conclusion is confirmed by results of experiments set up to determine the time T_c at low temperatures, when, owing to an increase in viscosity of the oil, the moment M_{fr} may attain an appreciable magnitude (Table 4.12).

2. Selection of Angles of Slope of Cage Seats /411

A prescribed rate of displacement of the cage is ensured by proper selection of the angles of slope of its seats. In this case, not only the rated values of the angles but also the allowances for manufacture, which have a noticeable effect on the time T_c, must be kept in mind. The remaining geometric parameters of the bearing, influencing the time T_c, are selected on the basis of design considerations.

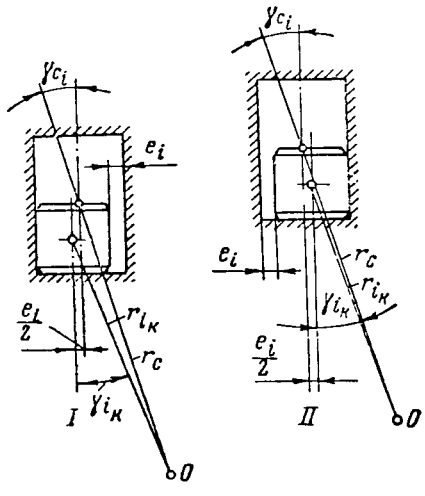

Fig.4.64 Determination of the Values of p with Clearance between Rollers and Cage.

Manufacturing deviations of the angles of slope of the cage seats, even with up-to-date technology and rigorous quality control of the finished articles, go as high as 7 - 10′. If no special measures are taken in the manufacture of bearings, such deviations may reach 20 - 30′.

The time T_c depends also on the clearance between rollers and cage. In the presence of clearance, the position of the rollers in the seats of the cage and hence the actual angles of slope of the rollers are determined by the forces of sliding friction exerted on the rollers by the races. Since, in the general case, a determination of these forces is difficult, we will assume that the rollers, with equal probability, can occupy any of two positions shown in Fig.4.64:

in position I:

$$p_{i_k}=\frac{l_{i_k}}{r_c\sin\gamma_{c_i}+\frac{e_i}{2}}\approx\frac{l_{i_k}}{r_c\sin\left(\gamma_{c_i}+\frac{e_i}{2r_c}\right)};$$

in position II:

$$p_{i_k}=\frac{l_{i_k}}{r_c\sin\gamma_{c_i}-\frac{e_i}{2}}\approx\frac{l_{i_k}}{r_c\sin\left(\gamma_{c_i}-\frac{e_i}{2r_c}\right)}.$$

It is obvious from these equalities that the effect of clearance on the time T_c can be taken into account by increasing the design deviations of the angles of slope of the cage seats to the quantity

$$\xi=\pm\xi_m+\frac{e_{max}}{2r_c},$$

where ξ_m is half of the manufacturing allowance, while e_{max} is the maximum clearance.

The most general case of arrangement of the cage seats of practical interest is the case where the cage contains z_1 seats with an angle of slope $\gamma_1 \pm \xi (\gamma_1 > 0)$ and z_2 seats with an angle of slope $0 \pm \xi$.

To simplify further calculations, let us assume that $l_{i_k} = l = \text{const}$. /412
If the quantity ξ is such that the difference $\Lambda' - \Lambda''$ is positive, then, provided that $l_{i_k} = l = \text{const}$, the time T_c can change from a certain

$$T_c^{(max)}=\frac{180}{\varphi_0 n v\mu'}\frac{2r_c}{d_r}\frac{A_{11}(p_1')+\chi A_{11}(p_2')}{A_{10}(p_1')+\chi A_{10}(p_2')} \qquad (6.13)$$

to a certain

$$T_c^{(min)}=\frac{180}{\varphi_0 n v\mu''}\frac{2r_c}{d_r}\frac{A_{11}(p_1'')+\chi A_{11}(p_2'')}{A_{10}(p_1'')+\chi A_{10}(p_2'')}. \qquad (6.14)$$

Here,

$$p_1'=\frac{l}{r_c\sin(\gamma_1-\xi)}; \qquad p_2'=-\frac{l}{r_c\sin\xi};$$

$$p_1''=\frac{l}{r_c\sin(\gamma_1+\xi)}; \qquad p_2''=\frac{l}{r_c\sin\xi};$$

$$\chi=\frac{z_2}{z_1} \quad \text{and} \quad v=\frac{\sum_{k=1}^{s}\frac{r_{i_k}}{r_c}}{\sum_{k=1}^{s}\frac{r_{i_k}^2}{r_c^2}}.$$

The coefficient v is usually close to unity (v = 0.98 - 1). This indicates that the time T_c depends little on the number of rollers s in one seat.

In the expressions for $T_c^{(max)}$ and $T_c^{(min)}$, the minimum and maximum values of the coefficient of sliding friction μ are denoted by μ' and μ''. With good lubrication, we have $\mu' \approx 0.05$ and $\mu'' \approx 0.08$.

Let the upper and lower limits of the range of optimal values of T_c be equal to T_c' and T_c'' respectively. As follows from test results, thrust bearings with slewed rollers operating in the feathering hinges of rotor hubs will have a time T_c' = 80 min and T_c'' = 40 min. It has been established that, to determine the maximum stability of the rate of displacement of the cage, the quantities γ_1 and χ should be selected such that, at a given value of ξ, $T_c^{(max)}$ will be equal to T_c'. At $T_c^{(max)} = T_c'$, the quantities γ_1, χ, and ξ are correlated by a definite relation. Setting $T_c^{(max)} = T_c'$ in eq.(6.13), this relation can be graphically represented as a family of corresponding curves*. Figure 4.65 which gives a family of such curves shows that the condition $T_c^{(max)} = T_c'$ imposes certain limitations on the selection of the quantities γ_1 and ξ. Thus in the case T_c' = = 80 min, the ratio χ should not exceed 1.28 for ξ = 0 and 0.77 for ξ = 15', and the angle γ_1 should not be less than some minimum angle $\gamma_1^{(min)} = \nu_1' + \xi$ (where γ_1' is the value of $\gamma_1^{(min)}$ for χ = 0 and ξ = 0). The range of time rate of change of cage displacement is characterized by the ratio $\eta = T_c^{(min)}/T_c^{(max)}$.

/413

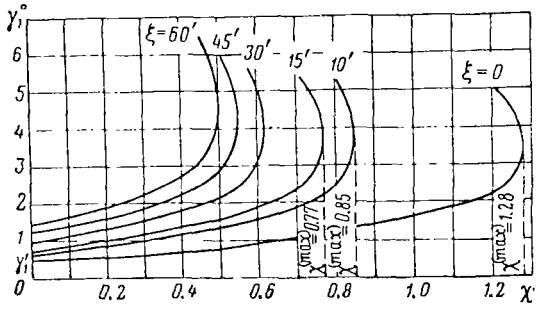

Fig.4.65 Curves of $\gamma_1 = \gamma_1(\chi)$ for Different Values of the Deviation of ξ.

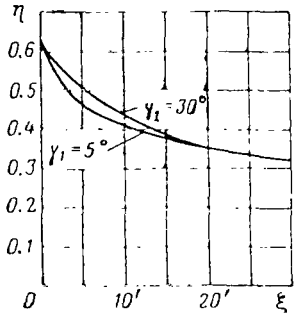

Fig.4.66 Dependence of the Ratio η on the Deviation of ξ for Different Angles of γ_1.

Figure 4.66 contains the curves of $\eta = \eta(\xi)$ for the angles $\gamma_1 = 5^\circ$ and $\gamma_1 = 30'$, plotted on the assumption that $T_c^{(max)} = T_c'$. Figure 4.66 shows that the ratio η depends mainly on the quantity ξ. The angle γ_1 has a rather minor effect on η. Thus, from the viewpoint of stability of the rate of cage displacement, different combinations of the angles of slope of the seats are approximately equivalent, provided they satisfy the conditions $T_c^{(max)} = T_c'$. According

* Everywhere where no special stipulations have been made, it is assumed that T_c' = 80 min. Here, all specific numerical values pertain to the case d_r = 9 mm, r_c = 40 mm, t = 8 mm, v = 1, $\varphi_o = 4.5^\circ$, n = 240 cyc/min, μ = 0.06.

to Fig.4.66, the deviation of ξ at which $T_c^{(min)} = T_c'' = 40$ min and thus $\eta = \frac{40}{80} = 0.5$, is about 5′. Hence, even with the most careful manufacture of cages, there might be cases in which the time T_c will exceed the limits of the optimal range.

In practice, we encounter two variants of arranging the cage seats. In the first, all seats have an identical angle of slope not exceeding 1° while in the second, several seats are arranged at an angle of 3 - 6° with all other seats being radial. Let us compare these variants for the following examples.

Let us examine a bearing for which $\gamma_1 = 45'$, $\chi = 0$, $d_r = 9$ mm, $r_c = 40$ mm, $l = 8$ mm, $e_{max} = 0.2$ mm, $\xi_m = 7'$, and $s = 2$; the bearing operates at $\varphi_0 = 4.5°$ and $n = 240$ cyc/min.

If all rollers have an angle of slope equal to γ, we have

$$T_c = \frac{180}{\varphi_0 n \mu v} \frac{2r_c}{d_r} \frac{A_{11}(p)}{A_{10}(p)}, \tag{6.15}$$

where

$$p = \frac{l}{r_c \sin \gamma}.$$

Figure 4.67 gives the curves of $T_c = T_c(\gamma)$, showing the variation in the time T_c as a function of the angle γ for $\mu = \mu' = 0.05$ and $\mu = \mu'' = 0.08$. We distinguish between the curves of $T_c = T_c(\gamma)$ a region bounded by vertical straight lines $\gamma = \gamma_1 + \xi_m + \frac{e_{max}}{2r_c} = 60'$ and $\gamma = \gamma_1 - \xi_m - \frac{e_{max}}{2r_c} = 30'$. The actual values of the time T_c should lie within this region. It is easy to note that, for such a bearing, $T_c^{(max)} = 74$ min and $T_c^{(min)} = 31$ min. These values are rather close to optimal. Results of experiments set up to determine the time T_c for several hundreds of bearings with the indicated parameters have shown that the actual values of T_c for all practical purposes do not extend beyond the limits of the indicated range, being grouped about average values of $T_c^{(av)} = 50 - 60$ min.

Now let the bearing have the following parameters: $\gamma_1 = 5°$, $\chi = 5$, $d_r = 5$ mm, $r_c = 28$ mm, $l = 4.2$ mm, $e_{max} = 0.2$ mm, $\xi_m = 7'$, $s = 2$ and let it operate at $\varphi_0 = 4.5°$ and $n = 300$ cyc/min.

We assume that the actual angles of slope of the radial seats are equal to ξ. Then, /414

$$T_c = \frac{180}{\varphi_0 n \mu v} \frac{2r_c}{d_r} \frac{A_{11}(p_1) + \chi A_{11}(p_2)}{|A_{10}(p_1) + \chi A_{10}(p_2)|}, \tag{6.16}$$

where

$$p_1 = \frac{l}{r_c \sin \gamma_1} \text{ and } p_2 = \frac{l}{r_c \sin \xi}.$$

Figure 4.68 which gives the curves of $T_c = T_c(\xi)$ plotted from eq.(6.16) shows that, at $\xi = 0$, the time is $T_c = 163 - 261$ min depending on the friction coefficient μ. If $\xi \approx -5'$, then the time T_c will tend to infinity. In other words, at small negative deviations of the angles of slope of the radial seats, the cage may stop moving. Such cases are often observed when testing bearings with large values of χ.

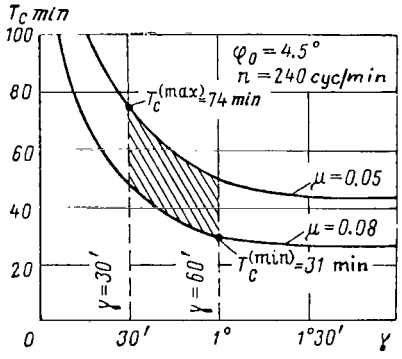

Fig.4.67 The Time T_c as a Function of the Angle of Slope of the Cage Seats γ.

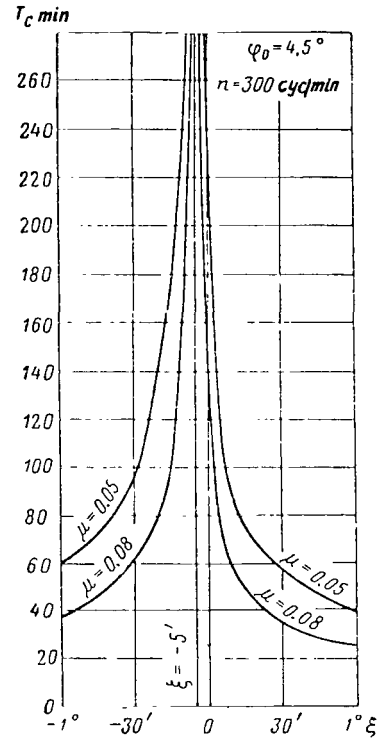

Fig.4.68 The Time T_c as a Function of the Deviation of ξ.

At $\mu = 0.08$ and $\xi = \xi_m + \frac{e_{max}}{2r_c} = 15'$, we have $T_c = 47$ min. Consequently, in the case in question the time T_c may vary from $T_c^{(max)} = \infty$ to $T_c^{(min)} = 47$ min.

These examples indicate that only the first variant of positioning the cage seats enables the bearings to operate under conditions close to optimal.

Positioning of the seats of the cage at identical angles will also reduce the friction losses and the nonuniformity of distribution of the normal load along the contact lines.

3. Friction Losses

Friction losses in thrust bearings with "slewed" rollers depend both on the

rate of the displacement of the cage and on the mode of selection of the quantities γ_1 and χ which provide cage displacement at a given rate.

The moment of friction of the bearing is usually written as /415

$$M_{fr} = f_{fr} N r_c, \tag{6.17}$$

where f_{fr} is the reduced friction coefficient.

Using the relations obtained in the preceding subsections, after a number of transformations we find

$$f_{fr} = f_{ro} + f_{sl} + \frac{M_{fr}}{2Nr_c}. \tag{6.18}$$

Here,

f_{ro} = coefficient of rolling friction;

f_{sl} = coefficient characterizing losses due to sliding friction.

The coefficient f_{sl} can be represented in the form [see (Ref.27)]

$$f_{sl} = \mu \frac{\sin\gamma_1 [B_{10}(p_1) - p_1 C_{10}(p_1)] + \frac{A_{11}(p_1)}{8} \cdot \frac{l}{r_c}\left[\frac{T_c}{T_c^{(0)}} \cdot \frac{A_{10}(p_1)}{A_{11}(p_1)} - 1\right]}{1 + \frac{A_{11}(p_1)}{2}\left[\frac{T_c}{T_c^{(0)}} \cdot \frac{A_{10}(p_1)}{A_{11}(p_1)} - 1\right]}, \tag{6.19}$$

where

$$T_c^{(0)} = \frac{180}{\varphi_0 n \mu v} \cdot \frac{2r_c}{d_r}.$$

On hand of Table 4.10 it is easy to demonstrate that, with an increase in angle of slope of the rollers, the ratio $\frac{|A_{10}(p)|}{A_{11}(p)}$ first increases rapidly, reaching, at $\gamma = \sin^{-1} 0.57\, l/r_c$, a value equal to unity. Upon a further increase in the angle, the ratio $\frac{|A_{10}(p)|}{A_{11}(p)}$ will not change. This means that the quantity $T_c^{(o)}$ represents the minimum time obtainable at a given value of the friction coefficient μ [see eq.(6.15)].

Figure 4.69 indicates that, at the same rate of cage displacement, the friction losses decrease with decreasing angle γ_1. Hence, the minimum friction losses actually occur when all cage seats are positioned at identical angles to the radial direction. At optimal rates of cage displacement $\left(\frac{T_c^{(o)}}{T_c} \approx 0.5\right)$,

non-observance of this arrangement of seats may lead to an increase in sliding friction losses by a factor of 1.5.

4. Additional Considerations of Optimal Thrust Bearing Design with "Slewed" Rollers

According to the above formulas, the coefficient K characterizing the non-uniformity of load distribution over the roller length, is equal to

$$K = 6\mu \frac{d_r}{2l}\left(2B_{10} + \mu \frac{d_r}{2l} B_{11} \frac{y_1 - y_2}{l}\right).$$

Since $|2B_{10}| \geq \left|\mu \frac{d_r}{2l} B_{11} \frac{y_1 - y_2}{l}\right|$, we can consider with sufficient accuracy that $K = 12\mu \frac{d_r}{2l} B_{10}$. Thus, the coefficient K depends only on the angle γ. It follows from the curve of $K = K(\gamma)$ plotted in Fig.4.70 that, on changing from an angle of 5° to an angle of $45'$ which corresponds to the positioning of all seats at identical angles, the coefficient K will decrease from 0.35 to 0.14.

The arrangement of all cage seats at equal angles is preferable also in view of the following considerations: If the angle of slope of the seats is identical, the forces $F_{1x} - F_{2x}$ driving the rollers against their lateral surfaces are very small. If $M_{fr} = 0$ and $s = 1$, these forces are theoretically absent. /416

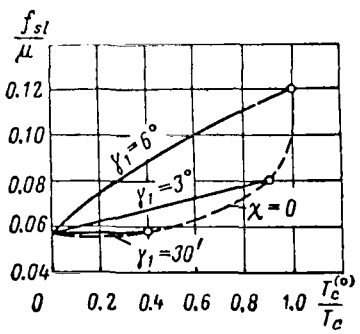

Fig.4.69 Losses Due to Sliding Friction.

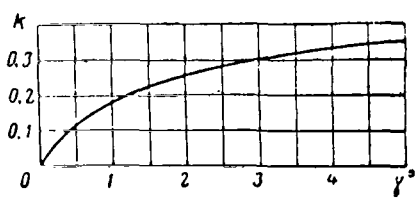

Fig.4.70 Coefficient K as a Function of the Roller Angle of Slope.

At different angles of slope of the seats, when the "slewed" rollers must overcome the resistance of radially arranged rollers, the forces $F_{1x} - F_{2x}$ may attain substantial magnitudes (up to $0.1\,\mu P$) and cause wear of the cage (especially at large χ).

So far, it has been assumed that all rollers are of identical length. Now let us see what happens at an alternation of long and short rollers in staggered sequence.

Table 4.13 shows that, in the latter case, the time T_c and the reduced coefficient of friction f_{fr} vary negligibly, whereas the coefficient K for short rollers increases by a factor of 3. This indicates that it is expedient to use rollers of the same length in thrust bearings with slewed rollers.

TABLE 4.13

EFFECT OF DISTRIBUTION OF ROLLER LENGTH ON T_c, f_{fr}, AND K

Variant of Distribution of Roller Lengths	T_c min	f_{fr} (when $f_{r0}=0.003$)	K
Rollers of identical length ($l_1=l_2=8$ mm)	48	0.00616	0.14
Long and short rollers alternating in staggered sequence ($l_1=11$ mm, $l_2=5$ mm)	45.7	0.00674	0.43 (for short rollers)

In estimating the effect of a nonuniform load distribution caused by the action of the moment $(F_{1y} + F_{2y}) \frac{d_r}{2}$ on the life expectancy of a bearing, one must not lose sight of the fact that the load at each contact point does not remain constant but changes with any change in direction of rotation. In particular, at the ends of the rollers the normal load varies in accordance with the law

$$q=\frac{P}{l} \pm \frac{1}{2}|K|\frac{P}{l}.$$

As a consequence, the nonuniformity of load distribution caused by the effect of the above moment should not excessively reduce the service life of the bearing. /417

The usual concentration of load on the ends of the rollers, which we have disregarded assuming that q = const at $\gamma = 0$, is of importance. To lessen the detrimental effect of the latter, it is preferable to use rollers with a camber.

5. Example of Calculating a Thrust Bearing with "Slewed" Rollers

In conclusion, let us give an example of calculating a thrust bearing with "slewed" rollers.

Given: axial load N = 20,000 kg, vibration amplitude of revolving race φ_0 = = 4.5°, frequency n = 180 cyc/min.

For the given conditions, we select a bearing with the following parameters: d_r = 12 mm, r_c = 61 mm, l = 10.5 mm (total length of rollers: l' = 12 mm), z = 20, and s = 2.

Wanted: to determine the angles of slope of the cage seats that will ensure optimal rate of displacement and maximum service life of the bearings.

We calculate the coefficient v:

$$v=\frac{\sum_{k=1}^{s}\frac{r_{i_k}}{r_c}}{\sum_{k=1}^{s}\frac{r_{i_k}^2}{r_c^2}}=\frac{1}{1+\left(\frac{l'}{2r_c}\right)^2}=\frac{1}{1+\left(\frac{12}{2\times61}\right)^2}=0.99.$$

Let us assume that all seats have an identical angle of slope. After substituting into eq.(6.15) $\varphi_0 = 4.5^\circ$, n = 180 cyc/min, v = 0.99, and $\mu = \mu'$ = = 0.05, we will construct the curve of $T_c = T_c(\gamma)$ by means of Table 4.11. From the curve we find the value γ' of the angle γ at which $T_c = T_c'$ = 80 min. In our case, $\gamma' = 46'$. Taking $\xi_m = 7'$ and e_{max} = 0.18 mm, we determine the deviation of ξ:

$$\xi=7+57.3\times60\,\frac{0.18}{2\times61}=12'.$$

The normal value of the angles of slope of the seats of the cage is

$$\gamma=\gamma'+\xi=46+12=58'.$$

The contact stresses in the bearing are

$$\sigma=860\sqrt{\frac{N}{zs\times d_r l}}=860\sqrt{\frac{20{,}000}{20\times2\times1.2\times1.05}}\approx17\,000\ \text{kg/cm}^2.$$

According to Fig.4.53, nh = 27×10^4 corresponds to this value of σ. Consequently, the service life of the bearing is

$$h=\frac{27\times10^4}{180}=1500\ \text{hrs}.$$

REFERENCES /418

1. Riz, P.M. and Pozhalostin, A.I.: Vibrations and Dynamic Strength of Propellers (Vibratsii i dinamicheskaya prochnost' vozdushnykh vintov). Tr. Tsentr. Aero-Gidrodinam. Inst., No.609, 1947.
2. Mil', M.L.: Dynamic Twisting of an Autogiro Rotor Blade in Flight (O dinamicheskom zakruchivanii lopasti rotora avtozhira v polete). Tekhn. Vozdushnogo Flota, No.2, 1937.
3. Bashkin, V.E.: Induced Velocities of a Propeller Exposed to Flow at an Angle to its Axis (Induktivnyye skorosti vozdushnogo vinta, obduvayemogo pod uglom k yego osi). Paper presented at the All-Union Congress on Theoretical and Applied Mechanics, Moscow, 1960.
4. Nekrasov, A.V.: Calculation of Natural Vibration Modes and Frequencies of Propeller Blades (Raschet form i chastot sobstvennykh kolebaniy lopastey vozdushnykh vintov). Tr. Tsentr. Aero-Gidrodinam. Inst., No.898, 1964.
5. Nekrasov, A.V.: Calculation of Natural Flexural and Torsional Vibration Modes and Frequencies of a Helicopter Blade in Vacuum (Raschet form i chastot sobstvennykh izgibno-krutil'nykh kolebaniy lopasti vertoleta v pustote). Tr. Tsentr. Aero-Gidrodinam. Inst., No.898, 1964.
6. Nekrasov, A.V.: Calculation of Stresses in a Helicopter Rotor Blade at High Flying Speeds (Raschet napryazheniy v lopasti nesushchego vinta vertoleta na bol'shikh skorostyakh poleta). Tr. Tsentr. Aero-Gidrodinam. Inst., No.898, 1964.
7. Nekrasov, A.V.: Calculation of Bending Stresses in a Helicopter Blade at Low and Moderate Flying Speeds (Raschet izgibnykh napryazheniy v lopasti vertoleta na malykh i srednikh skorostyakh poleta). Tr. Tsentr. Aero-Gidrodinam. Inst., No.913, 1964.
8. Galkin, M.S.: Solution of the Cauchy Problem for One Equation (O reshenii zadachi Koshi dlya odnogo uravneniya). Prikl. Mat. i Mekhan. Akad. Nauk SSSR, Vol.XX, No.2, 1956.
9. Lipskaya, M.E.: Determination of High Natural Frequencies of Propeller Blades and Turbine Buckets (Opredeleniye vysokikh sobstvennykh chastot vintovykh lopastey i turbinnykh lopatok). Tr. Mezhdunar. Assots. Pochvoved. SSSR, No.676, 1949.
10. Marchenko, V.M., Sarmina, L.A., and Vronskiy, G.V.: Calculation of Natural Blade Vibrations by Integral Equations on High-Speed Computers (Raschet sobstvennykh kolebaniy lopastey s pomoshch'yu integral'nykh uravneniy na bystrodeystvuyushchikh vychislitel'nykh mashinakh). Tr. Tsentr. Aero-Gidrodinam. Inst., No.898, 1964.
11. Ryzhik, I.M. and Gradshteyn, M.S.: Tables of Integrals, Sums, Series, and Products (Tablitsy integralov, summ, ryadov i proizvedeniy). GITTL, 1951.
12. Bogatyrev, B.V.: Static and Dynamic Strength of Rotor Blades of Rotary-Wing Aircraft (Staticheskaya i dinamicheskaya prochnost' lopastey rotorov vintokrylykh apparatov). Akad. Nauk SSSR, 1948.
13. Gureyev, D.I.: Self-Excited Oscillations of Helicopter Blades (Samokolebaniya lopastey gelikoptera). Izd. VVA im. Zhukovskogo, No.391, 1950.
14. Krasovskiy, A.A.: Vibration Method of Linearization of Certain Nonlinear Systems (O vibratsionnom sposobe linearizatsii nekotorykh nelineynykh sistem). Avtomatika i Telemekhanika, Vol.9, No.1, 1948.

15. Keldysh, M.V.: Shimmy of the Front Wheel of Aircraft Landing Gear (Shimmi perednego kolesa shassi samoleta). Tr. Tsentr. Aero-Gidrodinam. Inst., No.564, 1945.
16. Panovko, Ya.G.: Internal Friction during Vibrations of Elastic Systems (Vnutrenneye treniye pri kolebaniyakh uprugihh sistem). Fizmatgiz, 1960.
17. Grodko, L.N.: Forced Flexural Vibrations of a Bar in the Presence of a Linear Damper on a Hinge (Vynuzhdennyye kolebaniya izgiba sterzhnya pri nalichii lineynogo dempfera v sharnirnoy zadelke). Zh. Prikl. Mat. i Mekhan. Akad. Nauk,SSSR, Vol.XVII, No.5, 1953.
18. Belozerov, A.I., Grodko, L.N., and Litvakov, B.M.: Method of Eliminating Ground Resonance of Helicopters (Sposob ustraneniya zemnogo rezonansa vertoletov). Byul. Izobret., No.18, 1961; Patent No.141391.
19. Den-Gartog, Dzh.P.: Mechanical Vibrations (Mekhanicheskiye kolebaniya). Fizmatgiz, Moscow, 1960.
20. Babakov, I.M.: Theory of Vibrations (Teoriya kolebaniy). Gostekhteoret-izdat, 1958.
21. Belyayev, I.M.: Strength of Materials (Soprotivleniye materialov). Gostekhteoretizdat, 1958.
22. Kantorovich, L.V. and Krylov, V.I.: Approximate Methods of Higher Analysis (Priblizhennyye metody vysshego analiza). Gostekhteoretizdat, 1950.
23. Reshetov, D.N.: Combined Action of Radial and Axial Loads on Ball Bearings (Sovmestnoye deystviye na sharikovyye podshipniki radial'noy i osevoy nagruzki). Podshipnik, No.10-11, 1939.
24. Belyanchikov, M.P.: New Method of Calculating the Load-Carrying Capacity and Life Expectancy of Radial-Thrust Ball Bearings (Novaya metodika rascheta gruzopod"yemnosti i dolgovechnosti radial'no-upornykh shariko-podshipnikov). Podshipnik. Prom., No.3, 1960.
25. Beyzel'man, R.D. and Tsypkin, B.V.: Antifriction Bearings, Manual (Podshipniki kacheniya, Spravochnik). Mashgiz, 1960.
26. Spitsyn, N.A. and Sprishevskiy, A.I.: Antifriction Bearings, Textbook (Podshipniki kacheniya, Spravochnoye posobiye). Mashgiz, 1961.
27. Leykand, M.A. and Korostashevskiy, R.V.: Thrust Bearings of High Load-Carrying Capacity for Vibrations (Upornyye podshipniki povyshennoy gruzopod"yemnosti dlya kachatel'nogo dvizheniya). Tr. VNIPP, No.4, 1961. /419
28. Leykand, M.A., Kurova, I.V., and Komissarova, T.M.: Lubrication of Anti-friction Bearings Operating with Vibrations (Smazka podshipnikov kacheniya, rabotayushchikh pri kachatel'nom dvizhenii). Podshipnik. Prom., No.6, 1962.
29. Bochkov, V.S.: Theoretical Determination of Center-of-Gravity Shift of Radial-Thrust Ball Bearings under Combined Load (Teoreticheskoye opre-deleniye smeshcheniya tsentra tyazhesti radial'no-upornykh sharikopodship-nikov pri kombinirovannoy nagruzke). Tr. VNIPP, No.4, 1962.
30. Leykand, M.A.: Calculation of Ball Bearings Operating under Combined Loads (Raschet sharikopodshipnikov, rabotayushchikh pri kombinirovannykh nagruz-kakh). In Coll: Strength and Dynamics of Aircraft Propellers (Sbornik "Prochnost' i dinamika aviatsionnykh dvigateley"). No.3, Mashgiz, 1966.
31. Pal'mgren, M.: Ball and Roller Bearings (Sharikovyye i rolikovyye podship-niki). Mashgiz, 1949.
32. Morris, T. and Tye, W.: The Stressing of Rotor Blades. Aircraft Eng., Vol.X, No.112, 1938.
33. Horvay, G.: Stress Analysis of Rotor Blades. J. Aeron. Sci., Vol.14, 1947.

34. Horvay, G.: Chordwise and Beamwise Bending Frequencies of Hinged Rotor Blades. J. Aeron. Sci., Vol.15, 1948.
35. Coleman, R.P.: Theory of Self-Excited Mechanical Oscillations of Hinged Rotor Blades. NACA, ARR, July 1942; NACA, ARR, No.3029, 1943.
36. Coleman, R.P. and Feingold, A.M.: Theory of Ground Vibrations of a Two-Blade Helicopter Rotor on Anisotropic Flexible Supports. NACA, Tech. Note, No.1184, 1947.
37. Horvay, G.: Vibrations of a Helicopter on the Ground. J. Aeron. Sci., Vol.13, No.11, pp.605-619, Nov. 1946.
38. Howarth, R.M. and Jones, C.H.: Ground Resonance of the Helicopter. J. Helicopter Assoc. (Great Britain), Vol.7, No.4, April 1954.
39. Sibley and Jones: Some Design Aspects of Tandem Rotor Helicopters. J. Helicopter Assoc. (Great Britain), Vol.13, No.15, Oct. 1959.
40. Gilly, I. and Normand, Y.: Stability of Three-Blade Helicopters on the Ground (Stabilité au sol des hélicoptères tripales). Tech. Sci. Aéron., No.6, 1952.
41. Heinrich: Compensation of Friction by Auxiliary Oscillatory Motion (Über die Kompensation der Reibung durch zusätzliche Schwingbewegung). ZAMM, No.22, pp.136-142, 1942.
42. Meldau, E.: Pressure Distribution in Radial Roller Ball Bearings (Druck-verteilung im Radial-Rollen Kugellager). Werkstatt und Betrieb, No.87, 1954.
43. Weibull, W.: A Statistical Representation of Fatigue in Solids. Trans. Roy. Inst. Technol., No.27, 1949.
44. Lundberg, G. and Palmgren, A.: Dynamic Capacity of Roller Bearings. Acta Polytech., Vol.96, 1952.
45. Harris, A.: Predicting Bearing Reliability. Machine Design, No.1, 1963.
46. Larivière, J.S.: Calculation of Service Life of Helicopter Blades (Calcul de la durée d'utilisation des pales d'hélicoptères). Tech. Note STA/VT, No.165.
47. Selichov, A.F.: On the Theory of Calculation of Service Life of a Structure. Proc. 4th Congr. JCAS, Spartan Press, 1965.
48. Gessow, A. and Myers, G.: Aerodynamics of the Helicopter. Oborongiz, 1964.

Translated for the National Aeronautics and Space Administration by the O.W.Leibiger Research Laboratories, Inc.